Source book to the Forecasters' Reference Book

The Met.Office

Later reprint with some amendments (?)

SOURCE BOOK

to the

FORECASTERS' REFERENCE BOOK

Met.O.1024

Meteorological Office College

February 1997

ISBN 0 86180 321 3

Published by The Met. Office
London Rd
Bracknell
Berkshire
RG12 2SZ

PREFACE

This latest edition of the *Forecasters' Reference Book* (*FRB*) builds on the strengths of the previous editions and handbooks, incorporating the latest science, where this is available in 'forecaster-friendly' form. From the outset, in designing the contents and format, every regard has been paid to forecasters' suggestions; the draft chapters have been thoroughly reviewed by a panel of forecasters and specialists. In this review process it became apparent that, to do justice to the copious literature on forecasting techniques, it was sensible to present not only a *FRB* of selected forecasting techniques but also a more erudite account of techniques, alternatives and limitations in a *Source Book*. The Chapters of the *FRB* and the *Source Book* should be seen as complementing many of those in *Images in Weather Forecasting*, 1995 (Ed. M. Bader et al.).

Remote Sensing, and Numerical Weather Prediction, now integral parts of the the forecasters' armoury are constantly referred to in the text but, with many guides available (e.g. *Images in Weather Forecasting*), they are only touched upon in the *Source Book* and *FRB*. Other chapters reflect the increasing concern over Air Pollution (*Source Book* Chapter 12), as well as the customer demand for Probability Forecasting (*FRB* and *Source Book* Chapter 11). I am grateful to Eddie Carroll for contributing Chapter 8, reflecting his insight on the use of dynamical concepts in assessing development. Chapter 11, Probability Forecasts, is based on a lecture course prepared by Bob Riddaway.

Where appropriate, Sections have references to key published papers as well as useful general reading articles/books. Reference is often made to the *Handbook of Weather Forecasting*, 1975 (HWF), which contains detailed accounts of forecasting techniques, accompanied by copious references.

There are some topics, such as fog, stratocumulus, and airflow over hills, where a more-detailed physical and dynamical picture has been included in the *Source Book* to enable the forecaster to make more considered judgements in forecasting elements whose behaviour is at best capricious.

As with previous editions it should be noted that this *Forecasters' Reference Book* has been produced specifically for the UK Meteorological Office forecaster; thus, forecasting techniques and rules apply mainly to the British Isles and north-west Europe and will not necessarily be applicable in other areas.

John R. Starr
Meteorological Office College
Shinfield Park

February 1997

SOURCE BOOK

to the

FORECASTERS' REFERENCE BOOK

CONTENTS

CHAPTER 1 — WIND

CHAPTER 1 — WIND

1.1 Winds in the free atmosphere

1.1.1 Geostrophic wind (V_g)

V_g is defined as the steady (unaccelerating), horizontal wind which results from the balance of two forces only — namely the pressure gradient force and the Coriolis force, f. It follows that geostrophic wind is a good approximation to the actual wind only with isobars (or contours) which are straight, parallel and not changing with time. There are significant differences from V_g in strongly curved flow and flow near surfaces.

On MSL charts, or any other chart at a constant height level:

$$V_g = (1/\rho f)\,|\Delta p/\Delta n|$$

where Δn is measured normal to the isobars and V_g blows with low pressure to the left in the northern hemisphere; ρ is the air density. Similarly on charts at a constant pressure level:

$$V_g = (g/f)\,|\Delta z/\Delta n|$$

where $|\Delta p/\Delta n|$ is the scalar horizontal pressure gradient (in hPa m^{-1}), $|\Delta z/\Delta n|$ is the height gradient along a constant pressure surface (in m m^{-1}) and V_g is expressed in m s^{-1}.

(Note: The Rossby Number, V_g/fL (where L is a scale length) is a useful measure of the validity of the geostrophic approximation; the smaller the value the smaller the ageostrophic contribution.)

1.1.1.1 Tables for geostrophic winds

Table 1.1 may be used to derive V_g for charts on which no geostrophic wind scale is provided. It gives 'multipliers' corresponding to a pressure (contour height) change over a distance of 300 n mile (or 5° latitude) of 1 hPa (1 dam).

Examples:

(i) A gradient of 5 hPa per 300 n mile at 55° N corresponds to $V_g = 5 \times 2.4 = 12$ kn (approx.).

(ii) A gradient of 12 dam per 300 n mile at 50° N corresponds to $V_g = 12 \times 3.1 = 37$ kn (approx.).

Table 1.1. To derive V_g for charts with no geostrophic scale

	Pressure/height change over 300 n mile	
	Isobars (hPa)	Contours (dam)
Latitude (°)	multipliers	
70	2.1	2.5
60	2.3	2.7
55	2.4	2.9
50	2.6	3.1
45	2.8	3.3
40	3.1	3.7
35	3.4	4.1
30	3.9	4.7

If gradients are measured over shorter distances, the factors should be altered in proportion, i.e. for 150 n mile (2.5° latitude span) the factors are doubled. Correction factors for density variations may be applied to geostrophic wind values measured by scales based on the Standard Atmosphere (1013.2 hPa, 15 °C) as follows:

Table 1.2. Percentage corrections to geostrophic wind

Pressure	Temperature (°C)								
(hPa)	+40	+30	+20	+10	0	−10	−20	−30	−40
920	120	116	112	108	104	101	97	93	89
940	117	113	110	106	102	98	95	91	87
960	115	111	107	104	100	96	93	89	85
980	112	109	105	102	98	94	91	87	84
1000	110	107	103	100	96	93	89	85	82
1020	108	104	101	98	94	91	87	84	80
1040	106	102	99	96	92	89	86	82	79
1060	104	101	97	94	91	87	84	81	77

Example:
If the measured $V_g = 25$ kn at a location where the pressure is 1030 hPa and the temperature is −10 °C, then the true $V_g = 25 \times 90\% = 22.5$ kn.

1.1.2 Gradient wind

When its trajectory is curved, air must be subjected to a local centripetal acceleration, V^2/r, where V is the gradient wind velocity and r is the radius of curvature of the trajectory.

The gradient wind equations are:

(i) for cyclonic curvature:
$V_{gr} = 0.5[- rf + (r^2f^2 + 4rf\,V_g)^{0.5}]$ gradient wind is sub-geostrophic;

(ii) for anticyclonic curvature:
$V_{gr} = 0.5[+ rf - (r^2f^2 - 4rf\,V_g)^{0.5}]$ gradient flow is super-geostrophic.

1.1.2.1 Estimation of gradient wind (tabular method)

Corrections to be applied to the geostrophic wind to obtain the gradient wind are given in **Table 1.3**. The top section of the table (a) shows how changes in the Coriolis parameter affect the results. Thus a radius of **600** n mile at latitude 50° is equivalent to a radius of **489** n mile at latitude 70° or **919** n mile at latitude 30°.

1.1.2.2 Estimation of gradient wind (graphical method)

Fig. 1.1 is a graph for obtaining the gradient wind speed from the speed of the geostrophic wind and the radius of curvature. The graph is drawn for use at latitude 50°. For use at other latitudes the radius of curvature must be multiplied by a correction factor to obtain the equivalent value at latitude 50°.

To use the graph:

(i) Use the right-hand inset to find the equivalent radius of curvature for latitudes other than 50°. Multiply the actual radius by the factor shown against the value for latitude. If, for example, the radius at latitude 39.5° N is 1200 n mile, the correction factor is 0.83 and the equivalent radius at latitude 50° is about 1000 n mile.

(ii) Find the point of intersection of the geostrophic wind speed (shown along the left-hand axis) with the curve showing the radius of curvature. The cyclonic curves lie to the left and the anticyclonic curves lie to the right of the straight line denoting infinite radius. The gradient wind speed is shown along the bottom of the diagram. Thus with a radius of curvature of 1000 n mile and $V_g = 90$ kn, the gradient wind is 76 kn for cyclonic curvature and 136 kn for anticyclonic curvature.

The theoretical maximum gradient wind speed for anticyclonic curvature is twice the geostrophic wind. The graphs show that as the gradient wind approaches this value, small increases in the geostrophic wind can produce very large increases in the gradient wind.

Table 1.3. Gradient wind corrections

(a)

Latitude (°)	Radius of curvature of isobar or contour (n mile)											
70	98	147	196	245	367	**489**	737	978	1467	1957	2446	3261
60	106	159	212	265	398	531	796	1061	1592	2123	2654	3538
50	120	180	240	300	450	**600**	900	1200	1800	2400	3000	4000
40	143	215	286	358	536	715	1073	1430	2145	2860	3575	4767
30	184	276	368	460	689	**919**	1379	1839	2758	3677	4596	6128

The corrections are to be applied to the geostrophic wind to obtain the gradient wind when the system of isobars or contours is stationary.

(b)

Geostrophic speed (kn)	Cyclonic curvature correction (kn)											
10	−1	−1	−1	−1	0	0	0	0	0	0	0	0
20	−5	−4	−3	−3	−2	−1	−1	−1	−1	0	0	0
30	−9	−7	−6	−5	−4	−3	−2	−2	−1	−1	−1	−1
40	−14	−11	−10	−8	−6	−5	−4	−3	−2	−2	−1	−1
60	−25	−21	−18	−16	−12	−10	−8	−6	−4	−3	−3	−2
80	−37	−32	−28	−25	−20	−17	−13	−10	−7	−6	−5	−4
100	−51	−44	−39	−35	−28	−24	−18	−15	−11	−9	−7	−6
120	−64	−56	−50	−46	−38	−32	−25	−21	−15	−12	−10	−8
140	−78	−69	−62	−57	−47	−41	−32	−27	−20	−16	−13	−10
160	−93	−83	−75	−69	−58	−50	−40	−33	−25	−20	−17	−13
180	−108	−96	−88	−81	−69	−60	−48	−40	−31	−25	−21	−16
200	−123	−111	−101	−94	−80	−70	−57	−48	−37	−30	−25	−20

(c)

Geostrophic speed (kn)	Anticyclonic curvature correction (to be added) (kn)											
10	4	2	1	1	1	0	0	0	0	0	0	0
20	—	—	8	5	3	2	1	1	1	0	0	0
30	—	—	—	26	8	5	3	2	1	1	1	1
40	—	—	—	—	20	11	6	4	2	2	1	1
60	—	—	—	—	—	52	16	10	6	4	3	2
80	—	—	—	—	—	—	39	21	12	8	6	4
100	—	—	—	—	—	—	—	41	20	13	10	7
120	—	—	—	—	—	—	—	104	32	20	15	11
140	—	—	—	—	—	—	—	—	50	30	22	15
160	—	—	—	—	—	—	—	—	79	42	30	20
180	—	—	—	—	—	—	—	—	156	59	40	26
200	—	—	—	—	—	—	—	—	—	83	53	34

1.1.2.3 Curvature of trajectories for systems in motion

Significant differences occur between the curvature of trajectories and the curvature of isobars or contours when the systems are in motion (**Fig. 1.2**).

In (a) the eastward moving depression has a speed of half the geostrophic wind around it, while (b) has a speed twice the geostrophic. Calculated parcel trajectories take into account the locally changing pressure pattern. Trajectory curvature is much less than isobaric curvature on southern and western sides, greater on northern and eastern sides. Thus winds could be super-geostrophic on the south-western side (assuming even isobaric spacing) of a fast-moving depression, and certainly stronger than those in the north-eastern sector.

Holton (1992)

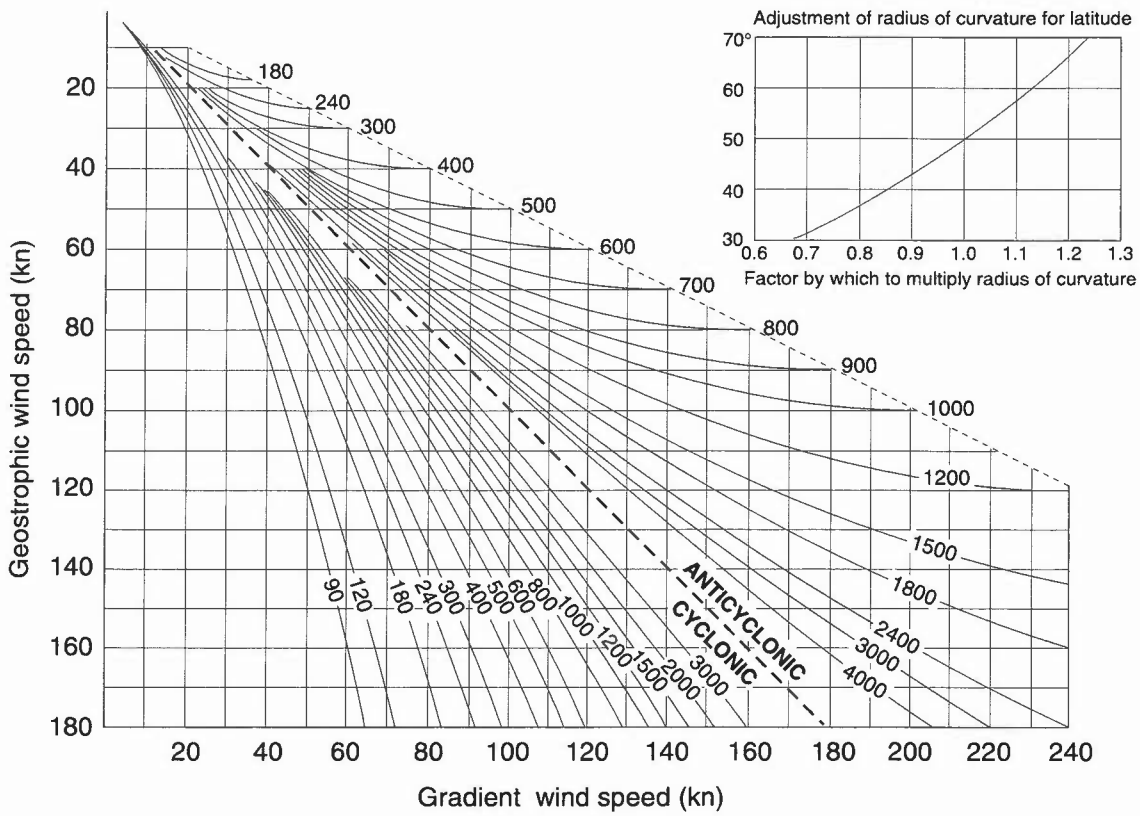

Figure 1.1. A graph to obtain the gradient wind speed from the speed of the geostrophic wind and the radius of curvature.

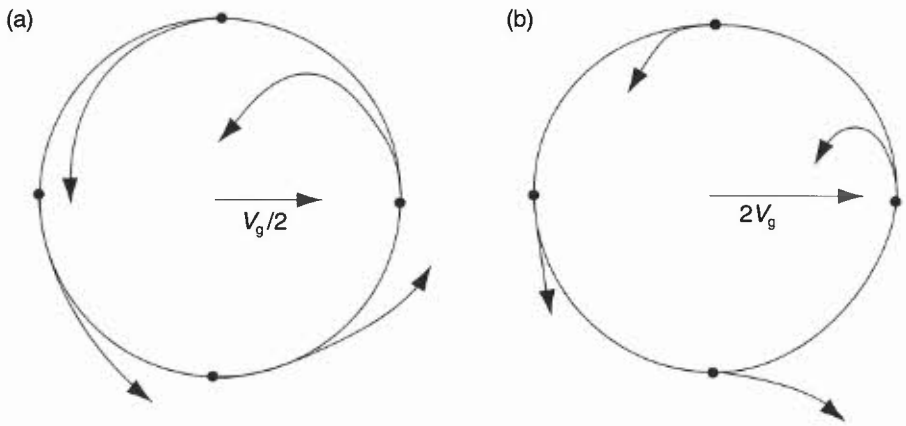

Figure 1.2. (a) Calculated trajectories of parcels of air around a depression moving eastwards at half the geostrophic wind speed. (b) Calculated trajectories of parcels of air around a depression moving eastwards at twice the geostrophic wind speed.

1.1.3 Variations in the mean wind

1.1.3.1 Ageostrophic winds (see Chapter 8)

An actual wind may be considered to have two components, one of which is geostrophic and the other ageostrophic (non-geostrophic).

1.1.3.2 Thermal winds

(i) The *thermal wind* in the layer between two pressure levels is the vector difference between the geostrophic winds at two levels B (upper level) and A (lower level) (**Fig. 1.3**).
Thus: $V_{\text{thermal}} = V_A - V_B$.

(ii) A geostrophic wind is proportional to the contour height gradient at a pressure level; a thermal wind, $V_{thermal}$, measures the difference in the contour gradient between two pressure levels. $V_{thermal}$ is proportional to the horizontal temperature gradient in the layer. It may be regarded as a steering wind for surface features.

(iii) A strong north–south temperature gradient implies a strong westerly thermal wind with a westerly wind component increasing with height in the layer. A reversed temperature pattern gives easterly thermal winds, and a westerly wind component decreasing with height.

(iv) Although the thermal wind is geostrophic, practical computations use the difference between the actual winds at two levels. This is normally acceptably accurate.

Holton (1992)

1.1.4 Use of the hodograph

Plotting

Wind vectors are plotted on a hodograph so that they end at the centre of the diagram. **Fig. 1.3** shows a 900 hPa wind of 240° 20 kn and an 800 hPa wind of 300° 30 kn. The thermal wind in this layer is the vector from B to A. A normal hodograph plot only shows the points at each pressure level, joined to show the thermal winds in each layer.

Identifying the direction of warm and cold air

In **Fig. 1.4** the colder air is shown by light stippling and the warmer air by heavy stippling. Arrows show the direction of the thermal winds in the different layers. Thus between 850 and 500 hPa the thermal wind direction is 240° which shows that the colder air lies towards the north-west. Between 500 and 400 hPa the thermal wind direction is 005° indicating that in that layer the colder air is towards the east.

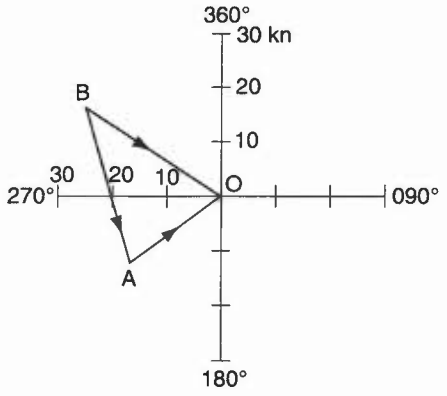

Figure 1.3. Plotting wind vectors on a hodograph. AO is the lower-level wind vector (say, 900 hPa). BO is the upper-level wind vector (say, 800 hPa). BA is the thermal wind vector (directed from the upper to the lower wind vectors).

Warm and cold advection

Between 900 and 850 hPa in **Fig. 1.4** the thermal wind direction is 315°, indicating colder air to the north-east. Since the mean wind direction between these levels is from the north-east, colder air is being advected towards the station. This cold advection is in fact taking place at all levels up to 500 hPa. (i.e. wind is backing with height). Between 500 and 400 hPa the thermal wind is from 005° while the mean wind is about 345° indicating weak warm advection (wind is veering with height).

1.1.4.1 Fronts and vertical motion

Fig. 1.5 shows a construction which can be useful when a frontal surface lies over the station at some level.

(i) Mark the surface front through the centre of the hodograph, its orientation being as shown on a surface chart.

(ii) Determine the upper and lower levels of the frontal zone from a tephigram (i.e. noting change of θ_w), and mark them on the hodograph. The thermal wind direction in the frontal zone is often roughly parallel to the front.

(iii) Measure the wind component normal to the front at each level in the frontal zone and in the warm air mass above.

(iv) The frontal speed at the surface approximates to the speed of the cold air normal to the front at the base of the frontal zone (although adiabatic effects often lead to this being an overestimate).

(v) If the wind component normal to the front increases with height in the warm air, then: a warm front is an anafront, and a cold front is a katafront.

(vi) If the wind component normal to the front decreases with height in the warm air, then: a warm front is a katafront, and a cold front is an anafront.

HWF (1975), Chapter 3.4.3

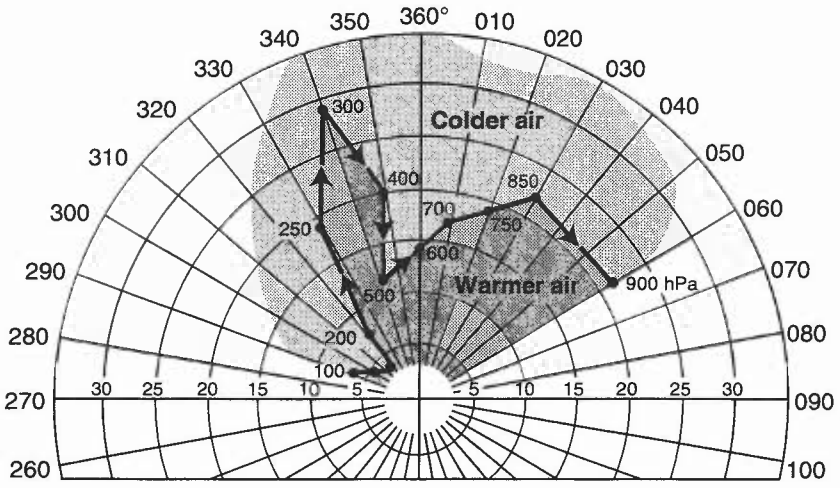

hPa	deg	kn
900	060	22
850	030	22
750	020	19
700	010	17

hPa	deg	kn
600	360	14
500	340	12
400	350	20
300	340	29

hPa	deg	kn
250	330	18
200	320	7
150	320	4
100	300	6

Figure 1.4. Hodograph example: Stornoway, 0600 UTC on 9 June 1961.

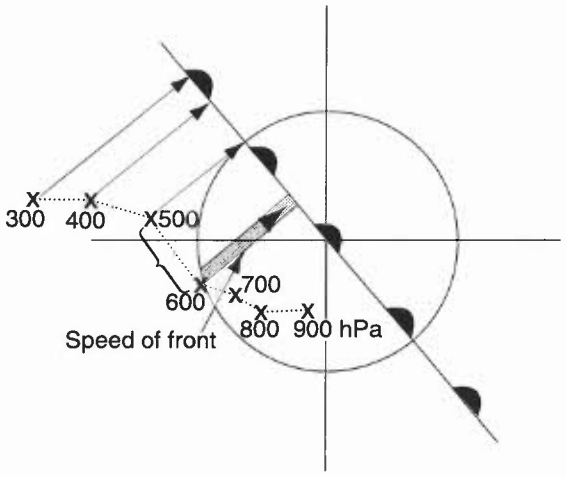

Figure 1.5. Assessment of ana- and kata-frontal characteristics from a hodograph.

1.1.5 Jet streams

1.1.5.1 The polar-front jet

(i) This is so named for its links with the polar front.
(ii) This jet is found over a wide range of latitudes between 35° and 70°.
(iii) The mean position is nearer the equator in winter than in summer.

A cross-section through a typical example of a polar-front jet is shown in **Fig. 1.6**, and the relationship between the location of surface fronts and jet core in a mature system in **Fig. 1.7**.

Height

(i) The jet core is located in the warm air about 3000 ft below the tropopause, usually between 300 and 250 hPa, and vertically above the position of the frontal zone at 500 hPa.
(ii) The level varies along the length of the jet, being higher round ridges and lower near troughs.

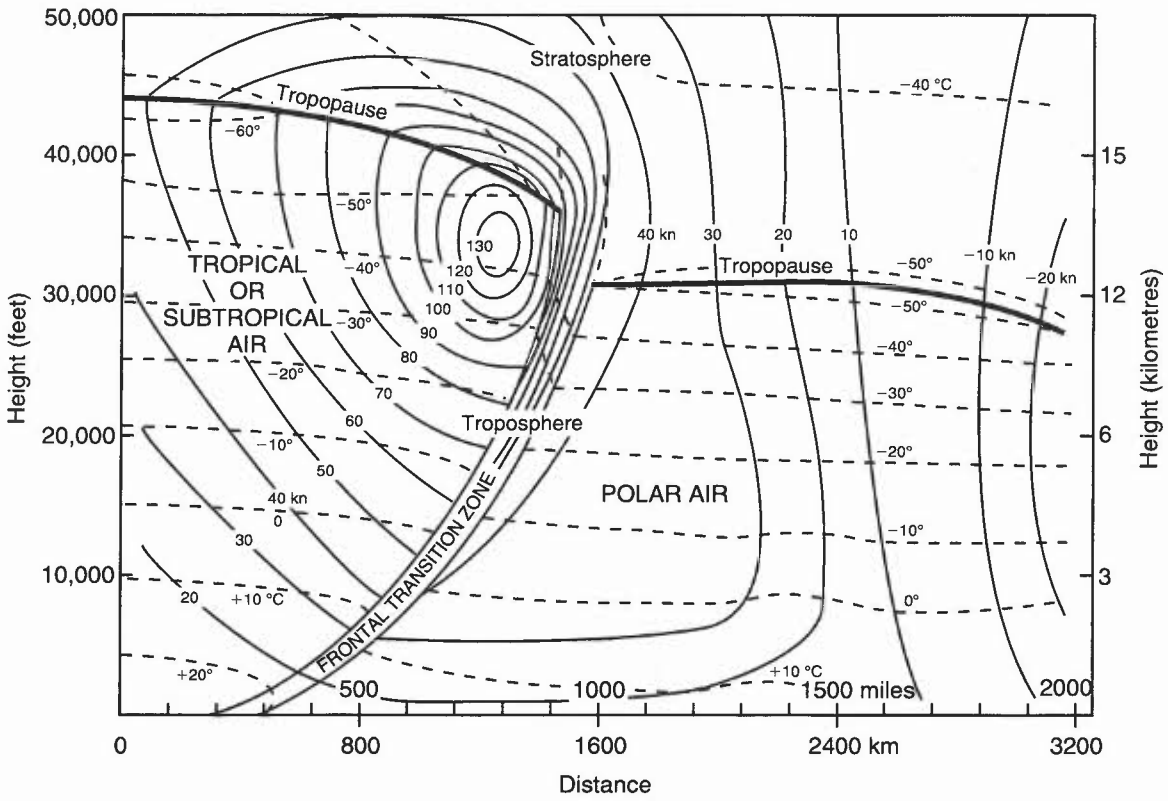

Figure 1.6. Cross-section across a polar-front jet stream. Solid lines are isotachs (knots) and broken lines isotherms (°C). Positive wind speeds have a component out of the plane of the page.

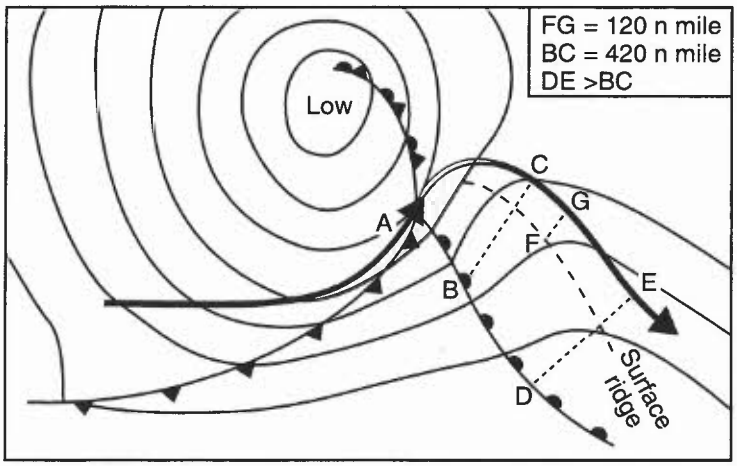

Figure 1.7. Polar-front jet in relation to surface fronts. The broad arrow represents the core of the jet at 300 hPa, which is weak or broken in the unshaded section. A is the tip of the warm sector.

Direction:

(i) The majority of jets have a component from between 190° and 350°.

(ii) Northerly or north-easterly jets occur at times in the winter months. South-easterly jets are rare.

Speeds

(i) Winter jets can often reach 150 kn and may sometimes exceed 200 kn.

(ii) The 300 hPa wind speed is approximately twice the maximum thermal wind in the 500 to 1000 hPa layer, but displaced some 60 n mile to the cold side of the thermal wind maximum.

(iii) The core of a jet at any level crosses the contour pattern on the entrance and exit regions of a jet, due to ageostrophic effects **(Fig. 1.8)**. (See 8.2).

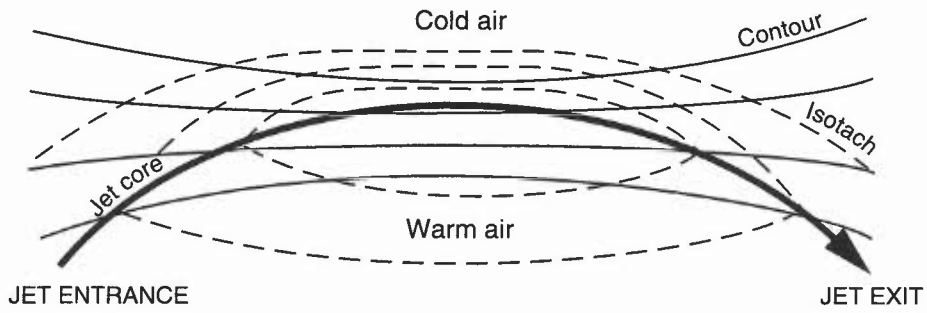

Figure 1.8. Position of the jet core on an upper-level chart, in relation to the contour lines. In the entrance and exit regions, ageostrophic effects produce cross-contour flows. In the steady part of the jet the core is displaced towards the cold side of the contour pattern.

Vertical shear

This varies in relation to the strength of the jet **(Table 1.4)**:

Table 1.4. Vertical shear associated with jet streams

Typical values:	
Normal	3–6 kn per 1000 ft
Large	10–15 kn per 1000 ft
Extreme	more than 20 kn per 1000 ft

(i) The maximum horizontal shear is generally on the cold side of the jet at about the core level, or slightly below.
(ii) On the warm side of the jet the maximum anticyclonic shear is slightly above the core level.
(iii) Theoretically the anticyclonic shear cannot exceed the Coriolis parameter which has values as follows **(Table 1.5)**.

Table 1.5. Coriolis parameters

Latitude (°)	30	35	40	45	50	55	60	65	70
Coriolis parameter (kn/100 n mile)	26	30	34	37	40	43	45	47	49

When the warm-side maximum shear values are attained, or exceeded, the flow becomes turbulent.

1.1.5.2 The subtropical jet

The subtropical jet generally occurs between latitudes 20 and 30° and is most marked during the winter months.

1.1.5 3 Overlapping of jets

(i) Satellite pictures show that a cyclonically curved polar-front jet may cross underneath the anticyclonically curved subtropical jet.
(ii) There are then two velocity maxima, one near 200 hPa and the other near 300 hPa.
(iii) Very sharp changes of wind direction can occur in the relatively shallow layer between the two jet cores, resulting in severe clear air turbulence (CAT).

HAM (1994)

1.2 Winds near the surface

Forecasts required will depend on what is at risk and the nature of the wind/gust hazard.

Hunt (1995)

1.2.1 *Surface wind and gradient wind*

(i) The surface wind is usually reduced in speed and backed in direction from the gradient wind (**Fig. 1.9**).

(ii) The magnitude of the change depends on the stability of the air and the roughness of the surface. Rough surfaces increase the frictional effect; greater stability reduces the turbulent exchange of energy between the flow aloft and that at the surface. An increase in stability near the surface implies a change in the vertical wind profile.

1.2.1.1 *Surface wind and 900 m wind (statistical relations)*

Table 1.6 shows some observed relationships between the speed of the surface wind (V_0) and the 900 m wind (V_9), together with the angle (α) between them.

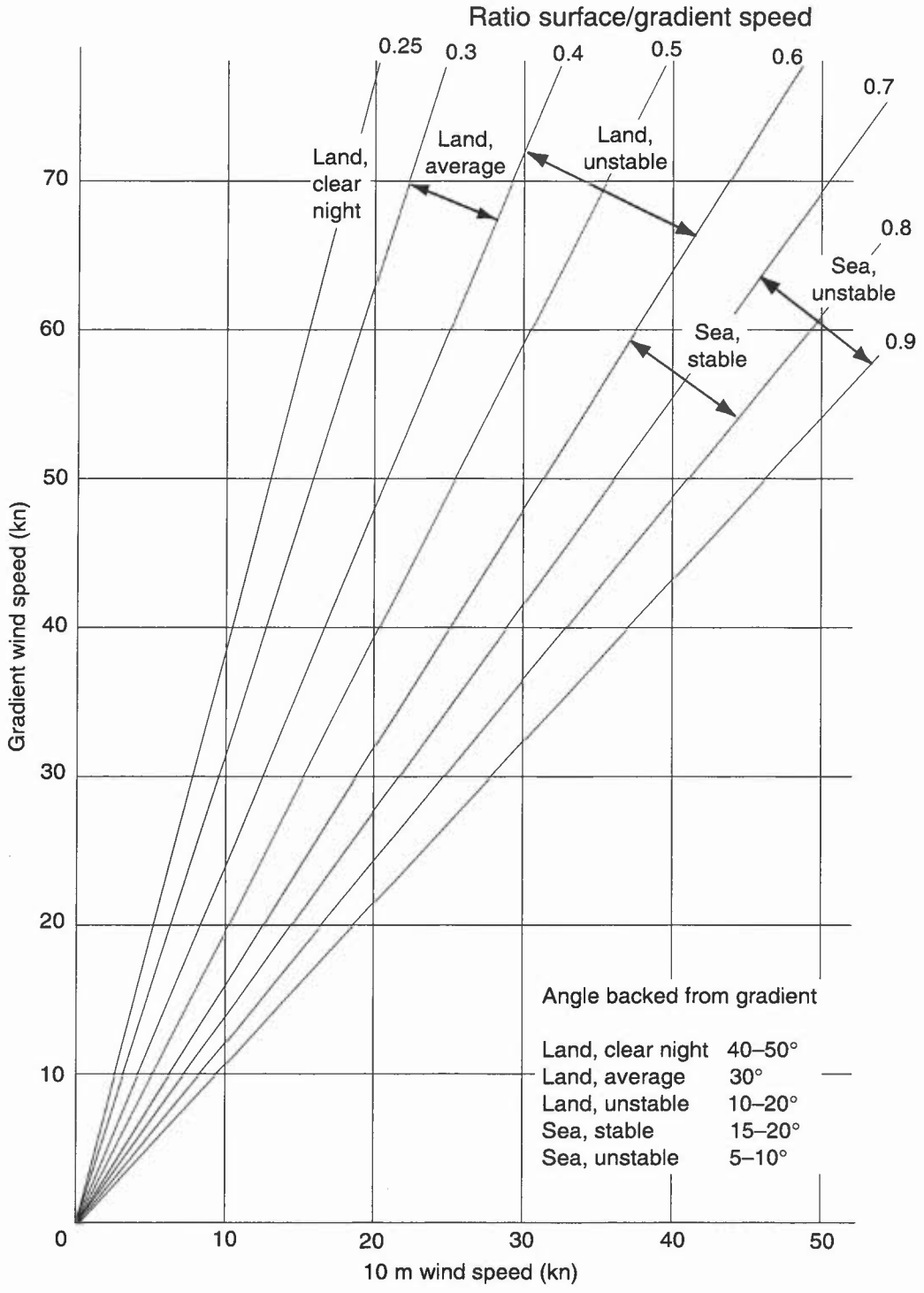

Figure 1.9. Nomogram for determining the 10 m wind speed and direction from gradient wind speed in various conditions of stability and surface roughness (the numbers on the diagonal lines represent the ratio of surface/gradient speed).

Lapse-rates are classified as:

1. Superadiabatic.
2. Conditionally unstable.
3. Conditionally stable.
4. Stable.
5. Isothermal/Inversion*.

*Important from the aviation point of view is the breaking up of the surface inversion with the consequent increase in mean surface wind

(The above lapse rate classes are based on the difference between surface and 900 hPa temperatures, differences which may not reflect the boundary-layer stability all that well.)

Table 1.6. Observed relationships between the speed of the surface wind (V_0) and the 900 m wind (V_9) together with the angle (α) between them

(a) Over the sea: at 59° N, 19° W and 52° N, 20° W

Lapse class	900 m wind speed (kn) 10–19		20–29		30–39		40–49		>50	
	V_0/V_9	α	V_0/V_9	α	V_0/V_9	α	V_0/V_9	α	V_0/V_9	α
1	0.95	0	0.90	0	0.85	0	0.80	0	0.80	0
2	0.90	5	0.85	5	0.80	5	0.75	5	0.75	5
3	0.85	10	0.75	10	0.70	10	0.65	10	0.65	10
4	0.80	15	0.70	20	0.65	20	0.60	20	0.60	20
5	0.75	15	0.70	20	0.65	20	0.60	20	0.55	25

(b) Over land: at London (Heathrow) Airport

Lapse class	900 m wind speed (kn) 10–19		20–29		30–39		40–49		>50	
	V_0/V_9	α	V_0/V_9	α	V_0/V_9	α	V_0/V_9	α	V_0/V_9	α
Daytime										
1, 2	0.65	5	0.55	5	0.50	10	0.50	10	0.35	15
3	0.50	20	0.45	20	0.45	20	0.45	20	0.45	15
4	0.45	35	0.45	30	0.40	25	0.30	20	0.40	25
5	0.35	45	0.40	35	0.35	35	0.40	30	0.40	30
Night-time										
1, 2	0.25	20	0.35	25	0.30	35	0.40	15	0.40	25
3	0.35	25	0.35	30	0.35	25	0.35	20	0.35	15
4	0.30	35	0.30	35	0.30	30	0.35	30	0.35	15
5	0.30	45	0.25	40	0.25	35	0.30	30	No obs	

(Some results based on less than 10 observations.)

Fig. 1.9 is a useful first-guide summary based on these figures.

Two sets of these analyses, using sectored wind directions with wind-speed bands to include the 2–10 kn range, and based on 3-monthly data sets from two appropriate radiosonde stations (for 00/12 UTC), enables a realistic estimate to be made (to be checked against model output) of the mean surface wind speed for local normal aircraft operations and TAFs.

Findlater et al. (1966)

1.2.2 Vertical wind shear

1.2.2.1 Vertical wind shear over surfaces with different roughness

(i) For neutral stability (defined as a dry adiabatic lapse rate throughout) the variation of wind speed (V) with height (z) may be expressed by: $V(z)/V(10) = \ln(z/z_o)/\ln(10/z_o)$ where z_o depends on the roughness of the terrain.

(ii) This relationship is considered reasonable to 100 m or so and is probably usable above that.

(iii) **Fig. 1.10** shows the calculated ratio V_z/V_{10} (the winds at z and 10 metres) for different surfaces.

(iv) The curves show that over wooded country:
if the 200 m wind is 18 kn, then the 100 m wind should be just under 16 kn and the 10 m wind should be 10 kn.

Table 1.7 gives the variation with height of the mean hourly wind and corresponding gusts, based on statistical data, and likely to be particularly applicable to open areas under neutral conditions.

Local Weather Manuals (1994)

Table 1.7(a). Variation with height of mean hourly wind speeds (knots) in open level situations calculated according to the formula $V_H = V_{33}((H^{0.17})/33)$

Standard effective height			Effective heights (H)			
33 ft	70 ft	100 ft	150 ft	200 ft	250 ft	300 ft
10	11	12	13	13	14	15
15	17	18	19	20	21	22
20	23	24	26	27	28	29
25	28	30	32	34	35	36
30	34	36	39	41	42	44
35	40	42	45	47	49	51
40	45	48	52	54	56	58
45	51	54	58	61	63	65
50	56	60	65	68	70	73
55	62	66	71	75	77	80
60	68	72	78	82	85	87

Table 1.7(b). Variation with height of gusts speeds (knots) in open level situations calculated according to the formula $V_H = V_{33}((H^{0.085})/33)$

Standard effective height			Effective heights (H)			
33 ft	70 ft	100 ft	150 ft	200 ft	250 ft	300 ft
30	32	33	34	35	36	36
35	37	38	40	41	42	43
45	47	49	51	52	53	54
50	53	55	57	58	59	60
55	58	60	62	64	65	66
60	64	66	68	70	71	72
65	69	71	74	76	77	78
70	74	77	80	82	83	84
75	80	82	85	87	89	90
80	85	88	91	93	95	96
85	90	93	97	99	101	102
90	95	99	102	105	107	109
95	101	104	108	111	113	115
100	106	110	114	117	119	121
105	111	115	119	122	125	127
110	117	121	125	128	131	133

Note: The above table represents a useful general guide, but may be misleading in very stable or very unstable conditions, in heavily built-up areas, very hilly ground, etc.

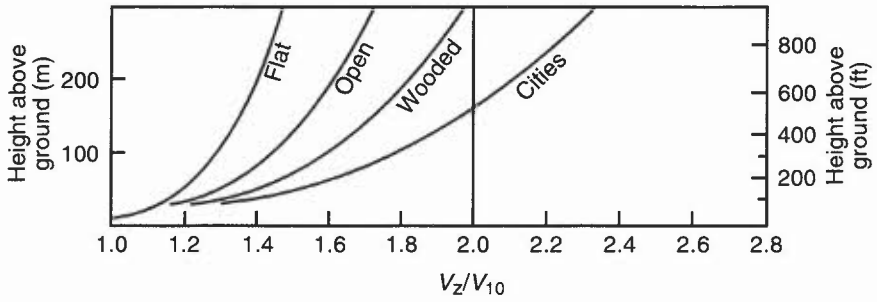

Figure 1.10. Calculated ratio of V_z/V_{10} over different surfaces in neutral stability conditions.

1.2.2.2 Vertical wind shear in different stability conditions

(i) Strong wind shears can be due to high stability, especially with increasing gradient winds.
(ii) There will be orographic/shelter influences.

Fig. 1.11 shows how the ratio V_z/V_{10} alters with changes of stability based on observations of wind changes between the surface and 400 ft with lapse rates ranging from +2 °C to −6 °C through that layer (lapse rate of −6 °C means a rise of 6 °C within the layer).

HWF (1975), Chapter 16.5.2
WMO (1969)

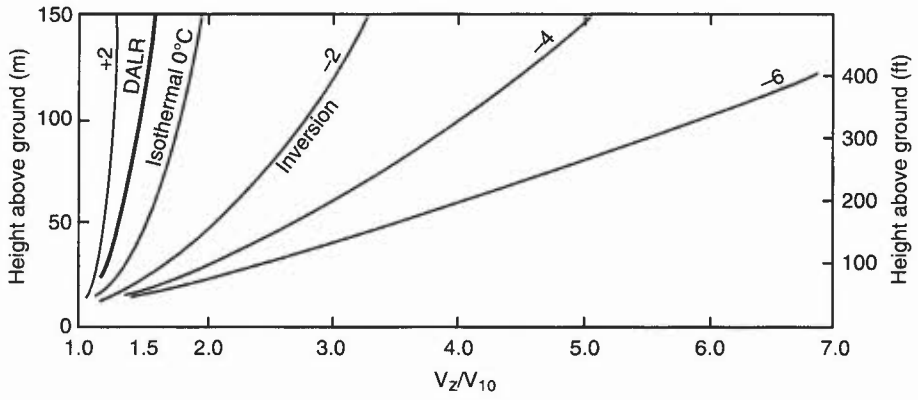

Figure 1.11. Observed ratio of V_z/V_{10} for different lapse-rates, measured at Cardington.

1.2.2.3 Criteria for airfield warnings of hazardous low-level wind shear/turbulence (see 6.2.1.1)

MO, Heathrow (198?)

1.2.2.4 The nocturnal jet and diurnal variations of vertical wind shear

Nocturnal jets can be an embarrassment to light aircraft when landing and will influence pollution transport (and bird migration).

(i) A nocturnal jet can occur overland when radiation cooling over a sufficient period of time (particularly during spring and autumn) stabilizes the near-surface flow (θ increases with height). The frictional force is greatly reduced in the upper part of the boundary layer where speeds become super-geostrophic and undergo an inertial oscillation about the geostrophic value.
(ii) Near the top of the stable layer the wind speed may be 1.5 and sometimes up to 3 times the geostrophic value **(Fig. 1.12).** The inertial period is about 17 hours in mid-latitudes; the magnitude of the geostrophic departure depends on the geostrophic wind departure at the end of the previous day. The jet will not be pronounced in light winds; the inversion cannot form if the wind is too strong.
(iii) The length of the night relative to the half inertial period determines whether the maximum super-geostrophic wind will occur by dawn when the jet becomes important in the subsequent boundary-layer evolution.

(iv) Wind in the lower layer has a cross-isobar angle of 60–70°. Over England speeds of 40 kn have been measured at heights usually below the top of the inversion (≈600 ft) by the end of a radiation night.
(v) By dawn the jet is more pronounced along a direction parallel to the surface geostrophic wind. The speed decreases rapidly after sunrise with jet break-down due mainly to convective activity from surface insolation reaching the jet level 2 to 3 hours after sunrise.
(vi) A helpful indicator of jet formation over rough terrain is if the 10 m wind decreases significantly after dark.

Above conditions are likely to be satisfied in an anticyclonic region of significant pressure gradient; warm advection forcing the development of mesoscale convective systems (4.7) is often associated with the nocturnal jet.

As an example of vertical wind shear: associated with a nocturnal 'jet', observed at Cardington on a radiation night, was a wind-speed shear of 0.42 kn m^{-1} (15 kn between 9 m (30 feet) and 45 m (150 feet)).

Downward momentum transfer is an important consideration for night aviation forecasts; it can maintain light surface winds over airfields on ridges and small hills, keeping them from visibility deterioration that might occur in the valley. Conversely, diurnal reversal after sunrise may result in deteriorating conditions of fog/low stratus.

Stull (1988)
Thorpe & Guymer (1977)

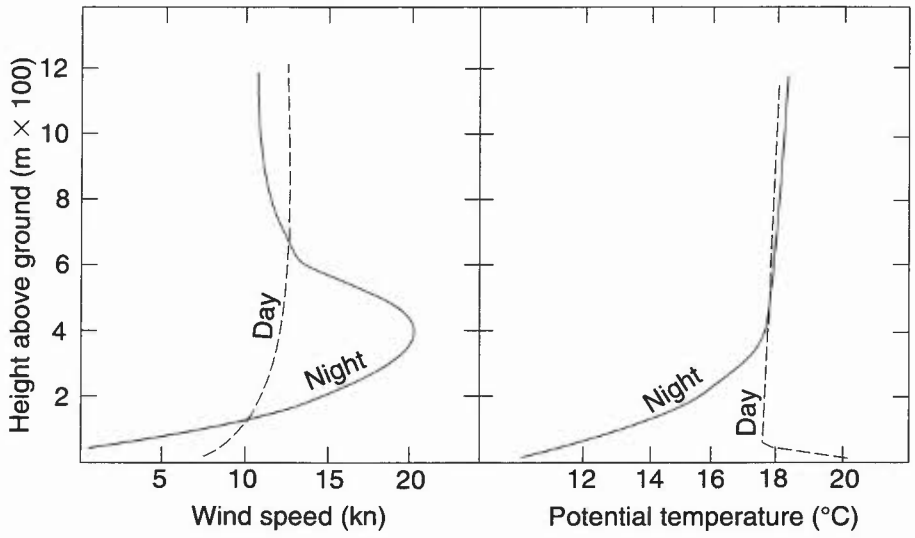

Figure 1.12. Vertical profiles of wind speed and potential temperatures by night and day under typical fair-weather conditions with little or no low cloud.

1.2.3 Low-level jets

(i) These are bands of strong winds in the lower troposphere.
(ii) Unlike high-level jets there is no specified minimum speed and many do not exceed 60 kn.
(iii) These jets are often associated with large vertical and horizontal wind shears.
(iv) Low-level jets occur in the warm conveyor belt just ahead of a surface cold front.
(v) There may be more than one core, each about 100 km wide.
(vi) Maximum speeds are in the range 50–60 kn and at a height of about 1 km.

A cross-section through one example of a low-level jet associated with a front is at **Fig. 1.13**.

1.3 Local winds

1.3.1 Sea and land breezes

Sea (and land) breezes are driven by the unequal diurnal heating and cooling of adjacent land and sea surfaces.

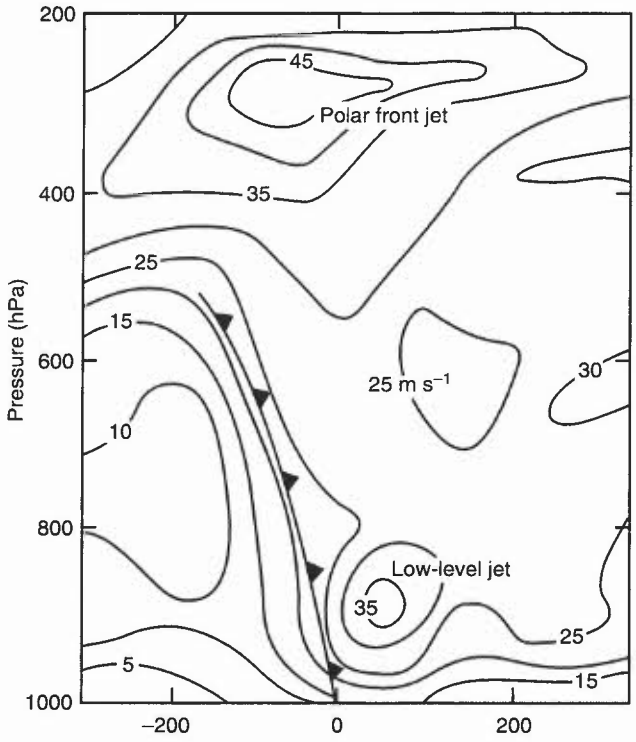

Figure 1.13. Low-level 'jet' associated with a front. Isotachs at intervals of 5 m s^{-1} show the wind flow into the paper.

1.3.1.1 Sea breezes

Criteria for sea breezes:

(i) inland temperatures greater than temperature of coastal waters;

(ii) a moderate depth of dry convection to, say, between 750 and 900 m (2500 to 3000 ft) is required before the sea breeze can become established;

(iii) if the air is so stable that the convection is confined to a very shallow layer there will be little or no penetration of the sea-breeze regardless of the temperature difference between land and sea;

(iv) only a weak offshore wind component of <14 kn at 3000 ft initially;

(v) convection to 1500 m (4000 ft) favours deep inland penetration (deep convection, leading to shower or thundery activity, tends to halt the sea-breeze);

(vi) significant inland penetration is only likely if offshore 3000 ft wind is <10 kn. This is typified by the following observations **(Table 1.8)** for the onset of sea breezes as a function of land/sea temperature contrast for the Lincolnshire coast.

Table 1.8.

Off-shore component (kn)	2	4	6	8	10	12	14	16
Temperature contrast (°C)	3.5	5.0	6.0	7.3	9.0	11	14	—

(sea surface temperature measured at light vessel in 19 m of water, 30 miles (48 km) offshore).

Providing these criteria are met the approximate time for a sea breeze to start to move inland is given by **Table 1.9:**

Table 1.9.

Off-shore wind component (kn) at 3000 ft	Time sea-breeze front crosses coast (UTC)
≥15	sea-breeze front unlikely
14	1600
10	1100–1200
5	0900 (or when convection penetrates 3000 ft)

Sea-breeze front

(i) The convergence line where incoming sea air meets the land air is often termed the sea-breeze front.

(ii) A small off-shore component to the geostrophic wind is generally needed for the development of a well defined front.

(iii) A narrow line of rising air occurs along the front producing enhanced convection; a distinguishing feature is a ragged line of 'curtain cloud hanging below the main cloud base'. Nearly all cloud disperses on the seaward side of the front.

Penetration inland

(i) Movement inland from the coast may extend to more than 50 n mile inland over the south and east of England (10.3.1.1).

(ii) The distance depends on the off-shore component of the geostrophic wind, the land–sea temperature contrast, the depth of convection and the topography.

(iii) High ground delays or deflects the flow of sea air which tends to move up wide valleys rather than climb over hills (**Fig. 1.14**).

(iv) The sea breeze will veer with time.

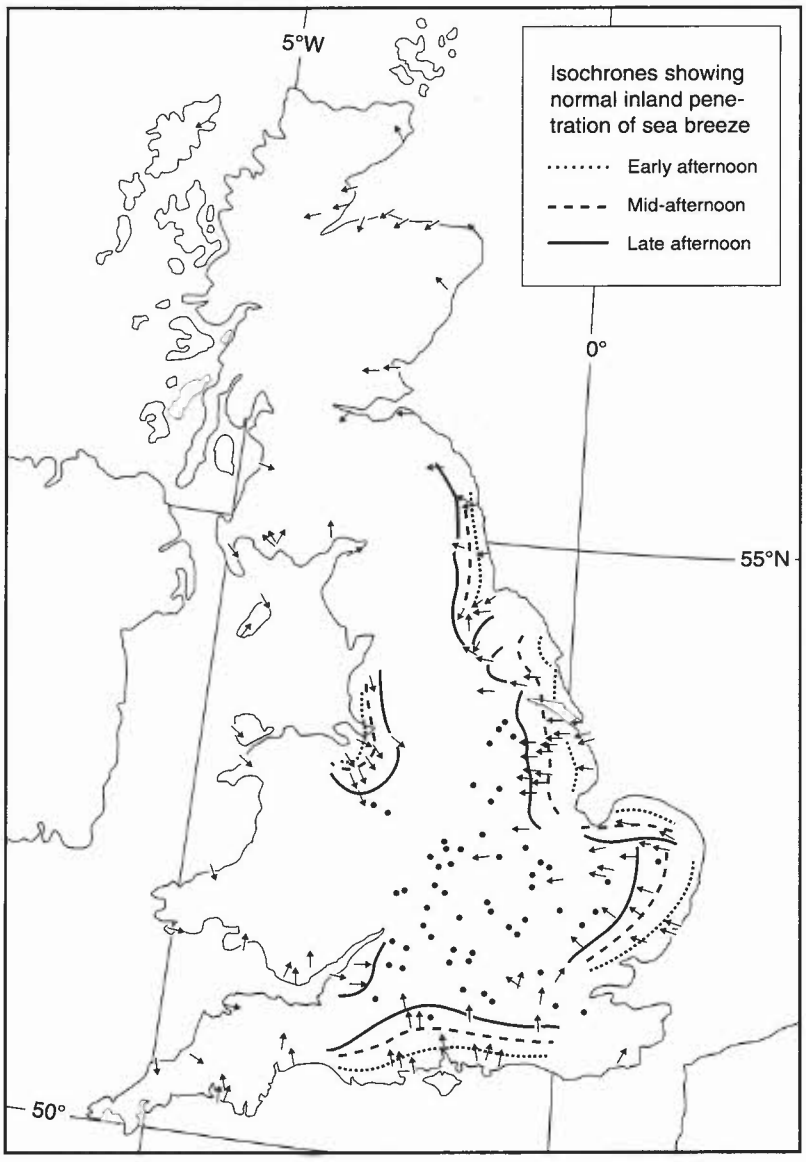

Figure 1.14. The normal direction and penetration of sea-breezes during summer months. Each arrow or dot represents an individual airfield. Arrows show the late afternoon direction of the sea-breeze (a few places having two preferred directions). Dots show airfields where sea-breezes have not been specially recorded in the local weather notes. The isochrones show the normal rate of progress inland of the sea-breeze on a summer afternoon.

Speed of movement

(i) The average in the United Kingdom is 4–8 km h^{-1} (2.2–4.4 kn).

(ii) The rate of advance is not constant. The front moves inland in a series of surges with a speed less than that of the incoming sea air.

Seasonal variation

(i) In the United Kingdom sea-breezes occur from March to late September.

(ii) The majority occur from May to August with the peak in June.

Depth of sea air

(i) The incoming sea air often extends to a height of 2000 ft (600 m), occasionally 3000 ft (900 m), at the front where the depth is greatest.

(ii) The top descends to about half the maximum after the front has passed; visibility may be reduced due to increased relative humidity of air and hygroscopic nature of salt aerosol or to smoke/haze trapped beneath the inversion (e.g. in south-east England) (3.9).

Coastal convergence/divergence effects

Fig. 1.15 shows typical cloud patterns generated by land and sea breezes along peninsulas and inlets; coastal convergence/divergence zones with associated cloudiness are illustrated in **Fig. 1.16.**

Bader et al. (1995), Chapter 6
Bradbury (1989)
Brittain (1970)
Findlater (1964)
HWF (1975), Chapter 16
MG (1991)
Pielke (1984)
Simpson (1994)

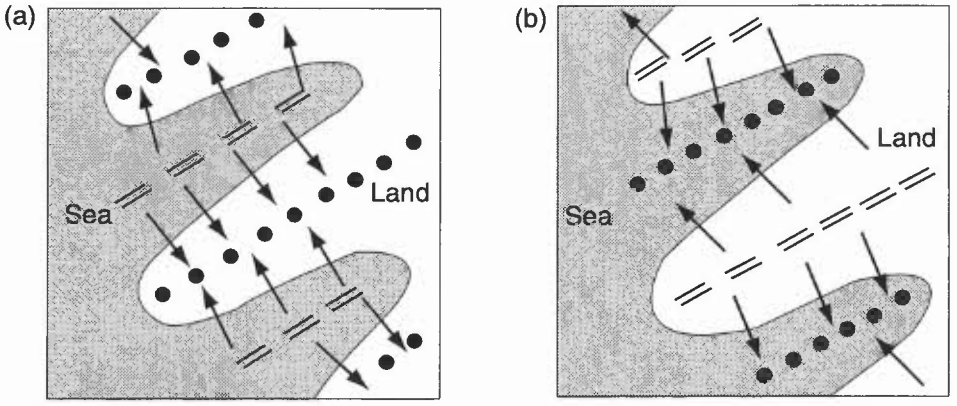

Figure 1.15. Peninsular and inlet convection patterns generated by coastal breezes, showing cloudy areas of surface convergence (····) and cloud-free area of surface divergence (====). (a) On a warm summer day, and (b) when land is relatively cold.

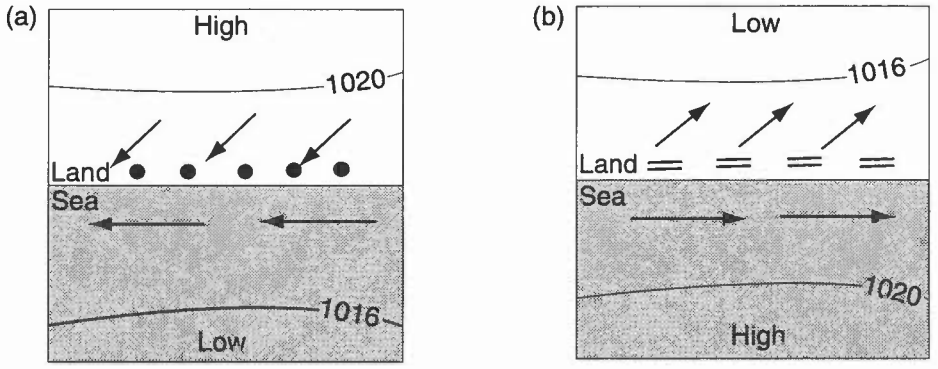

Figure 1.16. Coastal convergence/divergence zones, with cloudiness indicated as in Fig. 1.15. Nominal isobars in hectopascals; arrows are surface wind vectors.

1.3.1.2 The (nocturnal) land breeze

Occurrence

(i) usually sets in about midnight or later;
(ii) it is usually shallower and less well-developed than the sea breeze;
(iii) it is much influenced by topography and tends to increase during the night near flat coasts; a katabatic flow from hills parallel to the coast may reinforce it;
(iv) the strength and frequency depend, theoretically, on the land-sea temperature contrast, and thus might be expected to be greater in anticyclonic conditions in early autumn;
(v) snow-covered ground encourages persistent flow.

Moffitt (1956)

1.3.2 Airflow over hills

1.3.2.1 Mountain waves

Moving, statically stable air, within a boundary layer of thickness δ oscillating at its natural (Brunt–Väisälä) frequency, N:

$$N^2 = (g/\theta)d\theta/dz,$$

traces a wave which has a wavelength Λ. When the (undisturbed) air flow, V, encounters a hill, a useful parameter for identifying the subsequent wind flow, the internal *Froude number,* is defined by:

$$Fr = V/N\delta.$$

Fr represents the ratio of inertial to buoyant forces; high stability implies low Fr although high stability in combination with high V can result in $Fr \approx 1$. Thus, various combinations of stability and wind profile can combine to produce a single Fr value. **Fig. 1.17** shows the variety of flows possible for different stabilities (Fr numbers) for the case of an isolated hill.

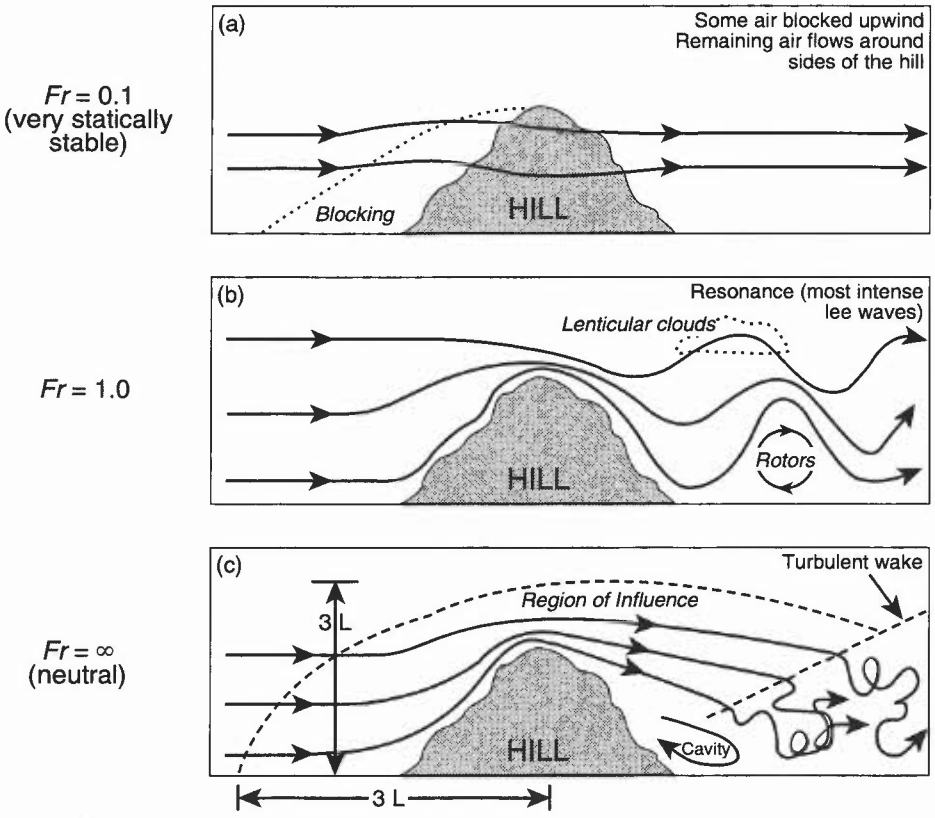

Figure 1.17. Idealized flow over an isolated hill. The Froude number (Fr) compares the natural wavelength of the air to the width of the hill (L). (a) $Fr = 0.1$ (very statically stable), (b) $Fr = 1.0$, and (c) $Fr = \infty$ (neutral).

Summary of guidance on forecasting.

(i) Two types of lee waves can form with different characteristics:
(a) *Trapped waves* form when wind speeds increase with height and/or a less stable layer overlies a stable layer (wave energy is trapped and propagates downwind, confined to low levels).
(b) *Untrapped waves* form if stability is high and/or wind speed low, or the hill width large. The wave energy is propagated upwards so that these waves are routinely observed in the stratosphere, having a characteristic orographic cirrus signature with a well defined boundary (**Fig. 6.1**).

(ii) The length scale of the hills is important — there will be a favoured width of hills depending on the wind and stability conditions.

(iii) An idea of the flow strength may be gained from the distance apart of wave elements on a satellite image. (Flight along the wave, i.e. against and across the flow, can result in experiencing prolonged ascent or descent.)

(iv) Beware of strong-wind situations over the hill top and to its lee where there is an inversion or stable layer not far above the hill or ridge top — this is most likely around the periphery of an anticyclone or ahead of an approaching warm front. Winds can be stronger than expected and quite gusty over the hill top and to its lee. Marked turbulence can be encountered, with perhaps a rotor where the wave flow leaves the ground downwind of the hill.

(v) Both wave types are accompanied by pronounced lee troughing in the surface isobaric field.

(vi) Even in the absence of a stable layer, there will tend to be a flow speed-up effect which may cause the winds over a hill or ridge crest to be as much as double or more the upwind values on occasion, depending on hill height and width.

Both these wave types can generate *severe downslope winds* as as discussed in 1.3.3.4.

Bader et al. (1995)
Barry (1981)
Bradbury (1989)
Bradbury et al. (1994)
Corby (1954)
Foldvick (1962)
Hunt (1980)
Scorer (1949)
Shutts & Broad. (1993)
Starr & Browning (1972)
WMO (1973)

1.3.2.2 Casswell's method for predicting mountain wave characteristics

(i) Casswell presents a graphical method for estimating the likely occurrence and properties of mountain (lee) waves. (This method has little credibility with specialists in the subject.)

(ii) The method involves estimating a parameter l, which is a function of the static stability, the wind speed and vertical wind shear.

(iii) l is allocated a value for two layers (1000–700 and 700–300 hPa) and the existence or not or lee waves read off from a graph. Vertical velocity is then found from a knowledge of the mountain height and wind flow at that height.

Procedure:

(i) From a representative sounding, obtain temperature differences $T_{1000} - T_{700}$ and $T_{700} - T_{300}$.

(ii) From upper-air data obtain:
V_o, the wind at the top of the mountain barrier (surface gradient wind is usually adequate);
V_{850} (or, preferably, mean wind between mountain top and 700 hPa);
V_{500} (or, preferably, the mean 700–300 hPa wind).

(iii) Marked lee waves are not expected if $V_o < 20$ kn or if the direction of V_o makes an angle of $>30°$ with the perpendicular to the mountain range. If lee waves are deemed possible then:
obtain l_{850} from **Fig. 1.18(a)** and l_{500} from **Fig. 1.18(b)**.

(iv) Using l_{850} and l_{500} enter **Fig. 1.18(c)** to obtain L_1, the wavelength (km) and h_1, the height of the maximum vertical velocity, and C_1 (which when multiplied by V_o, gives the maximum vertical velocity). In the figures the ridge height is taken as 300 m. For other values of H multiply the resulting maximum velocity by $H/300$.

(v) Note that $C_1 \times V_o$ m s^{-1} gives vertical velocity in m s^{-1}.

(vi) If the point (l_{850}, l_{500}) lies above tropopause line, no lee waves are expected. If h_1 is above or near the tropopause, any values derived graphically may be unreliable, but marked lee waves are not expected at lower levels.

(vii) If there is a marked decrease of wind speed or change of wind direction at any level, wave activity is not expected to extend beyond this height.

(viii) In a similar way **Fig. 1.18(d)** may be used to determine the likely existence and properties of any secondary wave train at another level above the primary.

(ix) Erroneous results are likely when there is a marked inversion within the wave region. (The maximum vertical velocity should then occur at the base of the stable layer.)

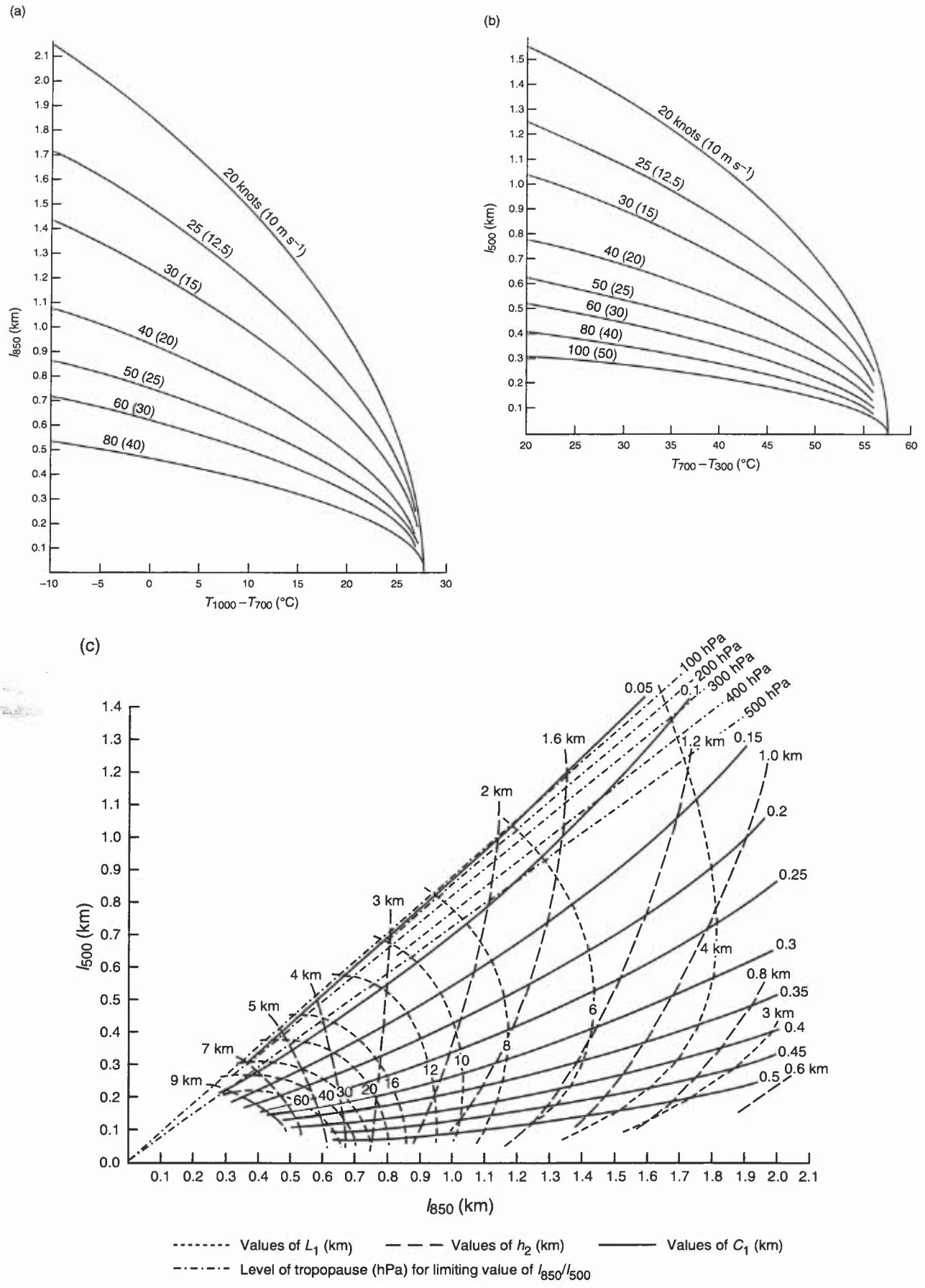

Figure 1.18. (a) Graphs for obtaining (a) l_{850} from $(T_{1000} - T_{700})$ and V_{850}, (b) l_{500} from $(T_{700} - T_{300})$ and V_{500}, (c) L_1, h_1 and C_1, and (d) L_2, h_2 and C_2.

(d)

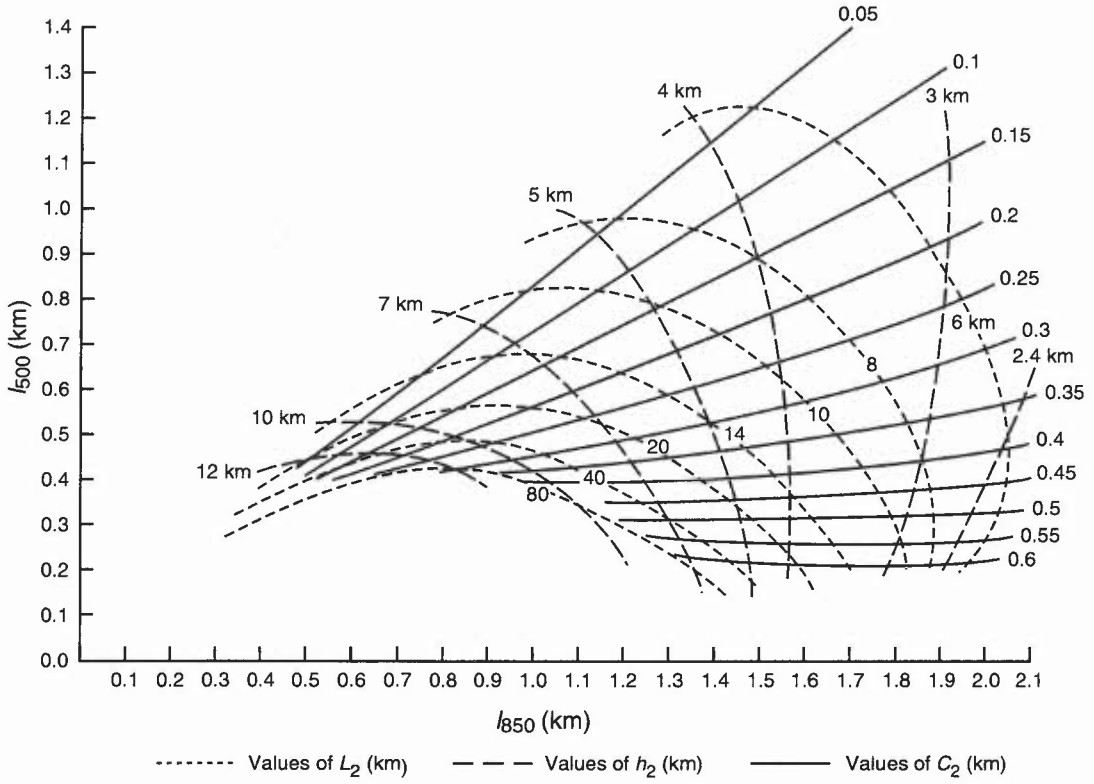

Figure 1.18. (Continued).

Lee waves are generally found when winds are fairly unidirectional, increase in strength with height and when the lowest 3 km has a higher static stability than normal, however, there are numerous cases reported which do not conform to these or other (e.g. HWF) simplified conditions but which are handled well by Shutts' method.

Casswell (1966)

1.3.2.3 Shutts' method for predicting mountain wave characteristics

(i) Shutts' model looks for trapped lee wave modes in a range of directions centred on the near-surface wind direction; it is available as a PC model.

(ii) In the simplified example in **Fig. 1.19** a wind profile that is linear with height is assumed (governed only by values specified at the surface and at a fixed tropopause height of 10 km). The temperature profile is fixed by three values at the surface (12 °C), at 3.5 km (−3 °C) and at the tropopause (−60 °C), the stratosphere being isothermal at that temperature.

(iii) **Fig. 1.19** shows (a) the resonant wavelength, and (b) the maximum vertical velocity and height for a range of surface and tropopause wind speeds. The figure confirms the tendency of the resonant wavelength to increase with wind speed; beyond a certain surface wind they are non-existent. At low wind speeds plots are complicated by the presence of multiple solutions. Between mode regimes, there appear to be regions with no trapped modes. Strong lower tropospheric stability leads to gigantic waves for strong height-independent flows.

The Sheffield storm of 1962 is an example when a lee wave system developed contrary to conventional wisdom, possibly due to trapping of lee waves by reflection off the tropopause (rather than by increasing wind speed with height). The condition for this is that the height of the tropopause should be about $\pi V/N$. This case is handled by Shutts' method.

Aanensen (1965)
Shutts (1992)
Shutts & Broad (1993)

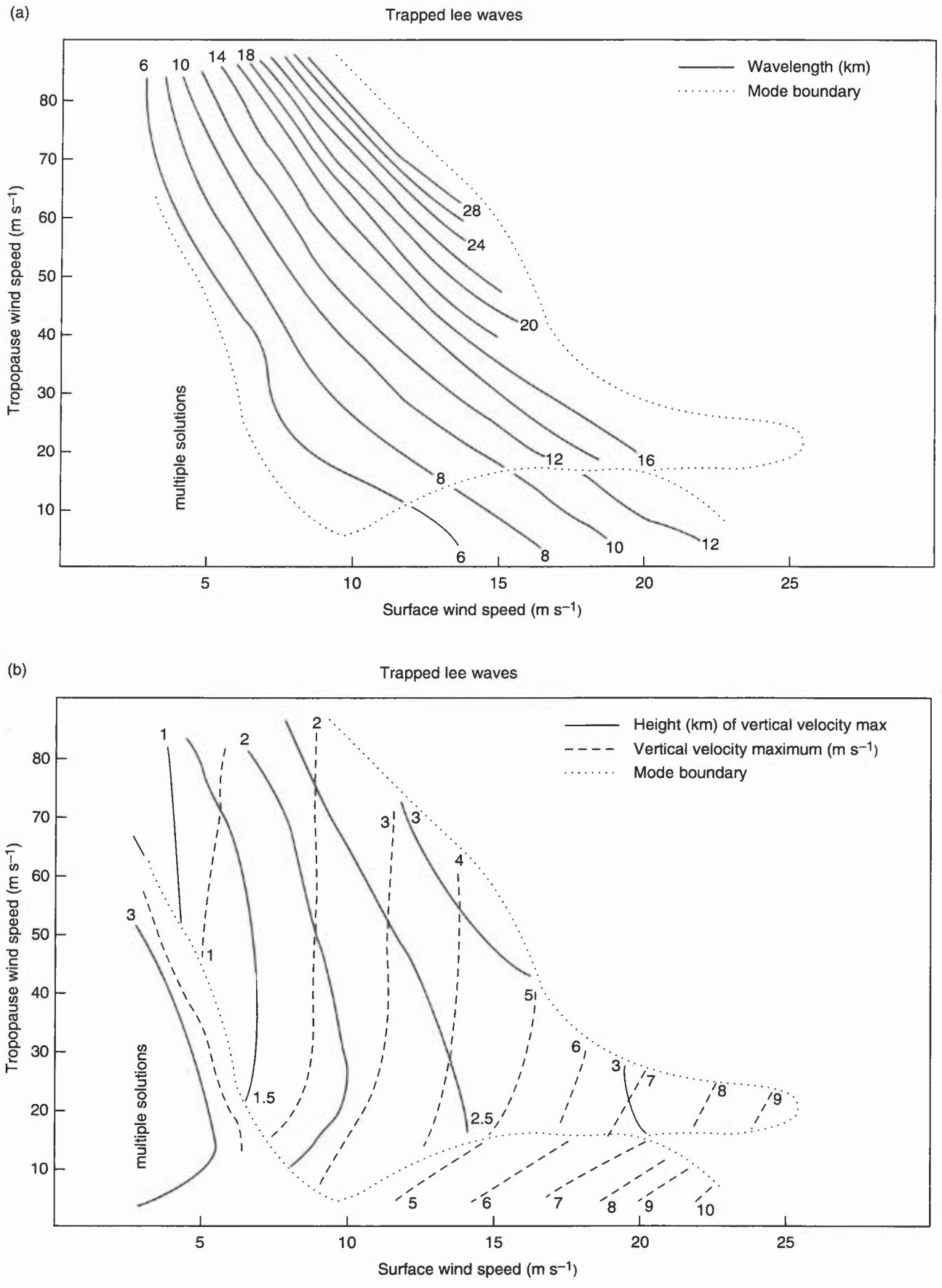

Figure 1.19. (a) Resonant wavelength, and (b) maximum vertical velocity for a range of surface and tropopause wind speeds.

1.3.2.4 *Convection and cloud street waves*

Thermals can act as temporary hills and set off gravity waves in a stable layer, propagating to an altitude of >9 km. (In turn the thermal activity may be stimulated in regions beneath ascending flow and suppressed where wave flow is descending.) This type of wave activity (cloud street waves) requires special criteria:

(i) thermal or cumulus streets lying along the line of the low-level flow;
(ii) the thermal/cloud tops inhibited by an inversion;
(iii) the flow at and above the inversion must blow across the thermal/cumulus streets.

Favourable synoptic conditions are:

(i) weak flow in the convective layer and a horizontal 850 hPa temperature gradient;
(ii) isotherms approximately at right angles to the surface isobars;
(iii) additionally the natural wavelength of the air above the cloud should be similar to the cloud-street spacing.

Booth (1980)
Bradbury (1990)

1.3.2.5 *Speed-up at the crest of an isolated hill*

(i) The fractional speed-up ratio, valid for small slopes (<20°), neutral stability and low hills, is defined as: $\Delta V_{hill} = [V_o(\Delta z)V_A(\Delta z)]/V_A(\Delta z)$
where Δz is the height above the local terrain, subscript 'A' denotes a point upwind where flow is undisturbed and subscript 'o' the hill top.
(ii) For gentle ridges: ΔV_{hill} equals about: 4 × hill height/L
For isolated hills: ΔV_{hill} equals about: 3.2 × hill height/L,
where L is the hill width at half the maximum height of the hill.
(iii) For a typical, gentle hill (height = 100 m, L = 250 m), the speed-up just above the crest can be 160% or more (especially if there is an inversion above summit height).

Stull (1988)

1.3.2.6 *Vertical velocities and slope*

Amplitude of the vertical velocities is determined by the slope of the topography and the undisturbed wind flow, V_A.

Roughly the same characteristics apply for unstable, neutral and slightly unstable lapse rates:

(i) magnitude of vertical velocity is roughly $V_A\tan\alpha$, (where α is ground slope), limited to V_A for $\alpha>45°$;
(ii) slopes <1 in 5 (α about 10°), flow attached to topography;
(iii) slopes 1 in 5 to 1 in 3, flow separation with recirculating eddies downwind; in moist conditions a banner cloud trails away downwind (e.g. Tenerife).
(iv) slopes >1 in 3 ($\alpha \approx 18°$), recirculating eddies down- and up-wind.

An associated characteristic pressure-change signature (a 'kick') of 0.5 to 1 hPa across the hill/ridge may be evident.

Stull (1988)

1.3.2.7 *Airflow over a series of hills*

A series of hills can modify the flow to yield a new profile that behaves in accordance with the characteristics of the rougher surface of the terrain.

Stull (1988)

1.3.2.8 *Airflow with a capping inversion*

An airflow approaching a ridge capped by an inversion will produce **(Fig. 1.20)**:

(i) for relatively slow winds:
acceleration over the ridge crest can locally draw down the inversion;
to the lee of the ridge light winds are found perhaps with flow reversal at low levels;
(ii) for faster winds with a strong capping inversion:
a shallow high velocity lee-slope flow develops, associated with an 'hydraulic jump'.
(iii) if the boundary layer depth is much greater than the hill height:
a flow which tends to evolve as if the hill were not present;

with a shallow boundary layer the air is constrained to flow around the hill, which can give rise to downwind streets of vortices (visible in satellite imagery).

These various responses will be amplified by hill/ridge assymetry.

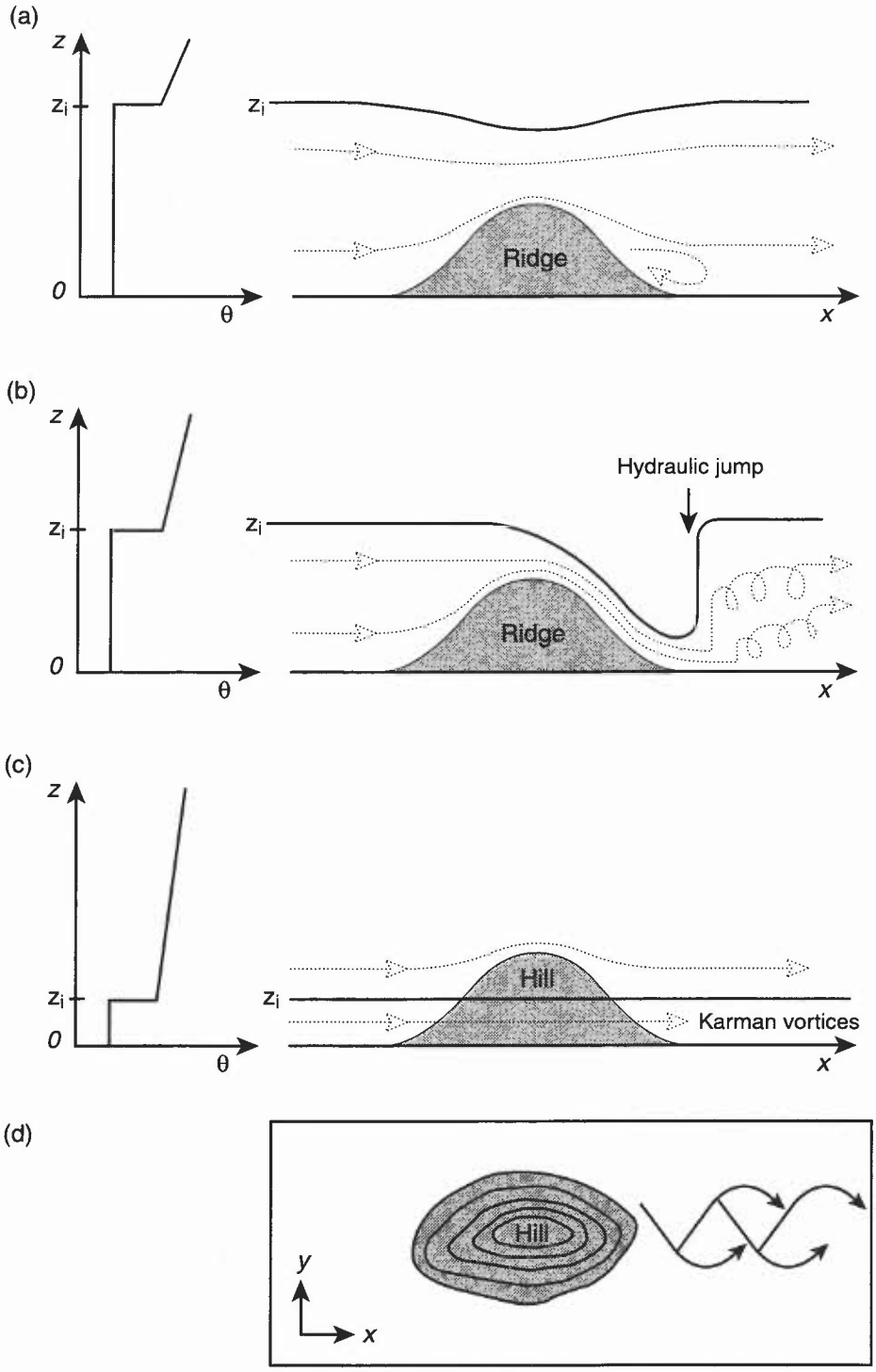

Figure 1.20. (a) Bernoulli effect as flow accelerates over a 2-D ridge, (b) hydraulic jump downwind of a 2-D ridge for greater ambient wind speed, (c) flow around the sides of an isolated hill, and (d) Karman vortex street downwind of the hill from (c). (After Hunt (1980)).

1.3.2.9 Airflow over other complex terrain

(i) Valleys and passes channel wind flows.
(ii) Cross-valley flows can generate both along-valley flow and cross-valley circulations.
(iii) Tall buildings in large cities act like steep valley walls, trapping and channelling air into 'urban canyons'.

1.3.2.10 Airflow over different surfaces

Low-level air flowing from a smooth to a rough surface results in convergence and upward motion above the rough/smooth boundary (the converse holds for rough to smooth flow).

Stull (1988)

1.3.3 Slope and valley winds

1.3.3.1 Anabatic winds:

(i) are generally shallow flows up slopes warmed by solar heating;
(ii) maximum speeds occur within a few metres of the slope surface.

In the United Kingdom these winds are less frequently observed than katabatic winds.

1.3.3.2 Katabatic winds:

These are generally shallow flows (<30 m deep) down slopes and along valleys (donor sites) cooled by nocturnal radiation.

(i) Screen-height fluctuations of temperature and relative humidity have been measured, with a period of about 1 hour, in antiphase.
(ii) An organized wind-shear, perhaps hazardous to aircraft, could be encountered at the bottom as well as at the top of a katabatic airstream, even though the anemometer has ceased to record katabatic flow.
(iii) Another mechanism operates when upper hill slopes are cooled by precipitation, by day or night; the temperature contrast between this cooled air and air at the same level above the lower slopes often results in vigorous katabatic flow.
(iv) A persistent flow results when ground adjacent to sea is snow-covered, resulting in a seaward thermal flow for most of the day.

Bader et al. (1995)
Dawe (1982)
Moffitt (1956)

1.3.3.3 Valley wind systems

On any occasion there may be anabatic or katabatic components complicated by the presence of a gradient wind flow above the level of the surrounding ridge tops and varying through the day as the sun's orientation changes.

Fig. 1.21 illustrates the general pattern, in which there are three main layers with different airflows:

(i) The lowest layer in contact with the slopes flows upwards while the slope is heated and descends towards the valley floor when radiation cools the slopes.
(ii) An intermediate layer where the flow is often reversed. This has been termed the 'anti-wind' which tends to balance the lowest-level flow.
(iii) At the top is the gradient wind, controlled by large-scale synoptic systems.

Bradbury (1989)

1.3.3.4 Severe downslope winds

Two types of mountain waves can generate severe downslope winds (1.3.2.1):

Untrapped lee waves may result in gusty, downslope winds. Conducive atmospheric conditions of high stability accompanying strong low-level flow with little increase in speed with height are frequently found in the lee of the Pennines during:

(i) strong anticyclonic south-westerlies;
(ii) warm-sector conditions;
(iii) in the low-level zone of strong winds a few hundred kilometres ahead of a cold front.

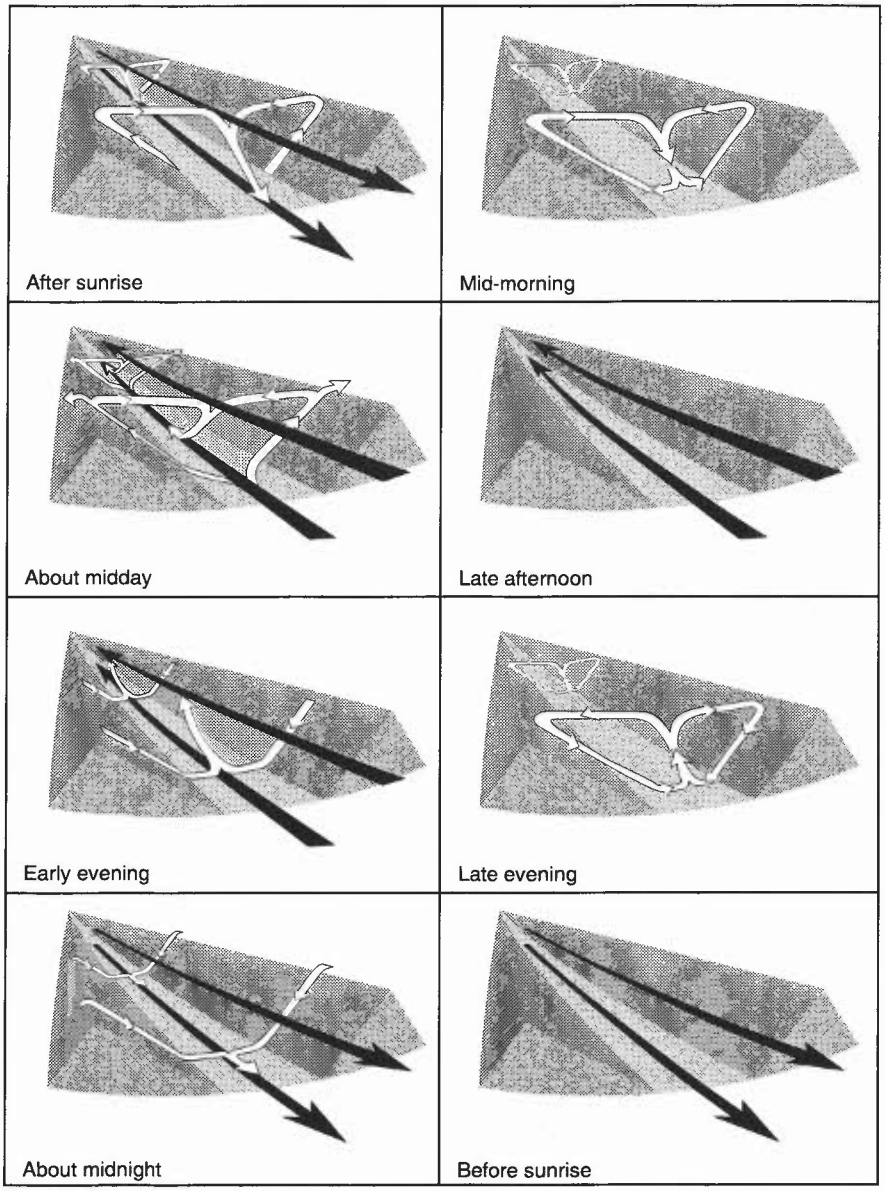

Figure 1.21. Valley wind systems. A schematic display of the diurnal variation of upslope and downslope winds forced by the changing effects of solar heating at the surface.

They are characterized in satellite imagery (e.g. of a frontal system lying across mountainous regions) by dense orographic cirrus in the lee of the mountains; the imagery may show a cloudless 'slot' where frontal cirrus is forced to descend in the lee wave system.

Trapped lee waves may give rise to severe downslope winds when the waves reach a critical amplitude and wavelength.

(i) When the Froude number, based on mountain height (1.3.2.1), is close to unity large amplitude trapped lee waves can form leading to severe downslope winds. UK mountain ridges are never much more than 1 km high so such winds can only occur for $V \approx 10$ m s^{-1}

(ii) The streamlines of flow are concentrated above and to the lee of large mountain ridges (particularly those with steep lee escarpment, such as the western side of the Cross Fell range in the Pennines).

(iii) These extreme winds may extend for some distance across the plain before the flow separates from the surface in an intense vertical current beyond which rotors may be found. Such flow type is analogous to the hydraulic theory of a single fluid layer of constant density as it flows over an obstacle such as a weir and rises again some distance downstream accompanied by turbulent motion.

(iv) Surface charts may show a marked lee trough (note that mesoscale model resolution limitations may result in the effect being underestimated).

Conditions conducive to severe downslope winds resulting from trapped lee waves:
(i) strong stable layer near hill-top height;
(ii) very light winds or flow reversal at some tropospheric level;
(iii) a mountain range with steep leeward escarpment.

The rotor may or may not be indicated by a long roll of ragged cumulus or stratocumulus parallel to the ridge; the 'Helm Bar' in Cumbria is a well-known example.

Both wind regimes require hilly regions of at least 30 km horizontal extent; typical lee-wave related downslope winds in the UK will be associated with a pressure 'kick' across a range of a few hectopascals.

Bader et al. (1995), Chapter 8
Bradbury (1989)
Corby (1954)
Förchtgott (1949)
HAM (1994)
Klemp (1978)
Stull (1988)

1.3.3.5 Rotor streaming (see 6.2)

1.3.3.6 Föhn winds

(i) Föhn winds occur on the lee side of mountain ranges when the winds aloft blow across the axis of the main ridges. Two examples are shown in **Fig. 1.22.**
(ii) In the more common 'subsidence' case **(a)**, low-level cold air flow is blocked upstream and only the higher-level flow crosses the ridge to plunge down the lee side as a very dry, adiabatically warmed, current.
(iii) In **(b)** all the upstream air crosses the ridge. Orographic lifting produces cloud; precipitation over the mountains then depletes the moisture content; the drier air then descends the lee side, warming adiabatically.

Bader et al. (1995), Chapter 8
Bradbury (1989)
Lawrence (1953)

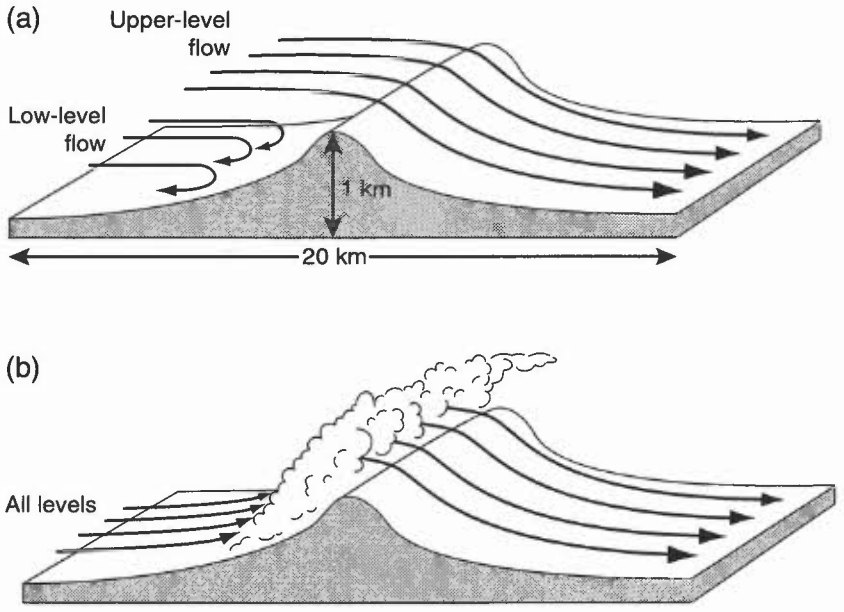

Figure 1.22. Föhn winds. (a) The low-level flow is blocked upstream of the hill barrier and only the higher-level air flows across the ridge, and (b) all the upstream air crosses the ridge.

1.3.4 Urban winds

Gusts and lulls due to channelling by buildings and streets result in eddies around the sides and in the precincts in front of (tall) structures, strengthening winds by up to a factor of three. Restricted and channelled air movement under appropriate synoptic conditions can result in high levels of air pollutants at ground level in the so-called 'canopy layer'.

The temperature differential due to the urban 'heat island' (2.11) can set up a 'country breeze', a low-level flow (<8 kn) of cool air from the rural area towards the city. Contrarotating eddies have been measured over opposite sides of a city. Frictional drag over large cities reduces wind speeds below that of the rural surroundings; pollution can be transported large distances downwind in the 'urban plume' which is as wide as the city, and whose boundary-layer characteristics vary diurnally **(Fig. 1.23)**.

Oke (1982)
Stull (1988)

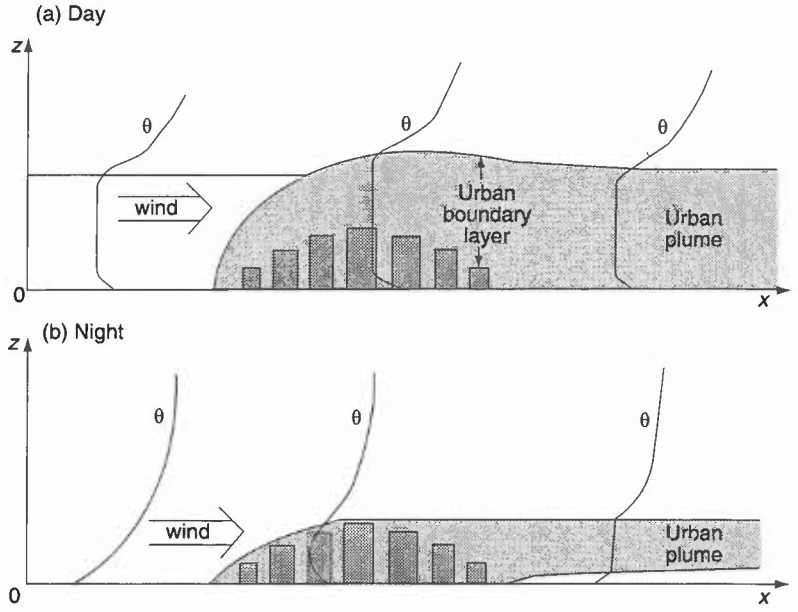

Figure 1.23. Sketch of urban boundary layer and urban plume for (a) a windy day and (b) a windy night (after Oke (1982)).

1.3.5 Wind-chill (see 2.10)

BIBLIOGRAPHY

CHAPTER 1 — WIND

Aanenson, C.J.M. (Editor), 1965: Gales in Yorkshire in February 1962. *Geophys Mem* No. 108, Meteorological Office

Bader, M.J., Forbes, G.S., Grant, J.R., Lilley, R.B.E. and Waters, J., 1995: Images in weather forecasting. Cambridge University Press.

Barry, R.G., 1981: Mountain weather and climate, Methuen.

Booth, B., 1980: Unusual wave flow over the Midlands. *Meteorol Mag*, **109**, 313–324.

Bradbury, T.A.M., 1989: Meteorology and flight, A & C Black.

Bradbury, T.A.M., 1990: Links between convection and waves. *Meteorol Mag*, **119**, 112–120.

Bradbury, W.M.S., Deaves, D.M., Hunt, J.C.R., Kershaw, R., Nakamura, K. and Hardman, M.E., 1994: The importance of convective gusts. *Meteorol Appl*, **1**, 365–378.

Brittain, O.W., 1970: Forecasting the inland penetration of a sea-breeze over Lincolnshire. Met. Office Forecasting Techniques Memorandum No. 20.

Carruthers, D.J. and Choularton, T.W., 1982: Airflow over hills of moderate slope. *QJR Meteorol Soc*, **108**, 603–624.

Casswell, S.A., 1966: A simplified calculation of maximum vertical velocities in mountain lee waves. *Meteorol Mag*, **95**, 68–80.

Corby, G.A., 1954: The airflow over mountains: A review of the state of current knowledge. *QJR Meteorol Soc*, **80**, 377–408.

Dawe. A.J., 1982: A study of a katabatic wind at Brueggen on 27 February 1975. *Meteorol Mag*, **111**, 491–521.

Findlater, J., 1964: The sea breeze and inland convection — an example of the interrelation. *Meteorol Mag*, **93**, 82–89.

Findlater, J., Harrower, T.N.S., Howkins, G.A. and Wright, H.L., 1966: Surface and 900 mb wind relationships. Scientific Paper No. 23. London, HMSO.

Foldvick, A., 1962: Two-dimensional mountain waves — a method for rapid computation of lee wavelength and vertical velocity. *QJR Meteorol Soc*, **88**, 271–285.

Förchtgott, J., 1949: Wave currents on the leeward side of mountain crests. *Bull met tchecoal, Prague*, **3,** 49–51.

HAM. Handbook of Aviation Meteorology, 1994: London, HMSO.

HWF. Handbook of Weather Forecasting, 1975: Met.O.875, Meteorological Office.

Holton, J.R., 1992: Introduction to dynamic meteorology (3rd edition). Academic Press.

Hunt, J.C.R., 1980: Wind over hills. Workshop on the Planetary Boundary Layer, pp. 107–144. Am Meteorol Soc.

Hunt, J.C.R., 1995: The contribution of meteorological science to wind hazard mitigation. *In* T. Wyatt (Ed), Proceedings of the Wind Engineering Society meeting on wind hazard, May 1995.

Klemp, J.B., 1978: A severe downslope windstorm and aircraft event induced by a mountain wave. *J Atmos Sci*, **35**, 59–77.

Lawrence, E.N., 1953: Föhn temperatures in Scotland. *Meteorol Mag*, **82**, 74–79.

Ludlam, F.H., 1980, Clouds and storms. Pennsylvania State University Press.

McCarthy, J. and Serafin, R., 1984: The microburst: hazard to aircraft. *Weatherwise*, **37**, 120–127.

Mason, P.J., 1986: Flow over the summit of an isolated hill. *Boundary Layer Meteorol*, **37**, 385–405.

Meteorological Glossary (MG) (6th Edition), 1991: London, HMSO.

Meteorological Office (Heathrow), 198?

Moffitt, B.J., 1956: The nocturnal wind at Thorney Island. *Meteorol Mag*, **85**, 268–271.

Oke, T.R., 1982: The energetic basis of the urban heat island. *QJR Meteorol Soc,* **108**, 1–24.

Pielke, R.A., 1984: Mesoscale meteorological modeling. Academic Press, Florida.

Scorer, R.S., 1949: Theory of waves in the lee of mountains. *QJR Meteorol Soc*, **75**, 41–56.

Shutts, G.J., 1992: Observations and numerical model simulation of a partially trapped lee wave over the Welsh mountains. *Mon Weather Rev*, **120**, 2056–2066.

Shutts, G.J. and Broad, A., 1993: A case study of lee waves over the Lake District in northern England. *QJR Meteorol Soc*, **119**, 377–408.

Simpson, J.E., 1994: Sea breeze and local wind. Cambridge University Press.

Starr, J.R. and Browning, K.A., 1972: Observations of lee waves by high power radar. *QJR Meteorol Soc*, **98**, 73–85.

Stull, R.B., 1988: An introduction to boundary layer meteorology. Kluwer Academic Publishers.

Thorpe, A.J. and Guymer, T.H., 1977: The nocturnal jet. *QJR Meteorol Soc*, **103**, 633–654.

WMO, 1969: Vertical wind shear in the lower layers of the atmosphere. Geneva, World Meteorological Organization, Technical Note 93.

WMO, 1973: Airflow over mountains. Geneva, World Meteorological Organization, Technical Note 127.

CHAPTER 2 — TEMPERATURE

CHAPTER 2 — TEMPERATURE

2.1 Thermodynamics and the tephigram

In the tephigram straight-line rectangular co-ordinates are T (temperature) and ϕ (entropy); dry adiabats are, therefore, perpendicular to the isotherms. Equal area represents equal energy at any point, simplifying geopotential calculations.

2.1.1 Constructions using a tephigram

Fig. 2.1 illustrates Normand's theorem and construction to obtain potential and equivalent temperatures. **Fig. 2.2** illustrates constructions to obtain vapour pressure and saturation vapour pressure. Temperatures are specified for a parcel of air at 850 hPa.

HWF (1975)

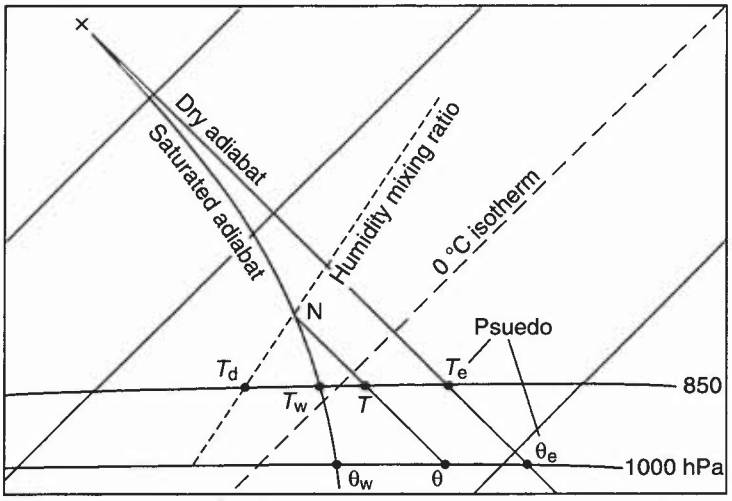

Figure 2.1. Construction on a tephigram to illustrate Normand's theorem, and to obtain potential temperature (θ, θ_w) and pseudo-equivalent temperatures (T_e, θ_e). The constructions are based on a parcel of air at 850 hPa, with temperature (T), wet-bulb temperature (T_w) and dew point (T_d).

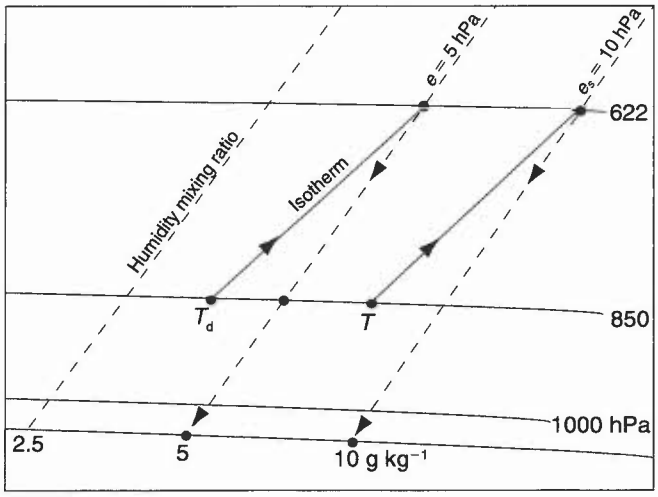

Figure 2.2. Constructions on a tephigram to obtain vapour pressure (e) and saturation vapour pressure (e_s) based on the air temperature (T) and dew point (T_d) of a parcel of air at 850 hPa.

2.1.2 Calculation of heights on a tephigram

This is illustrated in **Fig. 2.3**. After modifying the profile to show the virtual temperature (T_v):

(i) divide the temperature profile into a series of layers, 100 hPa deep up to the 300 hPa isobar, and then 50 hPa deep between 300 and 100 hPa.

(ii) Use a transparent scale marked with a straight line. Lay this over the temperature profile in each of the layers, parallel to the isotherms so as to create equal positive and negative areas either side of the mean isotherm.

(iii) Read off the layer thicknesses, in decametres, as marked along the intermediate isobars at 950, 850, 750 hPa, etc. The height of a standard pressure level is the sum of all the partial thicknesses below that level, plus the height of the 1000 hPa level. The height of the 1000 hPa surface may be read off from the nomogram printed on standard tephigrams. When the MSL pressure is less than 1000 hPa, the 1000 hPa heights are negative.

The formula for height calculations involving layers which are not at standard levels is:

$$H = 29.27\, T_v \ln(p_0/p_1)$$

where H is in metres and T_v is the mean virtual temperature (K) of the layer $p_0 - p_1$.

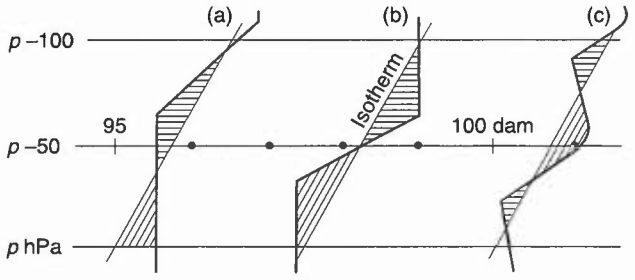

Figure 2.3. Calculating the thickness of a 100 hPa layer (base pressure = p). Shaded areas show equal positive and negative areas either side of a mean isotherm for three different shapes of environment curve. Thickness values are read off the scale on intermediate isobars. The examples show thickness values of (a) 95.7 dam, (b) 98.2 dam, and (c) 100.7 dam. See text for method of calculation.

2.2 Diurnal temperature variations in different air masses

(i) Statistics of temperature ranges occurring in various conditions can help in deciding whether forecast temperatures are reasonable.

(ii) In **Table 2.1** air-mass types are grouped according to whether trajectories on approaching the British Isles are curved cyclonically or anticyclonically. Data are pre-1950.

(iii) Forecasters may well have local data.

Table 2.1. Diurnal variation of temperature (°C) at Kew and Rye in different conditions

	Kew (1871–1940)					Rye (1945–1948)			Kew (1950–1954) Clear days		
Month	Polar (cyclonic)	Polar and tropical (anticyclonic)	Tropical (straight trajectory) maritime	Tropical (straight trajectory) continental	All occasions	All occasions	Clear days	Cloudy days	Average	Maximum	Minimum
Jan.	3.5	5	2	2	5	3	6	1	5	6.5	4.5
Feb.	4.5	5.5	3	5.5	5.5	3.5			7.5	8.5	7
Mar.	5	6.5	4.5	8.5	7	7			9.5	16.5	5.5
Apr.	6	8.5	4.5	10.5	8.5	8			11.5	18	7
May	7	9.5	8	11.5	9.5	8.5			12	16.5	8
June	7	9	6.5	10.5	9.5	7.5			12.5	17.5	8.5
July	6.5	9.5	6.5	11.5	9	8	13.5	3.5	11	14	8.5
Aug.	6.5	9.5	6.5	11.5	9	8.5			10.5	15	7.5
Sept.	6	8	6	9	8.5	7			10	15	7
Oct.	5.5	6.5	4	7	7	7			9.5	12	5
Nov.	4.5	5.5	2	5	5.5	4			7	11.5	4.5
Dec.	4	5	2	4	5	2.5			6	8	4

These data are summarized in the Local Weather Manual for S England, which also presents the 850 hPa WBPT by air-mass track and by season.

Belasco (1952)
Local Weather Manual (S England) (1994)

2.3 Daytime rise of surface temperature

2.3.1 Forecasting the hourly rise of temperature on sunny days, using a tephigram

This method relates the amount of solar energy available for heating the lower layers of the atmosphere to an equivalent area on a tephigram.

(i) **Table 2.2** gives the thickness of the layer (Δp in hPa) which is changed from an isothermal to an adiabatic state by insolation for each hour from dawn, to the time of day maximum temperature, for the middle of each month, assuming no cloud.

(ii) Marking isobars p_o (the QFE) and $p_o - \Delta p$ **(Fig. 2.4)**, point I is placed on the isobar ($p_0 - \Delta p$) with JIF along a dry adiabat and IH along an isotherm in such a way that it intersects the environment curve to form equal areas on either side, i.e. in this case area BAD equals area GHA plus area BIE. The point F then gives the value of the forecast surface temperature. This assumes no superadiabat at the surface (e.g. to F′). See note (i) below.

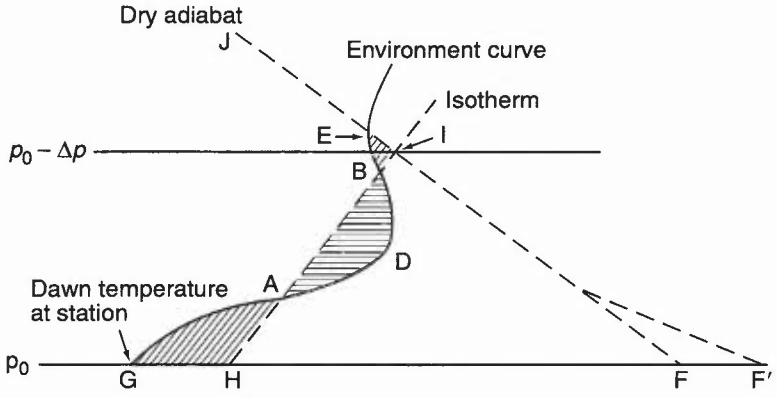

Figure 2.4. Estimating the rise of temperature on a sunny day by a tephigram construction. Δp is the thickness of the layer (hPa) and F is the forecast surface temperature. See text for details of construction.

Table 2.2 The thickness of the layer (Δp in hPa) which is changed from an isothermal to an adiabatic state by insolation at 52° N, 00° W

Month	Time (UTC)											
	05	06	07	08	09	10	11	12	13	14	15	Max
Jan.	—	—	—	—	03	18	35	48	58	61		61
Feb.	—	—	—	01	15	33	50	65	75	80		81
Mar.	—	—	02	17	35	53	68	81	90	95		97
Apr.	—	04	19	37	54	71	86	98	107	112	115	115
May	04	19	36	54	70	86	100	110	119	124	127	127
June	08	23	40	58	74	89	102	113	122	127	130	131
July	04	19	36	53	69	84	98	109	118	123	126	126
Aug.	—	08	24	41	59	75	89	101	110	116	119	119
Sept.	—	—	10	27	44	60	76	88	96	102	104	104
Oct.	—	—	01	13	29	45	60	72	80	85		86
Nov	—	—	—	—	11	25	38	49	57	61		61
Dec.	—	—	—	—	02	15	30	42	50	53		53

Notes:

(i) These values do not take into account any superadiabatic close to the surface. Add 2 °C (or more, according to local experience) to the resulting forecast temperature with clear skies and light winds in summer, to allow for superadiabats.

(ii) Approximate corrections to be applied to allow for cloud cover:

Table 2.3.

8/8 Ci	use	90% of depth (Δp in hPa)
8/8 As	use	60%
8/8 Sc	use	50%
8/8 Ns	use	35%

The value of Δp may be reduced if the ground is wet, covered in snow/hoar frost and/or the lowest layers of the atmosphere are very humid. In summer, if the ground is very dry and humidity in the bottom layers is low, the value of Δp may be increased. These changes are generally only significant in the first 3 or 4 hours of heating.

Inglis (1970)
Jefferson (1950)
Johnson (1958)

2.3.2 Forecasting the temperature rise on days with fog or low cloud (Jefferson's method)

(i) Use the method in 2.3.1 to draw a curve showing the rise of temperature to be expected if the sky were clear.

(ii) Evaluate a constant 'delay factor' f. This may be done from the observation of temperature at least 3 hours after sunrise (T_3). If h_0 is the time of sunrise, h_2 is the time at which the temperature is observed and h_1 is the time at which that temperature would have been observed on a sunny day, then

$$f = (h_1 - h_0)/(h_2 - h_0)$$

(iii) Plot points C, F, etc., as shown in **Fig. 2.5**, such that:

$$AB/AC = DE/DF = \ldots f.$$

(As a first estimate, take $f = 0.25$ for deep fog or thick stratus and $f = 0.35$ for shallow fog or thin stratus). Points C, F, etc. provide a forecast temperature curve for a foggy day.

(iv) If this curve reaches the temperature (T_c) at which the fog can be expected to disperse, the subsequent temperature rise will be steeper and more in line with conditions for a clear day (dotted line in **Fig. 2.5**).

(v) A note of caution: the local advection of fog will give large errors in T_c, the calculated value not being achieved.

Grant (undated)
Jefferson (1950)

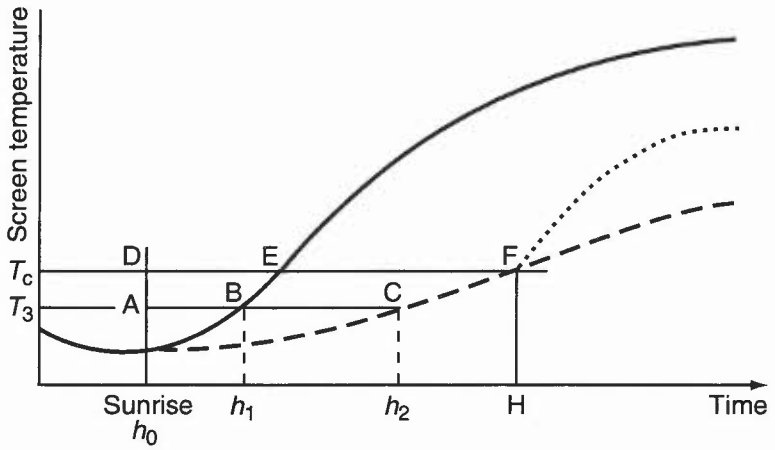

Figure 2.5. Constructing a forecast temperature curve on a foggy morning. The solid line is the forecast temperature curve for a clear day. The dashed line is the forecast for a foggy day, based on a delay factor of 0.35. The dotted line is the forecast for the later part of the day if the fog clears when the temperature reaches the critical value (T_c), at time H. See text for details of construction.

2.3.3 Forecasting T_{max} (Callen and Prescott's method, using 1000–850 hPa thickness)

This is an empirical method based on the maximum temperatures observed at Gatwick and the 1000–850 hPa thickness values at midday at Crawley.

There are three steps:

(i) Classify the cloud cover or presence of fog between dawn and 1200 UTC on a scale from 0 to 3 (**Table 2.4**), as follows:

Table 2.4.

Class 0	$C_L + C_M \leqslant 3/8$, $C_H \leqslant 5/8$; or any fog confined to dawn period.
Class 1	$C_L + C_M + C_H = 4/8$–$6/8$; or any fog clearing slowly during morning.
Class 2	$C_L + C_M \geqslant 6/8$; or any fog clearing before noon.
Class 3	Predominantly overcast with precipitation (not including very slight drizzle) or persistent fog.

(ii) Using **Fig. 2.6**, obtain the temperature adjustment for the month for the appropriate cloud class.
(iii) Apply this adjustment to the values given in **Table 2.5** to find the predicted maximum temperature.

The relationship between 1000–850 thickness (h) and the unadjusted maximum temperature (T_u) is given by

$$T_u = -192.65 + 0.156h.$$

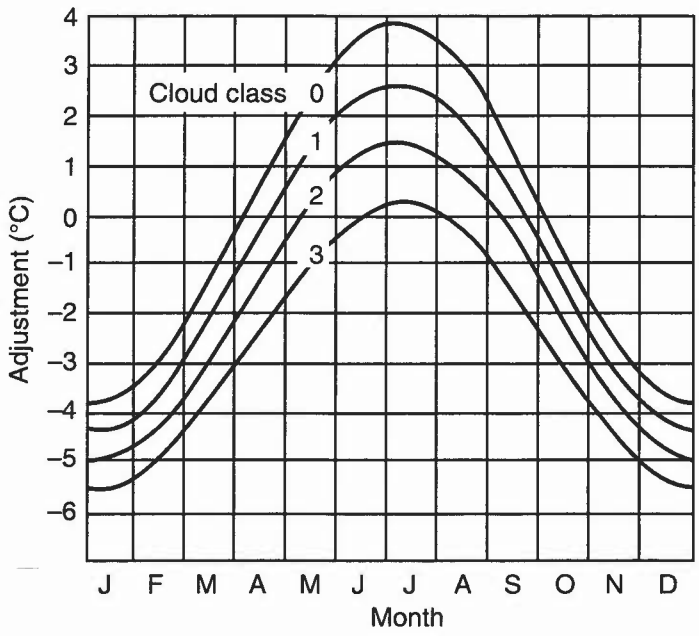

Figure 2.6. Adjustments to be applied to the values in Table 2.5 to allow for cloud classification and time of year.

Table 2.5. Unadjusted maximum temperature (°C) in terms of 1000–850 hPa thickness

Thickness (gpm)	Maximum temperature									
	0	1	2	3	4	5	6	7	8	9
1230	−0.8	−0.6	−0.5	−0.3	−0.1	0.0	0.2	0.3	0.5	0.6
1240	0.8	0.9	1.1	1.3	1.4	1.6	1.7	1.9	2.0	2.2
1250	2.3	2.5	2.7	2.8	3.0	3.1	3.3	3.4	3.6	3.8
1260	3.9	4.1	4.2	4.4	4.5	4.7	4.8	5.0	5.2	5.3
1270	5.5	5.6	5.8	5.9	6.1	6.2	6.4	6.6	6.7	6.9
1280	7.0	7.2	7.3	7.5	7.7	7.8	8.0	8.1	8.3	8.4
1290	8.6	8.7	8.9	9.1	9.2	9.4	9.5	9.7	9.8	10.0
1300	10.1	10.3	10.5	10.6	10.8	10.9	11.1	11.2	11.4	11.6
1310	11.7	11.9	12.0	12.2	12.3	12.5	12.6	12.8	13.0	13.1
1320	13.3	13.4	13.6	13.7	13.9	14.0	14.2	14.4	14.5	14.7
1330	14.8	15.0	15.1	15.3	15.5	15.6	15.8	15.9	16.1	16.2
1340	16.4	16.5	16.7	16.9	17.0	17.2	17.3	17.5	17.6	17.8
1350	17.9	18.1	18.3	18.4	18.6	18.7	18.9	19.0	19.2	19.4
1360	19.5	19.7	19.8	20.0	20.1	20.3	20.4	20.6	20.8	20.9
1370	21.1	21.2	21.4	21.5	21.7	21.8	22.0	22.2	22.3	22.5
1380	22.6	22.8	22.9	23.1	23.3	23.4	23.6	23.7	23.9	24.0
1390	24.2	24.3	24.5	24.7	24.8	25.0	25.1	25.3	25.4	25.6
1400	25.7	25.9	26.1	26.2	26.4	26.5	26.7	26.8	27.0	27.2
1410	27.3	27.5	27.6	27.8	27.9	28.1	28.2	28.4	28.6	28.7
1420	28.9	29.0	29.2	29.3	29.5	29.6	29.8	30.0	30.1	30.3
1430	30.4	30.6	30.7	30.9	31.1	31.2	31.4	31.5	31.7	31.8
1440	32.0	32.1	32.3	32.5	32.6	32.8	32.9	33.1	33.2	33.4

Callen et al. (1982)

2.3.4 Forecasting T_{max} from the 850 hPa wet-bulb potential temperature

The maximum temperature derived from the 850 WBPT is presented in **Table 2.6**, with corrections for wet and sunny conditions (based on London Weather Centre data for southern England).

Table 2.6. Maximum temperatures derived from 850 hPa wet-bulb potential temperatures

850 hPa θ_w	Equivalent thickness (m) 1000–850 hPa	Jan.	Feb.	Mar.	Apr.	May	Jun.	Jul.	Aug.	Sept.	Oct.	Nov.	Dec.	Correction Wet	Correction Sunny
18	1390	19	20	21	23	25	26	26	25	24	22	20	19	−5	+3
16	1380	17	19	19	21	23	25	25	23	23	21	19	17	−5	+2
14	1370	16	17	18	20	22	23	23	22	21	19	17	16	−4	+2
12	1360	15	15	17	19	21	21	21	21	19	17	15	17	−4	+2
10	1350	13	14	15	17	19	20	20	19	18	16	14	13	−4	+2
8	1340	11	13	13	15	17	19	19	17	17	15	13	11	−3	+2
6	1325	9	10	11	13	15	16	16	15	14	12	10	9	−3	+1
4	1320	8	9	10	12	14	15	15	14	13	11	9	8	−3	+1
2	1305	6	7	8	10	12	13	13	12	11	9	7	6	−3	+1
0	1295	4	5	6	8	10	11	11	10	9	7	5	4	−2	+1
−2	1285	3	4	5	7	9	10	10	9	8	6	4	3	−2	+1
−4	1270	−1	1	1	4	6	7	7	6	5	3	1	1	−2	+1

2.4 Nocturnal fall of surface temperature

(i) A number of techniques have been developed, based on empirical methods, to estimate the night minimum temperature during a clear night.

(ii) These depend on solving an equation of the form: $T_{min} = aT + bT_d + C$, where T is an afternoon temperature, T_d is the dew point at a particular time or a mean dew point over a cooling period and C is a quantity depending only on wind speed and cloud amount. a and b are constants.

(iii) Various methods for estimating T_{min} are presented, each using different ways of determining the constants a, b, and C. A useful approach is to estimate the dusk temperature as one of the points on the Saunders' cooling curve.

(iv) The methods are applicable only when the ground is not snow covered; the effect of fresh snow cover is discussed later. Exceptionally low minima may also occur when there is a large catchment area for katabatic drainage and when the lowest layers (950–850 hPa) are very dry (dew-point depressions >20 °C).

Boyden (1937) **McKenzie (1944)**

2.4.1 Forecasting dusk temperature, T_R, by Saunders' method

Saunders based his graphical method for determining a cooling curve on the idea of a discontinuity occurring in the rate of cooling at grass level within an hour after sunset, an effect particularly well defined on clear, windless nights (and possibly related to the deposition of dew).

He obtained regression equations relating the maximum temperature, T_{max}, and corresponding dew point, T_d, to T_R:

$$T_R = 0.5\,(T_{max} + T_d) - C$$

and C = 0.3 °C when no inversion with base below 900hPa
C = 2.2 °C when there is an inversion base below 900hPa.

Consider whether observed T_{max} and T_d will be representative of air mass expected over the site during the night.

Saunders established the approximate times for T_R (at Northolt) to be:

Table 2.7.

	Jan.	Feb.	Mar.	Apr.	May	June	July	Aug	Sept.	Oct.	Nov.	Dec.
UTC	1645	1800	1930	2045	2100	2115	2115	2045	1930	1745	1700	1630

If topsoil is wet T_R occurs about 1 hour earlier in late spring and early summer, and about ½ hour earlier in late summer.

Barthram refined this T_R technique to produce night-cooling nomograms for summer and winter, allowing for the effect of the geostrophic wind and cloud cover.

Barthram (1964) **Saunders (1952)**

2.4.2 Forecasting minimum temperature

2.4.2.1 Forecasting T_{min} (McKenzie's method)

(i) The night-time minimum air temperature (T_{min}) can be forecast as follows:

$$T_{min} = 0.5(T_{max} + T_d) - K$$

where T_{max} = maximum temperature, T_d = air-mass dew point at time of T_{max}, and K = local constant depending on forecast surface wind and low cloud amount).

(ii) Although originally for Dyce (Aberdeen) many inland low-level airports have values similar to those for Birmingham (**Table 2.8(a)**). Kensett has published K values for 90 UK stations.

Table 2.8(a). Values of local constant (K) for Birmingham Airport

Mean overnight surface wind (kn)	Average cloud amount overnight (oktas) 0	1–2	3–4	5–6	7–8
Calm	8.8	8.0	7.3	6.7	3.2
1–3	8.2	7.7	6.7	5.1	2.8
4–6	6.5	5.8	5.2	4.0	2.3
7–10	4.7	4.3	3.9	3.1	1.8
11–16	2.3	2.8	2.5	2.1	1.4
17–21	0.5	0.8	2.0	1.1	0.8

Monthly variations have been found which apply at all stations. The value of K may usefully be corrected by the following amounts:

Table 2.8(b).

	Jan.	Feb.	Mar.	Apr.	May	June	July	Aug.	Sept.	Oct.	Nov.	Dec.
A	−1.0	−0.5	+0.5	0.0	0.0	0.0	0.0	0.0	+0.5	+1.0	0.0	−1.0
B	−0.5	−0.5	0.0	0.0	+0.5	+0.5	+0.5	+0.5	0.0	0.0	−0.5	−0.5

A = 'Good radiation nights' B = 'Poor radiation nights'

Kensett (1983) **McKenzie (1944)**

2.4.2.2 Forecasting T_{min} (Craddock and Pritchard's method)

(i) The following regression equation was obtained from a statistical investigation of 16 stations in eastern England not close to the sea; it is considered valid for a wide area of eastern England:

$$T_{min} = 0.316\,T_{12} + 0.548\,T_{d12} - 1.24 + K$$
$$= X + K$$

where T_{12} = screen temperature at 1200 UTC and T_{d12} = dew-point temperature at 1200 UTC.

(ii) For ease of use, the value for X may be obtained from **Table 2.9** while the values for K, which depend on forecast values of the mean geostrophic wind and mean cloud amount, are given in **Table 2.10.** The means are forecast values for 1800, 0000 and 0600 UTC.

Table 2.9. Computation of the value of X (°C)

Air temp. at 1200	Dew-point at 1200 UTC −3	−2	−1	0	1	2	3	4	5	6	7	8	9	10	11	12	13	14	15	16
27	5.7	6.2	6.7	7.3	7.8	8.4	8.9	9.5	10.0	10.6	11.1	11.7	12.2	12.8	13.3	13.9	14.4	15.0	15.5	16.1
26	5.4	5.9	6.4	7.0	7.5	8.1	8.6	9.2	9.7	10.3	10.8	11.4	11.9	12.5	13.0	13.6	14.1	14.6	15.2	15.7
25	5.1	5.6	6.1	6.7	7.2	7.8	8.3	8.9	9.4	9.9	10.5	11.0	11.6	12.1	12.7	13.2	13.8	14.3	14.9	15.4
24	4.8	5.2	5.8	6.3	6.9	7.4	8.0	8.5	9.1	9.6	10.2	10.7	11.3	11.8	12.4	12.9	13.5	14.0	14.6	15.1
23	4.5	4.9	5.5	6.0	6.6	7.1	7.7	8.2	8.8	9.3	9.9	10.4	11.0	11.5	12.1	12.6	13.2	13.7	14.2	14.8
22	4.1	4.6	5.2	5.7	6.3	6.8	7.4	7.9	8.5	9.0	9.5	10.1	10.6	11.2	11.7	12.3	12.8	13.4	13.9	14.5
21	3.8	4.3	4.8	5.4	5.9	6.5	7.0	7.6	8.1	8.7	9.2	9.8	10.3	10.9	11.4	12.0	12.5	13.1	13.6	14.2
20	3.5	4.0	4.5	5.1	5.6	6.2	6.7	7.3	7.8	8.4	8.9	9.5	10.0	10.6	11.1	11.7	12.2	12.8	13.3	13.8
19	3.2	3.7	4.2	4.8	5.3	5.9	6.4	7.0	7.5	8.1	8.6	9.1	9.7	10.2	10.8	11.3	11.9	12.4	13.0	13.5
18	2.9	3.4	3.9	4.4	5.0	5.5	6.1	6.6	7.2	7.7	8.2	8.8	9.4	9.9	10.5	11.0	11.6	12.1	12.7	13.3
17	2.6	3.0	3.6	4.1	4.7	5.2	5.8	6.3	6.9	7.4	8.0	8.5	9.1	9.6	10.2	10.7	11.3	11.8	12.4	12.9
16	2.3	2.7	3.3	3.8	4.4	4.9	5.5	6.0	6.6	7.1	7.7	8.2	8.7	9.3	9.8	10.4	10.9	11.5	12.0	12.6
15	1.9	2.4	3.0	3.5	4.0	4.6	5.1	5.7	6.2	6.8	7.3	7.9	8.4	9.0	9.5	10.1	10.6	11.2	11.7	
14	1.6	2.1	2.6	3.2	3.7	4.3	4.8	5.4	5.9	6.5	7.0	7.6	8.1	8.7	9.2	9.8	10.3	10.9		
13	1.3	1.8	2.3	2.9	3.4	4.0	4.5	5.1	5.6	6.2	6.7	7.3	7.8	8.3	8.9	9.4	10.0			
12	1.0	1.5	2.0	2.6	3.1	3.6	4.2	4.7	5.3	5.8	6.4	6.9	7.5	8.0	8.6	9.1				
11	+0.7	1.1	1.7	2.2	2.8	3.3	3.9	4.4	5.0	5.5	6.1	6.6	7.2	7.7	8.3					
10	+0.4	+0.8	1.4	1.9	2.5	3.0	3.6	4.1	4.7	5.2	5.8	6.3	6.9	7.4						
9	−0.0	+0.5	1.1	1.6	2.2	2.7	3.2	3.8	4.3	4.9	5.4	6.0	6.5							
8	−0.4	+0.2	+0.7	1.3	1.8	2.4	2.9	3.5	4.0	4.6	5.1	5.7								
7	−0.7	−0.1	+0.4	1.0	1.5	2.1	2.6	3.2	3.7	4.3	4.8									
6	−1.0	−0.4	+0.1	+0.7	1.2	1.8	2.3	2.8	3.4											
5	−1.3	−0.8	−0.2	+0.3	+0.9	1.4	2.0	2.5	3.1											
4	−1.6	−1.1	−0.5	+0.0	+0.6	1.1	1.7	2.2												
3	−1.9	−1.4	−0.8	−0.3	+0.3	+0.8	1.4													

Table 2.10. Values of K (°C) based on mean forecast values of wind speed and cloud amount for 1800, 0000 and 0600 UTC

Mean geostrophic wind speed (kn)	Mean cloud amount (oktas) 0–2	2–4	4–6	6–8
0–12	−2.2	−1.7	−0.6	0
13–25	−1.1	0	+0.6	+1.1
26–38	−0.6	0	+0.6	+1.1
39–51	+1.1	+1.7	+2.8	—

The development of appropriate regression equations is required if the method is to be applied to other areas of the country.

Craddock et al. (1951)

2.4.2.3 Forecasting the hourly fall of temperature during the night (Barthram's method)

The following steps are used in conjunction with the Night Cooling Nomogram (**Fig. 2.7**), to obtain a cooling curve, drawn realistically through T_{max}, T_R (the Saunders' discontinuity temperature) and T_{min}:

(i) Use a representative upper-air sounding to determine whether there is an inversion with its base below 900 hPa at the time of maximum temperature.
(ii) Decide if nocturnal cloud cover will be best described as cloudless or 8/8.
(iii) From steps (i) and (ii), select one of the four rows marked 'Dew-point at time of maximum temp'. A series of vertical lines descends from these dew-point values.
(iv) Follow a horizontal line from the value for the maximum temperature (marked on the left-hand side) until it cuts the vertical line descending from the dew-point value selected in step (iii). From this point, follow one of the diagonal lines to the line marked 'Saunders' discontinuity temperature T_R'. Ignore T_R on cloudy, windy nights.
(v) The time of this discontinuity depends on the date. Use the small graph at the bottom of the nomogram where the months are marked. Find the time of T_R for the required date from the curve marked 'time of discontinuity'.
(vi) Follow the vertical line upwards from the time of T_R and extend it to the main graph to meet the value of T_R established in step (iv).
(vii) The next stage brings in a correction for the forecast gradient wind overnight. Select one of the diagonal lines on the right-hand side of the nomogram marked 'gradient wind speed'.
(viii) Follow the horizontal line from T_R until it cuts the selected diagonal line marked 'gradient wind speed'. From this point of intersection, descend along a vertical line to the diagonal marked 'Minimum temp. under clear skies'. The preliminary value for T_{min} can be read off here.
(ix) The preliminary value for T_{min} needs corrections for cloud amount and wind speed. The two small graphs (lower left) show amounts to be added to the preliminary T_{min} value to allow for the effect of nocturnal cloud cover and wind.
(x) In summer a further correction is needed because the short nights give a reduced period for cooling. Use the small graph (lower right, **Fig. 2.7(b)**) to find this value.
(xi) After raising the preliminary T_{min} by adding the corrections in steps (ix) and (x) the final value of T_{min} is plotted on the main graph above the time for sunrise shown on the lower graph.
(xii) This fixes three points on the cooling curve: T_{max} at approximately mid afternoon, T_R and T_{min}. The cooling curve can be drawn through these three points.

There are small differences between cooling for summer and winter and separate diagrams are provided for winter (October to March) (**Fig. 2.7(a)**) and for summer (April to September) (**Fig. 2.7(b)**).

Notes:
(a) The method applies to nights without fog.
(b) Effect of snow cover is discussed next.

Barthram (1964)

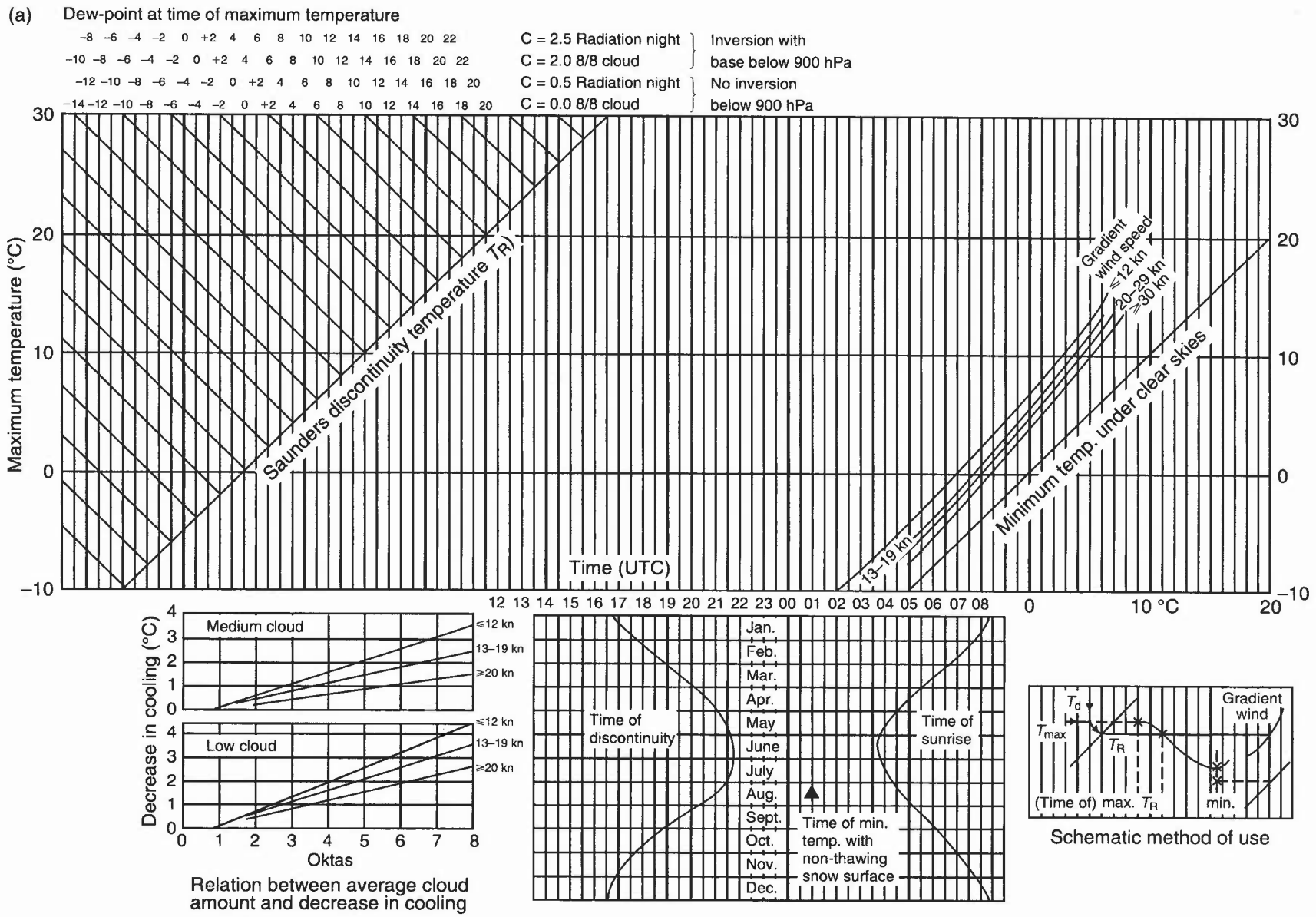

Figure 2.7(a). Night cooling nomogram for winter (October–March). See text for method of use.

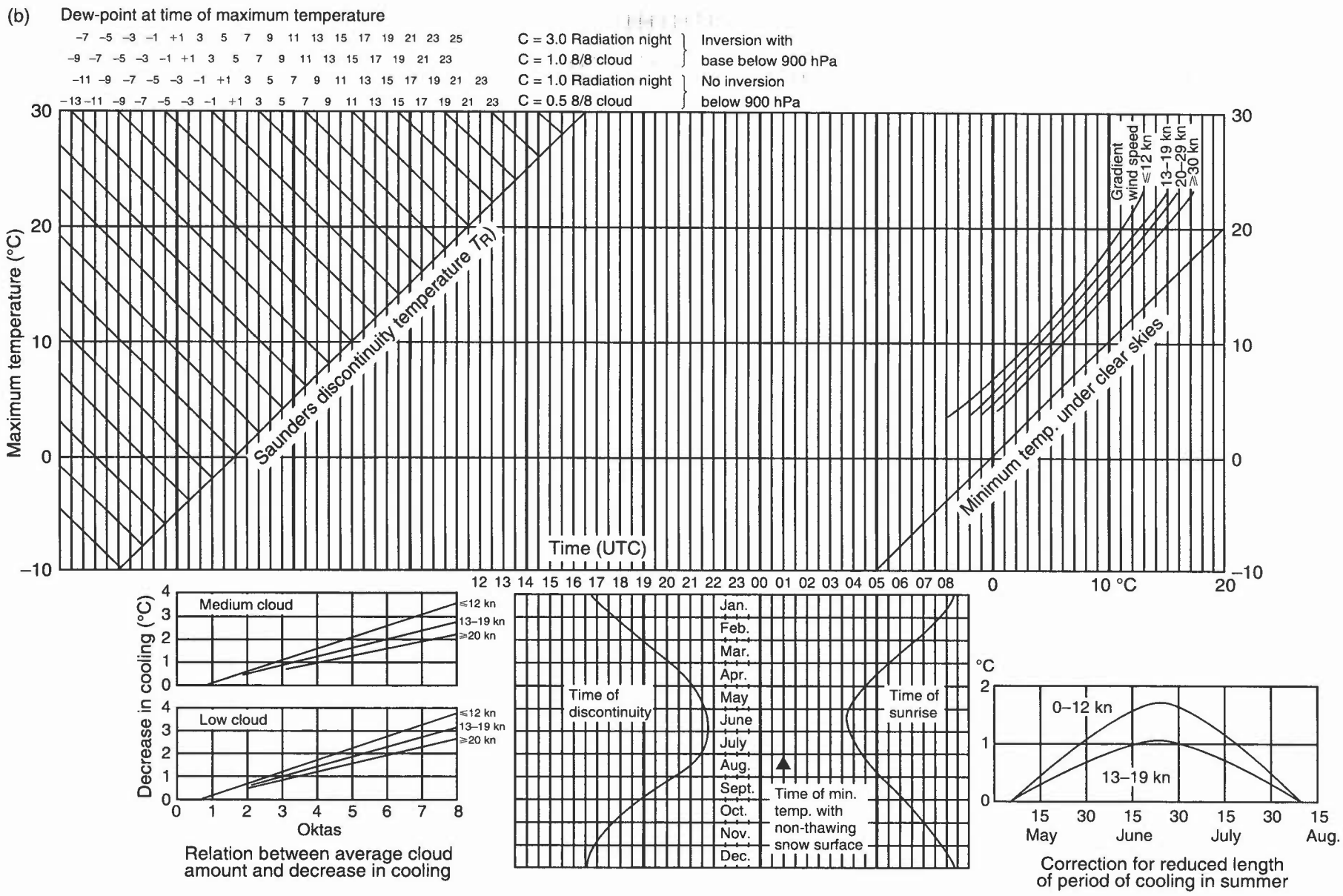

Figure 2.7(b). Night cooling nomogram for summer (April–September). See text for method of use.

2.4.3 *Effect of snow cover*

(i) Under clear skies and light winds, screen temperature over a snow surface is likely to fall 2 to 4 °C below the minimum calculated by the methods in 2.4 and to be reached earlier than if snow free.

(ii) With cloud present the minimum is likely to be about 1 °C lower than over snow-free surface; it may be less than that for wind speeds of 15 kn or so.

HWF (1975), Chapter 17.7.4

2.4.4 *Description of the severity of air frost*

When actual or forecast air temperatures fall below 0 °C, the severity of the frost is described arbitrarily by the terms 'Slight', 'Moderate', 'Severe' or 'Very severe' according to the temperature and the surface wind speed at the time, as illustrated in **Fig. 2.8.**

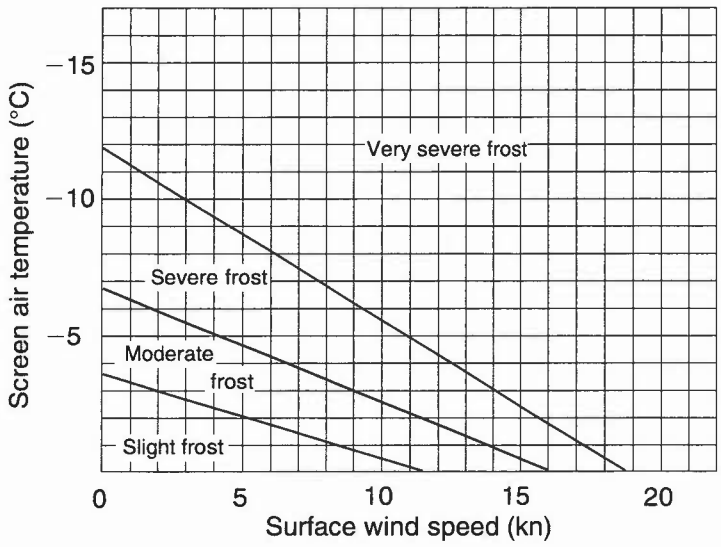

Figure 2.8. Diagram for determining the severity of air frost for actual or forecast wind speeds and air temperatures.

2.5 Grass- and concrete-minimum temperatures

2.5.1 *Forecasting the grass-minimum temperature, using the geostrophic wind speed and cloud amount*

T_g, the grass-minimum temperature is calculated from:

$$T_g = T_n - K$$

where T_n is the air-minimum temperature, and K is a constant which depends on forecast values of geostrophic wind speed and cloud amount.

Table 2.11. Values of K (°C)

V_g	N (oktas)			
(kn)	0–2	2–4	4–6	6–8
0–12	5.0	5.0	4.0	4.0
13–25	4.0	4.0	3.0	2.0
26–38	3.5	3.0	2.5	2.5
39–52	2.5	2.5	2.5	3.0

Values of V_g and N are means of the 1800, 0000 and 0600 UTC values.

Craddock & Pritchard (1951)
HWF (1975), Chapter 14.7.3

2.5.2 *Forecasting the grass-minimum temperature from the geostrophic wind speed (graphical method)*

Fig. 2.9 shows isopleths of the depression of the grass-minimum temperature below the air-minimum temperature at Cottesmore in eastern England. Only low-cloud cover is considered, and 'sky obscured' is taken to be the same as 8 oktas.

Sills (1969)

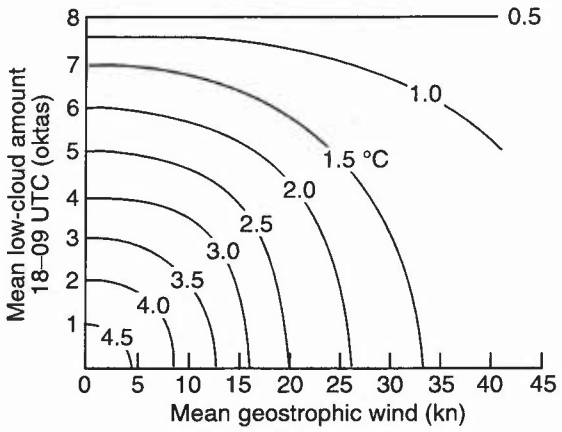

Figure 2.9. Depression (°C) of the grass-minimum temperature below the air-minimum temperature at Cottesmore.

2.5.3 *Forecasting the grass-minimum temperature from the surface wind speed*

Use the same formula as in 2.5.1 above but with values of K as follows:

Table 2.12. K values (°C) as a function of surface wind speed and cloudiness

Surface wind (kn)	Clear sky (up to 2/8)		Cloudy (8/8 cloud)
	Mean	(Max)	Mean
1–5	5.0	(8.0)	1.0
6–10	3.5	(8.6)	1.0
11–15	2.5	(3.5)	1.0
>15	1.5	(2.8)	1.0

Cloud cover is C_L, C_M or $C_L + C_M$

The mean values, averaged for six stations in England, have been rounded to 0.5 °C.

FRB (1993)

2.5.4 *Minimum temperature on roads*

At Watnall (near Nottingham), it was found that the difference between screen minimum, T_{min}, and (concrete) road minimum temperatures varied with the length of night. The following regression equation was obtained **(Table 2.13)**:

$$T_{min} - T_r = 0.28t - 2.9$$

where T_r = minimum temperature on the road, t is the length of night (in hours).

Table 2.13. Minimum temperature on roads (°C)

	Jan.	Feb.	Mar.	Apr.	May	June	July	Aug.	Sept.	Oct.	Nov.	Dec.
$T_{min} - T_r$ (observed)	2.0	1.5	1.0	0.0	—	—	—	—	—	0.5	1.5	2.0
From the formula for length of night for 52° N	1.5	1.1	0.5	0.0	−0.6	−1.1	−0.7	−0.3	0.3	0.8	1.4	1.6

Parrey (1969)
Ritchie (1969)

2.6 Forecasting road surface conditions

Forecasting the temperature of road surfaces is especially important in winter when icy conditions may occur. It is not straightforward, because of the wide variations in meteorological conditions which are found over short distances on the same night as well as variations in the thermal capacity and conductivity of different types of road and the road state (wet, ice-covered, salted, dry). Evaporation from the surface into dry ambient air will cool the surface.

2.6.1 Site differences

Site-specific ice prediction lies at the core of forecasting road surface conditions. There are three types of night for which forecasts are required: *Extreme, Damped and Intermediate.* **Fig 2.10** (for high and low sites).

2.6.1.1 Urban, rural and coastal sites and bridges

The following factors are important:

(a) *Urban and rural*
  (i) urban heat island (2.11) will give warmer air temperatures overnight;
  (ii) increased traffic flows cause increased turbulence; to simulate this forecast winds should be stronger in cities by 5 kn — even 10 kn on extreme radiation nights;

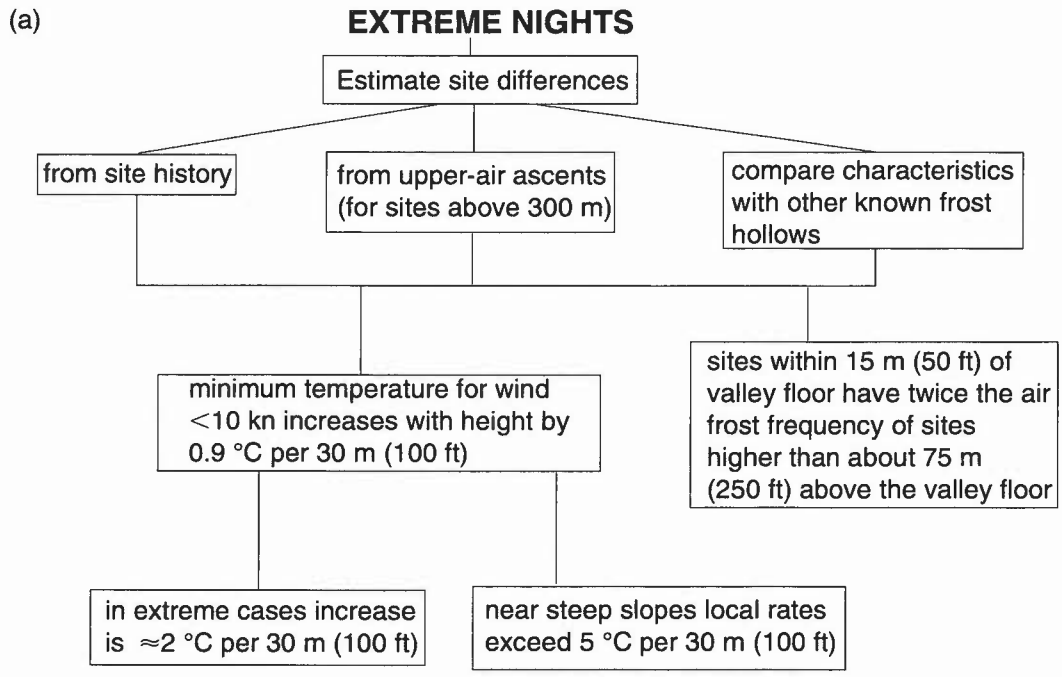

Figure 2.10. Forecasting road surface conditions — site differences. Select 'type of night'. EXTREME: clear, calm; generally katabatic drainage will ensure lowland sites colder than more elevated sites. Refer to Fig. 2.10(a). DAMPED: overcast, windy; giving well-mixed boundary layer. Refer to Fig. 2.10(b). INTERMEDIATE: wind/no cloud or cloud/no wind or rapidly changing conditions. Refer to Fig. 2.10(c). Note: high-level valleys will be subject to katabatic drainage from higher sites and show frost-hollow characteristics. Since these sites may be colder than lower sites due to altitude, they are often the coldest type of site, especially if sheltered. If not sheltered this will be similar to other high-altitude sites. Site history will be a useful indicator.

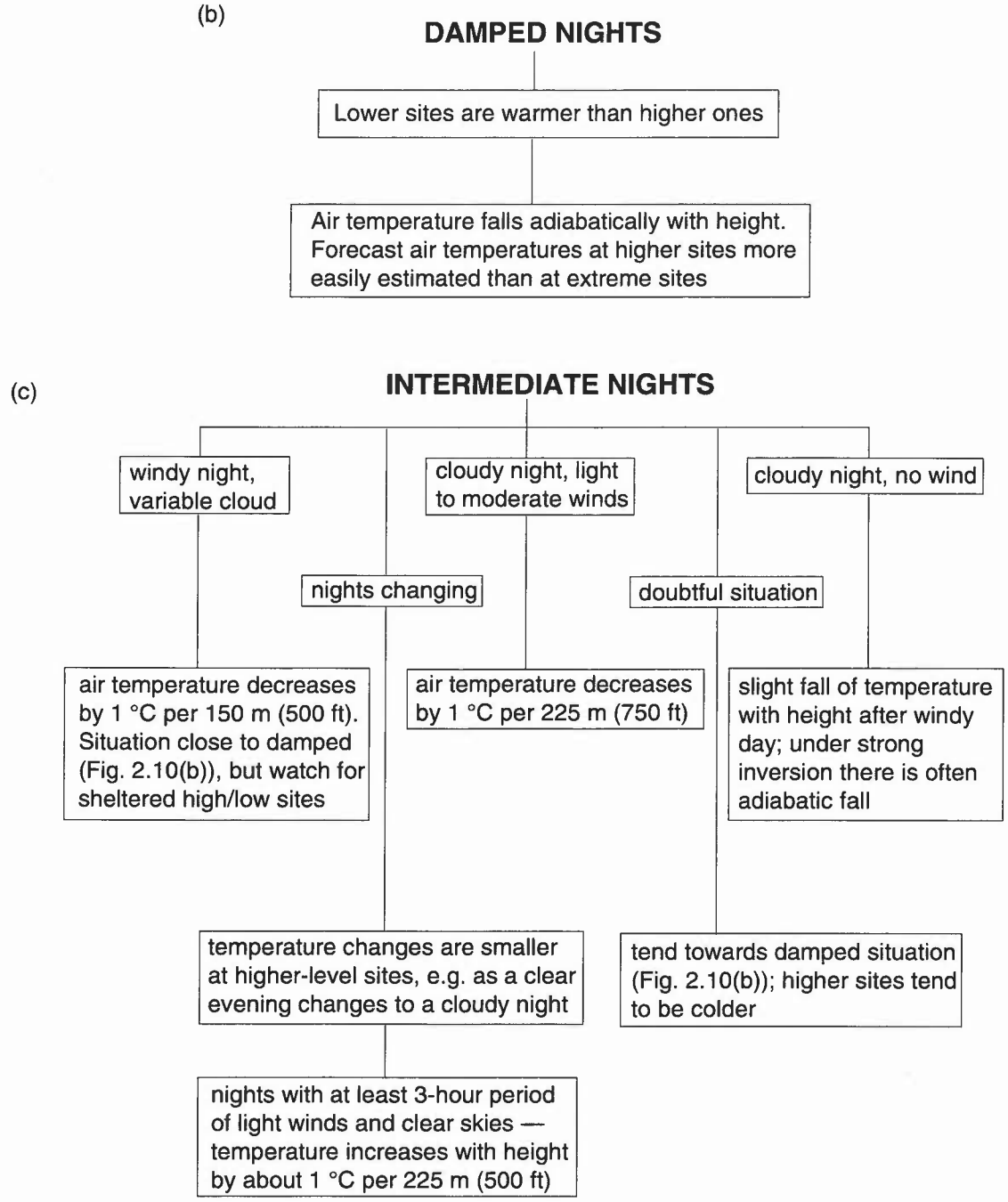

Figure 2.10. (Continued).

(iii) heavier traffic flows and buildings impede outgoing long-wave radiation; forecast clouds should be increased by 2 oktas to compensate (more for exceptional traffic flows);

(iv) well exposed *rural* sites will be the standard, requiring little adjustment although busy rural roads (e.g. motorways) may need adjustment which will be indicated by site history; these adjustments may need toning down to allow for the 'Sunday Effect'.

(b) *Coastal sites*

(i) can be warmer than inland sites when the wind comes off the sea;

(ii) sandy soils can point to a rapid drop of temperature on favoured nights;

(iii) greater dew points and greater likelihood of daytime showers favour widespread icing compared with inland;

(iv) site history is important;

(v) the forecasting aim is to determine the overnight wind direction.

(c) *Bridge decks*
   (i) have no ground heat flux, a small heat capacity;
   (ii) road surface temperatures (RST) will respond quickly to external forcing factors;
   (iii) the difference between bridges and roads will be greatest at times of greatest soil heat fluxes (especially late October/early November);
   (iv) location factor is dominant (e.g. estuarine, elevated urban).

Astbury (1994)
Perry & Symons (1991)

2.6.2 Forecasting for icy roads

Sources of moisture leading to road icing: precipitation; dew; hoar frost; freezing fog; moisture advection; melting snow; seepage; other sources (springs etc.).

(a) *Precipitation*
   (i) Widespread ice only forms twice in an average southern England winter.
   (ii) The central crown of the road will dry quickly after rain; ice will not become widespread, but will form in prone locations.
   (iii) Road temperatures need to fall below freezing within 2 hours of the cessation of rainfall for widespread ice.
   (iv) Late, prolonged showers from a trough followed by clear skies and light winds in the early evening can present a dangerous combination; salt may be washed off by later showers, with possible freezing following.
   (v) Forecasters must be aware of the necessity to update local authorities.
   (vi) Particular scenarios to note:
   rapid frontal clearance —
   heavy precipitation associated with a slow moving ana-front may be followed by rapid clearance and light winds;
   low road temperatures during precipitation —
   if rain turns to sleet or wet snow before clearing or under wintry showers, the latent heat to melt ice/snow will cool the road; a rapid drop of surface temperature below zero may result if skies then clear (even if a breeze persists or the cloud break is not continuous).

(b) *Freezing rain/drizzle*
   (i) The type of ascent involved is, typically, when a warm front approaches a surface intensely cooled due to radiation or by low-level cold advection.
   (ii) It is possible to get freezing drizzle from a complete sub-zero ascent. If no ice particles are present in the stratiform cloud (likely if temperatures are just below zero), then coalescence can still occur with supercooled droplets which then freeze on contact with the ground.

(c) *Dew*
Not common; it requires road surface temperature (RST) to fall below dew point and sufficient breeze to mix air in vicinity of road surface.

(d) *Hoar frost*
Not common; problems occur after traffic has traversed it, changing it to ice/water.

(e) *Freezing fog*
   (i) Although adjacent grass verges may be coated with rime, roads may be unaffected.
   (ii) As the fog thickens the ground temperature will rise as outgoing long-wave radiation is shut off.
   (iii) The RST may go above 0 °C even with a screen temperature as low as −1 °C.
   (iv) Widespread rime on roads is only expected if freezing fog is expected to remain shallow, or if the screen temperature is −1 °C or less.

(f) *Moisture advection over a cold surface*
   Particularly under increasing gradient with little cloud towards the end of a long radiation night. This process can also lead to ice formation after sunrise.

(g) *Melting snow*
   (i) Following snowfall the air temperature generally rises a little to give a slight daytime thaw and hence a source of moisture, leading to widespread icing after dark.
   (ii) Residual snow mounds left by snow ploughs can be very persistent and thus a potential source of road icing for days/weeks.

(h) *Seepage, springs, etc.*
Not strictly a meteorological problem, but can follow a prolonged period of winter rain, maintaining a verge or road wet even when conditions are dry.

Astbury (1994)
Hewson & Gait (1992)

2.6.2.1 Forecasting hoar frost

The following are necessary for hoar frost:
RST to be below air-mass dew point and to be at or near freezing; breeze sufficient to cause mixing.

These conditions are likely if five or more of the following conditions are satisfied:
(i) long night;
(ii) low road-depth temperature (RDT) ($\leq$4.5 °C);
(iii) clear sky $\leq$2/8 cloud cover;
(iv) wind $\geq$4 kn at 10 m;
(v) high dew point $\geq$1 °C;
(vi) small dew-point depression $\leq$1.5°C;
(vii) cold and clear previous night.

Adjacent moisture sources, such as small lakes, rivers, edges of woods, etc. are important.

Local variations: more likely to be encountered on higher ground, in coastal regions, on bridge decks.

Note that:
(i) Hoar frost is unlikely in very cold, dry air; early or late in the season.
(ii) The five conditions are most likely during polar maritime and arctic maritime outbreaks when the higher, colder more exposed sites become frosty first.
(iii) Most severe events occur when moister air with RDT higher than RST is being advected over a cold surface after a cold spell.
(iv) During several days of clear skies north facing slopes, sheltered urban and rural roads can accumulate hoar frost over several days and nights.

Thermal maps can aid the forecaster in constructing the likely spatial variability to be anticipated in road-surface temperatures under clear, cloudy, windy, wet, etc. nights.

Astbury (1994)
Hewson & Gait (1992)
Perry & Symons (1991)

2.7 Modification of surface air temperature over the sea

2.7.1 Advection of cold air over warm sea

2.7.1.1 Frost's method

If T_o (°C) and r_o (g kg^{-1}) are the temperature and humidity mixing ratio of the air before crossing the sea, T and r the values after crossing at least 60 miles of sea; T_s and r_s are the sea temperature and humidity mixing ratio of saturated air at temperature T_s, then:

$$T = T_o + 0.6\,(T_s - T_o)$$
$$r = r_o + 0.6\,(r_s - r_o).$$

Notes:
(a) These formulae apply to all cold airstreams crossing a warmer sea surface, e.g. a cold northerly outbreak reaching north Scotland or a cold westerly current reaching Norway.
(b) In applying these formulae, make the best estimate of the sea-surface temperature along the trajectory. Determine r_o and r_s by using a tephigram.
(c) Although this method is simple to use it has been criticized because:
(i) The factor of 0.6 only applies to sea crossings of over 300 n mile (550 km).

(ii) The presence of any inversion is ignored.
(iii) The values of r can exceed the saturated humidity mixing ratio at the temperature T_s.

Frost (1941)

Blackall put forward a more empirically based method to overcome these objections.

2.7.1.2 Blackall's method

This is an empirically based method which takes into account both the duration of the sea crossing and the depth of convection. The method uses the equation

$$T = T_s - (T_s - T_o) \exp(-12t/d)$$

where T_s = sea temperature (°C), t is the duration of the sea crossing (hours), d is the depth of convection in hectopascals, and T is the final and T_o the original air temperature.

The procedure is as follows:

(a) On a sounding in the air upwind of the sea crossing, draw in the MSL isobar and, if necessary, extend the ascent downwards to meet this isobar at the coastal temperature.
(b) Draw a dry adiabatic through the sea temperature T_s **(Fig. 2.11)**. The pressure at which this line meets the environment curve is subtracted from the surface pressure to give the depth of convection d in hectopascals.
(c) Establish the expected lapse rate; if the air already has a lapse rate implying convection through the layer d, the environment curve should not be changed. If a lapse rate needs to be forecast modify the environment curve as follows: draw a line through the layer d with an appropriate lapse (use **Table 2.14**) such that the environment curve encloses equal areas (A and B in **Fig. 2.11(b)**) on each side of the line. Where this line meets the surface isobar is T_o. This step represents complete mixing without the addition of heat.
(d) Determine the time t that the air will spend over the sea from the wind in the layer d and the fetch. Using gradient winds from the isobars and 850 hPa contours should be sufficiently accurate in most cases.
(e) From **Table 2.14** look up the value of $\exp(-12t/d)$ using the appropriate values of t (hours) and d (hectopascals). Then find T from the equation, above.
(f) From temperature T on the surface isobar, draw a line parallel to the environment curve produced in step (c); this is the predicted environment curve when the air finishes its crossing.
(g) A mean value of the sea temperature will often give good answers; however, if changes in T_s alter the value of d and thus $\exp(-12t/d)$ it will be necessary to proceed by steps. This will also be necessary when the sea passage is expected to take more than 24 hours.

Note:
The procedure above does not allow for fronts and other dynamic means of heating and cooling. The increase in surface humidity mixing ratio is taken to be

$$r - r_o = 0.18\,(T - T_o)$$

with the dew point remaining constant with height.

Blackall (1973)

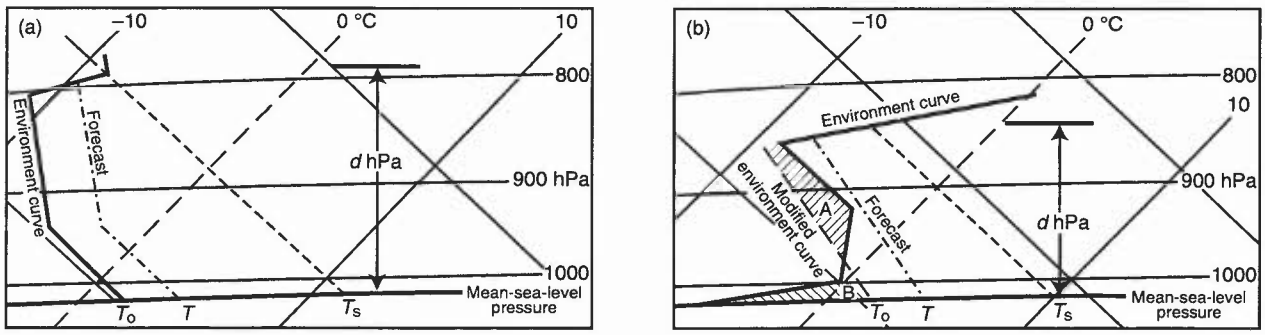

Figure 2.11. Forecasting the warming of cold air moving over a warm sea (Blackall's method) when (a) the upstream environment curve already indicates convective mixing is occurring, and (b) the environment curve is initially stable and needs modification. See text for details of construction.

Table 2.14. Values of exp (−12*t*/*d*).

Temp. lapse in the layer with depth *d* (°C)	*d* (hPa)	Duration of crossing *t* (hours)													
		1	2	3	4	5	6	7	8	9	12	15	18	21	24
	700	0.98	0.97	0.95	0.93	0.92	0.90	0.89	0.87	0.86	0.81	0.77	0.73	0.70	0.66
	600	0.98	0.96	0.94	0.92	0.90	0.89	0.87	0.85	0.84	0.79	0.74	0.70	0.66	0.62
40	500	0.98	0.95	0.93	0.91	0.89	0.86	0.84	0.82	0.81	0.75	0.70	0.65	0.60	0.56
31	400	0.97	0.94	0.91	0.89	0.86	0.84	0.81	0.79	0.76	0.70	0.64	0.58	0.53	0.49
26	350	0.97	0.93	0.90	0.87	0.84	0.81	0.79	0.76	0.73	0.64	0.60	0.54	0.49	0.44
22	300	0.96	0.92	0.89	0.85	0.82	0.79	0.76	0.73	0.70	0.62	0.55	0.49	0.43	0.38
17	250	0.95	0.91	0.86	0.83	0.79	0.75	0.71	0.68	0.65	0.57	0.49	0.42	0.36	0.32
14	200	0.94	0.89	0.84	0.79	0.74	0.70	0.66	0.62	0.58	0.49	0.41	0.34	0.28	0.24
13	180	0.94	0.88	0.82	0.77	0.72	0.67	0.63	0.59	0.55	0.45	0.37	0.30	0.25	0.20
12	160	0.93	0.86	0.80	0.74	0.69	0.64	0.59	0.55	0.51	0.41	0.33	0.26	0.21	0.17
10	140	0.92	0.84	0.77	0.71	0.65	0.60	0.55	0.50	0.46	0.36	0.28	0.21	0.17	0.13
9	120	0.90	0.82	0.74	0.67	0.61	0.55	0.50	0.45	0.41	0.30	0.22	0.17	0.12	0.09
8	100	0.89	0.79	0.70	0.62	0.55	0.49	0.43	0.38	0.34	0.24	0.17	0.12	0.08	0.06
6	80	0.86	0.74	0.64	0.55	0.47	0.41	0.35	0.30	0.26	0.17	0.11	0.07	0.04	0.03
5	60	0.82	0.67	0.55	0.45	0.37	0.30	0.25	0.20	0.17	0.09	0.05	0.03	0.01	
4	50	0.79	0.62	0.49	0.38	0.30	0.24	0.19	0.15	0.12	0.06	0.03	0.01		
4	40	0.74	0.55	0.41	0.30	0.22	0.17	0.12	0.09	0.07	0.03	0.01			
1	30	0.67	0.45	0.30	0.20	0.14	0.09	0.06	0.04	0.03	0.01				

2.7.1.3 Grant's method

(a) Use air trajectory and wind speed to find length of fetch(es).

(b) Use sea temperature charts to find the mean sea temperature (T_s) and from a tephigram, determine the saturated humidity mixing ratio (r_s) at this temperature.

(c) On a representative upstream sounding:
  (i) Draw in the MSL isobar (p_s).
  (ii) Draw a dry adiabat from T_s to meet the environment curve.
  (iii) Draw the isobar through this meeting point and note the depth of convection (d) in hectopascals.

(d) Modify the initial air temperature (T_o) by
  (i) Drawing the expected condensation level (CL) at end of sea crossing. Use $p_s - 60$ hPa as a first guess.
  (ii) If the sounding is well inland, modify the lower part to fit the reported temperatures at the upwind coast.
  (iii) Draw the path followed by a parcel of air condensing at the expected CL so that equal areas (A = B) are enclosed between the path curve, the environment curve and the isobar $p_s - d$ (**Fig. 2.12**).
  (iv) Note value of modified initial temperature (T_o).
  (v) Note value of $T_s - T_o$. This is used in (f)(ii) below.

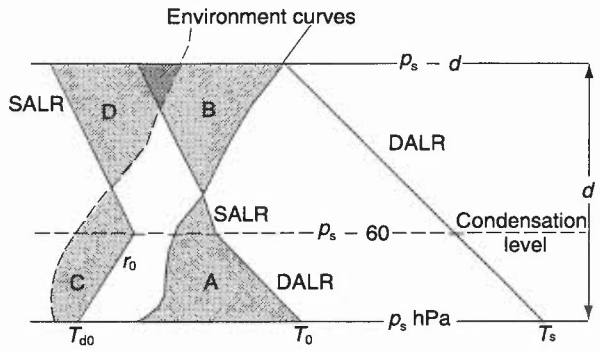

Figure 2.12. Forecasting the warming of cold air moving over a warm sea (Grant's method) — the modification of an initially stable temperature and moisture structure where T_s is the sea temperature at mean-sea-level pressure (p_s), ($p_s - 60$) is a first estimate of condensation level and ($p_s - d$) is the expected top of the convective layer. See text for method of construction.

(e) Modify the initial mixing ratio (r_o)
   (i) Draw a constant-mixing-ratio line up to the CL and a saturated adiabat above, so that the total water-vapour content between the isobars p_s and $p_s - d$ is unchanged. Since water content is not proportional to area this construction is not an 'equal area' one, but the lower area where water content is large must be less than the upper one where water contents are smaller, i.e. area C<area D.
   (ii) Note the modified value of r_o.

(f) Use the nomogram in **Fig. 2.13**.
   (i) Starting from the scale for 'fetch', move horizontally to 'd', the depth of convection, and from this point draw a line downward to the lower part of the nomogram.
   (ii) Enter left-hand scale for $(T_s - T_o)$ and draw a horizontal line to meet the vertical. The meeting point is marked by a small circle on the example plotted on **Fig. 2.13**
   (iii) Read off the value ΔT from the family of full curves. The downwind temperature is then $T_o + \Delta T$.
   (iv) Read off Z to the nearest 0.01 from the family of pecked curves.
   The final mixing ratio is given by

$$r = r_o + Z\,(r_s - r_o).$$

   (v) Use a tephigram to convert 'r' to the corresponding dew point T_d.
   (vi) The final CL is given approximately by 120 $(T - T_d)$ m
   or 400 $(T - T_d)$ ft.

This method of forecasting coastal temperatures in cold-air advection with onshore winds appears to perform better than Blackall's method, though giving no real improvement in showery northerlies.

Grant (1975)

2.7.2 Advection of warm air over a cold sea (Lamb and Frost's method)

For surface winds less than 20 kn

$$T - T_s = (T_s - T_o)\,\mathrm{f}(d)$$
$$r - r_s = (r_s - r_o)\,\mathrm{f}(d)$$

where d is the fetch (km) over the sea and other symbols are as in Frost's method.

Table 2.15. Values of f(d)

d (km)	100	200	300	400	500	600	700	800	900	1000
f(d)	0.175	0.152	0.141	0.133	0.127	0.123	0.119	0.116	0.113	0.110

Note: A cool sea surface exerts a powerful and rapid control on the temperature at screen height.

Lamb (1943)

2.8 Cooling of air by precipitation

2.8.1 Cooling of air by rain

A dry-bulb temperature close to the wet-bulb value is reached after about half an hour of very heavy rain or about 1 to 2 hours of rain of lesser intensity.

HWF (1975) Chapter 14.9.3

2.8.2 Cooling of air by snow

Falling snow gradually lowers the 0 °C level. However, the reduction of the surface temperature to 0 °C is unlikely if:
(i) the wet-bulb temperature at the surface is higher than 2.5 °C in prolonged frontal precipitation;
(ii) the wet-bulb temperature at the surface is higher than 3.5 °C within extensive areas of moderate or heavy instability precipitation.

Note: The relation between wet-bulb temperature and the form of precipitation is given in 5.10.1.

Lumb (1963)

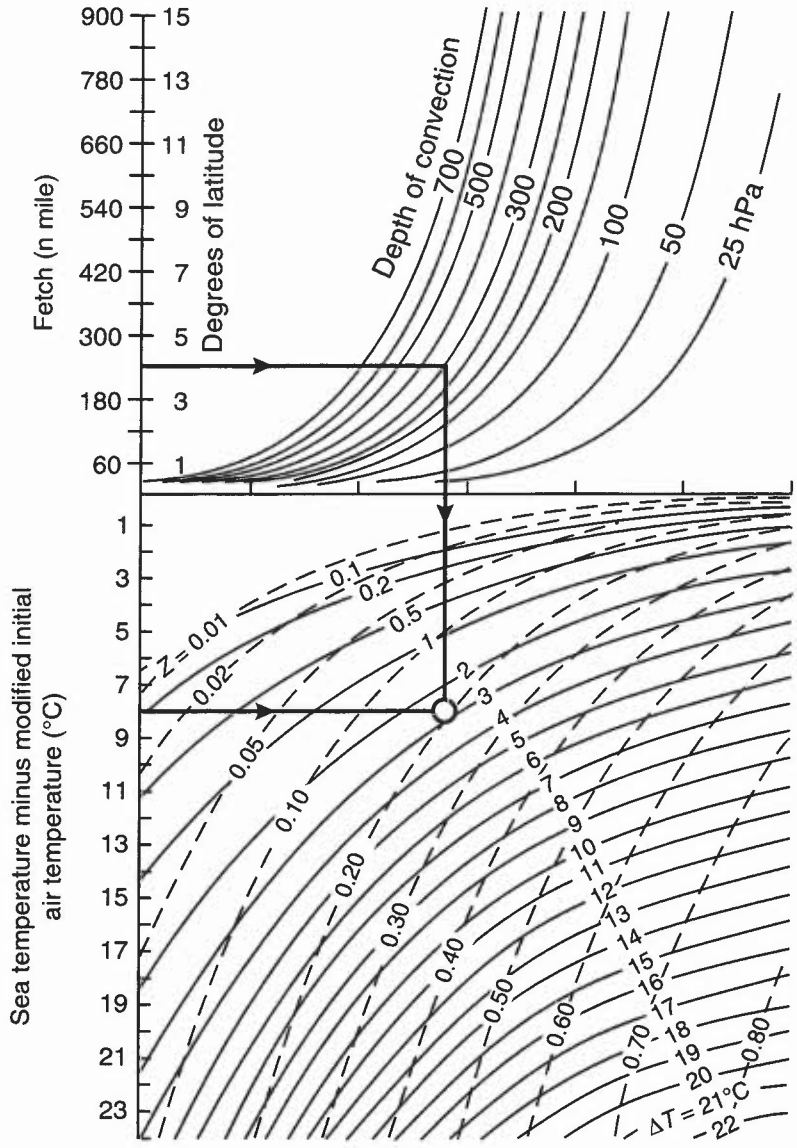

Figure 2.13. Nomogram for determining the surface temperature increase (ΔT) from the fetch(es), the depth of convection and the sea–air temperature difference. The pecked lines show isopleths of the moisture lines, Z. See text for method of use.

2.8.3 Downdraught temperatures in non-frontal thunderstorms

The temperatures of strong downdraughts reaching the ground are very close to the surface temperature of the saturated adiabatic through the intersection of the wet bulb and the 0 °C isotherm (6.2.2.4) **(Fig. 6.4)**.

Fawbush & Miller (1954)

2.9 Ice accretion

2.9.1 Types of icing

Table 2.16. Types of icing

Type	Source	Formation and properties
Hoar frost	Vapour	Direct deposition on surface with temperature below frost point of ambient air. White crystalline coating.
Rime	Supercooled droplets	Impact on surface with temperature <0 °C. Variable properties. Two extreme forms are: (a) *Opaque rime*: Drops freeze rapidly without much spreading; light porous texture with a lot of entrapped air; the smaller the droplets and the lower the temperature the rougher and more cloudy will be deposit. (b) *Clear, or glazed, ice*: Drops spread and freeze more slowly; smooth and glassy deposit sticks strongly to surface (temperatures near 0 °C).
Rain ice	Supercooled	Formation similar to clear ice. Substantial deposits may form over an extensive region. The resulting low-level icing may be severe; it is not common, but is a very important forecasting challenge in the UK and near continent (see 2.9.9).
Cloudy or mixed ice	Supercooled and ice	Ice crystals may adhere to wet surface and freeze in with droplets to give a rough, cloudy ice.
Pack snow	Supercooled drops and snowflakes	Drops freeze on impact, embedding the snowflakes, giving deposit like tightly packed snow.

HAM (1994)

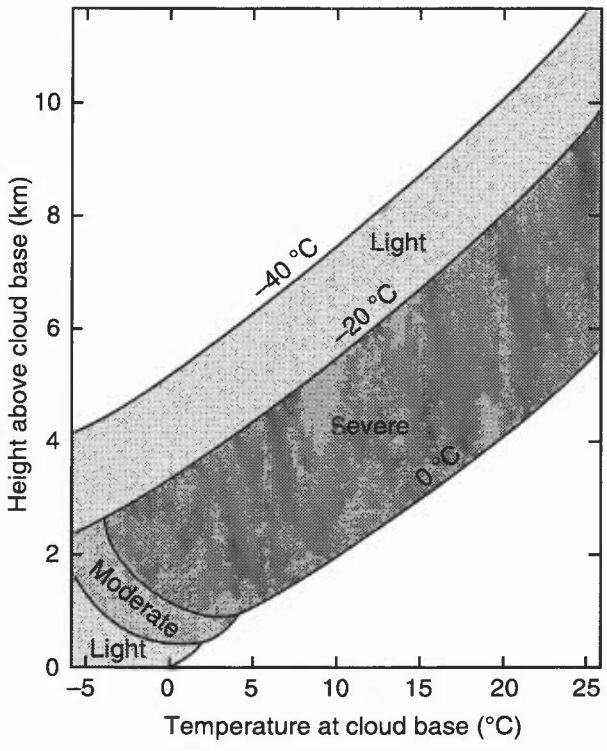

Figure 2.14. Airframe icing in convection cloud. Approximate thickness of layers within which various degrees of icing may be expected to occur. Base of cloud = 950 hPa, ambient relative humidity = 70%.

2.9.2 Airframe icing

Ice accretion on an airframe is possible whenever flight occurs through cloud or rain at sub-zero temperatures **(Fig. 2.14)**, and on a rapid move from regions of low temperature to warm, moist regions. Potentially dangerous effects are:

(i) ice may alter the wing profile, reducing the available lift;
(ii) engine intakes may be blocked, causing loss of power;
(iii) weight of ice may overload the aircraft;
(iv) forward facing windows may be made opaque.

Pike (1995)

2.9.2.1 Icing risks for helicopters

Additional risks for helicopters are:

(i) Ice on rotating blades is especially dangerous, as they are more heavily loaded than a fixed aircraft wing. Uneven ice accretion, compounding the centrifugal loads, may cause severe vibration.
(ii) Cyclic pitch controls may become jammed, causing loss of control.

For commercial operations, principally in the North Sea, forecasts of liquid-water content and temperature are made available from numerical models.

HAM (1994)

2.9.2.2 'Cold-soak' icing as a result of 'Hi-Lo' profile flying

(i) Fast descent of military aircraft after prolonged flight at high levels with sub-zero temperatures can result in 'cold-soak' icing in no-cloud conditions.
(ii) Although the effect is usually short-term until ambient warming is effected, it becomes more important when descent temperatures are around the 0 °C level.
(iii) Kinetic airframe heating (typically at least 10 °C for transport aircraft) will offset the effect.

HAM (1994)

2.9.3 Engine icing

Engine icing can occur at temperatures above zero and in clear air. Many oceanic flights are now undertaken by twin-engined jets whose engines rely on their own power for anti-icing; engine loss forces descent to regions of high potential icing where ice build-up on an inoperative engine could attain 30 cm (1 ft) in a North Atlantic diversion.

2.9.3.1 Piston engines

In addition to *impact icing* piston engines are subject to:

(a) *Fuel icing* — due to water in fuel freezing — not common,
(b) *Carburettor icing* —
  (i) There are several types of carburettor with very different icing characteristics.
  (ii) Pressure reduction through venturi effect can reduce air temperature within (particularly float-type) carburettors by as much as 30 °C.
  (iii) There is thus a potential hazard for some types of aircraft even when temperatures are $\gg 0$ °C and is likely to present a greater hazard on humid summer days than on cold winter days.
  (iv) The pilot should be alert to clues that might suggest high ambient humidity such as: poor visibility; wet ground; nearby extensive water surface; just below cloud base; in clear air just after fog dispersal.

CAA (1991)

2.9.3.2 Turbine and jet engines

(i) Susceptible parts are intake rim and struts; icing will be proportional to rate of airflow through engine.
(ii) Adiabatic expansion in the intake can cause temperature drop of up to 5 °C.
(iii) Prolonged flight near 0 °C in moist air might result in icing of engine while not occurring on the airframe.

2.9.4 Intensity of ice accretion

Terms used to describe ice accretion are: Trace of icing, light, moderate and severe icing.

(i) These terms can be used to *report* ice accretion but not for *forecasting* purposes since icing intensity is dependent on aircraft type and velocity vector.

(ii) The *depth* of the icing layer ('icing band') is always required by aircrew in order to plan for avoidance or rapid transit of the band.

HAM (1994)
WMO (1968)

2.9.5 Icing and liquid-water content

(i) The relationship between the intensity of icing in clouds and supercooled liquid water content (LWC) is not simple.

(ii) It depends on the integral of the LWC (or rather that fraction that consists of droplets large enough to accrete to the aircraft) along the aircraft trajectory. Thus Fig. 2.14 is only a guide.

(iii) Critical value of the integral is 7.5 g cm^{-3}.

(iv) Forecasters should, in principle, forecast LWC using model guidance and/or methods in 2.9.6 and 2.9.7.5, allowing the user to calculate integrals along aircraft trajectories (consistent methodology required of the user).

(v) Forecasters must be aware that the propensity for droplets to accumulate on an aircraft depends critically on both drop size and the size of the aircraft component; a large proportion of cloud drops are of sizes that are efficiently collected by small components (e.g. pitot-static tubes) on fast aircraft but are collected much less efficiently on large components on slow-moving aircraft.

2.9.6 Estimating the maximum liquid-water content of a cloud

On a tephigram:

(a) Plot the pressure and temperature at cloud base.

(b) Ascend along a saturated adiabat to the cloud-top level.

(c) The difference in HMR between the base and top of the cloud gives the maximum (adiabatic) liquid-water content of the cloud, in units of g kg^{-1}.

Since at 800 hPa (a typical wet-cloud level) 1 kg of air occupies about 1 m^3, the number obtained in (c) may simply be relabelled in units of g m^{-3}, which is a more useful measure of liquid water content for practical measurement.

Modifying factors

(i) Mixing with dry air at cloud top may reduce the actual cloud water content to around half the theoretical maximum value.

(ii) Maximum values are only approached in a tiny fraction of the cloud volume.

(iii) Upward motion of the cloudy air increases the water content and the risk of icing at any level.

(iv) Strong upcurrents in convective clouds produce the most severe icing, but orographic and frontal upslope motions may also produce severe ice accretion at times.

Note that orographic uplift can significantly lower the freezing level, giving icing at unexpectedly low levels. The importance of the increase in icing severity thus encountered cannot be overemphasized.

2.9.7 Cloud temperature and icing risk

2.9.7.1 Convective clouds

(i) Cloud-base temperature influences the risk and severity of ice accretion; the average liquid-water content/unit volume shows little variation with that over most of the cloud depth.

(ii) However, there is a higher liquid-water content in newly developing parts of a Cu cloud than in the more mature regions; liquid droplets predominate down to about −15 °C.

(iii) Large cloud-water mixing ratios can exist at high altitude. Incidents of severe icing have been reported in developing Cb anvils, the tropopause restricting vertical development, thereby producing an extensive layer of liquid and frozen water.

The following rules are generally accepted:

Table 2.17.

Cloud temperature (°C)	Nature of cloud particles: Supercooled water	Nature of cloud particles: Ice crystals	Icing risk
0 to −20	many	few	High
−20 to −40	few	many	Low (but High in Cb cells and see (iii) above))
<−40	nil	all	nil

Fig. 2.14 illustrates the potential for airframe icing in convective clouds under various cloud-base temperature conditions, but see 2.9.4 and 2.9.5.

Lunnon et al. (1994)

2.9.7.2 Layer cloud

Generally the icing severity in layer clouds of about 3000 ft thickness and tops at 850 hPa is:

(a) *moderate* for tops between 0 and −10 °C;
(b) *light* for tops <−10 °C.

Satellite imagery is useful in pinpointing the rapid build-up of cloud frequently responsible for icing.

It is important to note:

(i) The risk of icing increases above the lowest 300 m of the cloud.
(ii) Even in layer cloud, such as anticyclonic stratocumulus forming over the sea in winter, the icing in the upper part of the cloud may be severe. This is due both to the high liquid-water content and to duration of flight possible within extensive cloud layers. A capping inversion will further encourage the maintenance of a high liquid-water content by restricting the depth for drop growth by the Bergeron–Findeisen method.
(iii) Altocumulus and nimbostratus, formed by mass ascent, may be extensive and deep; icing will be further enhanced by orographic lifting. Severe icing has been reported at temperatures as low as −20 to −25 °C.

2.9.7.3 Cirrus

Cirrus clouds seldom constitute an icing hazard.

2.9.7.4 Orographic cloud

Icing is likely to be more severe in clouds subject to orographic lift than in similar clouds away from high ground.

2.9.7.5 Cloud type: summary table of icing probability and intensity

Liquid water content increases from zero at just below cloud base roughly linearly for the first 200–300 m above cloud base. In this region there is little or no icing, unless there is orographic uplift or embedded convective cloud.

Table 2.18.

Cloud type	Probability of icing	Intensity	Water content ($g\ m^{-3}$)
Cb, Ns	High	May be severe	0.2–4.0
Cu, Sc, Ac, AcAs	50%	Rarely more than moderate	0.1–0.5
As	Low	Moderate or light	0.1–0.3
St	Low	Light	0.1–0.5
Upper regions of layer cloud	High	May be severe	0.5–1
Orographic	High	probably moderate	0.1–0.5

Note that the severity is also a function of other non-meteorological factors: aircraft type and duration of flight within the cloud (2.9.4).

HAM (1994)

2.9.8 Freezing rain in elevated layers (see 5.9.7)

Ahmed et al. (1993)

2.9.9 Severe low-level icing (rain ice) (see 5.9.8)

HWF (1975), Chapter 19.7.8

2.9.10 Slantwise convection (conditional symmetric instability)

Generally θ_w surfaces are roughly parallel to the earth's surface while surfaces of constant momentum are vertical. Occasionally, however, θ_w surfaces can become more vertical than the momentum surfaces (e.g. in association with fronts), and air parcels can then move considerable distances up these θ_w surfaces (slantwise convection) without experiencing any restoring force. Severe icing events are often associated with this slantwise convection.

Bohorquez & McCann (1995)

2.9.11 Icing on ships

(i) In rough seas when the wind is strong and the air temperature below −2 °C, spray may freeze on the superstructure of a vessel. The weight of accumulated ice may eventually become a considerable hazard.

(ii) The degree of icing depends on both temperature and wind speed, as shown in **Fig. 2.15**. The icing is classified in terms of thickness of accumulation per day (**Table 2.19**).

Table 2.19.

Degree of icing	Accumulation (cm per 24 hours)
Light	1–3
Moderate	4–6
Severe	7–14
Very severe	15 or more

HWF (1975), Chapter 21.5.2

2.10 Wind chill and heat stress in man and animals

2.10.1 Human perception of wind chill

The influence of wind on the human perception of temperature gives rise to an 'equivalent temperature' (not applicable to inanimate objects). Steadman's data (**Table 2.20, Fig. 2.16**) relate to the still air temperature for which the rate of heat loss from a human is the same as that for the observed wind and temperature.

C & PSH, Chapter 3.10.3
Dixon & Prior (1987)
Steadman (1984)

2.10.2 Heat stress, mass participation events

Many heat stress indices have been devised. The Temperature–Humidity Index (THI) is applicable to sedentary workers indoors, or outside in the shade in light winds and can be forecast from the dry- and wet-bulb temperatures (T and T_w) as follows:

$$\text{THI} = 0.4(T + T_w) + 4.8 \text{ (in °C)}.$$

As THI increases above 20, increasing discomfort is felt; at THI = 24 some 50% of people are expected to feel discomfort; for THI >27 all are likely to be distressed.

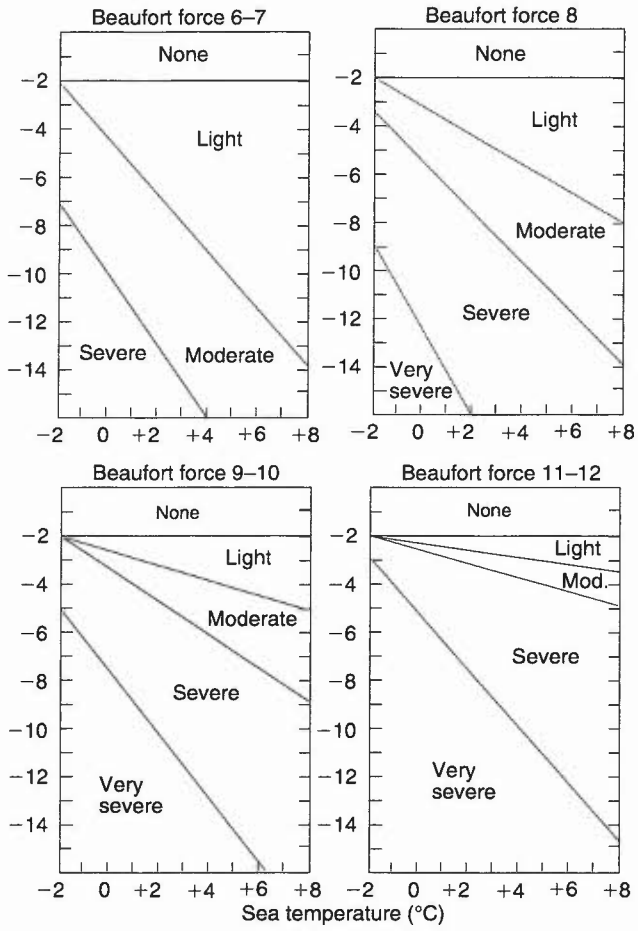

Figure 2.15. Icing on slow-moving fishing vessels in various wind conditions.

Table 2.20. Wind-chill equivalent temperatures (Steadman)

Screen temp. (°C)	10-metre wind (knots)							
	5	10	15	20	25	30	35	40
20	19.1	17.4	15.9	14.9	14.0	13.3	12.8	12.3
18	17.0	15.2	13.7	12.5	11.5	10.8	10.2	9.7
16	14.9	13.0	11.4	10.1	9.0	8.2	7.6	7.0
14	12.9	10.8	9.1	7.6	6.5	5.6	4.9	4.2
12	10.8	8.6	6.7	5.2	4.0	3.0	2.1	1.4
10	8.7	6.4	4.4	2.7	1.4	0.2	−0.6	−1.4
8	6.7	4.2	2.0	0.2	−1.2	−2.5	−3.4	−4.2
6	4.6	2.0	−0.4	−2.3	−3.9	−5.2	−6.3	−7.0
4	2.5	−0.3	−2.8	−4.8	−6.5	−7.9	−9.1	−10.0
2	0.4	−2.5	−5.2	−7.3	−9.1	−10.7	−11.9	−12.9
0	−1.7	−4.8	−7.5	−9.9	−11.8	−13.3	−14.6	−15.8
−2	−3.7	−7.1	−9.9	−12.3	−14.4	−16.1	−17.4	−18.6
−4	−5.8	−9.3	−12.3	−14.8	−17.0	−18.8	−20.2	−21.4
−6	−7.9	−11.6	−14.6	−17.3	−19.6	−21.3	−22.9	−24.2
−8	−10.0	−13.9	−17.0	−19.9	−22.2	−24.0	−25.6	−27.0
−10	−12.1	−16.1	−19.4	−22.4	−24.7	−26.6	−28.3	−29.5
−12	−14.2	−18.3	−21.7	−24.9	−27.3	−29.3	−31.0	−32.6
−14	−16.3	−20.6	−24.1	−27.3	−29.9	−31.9	−33.8	−35.3
−16	−18.3	−22.8	−26.5	−29.7	−32.4	−34.6	−36.5	−38.0
−18	−20.4	−25.0	−28.9	−32.2	−34.9	−37.2	−39.1	−40.8
−20	−22.5	−27.2	−31.2	−34.7	−37.4	−39.7	−41.7	−43.5

The potential for heat stress in mass participation 'fun-run' events is considerable and this must be pointed out in any forecasts specifically for such events; crowding restricts airflow and the ability of the body to dissipate the heat load imposed by high levels of temperature, humidity and solar radiation.

Driscoll (1985)
de Freitas et al. (1985)
Kerslake (1972)
Steadman (1984)

2.10.3 Wind chill and heat stress in livestock

Heat loss from lambs, particularly if wet, in the first few hours after birth can impose enormous stress which may result in death. Forecast advice is available to farmers. Housed livestock, including chickens, are liable to heat stress, particularly under crowded conditions; warnings to livestock managers are available when temperatures of >23 °C are expected for more than 3 hours.

C & PSH, Chapter 6
Starr (1988)

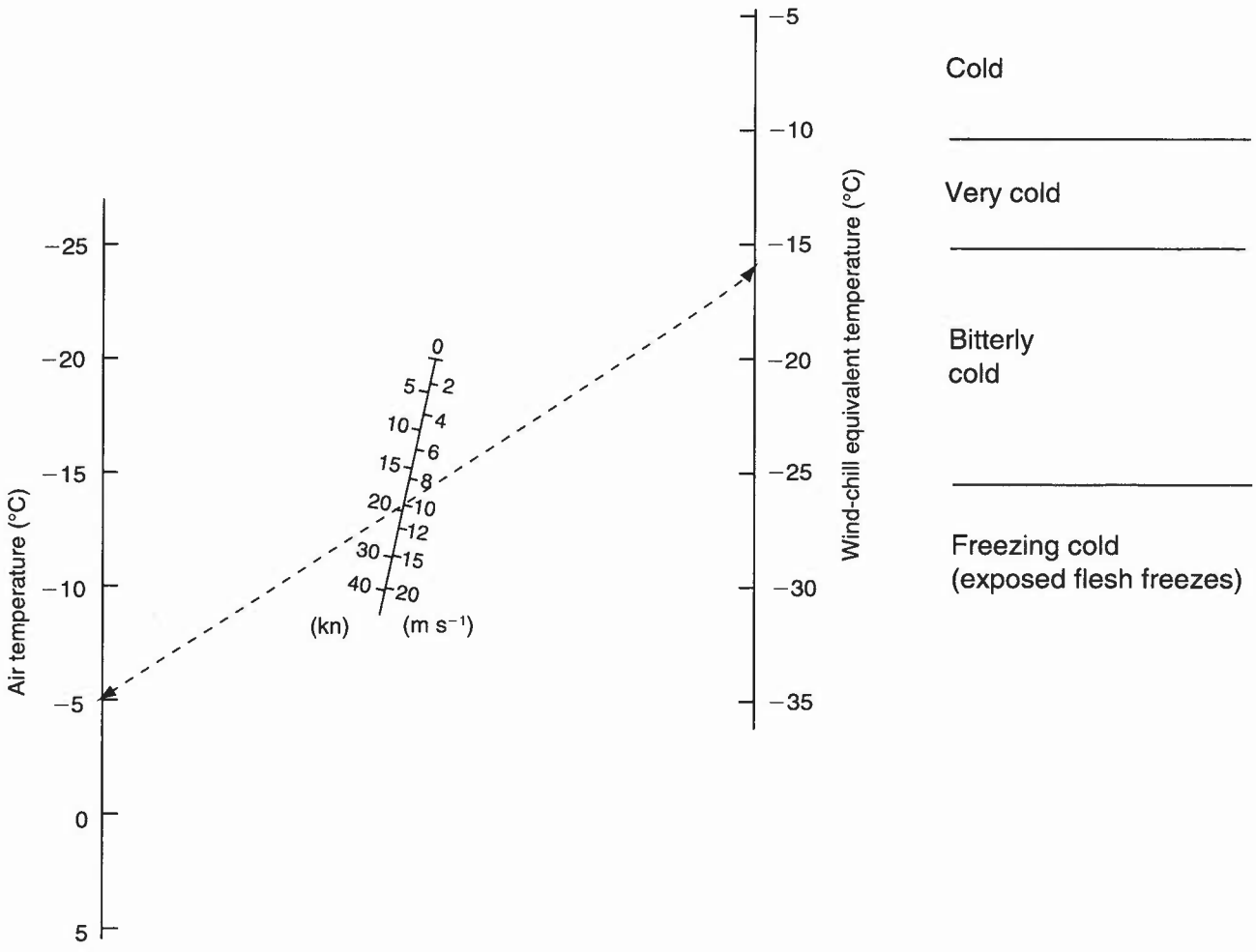

Figure 2.16. Nomogram for obtaining Steadman (1984) wind-chill equivalent temperatures and associated sensations for various combinations of air temperature and 10 m wind speed. The example shows an equivalent temperature of −16 °C, which would be termed 'bitterly cold', resulting from an air temperature of −5 °C and a wind speed of 20 kn.

2.11 The urban 'heat island'

The urban environment will influence heat storage and the radiation balance; the result is a modified local (micro-) climate compared with the surrounding rural environment:

(i) Rural areas typically form surface inversions under good nocturnal radiation conditions.
(ii) Over the city this 'heat island' maintains a shallow, convectively mixed, approximately isothermal, layer. Hence at about 50 m rural air may be warmer than city air (**Fig. 2.17**).
(iii) The layer is a function of population density, is less than 100 m deep and is most pronounced in the evening about 4 hours after sunset.
(iv) On a clear night over London temperature differences of more than 7 °C over the surrounding country have been measured.
(v) Under appropriate synoptic conditions this 'heat island' effect gives rise to thermal circulations and influences advection so as to, for example, induce severe storms.
(vi) Another effect is that the inner city may have its last frost several weeks earlier than the suburbs.
(vii) During the day the heat island effect is observable but, because of natural convection, is only 0.5 to 1 °C.
(ix) If a wind is present the 'heat island' might be eliminated; the breakdown depends on the size of the town. Limiting wind speeds are presented in **Table 2.21.**
(x) However, the presence of wind may cause excesses of temperature and deficits of humidity to be carried downwind with the urban pollution plume — which can be as wide as the city and transport for hundreds of kilometres. (1.3.4).
(xi) An implication is that visibility may be reduced in the plume core by a factor of two compared with conditions in the country well away from the plume (3.9.1).

Table 2.21. Limiting wind speed for development of heat islands

Population	Surface wind (kn)
10 million	25
2 million	22
500 thousand	16
250 thousand	12
100 thousand	10
50 thousand	9
25 thousand	8

Landsberg (1981)
Oke (1987)

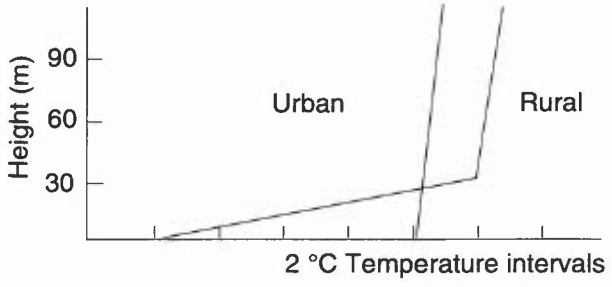

Figure 2.17. The difference of the urban heat-island on an urban and an adjacent rural temperature profile (see text).

2.12 Model Output Statistics (MOS)

(i) MOS models match observations and forecast parameters; a statistical relationship is established, the MOS technique thus allowing for bias in the model forecast by the post-processing of model data. Station-specific maximum and minimum temperatures are available.

(ii) Current parameters used in MOS regressions are:
MSLP (of little value);
level 1 (997 hPa): temperature, dew point, wind speed and direction;
level 4 (870 hPa): temperature, dew point, wind speed and direction;
vertical shear parameter (of minor significance).

(iii) MOS are not well equipped to forecast extreme temperatures.

(iv) MOS temperatures from the LAM are occasionally misleading due to poor representation of boundary layer cloud, particularly when Sc is trapped below an inversion lower than model level 4, with dry air above (giving too low minima).

(v) Changes in model formulation can affect maximum temperatures, giving a temporary deterioration in accuracy until the new model characteristics have been 'learnt' by the MOS model.

(vi) Forecasters must examine structure of low-level flow before using MOS values.

(vi) MOS forecasts are based on midday and midnight ascents for maximum and minimum temperature, respectively. Changes after these times, e.g. the passage of a cold front in the early hours of the morning, cannot be taken into account; beware situations when the base of an inversion is lower than 870 hPa (level 4).

(vii) MOS algorithms are updated monthly.

(viii) Around equinoxes rapid changes in insolation may lead to inaccurate forecasts, e.g. too cold at beginning of September, too warm at end of that month.

Glahn & Lowry (1972)
Ross (1989)

BIBLIOGRAPHY

CHAPTER 2 — TEMPERATURE

Ahmed, M., Graham, R.J. and Lunnon, R.W., 1993: Creating a global climatology of freezing rain using numerical model output. Proc. of Fifth Conference on Aviation Weather Systems, Am Meteorol Soc, Vienna (Virginia), USA.

Astbury, A., 1994: OpenRoad Manual, Meteorological Office (continuously updated).

Barthram, J.A., 1964: A method of forecasting a radiation night cooling curve. *Meteorol Mag*, **93**, 246–251.

Belasco, J.E., 1952: Characteristics of air masses over the British Isles. *Geophys Mem*, No. 87, London, Meteorological Office.

Blackall, R.M., 1973: Warming of the lower troposphere by the sea. *Meteorol Mag*, **102**, 65–73.

Bohorquez, M.A. and McCann, D.W., 1995: Model proximity soundings near significant aircraft icing reports. Proc. of Sixth Conf. on Aviation Weather Systems, Am Meteorol Soc, Dallas, Texas, USA.

Boyden, C.J., 1937, A method for predicting night minimum temperatures. *QJR Meteorol Soc,* **63**, 383–392.

CAA, 1991: Piston engine icing. Safety Sense Leaflet No. 14, Civil Aviation Authority.

Callen, N.S. and Prescott, P., 1982: Forecasting daily maximum surface temperatures from 1000–850 mb thickness lines and cloud cover. *Meteorol Mag*, **111**, 51–58

C&PSH: Commercial and Public Services Handbook, Met.O.868, Meteorological Office (continuously updated).

Craddock, J.M. and Pritchard, D.L., 1951: Forecasting the formation of radiation fog — a preliminary approach. *Meteorological Research Paper* No. 624. Meteorological Office (unpublished).

de Freitas, C.R., Dawson, N.J., Young, A.A. and Mackey, W.J., 1985: Microclimate and heat stress in runners in mass participation events. *J Clim Appl Meteorol*, **24**, 184–191.

Dixon, J.C. and Prior, M.J., 1987: Wind-chill indices: a review. *Meteorol Mag*, **116**, 1–16.

Driscoll, D.M., 1985: Human health. Handbook of Applied Meteorology, pp. 778–814. John Wiley & Sons.

Fawbush E.J. and Miller, R.C. 1954: A basis for forecasting peak wind gusts in non-frontal thunderstorms. *Bull Am Meteorol Soc*, **35**, 14–19.

Frost, R., 1941: The influence of the North Sea on winter temperatures and dew points. Meteorological Office (unpublished).

Glahn, H.R. and Lowry, D.A., 1972: The use of MOS in objective weather forecasting. *J Appl Meteorol*, **11,** 1203–1211.

Grant, K., Fog frequencies in the UK relative to time of sunrise. *Special Investigations Paper*, Meteorological Office, (unpublished).

Grant, K., 1975: The warming and moistening of cold air masses by the sea. *Meteorol Mag*, **104**, 1–9.

HAM. Handbook of Aviation Meteorology, 1994: London, HMSO.

Hewson, T.D. and Gait, N.J., 1992: Hoar-frost deposition on roads. *Meteorol Mag*, **121**, 1–21.

HWF. Handbook of Weather Forecasting, 1975: Met.O.875, Meteorological Office.

Inglis, G.A., 1970: Maximum temperatures on clear days. *Meteorol Mag*, **99**, 355–363.

Jefferson, G.J., 1950: Temperature rise on clear mornings. *Meteorol Mag*, **79**, 33–41.

Johnson, D.W., 1958: The estimation of maximum day temperatures from the tephigram. *Meteorol Mag*, **87**, 265–266.

Kensett, C.H., 1983: Forecasting night minimum temperatures — a revision of McKenzie's method for 90 stations in the UK. Forecasting Techniques Memorandum No. 21. Meteorological Office.

Kerslake, D. McK., 1972: The stress of hot environments. Cambridge University Press.

Lamb, H.H., 1943: Haars or North Sea fogs on the coast of Great Britain. Meteorological Office (unpublished).

Landsberg, H.E., 1981: The Urban Environment. Academic Press.

Local Weather Manual (S England), 1994: Meteorological Office (PSP) publication.

Lumb, F.E. 1963: Downward penetration of snow in relation to the intensity of precipitation. *Meteorol Mag*, **92**, 1–14.

Lunnon, R.W., Holpin, G.E. and Anderson, S., 1994: Study of the meteorological conditions pertaining to 25 January 1994 BAe ALF502 rollback incident. Meteorological Office Research Tech. Report No. 102.

McKenzie, F., 1944: A method of estimating night minimum temperatures. *SDTM* No. 68. Meteorological Office, London (unpublished).

Oke, T.R., 1987: Boundary layer climates (2nd edition). Methuen.

Parrey, G.E., 1969: Minimum road temperatures. *Meteorol Mag*, **98**, 286–290.

Perry, A.H. and Symons, L.J., 1991: Highway meteorology. E & F.N. Spon.

Pike, W.S., 1995: Extreme warm frontal icing on 25 February 1994 causes an aircraft accident near Uttoxeter. *Meteorol Appl*, **2**, 273–279.

Ritchie, W.G., 1969: Night minimum temperatures at or near various surfaces. *Meteorol Mag*, **98**, 297–304.

Ross, G.H., 1989: Model Output Statistics. An updatable scheme. Am Meteorol Soc. 11th Conference on Probability and Statistics in the Atmospheric Sciences, Monterey, Ca, USA.

Saunders, W.E., 1952, Some further aspects of night cooling under clear skies. *QJR Meteorol Soc,* **78**, 603–612.

Sills, A.G., 1969: An investigation into the depression of the grass minimum temperature below the air minimum at Cottesmore. *Meteorol Mag*, **98**, 348–351.

Starr, J.R., 1988: Weather, climate and animal performance. Geneva, World Meteorological Organization, Technical Note 190.

Steadman, R.G., 1984: A universal scale of apparent temperatures. *J Clim Appl Meteorol,* **23,** 1674–1687.

WMO, 1968: Ice formation on aircraft. Geneva. (Reprint of 1961 publication). World Meteorological Organization, Technical Note 139.

CHAPTER 3 — VISIBILITY

CHAPTER 3 — VISIBILITY

3.1 Factors reducing visibility

Reduction in visibility depends on the concentration and size of hydrometeors, particulates or moisture in the atmosphere as well as the viewing path and the time of day. Factors reducing visibility are:

(i) Precipitation — rain, snow, hail.
(ii) Haze — condensation on dry particulates. Haze particles shrink and grow with changes in relative humidity (RH), high RH leading to poor visibility. Hygroscopic particles will encourage condensation at relative humidities well below 100% (3.9.2).
(iii) Haze in the dry atmosphere due to industrial pollutants and vehicle exhaust products — photochemical reactions can reduce visibility to <5 km.
(iv) Smoke.
(v) Moisture — mist, fog.
(vi) Blowing snow (3.10) or soil/sand (e.g. 'fen blows') (see 10.3.6.3).
(vii) Spray, at sea and at coastal sites (3.10).

In forecasting visibility, air-mass characteristics and history must be noted, particularly the possibility of importing pollution from continental sources and allowing for local sources. Fog forming in a polluted boundary layer is likely to have more, but smaller drops than fog forming in a cleaner air mass, hence the poorer visibility.

Much information on local visibility incidence (albeit prior to the 'Clean Air Act') is available in *Airfield Weather Diagrams and Characteristics* (extracts in Local Weather Manual for Southern England).

AWDC (1960)
Local Weather Manual for Southern England (1994)

3.2 Fog

Fog formation is complex; its occurrence is widely variable in space and time, forming under a wide range of meteorological circumstances. In all cases it forms as a result of air near the surface becoming saturated and being cooled below its dew point (see 10.3.3).

3.2.1 Classification

The basic fog classifications are: air mass fog((i) to (iii)) and frontal fog (iv):

(i) *Radiation fog* — loss of heat from the air, to ground cooled by nocturnal radiation, causes air to become saturated
(ii) *Advection fog* (warm and cold) — movement of air over a surface with different temperature and moisture regimes.
(iii) *Upslope fog* — air is forced, under stable conditions, up a land slope, resulting in adiabatic cooling and saturation.
(iv) *Frontal fog* — developing in frontal zones when precipitation from warmer air falls into very cold, stable air beneath, saturating the layer.

(*Mixing fog* — two unsaturated masses of air becoming saturated on mixing, is not a recognized mechanism for fog formation on the synoptic scale.)

On many occasions the development of fog is due to more than one factor.

Bader et al. (1995), Chapter 7
Perry & Symons (1991)
Thomas (1995)

3.3 Radiation fog

Radiation fog can occur at any time of the year but is most frequent in autumn and early winter; it is likely to be more widespread and persistent when *advection* brings an increase in vapour content just above the surface. Low-lying stations in eastern England experience an increased frequency of radiation fogs when there is a weak flow from the North Sea.

3.3.1 Physics of formation of radiation fog

(a) *Radiative cooling and dew deposition phase (Stage 1)*

(i) Under favourable conditions the absence of cloud permits strong radiative nocturnal cooling at the ground. Cooling is initially rapid; with (10 m) winds <7 kn a temperature inversion forms in the lowest levels near the ground.

(ii) Once the ground is at the dew point of the air, dew deposition onto the surface begins. This dries the air in contact with the ground and slows down surface cooling by the addition of latent heat.

(iii) Continuation of this process depends on the degree and effectiveness of the vertical mixing in the lowest layers; if sufficient mixing turbulence is present fresh supplies of moisture will be brought into contact with the ground and deposition of dew will continue. Hence the amount of water vapour in the atmosphere decreases (as shown by falling dew points) and air temperatures must fall further before fog can begin to form.

(b) *Initial formation (Stage 2)*

(i) Fog formation now depends on a delicate balance of several factors: principally the spreading upwards of radiative cooling by turbulence, and the drying out and warming of near-surface layers by dew deposition.

(ii) Initial formation often occurs when there is a lull in the 2 m surface wind to around 1 kn or less. This causes turbulence to cease and markedly reduces rate of dew deposition; with no significant air motion, any further radiative cooling in the lowest layers leads to supersaturation of those layers and hence condensation in the form of thin, shallow wisps of fog at a height of some 20 cm above the ground. (Note that there may not be a 2 m anemometer; under fog formation conditions it will not be possible to deduce the 2 m wind from a 10 m reading.)

(c) *Mature stage.*

With sky visible (Stage 3(i))

(i) Radiative cooling continues from the ground and the inversion base remains close to the surface.

(ii) As the screen temperature falls, fog gradually deepens. The upward heat flux decreases with time but may still be sufficient to halt the fall in surface temperature.

With sky obscured (Stage 3(ii))

(i) After a few hours the fog may be deep enough (65–165 ft; 20–50 m) to obscure the sky. The fog top now becomes the radiating surface, radiative cooling at the ground ceases and the surface temperature may start to rise, if the upward soil heat flux is large enough. The resulting heating at the ground and cooling aloft gives rise to convective overturning. In fact if the fog is deep enough to have an effective emissivity of ≈ 1, then cooling from the fog top can be sufficient alone to cause overturning.

(ii) This raises the inversion away from the surface as an SALR profile develops. Continued radiative cooling from the fog top causes the inversion to rise further and fog to continue to deepen.

(iii) Maximum inversion height of 230–750 ft (70–230 m) is generally reached in 2–3 hours after lifting from surface, with fog top about 80 ft (25 m) above base of inversion; there is a marked wind shear at the fog top.

The above stages are represented diagrammatically in **Figs 3.1(a)–(d)**.

Fig. 3.2 shows the conditions observed in a fog at Bedford in November 1983, which passed from its formative to its mature stage at about 01 UTC. Large-amplitude variations in fog top may be superimposed on the general upward growth.

Bradbury (1989) **Findlater (1985)**
Brown (1987) **Roach (1994, 1995)**

3.3.2 Conditions observed during radiation fog formation

F*actors favourable for formation*:

(i) Clear skies or just thin, high cloud.

(ii) Moist air in the lowest 100 m or so.

(iii) Moist ground (e.g. after rain, or over marshes).

(iv) Favourable local topography.

(v) Slack pressure gradient, allowing the surface wind (preferably measured at 2 m) to decrease to near calm.

The frequency of geostrophic wind speeds (V_g) at Cardington during periods of fog were found to be as shown in **Tables 3.1 and 3.2**).

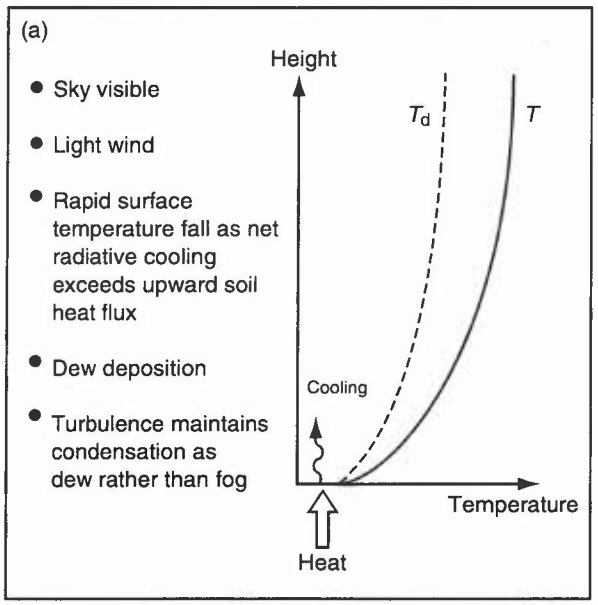

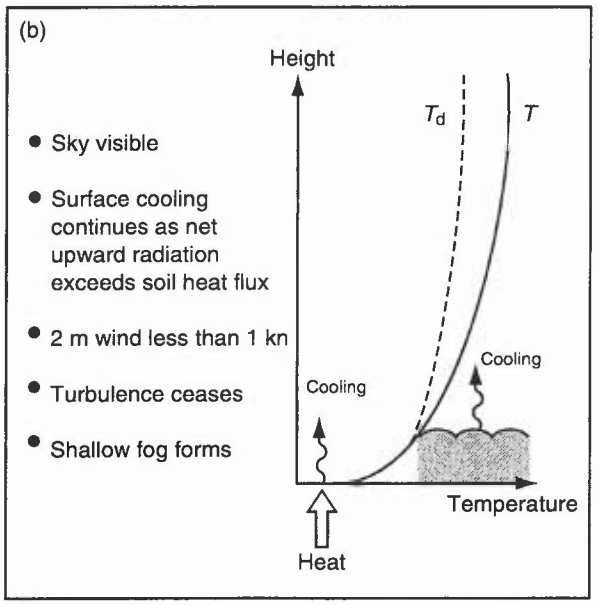

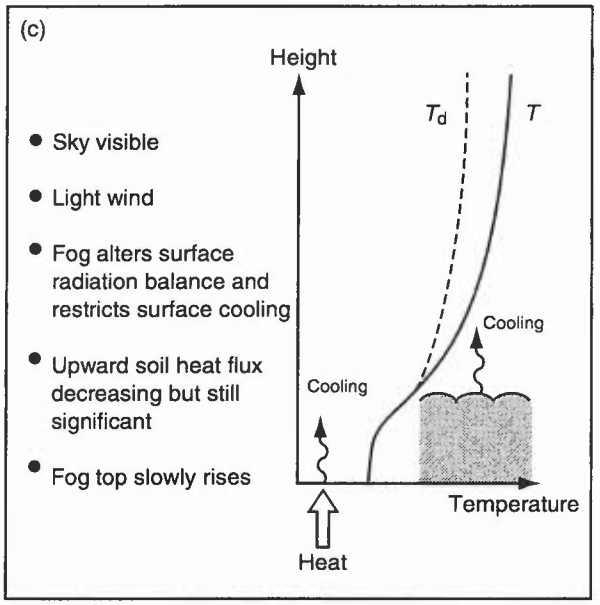

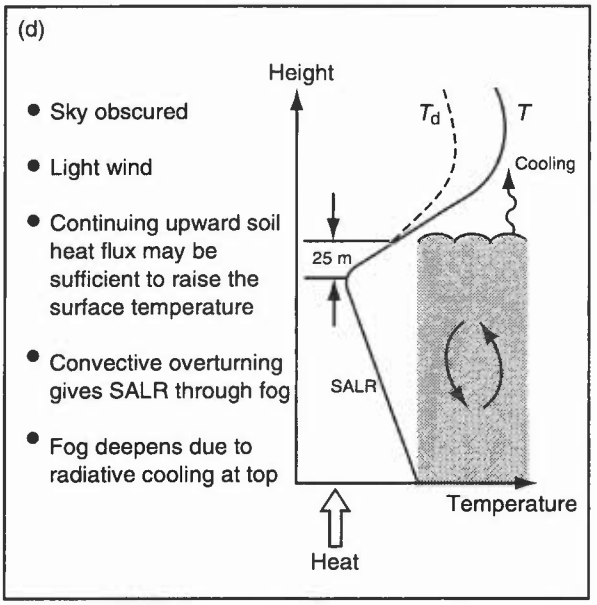

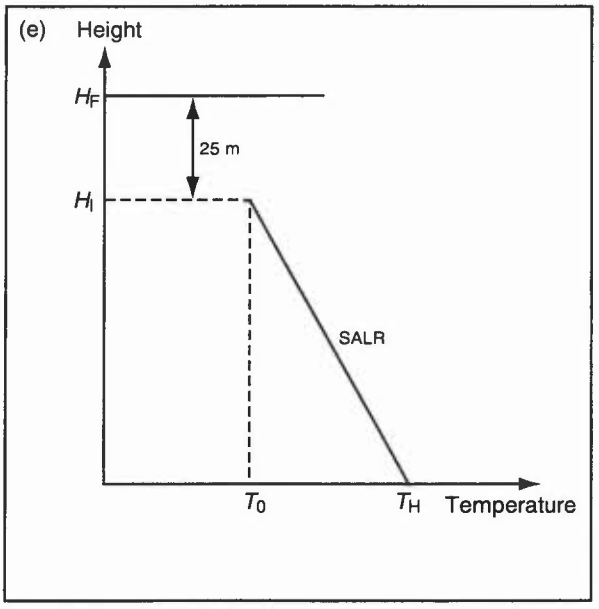

Figure 3.1(a–d). Schematic representations of (a) Stage 1 — radiative cooling and dew deposition, (b) Stage 2 — initial formation, (c) Stage 3(i) — development of a mature fog (sky visible), and (d) Stage 3(ii) development of mature fog (sky obscured).

Figure 3.1(e). Schematic daigram to estimate the height of the inversion base during sky obscured/fog deepening phase (Stage 3(ii) — Fig. 3.1(d)).

H_I Height of inversion base
H_F Height of fog top (H_I + 25 m)
T_0 Screen temperature when sky became obscured
T_H Screen temperature at time H after sky became obscured

See 3.3.2.1.

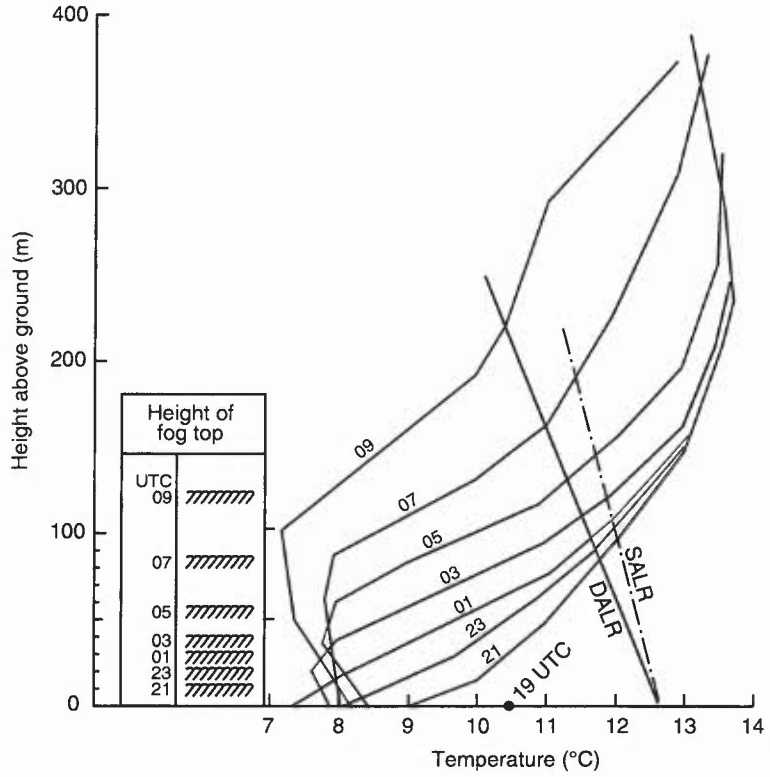

Figure 3.2(a). Temperature–height diagram showing the temperature structure and fog top at Bedford at various times during the night of 9/10 November 1983.

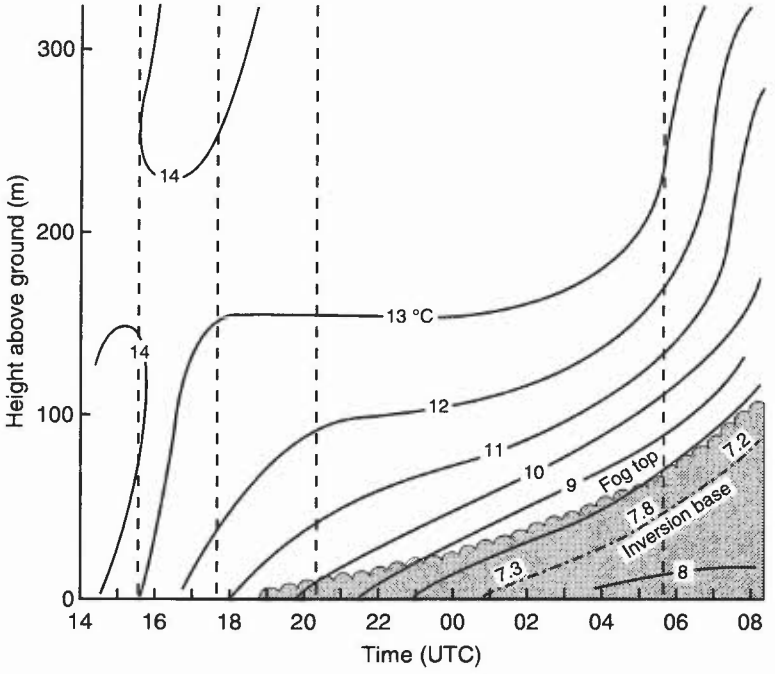

Figure 3.2(b) Time-section of the vertical temperature profile and fog depth at Bedford on the night of 9/10 November 1983. Fog formed at about 1830 UTC. The change from 'sky visible' to 'sky obscured' occurred just before 0100 UTC, which was also the time of the minimum surface temperature. The fog-top temperature from this time on remained steady, with the coldest temperature just below the fog top.

Table 3.1. Percentage frequency of V_g in various speed ranges

	knots										
	0–2	3–5	6–8	9–11	12–14	15–17	18–20	21–23	24–26	27–29	30+
A	7.1	16.7	23.8	23.0	18.3	10.3	0.8	—			
B	6.7	16.0	18.0	20.0	16.3	11.3	6.7	2.5	1.5	0.5	0.7

A = when fog first formed, B = while fog persisted

The wind speed at 10 m during the same fogs had the following frequency distribution:

Table 3.2. Percentage frequencies of surface wind in various speed ranges

knots	0–2	3–5	6–8	9–11	12–14	15–17
%	58.5	28.6	10.5	2.1	0.3	—

The stronger winds occurred when North Sea stratus spread inland replacing local radiation fog with widespread advection fog.

(i) Recent studies have shown that the wind speed at 1–2 m is more important than the 10 m wind. Fog forms when the 2 m wind falls below 2 kn. The wind at 10 m may be significantly stronger than the 2 m wind on radiation nights.
(ii) Synoptic studies demonstrate the preferred occurrence of radiation fog to be with anticyclonic pressure patterns, particularly on the western side (to where, generally, air of higher RH is moving).
(iii) Only about one fog in seven occurs in a cyclonic situation. Within these pressure patterns there is a greater tendency for fog to form in those sectors where there is a southerly component to the geostrophic wind (East Anglia/Lincolnshire) by a factor of about 3 to 1.

Findlater (1985)

3.3.2.1 Height of fog top (Findlater's method)

(i) During the period of fog deepening, and with minimum advective effects, the temperature at the base of the inversion was observed by Findlater to remain constant to within ±0.5 °C while the screen temperature rose slightly. In many cases, however, screen temperatures continue to fall, in which case the following technique is not appropriate.
(ii) Findlater's technique (based on only a small number of cases) is to draw the SALR temperature profile from the known screen temperature T_t at time t after sky obscuration to intersect an assumed temperature at the inversion base (i.e. the screen temperature when sky became obscured). The height of the inversion base, H_I, may then be estimated and fog top is taken as: H_I + 25 m (**Fig. 3.1(e)**) (this only applies while fog is still deepening and if advective effects are minimal).

Findlater (1985)

3.3.2.2 Factors modifying fog formation

Four specific factors which complicate and modify the radiative progress of fog formation are:

(a) *Advective effects*:
  (i) of fog formed upwind;
  (ii) of air with different temperature/moisture characteristics at low level;
  (iii) of sea fog inland before locally produced fog has formed;
  (iv) due to upslope motion (3.5).
(b) *Sunrise*: turbulence and added moisture due to the evaporation from the surface often give a sudden deepening soon after sunrise. Sudden fog formation may result if turbulence mixes cold surface air and warmer aloft.
(c) *Fog aloft*: very low stratus may be found with moderate winds; once formed continued cooling and turbulent mixing act to lower the base to ground level. The fog will only persist if winds become light.
(d) *Fog forming in smoky boundary layers* will have very poor visibility; formation of fog is less rapid in such cases possibly due to the reduction of the rate of radiative cooling of the ground and the distribution of condensing water among a large number of nuclei.

Findlater (1985)

3.3.3 Forecasting the formation of radiation fog

3.3.3.1 Calculation of fog point (Saunders' method)

The method takes account of moisture throughout the cooling layer; it is based on Mk. IIb radiosonde profiles; Mk. III T_d data may differ.

(i) Select a representative upper-air sounding and find the condensation level from the maximum temperature and the dew point at that time, using Normand's theorem (2.1.1).
(ii) Find the humidity mixing ratio at the condensation level and read off the temperature where the humidity mixing ratio line cuts the surface isobar. This is the expected fog-point temperature.

This procedure needs modification to allow for different types of sounding (see **Fig. 3.3**):

(a) *Type I* has a constant dew-point lapse rate except near the ground where the surface dew-point lies on, or to the right of, a downward extension of the upper dew-point curve. T is the maximum temperature and T_d is the surface dew-point. If there is a superadiabatic, use the value T_c instead of T to eliminate the superadiabatic section. The pecked lines through T_c and the dew point T_d meet at the condensation level A. The humidity mixing ratio at this level is at B and the fog point is at C.

(b) In *Type II* the dew-point lapse rate increases aloft. Point B is found by extrapolating the lower part of the dew-point curve above the point at which the lapse rate increases.

(c) In *Type III* the surface dew point lies to the left of the downward extension of the upper dew-point curve, two possibilities are illustrated:

  (i) If the temperature lapse in the lowest layers is less than a dry adiabatic, the construction follows the basic principles as for *Type I*.

  (ii) If the temperature lapse rate in the lowest layer is equal to or greater than a dry adiabat, then no Normand construction is drawn and the fog point is taken to equal the dew-point.

Normally, if the boundary layer is mixed at the time of the midday sounding, extending the mean mixing-ratio through the boundary layer to the surface will give an acceptable fog point. As a rough guide, the afternoon dew point at screen level minus 2 °C gives a good first guess for $T_f > -2$ °C.

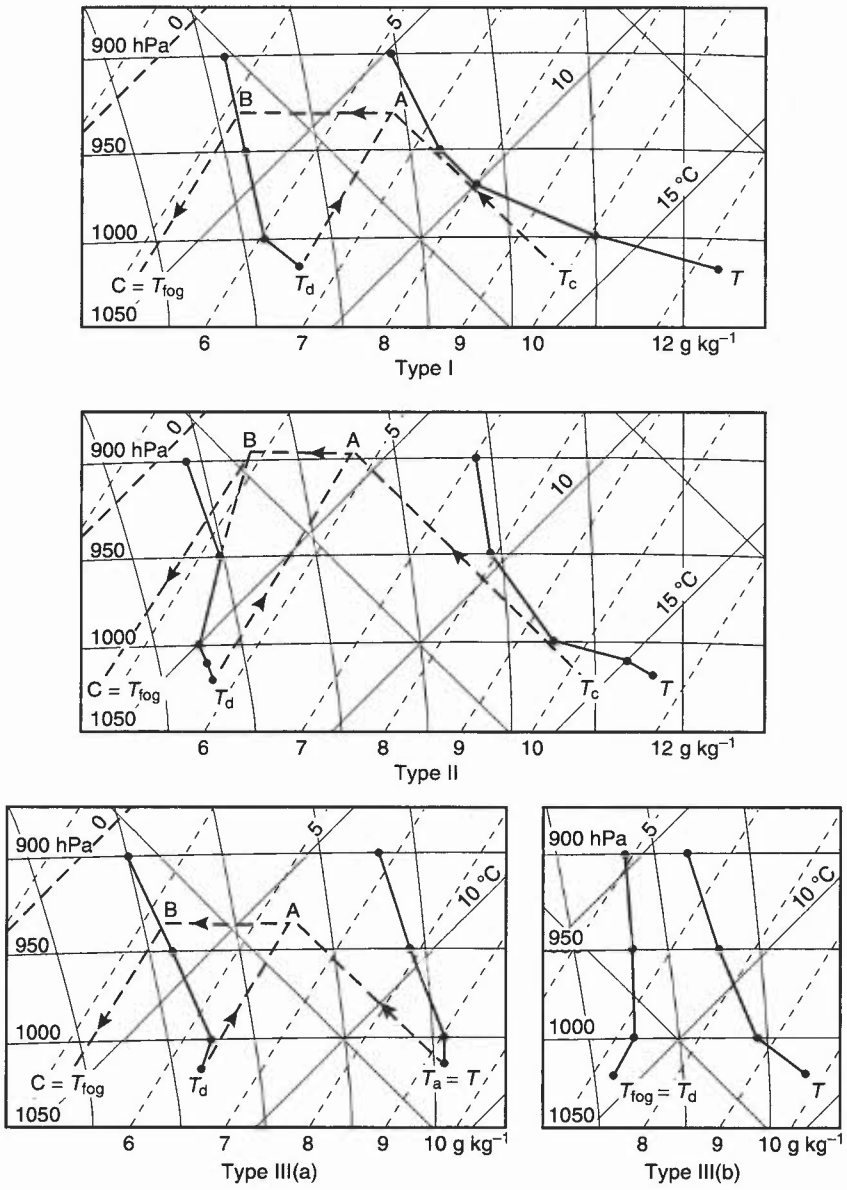

Figure 3.3. Estimation of fog-point (Saunders' method) with adjustments to midday soundings under various conditions. See text for explanation of types.

Notes:

(i) If a subsidence inversion has brought dry air down to within 30 hPa of the ground, use the dew point (T_d) as the fog-point.

(ii) If rain falls during the afternoon leaving the ground wet, the actual fog point may be higher than the calculated value.

(iii) If a sea-breeze reaches the area later in the day, the fog point may be much higher than calculated; use the coastal dew point.

(iv) The dew-point temperature 60 hPa above the surface nearly always gives a fog-point value close to Saunders' value, exception being *Type IIIb* when the surface dew-point is used.

(v) If the calculated temperature is ≤0 °C, then the actual fog point may well be lower (due to deposition by hoar frost).

Saunders (1950)

3.3.3.2 Calculation of fog-point (Craddock and Pritchard's method)

If T_f is the fog point, T_{12} is the screen temperature at 1200 UTC, and T_{d12} is the dew point at 1200 UTC, then

$$T_f = 0.044\,(T_{12}) + 0.844\,(T_{d12}) - 0.55 + A = Y + A.$$

Values of A and Y can be obtained from **Table 3.3**.

Table 3.3(a). Values of Y (°C) corresponding to the observed values of T_{12} and T_{d12}

	T_{12}								
T_{d12}	30	25	20	15	10	5	0	−5	−10
20	17.7	17.4	17.2						
18	16.0	15.7	15.5						
16	14.3	14.1	13.8						
14	12.6	12.4	12.1	11.9					
12	10.9	10.7	10.5	10.2					
10	9.2	9.0	8.8	8.6	8.3				
8	7.5	7.3	7.1	6.9	6.6				
6	5.8	5.6	5.4	5.2	5.0				
4	4.1	3.9	3.7	3.5	3.3	3.0			
2	2.5	2.2	2.0	1.8	1.6	1.4			
0	0.8	0.6	0.3	0.1	−0.1	−0.3	−0.6		
−2	−0.9	−1.1	−1.4	−1.6	−1.8	−2.0	−2.2		
−4	−2.6	−2.8	−3.0	−3.3	−3.5	−3.7	−3.9		
−6	−4.3	−4.5	−4.7	−5.0	−5.2	−5.4	−5.6	−5.8	
−8	−6.0	−6.2	−6.4	−6.6	−6.9	−7.1	−7.3	−7.5	
−10	−7.7	−7.9	−8.1	−8.3	−8.6	−8.8	−9.0	−9.2	−9.4

The number A (°C) is an adjustment which depends upon the forecast cloud amount and geostrophic wind speed, as tabulated below.

Table 3.3(b).

*Mean cloud amount (oktas)	*Mean geostrophic wind speed (kn)	
	0–12	13–25
0–2	0.0	−1.5
2–4	0.0	0.0
4–6	+1.0	+0.5
6–8	+1.5	+0.5

*Mean of forecast values for 1800, 0000 and 0600 UTC.

Notes:

(a) The equation for T_f was derived from the combined data for 13 widely separated stations in England. There was considerable variation from station to station in their proximity to major smoke sources.

(b) Account was not taken of variations in atmospheric pollution so that, in effect, an average degree of pollution is assumed in using this technique (in contrast to Saunders' method which refers mainly to fog in clean air).

(c) If the minimum temperature is predicted using Craddock and Pritchard's method it is suggested that:
   (i) if T_f is 1 °C or more above T_{min}, forecast fog;
   (ii) if T_f is 0.5 °C above to 1.5 °C below T_{min}, forecast a risk of fog;
   (iii) if T_f is 2 °C or more below T_{min}, do not forecast fog.

(d) When forecasting for a region, rather than a specific airfield, allow a larger safety margin, since there is always more low-level moisture present near streams and in lush valleys than over flat airfields with trimmed grass.

Craddock & Pritchard (1951)

Other fog prediction techniques (Banks, Swinbank) are given in HWF; a 'probability predictor' diagram for Waddington, while not being statistically rigorous has operational credibility.

HWF (1975) Chapter 20.7

3.3.3.3 Inferred fog prediction from $T_f - T_{min}$

Table 3.4. Fog prediction summary

$T_f - T_{min}$ (°C)	Inferred fog prediction
$\geq +1$	widespread fog expected
$=0.5$	fog probable late in the night
$=0$	patchy fog likely by dawn
-0.5 to -1.5	fog patches possible in fog-prone areas
≤ -2	fog not expected

If T_f is significantly greater than T_{min} the time of formation can be predicted from the night cooling curve.

Craddock& Pritchard (1951)

3.3.3.4 The fog point in relation to the 850 hPa wet-bulb potential temperature

(i) The 850 hPa wet-bulb potential temperature is useful as a means of identifying air masses.

(ii) The probability of fog occurring increases as the temperature difference of the surface temperature below the 850 hPa WBPT increases, see **Fig. 3.4**.

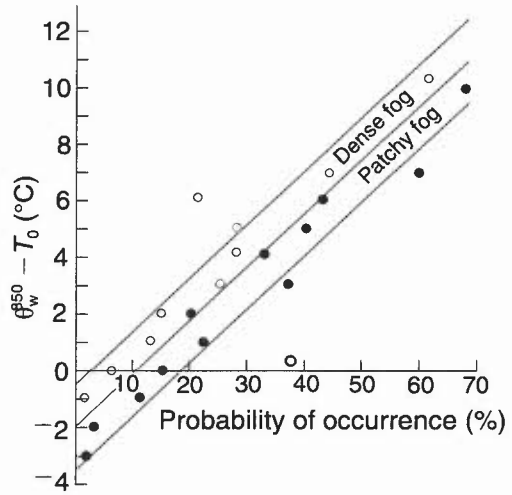

Figure 3.4. The probability of fog corresponding to a given depression of the surface temperature (T_0) below the 850 hPa wet-bulb potential temperature (θ_w^{850}).

3.3.3.5 Summary of forecasting procedures for fog formation

(i) Forecast the synoptic situation overnight
Air-mass characteristics
Cloud type and amount
Pressure pattern, gradient and surface winds
(ii) Consider history
Did fog form last night in the same air mass?
If so, was it widespread or patchy?
How will conditions differ tonight?
— Warmer or colder?
— Moister or drier?
— Cloudier or clearer?
— More or less windy?
(iii) Consider local factors
Look at local weather diagrams etc.
Topography, smoke sources, etc.
(iv) Estimate the fog point
Craddock–Pritchard
Saunders' technique
Any others available?
(v) Will the fog point be reached?
Construct night cooling curve
If $T_f > T_{min}$, what time will fog form?
(vi) Once the fog forms, what will the visibility be?
Large variations over short distances
Visibility often falls rapidly once fog forms
Usually less than 200 m in clean air
— Decrease in visibility may be slower in smoky air
If temperature <0 °C, 200 to 1000 m more common
(vii) Keep the forecast under review
Synoptic developments
Observations at your station
Observations from other stations nearby
Satellite imagery
Amend the forecast if necessary

The potential of a given location for thick radiation fog (visibilities <200 m) can be assessed by a Fog Potential Index.

Meteorological Office (1985)

3.3.4 Forecasting the clearance of radiation fog

Four main mechanisms for dispersing radiation fog:
(i) Solar radiation.
(ii) Advection of cloud cover over the fog top.
(iii) Increasing gradient wind.
(iv) Advection of drier air.

3.3.4.1 Fog clearance by insolation

Satellite imagery shows that extensive areas of radiation fog and stratus dissipate from their outer edges inward due to mixing generated by insolation (this can be a more-efficient mechanism than the absorption of solar radiation by fog and underlying surfaces). The time of clearance depends on the thickness of the fog, the location of the site relative to the fog boundaries and the insolation available at a particular latitude and time of year; hill/valley circulations complicate matters for valley fog. Estimates of fog duration may be made from fog brightness in VIS imagery.

Bader et al. (1995), Chapter 7
Gurka (1986)

The fog depth must be known or estimated, together with a fog-clearance temperature.

(a) *Estimation of fog top.*

(i) Visual estimation: if the sky is visible, the fog depth is probably about 5 hPa in dense fog, and 10 hPa in thin fog.

(ii) If the sky is obscured at dawn, and no local mini-sonde ascent is available, the most representative midnight sounding should be modified as in (b) below to allow for changes between midnight and the time of minimum temperature (note height of fog top is 25 m above top of inversion).

(b) *Modifying the temperature profile on a tephigram.*

Heffer's estimate is probably appropriate:

(i) If the nose has already formed on the temperature ascent curve, the level is raised by 5 hPa and the temperature decreased by 1.5 °C; this point is joined to the night-minimum temperature by a straight line on the tephigram. The point where this line and the downward extension of the dew-point curve intersect (O in **Fig. 3.5(a)**) represents the fog top.

(ii) If a nose has not yet formed on the midnight ascent, the point 35 hPa above the ground is joined to the night minimum surface temperature and the fog top at dawn estimated as before (O in **Fig. 3.5(b)**).

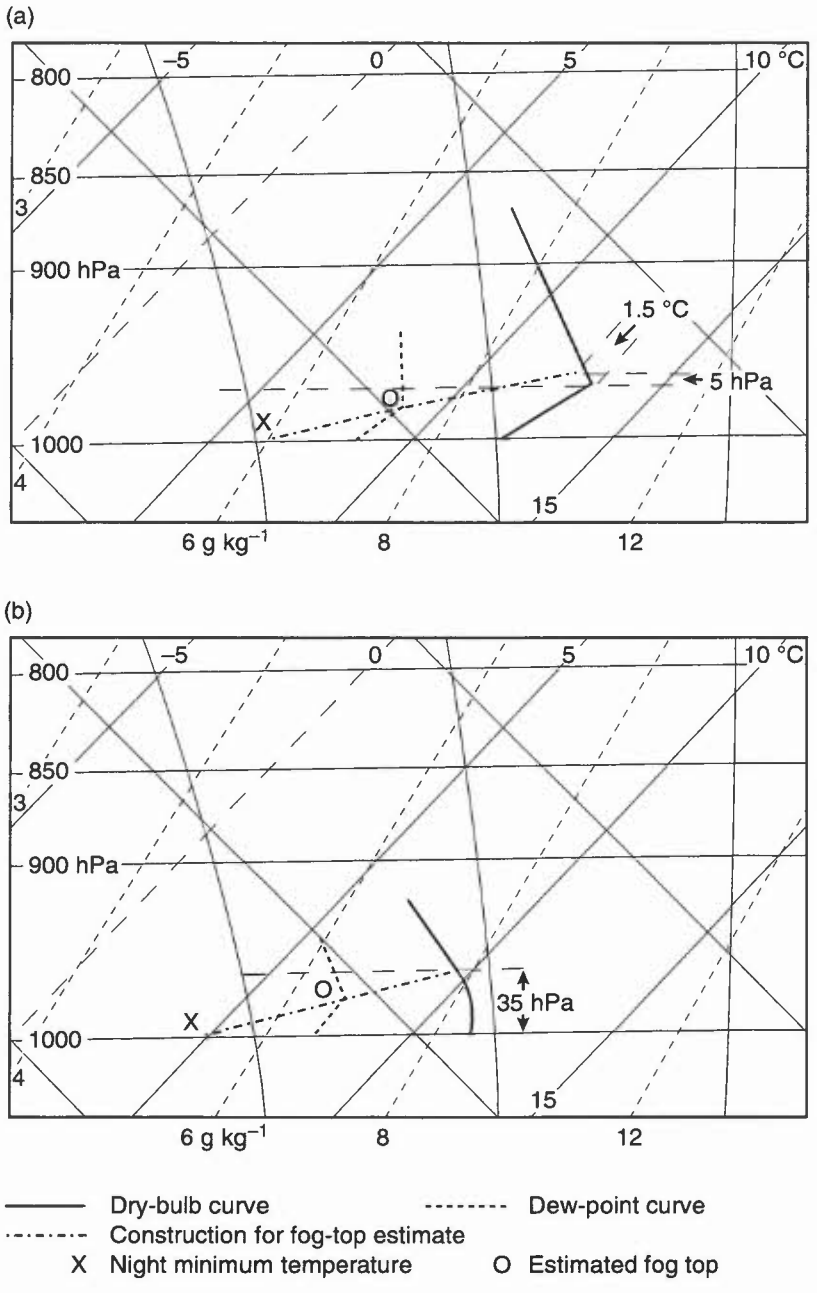

Figure 3.5. Construction for fog-top estimate from a midnight BALTHUM when (a) the inversion nose has already formed, and (b) the inversion nose has not yet formed.

(c) *Estimation of fog-clearance temperature (Jefferson).*

(i) From the fog-top estimate, the clearance temperature is estimated on the assumption of a dry adiabat from the surface to fog top. Temperature rise is estimated from 2.3 **(Fig. 2.5)**.

(ii) The surface temperature thus obtained represents the probable value above which the fog will lift to very low stratus.

(iii) The fog or low stratus should disperse entirely when the condensation level reaches the level of the inversion base (fog top will rise as fog lifts into stratus).

Caution: During winter when the sun is at a very low angle, the fog top will continue to radiate after sunrise. The fog will increase in depth for some time before the absorption of insolation is effective in starting the clearance process.

Barthram (1964) **Heffer (1965)**
Brown (1987) **Jefferson (1950)**
Findlater (1985) **Kennington (1961)**

(d) *A nomogram for forecasting clearance of fog by insolation*

Fig. 3.6 is a nomogram, due to Barthram, for predicting the time of fog clearance due to insolation, where:
T_1 = surface temperature at dawn
T_2 = fog-clearance temperature
d = depth of fog at dawn in hectopascals.

To use the nomogram:

(i) Enter the fog-depth on the left-hand diagram and move to the right to meet the vertical from the value $(T_2 - T_1)$. From this point move downwards and to the right following the curved lines representing Q to the right-hand edge of the diagram.

(ii) Move horizontally across to the middle diagram and then as far as the vertical from the value $T_2 + T_1$. Then follow the curves for fQ to the right-hand edge of the diagram.

(iii) From this point move horizontally across to the right-hand diagram to meet one of the curves marked with dates. From this curve go down to the baseline where the time of clearance is marked.

If the fog is thin (visibility more than 600 m or depth <20 hPa) the insolation needed is reduced by one third. Take the value on the left-hand margin and follow one of the diagonal pecked lines down to the inner (thin fog) scale and continue as before.

Barthram (1964)

3.3.4.2 Fog clearance without insolation

(a) *Fog clearance following the spread of cloud*

(i) The arrival of a cloud sheet over water fog often leads to the most rapid and efficient clearance of the fog because it stops, or reverses, the continual radiative cooling of the fog.

(ii) The lower the cloud sheet the more effective it is in clearing the fog, provided the ground is not frozen.

(iii) Heat flux from the soil, causing warming of the air by weak convective motions, may lift the fog into low stratus before its complete dispersal.

(iv) The time taken for fog to clear decreases with higher temperatures, as is shown by the following observations (**Table 3.5**) made at Exeter Airport (south-west England).

Table 3.5.

	Initial grass temp. (°C)					
	<0	0–2	3–5	6–8	9–10	11–13
Average time (hours) for fog to clear after arrival of cloud sheet	3.1	2.2	1.1	1.5	0.9	0.5
Number of cases	10	10	5	10	5	3

Saunders (1957, 1960)

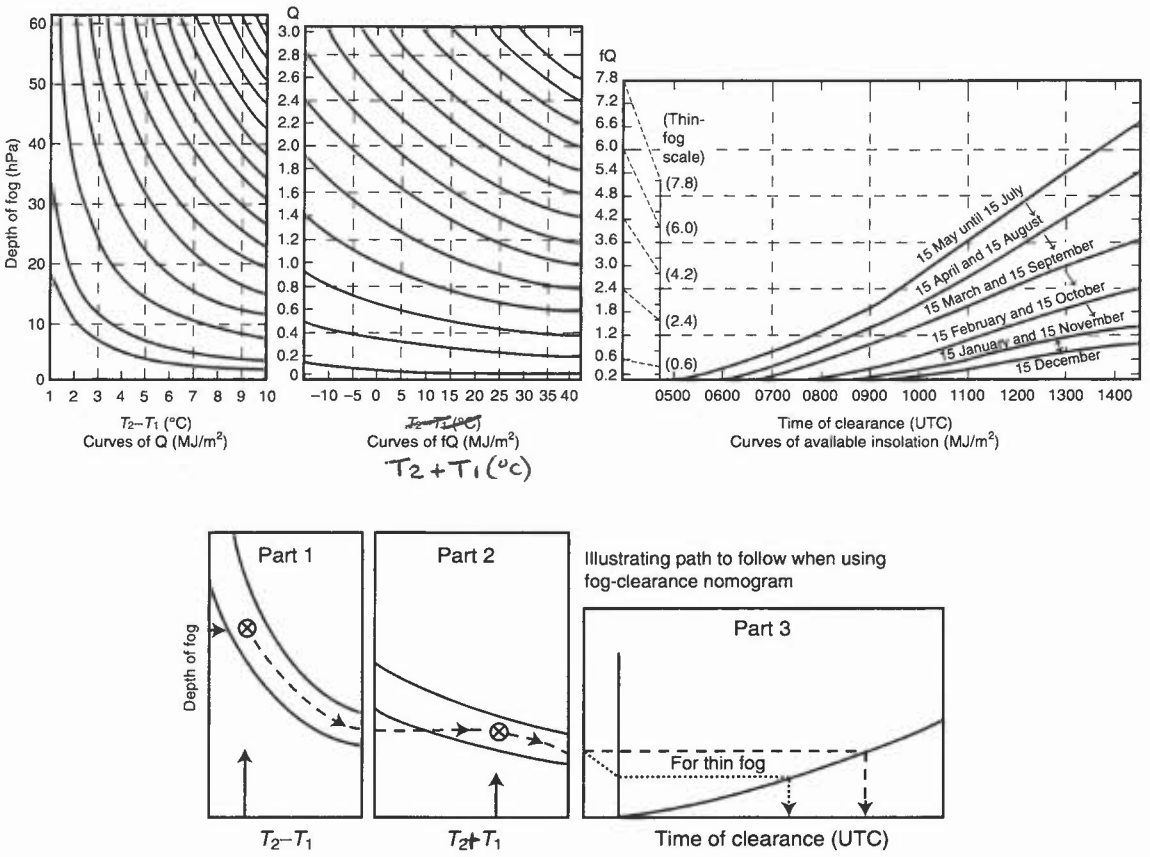

Figure 3.6. Nomogram for forecasting the clearance of radiation fog by insolation.

(b) *Fog clearance due to increase of gradient wind*

Although fog does not normally form unless the wind falls very light, its dispersal may be delayed until the winds aloft are quite strong. Mature fog has a well developed inversion capping it; through this mixed layer, a strong wind shear can be maintained. The more intense the inversion, the greater must be the wind above in order to produce turbulent mixing and dispersal of fog.

As a guide, the geostrophic wind speed required for fog to be dispersed by the increasing wind is:

(i) 15–20 kn over flat coastlands;
(ii) 20–25 kn inland;
(iii) 30–40 kn in deep valleys lying across the wind flow.

Even over the flat terrain at Cardington a peak geostrophic wind of 37 kn was estimated on one occasion before the fog cleared.

While increasing winds may lift fog into a layer of low stratus, localities downstream, especially where the ground has a gradual slope upwards, are liable to experience a delay in clearance, or the arrival of stratus if there was no fog initially.

HWF (1975) Chapter 20.8.5

(c) *Fog clearance due to dry-air advection*

(i) Local variations in air-mass surface characteristics and moisture content can create mesoscale patches of drier air which cannot be detected on synoptic-scale charts.
(ii) Unexpected nocturnal clearance of fog may occur when advection brings in drier air.
(iii) The gradual advection of progressively drier air can be effective in fog clearance.
(iv) The passage of a cold front can produce rapid fog clearance, by combining effects of dry air advection, increasing cloud cover and, often, increased wind speed.

3.3.4.3 Persistent fogs

Defining a persistent fog as one which forms one night and lasts all through the following day, not clearing until after dusk, then persistence occurs most commonly in eastern districts of England in winter.

(i) In December and January, one third of all fogs are persistent (according to this definition).
(ii) In November and February the proportion is about one sixth.
(iii) Care must be exercised in predicting whether overnight fogs between late November to early February will clear during the morning — the question is more 'if the fog lifts' than 'when'.
(iv) Most of these fogs are found to clear during the second night (44% by midnight and 80% by 0900 UTC on the next morning).
(v) Only 5–10% persist beyond 1700 UTC on the second day.
(vi) Radiation fog clearance in the summer half-year is infrequent and unlikely to persist after sunrise.
(vii) In autumn/winter it may persist overnight, although it tends to disperse next day.
(viii) Fog may thicken or, following a quiet, clear night, suddenly form soon after sunrise.
(ix) Most clearances are associated with the strengthening of winds aloft and/or an increase in low cloudiness, often (but not always) associated with a front within 200 km.
(x) Subtle indications of an impending clearance will include a slightly bigger pressure tendency or a change in wind drift at a particular station.

Note that, generally, the incidence of fog (and thick fog) has decreased markedly over the last 30 years as a result of the Clean Air Act legislation (1956).

Brown (1979) **HAM (1994) Fig. 59**
Kennington (1961)

3.3.4.4 Summary of forecasting procedures for fog clearance

(i) Study the synoptic situation
Will fog clear by any other mechanism?
— Increasing gradient wind?
— Advection of cloud cover over fog top?
— Advection of drier air?
(ii) Obtain a dawn temperature
Actual for your station if available
Otherwise forecast value
(iii) Choose a representative upper-air sounding
Latest time available (usually 2300 hrs)
Close to, or upwind of, station
Same air mass
Similar cloud/weather conditions
Beware of coastal influences
(iv) Modify the sounding
Sky visible or obscured?
Station dawn temperature
(v) Find fog clearance temperature and time
Kennington–Barthram technique
Other techniques available
Which one works best at your station?
(vi) Find stratus clearance temperature
— if fog is deep and widespread
(vii) Will local factors delay or advance clearance?
Upslope effects
Local wind circulations
Frost melt
Freezing fog can precipitate out
(viii) Keep the forecast under review
Synoptic developments
Observations at your station
Observations from other stations nearby
Satellite imagery
Amend the forecast if necessary

3.3.4.5 Large temperature falls associated with periods of weak advection on radiation nights

Sudden, large temperature falls (≥3.5 °C) have been recorded inland (at Lyneham, southern England) on radiation nights due to either:

(i) fog-free cold air being advected from adjacent low ground by an increase in wind, or:
(ii) fog forming in the same low area and deepening sufficiently to suddenly engulf the airfield.

On such nights it is clearly inadvisable to take a single station's observations as representative of an area.

Booth (1982)

3.4 Advection fog

3.4.1 Warm advection fog

Typical examples are sea fog and fog over very cold land. Thawing snow is commonly associated with advection fog over land.

(a) Factors favourable for *formation*:
  (i) Air-mass dew point greater than temperature of surface.
  (ii) Stable lapse rate, slight hydrolapse in lowest layers.
  (iii) Moderate winds (10–15 kn) — low stratus likely in winds greater than 15 kn.
  (iv) Suitable wind direction.

  Note that: The advection of moist air also renders *radiation fogs* more frequent.

(b) Factors favourable for *clearance*:
  (i) Change of air mass — the most common and reliable means.
  (ii) Change of track of air mass to drier source.
  (iii) Over land — solar heating; radiation fog clearance techniques may be used. (Over snow the surface temperature may not rise above 0 °C).

HWF (1975), Chapter 20.9

3.4.1.1 Sea fog

There are four main sources of warm, moist air giving sea fog over coasts and waters around the British Isles:

(i) A south-westerly flow from the Atlantic west of the Iberian Peninsula; the air should have originated from, or spent some time over, warm waters south of 40° N. It is often associated with the warm sector of a frontal depression; it gives rise to widespread fog around southern and western coasts.
(ii) With high pressure to the west of the British Isles, mild air may circulate around northern Britain and come southwards as a north to north-east wind, bringing low stratus and fog ('haar') to exposed eastern coasts of Scotland and north-east England.
(iii) Warm continental air during spring and early summer in a south-easterly flow from the Mediterranean across Europe may become sufficiently moist and stable at low levels to affect east coast areas of the United Kingdom.
(iv) In summer very high dew-point air often accompanies thundery lows moving north from France, giving rise to sea fog in the English Channel and southern North Sea which may spread inland at night.

Bader et al. (1995), Chapter 7
HWF (1975), Chapter 20.9
Roach (1995)

3.4.1.2 Prediction of sea fog

Satellite imagery (VIS) is invaluable for locating the boundaries of existing areas of sea fog:

(i) The shape of the foggy areas may correspond to areas of particularly low sea temperature (for example along the coast of north-east England).
(ii) Other patterns are due to the incursion of tongues of much drier air, usually of continental origin.

For prediction:

(i) A detailed and up-to-date chart of sea surface temperatures is essential, combined with an analysis of the dew-point distribution over the sea and a prediction of the low-level air flow.

(ii) Wind speed in sea fog is most commonly 10–15 kn, but it is not unusual to find winds of 25 kn. In some cases the wind speed may reach gale force, though such observations are usually confined to ships in mid-Atlantic.

3.4.1.3 Advection of fog from land to sea

(i) Radiation fog carried out to sea by a light offshore wind may drift considerable distances over a slightly warmer sea before being dispersed.

(ii) Radiation from the fog top may effectively disperse heat supplied to the lower layers of the fog by warmer waters. This results in a mature fog type of profile.

(iii) Occasionally such fogs may be carried back to land by a sea-breeze.

3.4.1.4 Advection of fog from sea to land

(i) Sea fog is frequently carried inland over coastal districts by winds off the sea (during the summer months sea-breezes may be responsible for this).

(ii) Nocturnal penetration may be extensive over low-lying ground where the liability to fog will be increased by radiational cooling.

(iii) By day sea fog usually lifts to low stratus overland and 'burns off' with adequate insolation.

(iv) Such clearances start off well inland and gradually spread upwind towards the coast.

3.4.1.5 Advection fog over land

(i) For advection fog over land to be at all widespread or persistent it is generally necessary for the ground to be very cold — either frozen or snow covered. Particularly widespread and persistent fog may occur when warm air starts snow cover thawing.

(ii) In summer the fog tends to spread inland in the evening and burn back to the coast in the morning. Fog often returns to an inland station when the temperature falls to the value at which the fog cleared in the morning.

(iii) During the coldest months, when insolation is too weak to disperse mature fogs, any change in wind speed or direction needs to be watched for signs that persistent fog patches may be advected into previously clear zones. Such movements can occur even in the middle of the day when a deterioration is least expected.

3.4.2 Cold advection fog

Cold advection fog forms when cold dry, stable air flows over a much warmer water surface (warmer by 10–15 °C at least).

(i) The evaporating vapour immediately condenses again to form *steam fog*, with convective whirls and a top at a few metres.

(ii) In polar regions the same process gives rise to 'Arctic Sea Smoke'.

HWF (1975) Chapter 20.9

3.5 Upslope fog

3.5.1 Requirements

(i) flow of moist air over gently rising ground over a wide area **(Fig. 3.7)**;

(ii) a stable lapse rate in the lowest layers.

(Very stable air may be deflected around the edge of steeply rising ground if there are gaps in the escarpment.)

On radiation nights, weak moist advection may be combined with gentle upslope motion producing multiple conditions favourable for fog; the likelihood of formation of upslope fog may be determined from a representative tephigram — the height of the base being given by the lifting condensation level of the upwind air.

3.5.2 Hill fog

(i) Hill fog does not necessarily require upslope motion.

(ii) It occurs when the cloud base happens to be lower than the hill top **(Fig. 3.8(a))**.

(iii) Depending on the humidity profile below the general cloud base, upslope motion may generate cloud on hills at a lower level, either merging with the general cloud layer or as a separate layer well beneath it.

(iv) Radiation fog which has formed overnight in valleys may lift into low stratus during the morning, covering hills temporarily before dissipating **(Fig. 3.8(b))**.

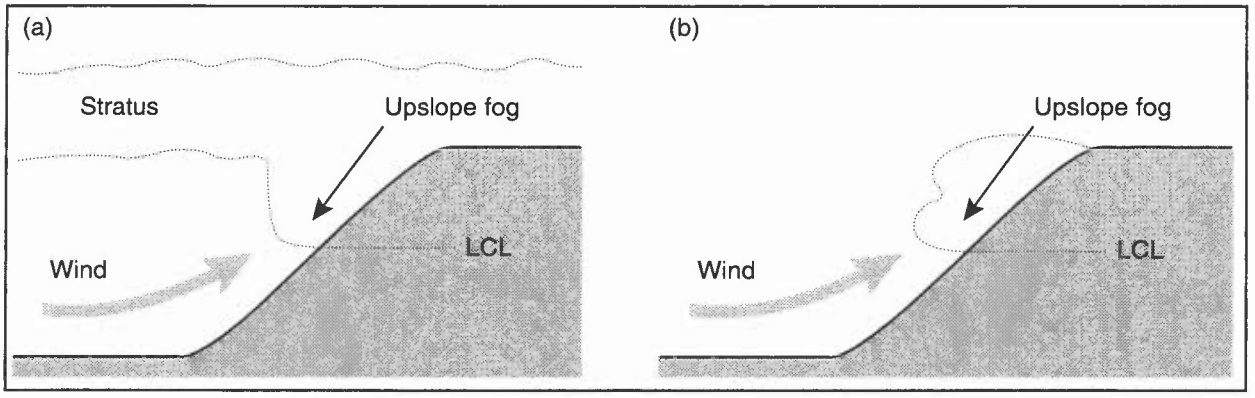

Figure 3.7. Upslope fog formation. (a) If turbulence is already causing stratus over flat ground, the effect of upslope motion will be to lower the cloud base on the windward side. (b) If turbulence is insufficient to form stratus, the extra uplift generated by upslope motion may cause patchy upslope fog to form. This can sometimes be the first sign of stratus forming more generally.

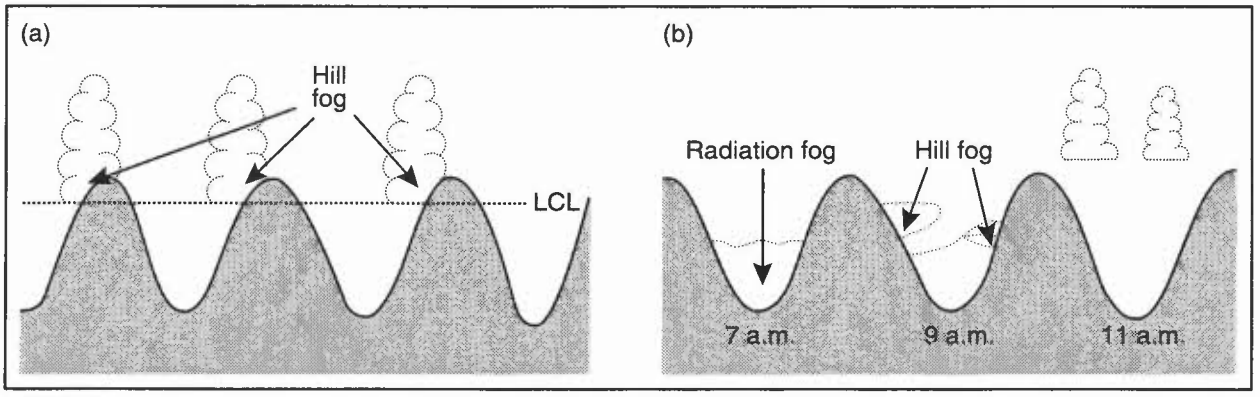

Figure 3.8. Hill fog formation. (a) Hill fog can occur in any air mass provided the hills are high enough, or the cloud base low enough. Here the base of the cumulus clouds is low enough to give hill fog patches. (b) Radiation fog which has formed overnight in valleys may lift into low stratus during the morning, covering hills temporarily before dissipating.

In the presence of strong winds the empirical relationship is suggested for the height of the cloud base in kilometres:

Cloud base (km) = dew-point depression (°C)/8;

thus in a southerly airstream ahead of a depression, with dew-point depression near a coast of <2 °C, cloud base may develop only 250 m asl.

Pedgley (1967)

3.6 Frontal fog

(i) Frontal rain falling into very cold stable air beneath eventually saturates the layer, frequently forming *pannus*, with fog confined to higher ground **(Fig. 3.9)**.
(ii) Occasionally winds may be light enough to give fog at low levels.
(iii) Visibility is often several hundred metres; forced ascent may reduce this.

3.6.1 Summary of factors favourable for frontal fog development:

(i) Ahead of active warm front or warm occlusion.
(ii) Very cold (or snow-covered) ground.
(iii) Large temperature contrast between cold and warm air masses.
(iv) Light surface winds.

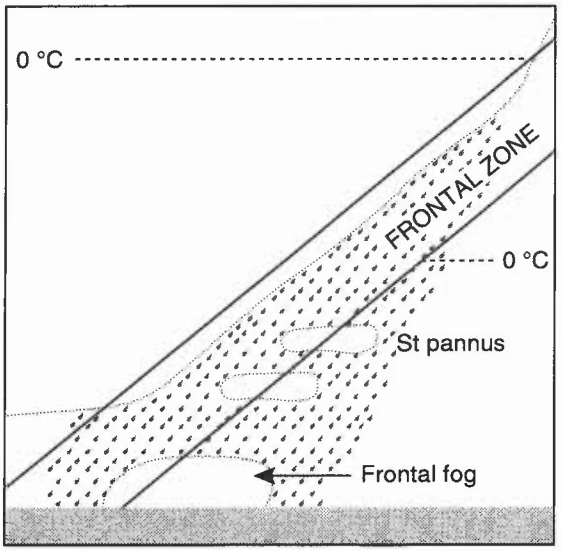

Figure 3.9. The formation of stratus pannus and frontal fog.

3.7 Convective activity above fog

(a) Although fog is normally associated with a stable air mass, the top of the inversion may be below the level of adjacent hills. During the day fog-free high ground may become warm enough to set off cumulus clouds.
(b) Beware of the development of thermally induced circulations in the low-level air flow; these may start the fog bank moving.
(c) Where large areas of low-lying fog persist throughout the day the heating of fog-free areas may result in the development of a pseudo sea-breeze effect during the afternoon. In winter, foggy air may be advected for many miles to produce sudden deteriorations in previously clear localities.
(d) In south and east England, wind speeds in excess of 15 kn have been observed as the fog front advanced.
(e) Fog formed in warm moist air advected over the sea may be overlain by a potentially unstable layer at higher levels. Convergence in the layers above the fog may set off vigorous convective activity and thunderstorms. In the early stages these may not affect the fog but the downrush of air associated with heavy storms will lead to localized clearances.

The following features may be used as a guide:
(i) Upper-level convective developments occur with a south-easterly flow at low levels and relatively high dew points near the surface.
(ii) Wet-bulb potential temperatures show a decrease with height in the middle levels.
(iii) The potential instability is realized if an upper low or trough in the contours at 500 and 300 hPa moves across the area.
(iv) This development will become apparent on infrared satellite imagery where the cold tops of instability cloud appear white above the grey of sea fog. Beware of situations of fog and thunder giving rise to 'anaprop' on the radar screen (10.6).

3.8 Guidance on the formation and detection of fog through imagery

Satellite imagery will help to determine several atmospheric conditions that can lead to fog formation:
(i) *Low-lying moisture* — prior to fog formation surface appears warmer under low-level moist air than where air is drier. Fog boundaries are generally more distinct than moisture boundaries.
(ii) *Cloud cover* — likely locations are areas with daytime cloud cover, or with a trajectory from cloud-covered areas, followed by clear skies at night.
(iii) *Snow cover* — snow cover can be a source of cooling that leads to fog formation.
(iv) *Precipitation* — if during the late afternoon or evening, followed by clearing skies will often lead to fog formation.

Extra information may be deduced from satellite multi-spectral channels.

Bader et al. (1995), Chapter 7

3.9 Haze

3.9.1 Haze particles

These may be produced by:

(i) Industrial pollution (of local and/or continental origin) and vehicle exhausts and may develop due to photolytic reagents; thus visibility may be substantially reduced in the 'urban plume' downwind of a city (2.11).

(ii) Smoke concentration near the ground will be less in stronger winds; it will only seriously affect visibility when atmosphere is stable at some level in the lowest 500 to 1000 m (1650 to 3300 ft).

(iii) Dust and fine sand raised by the wind during prolonged dry weather (e.g. 'fen blows').

(iv) Salt spray produced by rough seas and carried inland by strong winds.

3.9.2 Haze occurrence

(i) Haze is often concentrated where RH is high (e.g. under an inversion); hygroscopic particles can result in haze at relatively low RH. Injection of aerosols through the inversion by convective activity can lead to haze in stable layers well up in the troposphere.

(ii) The concentration of particulates will be modified by diurnal variations in temperature and RH as well as cloud cover (affecting the temperatures in the lowest layers) and precipitation (wash-out agent).

(iii) Urban haze may thicken in the afternoon due to photochemical reagents.

(iv) Haze is a problem for aircraft in low-level flight, especially viewing objects through a slant-path and particularly when looking towards the sun.

(v) Haze boundaries are often sharply defined, and may be associated with convergence lines (e.g. sea-breeze fronts).

(vi) The position of weak synoptic-scale fronts may also be located at times by haze boundaries.

AWDC (1960) **HAM (1994)**
Bradbury (1989) **Hänel (1976)**

3.9.3 Depth of haze

(i) With a well-marked stable layer near the ground, the haze top is often very clear-cut.

(ii) The tops of shallow cumulus generally extend just above the haze layer, **Fig. 3.10(a)**. If the air above is conditionally unstable, large cumulus or cumulonimbus may rise many thousands of feet above the haze top, which is usually at, or below, the level where the environment lapse rate decreases to less than the SALR.

(iii) Dispersing layer clouds may leave thin layers of elevated haze. These are rarely apparent from the ground but can be seen from aircraft when viewed horizontally during climb or descent.

Bradbury (1989)

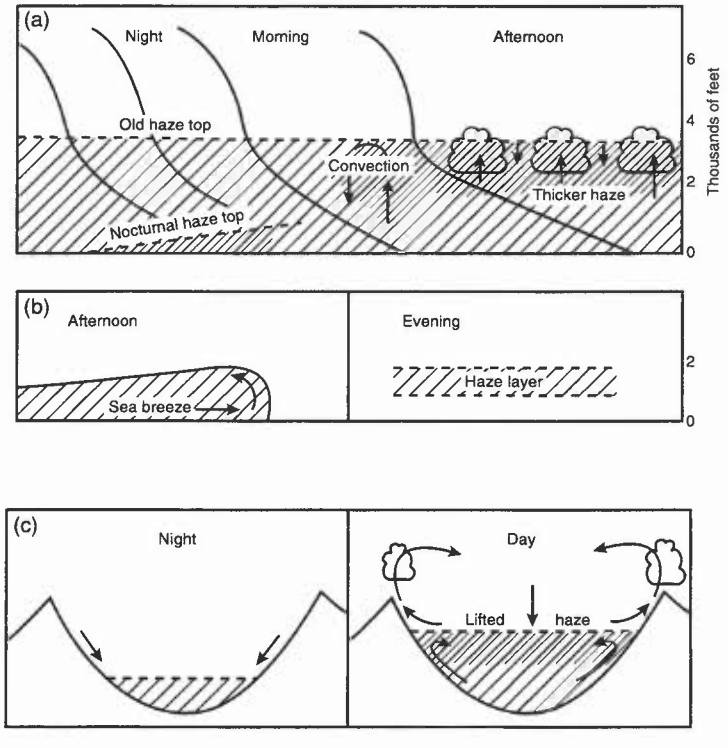

Figure 3.10. Idealized patterns of the diurnal variation of haze. (a) Under calm conditions with a stable layer at 3000–4000 ft. Curved full lines give an impression of the temperature profiles. (b) Association of haze with sea-breezes, which degenerate in the evening leaving an elevated haze layer. (c) Valley haze. Daytime convection over surrounding high ground generates subsidence over the valley which keeps the haze trapped in a restricted depth.

3.9.3.1 Airborne visibility

A forecaster should be aware of the effect on visual contact with the runway of slant visibility and be able to give guidance as to the likely height at which poor visibility may be encountered. Air-to-ground visibilities are made worse into the sun by reflection and scattering from the haze/fog top. Flight below an inversion may make target acquisition impossible, while above the inversion visibility may be much improved. (Visibility air-to-ground and air-to-air is also a function of column size, illumination, etc.)

HAM (1994) Chapter 9.2

3.9.4 Diurnal variation of haze

(i) At the surface, haze thickens during the night as RH increases and the nocturnal low-level inversion intensifies.
(ii) It thins out during the day when the RH decreases and the inversion is destroyed by solar heating.
(iii) Mesoscale weather systems exert important controls on the distribution of haze. The sea-breeze circulation, for example, with its diurnal rhythm, often very clearly distinguishes the well mixed, convective air inland from the much hazier, stable sea air (**Fig. 3.10(b)**).
(iv) Daytime convective mixing increases the haze depth and improves the horizontal visibility reported at the surface, but during the day the haze thickens at the inversion level where RH is highest. This effect is particularly marked when the inversion is low and haze is being channelled into the valleys intersecting areas of high ground. Valley haze (**Fig. 3.10(c)**) is due to subsidence generated by daytime convection over surrounding high ground.

HWF (1975), Chapter 20

3.9.5 Dispersal of haze

Continuous rain is effective in washing out most of the haze particles from the air. Showers, and even heavy thunderstorms, are much less effective.

3.9.6 Synoptic situations favourable for haze

(i) Haze is usually thickest in anticyclonic conditions when low-level winds are light. An increase in surface wind often leads to improved visibility, and a decrease in wind to poorer visibility at the surface.
(ii) Ahead of a warm front, when the clouds are increasing, the visibility from the air often deteriorates in the layer extending about 300 ft below the cloud base.
(iii) In the United Kingdom a high proportion of haze days are associated with winds from Europe (**Fig. 3.11**). Surface wind directions from 060–120° commonly bring the worst haze.

3.9.7 Visibility forecasting methods

3.9.7.1 The File method

Based upon data for five stations in southern England, the method is intended to be used 6–8 hours before the forecast time. Part I requires prediction of afternoon and evening wind speed and relative humidity. Forecast values are read from **Fig. 3.12.** In Part II a correction factor for those results is obtained by considering the surface chart and inspecting upwind humidity and wind speed and then applying these to the nomogram.
Example: actual visibility is 20 km, relative humidity about 60% and surface wind 10 kn. **Fig. 3.12(a)** gives a visibility of 13 km. The correction factor is then 20/13 = 1.5; this is applied to all subsequent forecasts. (A good forecast of advective changes to the airstream is necessary.) File recommends that in highly polluted airstreams visibility derived from the graphs be halved.

File (1985)

3.9.7.2 A (non-frontal) visibility forecasting method devised at Middle Wallop

(i) Construct a forecast night-cooling curve; find intercept of expected air-mass dew point with cooling curve.
(ii) Find out visibility at time of the maximum temperature (Vis_{max}); allow for areas of differing visibilities advecting across area.
(iii) Forecast overnight surface wind.

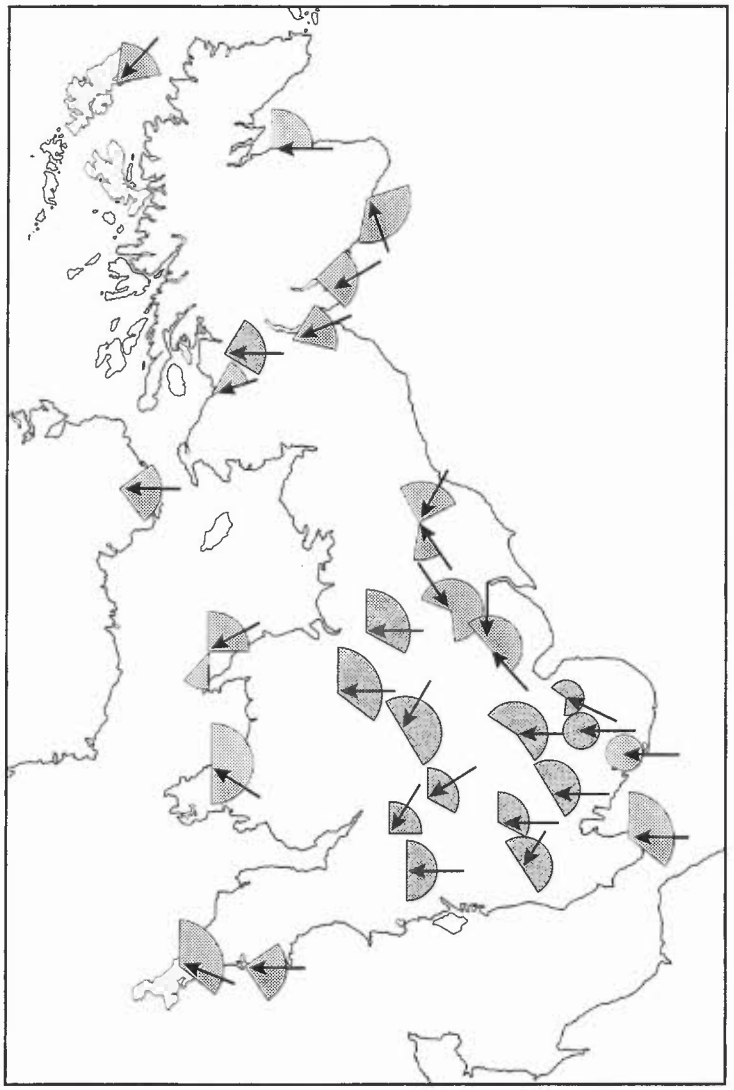

Figure 3.11. Surface wind direction and summer haze. Shaded sectors show the range of directions most often associated with visibilities in the range 1.8 to 9.9 km. Where variations are small the area shown is circular, and the arrows denote the worst directions. The radius of the sector arcs has no significance.

Then visibility, when temperature has fallen to air-mass dew point, depends on wind speed (**Table 3.6(a)**):

Table 3.6(a).

Wind (kn)	Visibility
0–5	⅓ of Vis_{max}
6–9	½ of Vis_{max}
≥10	¾ of Vis_{max}

Thereafter for each °C below the intercept temperature halve the visibility, noting time from curve.
For example, dew point at T_{max} is +4 °C, when visibility was 25 km; forecast wind speed: 3 kn.

Table 3.6(b).

At forecast temperature of 4 °C, forecast visibility is 8 km
At forecast temperature of 3 °C, forecast visibility is 4 km
At forecast temperature of 2 °C, forecast visibility is 2 km

A further proposition is that visibility at dusk is 80% of Vis_{max}.

Perry & Symons (1991)

3.9.7.3 Changes in horizontal visibility with height associated with relative-humidity changes

An untested, but theoretically sound, method for inferring the variation of visibility with height from a given surface observation is derived as follows:

(i) Aerosol is assumed well mixed, relative humidities (RH) >75% (0.75) and <98% (0.98) and with no local sources.

(ii) The relationship between the horizontal visibilities V_1 and V_2 at RH_1 and RH_2 is:

$$V_2 = V_1[(1 - RH_2)/1 - RH_1]^N$$

where $RH_2 > RH_1$ and N applies to a particular location, possibly varying with season, wind direction, etc. (German studies for an urban aerosol give $N = 0.7$; this may be ascertained for the local area by plotting log of visibility against log of $(1 - RH)$, when the slope will give N).

(iii) Using **Fig. 3.13**, plot starting surface visibility and associated RH.

(iv) Draw a line through this plot whose slope corresponds to the local N (shown here for values 0.6, 0.7 and 0.8; illustrated are other V', RH' relationships, where V at $RH = 0.8$ is assumed known, perhaps typifying local wind directions etc).

(v) Read off visibilities at other heights, corresponding to the (higher) RHs at these heights (derived from tephigram estimates).

Hänel (1976)
Reichert (1978)

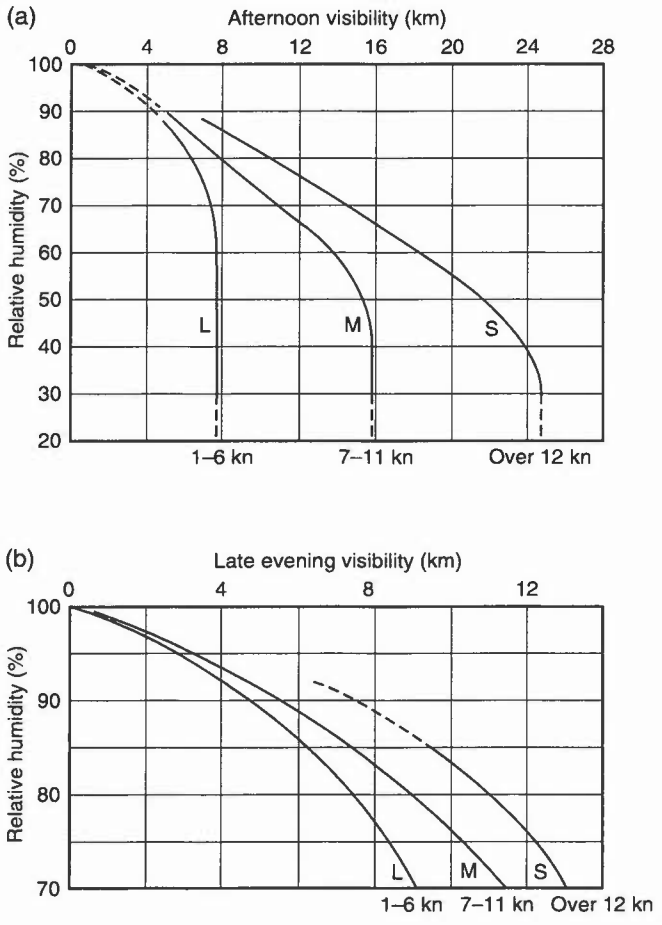

Figure 3.12. (a) Afternoon visibility against relative humidity for three classes of wind speed in 'easterly' synoptic situations. Median values are represented by L, M and S for light, moderate and strong wind speeds, respectively. The curves should be regarded as provisional for relative humidities above 87% and below 30%. (b) Late evening visibility against relative humidity for three classes of wind speed in 'easterly' synoptic situations. Median values are represented by L, M and S for light, moderate and strong wind speeds, respectively. The curve for strong winds should be regarded as provisional for relative humidities above 87% where data were sparse.

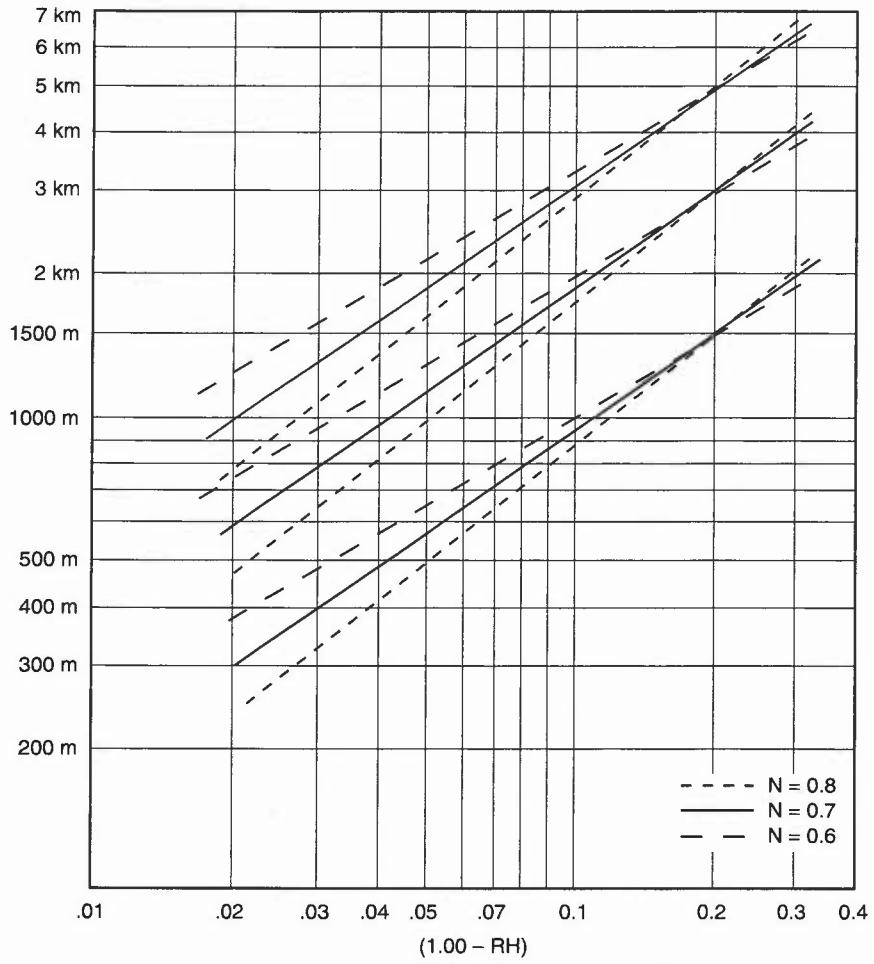

Figure 3.13. Diagram for estimating changes in horizontal visibility associated with changes in relative humidity.

3.10 Visibility in precipitation and spray

Rain — visibility is inversely proportional to total water content and number of raindrops; thus deterioration is greatest in heavy rain and in drizzle. **Fig. 3.14** summarizes experience in various countries; in moderate rain visibility is between 5 and 10 km, while heavy showers can reduce visibility to 1000 m, assuming no pre-existing pollution.

Snow — has a greater impact, visibility commonly falling below 1000 m even in moderate snow; in heavy snow this may fall to 200 m or less. Dry snowflakes result in visibilities only about one half of those illustrated in **Fig. 3.14** (wet snowflakes collapse to a smaller volume and become translucent). Blowing snow gives very low visibilities. It is most likely to occur when snow is dry and powdery.

In drizzle visibility ranges from about 3000 m to 500 m although simultaneous presence of fog droplets will still further reduce range.

In *low cloud* (hill fog) visibility is reduced to below 30 m.

In *spray* at sea and at coastal sites — winds >50 kn reduce visibility to <5 km
winds >70 kn reduce visibility to <1 km.

Jefferson (1961)

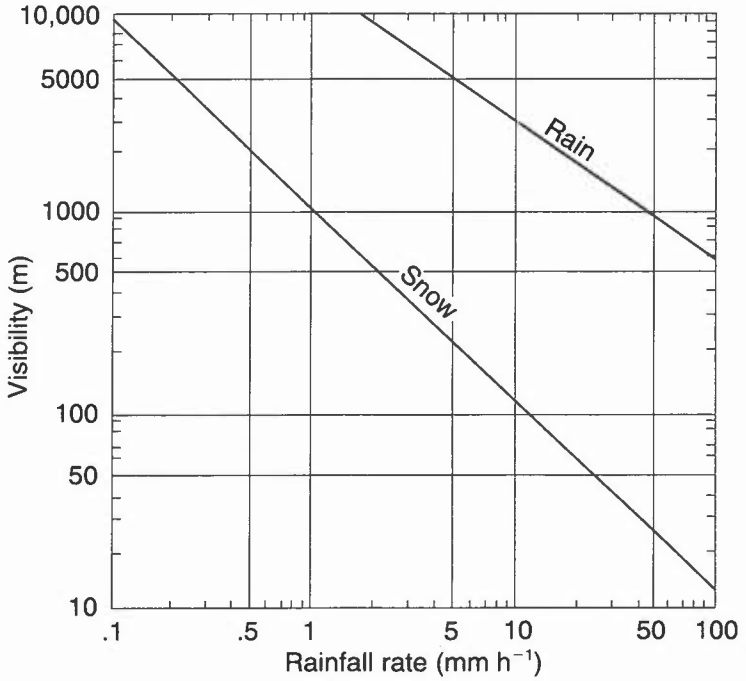

Figure 3.14. Visibility in rain and snow.

BIBLIOGRAPHY

CHAPTER 3 — VISIBILITY

Aerodrome Weather Diagrams and Characteristics (AWDC), 1960: Meteorological Office, London, HMSO (also Airfield Weather Diagrams, Met.O.564).

Bader, M.J., Forbes, G.S., Grant, J.R., Lilley, R.B.E. and Waters, J., 1995: Images in weather forecasting. Cambridge University Press.

Barthram, J.A.,1964: A diagram to assess the time of fog clearance. *Meteorol Mag,* **93**, 51–56.

Booth, B.J., 1982: An analysis of sudden, large falls in temperature at Lyneham during periods of weak advection. *Meteorol Mag,* **111**, 281–290.

Bradbury, T., 1989: Meteorology and flight. A & C Black.

Brown, A.A., 1979: The clearance of persistent fog. *Meteorol Mag,* **108**, 201–208.

Brown. R., 1987: Observation of the structure of a deep fog. *Meteorol Mag,* **116**, 329–338.

Craddock, J.M. and Pritchard, D.L., 1951: Forecasting the formation of radiation fog — a preliminary approach. Meteorological Research Paper No. 624. Meteorological Office (unpublished).

File, R.F., 1985: Forecasting visibility over southern England in polluted easterly airstreams. *Meteorol Mag,* **114**, 13–23.

Findlater, J., 1985: Field investigations of radiation fog formation at outstations. *Meteorol Mag,* **114**, 187–201.

Gurka, J.J., 1986: The role of inward mixing in the dissipation of fog and stratus. *Meteorol Monogr*, 2-86, Satellite imagery interpretation for forecasters, Vol. 3, National Weather Assoc. Temple Hills, MD.

HAM. Handbook of Aviation Meteorology, 1994: London, HMSO.

Hänel, G., 1976: The properties of atmospheric aerosol particles as functions of the relative humidity at thermodynamic equilibrium with the surrounding air. *Adv in Geophys*, **19**, 73–188.

Heffer, D.J., 1965: A test of Kennington's method of forecasting the time of clearance of radiation fog. *Meteorol Mag,* **94**, 259–264.

HWF. Handbook of Weather Forecasting, 1975: Met.O.875, Meteorological Office.

Jefferson, G.J., 1950: Method for forecasting the time of decrease of radiation fog or low stratus. *Meteorol Mag,* **79**, 102–109.

Jefferson, G.J., 1961: Visibility in precipitation. *Meteorol Mag,* **96**, 19–22.

Kennington, C.J., 1961: An approach to the problem of fog clearance. *Meteorol Mag,* **90**, 70–73.

Local Weather Manual for Southern England, 1994: Meteorological Office.

Meteorological Office, 1985: The susceptibility of fog on the M25 motorway. Met O 3, Building, Construction Climat Unit.

Pedgley, D.E., 1967: Weather in the mountains. *Weather*, **22**, 266–275.

Perry, A.H. and Symons, L.J., 1991: Highway meteorology. E. and F.N. Spon.

Reichert, B, 1978: A method of forecasting flight visibility in bad weather. Porz-Wahn, *Amt Wehrgeoph*, Fachl. mitt. Nr. 187, 157–162.

Roach, W.T., 1994/95: Back to basics: Fog.
1994: Part 1: Definitions and basic physics. *Weather*, **49,** 411–415.
1995: Part 2: Formation and dissipation of land fog. *Weather*, **50**, 7–11.
1995: Part 3: Formation and dissipation of sea fog. *Weather*, **50**, 80–84.

Saunders, W.E., 1950: A method of forecasting the temperature of fog formation. *Meteorol Mag,* **79**, 213–219.

Saunders, W.E., 1957: Variation of visibility in fog at Exeter airport and the time of fog dispersal. *Meteorol Mag,* **86**, 362–368.

Saunders, W.E., 1960: The clearance of water fog following the arrival of a cloud sheet during the night *Meteorol Mag,* **89**, 8–10.

Thomas, N., 1995: Fog and fog forecasting. MSc dissertation, University of Reading (also available as Meteorological Office NWP publication).

CHAPTER 4 — CONVECTION AND SHOWERS

CHAPTER 4 — CONVECTION AND SHOWERS

4.1 Forecasting convective cloud

The initial upward motion of an air parcel is provided by buoyancy from surface heating, convergence on a range of scales, mass ascent or orographic forcing. Condensation and entrainment mark the subsequent progress of the parcel upwards under various instability criteria until it achieves its upper limit. A simple model of the thermodynamic processes which occur can be represented on the tephigram which, however, shows only the static stability which does not always give a complete description of the true stability of moving air.

4.1.1 Instability definitions

Conditional describes a temperature sounding in a layer where the actual lapse rate lies between the SALR and the DALR.

Potential is shown by the decrease of wet-bulb potential temperature with height through a layer. This form of instability is released during mass ascent of air (e.g. over a hill, or in a rising frontal air current).

Latent an atmosphere that possesses potential instability may also possess latent instability (the converse is not necessarily true); a parcel of air with negative buoyancy may undergo forced ascent past its level of free convection. It then continues under its own buoyancy. The SALR through the wet-bulb temperature at any level on an ascent cuts the environmental temperature curve higher up. Latent instability describes, for example, a temperature sounding which is stable near the ground and unstable above, typically at night. Even though no convection is occurring at the time of the sounding, it may be released later in the day as a result of solar heating.

Met. Glossary (1991)

4.2 Constructions on a tephigram

4.2.1 Parcel method

Fig. 4.1 illustrates the general 'parcel' method, using a temperature sounding made before dawn (usually midnight) to forecast cumulus cloud during the day. ABCD is the environment curve. T and T_d are the surface temperature and dew point expected as a result of daytime heating. BU is the condensation level, CV is the level where the lapse-rate of the environment decreases to less than the SALR.

(i) This method assumes that a small parcel of air, of negligible mass, is warmed at the surface and becomes buoyant, rising up through the environment without disturbing it or mixing with it.

(ii) In **Fig. 4.1** the path curve of the rising parcel is shown by TUVWX. At T the parcel is warmer than the environment at that level (A) and it rises. From T to U its temperature falls at the DALR. U is the condensation level and cloud base, at which point it is still buoyant and continues to rise, but cooling at the SALR. At W (Parcel Tops) the rising parcel has a temperature equal to that of the environment and it is no longer buoyant, but theoretically, it will continue to rise to X because of momentum gained during ascent.

(iii) Some tops may reach W and, in extreme cases, vigorous convection cloud may penetrate to X, which is defined as the level which is such that the 'negative area' XDWX equals the 'positive area' WVTACW. This latter area defines the convectively available potential energy, CAPE.

(v) For practical use a modification to this method assumes that entrainment, detrainment and frictional drag slow the ascent. As a result the ascent ceases at a lower level than that predicted by the parcel method. The level C in **Fig. 4.1**, where the lapse-rate of the environment becomes less than the SALR, is the cloud-top level for most cumulus (Slice Tops).

Summary:

U is Normand's point

V is taken as the tops of most of the clouds

W is forecast for the tops of occasional large clouds

X is forecast only when conditions seem favourable for exceptionally vigorous and deep convection (e.g. θ_w lapse rate ≥ 0).

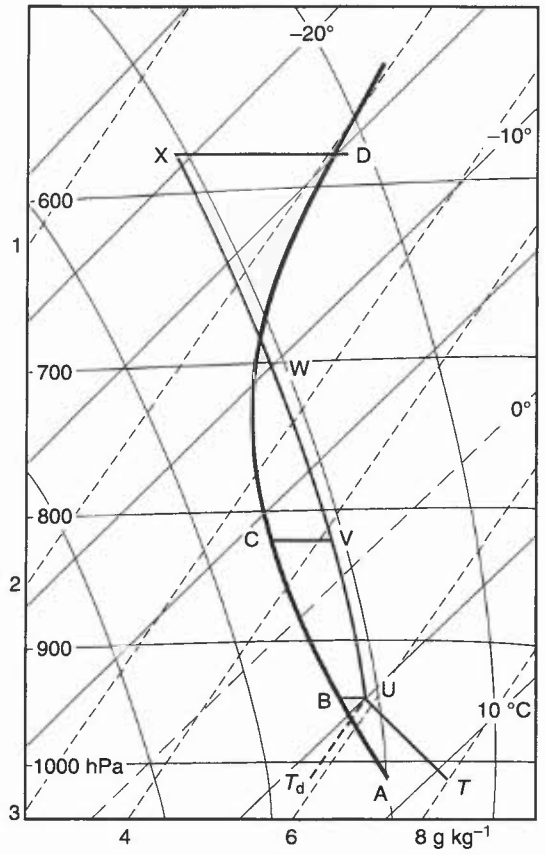

Figure 4.1. Tephigram construction for estimating the base and tops of convection cloud. See text for method of use.

4.2.2 Forecasting the cloud base of cumulus

4.2.2.1 Estimating the condensation level

The surface temperature (T) and dew-point (T_d) may be used to estimate the condensation level (H).

As a rough approximation:

$$H = 4\,(T - T_d)$$
$$H_m = 1.22\,(T - T_d)$$

where T, T_d are in degrees Celsius and H in hundreds of feet (H_m in hundreds of metres).

On a tephigram, Normand's theorem gives the condensation level at the intersection of a dry adiabat through T and a humidity mixing ratio (HMR) line through T_d. This is the level BU in **Fig. 4.1.**

4.2.2.2 Relationship between condensation level and cloud base

(i) While surface temperatures are rising quickly during the morning, the base of cumulus cloud is close to the calculated condensation level.

(ii) During the afternoon, when convective upcurrents are strongest, the base of cumulus may be up to 700 ft (25 hPa) above the condensation level as the moisture flux from the surface causes the mixing ratio to decrease in the lowest tens of metres near the ground.

(iii) These relationships are based on data from gliding sites where light aircraft and sailplanes provided frequent reports of cloud base. Aircraft observations from Bircham Newton and Aldergrove, made during the months from April to September, showed an average cloud base 25 hPa above the condensation level.

(iv) After the time of maximum temperature the cloud base remains almost constant although the falling surface temperatures imply a lowering of the condensation level.

(v) Even in an apparently homogeneous air mass there may be significant variations in the cumulus cloud base over short distances. The difference is usually greatest during the morning when the air is not well mixed. Different

rates of heating over hilly and over low-lying areas can lead to temporary variations of the cloud base by as much as 2000 ft (600 m) within a distance of 1 km.

(vi) The daytime ground surface temperature and dew point of fairly extensive areas of elevated ground may not be greatly different from surrounding low-ground values; condensation levels may thus be at a similar height above elevated ground as condensation levels above adjacent lower ground — the 'plateau effect'.

4.2.3 Forecasting the heights of convective cloud tops

4.2.3.1 First estimates — using a tephigram

(i) An initial estimate of the cumulus/cumulonimbus cloud tops may be made following the method illustrated in **Fig. 4.1,** paying due regard to the limitations imposed on cloud-top height by entrainment etc. (the 'Slice Tops' approach). Observations often confirm the irregular level of actual cumulus tops.

(ii) It is suggested that, as a first estimate, the construction shown in **Fig. 4.1** is adopted.

(iii) Workstation satellite imagery can be used to see the spatial distribution of showers. By using temperature slicing of IR images an estimate of the cloud-tops temperature can be found. Then an estimate of cloud height may be made from an adjacent tephigram.

4.2.3.2 Choosing a representative ascent

(i) At the time a forecast is being prepared, the appropriate sounding will be upwind of the area and in the correct air mass. If there is cold advection, as indicated by wind backing with height, then the environment is likely to become more unstable with time.

(ii) Even if no fronts are expected to cross the area bringing major air-mass changes, there may be significant variations in the convective activity within the same air mass.

(iii) Enhanced convection may be associated with the occurrence of synoptic-scale features such as upper troughs or lows.

(iv) Similarly, suppressed convection may accompany an upper ridge.

(v) Mesoscale variations are also common, and may be associated with regions of low-level convergence/divergence or variations in low-level moisture content.

Local Weather Manuals (1994)

4.2.3.3 Prediction of surface dew points

(i) **Fig. 4.2** shows a tephigram construction for finding a representative daytime dew point from a night-time sounding.

(ii) The full line is the dry-bulb curve and the pecked line is the dew-point curve at dawn. The maximum surface dew point may be found by extrapolating down to the surface that part of the dew-point curve (DX) which has been unaffected by nocturnal cooling in the boundary layer. The dew point so obtained, A, is the maximum daytime value of the dew point. This will occur in the late morning when cumulus cloud first forms. The temperature T_{Cu}

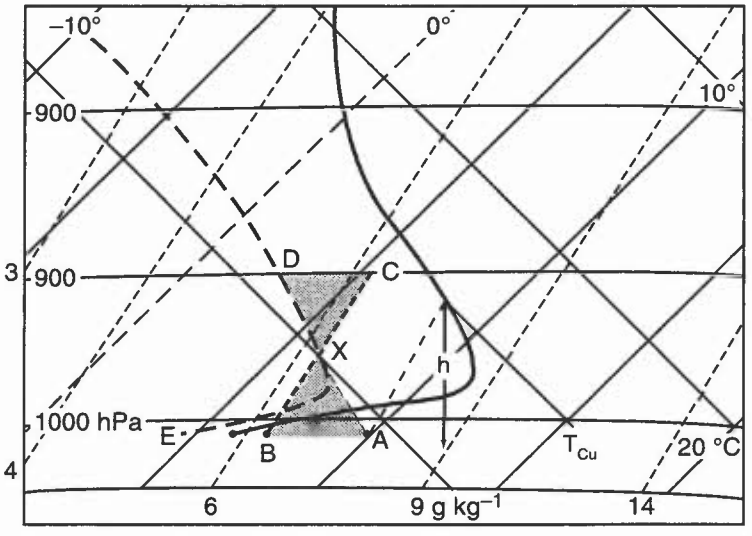

Figure 4.2. Tephigram construction for estimating a representative daytime value of the surface dew point, and temperature of first formation of cumulus. See text for method of use.

and height, h, at which the first Cu form is estimated by drawing up a constant HMR from A to the environment curve (for h) and then down to the surface along a DALR (for T_{Cu}).

(iii) With the onset of vigorous convection, at midday or soon after, the boundary layer develops an almost constant HMR. The afternoon value of the dew point (B) may be found by drawing a line of constant HMR (CXB) such that the total moisture content represented by the values along DX equals that represented by the values along XA. Since the HMR scale is not linear, DX should be slightly longer than XA. In practice it may be assumed that DX equals XA to a first approximation.

(iv) In this example it has been assumed that the mixed layer extends up to 900 hPa. In midsummer it may be necessary to raise this level to a point 150 hPa above the surface.

(v) On days with strong heating the reported dew points may show wide differences between adjacent inland stations by mid afternoon, especially if winds are light. Stations on or near the coast report much higher dew points when there is an influx of air from the sea.

4.3 Forecasting considerations

4.3.1 Synoptic-scale indicators of enhanced or suppressed convection

Note that two factors are sought — changing stability and a trigger mechanism. The forecast height of convective cloud tops suggested in **4.2.3** should be modified according to the synoptic-scale and mesoscale developments expected during the day. Such developments are, for example:

(a) Synoptic-scale ascent makes the air mass less stable. Thus, factors indicating an increased depth of convection are:
  (i) Approach of a trough, or low, in the 500, 300 or 200 hPa contour pattern (i.e. positive vorticity advection); convection decreasing rapidly after its passage.
  (ii) Advection of warm, moist, air at low levels.
  (iii) Advection of cold air at medium levels: the approach of a 1000–500 hPa thickness trough or ridge moving away.
  (iv) A trough, or increased cyclonic curvature, on the surface chart, or at time of maximum heating.
  (v) A convergence zone (e.g. due to a sea-breeze front, topography, or cold air drainage converging over a warmer sea surface, as in the Bristol Channel area).
  (vi) Over mountains in summer when the winds are light (4.6).
  (vii) Airflow over the sea across the isotherms towards warmer water.

(b) Synoptic-scale descent makes the air mass more stable. Thus, factors indicating a decreased depth of convection are:
  (i) Approach of a ridge in the 500, 300 or 200 hPa contour pattern (i.e. negative vorticity advection).
  (ii) Advection of dry air at low levels, tending to evaporate cloud.
  (iii) Advection of warm air at medium levels: 1000–500 hPa trough moving away or ridge approaching.
  (iv) Increasing anticyclonic curvature, or the approach of a ridge, on the surface chart. (Inversions will inhibit convection even if parcel stays to right of environment curve.)
  (v) Strong wind shear will often inhibit vertical extent of convection; however, marked shear is necessary for supercell storms.
  (vi) At the left entrance or right exit of a jet stream.
  (vii) Over valleys or lower ground surrounded by mountains when upper winds are light in summer.
  (viii) Airflow over the sea across the isotherms towards cooler water.

Note: continued convection will gradually stabilize the air due to the adiabatic warming by subsidence between the clouds, and transport upwards of latent heat from the surface (but not if synoptic-scale ascent is taking place).

Differential heating between wet and drier ground, or vegetation differences, can result in the development of mesoscale thermal gradients and corresponding circulations, and convergence zones.

Bader et al. (1995), Chapter 6

4.3.1.1 Summary of forecasting pointers — convective cloud

Decide which air mass will affect the station. Look at its history: did showers develop in it yesterday? If so:

Where? Over sea/coasts/hills/inland?
When? Throughout 24 hours or only at the time of maximum temperature?
At what temperature?
What factors since yesterday have changed the stability?
Heating/cooling from below — advection over warm sea, etc.
Warming/cooling aloft — warm or cold advection.
Increase/decrease in moisture content — by evaporation from a surface/advection of moister air aloft.
Wind direction change may have brought air with markedly different low-level characteristics into the local area, or may do so later in the day.

From representative ascents: what factors might release potential/latent instability?

Low-level convergence due to:
(i) Cyclonic curvature of isobars.
(ii) Along sea-breeze front or where two sea-breeze fronts meet.
(iii) Falling surface pressure.
(iv) Coastal convergence.

Forced mass ascent due to:
(i) Orographic uplift.
(ii) Divergence aloft — upper troughs, etc.
(iii) Along a front.
(iv) Intense surface heating — over a plateau.

HWF (1975), Chapter 19.7

4.3.2 Organization of shallow convection

4.3.2.1 Convection and waves (see 1.3.2.4 and 10.3.1.1)

Thermal activity can be modified by the gravity waves that have, in turn, been generated by the convective activity.

Down-wind patterns (streets)
If the depth of convection is limited by a stable layer and cloud streets form, the waves form parallel to the streets when the winds (usually constant in direction with moderate speed increasing slightly with height) blow across them.

Cross-wind patterns (waves)
If there is no change of wind direction with height and convection increases to 3 to 4 km, transverse waves may form at right angles to the cloud streets. Such waves are influenced by topography but can form even when strong convection extends far above any mountain summits.

Cumulus development will be enhanced in the ascent regions of the waves, and suppressed in the descent regions; the resulting cloud pattern is unlikely to be very well defined.

Booth (1980)
Bradbury (1990)
Ludlam (1980)

4.3.2.2 Sea breezes and other convergence zones (see 1.3.1.1 and 4.6)

4.3.2.3 Convection over the sea (see 10.3.1.2)

4.3.3 Forecasting thermals for glider flights

The best gliding conditions usually occur when the top of the convective layer is marked by an inversion between 5000 and 8000 ft, and thermals are marked by shallow Cu.

Thermal strengths are classified as nil, weak, moderate or strong as follows:

Table 4.1.

Thermal category	Max. rate of climb (kn)	(m s^{-1})	Cu bases at, or dry adiabatic conditions to (feet agl)
Nil	0	0	<2000
Weak	≤3	≤1.5	≥2000<3000
Moderate	>3≤6	>1.5≤3	≥3000<5000
Strong	>6	>3	≥5000

Mean rate of ascent will be less.

Fig. 4.3 illustrates maximum lift (a) in cloudless thermals, and (b) in cumulus clouds, the latter deduced from the tracking of free balloons by radar. Thermal activity begins to decrease about an hour after maximum surface temperature has been reached. After 1700 UTC thermals usually subside quickly; lift may still be found over towns and south-west facing slopes well into the evening.

An empirical method for estimating thermal strength, based on numerous French glider pilot reports, is illustrated in **Fig. 4.4.** The prediction requires an estimate of cloud base:

(i) Move horizontally across from an estimate of cloud base (e.g. 5500 ft) to one of the diagonal line labelled with the cloud amount (e.g. 1/8).
(ii) Follow line from intersection vertically to the Average Lift scale (e.g. 4.25 kn).
(iii) Continue down to intersect the diagonal lie and read off the Max Lift (e.g. 7 kn).

Summary: a prediction of 1/8 cloud at 5500 ft gives a forecast average lift of 4.25 kn, peaking at about 7 kn.

Lee waves enable gliding to high altitudes in the lee of quite moderate hills; vertical velocities are generally between 5 and 10 kn (2.5 to 5 m s^{-1}), exceptionally speeds >25 kn (12.5 m s^{-1}) and heights in excess of 30,000 ft have been recorded. Often associated with such systems, however, are flight hazards such as rotors and severe downslope winds (1.3.3.4). Waves above isolated cumulus, cumulus streets and waves, enhanced by cumulus over mountains, offer good opportunities, for example, for cross-country flights.

Local Weather Manual for Southern England (1994)

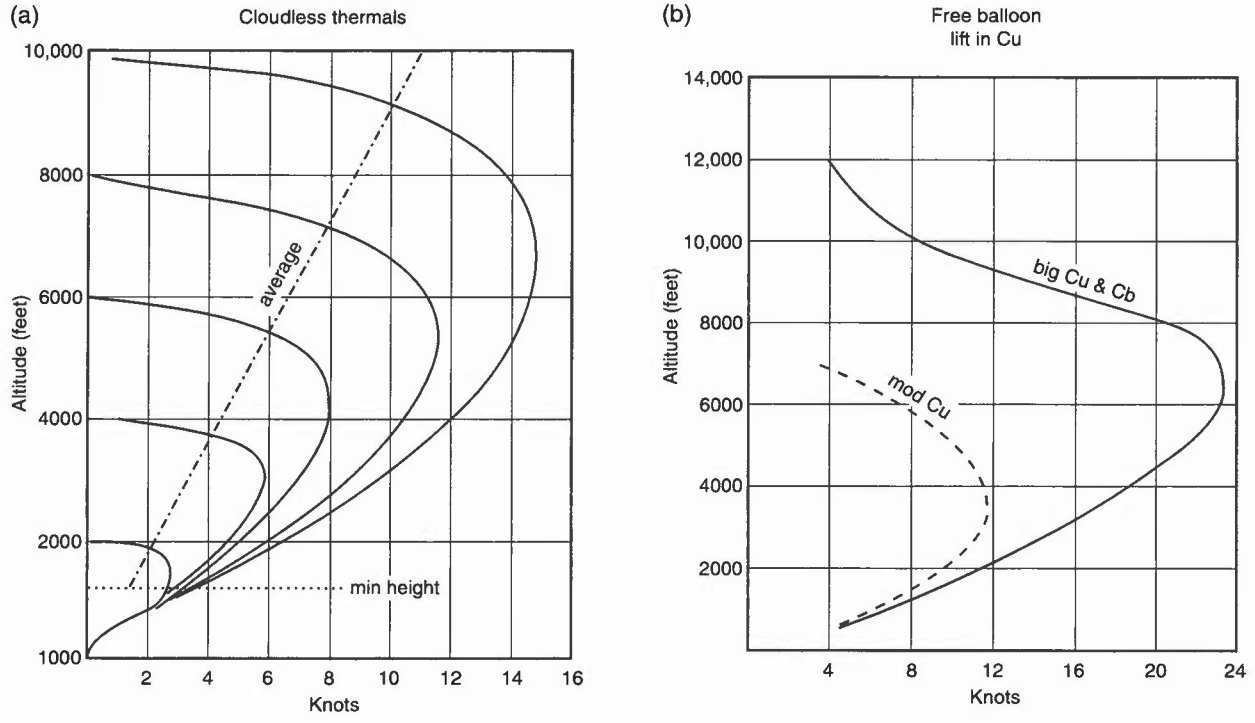

Figure 4.3. (a) Lift in cloudless thermals, and (b) lift in cumulus cloud.

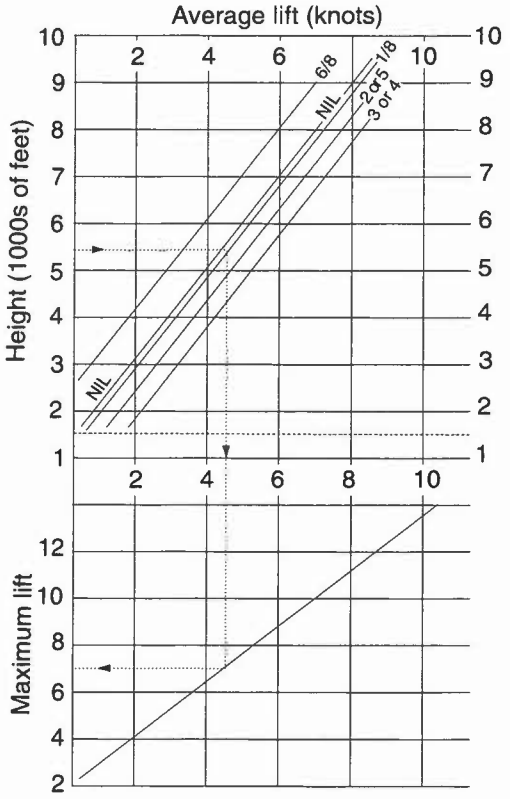

Figure 4.4. Empirically derived average and maximum thermal lift as a function of cloud base and cloud cover (see text for details).

4.3.3.1 Cross-country flights

Prediction diagrams of air trajectory, isobaric curvature, 850 hPa wind speed/direction, and potential temperature/dew-point depression data (due to Bradbury) may be 'scored' to assess long-distance prospects. **Table 4.2** summarizes favourable conditions over closed-circuit routes.

Table 4.2. Long cross-country flights over closed-circuit routes: favourable conditions

Previous air trajectory	From NW, N or NE (never from S).
Curvature of isobars	Anticyclonic.
Mean sea-level pressure	1023 hPa (±7 hPa).
850 hPa wind	Speed not more than 16 kn, direction between WNW and ENE through N.
Stability	Potential temperature decreasing about 3 °C between surface and 850 hPa at the time of maximum temperature. Depth of instability restricted to a stable layer below 700 hPa to prevent any shower activity.
Surface dew-point depression	11 to 18 °C by mid-afternoon.
Surface moisture and rainfall	State of ground dry at 06 UTC, no overnight rainfall.
Sunshine	At least 8 hours bright sunshine.
Visibility	More than 20 km.

Booth (1978)
Bradbury (1978, 1991a, 1991b)
Met O 6 Gliding Notes (1989)

4.4 The spreading out of cumulus into a layer of stratocumulus

4.4.1 Cloud cover beneath an inversion

When the depth of convection is limited by an inversion, cumulus tops may spread out to form an almost unbroken sheet which covers large areas and persists for long periods. This is common in subsided polar maritime air masses, particularly on the eastern flanks of anticyclones. **Fig. 4.5** illustrates an empirical method for estimating the cloud cover beneath an inversion. B is the condensation level, derived from the expected surface temperature, T, and dew point, T_d, BC is a saturated adiabat from cloud base to cloud top. DE is a dry adiabat from the base of the capping inversion, cutting BC at E.

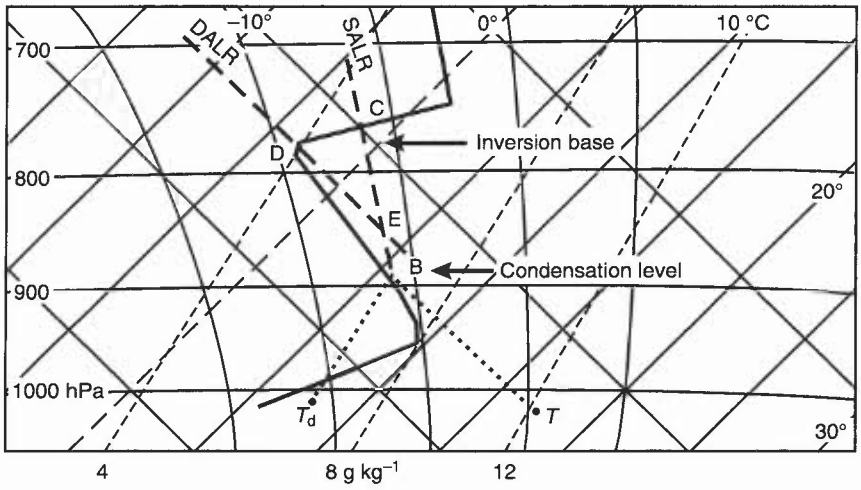

Figure 4.5. Estimating the spread out of cumulus cover beneath an inversion. See text for method of construction.

The expected cloud amount equals CE divided by CB, where the depths are conveniently measured in hectopascals and the answer is a fraction which can be expressed in terms of oktas.

4.4.2 Criteria for development of stratocumulus spread-out (see 5.8)

(i) An inversion or well-marked stable layer strong enough to halt all convective upcurrents even at the time of maximum insolation.
(ii) A lapse-rate close to the DALR from the surface to near the base of the inversion when convection starts.
(iii) Condensation level at least 2000 ft below the level of the inversion.
(iv) A dew-point depression of 5 °C or less in the layer between the condensation level and the base of the inversion.

4.4.3 Criteria for break-up of cloud sheet

(i) Decreasing surface dew points, lifting the condensation level to within 30 hPa of the inversion.
(ii) Increasing surface temperatures, sufficient to lift the condensation level to within 30 hPa of the inversion.
(iii) Continued subsidence, bringing the inversion down to within 30 hPa of the condensation level.
(iv) A weakening of the inversion, allowing cumulus tops to break through to a higher level.
(v) If the cloud layer is formed due to diurnal heating over land, nocturnal cooling usually results in the dispersal of the layer.
(vi) Cloud formed by convection over the sea shows no such diurnal variation.

HWF (1975)

4.5 Forecasting showers

4.5.1 Precipitation processes within continental and maritime clouds

(i) Concentrations of cloud condensation nuclei (CCN) decline over land by a factor of about five between the surface and 5 km while they remain fairly constant in maritime air where the average cloud droplet size is larger.
(ii) These factors have an important influence on precipitation development; precipitation may fall from a warm cloud of maritime origin with limited depth, due to the more efficient coalescence process with larger droplet size, while a similar cloud over land will not rain.
(iii) Air masses quickly acquire the CCN characteristics of the surface over which they are passing; for example, aerosol collected over the Irish Sea in a polar maritime north-westerly were found to be predominantly of a continental type.
(iv) Clouds with tops between 0 and −4 °C generally consist entirely of water drops; it is within this temperature range that the worst aircraft icing conditions are most likely.

4.5.2 Depth of cloud needed for showers

(i) The diagram at **Fig. 5.15** may be used as a rough guide to the intensity of both convective and non-convective precipitation, even though cloud-top temperature is not considered.
(ii) Showers are likely to be heavier in intensity than layer-cloud precipitation for the same thickness of cloud.

(iii) The diagram only applies if the difference in water content at the base and top of a shower cloud exceeds 1.5 g kg^{-1}.
(iv) Moderate Cu of maritime origin may give more precipitation than indicated.
(v) If the cloud depth is <5000 ft (1500 m) with cloud-top temperature warmer than −12 °C there is a 10% probability of showers; the figure rises to 90% for cloud depth >10,000 ft (3000 m). Exceptions to this rule are the 'drizzly' showers from warm maritime clouds and the shallow winter maritime/coastal showers common in northern areas in northerly polar flows with limited instability.
(vi) It is important that the top should certainly be <−4 °C, and generally <−10 °C, for any likelihood of showers by the Bergeron–Findeisen mechanism.

See 4.7.1.2 for guidance on the probability of thunderstorms related to the height of cumulonimbus tops.

Pettersen et al. (1945)

4.5.2.1 Cloud cover and lifetime

(i) Cover — if RH at cloud level is 50% suggest 2 oktas;
if 75% suggest 5 oktas.
(ii) Surface observations routinely give larger amounts of convective cloud than are seen from the air or satellite, since the gaps between distant Cu are obscured from the ground-based observer by adjacent Cu.

Table 4.3. Depths, updraughts and lifetimes of Cu and Cb

Cloud type	depth (ft)	updraught (m s^{-1})	lifetime
Small Cu	1500	1–5	20 min
Large Cu	6000–15,000	5–10	1 hour
Cb	15,000 upwards	10–20	>1 hour
Supercell Cb	15,000 upwards	>50	>>1hour

4.5.2.2 Intensities of showery precipitation (UK Met. Office definitions)

Table 4.4.

Rain showers	Intensity (mm h^{-1})
Slight	<2.0
Moderate	2.0 to 10.0
Heavy	10.0 to 50.0
Violent	>50.0

Meteorological Glossary (1991)
Observer's Handbook (1982)

4.5.3 Showers and wind shear

The wind shear in the cloudy convective layer is a useful key to the persistence of individual showers:

(i) *No change in wind speed or direction* — there is mutual interference between coincident updraughts and downdraughts. This occurs with shallow clouds. Showers are very light and last only a few minutes.
(ii) *Increasing wind speed but little change in direction with height* — the clouds slope forwards; thus downdraughts fall into the inflowing surface air, cutting off the updraughts and reducing the lifetime of the showers. This commonly occurs in maritime airstreams with moderately deep convection and light/moderate showers. Though each shower may have a life-span of 20–30 minutes, specific places are affected for a shorter time.
(iii) *Strong vertical wind shear* — usually associated with strong isobaric temperature gradients and an upper stable layer. Not compatible with showers (although intrinsic to severe storm development — see 4.7.7.2).

HWF (1975), Chapter 19.7.3.3 Ludlam (1980)

4.6 Topographically related convection

Satellite and radar imagery confirm that the distribution of convection is rarely random. Cloud bands and precipitation repeatedly occur in similar air masses relative to the same topographic features **(Figs 4.6 and 4.7** — radar data were not available for Scotland at the time). Forecasters may be familiar with other local patterns.
Topographically induced cloud forms as a result of:

(i) convection generated in unstable air over relatively warm surface;
(ii) thermally driven land or sea breeze;
(iii) frictional convergence induced by coasts (cloud bands giving intense showers inland can result from a winter airstream with a long fetch down the North Channel);
(iv) deflection of airstream by hills or headlands.

Isolating the particular cause may not be possible but satellite imagery may provide some clues, e.g. (i) and (ii) will be seasonal and diurnal, (iii) will depend on wind direction (10.3).

(a) Bands of enhanced convection (either in an otherwise cloud-free area or in an area of abundant showers) are most common in polar maritime air masses (wind directions between south-west and north).
(b) Location of convective band maxima for airstreams from four directions are shown in **Figs 4.8 and 4.9**; they provide a fairly comprehensive picture of favoured locations and downwind penetration for cloud.
(c) When winds exceed 20 kn on windward coasts, dominant cloud areas are over high ground; such strong winds also disrupt the summer cloud pattern, correlated with the coast line, because the sea breeze cannot become established (double-headed arrows indicate that bands occur within a range of wind directions; single-headed arrows denote where successive areas of activity follow similar paths).
(d) Note that shallow summer convection often produces a pattern of Cu clouds which imitates the shape of the topography, but is displaced by 10 to 20 n mile (18.5 to 37 km) downwind.
(e) When off-shore winds are light, sea breezes may develop, enhancing the Cu just inland from the coast and delaying the downwind drift of Cu.

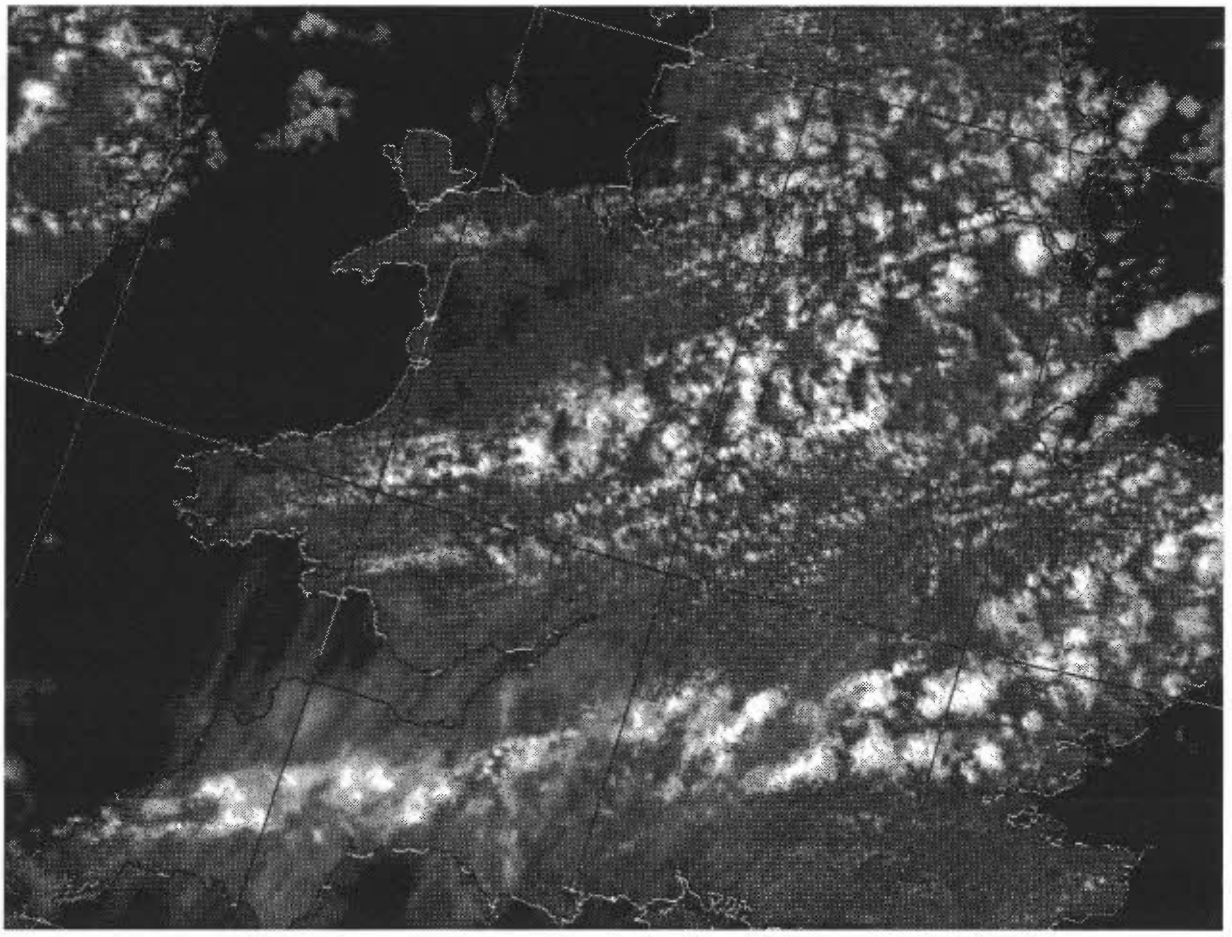

Figure 4.6. NOAA-9 visible image at 1406 UTC on 13 May 1986. (Photograph by courtesy of University of Dundee.)

(f) The approach allows a general forecast of 'sunny (or clear) periods and showers' to be more specific, with emphasis on the distribution of cloud and precipitation.
(g) Severe weather may develop if the steering level of convection lies along a convergence zone.

Bader et al. (1995), Chapter 6
Browning et al. (1985)
Hill (1983)
Monk (1987)
Orographic Processes (1993)

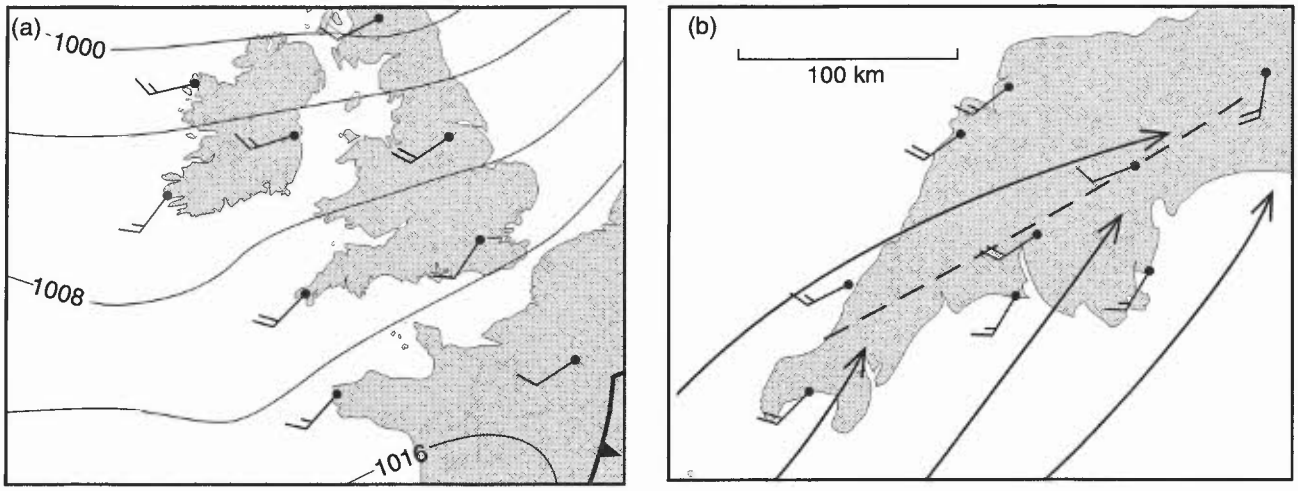

Figure 4.7. Surface analyses at 1400 UTC on 13 May 1986. (a) Isobaric analysis, and (b) available wind observations and streamlines over south-west England. The convergence line suggested by the cloud and precipitation is shown by the dashed line.

4.7 Forecasting cumulonimbus and thunderstorms

4.7.1 Main factors

At around −20 °C a significant proportion of cloud particles in an air parcel will be composed of ice crystals, giving the cloud boundary a fibrous appearance. This marks the transition of the cloud from large cumulus to cumulonimbus. The vertical wind structure will determine the lifetime and severity of the storm and whether it exists as a single cell or develops as a multicell storm.

4.7.1.1 Movement of thunderstorms: the steering level

With a cumulonimbus extending through a deep layer in which there is marked wind shear, the storm cloud is steered by the wind at the level approximately one third of its depth, measured from the base of the cloud, i.e.

$$H_{base} + 1/3\ (H_{top} - H_{base}).$$

In the United Kingdom, the steering level is often around 700 hPa. However, for a storm with a 5000 ft (1500 m) base and top at 40,000 ft (12,000 m) this gives a steering level of 16,600 ft (5000 m; 550 hPa).

Ludlam (1980)

4.7.1.2 Depth of cumulonimbus giving thunder

A useful guide is given by:

Table 4.5.

If cumulonimbus tops are at:	
<13,000 ft	— thunder unlikely
14,000–18,000 ft	— thunder probable
>18,000 ft	— thunder highly probable

A better guide may be: cloud-top temperature ≤ −18 °C.

HWF (1975), Chapter 19.7.5

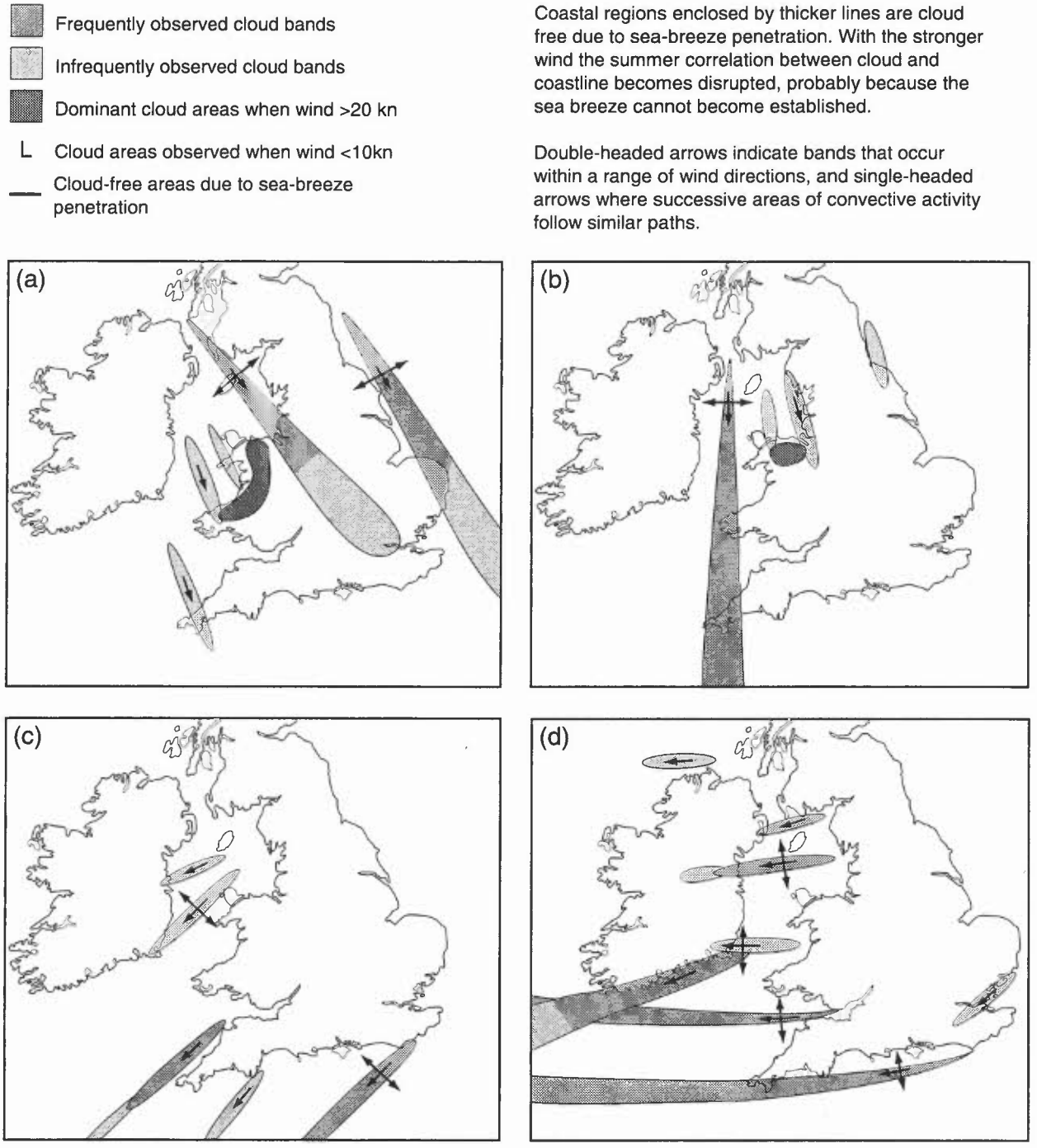

Figure 4.8. Winter convection generated due to air which is unstable to sea temperatures. (a) North-westerly airflow, (b) northerly airflow, (c) north-easterly airflow, and (d) easterly airflow.

4.7.2 Forecasting thunderstorms — instability indices

(a) *Boyden Index*

A measure of the instability below 700hPa is:

$$I = (Z - 200) - T$$

where Z = 1000–700 hPa thickness (dam); T = 700 hPa temperature (°C).

Thunder is probable if $I \geq 94/95$ (in the UK).

Forecasts should be made assuming that index isopleths move with the 700 hPa wind. A main advantage claimed for this method is its usefulness in mobile situations, regardless of whether fronts are involved. It should not be used in Mediterranean or tropical areas, or where the ground level is high.

Boyden (1966)

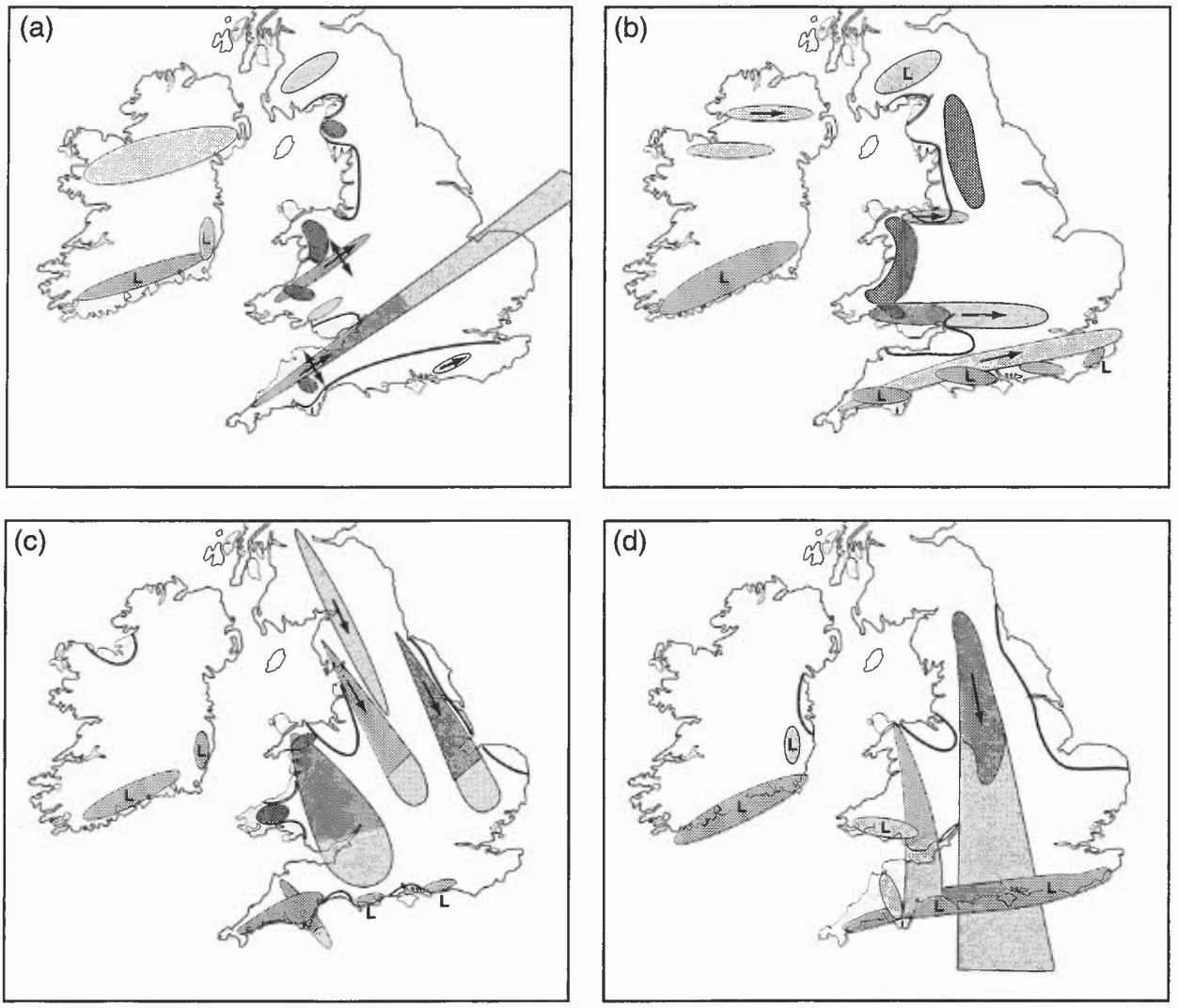

Figure 4.9. Summer convection generated due to air which is unstable to land temperatures. (a) South-westerly airflow, (b) westerly airflow, (c) north-westerly airflow, and (d) northerly airflow.

(b) *Rackliff Index*

The index is related to temperature as well as instability:

$$T = \theta_{w900} - T_{500}$$

where θ_{w900} is the 900 hPa wet-bulb potential temperature (°C); T_{500} is the 500 hPa temperature (°C).

In non-frontal situations significant showers accompanied by thunder are probable if $T \geq 29/30$ in the UK.

Rackliff (1962)

(c) *Modified Jefferson Index*

An amended form of Rackliff's index: values of that index for neutral stability air decrease almost linearly as WBPT increases. Jefferson's index gives an index independent of temperature (with same thunderstorm threshold value over a wide range of temperature). The formula was later amended to incorporate the 700 hPa dew-point depression to allow for middle-level humidity:

$$T_{mj} = 1.6\theta_{w900} - T_{500} - 0.5D_{700} - 8$$

where D_{700} = dew-point depression (°C) at 700 hPa.

Thunder is probable if T_{mj} = 27 to 28, in the United Kingdom although 26 to 27 is better in returning polar maritime air.

The formula can be reduced to $T_{mj} = \Delta T + X$ and computed more easily by using **Fig. 4.10,** where the value of $(-0.5D_{700} - 8)$ is replaced by the constant -11.

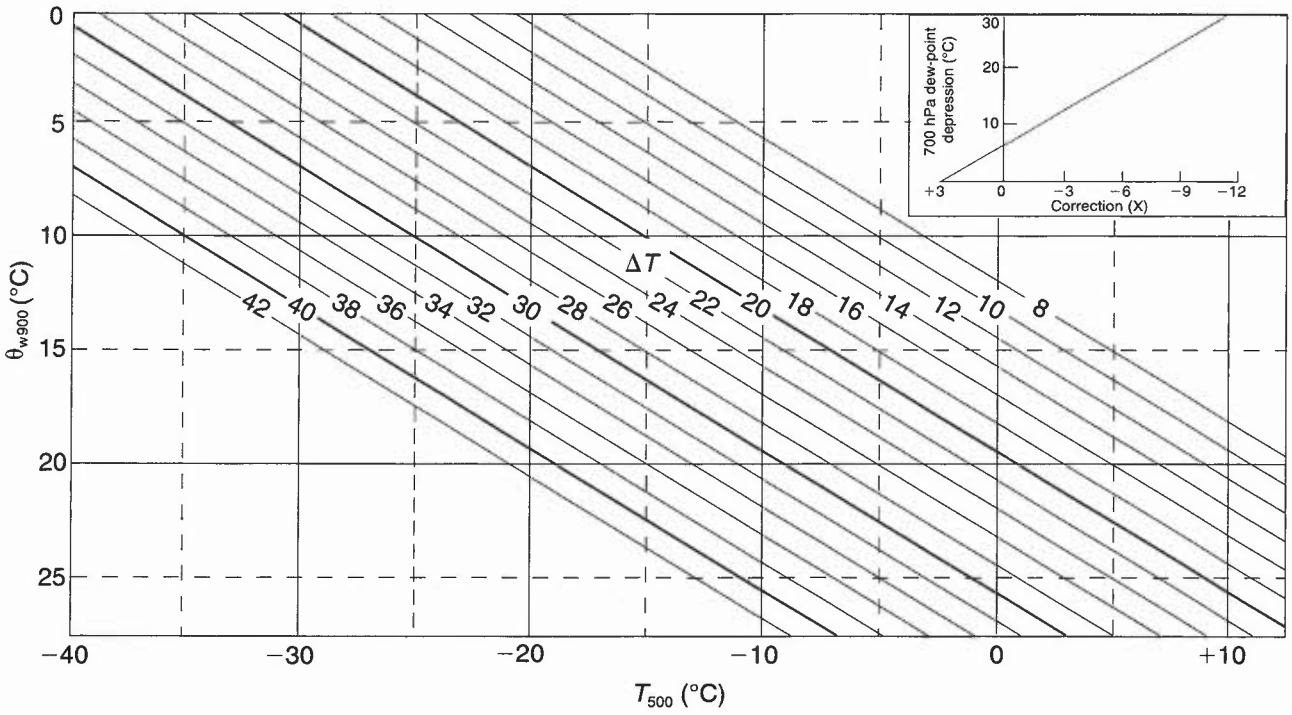

Figure 4.10. Computing the modified Jefferson Instability Index. See text for method of use.

(i) From the values of 500 hPa temperature (x-axis) and 900 hPa θ_w (y-axis), obtain a value of ΔT given by the sloping lines.

(ii) Correct this value of ΔT, according to the actual 700 hPa dew-point depression, using the small graph (top right) to obtain the correction X.

Jefferson (1963)

(d) *Potential instability index*

$P = \theta_{w500} - \theta_{w850}$

Thunder is possible if: P is ≤ -2 °C (summer)
P is $\leq +3$ °C (winter)

Bradbury (1977)

(e) *K index*

$K = (T_{850} - T_{500}) + T_{d850} - (T_{700} - T_{d700})$, where: T_{d850} is 850 hPa dew-point temperature etc.
Thunder possible for $K \geq 20$

George (1960)

4.7.2.1 Tests of different instability indices

Operationally indices offer only a guide to the degree of static instability at the time of a sounding. Other measures of convective development, such as radar and satellite imagery, as well as numerical weather prediction models, must provide supporting information.

Bradbury (1977)
Collier & Lilley (1994)

4.7.3 Hail

Deep and vigorous convection is required. The following criteria are a guide:

(i) Cumulonimbus tops are colder than −20 °C.

(ii) The 'parcel' path curve is warmer than the environment curve by 4 °C at some level (CV in **Fig. 4.1**) and gives cloud tops of 15,000 ft (4500 m) or more.

A similar method, based on the parcel curve, is:

(i) At the point where the curve reaches −20 °C measure the difference between this temperature and the environment temperature.

(ii) If this difference is:

≥5 °C	forecast hail;
from 5 °C to 2.5 °C	forecast soft hail or rain;
if difference ≤2.5 °C	forecast rain.

(large hail requires a 'steady state', but not necessarily slow-moving, storm).

In both methods vertical wind shear exists between the base and top of cumulonimbus.

Browning (1963) **Ludlam (1980)**

4.7.4 Lightning

Lightning occurs in vigorous convective cloud; ice particles and hail are considered to play a key role in charge generation and, indeed, the vast majority of lightning emanates from thunderstorms extending well above the freezing level. However, there are well documented UK observations of lightning discharges from all-water clouds.

4.7.4.1 Detection and forecasting

(i) Often it is a reliable assurance that lightning is not going to occur that is required.

(ii) The Arrival Time Difference (ATD) system can detect both ground and cloud-to-cloud lightning strokes.

(iii) The current system detects about one third of all strokes, being limited by computer processing speed and station locations; the low false-alarm rate allows the detection of smaller thunderstorms earlier.

Atkinson et al. (1989) **Ludlam (1980)**
Lee (1986) **Mason (1971)**

4.7.4.2 Static risk for towed targets

Many incidents of aerial-towed targets glowing and then disintegrating are due, apparently, to static discharge associated with the following conditions:

(i) preceding a fairly lengthy dry spell;

(ii) too dry below cloud (Cu or Ac cast) level for thunder forecast;

(iii) cloud structure exhibits convective instability, but of shallow extent;

(iv) cloud form suggests a history of significant vertical development;

(v) aircraft is usually operating below cloud which has supercooled water or ice crystals present near the base;

(vi) some weak precipitation is often observed, usually slight showers or virga.

Both conducting and non-conducting tow lines have been used at the Aberporth Test and Evaluation ranges, but the influence of the conducting nature of the tow line has yet to be determined.

Static risk is also reported for helicopters but associated weather criteria await evaluation.

Aberporth Met. Office (1993) **Rogers (1967)**

4.7.5 Gust fronts

(i) Air from well-developed downdraughts spread out as a cold density current; leading edge convergence and uplift in this 'gust front' are marked by wind vector changes of, commonly, 10 m s^{-1} over a few hundred metres, with temperature falls of several degrees and pressure rises of up to 4 hPa. Downdraught temperature can be estimated from Fawbush & Miller, **Fig. 6.4**.

(ii) On average the gust front extends to 5 km ahead of the precipitation area, and so is often the precursor of rain. It is a region of potential daughter cell development (4.7.7), and may possibly be identifiable in imagery by an arc-cloud formation.

Bader et. al (1995), Chapter 6.4.3

4.7.6 Squall lines

Associated with *thunderstorms* as follows:

(i) Lines of Cb may form into 'squall lines', typically 30 km wide and 200 km long.

(ii) As they advance, moving in the direction of the shear, the systems force high θ_w surface air to the level of free convection, where it joins the updraught, cooler air from aloft being brought down behind the system.

Associated with *cold active fronts* with rearward-sloping warm conveyor belt (7.1):

(i) Line convection, marked wind shift and sharp pressure changes indicate the likelihood of a squall.

(ii) The severity of the squall probably depends on:
Wind speed in the low-level jet ahead of the cold front.
Wind speeds in the medium-level layers near the frontal surface.

See also 6.2.2.3 — *Gust forecasting in strong wind situations.*

HWF (1975) Chapter 16
Ludlam (1980)

4.7.7 Single- and multi-cell development

4.7.7.1 Effect of vertical wind shear

(i) With *no shear,* the updraught and downdraught in a cumulonimbus are coincident. The precipitation falls through the updraught which is weakened by the drag of the falling precipitation, and the cloud quickly decays.

(ii) With *wind speeds varying with height but no directional shear,* the updraught is tilted and the precipitation falls down beside the updraught. The cloud persists longer than in a no-shear situation. Eventually the updraught may be cut off at the surface by the spreading out of the cold downdraught beneath the storm.

(iii) With *directional and speed shear*, some complex mesoscale storm systems may result. These may develop into self-generating steady-state systems, multi-cell storms, which can persist for many hours, quite independently of any surface heating.

4.7.7.2 Changing wind direction and speed with height

(i) Under conditions of directional and speed shear the storm-cloud motion vector is found within the triangle formed by the wind vectors LMH (**Fig. 4.11(a)**); the downdraught falls to one side of low-level inflow (**Fig. 4.11(b)**).

(ii) Successive daughter cells may be generated where the surface outflow from the downdraught meets the inflow. Very high precipitation totals may result if cells are continuously generated in the same position. The storm area moves to the right of the track of individual cells if the wind veers with height, the most common case (**Fig. 4.12**).

(iii) The arrival of this mesoscale convective complex (MCC) system is preceded by extensive anvils, visible on satellite imagery as vast, long-lived areas which hide the elongated squall line producing them.

4.7.7.3 MCC systems: characteristics

Whether the MCC is a 'forward' or 'backward' propagating system will depend on whether new developments occur downwind or upwind (respectively) of the existing MCC system relative to the mean tropospheric wind.

Table 4.6. Characteristic properties of MCC systems near the British Isles

Dimensions	overall ≈300 km, with embedded cells ≈50 km
Cloud-top temperature	<-30 °C over wide area, locally <-50 °C
Duration as an active system	≈12 hours

Bader et al. (1995) Chapter 6

4.7.7.4 Supercells

(a) A very small proportion of MCC systems will develop into 'supercells' that propagate continuously with highly organized internal circulation with low θ_w downdraught coexisting with the high θ_w updraught, forming a mini-frontal system.

(b) A distinguishing feature is that cell movement is in a different direction from winds at any particular level (i.e. the storm motion vector falls outside the triangle formed by the wind vectors LMH, **Fig. 4.11(a)**, possibly due to effects induced by the rotating of the cell.

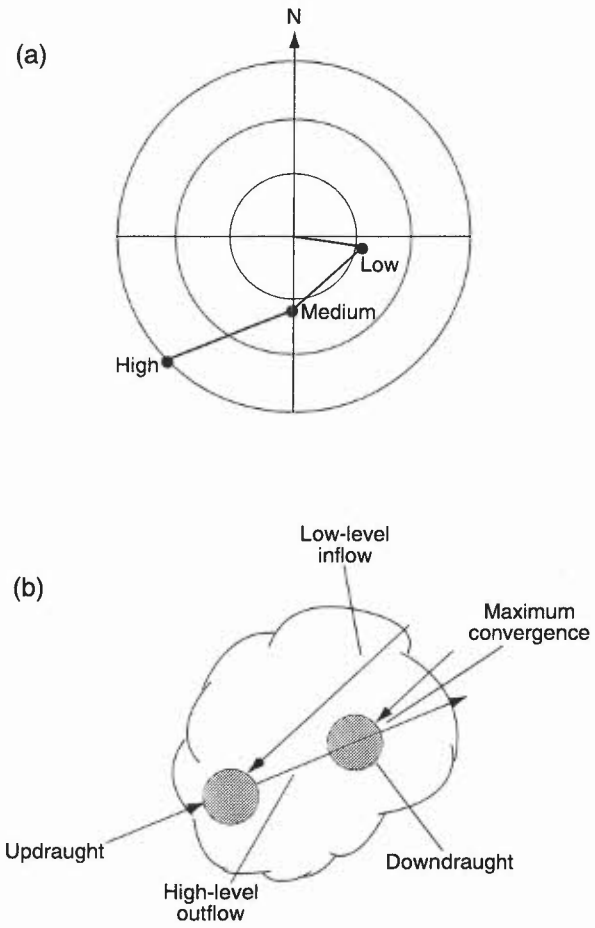

Figure 4.11. (a) Wind environment for multi-cell storm represented on a hodograph, and (b) configuration of updraughts and downdraughts from consideration of system-relative winds.

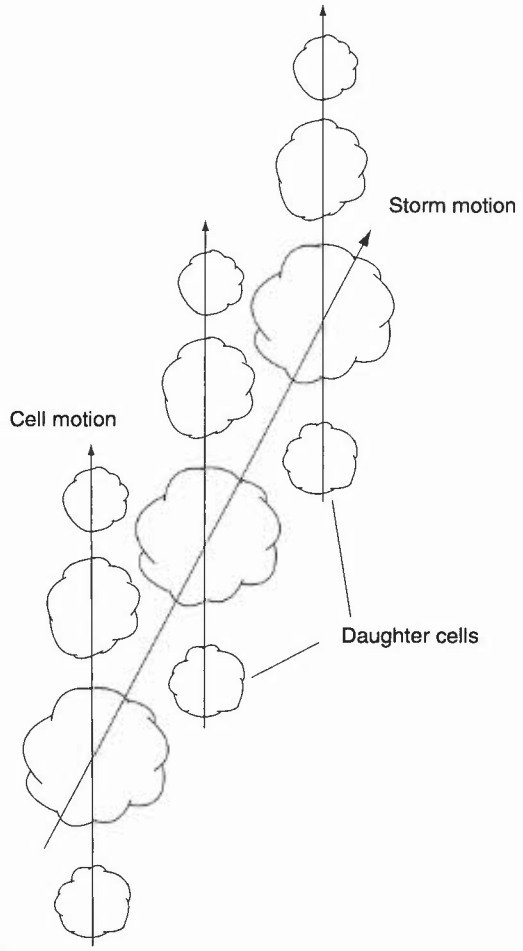

Figure 4.12. Multi-cell storm travelling to right of individual cells.

(c) The 'supercell' is responsible for the most severe summertime thunderstorms with localized flooding. Southern England is a favoured location with a low-level flow of warm, continental south-easterly winds overridden by cooler, oceanic south-westerlies aloft. In extreme cases with light winds storms may persist at a particular place for several hours with heavy rain and hail, although such storms are not common in the UK.

(d) Typical synoptic-scale environment for supercell storms:
- (i) Strong instability with parcel theory indicating >4 °C excess buoyancy at 500 hPa.
- (ii) Strong mean sub-cloud winds (order of 10 m s^{-1}).
- (iii) Strong environmental shear through cloud layer of 2.5 to 4.5 m s^{-1} per km (hence strong upper winds).
- (iv) Strong veer of wind with height.

Bader et al. (1995), Chapter 6
Browning & Ludlam (1962)
Ludlam (1980)

4.7.7.5 CAPE and development of severe storms

Severe storms may spawn 'daughter cells' to their north-east flank, due to convergence; the maximum area of convective activity (as tracked, for example, by radar) will move to the right of the individual cell motion, typically by 20 to 30° **(Fig. 4.12)**.

Development of severe storms depend on:
(i) Vertical wind shear through the depth of the convective layer ΔU **(Figs 4.11 and 4.13)**.
(ii) Large quantities of Convectively Available Potential Energy (CAPE), which can be released through convection. On a tephigram this energy is represented by the area between the environment curve and the path curve of a

rising parcel (ATUVWCB in **Fig. 4.1**). The severity of the storms depends on whether the CAPE is released by many small cumulonimbus clouds or by a few giant ones.

(iii) A measure of whether or not a storm will be single- or multi-cell is estimated from:
$R > 3$ — storms likely to be multi-celled;
$0.5 < R < 1$ — single cell likely,
where: R (the bulk Richardson number) $= \text{CAPE}/[0.5(\Delta U)^2]$, i.e a measure of the wind shear required to organize flow, against buoyancy forces tending to disrupt the flow.

Collier & Lilley (1994)
Galvin et al. (1995)
Ludlam (1980)

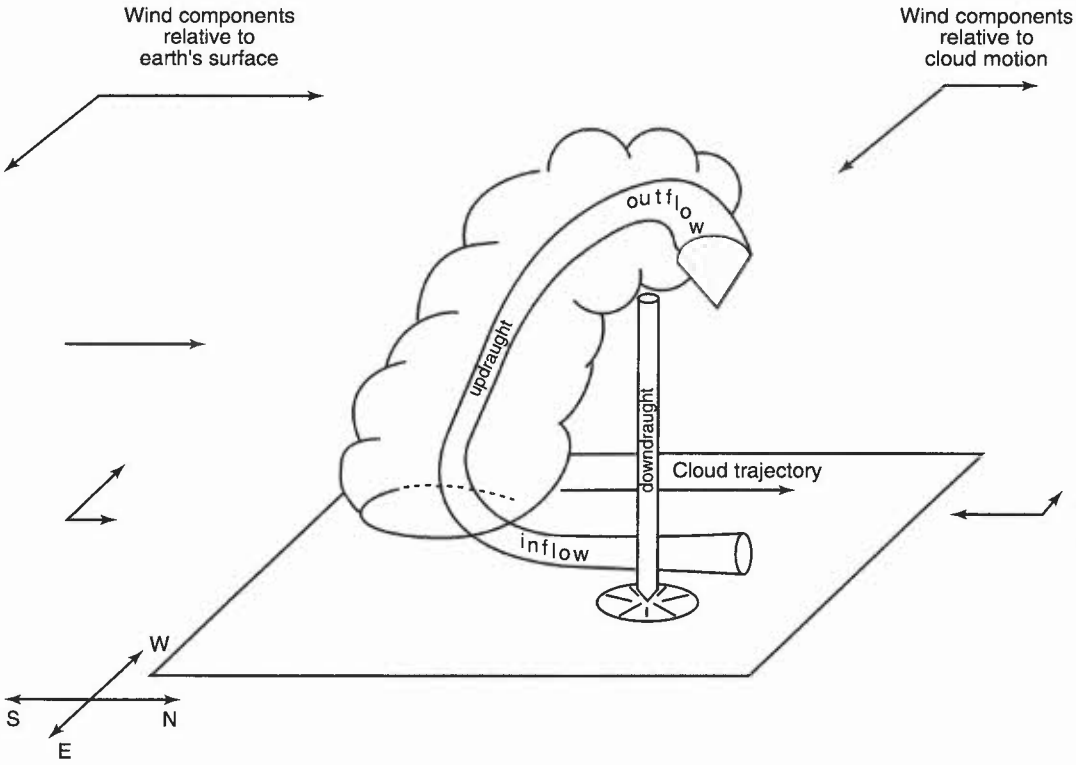

Figure 4.13. Cumulonimbus cloud in directional shear.

4.7.8 Forecasting thunderstorms — synoptic features

The objective forecasting techniques should not be used in isolation. Their value is greatly enhanced when they are used in conjunction with features which can be analysed on synoptic charts. Upper-air soundings alone do not always reveal the extent of the thunder risk, the soundings available before a thundery outbreak failing to show exceptional instability.

Consideration should be given to factors likely to release the energy available for convection, such as:

(i) The position and movement of upper-level troughs or lows. Thunderstorms are much more likely to break out along or ahead of an upper trough, or near an upper low.
(ii) The existence and movement of low-level convergence lines, such as surface fronts, or sea-breeze fronts.
(iii) Areas of high ground which may become very warm by day in the summer months.

Other useful synoptic tools are:

(iv) Dew-point analysis: the movement of a tongue of air with high dew points may help to define a thunder-threatened area.
(v) Charts of θ_w at 850 hPa: these serve a similar purpose as surface dew-point analyses.
(vi) Charts of the difference between θ_w at 500 and 850 hPa: these show where θ_w decreases with height over a significant depth of the atmosphere, and potential instability exists. Be on the lookout for $\theta_w \geq 18$ °C.
(vii) Cyclonic curvature of surface isobars: minor troughs are associated with convergence and enhanced convection.

4.7.8.1 *Conditions favouring severe thunderstorms*

This section is concerned only with the synoptic-scale setting in which the storms occur. Over Britain, severe storms are often associated with a cold front over, or close to, north-western parts with an attendant upper trough to the west. Under these conditions:

(i) Baroclinicity ensures a fairly strong south-west flow at upper levels.
(ii) At medium levels, air of Saharan origin passes over the Spanish plateau.
(iii) This air limits convective depth over south-west France and θ_w values attain as much as 24 °C there, leading to a heat low over France.
(iv) Overnight the low-level high θ_w air is advected northwards around the low, approaching southern England from the south or south-east next day.
(v) The warm, dry air of low θ_w (the 'Spanish Plume') has undergone mass ascent with its northward progression. It cools, moistens, sometimes producing bands of Ac castellanus and thundery outbreaks as it approaches the UK from across the Bay of Biscay.
(vi) By the time it reaches the UK the 'lid' produced by warming over the Spanish plateau has been removed; potential instability can then be realised.

A representation of synoptic-scale air flow associated with outbreaks of severe convection over southern Britain is shown in **Fig. 4.14**. Sometimes thunderstorms break out over northern France and advect northwards, becoming more organized and severe on encountering the stronger upper-level winds. Thunderstorms are most likely to break out within the tongue of highest θ_w air and where there is low-level convergence due to isobaric troughing or mesoscale effects such as sea-breezes.

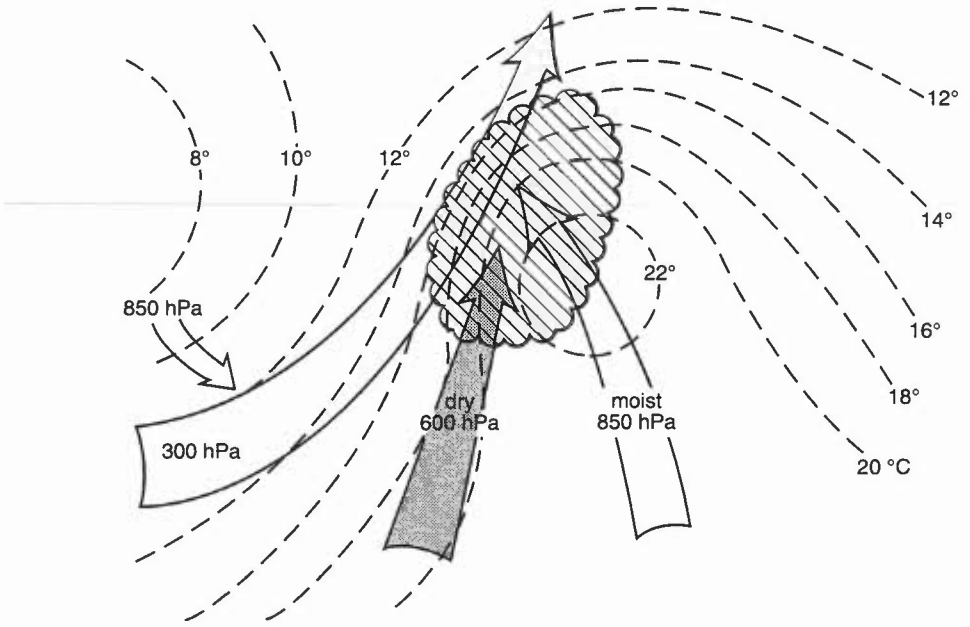

Figure 4.14. A schematic diagram of the three main synoptic-scale currents associated with the development of severe thunderstorms over southern England, together with typical isopleths of θ_w at 850 hPa. The hatched area indicates the the location of the storms.

Pointers to forecasting thunderstorms over southern England:

(i) *Upper-air soundings*
Some of the most severe and widespread outbreaks of thunder have occurred some 12–18 hours after a sounding showed a layer of warm air capping a shallow convective layer. This cap can prevent the early release of the convective energy, allowing it to build up with continued surface heating and be released explosively in one big storm later.

(ii) *Advection of low-level moisture*
Surface dew points should exceed 13 °C, but often reach 18 °C or more in severe storms over southern England. At 850 hPa, similar values of θ_w are experienced. The winds at this level are usually in the sector SE–SSW, with a speed of 20–30 kn, often in a narrow tongue.

(iii) *Medium-level advection of dry air*
With potential instability present, θ_w values at 500 hPa may be 2–5 °C lower than at 850 hPa. Winds at 500 hPa should be 20–40° veered from those at 850 hPa, with speeds of 35–50 kn.

(iv) *Upper-level strong winds*
Further veering above 500 hPa, with 300 hPa winds in the sector SSW–W and speeds 50–85 kn, are good conditions for positioning the downdraughts in the favoured position for generating severe storms.

(v) *Positive vorticity advection (PVA) at 500 and 300 hPa*
This usually occurs in the region in advance of an upper trough or upper low. Isopleths of vorticity cross the contour lines at an angle of 30° or more.

(vi) *'Dry lines'*
Mesoscale areas of dry air within an otherwise moist air mass, and the resulting production of strong horizontal moisture gradients (*dry lines*) by deformation in the air ahead of a (summer) cold front, may provide a preferred position for triggering intense thunderstorm activity in the already unstable air. Satellite, radar and model data should distinguish the deep, dry areas well before the outbreak.

Bader et al. (1995), Chapter 6
Grant (1995)
Ludlam (1980)
Morris (1986)
Scorer & Verkaik (1989)
Young (1995)

BIBLIOGRAPHY

CHAPTER 4 — CONVECTION AND SHOWERS

Aberporth Met. Office, 1993: Local Staff Instructions.

Atkinson,N.C, Blackburn, M.R. and Kitchen, M., 1989: Wide area lightning location using the UK Met. Office arrival time difference system. International Conference on Lightning and Static Electricity, University of Bath, 26/28 September 1989.

Bader, M.J., Forbes, G.S., Grant, J.R., Lilley, R.B.E. and Waters, J., 1995: Images in weather forecasting. Cambridge University Press.

Booth, B.J., 1978: On forecasting dry thermals for gliding. *Meteorol Mag*, **107**, 48–61.

Booth, B., 1980: Unusual wave flow over the Midlands. *Meteorol Mag*, **109**, 313–324.

Boyden, C.J., 1966: A simple Instability Index for use as a synoptic parameter. *Meteorol Mag*, **92**, 198–210.

Bradbury, T.A.M., 1977: The use of wet-bulb potential temperature charts. *Meteorol Mag*, **106**, 233–251.

Bradbury, T.A.M., 1978: Weather conditions for long glider flights over England. *Meteorol Mag*, **107**, 340–353.

Bradbury, T.A.M., 1990: Links between convection and waves. *Meteorol Mag,* **119**, 112–120.

Bradbury, T.A.M., 1991a: Thermal prediction from the tephigram. *Sailplane & Gliding*, **June/July**, 122–126.

Bradbury, T.A.M., 1991b: Meteorology and flight. A & C Black.

Browning, K.A., 1963: The growth of large hail within a steady updraught.*QJR Meteorol Soc*, **89**, 490–506.

Browning, K.A. and Ludlam, F.H., 1962: Airflow in convective storms. *QJR Meteorol Soc*, **88**, 117–135.

Browning, K.A., Eccleston, A.J. and Monk, G.A., 1985: The use of satellite and radar imagery to identify persistent shower bands downwind of the North Channel. *Meteorol Mag*, **114,** 325–331.

Collier, C.G. and Lilley R.B.E., 1994: Forecasting thunderstorm initiation in NW Europe using thermodynamic indices, satellite and radar data. *Meteorol Appl,* **1**, 75–84.

Galvin, J.F.P., Bennett, P.H. and Couchman, P.B., 1995: Two thunderstorms in summer 1994 at Birmingham. *Weather*, **50,** 239–250.

George, J.J, 1960: Weather forecasting for Aeronautics. Academic Press (K Index).

Grant, K., 1995: The British 'dry line' and its role in the genesis of severe local storms. *J Meteorol*, **20**, 241–259.

Hill, F.F., 1983: The use of average annual rainfall to derive estimates of orographic enhancement of frontal rainfall over England and Wales for different wind directions. *J Climatol*, **3**, 113–129

Jefferson, G.J., 1963: A further development of the Instability Index. *Meteorol Mag*, **92**, 313–316.

Lee, A.C.L., 1986: An operational system for the remote location of lightning flashes using a VLF arrival time difference technique. *J Atmos and Oceanic Technol*, **3**, 630–642.

Local Weather Manual for Southern England, 1994: Meteorological Office.

Ludlam, F.H., 1980: Clouds and storms. Pennsylvania State University Press.

MacIntosh, D.H. and Thom, A.S., 1972: Essentials of meteorology. London, Wykeham Pubs.

Mason, B.J, 1971: The physics of clouds (2nd edition). Clarendon Press, Oxford.

Met O 6, 1989: Notes on the preparation of gliding forecasts for RAF gliding schools. Meteorological Office (Met O 6), Unpublished.

Meteorological Glossary, 1991: London, HMSO.

Monk, G.A., 1987: Topographically-related convection over the British Isles. *In* Workshop on 'Satellite and Radar Imagery Interpretation' at the Meteorological Office College, Shinfield, Ed: M. Bader and A. Waters; pub: EUMETSAT.

Morris, R.M., 1986: The Spanish plume — testing the forecaster's nerve. *Meteorol Mag*, **115**, 349–357

Observer's Handbook, 1982: London, HMSO.

Orographic Processes in Meteorology (Pre-prints), 1993: Summer School, Meteorological Office College.

Pettersen, S., Knighting, E., Jones, R.W. and Herlofson, N., 1945: Convection in theory and practice. *Geofys Publ*, Oslo, **16**, No. 10.

Rackliff, P.G., 1962: Applications of an Instability Index to regional forecasting. *Meteorol Mag*, **91**, 113–120.

Rogers, M.E., 1967: Interim report reviewing the present position on helicopter static electrification. RAE Technical Report 67292.

Scorer, R.S. and Verkaik, A., 1989: Spacious skies. David and Charles.

Young, M.V., 1995: Severe thunderstorms over south-east England on 24 June 1994: A forecasting perspective. *Weather*, **50,** 250–256.

CHAPTER 5 — LAYER CLOUDS AND PRECIPITATION

CHAPTER 5 — LAYER CLOUDS AND PRECIPITATION

5.1 Layer cloud formation

Low stratus forms when air with a lapse rate less than the SALR is either cooled below its dew point or has extra moisture added by the evaporation of falling precipitation or by evaporation from wet surfaces, especially when snow or heavy frost begins to thaw.

Much information on the relation of stratus to local wind direction is available in *Aerodrome Weather Diagrams and Characteristics* (extracts in Local Weather Manuals).

AWDC (1960)
Mansfield (1988)

5.2 Large-scale ascent

5.2.1 Frontal cloud

Gentle ascent will often produce layer clouds throughout an extensive tropospheric depth; the following are forecasting techniques for short and longer term:

(a) Short term:
  (i) Tephigram analysis — **Table 5.1** may give an indication of cloud structure; high cloud may obscure lower cloud on satellite imagery; a general sense of cloud structure may be inferred from radar rainfall.
  (ii) Advection — apply gradient wind component normal to front; actual/forecast winds at cloud level; speed of warm/cold advection from hodograph.
  (iii) Development — refer to pressure tendencies; frontal waves; upper-air development; local effects.

(b) Longer term — beyond 12 hours:
  (i) Model output to position systems and indicate their likely activity.
  (ii) Conceptual models (7.1) and local knowledge to estimate likely cloud structure.

Table 5.1. Cloud structure from a tephigram

The following guidelines should give a reasonable assessment of the likely cloud structure from dew-point depressions on a representative tephigram.

Dry bulb >0 °C	
$(T - T_d) \leq 1$ °C	8/8 layer
$(T - T_d)$ 1 to 5 °C	Thin layers
$(T - T_d) > 5$ °C	No cloud
Dry bulb <0 °C	
$(T - T_d) < 3$ °C	8/8 layer
$(T - T_d)$ 3 to 5 °C	Thick layers
$(T - T_d)$ 6 to 10 °C	Thin layers
$(T - T_d) > 10$ °C	No cloud

5.2.2 Cloud formed in precipitation

(a) In rain:
  (i) Evaporation of precipitation can cool the air to its wet-bulb temperature. A temperature close to the wet-bulb value is reached after about half an hour of very heavy rain or 1–2 hours of moderate rain and results in ragged stratus *pannus*. A rough guide to the base of the stratus *pannus* is:
    2 hours continuous rain — base 800 feet (245 m).
    3 hours continuous rain — base 400 feet (120 m) (no account taken of upslope or advective effects).
  (ii) Prolonged drizzle and light winds frequently lead to the formation of very low stratus even when upslope motion is apparently negligible.

Advection of warm air across lying/thawing snow often results in stratus forming at or very near the surface.

(b) In snow:
  (i) Melting of falling snow into warm sub-cloud layer will produce an isothermal (along 0 °C isotherm) 600 feet deep after 1 hour, increasing to a maximum of 1200 feet after 4 hours.
  (ii) Extension of the 0 °C isotherm results in a DALR between cooled and unmodified air; at saturation instability causes fractocumulus of a few hundred feet thickness to form near the 0 °C isotherm below cloud base. The modified temperature profile is illustrated in **Fig. 5.1**; the surface temperature will fall as a result of the cooling.
  (iii) If snow reaches the ground, *pannus* forms at or very near the ground.

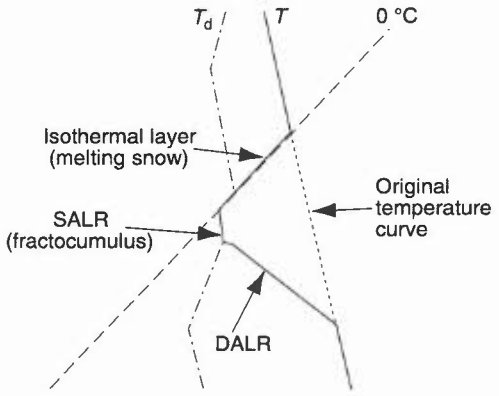

Figure 5.1. Schematic temperature profile produced by melting snow.

5.2.3 Non-frontal medium and high cloud

Most medium and high cloud is associated with mass ascent but may also occur in regions where instability is limited by a capping stable layer. Non-frontal cloud is hard to predict, especially when occurring in thin layers; it is often associated with medium- or upper-level instability or wind shear.

The following may be of help in forecasting its occurrence:
(a) Use of satellite imagery, especially IR (see 10.3.4 and 10.3.5).
(b) Use actual or forecast ascents: $(T - T_d) < 10$ °C, with:
  (i) wind increasing strongly with height;
  (ii) conditional or potential instability at medium/high levels.
(c) Use model cloud or RH fields.
(d) Favourable areas for cloud are:
  (i) cold pools or sharp thickness troughs;
  (ii) on warm side of jet;
  (iii) on, or just to rear of, a sharp upper ridge.
(e) Relate cirrus tops to tropopause (5.2.4.1):
  (i) low tropopause (<30,000 ft, 9 km) — Ci extends to tropopause;
  (ii) high tropopause (>35,000 ft, 10.7 km) — Ci tops a few thousand feet below tropopause.

HWF (1975), Chapter 19.5

5.2.4 Cirrus forecasting

James' technique requires scores to be allotted to a series of questions:
(a) 6–12 hours ahead:
  (i) Is forecast in area of, or just to rear of, an upper ridge?
  (ii) Is forecast area on the anticyclonic side of a 200 hPa jet stream and within 500 km of the jet axis?
  (iii) Is the forecast area within 500 km ahead of a surface warm front or occlusion?

  Score: 0, 0.5 or 1 for 'no', 'uncertain', or 'yes'.
  On adding scores, cirrus amounts are roughly as follows (**Table 5.2**):

Table 5.2.

Total score	0	0.5	1	1.5	2	2.5	3
Amount (oktas)	0	1	2	3	4	5	6–7

(b) 24–36 hours ahead:
- (i) Is the air likely to be moist? — Is the dew-point depression ≤10 °C at or above 500 hPa?
- (ii) Will area be up to 300 miles (480 km) ahead of a surface warm front or occlusion?
- (iii) Will area be on anticyclonic side of a 300 hPa jet and within 300 miles (480 km) of the jet axis?
- (iv) Will area be in, or just to the rear of, a 300 hPa ridge?
- (v) Will area be in a thermal ridge as suggested by the 1000–500 hPa thickness chart?
- (vi) Will the 300 hPa wind over the area be veered from that at 500 hPa by 20° or more?

If two or more affirmative answers are made, cirrus should be forecast 4/8 to 8/8; if not, forecast NIL to 3/8.

James (1957)

5.2.4.1 Tops and bases of cirrus

(i) 50% of all cirrus is likely to be within 5000 ft (1500 m) of the tropopause.

(ii) Thickness is likely to fall within the three ranges: 0–2000 ft, 2000–4000 ft or 4000–6000 ft (0–600, 600–1200 or 1200–1800 m) on roughly an equal number of occasions.

(iii) Mean tops reach the tropopause for tropopause heights up to about 30,000 ft (9 km), becoming relatively lower, until at 39,000 ft (12 km) they are some 4000 ft (1200 m) below the tropopause.

(iv) Mean bases tend to be about 1200 m below the tropopause up to 9 km; at higher levels mean base seems to be in the region of 9 km.

(v) Occurrence of cirrus is favoured in a layer through which wind speed increases rapidly with height **(Fig. 5.2)**.

HWF (1975), Chapter 19.6.4.2

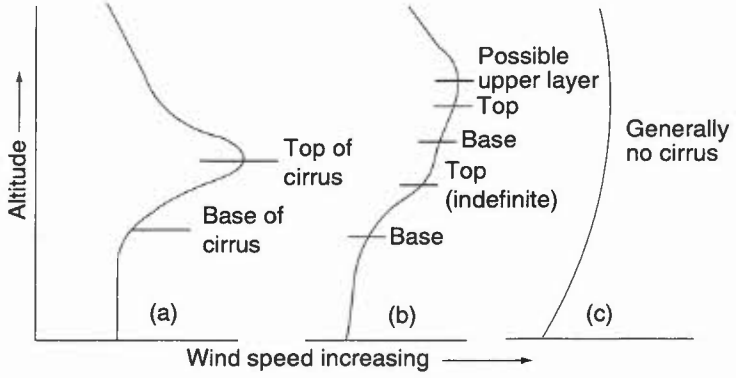

Figure 5.2. Association between cirrus levels and profiles of wind speed.

5.3 Condensation trails

(i) The condensation of water vapour from the exhaust of any aircraft engine can produce long and persistent trails (contrails), the formation and persistence depending on factors such as the ambient air temperature, RH and the amount of exhaust moisture from combusting fuel (see 10.3.5.1).

(ii) The MINTRA line printed on tephigrams gives the critical temperatures for old piston-engined aircraft, based on condensation with respect to ice.

(iii) The continuing usefulness of this line lies in the fact that it represents the limiting temperature above which contrails are unlikely to be formed by any aircraft. In practice, contrails do not normally appear until the ambient temperature is several degrees lower than the printed MINTRA value.

(iv) Recent work by USAF and UK workers has resulted in updated nomograms for the modern turbofan engine, which has a significantly different moisture and heat output.

HAM (1994)

5.3.1 Forecasting contrails

(a) *Using corrections to the MINTRA value*
On a tephigram, draw two lines that are, respectively, 11° and 14 °C colder than the MINTRA critical temperature (T_C) at any level. Plot a representative upper-air sounding. If the air temperature at any level is T, then:

Table 5.3.

		Forecast
If	$T>(T_C - 11)$	contrails unlikely
	$(T_C - 11)>T>(T_C - 14)$	short, non-persistent trails likely
	$T<(T_C - 14)$	long, persistent trails likely

Persistent trails are likely with high humidity and are common when aircraft fly near existing layers of cirriform cloud. Updated corrections show that contrails may form at temperatures warmer than T_C-11 (**Fig. 5.3**); for a dry environment, contrails may not form until significantly cooler. Thus at 200 hPa, with an environmental dew-point depression of 2 °C and a modern, high-bypass engine, trails may be expected at temperatures as warm as T_C-9. With a dew-point depression of 10 °C and a low-bypass engine, trails are not expected until the temperature is less than T_C-13. (Fighters and air-to-air transport refuelling aircraft are examples of the respective engine categories.) If conditions are suitable for contrail formation, then the contrails would be expected to persist for a significant time.

(b) *Graphical method*
Fig. 5.3(a) (after Appleman), includes the effect environmental dew-point depression. Five lines are drawn to show the critical temperature for jet aircraft at different values of dew-point depression. Contrails should always form if the temperature lies to the left of relevant dew-point depression line. No trails are to be expected if the temperature lies to the right of the 0 °C dew-point depression line.

5.3.2 Revised rules for modern engines

Contrail forecasting rules have been revised for two turbofan engine categories (low- and high-bypass) and their associated moisture output and heating; nomograms are illustrated in **Figs 5.3(b) and (c).**

Appleman (1953)
Ferris (1996)
HAM (1994)

5.4 Orographic uplift

5.4.1 Upslope stratus

Factors favourable for development are:
(i) stable atmosphere;
(ii) air near to saturation at lowest levels;
(iii) sloping terrain for the given wind direction;
(iv) moderate wind.

Note that where turbulent mixing maintains extensive low stratus over low-lying terrain, base will be at the mixing condensation level (MCL) (**Fig. 5.4**); the base on windward slopes is often lower (lifting condensation level, LCL, **Section 4.2**). Also the Föhn effect in precipitation (**Fig. 5.5**) will give a higher base or smaller cloud amount on the lee side (1.3.3.6).

To determine stratus base:
(i) From selected representative sounding modify temperature and moisture profiles near ground to fit local values.
(ii) Find LCL for a series of levels near the surface (**Fig. 5.6**).
(iii) Upslope base is given by lowest LCL.

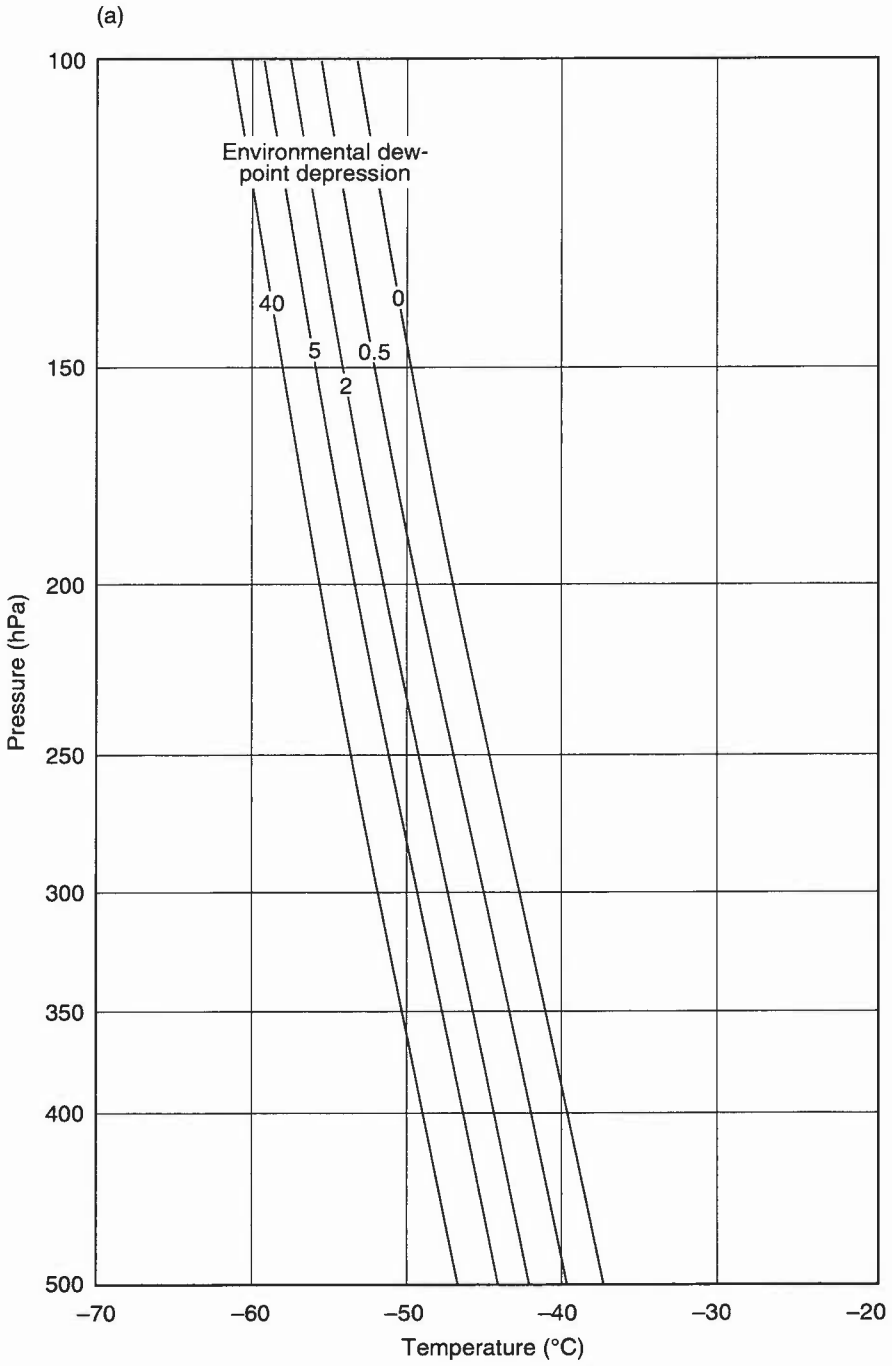

Figure 5.3. (a) The Appleman contrail forecast nomogram.

5.4.2 Orographic clouds

Cap, lenticular, rotor and banner clouds are discussed in 1.3.3 and 10.3.2.

Browning (1975) **Smith (1989)**

5.5 Turbulent mixing

(i) Turbulence tends to establish DALR and constant HMR profiles; RH increases with height, with any cloud base being at the mixing condensation level (MCL) of the layer.

(ii) To assess the MCL requires knowledge of the mixing layer depth, *d*, comparatively easy if top is marked by a sharp inversion. If this is not the case, there are several empirical techniques available, for example:

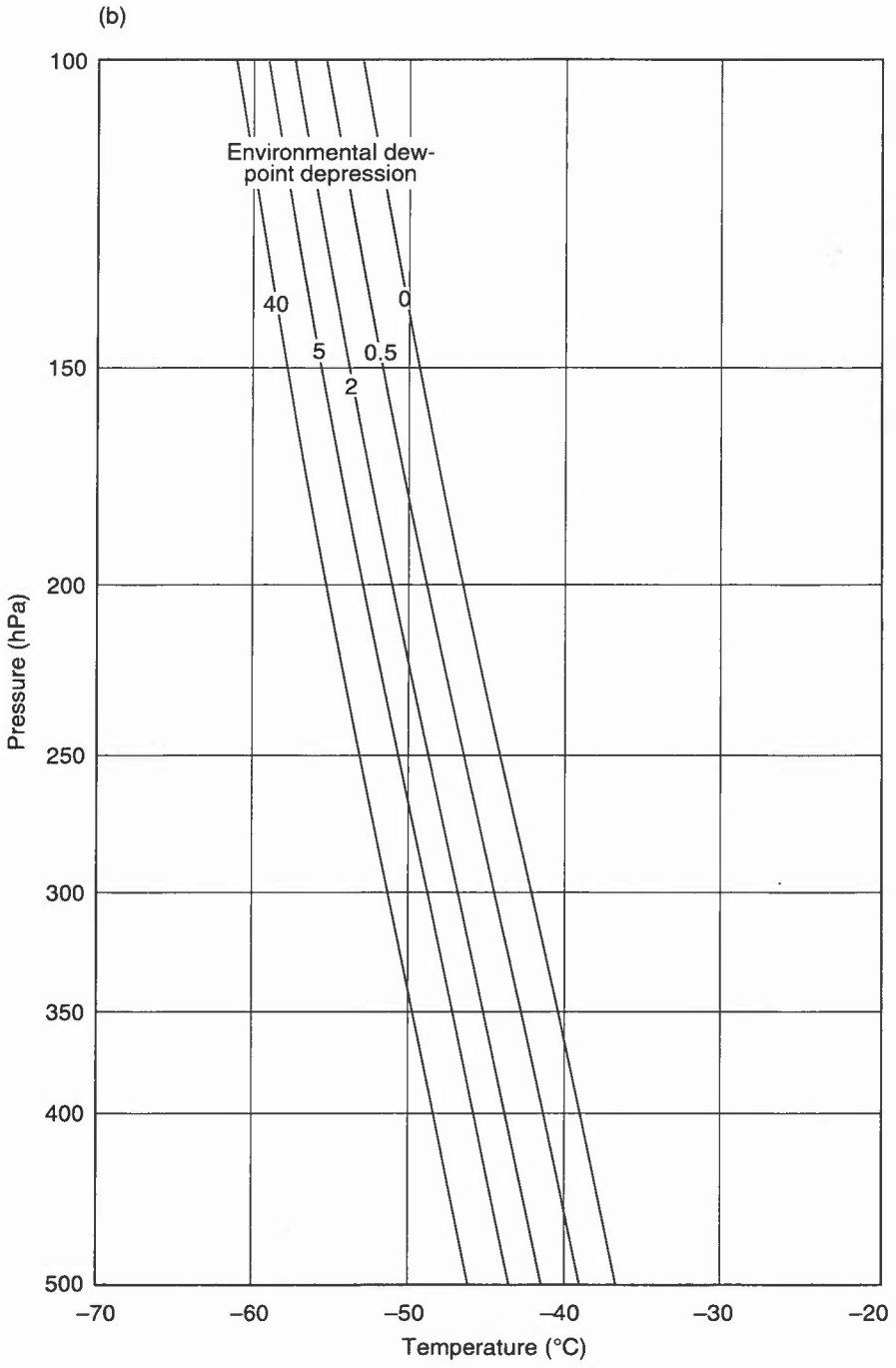

Figure 5.3. (b) low-bypass engine contrail algorithm.

for surface wind, $V_S \leq 16$ kn, $d = 200\ V_S$ feet;
for surface wind, $V_S \geq 16$ kn, $d = 3300$ to 3600 feet by night
$d = 4000$ feet by day.

(iii) In view of difficulty in deriving the MCL, locally derived empirical methods may prove more satisfactory.

HWF (1975), Chapter 19

5.5.1 Air-mass stratus

Cooling and turbulent mixing act to lower the boundary layer temperature, with stratus forming below the inversion (**Fig. 5.7**) (see 10.3.3). Three principal regimes identified for the cooling of a turbulent boundary layer below its dew point are illustrated in **Fig. 5.8.** They are:

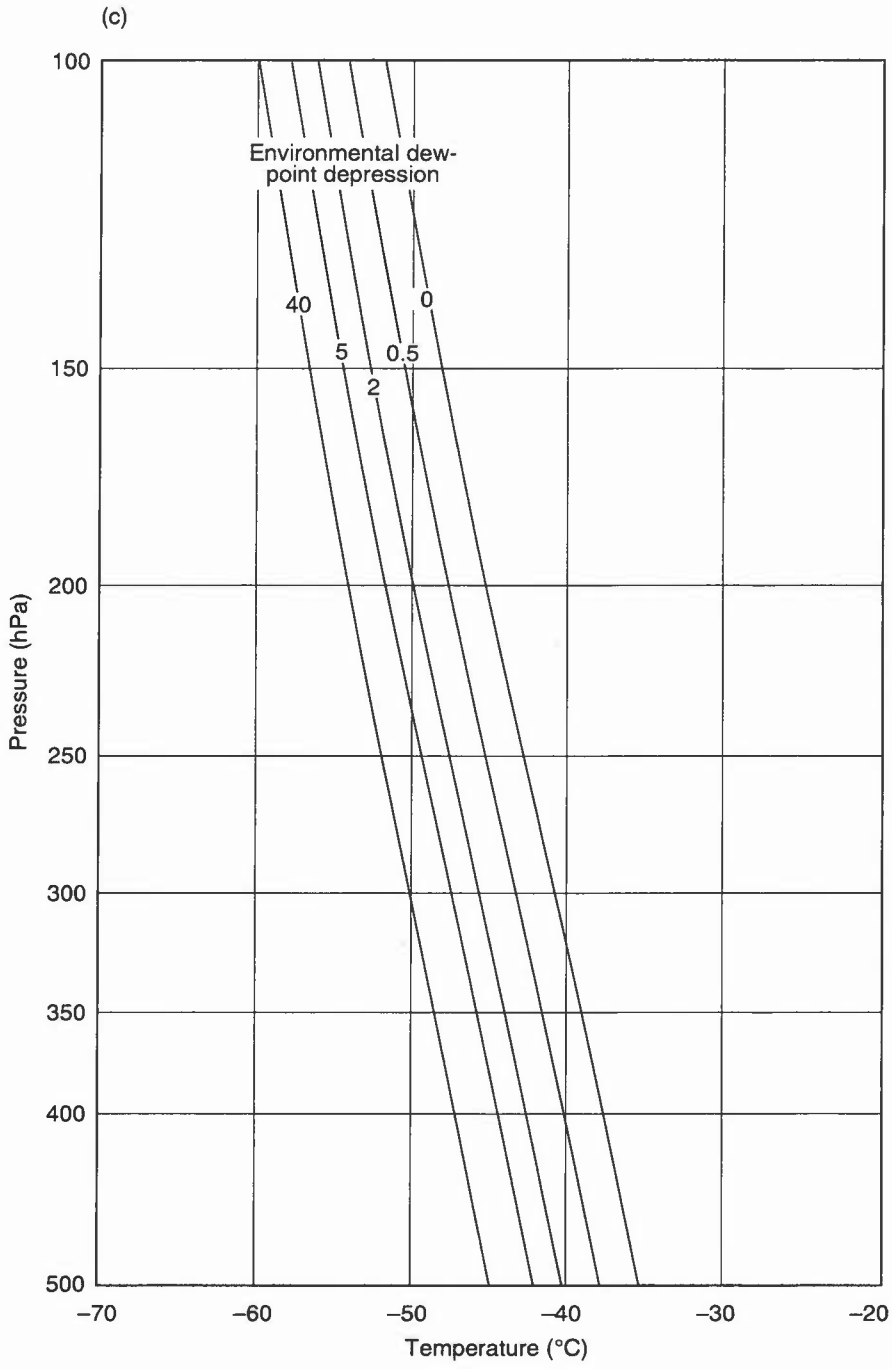

Figure 5.3. (c) high-bypass engine contrail algorithm.

In Fig. 5.8

(**a**) Moist south-westerlies giving widespread stratus around southern and western coasts, and sometimes sea fog. In autumn and winter inland penetration can give rise to widespread and persistent cover over southern England.

(**b**) Cold easterlies: in spring and summer relatively warm air advected from the east may be cooled sufficiently by cold sea passage to form stratus on the east coasts of England and Scotland; frequently a problem for airfields in eastern districts.

(**c**) Winter south-easterly; cloud most likely to form overnight, or when snow is lying. Airfields situated on ground sloping down to the south-east are particularly prone.

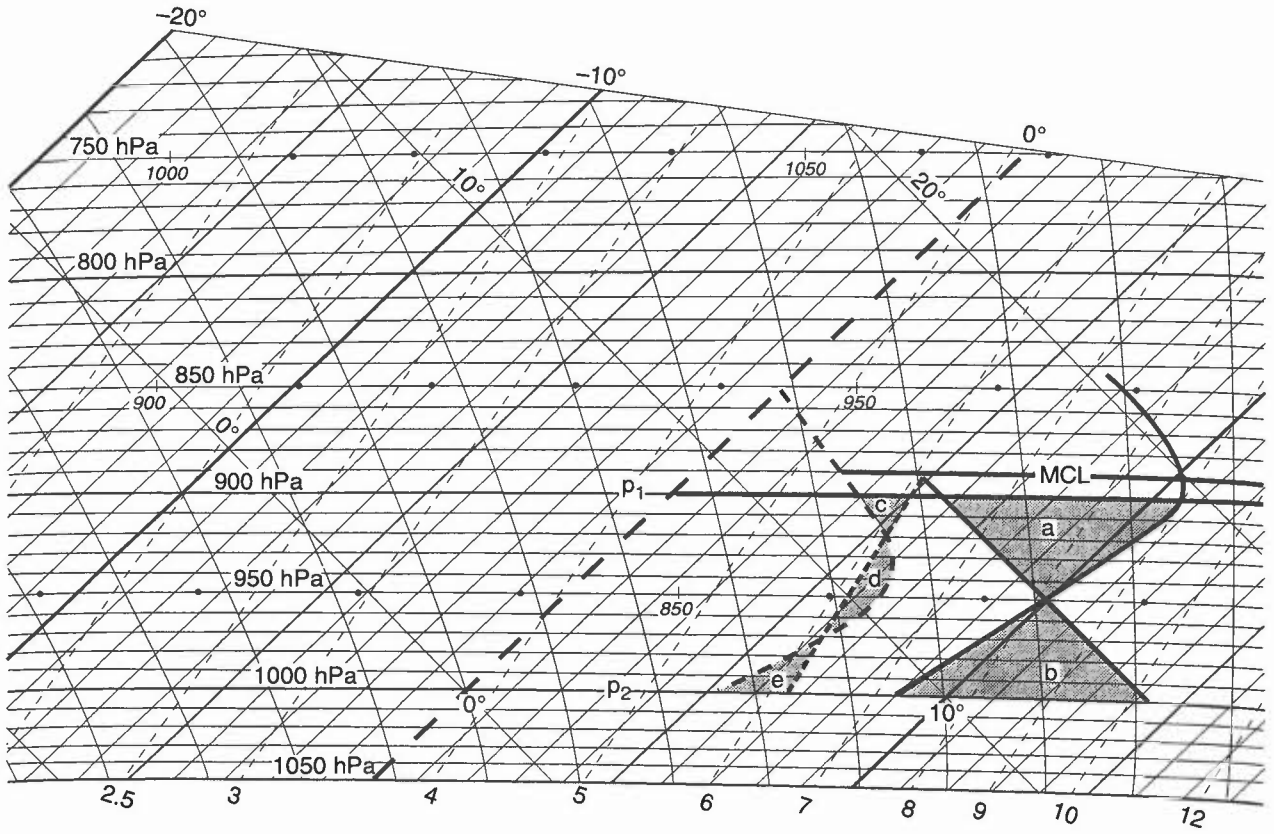

Figure 5.4. Mixing condensation level (MCL) for a layer is found by determining the level at which average HMR and θ_w lines for the layer intersect. The averages are determined by equalizing areas as indicated (area a = b, areas c and e = d).

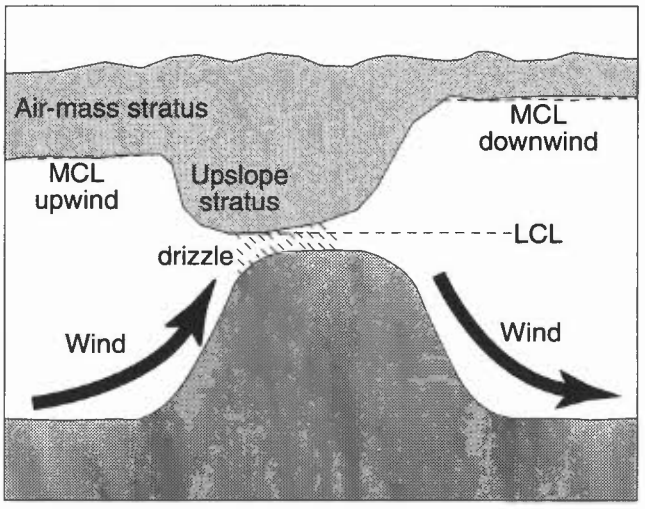

Figure 5.5. The variation of stratus base in response to upslope motion and the Föhn effect.

5.6 Stratus forecasting techniques

5.6.1 Formation of low stratus

To predict the formation of stratus, the following data are needed:

(i) vertical temperature and dew-point profiles of the air mass expected;
(ii) sea temperature (if flow is from over the sea);
(iii) predicted wind field;
(iv) predicted amount and depth of nocturnal cooling overland;
(v) knowledge of the topography.

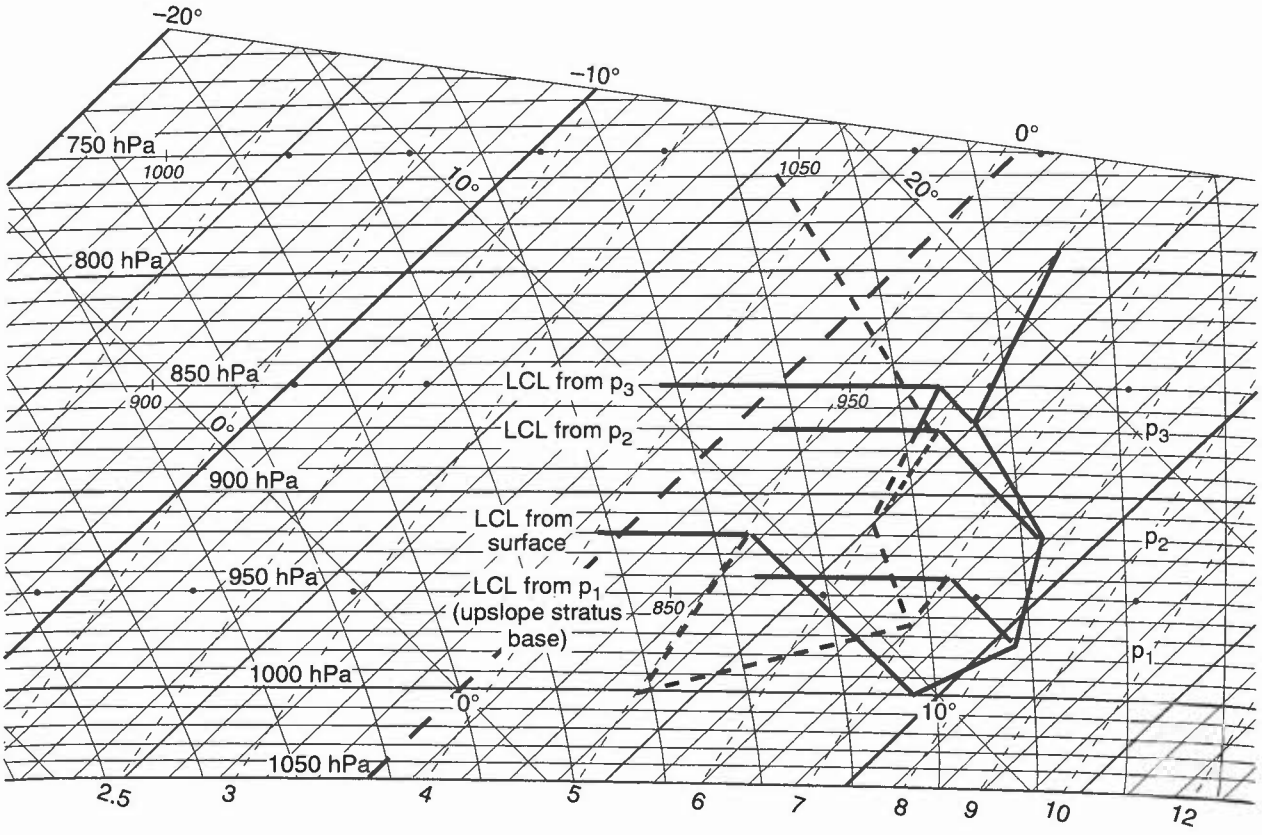

Figure 5.6. Determining the base of upslope stratus (given by the lowest lifting condensation level (LCL) in the lifted layer).

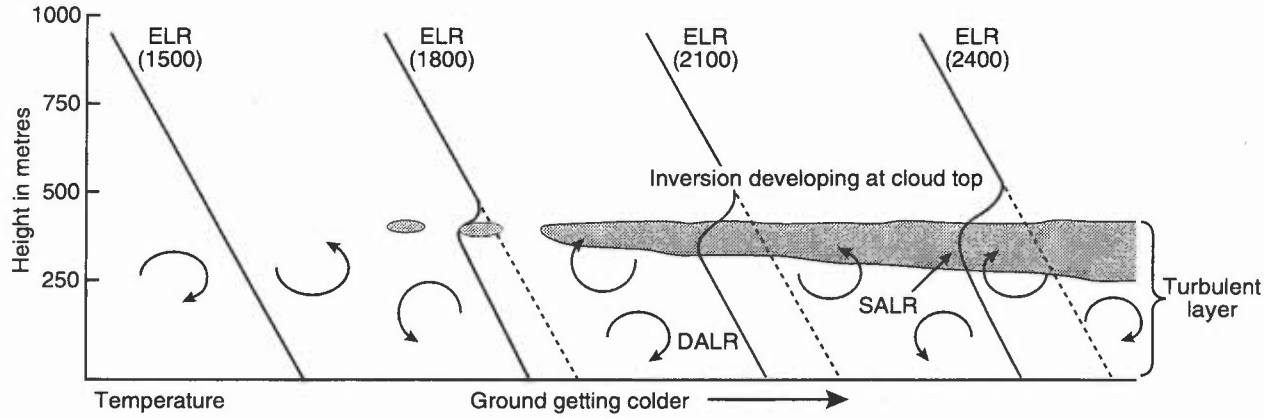

Figure 5.7. The formation of stratus by nocturnal cooling. Temperature profiles are shown every three hours as surface cooling and turbulent mixing act to lower the temperature layer, with stratus forming beneath the inversion.

5.6.2 Forecasting the temperature of stratus formation over land

Formation temperature may be found from a number of sources, the choice of which depends on location and synoptic situation. Stratus may form at:

(i) temperature at which stratus is already present on the chart;
(ii) the stratus clearance temperature earlier in the day (minus 1 or 2 °C);
(iii) the sea temperature if advection is likely;
(iv) the temperature derived from a representative ascent; a technique is given below.

To forecast the temperature at which stratus will form as a result of nocturnal cooling over land **(Fig. 5.9)**:

(i) Obtain the fog-point T_f by Saunders' method (3.3.3.1) from a representative ascent.
(ii) Assess the pressure level at which stratus is expected to form.

(iii) On a tephigram draw the constant mixing ratio line through the fog-point temperature (plotted on the surface isobar).
(iv) From the intersection of this line with the isobar corresponding to the top of the surface turbulent layer (point A), draw a dry adiabatic. The intersection of this adiabatic with the surface isobar indicates the temperature at which stratus will form. This is T_{st}.

The following technique is based on constructing a 'Critical θ_w' (CTW) **(Fig. 5.10)**:
(i) Construct the night cooling curve and find best upwind ascent.
(ii) Draw saturated adiabatic through wet-bulb temperature from the base of the boundary layer inversion to the surface isobar — this is the CTW.
(iii) Mark fog point, F, on surface isobar using Saunders' method.
(iv) Assess mean depth of nocturnal mixing layer by taking depth of 10 hPa for every 6 kn of gradient wind.
(v) Draw top of this mixing layer L′L′. Note where this line cuts environment curve at L; join this point to fog point F.
(vi) This line LF represents the top of any stratus that may form; Normand's point represents the cloud base. Stratus forms when the Normand point passes to a level below this line.
(vii) Monitor cooling by plotting successive Normand points; note where the Normand point seems likely to pass below the line: read off corresponding surface temperature and the time from the cooling curve.

HWF (1975), Chapter 19.6
Warne (1993)

5.6.3 Forecasting the stratus base

The base height is principally a function of wind, which affects the efficiency of turbulent mixing, and RH, which determines the height of the MCL. Generally, the stronger the wind, the higher the base, as given by the guide:

h (ft) = 75 V_S, for forecast surface wind in knots.

The surface temperature/dew-point difference may be used: $h = \alpha(T - T_d)$, α = 420 feet (130 m), although work at Shawbury has given values between 395 and 450 (the latter for tropical maritime air). However, the surface dew-point depression may not be representative of the mixing layer, and base estimates will be under- or over-estimated depending on whether the ground is cooling or warming. The observed base of stratus that has already formed upwind may be a more useful guide, adjusted to local effects.

HWF (1975), Chapter 19.6

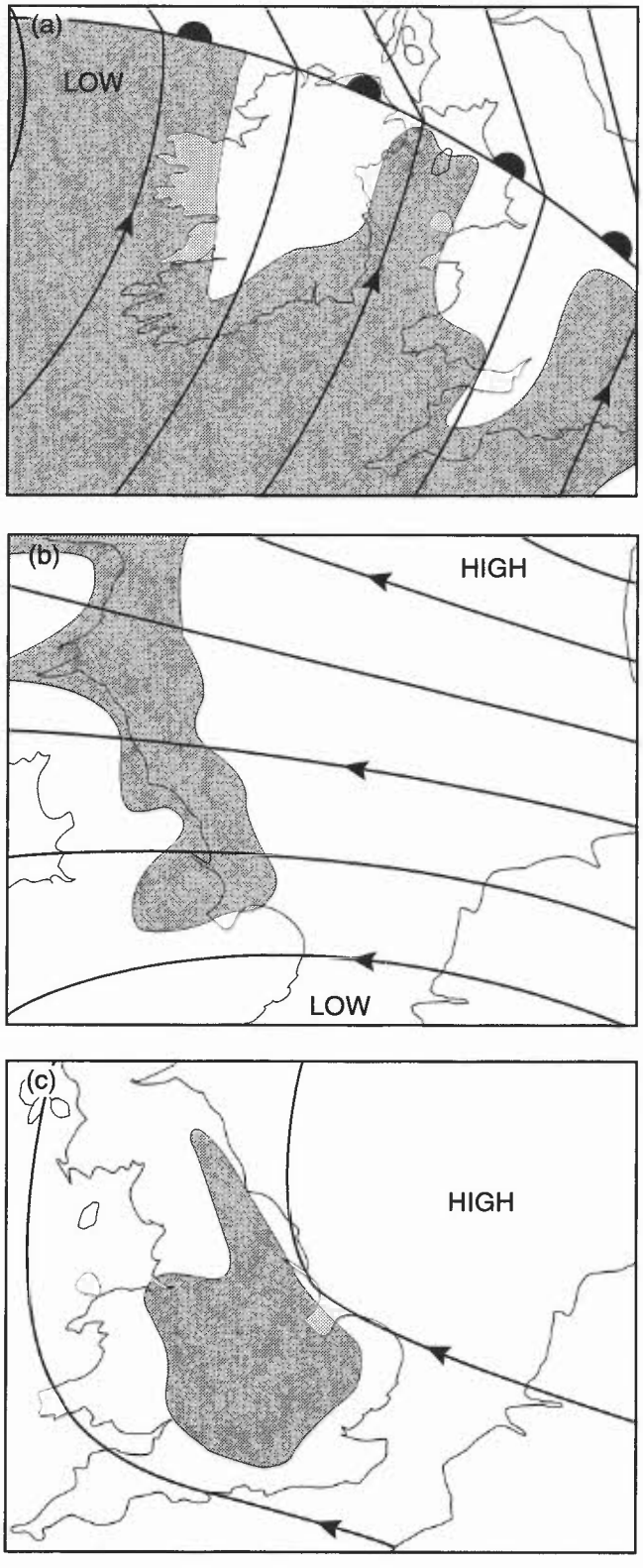

Figure 5.8. Areas of the British Isles prone to stratus (stippled) in the three principal regimes, (a) moist south-westerly, (b) cold easterly, and (c) winter south-easterly.

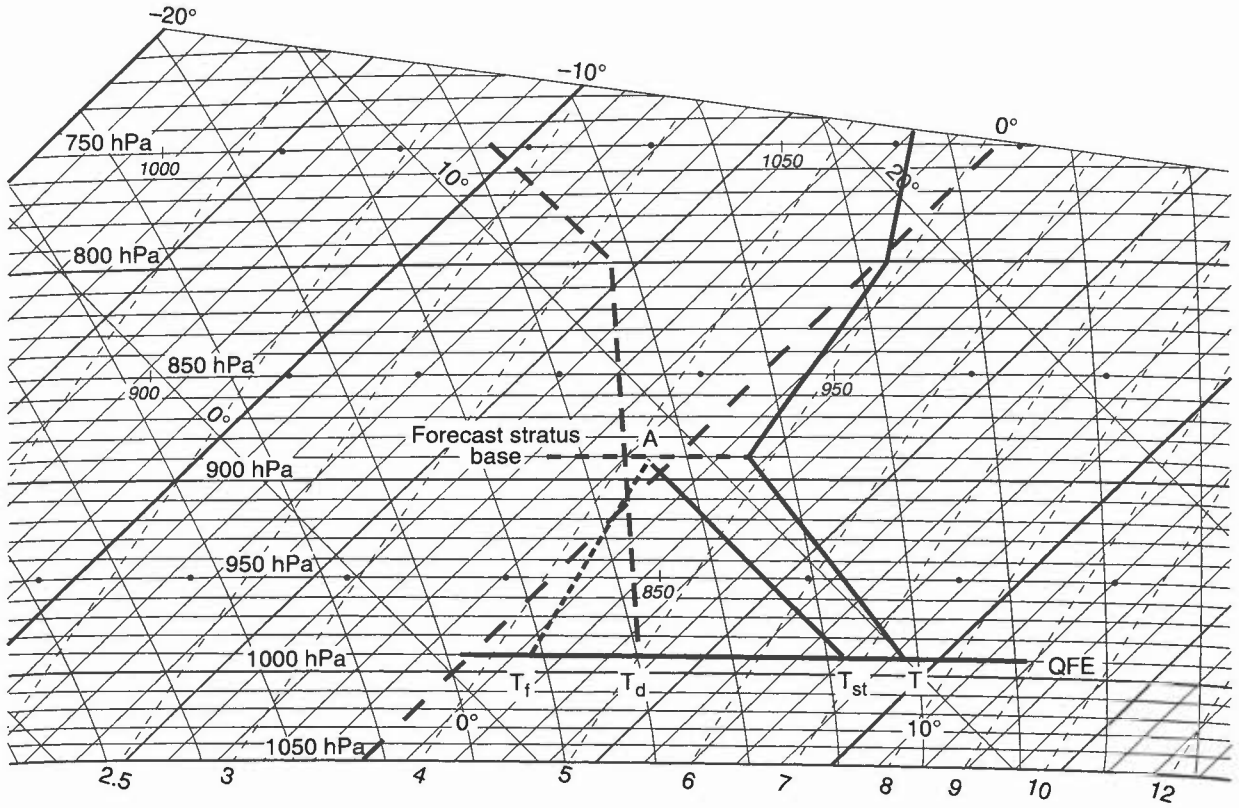

Figure 5.9. Determination of the stratus formation temperature (T_{st}) from a representative ascent. See text for details.

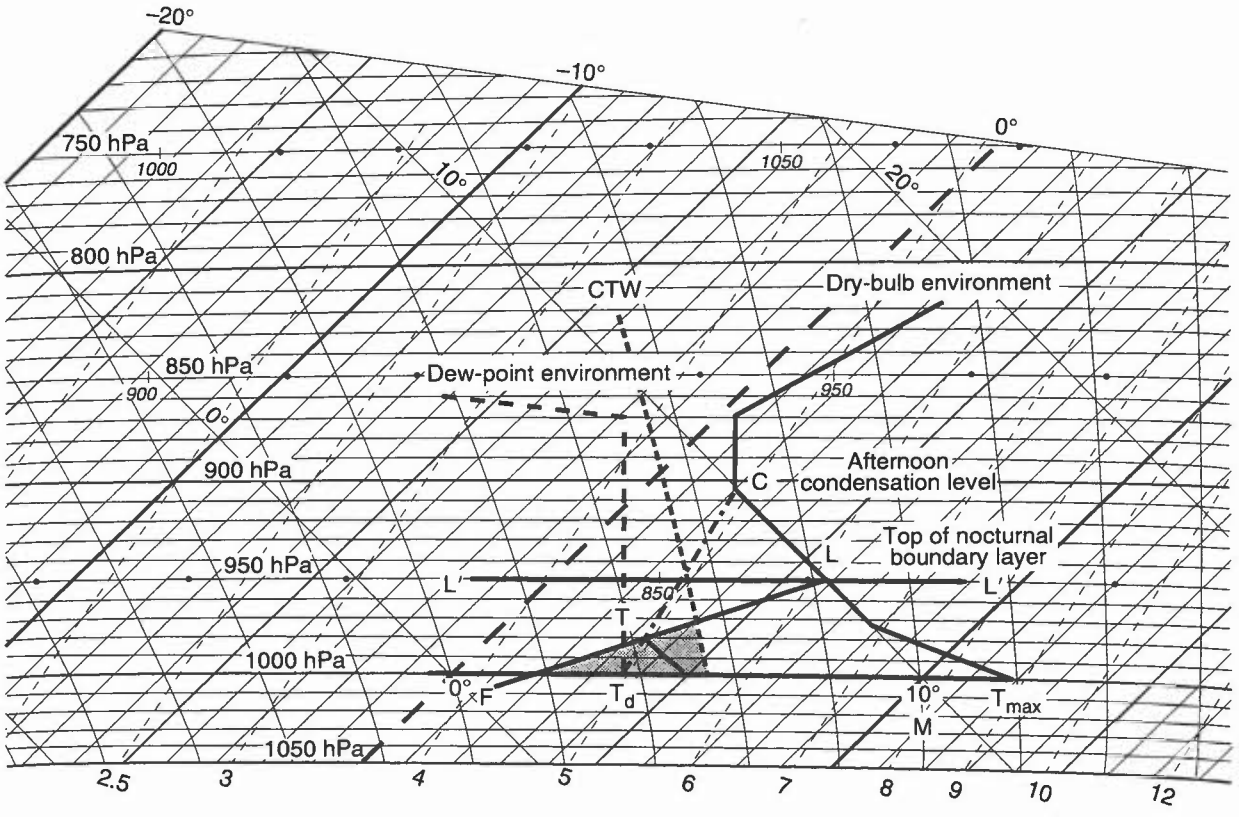

Figure 5.10. The stratus construction lines (on a tephigram) on an ideal sounding with a gradient wind of 30 kn. True stratus forms in the shaded area, 'cumulostratus' in the area between ML at the CTW.

5.6.4 Forecasting stratus tops

The top of the mixing layer will mark the stratus tops; it should be noted that, in most situations, stratus is likely to be no more than a few hundred feet thick. The 'critical θ_w' technique also gives stratus tops.

5.6.5 Forecasting the advection of stratus from the sea

(i) If there has been little change in the synoptic situation during the day, the temperature at which stratus cleared in the morning (minus 1 or 2 °C) is a good estimate of the threshold temperature at the coast when the stratus will start again to move inland from the coast. (If coastal temperature is not known use the (representative) sea temperature.)

(ii) The movement of stratus inland can be forecast from the direction and speed of the 10 m wind at the time when convection and turbulence are still operative in the lowest layers, and before the surface temperature begins to fall towards evening. Valleys aligned at right angles to the coast facilitate deep inland advances.

(iii) If there is upslope motion, stratus may form over higher ground before the main cloud sheet spreads in from the coast (giving the impression that the movement inland occurs at greater than the geostrophic speed).

(iv) The level at which stratus will form can be determined from a representative vertical profile of temperature and dew-point. Use a Normand construction to determine the condensation levels of air lifted from several levels. The lowest condensation level represents the pressure at the base of any orographic stratus.

(v) Studies around the Eden estuary (east Scotland) have shown that 'haar' may recede with the ebbing tide as estuarine muds and sands are exposed and warm rapidly; the haar advances with the next tide.

Alexander (1964) **Lamb (1945)**
Sparks (1962)

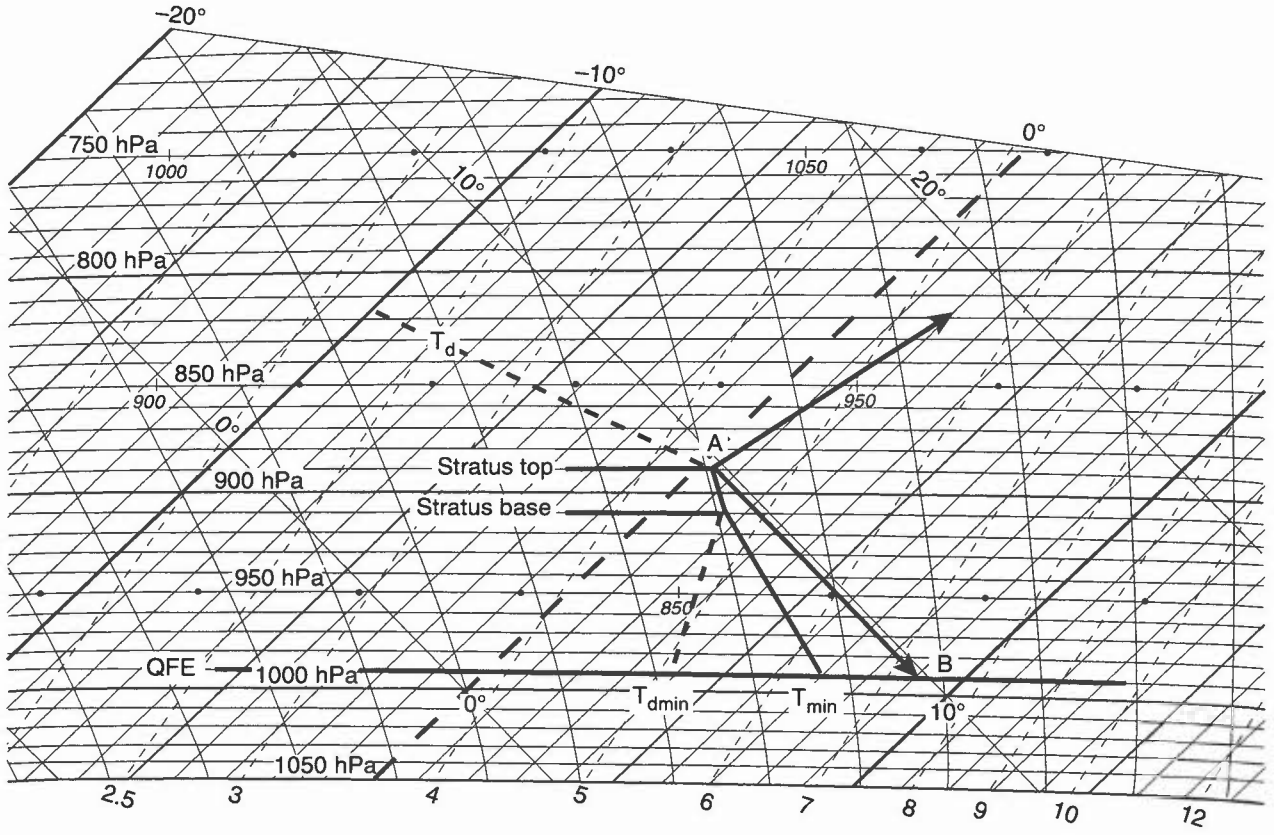

Figure 5.11. (a) Determination of the stratus clearance temperature from a representative ascent: construct a dry adiabat from the level of the stratus top on the temperature curve (point A) to the surface pressure level QFE (point B); the temperature at B is the stratus clearance temperature.

5.6.6 Stratus clearance

The three main clearance mechanisms are: *Insolation; Increased wind; Advection of drier air*

(a) *Insolation* — from a representative ascent construct a dry adiabat from the level of the stratus top to surface; this is clearance temperature. If a day heating curve is constructed assuming cloudy conditions, the time of clearance

will be that at which stratus clearance temperature is reached (point B in **Fig. 5.11**). In winter stratus often persists most of the day, clearing briefly at the time of maximum temperature.

(b) *An increased wind speed* — will deepen the mixing layer, mixing in drier air from above.

(c) *Advection of drier air* — in such cases the rear edge may be followed on satellite imagery and/or charts. One common example is the clearance of North Sea stratus by the backing or veering of the wind to give a shorter sea track from the continent.

Mansfield (1988)

5.7 Stratocumulus: physical and dynamical processes of formation and dissipation

Through its significant effect on the radiation balance Sc affects boundary layer structure and hence fog formation and dispersal, maximum and minimum temperatures, etc. Since Sc still presents a formidable forecasting challenge, it is important that forecasters be aware of the latest thinking on the physical and dynamical processes of formation and dissipation so as to be able to base Sc forecasts on as much physical insight as is currently available (see 10.3.1.3).

5.7.1 Features of formation

Sc formation is usually associated with either:

(i) cooling/moistening of the boundary layer or

(ii) spreading of Cu beneath an inversion.

Figs 5.12 and 5.13 show five regions of interest:

A— just above cloud; air is warm and dry through subsidence, thus stable with little turbulence.

B— at cloud top; marked inversion and hydrolapse. Very stable; local perturbations strongly damped although small-amplitude gravity waves are often present. Wind shear, sometimes large, is confined to this inversion layer.

C— within cloud; well mixed, constant WBPT. Liquid-water content slightly below the adiabatic value due to entrainment. Aircraft icing a danger with temperatures in the range 0 to −15 °C.

D— cloud base; transition to clear air poorly defined, no strong temperature gradients. Perturbations can grow as is evident from rolls frequently observed.

E— below cloud base; well mixed with same WBPT as in cloudy layer. Potential temperature profiles show discontinuity but within- and below-cloud regions may be treated as one.

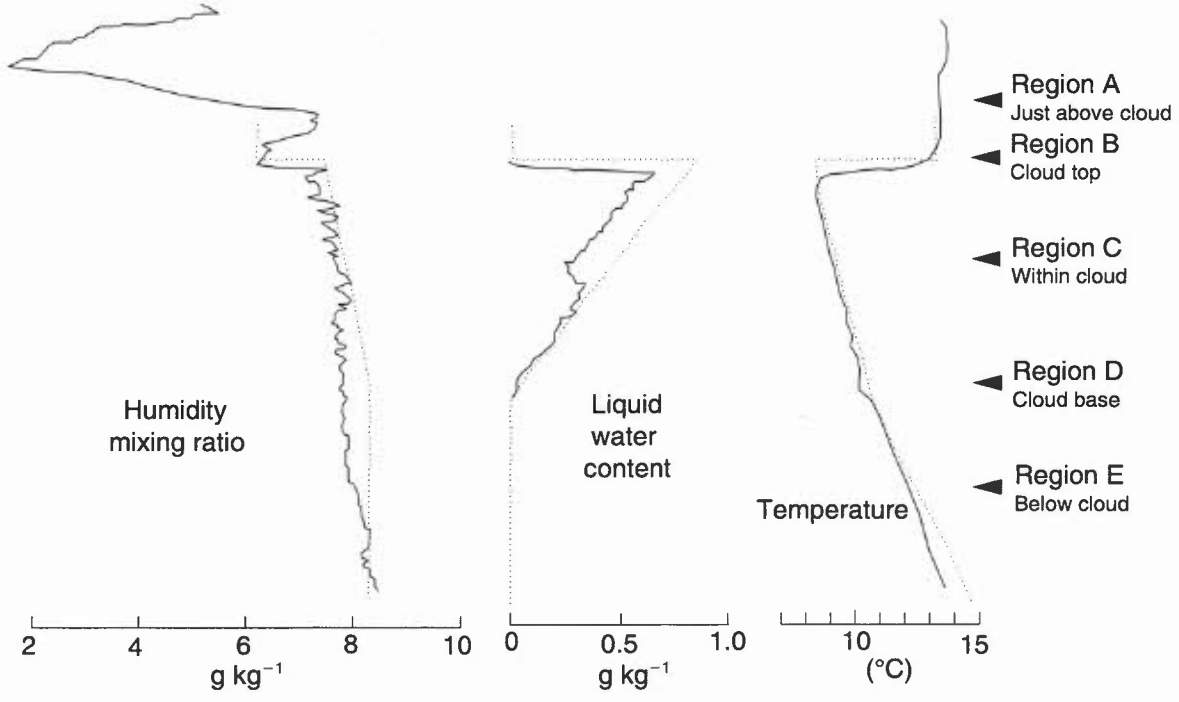

Figure 5.12. An example of the humidity mixing ratio, liquid water content and temperature profiles in stratocumulus. The solid lines show the structure as measured by the Meteorological Research Flight C-130 aircraft. The dotted lines show an idealized representation for stratocumulus.

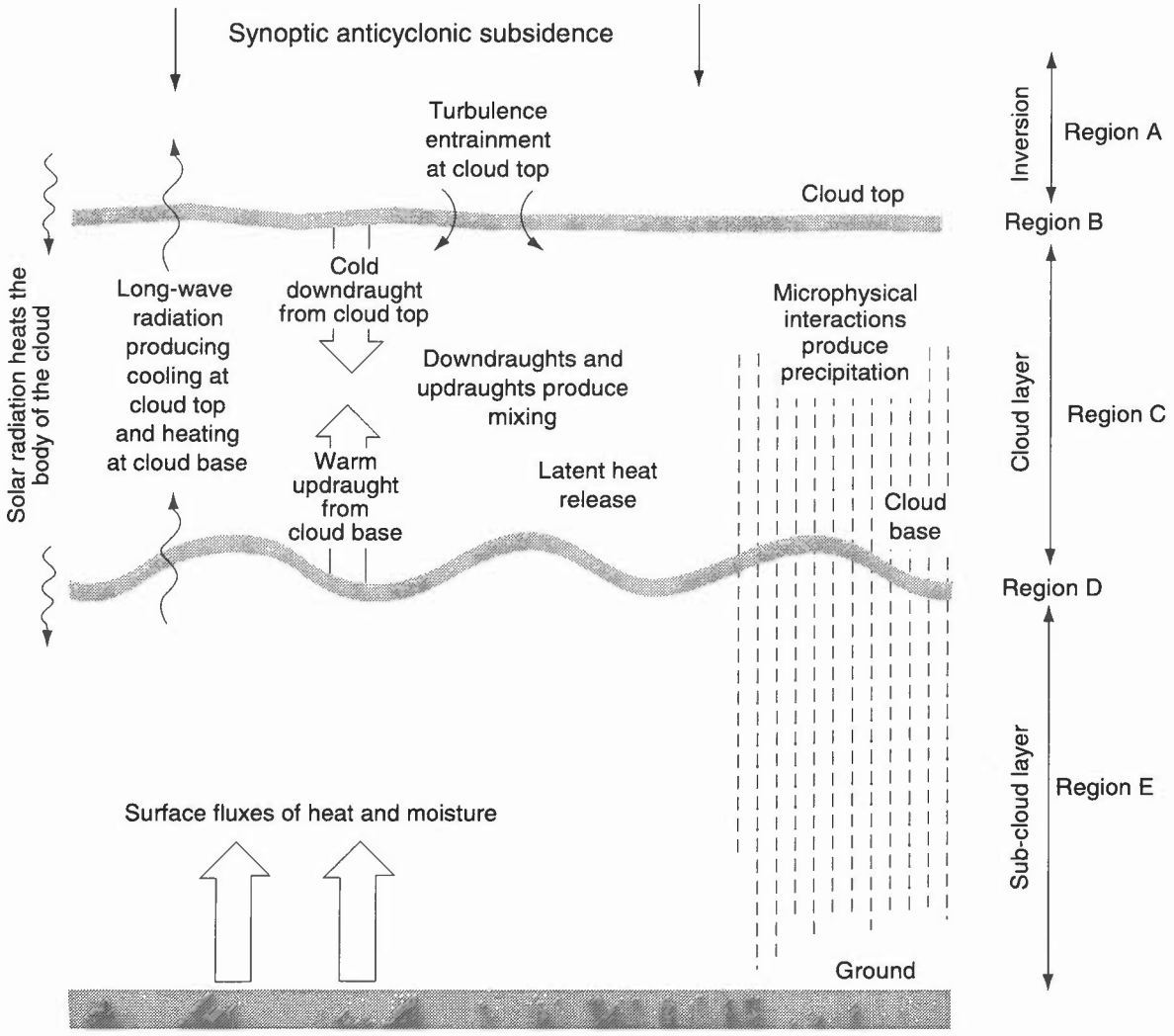

Figure 5.13. Summary of physical processes important to the development of stratocumulus.

5.7.2 Control mechanisms of Sc development

Processes include:

(a) synoptic-scale subsidence (tending to lower cloud top)
(b) radiative effects important (lifetime of Sc several days)
(c) turbulent mixing raises cloud top
(d) detailed structure defined by microphysical processes.

In more detail:

(a) Radiative heating and cooling generates convective instability, mixing and thickening clouds; this is opposed by large-scale subsidence. Thus cloud layer will basically rise and fall depending on which mechanism temporarily dominates.
(b) (i) When cloud thickness is >400 ft (150 m), it becomes important to consider the long-wave radiation balance between cloud top, base and within the cloud layer. Radiative cooling rate at cloud top is about 5 °C h^{-1}, with a slight warming at the base since surface is warmer than cloud base.
(ii) Of the solar radiation penetrating, 13–15% is absorbed; remainder reaches ground. In June in the UK balance of solar radiation emitted/absorbed nearly equal. Sc will display significant diurnal changes.
(c) Turbulence and entrainment generate convective instability; long-wave cooling and solar heating will rarely be in exact balance and cloud experiences a net cooling.
(d) Aircraft measurements show there to be little variation of droplet concentration with height, although drops become bigger towards cloud top. Whether there is drizzle at the ground will depend on the humidity of air below cloud base and local orographic effects.

Fig. 5.14 is a summary of the physical processes important to Sc development.

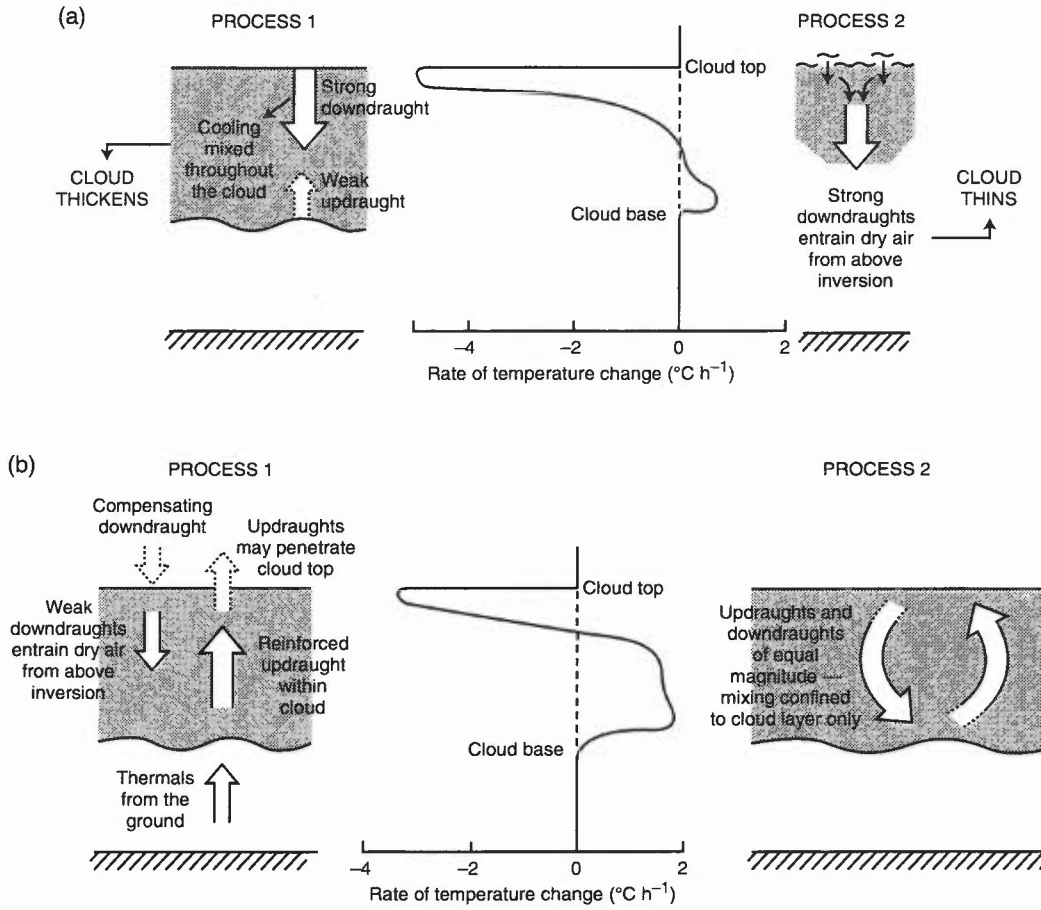

Figure 5.14. (a) Outline sketch showing the effect of the two competing processes on a sheet of nocturnal stratocumulus: Process 1 — radiative cooling at cloud top produces downdraughts which mix cold air throughout the cloud layer and cause stratocumulus to thicken, and Process 2 — strong downdraughts entrain air which when mixed with cloudy air may disperse the stratocumulus. (b) Outline sketch showing the effect of the two competing processes on a sheet of daytime stratocumulus: Process 1 — updraughts are enhanced due to warming and may penetrate the cloud top causing compensating downdraughts to entrain dry air, and Process 2 — updraughts and downdraughts are of equal magnitude confining mixing to the cloud layer only.

5.7.2.1 Night-time effects (Fig. 5.14(a))

Two competing processes are to be considered:

Process 1

(i) At night there is a net cooling in cloud layer.
(ii) Since water vapour content remains basically constant, cloud formation is enhanced.
(iii) Net effect: cloud becomes denser and cloud base lowers.

Process 2

(i) Net cooling at the top changes stability of layer and leads to enhanced instability, principally through the presence of stronger downdraughts.
(ii) Stronger downdraughts increase entrainment of dry air from above inversion,
(iii) If air above the inversion is sufficiently dry the Sc disperses through mixing.

From forecasting point of view:

Process 1 — precise details of cloud layer are unimportant once persistence is assured.
Process 2 — basis of James' rule (5.8.2.1): if $D_m > D_c$ then air above the cloud layer is dry enough to evaporate the cloudy layer completely; applicable over land only. Not very reliable because of difficulty of making measurements accurate enough to distinguish between the competing processes.

5.7.2.2 Daytime effects (Fig. 5.14(b))

Starting with night-time Sc two processes can be envisaged as the sun warms cloud and ground:

Process 1

(i) Both main body of cloud and the ground warm, achieving a radiation balance.
(ii) The turbulence structure changes; updraughts are enhanced by thermals from the ground; downdraughts weaken.
(iii) If the updraughts are strong enough, they may penetrate inversion, inducing compensating downdraughts and forcing dry air from above the inversion into the cloud layer.

If updraughts do not reach cloud top then no clearance possible; if they do penetrate inversion, air above top may not be either dry enough or warm enough to induce clearance. It is crucial that updraughts should be strong enough and air sufficiently warm and dry in order to clear the cloud. This delicate balance is reflected in Kraus' rule (5.8.2.2) which, however, only uses temperature change across the inversion (although, in subsiding air, hydrolapse and temperature inversion are often closely linked).

Process 2

(i) Insolation heating and long-wave cooling will sometimes be comparable, inducing updraughts and downdraughts of similar strength, thus confining mixing to the cloud layer. Sub-cloud moisture then no longer enters the cloud so cloud base will rise and cloud will thin and possibly disperse. A weak inversion will develop beneath cloud base.
(ii) Daytime observations may then suggest that the main cloud layer is beginning to thin and will eventually clear.

This section has concentrated on radiatively-driven convection; other forms of mixing (e.g. through wind shear) may also be important, but the cloud will then have a different structure and behaviour.

Bennetts et al. (1986)
James (1959)
Kraus (1943)

5.8 Non-frontal stratocumulus

In the formation of stratus, the turbulence is generally purely mechanical; in the case of stratocumulus, convection and radiation often play major roles.

5.8.1 Formation and dispersal

Two main categories of Sc are:

(a) Sc formed by spreading out of Cu — this is a common occurrence in subsiding Pm air masses, particularly on the eastern flank of anticyclones (4.4).
(b) Anticyclonic Sc:
Formation: is by mechanical turbulence in the mixing zone, by convection due to surface heating, or a combination of both. Convection is particularly important when cold air advects over warm sea and the inversion limits convective depth.

Forecasting notes:

(i) Advect the cloud edge with the wind at cloud level.
(ii) Use satellite imagery.
(iii) Best to forecast NIL or 8/8.
(iv) Sheet usually reduces insolation and inhibits night cooling.
(v) May be very persistent, especially in winter.

Dispersal: prediction is difficult, especially in winter.
Forecasting notes:

(i) Look for rear edge and advect with wind at cloud level, or by continuity (from satellite pictures or upwind observations)
(ii) If surface temperatures rise to give DALR profile to cloud top, break-up may start but re-form when temperature drops.

(iii) Continued subsidence may lower the inversion sufficiently to bring down drier air and disperse the cloud (unusual).
(v) James', and Kraus' rules are two forecasting techniques discussed next; neither is particularly reliable.

Bennetts et al. (1986)

5.8.2 Dispersal of stratocumulus

5.8.2.1 Nocturnal dispersal of stratocumulus over land (James' rule)

Only use this technique if the stratocumulus sheet is bounded by a dry inversion, there is no surface front within 400 miles and the cloud sheet is extensive, giving almost complete cloud cover (>6/8 for 2 or more hours).

The cloud will break if: $D_m > D_c$

where:
D_m is the maximum dew-point depression (°C) in the 50 hPa layer above cloud
D_c is the value given in the **Table 5.4** below, in which
b is the difference (g kg^{-1}) between HMR at top and bottom of the 50 hPa layer below cloud
z is the cloud thickness (hPa).

Table 5.4. Values of D_c (°C) for use with James' rule

z	b (g kg^{-1})					
(hPa)	0.25	0.50	0.75	1.00	1.25	1.50
10	—	—	1	3	6	8.5
20	0	2.5	5	8	10	13
30	4	7	9	12	14.5	17
40	9	11	14	16	19	21
50	13	15	18	20.5	23	26
60	17	20	22	25	27	30
70	21	24	26.5	29	32	34

Note: a linear hydrolapse in the layer is assumed.

James (1959)

5.8.2.2 Dispersal of stratocumulus by convection (Kraus' rule)

A cloud layer will not disperse by convective mixing with the air above if the pressure (hPa) at the cloud top is less than P_c, as given below. (If the pressure at cloud top is greater than P_c the cloud may or may not disperse.)

$$P_c = P + a(P_0 - 1000)$$

where P_0 is the surface pressure (hPa) and P and 'a' are given in **Table 5.5** below.

Kraus (1943)

Table 5.5. Values of *P* and '*a*' (for use with Kraus' rule) for given cloud-top temperatures (water or ice cloud) and strength of inversion.

	Temp. at cloud top (°C)	Magnitude of inversion containing the cloud layer (°C) 10		8		6		4		2	
		P	*a*	*P*	*a*	*P*	*a*	*P*	*a*	*P*	*a*
Water cloud	20	833	0.80	861	0.83	891	0.87	924	0.90	960	0.95
	10	803	0.75	834	0.79	869	0.82	906	087	951	0.93
	0	755	0.67	789	0.71	830	0.76	877	0.82	932	0.90
	−10	680	0.56	719	0.60	765	0.66	823	0.73	898	0.84
Ice cloud	0	779	0.71	812	0.75	850	0.79	891	0.85	941	0.91
	−10	702	0.59	739	0.63	786	0.69	839	0.76	908	0.85
	−20	586	0.45	628	0.49	679	0.54	747	0.62	841	0.74
	−30	451	0.30	489	0.34	540	0.38	613	0.45	728	0.58

5.9 Precipitation from layered clouds

5.9.1 Frontal and non-frontal precipitation

5.9.1.1 Definition of intensities of (non-showery) precipitation (UK Met. Office)

Table 5.6. Definition of intensities of (non-showery) precipitation (UK Met. Office)

(a) *Rain*	
Slight	<0.5 mm h^{-1}
Moderate	0.5 to 4.0 mm h^{-1}
Heavy	>4.0 mm h^{-1}
(b) *Snow*	
Slight	<0.5 cm h^{-1}
Moderate	about 0.5 to 4.0 cm h^{-1}
Heavy	>4.0 cm h^{-1}

Note: 1.25 cm of fresh snow ≈1 mm water.
1 foot of fresh snow ≈1 inch of rain.

Observer's Handbook (1982)

5.9.1.2 Precipitation in frontal depressions

Synoptic observations, satellite imagery, continuity, tephigrams and upper-air information will confirm the presence or otherwise of any jet streams or upper troughs that will encourage a front to become more active. The amount and intensity of the precipitation depends on:

(i) large-scale ascent of air;
(ii) the continued availability of moist air, originating at low levels;
(iii) the release of potential instability aloft;
(iv) orographic enhancement over high ground.

Frontal precipitation often occurs in bands, usually but not always parallel to, or coincident with, one of the surface fronts. (Bands of rain ahead of a cold front may penetrate well into the warm sector or even ahead of the warm front. These bands are mesoscale phenomena.) (Chapter 7).

Browning (1985)
Browning et al. (1974) **Browning et al. (1975)**

5.9.1.3 Non-frontal precipitation

If non-frontal precipitation is tied to a significant (organized) feature, a surface trough or polar low, for example, then a reasonable forecast of precipitation changes can be made, often by advecting the precipitation area with the 700 hPa wind.

5.9.1.4 Quantity of precipitation

Synoptic data and radar rainfall displays are the best guide to timing the onset and cessation of precipitation and for assessing development, movement and intensity of precipitation areas.

5.9.2 Forecasting drizzle

(i) Precipitation from stratiform cloud is related more to the microphysics than broader-scale dynamics.

(ii) Drizzle is often associated with haar/sea fog (fret), affecting exposed coasts, being cleared inland by insolation and, near coasts, by advection. It thus tends to be more frequent during the latter part of the night and early morning.

(iii) For drizzle to reach the ground it must fall from stratus cloud with its base less than about 1500 ft (450 m) and a minimum depth of 2000 ft (600 m). The dew-point depression in the air below cloud should be less than 2 °C, otherwise the very small drizzle droplets (0.2–0.5 mm diameter) will evaporate.

(iv) Clouds of thickness <7500 ft (2250 m), cloud-top temperatures <-12 °C and bases colder than 0 °C rarely give rain (**Fig. 5.15**).

(v) Satellite imagery can help to identify areas of colder cloud tops where precipitation is more likely. Heavy drizzle mostly occurs within clouds that are covering high ground but radar imagery often underestimates drizzle intensity due to the 'overshooting' of the beam (10.6).

HWF (1975), Chapter 19.7

5.9.3 Depth of cloud for precipitation

Fig. 5.15 gives a guide to the intensity of precipitation at ground level, over flat terrain, associated with different thicknesses of cloud; it thus defines criteria that distinguish precipitating from non-precipitating cloud although cloud-top temperature is not considered. It is constructed for layer clouds in which the difference in water content between the base and the top is over 1.5 g kg^{-1}. Precipitation intensity in polar air masses is likely to be enhanced by ice processes even in quite shallow clouds (about 2000 feet).

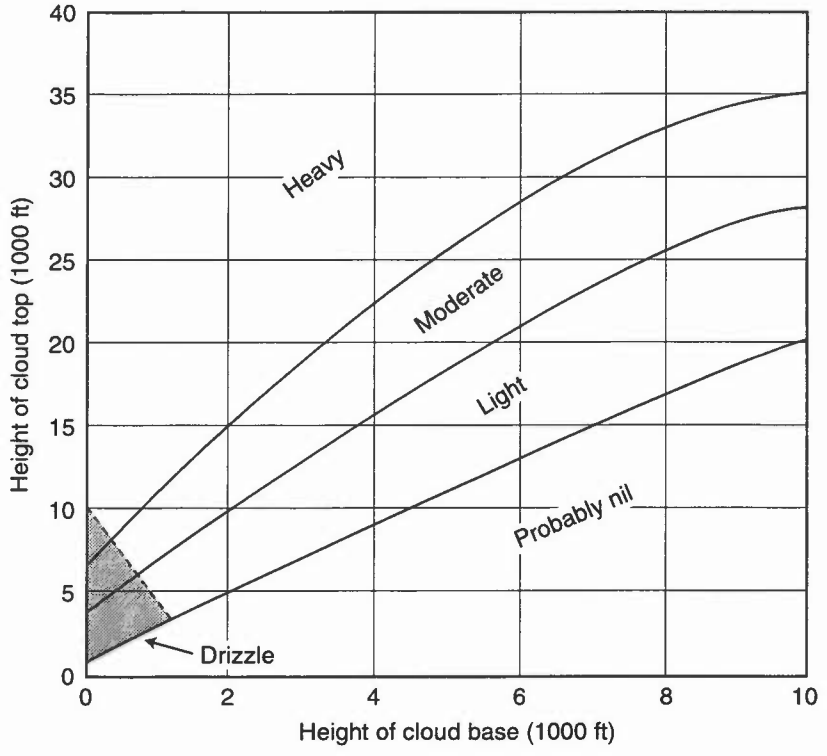

Figure 5.15. The depth of cloud related to intensity of precipitation. The stippled area indicates the conditions for the precipitation to be mainly drizzle.

In summary:

(i) There is a high probability of precipitation from clouds with thickness >7500 feet (2250 m) with cold tops (<−10 °C).

(ii) Deep clouds with bases <3300 feet (1 km) above the 0 °C isotherm — precipitation likely, while such clouds with bases >3300 feet above the 0 °C isotherm — precipitation unlikely.

HWF (1975), Chapter 19.7

Whether there is drizzle at the ground from Sc will depend on the humidity of air below cloud base and local orographic effects (**Table 5.7**).

Table 5.7. An estimate of stratocumulus depth to produce drizzle at cloud base (taking cloud top at −5 °C)

Air mass	Minimum depth to produce drizzle at cloud base	
	(m)	(ft)
Clean maritime	500	1600
Maritime	1000	3300
Continental	2000	6600
Industrial continental	2500	8200

Bennetts et al. (1986)

5.9.4 Lowering of cloud base

(a) during continuous *rain*:

(i) Base will be at height where temperature lapse changes from positive to less positive or to negative.

(ii) Base will be at a height where wet bulb or dew point is a minimum.

(iii) If rain is of sufficient duration a ceiling will occur below 2000 feet; most frequently it is a ceiling below 800 feet.

(iv) During continuous rain a ceiling does not generally occur at the height of temperature discontinuity and/or maximum humidity until after the occurrence of a ceiling corresponding to the next higher level of temperature and/or maximum humidity.

(v) Ceiling remains practically constant until the next lower cloud layer appears and increases in amount for its base to become the ceiling.

Note: Ceiling is the height above ground of the base of lowest cloud layers covering more than half the sky. (Method devised for USA).

(b) In intense *showers*: the cloud base may lower rapidly by 300 m (1000 ft) or more, rising rapidly again as the shower moves on.

(c) *Falling snow*: tends to establish an isothermal lapse rate just beneath the initial 0 °C level (see 5.2.2, Fig. 5.1).

Findeisen (1940)
Goldman (1951)
HWF (1975), Chapter 19.6.2

5.9.5 Seeder and feeder clouds

When a very moist low-level air flow is forced to rise over high ground, thick stratus/stratocumulus layers form. By itself this cloud may produce rather little precipitation, especially if the wind speed is strong and there is insufficient time for precipitation to form before the air flows down the lee side of the hills. If, however, rain is already falling from upper-level cloud layers (seeder clouds) above the stratus/stratocumulus, it will fall through the low-level (feeder) cloud, capturing the droplets within, considerably enhancing the rainfall rate at the surface.

The degree of enhancement depends on:

(i) seeder rate >0.5 mm h^{-1};

(ii) high θ_w in low-level air;

(iii) near-saturated air upwind;

(iv) strong low level wind ahead of cold front >30 m s^{-1} at 900 m for heaviest rain;

(v) favourable topography — not too steep.

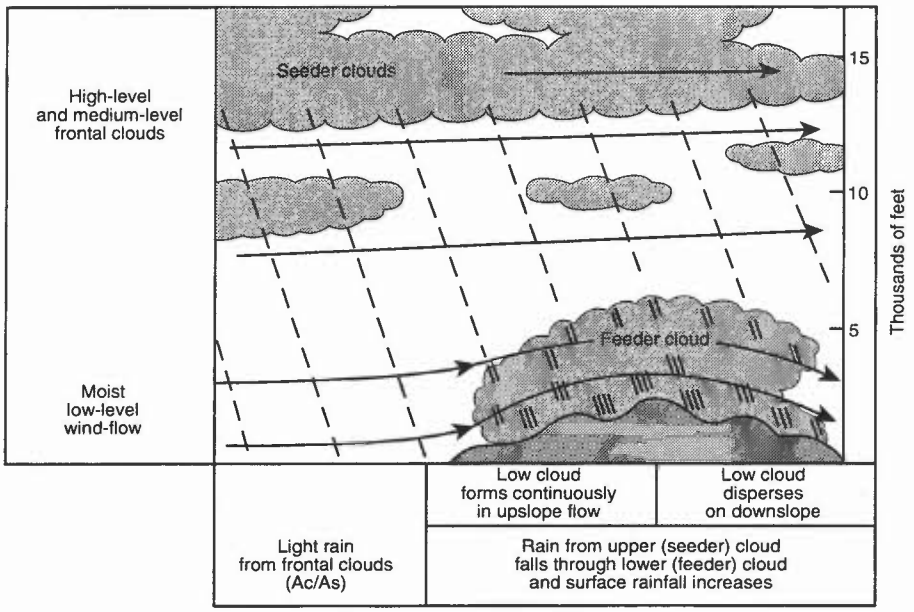

Figure 5.16. The seeder–feeder rainfall effect over hills.

This is a common mechanism for producing heavy rain over high ground in warm sectors approaching the UK from the south-west quadrant and is illustrated in **Fig. 5.16.**

Horizontal variations in surface rainfall intensity over high ground are on the same scale as the hills and valleys.

Curruthers & Choularton (1983) **Smith (1989)**
Robichaud & Austin (1988)

5.9.6 Mountain complications

A 'bad scenario' is as follows (**Fig. 5.17**): a freezing level may exist in free air at about 1000 m. A warm front from the west, with low dew-point south-easterly air undercutting ahead of the front, gives cloud cover producing snow on hill tops down to 500 m. Below freezing level the melting snow lowers the air temperature and delays melting; as the freezing level descends, the snow level also lowers. Undercutting dry air also encourages further reduction in air temperature. It is not unusual for the freezing level to descend to the surface, with snow at all levels, resulting in widespread hill fog at sub-zero temperatures.

Local Weather Manual for Scotland (1994)

5.9.7 Freezing rain from elevated layers

(i) Rain at the surface at temperatures >0 °C is quite possible when there is freezing rain aloft; typically snow, falling through the melting level in a warm sector, encounters polar/arctic air beneath the warm/occluded front and re-freezes before melting again in the lower-level melting band. Freezing rain in such elevated layers from mid-latitude storms occurs about 1% of the time in the UK; oceanic freezing rain will not, generally, be a threat to high-flying transport aircraft.

(ii) Cumulonimbus clouds have sometimes been reported to have large water contents composed of precipitation-sized drops well below 0 °C.

Ahmed et al. (1993)

5.9.8 Severe low-level icing (rain ice)

(i) The forecaster must identify the contrast between low-level, dry pre-frontal air and moist air aloft. In the example (**Fig. 5.18(a)**), an occluding warm sector was pushing slowly east across England and France over an increasingly cold continental south to south-easterly airstream. Freezing rain became widespread over northern France.

(ii) The necessary detail will not be resolved from numerical forecast ascents (**Fig. 5.18(b)**); furthermore any ascent is a 'snapshot' and allowances must be made for this.

HWF (1975), Chapter 19.7.8

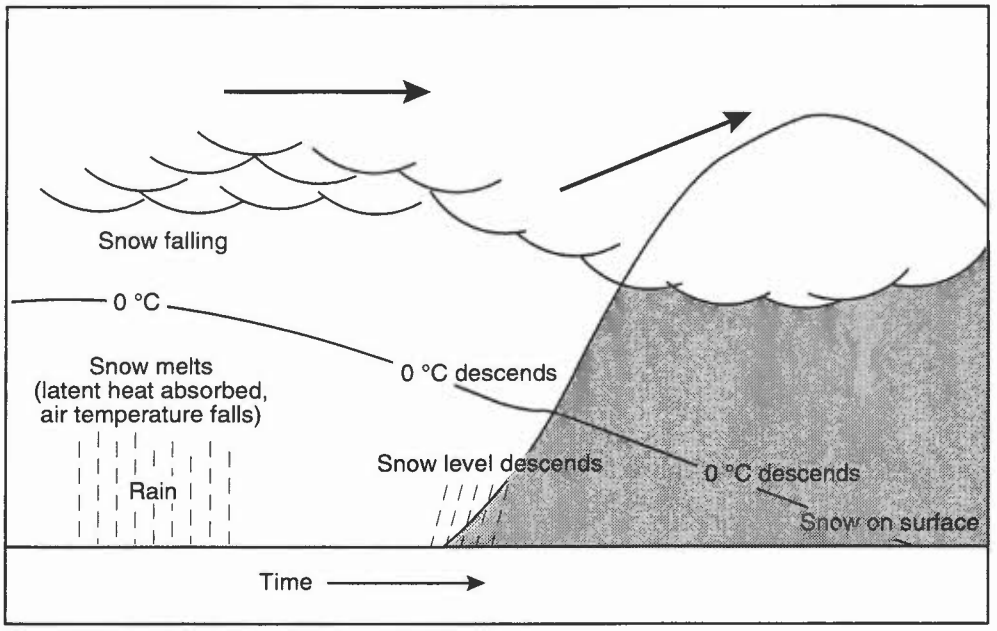

Figure 5.17. Mountain weather — the 'bad scenario' (see 5.9.6 for details).

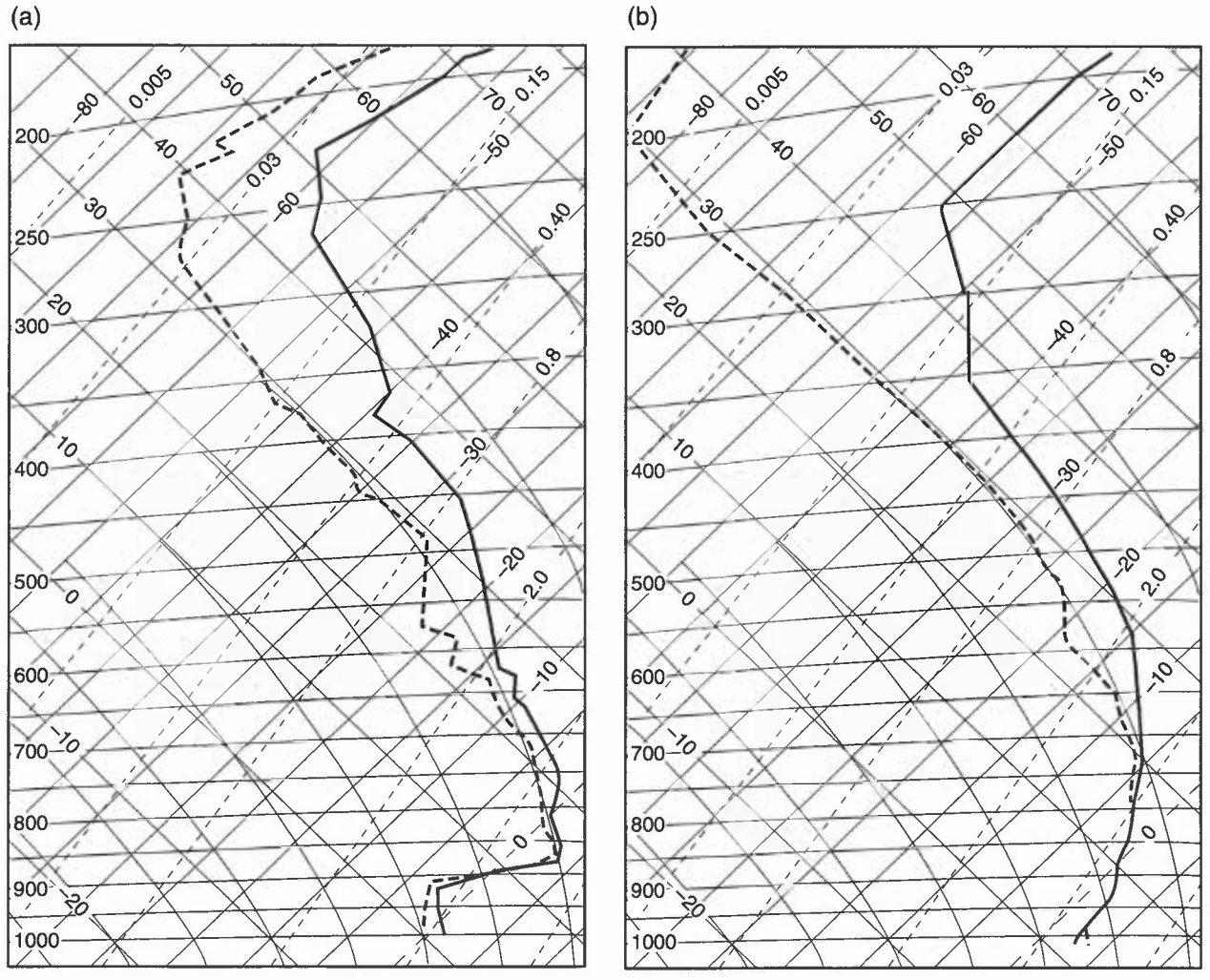

Figure 5.18. Actual ascent (a) at Herstmonceux at 1800 UTC on 5 January 1995 and mesoscale model T + 6 forecast ascent (b) with the same verification time.

5.10 Criteria for precipitation reaching the surface as snow or rain

5.10.1 Factors to consider:

(i) Site — high inland more prone than low coastal.
(ii) Orographic uplift can significantly lower the freezing level.
(iii) Snow cover — cover chills lowest layers implying that snow can be forecast with a slightly higher 1000–850 hPa thickness than would be expected.
(iv) Warm front approaching — if air preceding front is cold then precipitation can start as snow or freezing rain before turning to rain. A slow-moving warm front may develop a shallow wave and dramatically increase the potential for significant snow accumulations.
(v) In a tropical maritime air mass with wet-bulb temperatures of 10 °C or more, snow rarely falls within 50 miles of the front; if the 'warm' air mass is polar maritime then a wet-bulb temperature of about 4.5 °C in the cold air may give snow right up to the front.
(vi) Polar lows — note that NWP models cannot handle small-scale features well. Satellite and radar imagery will aid identification.
(vii) In winter a major problem is determining whether the precipitation will reach the ground as rain, snow, or rain and snow mixed; if no ice particles are present in a stratiform cloud, coalescence can still produce supercooled droplets that freeze on reaching the ground.

Various criteria have been derived for estimating the probability of precipitation in the United Kingdom falling as snow rather than rain. The following summary lists them in a rough order of merit; other techniques are presented.

Table 5.8.

Technique		Percentage probability of snow 90%	70%	50%	30%	10%
Adjusted value of 1000–850 hPa thickness (Boyden)	(gpm)	1281	1290	1293	1298	1303
Height of 0 °C isotherm (see Note (ii))	(hPa)	12	25	35	45	61
Surface temperature	(°C)	−0.3	1.2	1.6	2.3	3.9
1000–500 hPa thickness	(gpm)	5180	5238	5258	5292	5334

Lowndes et al. (1974)

5.10.1.1 Boyden's technique

The 1000–850 hPa thickness needs adjustment for the 1000 hPa height (H_{1000}) and the height of the ground above sea level (H_{GR}). The adjustment (m) is given by $(H_{1000} - H_{GR})/30$ and this quantity may be conveniently read off from **Fig. 5.19(a)**. Alternatively, the snow predictor nomogram, **Fig. 5.19(b)**, incorporates these corrections; it illustrates how a snow probability may be estimated.

Boyden (1964)

5.10.1.2 Height of 0 °C wet-bulb temperature technique

The height of the 0 °C wet-bulb temperature additionally takes into account latent cooling effects.

Table 5.9.

Height of 0 °C wet-bulb temperature	Form of precipitation
3000 ft or over	Almost always rain; snow rare
2000–3000 ft	Mostly rain; snow unlikely
1000–2000 f	Persistent rain readily turns to snow
Below 1000 ft	Mostly snow; only light or occasional precipitation falls as rain.

Beware of cold surface air undercutting warm; Hand uses mean temperature of the lowest 100 hPa (5.10.1.3).

HWF (1975), Chapter 19.7

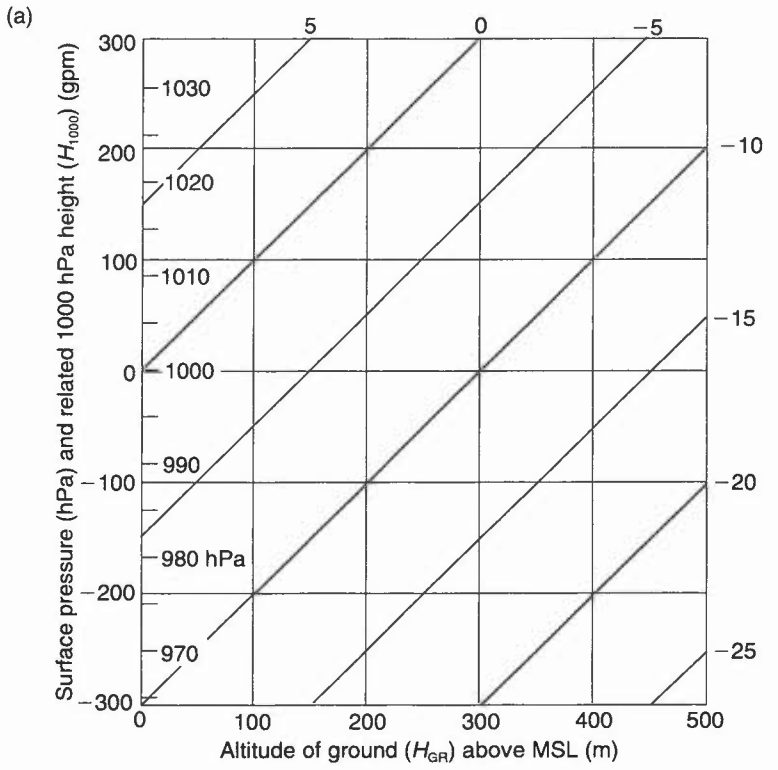

Figure 5.19(a). Forecasting the probability of precipitation as snow. This nomogram indicates the adjustment to be made to the 1000–850 hPa thickness to allow for the 1000 hPa height (or surface pressure) and altitude of ground above sea-level.

5.10.1.3 Hand's rule

Table 5.10. Use of mean temperature of lowest 100 hPa above ground to predict type of precipitation at the surface.

Mean temperature (°C) in lowest 100 hPa above surface	Precipitation type usually reaching surface
<-1.5	snow
-1.5 to 0.5	sleet
>0.5	rain

In heavy and persistent precipitation lowest layers will be further cooled by latent heat of evaporation.

Hand (1986)

5.10.1.4 Initial wet-bulb potential temperature level technique

Initial wet-bulb temperatures at which snow is likely for prolonged frontal precipitation are given in **Table 5.11**; the influence of frequent heavy showers/cold downdraughts can turn precipitation to snow with higher initial temperatures than from frontal precipitation.

Table 5.11. The relationship between downward penetration of snow beneath the 0 °C level and the initial wet-bulb temperature.

Type of precipitation	Initial wet-bulb temperature level (°C)	
	to which snow will descend	below which snow is unlikely
Prolonged frontal	+2.0 °C	+2.5 °C
Extensive moderate or heavy instability	+3.0 °C	+3.5 °C

HWF (1975), Chapter 19.7.6.1

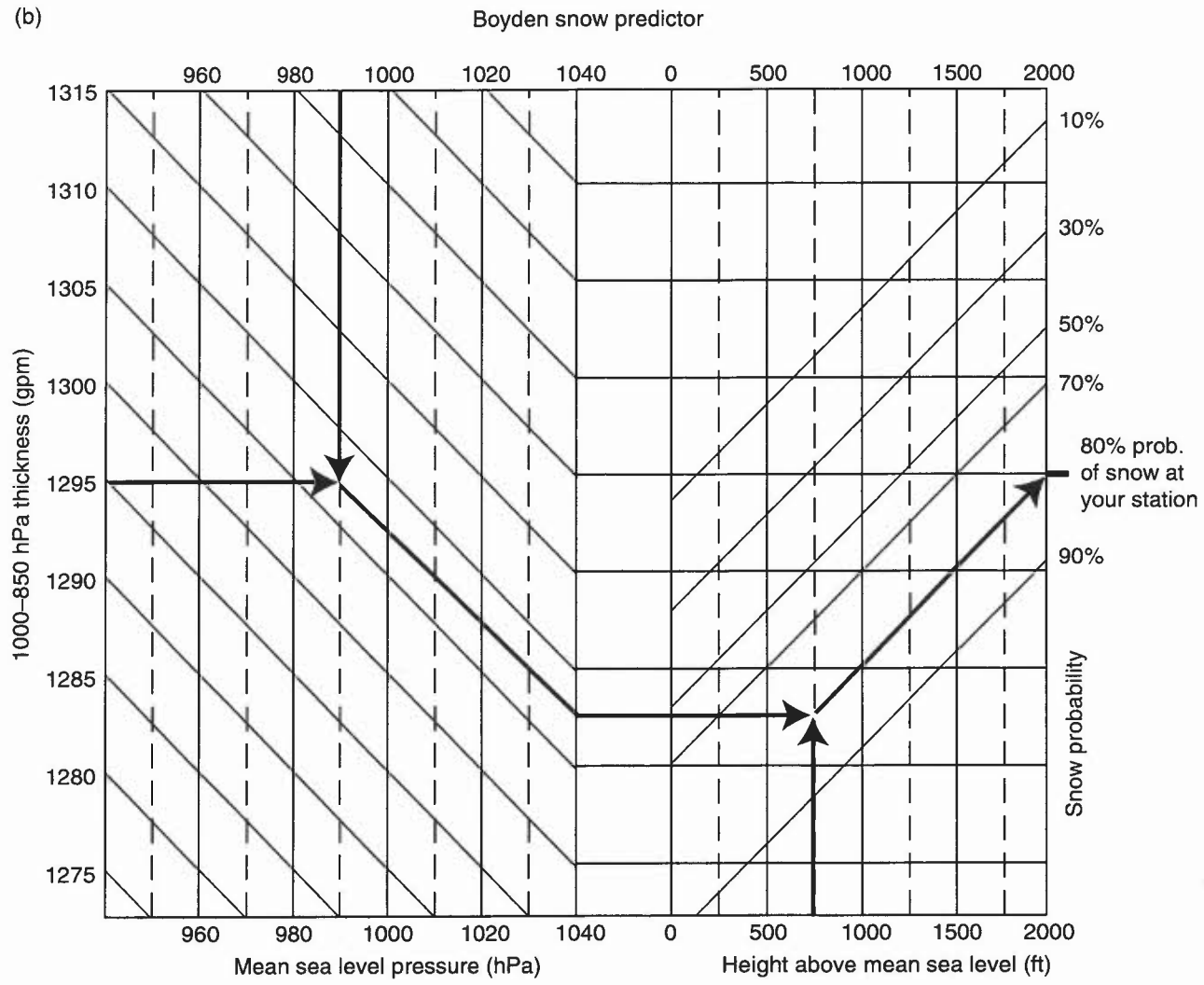

Figure 5.19(b). Forecasting the probability of precipitation as snow. How to find the probability of snow at a station with an elevation of 750 ft (230 m), a surface pressure of 990 hPa and a 1000–850 hPa thickness of 1295 gpm.

5.10.1.5 Screen wet-bulb temperature technique (Lumb)

For an exposed station at height H (in hundreds of metres) in central and western regions of the UK under moderate easterly, or stronger, winds:

(i) for elevations up to 170 m:
Rain turns to melting snow if: $T_w < (2.1 - 0.6H)$ °C
Rain turns to lying snow if: $T_w < (0.6H)$ °C
where T_w is surface wet-bulb temperature when precipitation begins.

(ii) for elevations 170 to 350 m:
Snow probable if: $T_w < (2.1 - 0.6H)$ °C.

(iii) If $T_w > 2.5$ °C rain is more likely than sleet, irrespective of elevation.

Winds should be at least moderate with a good cover of low- or medium-level cloud.

The method is summarized in **Fig. 5.20**.

Lumb (1986)

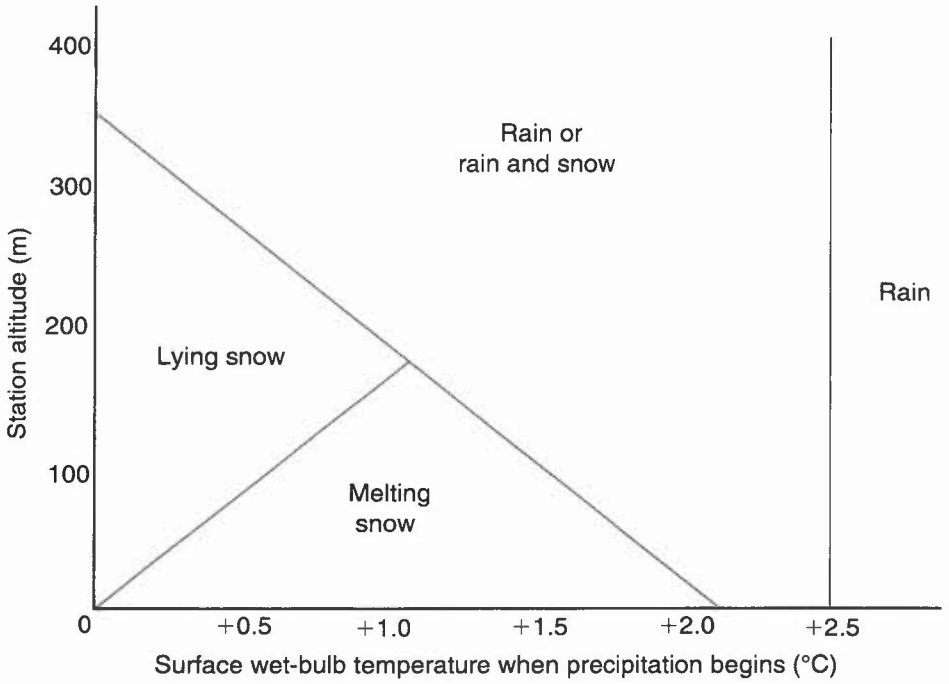

Figure 5.20. Diagrammatic form of Lumb's method for snow prediction.

5.10.1.6 Booth's snow predictor

A well tried snow predictor index, I_s, is based on the relationship: $T_w \approx (T + T_d)/2$ and I_s is defined as: $T + T_d$. The predictor can be plotted on a surface chart to show the most likely areas of rain, snow or rain turning to snow according to the **Table 5.12**:

Table 5.12.

Precipitation expected		I_s
Light intensity:	(i) probably rain if:	≥ 2
	(ii) probably snow if:	≤ 0
If continuous moderate or heavy precipitation is expected: (if there is no warm advection at or near the surface).		≤ 7

Rain may also turn to snow over areas into which colder air with $I_s \leq 7$ is advected.

Booth (1973)

5.10.1.7 Varley snow predictor

This predictor has proven skill in forecasting the level above which moderate or heavy snow (frontal or convective) will fall in the SW Midlands–Wales area. It is used for the lowest 2000 feet (610 m) and assumes:
$T_w \approx (T + T_d)/2$, lapse rate near the surface $\approx$ 2 °C per 1000 ft, and the snow will fall when T_w is 2 °C or below.
The height of the melting layer above the station in terms of T and T_d is:

$$250 \times (T + T_d - 4\ °C) \text{ feet} \qquad [\text{or } 76 \times (T + T_d - 4\ °C) \text{ metres}]$$

or, in terms of T and T_d: $[((T + T_d)/4) - 1]$ in thousands of feet
where T is the surface dry bulb, T_d the surface dew-point temperature and T_w the surface wet-bulb temperature. If, for example, $T + T_d$ in rain at a station at 20 feet is 8 °C, then snow in that area is likely at levels above about 1000 ft.

Table 5.13. An at-a-glance estimate of the height above which snow is likely in terms of T and T_d

$T + T_d$ (°C)	4	5	6	7	8	9	10	11	12
Melting height (ft)	surface	250	500	750	1000	1250	1500	1750	2000

5.11 Snow

5.11.1 Synoptic situations for snow in the United Kingdom

Over Britain, over 70% of substantial and extensive falls of snow are associated with a warm front or warm occlusion approaching from between south and west (cold fronts being less important). In such situations a large supply of moisture is available. Frontal progress is very slow as the warm air rises over a much colder continental easterly flow at low levels, so that snowfall is prolonged.

On 20% of occasions snow/blizzard conditions are due to polar lows which, in a northerly airstream, can produce substantial but more localized snowfalls — more frequently in Scotland than further south.

Easterly winds bring snow showers, intensified by the passage of troughs, and give substantial falls of snow in eastern Scotland and England. Exposed north-facing coasts as far south as Norfolk and Kent can be seriously affected when there is an unstable northerly airflow in winter.

Fig. 5.21 illustrate the annual incidence of days with (a) snow falling, and (b) lying.

Chandler & Gregory (1976)
Wild et al. (1996)

5.11.2 Lying snow

Large amounts of lying snow will greatly distort temperature-level structure, lowering the natural condensation level, the cloud base and increasing hill fog.

Local Weather Manual — Scotland (1994)

5.11.3 Snow over high ground

The 80%, 50% and 20% snow probability lines on numerical model forecast charts are based on forecast 1000–850 hPa thickness values and refer to mean sea level. The graph **(Fig. 5.22)** has been prepared to help forecasters to adjust these values in order to estimate the probability of snow at higher levels. Thus a snow probability forecast of 20% at mean sea level from the grid-point output of a numerical model becomes 50% at 500 ft (150 m) (e.g. most of the Marlborough Downs and the Cotswolds) and over 70% at 1000 ft (300 m).

5.11.4 Drifting of snow

With the temperature below 0 °C, drifting of dry/loose snow starts when the wind speed exceeds 12 kn. Serious drifting occurs with winds above 17 kn.

A *blizzard* is defined by the UKMO as 'the simultaneous occurrence of moderate or heavy snowfall with winds of at least force 7, causing drifting snow and reduction of visibility to 200 m or less'

Met. Glossary (1991)

5.11.5 Visibility in snow (see 3.10)

5.11.6 Thawing of snow

(i) Generally warm rain is the most effective agent for removing snow in winter since screen temperatures will not rise much above 0 °C over extensive areas of snow.
(ii) Insolation is most effective in other seasons, although it will have a negligible effect in hollows and north-facing slopes.
(iii) A depth of 150 mm (6 in) of snow requires either a continuous mild environment for several days or about 25 mm of rain to dispel it.
(iv) Since the advancing air will be cooled, thawing is less away from the windward edge of the snow cover.
(v) A screen temperature of 3 °C thaws 25 mm of snow in 24 hours, but if this warm air invasion is combined with appreciable rain, then 50 to 100 mm of snow thaws over the same period.

HWF (1975), Chapter 19.7.7

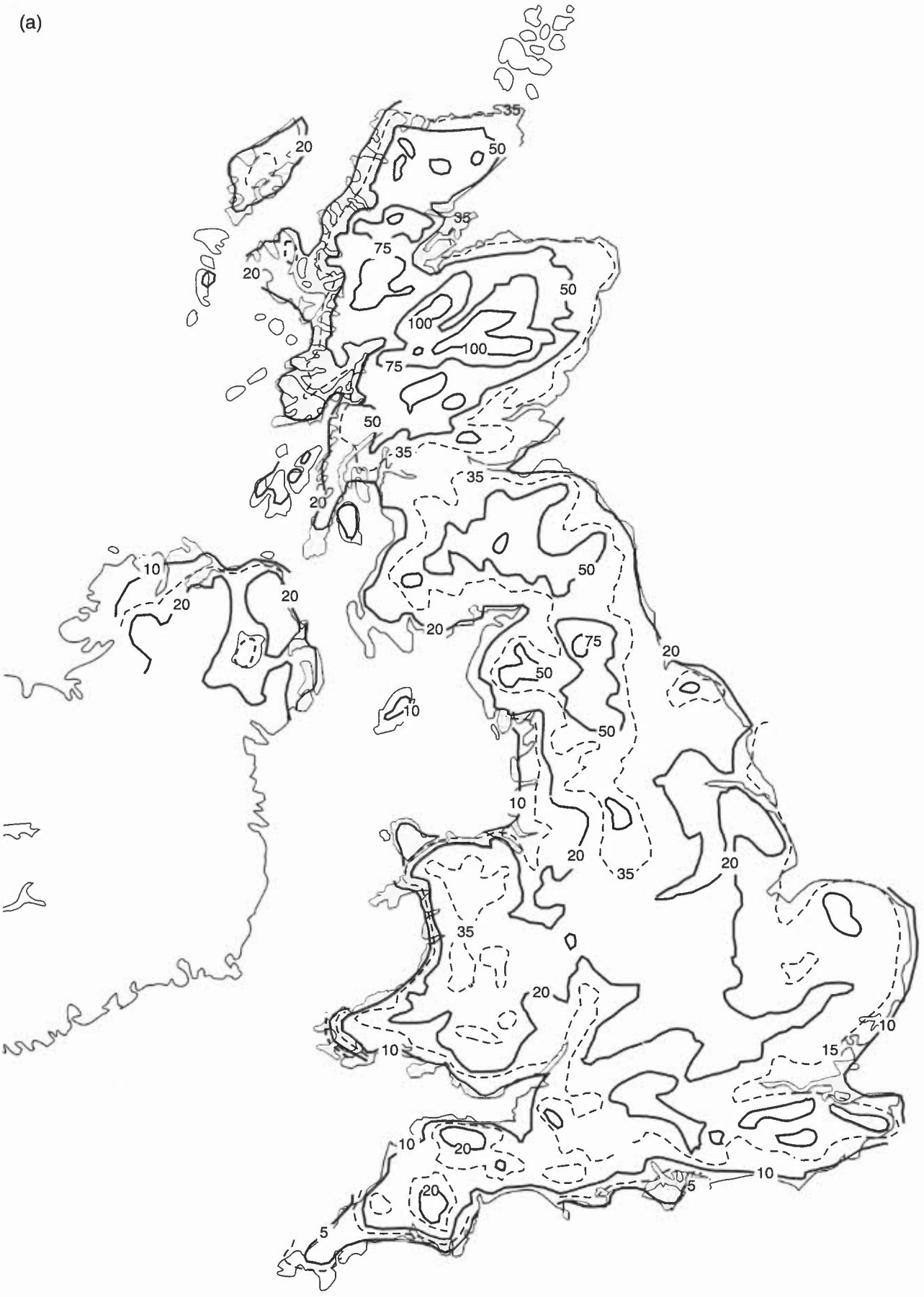

Figure 5.21(a). Annual incidence of days with snow falling.

(b)

Figure 5.21(b). Annual incidence of days with snow lying (October–May).

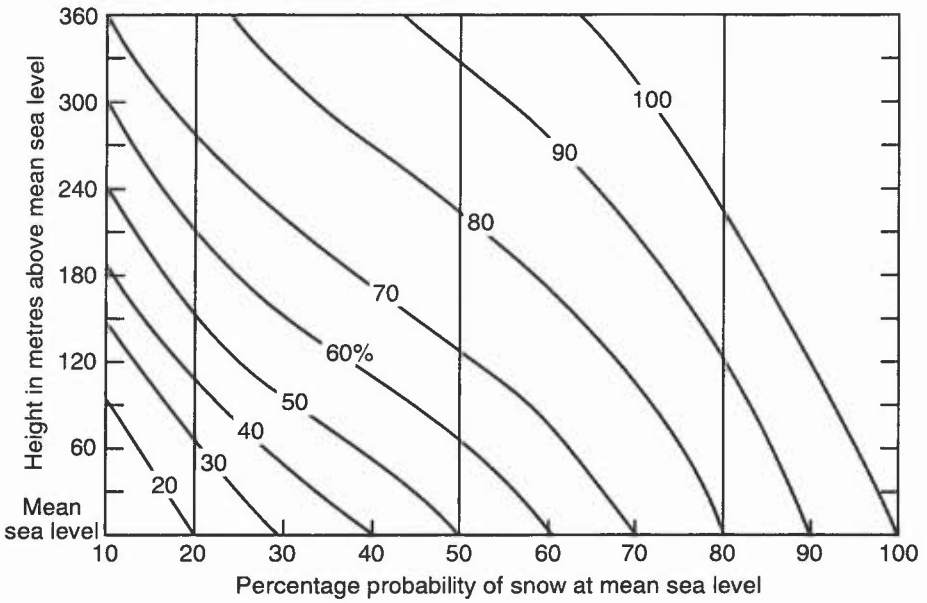

Figure 5.22. Snowfall over high ground. The increased probability of precipitation falling as snow over high ground, given its probability of occurrence at mean sea level.

BIBLIOGRAPHY

CHAPTER 5 — LAYER CLOUDS & PRECIPITATION

Aerodrome Weather Diagrams and Characteristics (AWDC), 1960: Meteorological Office, London, HMSO (Also Airfield Weather Diagrams, Met.O.564).

Ahmed, M., Graham, R.J. and Lunnon, R.W., 1993: Creating a global climatology of freezing rain using numerical model output. *In* Proceedings of the Fifth Conference on Aviation Weather Systems. American Meteorological Society, Vienna (Virginia), USA.

Alexander, L.L., 1964: Tidal effects on the dissipation of haar. *Meteorol Mag*, **93**, 379–380.

Appleman, H.S., 1953: The formation of exhaust condensation trails by jet aircraft. *Bull Am Meteorol Soc*, **34**, 14–20.

Bennetts, D.A., McCallum, E., Nicholls, S. and Grant, J.R., 1986: Stratocumulus: an introductory account. *Meteorol Mag,* **115**, 65–76.

Booth, B.J., 1973: A simplified snow predictor. *Meteorol Mag,* **102**, 330–340.

Boyden, C.J., 1964: A comparison of snow predictors. *Meteorol Mag,* **93,** 353–365.

Browning, K.A., Hill, F.F and Pardoe, C.W., 1974: Structure and mechanism of precipitation and the effect of orography in a wintertime warm sector. *QJR Meteorol Soc,* **109**, 309–330.

Browning, K.A., Pardoe, C.W. and Hill, F.F., 1975: The nature of orographic rain at wintertime cold fronts: *QJR Meteorol Soc,* **101**, 333–352.

Browning, K.A., 1985: Conceptual models of precipitation systems. *Meteorol Mag*, **114**, 293–318.

Carruthers, D.J. and Choularton, T.W., 1983: A model of the seeder-feeder mechanism of orographic rain including stratification and wind-drift effects. *QJR Meteorol Soc,* **109**, 575–588.

Chandler, T.J. and Gregory, S., 1976: The Climate of the British Isles, Longman.

Ferris, P.D., 1996: The formation and forecasting of condensation trails behind modern aircraft. *Meteorol Appl*, **3**, (to be published).

Findeisen, W., 1940: Die Entstehung der 0 °C-Isothermie und Fraktocumulus-Bildung unter Nimbostratus. *Meteorol Z.*, **57**, p. 49.

Goldman, L, 1951: On forecasting ceiling lowering during continuous rain. *Mon Weather Rev*, **79**, 133–142.

Hand, W., communication in: Davies, T. and Hammon, O.M., 1986: Snow forecasting from the Meteorological Office fine-mesh model during the winter of 1985/86. *Meteorol Mag,* **115**, 396–404.

Handbook of Aviation Meteorology (3rd edition), 1994: London, HMSO.

James, D.G., 1957: Forecasting cirrus cloud over the British Isles. *Prof Notes*, Meteorological Office, **8**, 123.

James, D.G., 1959: Observations from aircraft of temperatures and humidities near stratocumulus clouds. *QJR Meteorol Soc,* **85**, 120–130.

Kraus, E., 1943: Some contributions to the physics of non-frontal layer clouds. *SDTM* No. 67 (Meteorological Office, London, Unpublished).

Lamb, H.H., 1945: Haars or North Sea fogs on the coast of Great Britain. Meteorological Office report (M.O.504).

Local Weather Manual — Scotland, 1994: Meteorological Office.

Lowndes, C.A.S., Beynon, A. and Hawson, C.L., 1974: An assessment of some snow predictors, *Meteorol Mag*, **103**, 341–358.

Lumb, F.E., 1986: Local snow forecasting. *Weather*, **41**, 29–30.

Mansfield, D.A., 1988: An investigation into stratus distribution over the UK. *Meteorol Mag*, **117**, 236–245.

Robichaud, A.I. and Austin, G.L., 1988: On the modelling of warm orographic rain by the seeder-feeder mechanism. *QJR Meteorol Soc,* **114**, 967–988.

Smith, R.B., 1989: Mechanisms of orographic precipitation. *Meteorol Mag,* **118**, 85–88.

Sparks, W.R., 1962: The spread of low stratus from the North Sea across East Anglia. *Meteorol Mag*, **91**, 361–365.

Warne, D.V., 1993: Stratus forecasting. *Meteorol Mag,* **122**, 113–116.

Wild, R., O'Hare, G. and Wilby, R., 1996: A historical record of blizzards/major snow events in the British Isles, 1880–1989. *Weather*, **51**, 82–91.

CHAPTER 6 — TURBULENCE AND GUSTS

CHAPTER 6 — TURBULENCE AND GUSTS

6.1 Turbulence in the free atmosphere

The sources are deep convection, wave motion and clear air turbulence (CAT).

6.1.1 Turbulence due to convection

This occurs at the boundaries of vertical convective currents:

(i) in cloud; cumulonimbus clouds can extend above 40,000 ft (12,200 m) in the United Kingdom, and above 60,000 ft (18,300 m) in the USA and some tropical areas;
(ii) outside cumulonimbus clouds, especially in clear air around the anvil and just above a storm top;
(iii) in dry thermals below cloud base, or in a cloudless region over any heated land mass (over deserts, dry convection may extend up to 15,000–20,000 ft (4600–6100 m)).

The magnitude of typical vertical currents in convective clouds, based on aircraft reports, are (**Table 6.1**):

Table 6.1.

Regime	Vertical velocity ($m\ s^{-1}$)	Description of turbulence
Stratocumulus		Light/moderate, occasionally severe over rugged terrain or due to instability
Altocumulus		Light/moderate, occasionally severe in unstable medium-level layers
Cumulus (humilis/mediocris)	1–3	Light
Cumulus (congestus)	3–10	Moderate
Cumulonimbus	10–25	Severe
Severe storm (USA)	>>25	Extreme
Dry thermals	1–5	Light/Moderate
Downdraughts	3–15	Moderate/Severe
Downdraughts (USA)	up to 40	Extreme

6.1.2 Wave-induced turbulence

Both *trapped* and *untrapped* waves may induce turbulence (see 1.3.2.1). Although both types are characterized by smooth, laminar flow, severe turbulence is often associated with convective instability or shearing instability of these waves. Turbulence due to mountain waves will be found:

(i) throughout middle and lower troposphere in the lee of a mountain range experiencing a severe downslope windstorm;
(ii) above the main tropospheric jet during conditions of strong mountain flow (with little change of wind vector with height);
(iii) at an elevated layer of very light winds (or flow reversal) when surface flow is strong and stably stratified;
(iv) in a layer of strong stability (or inversion) when surface flow is strong and stably stratified.

Bailey (1970) **Shutts & Broad (1993)**
Bradbury (1989) **Stull (1988)**

6.1.2.1 Inferring turbulent areas from imagery

High mountains with steep lee slopes may generate turbulence indicated on imagery by a narrow stationary clearing of jet cirrus to the lee (**Fig. 6.1(a)**); this will contrast with the cloud pattern with turbulence absent (**Fig. 6.1(b)**).

Bader et al. (1995), Chapter 8

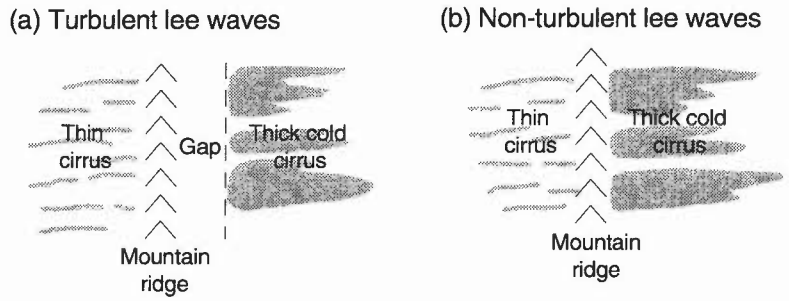

Figure 6.1. The relation between cloud patterns and possible turbulence, (a) pattern associated with turbulence and (b) pattern associated with turbulence absent.

6.1.3 Clear Air Turbulence (CAT)

Although this term can refer to any turbulence not associated with cloud, it is usually applied only to medium- and high-level disturbances.

Table 6.2(a). Typical dimensions of regions within which CAT may be encountered

Horizontally:	80–500 km (50–300 miles) along the wind direction, but only 20–100 km (12–60 miles) across the wind flow.
Vertically:	500–1000 m (1600–3300 ft), but they may be as shallow as 25 m (80 ft), or as deep as 4500 m (15,000 ft) near mountains.

Table 6.2(b). Mean percentage duration of CAT encounters experienced by jet transport aircraft on North Atlantic flights

Light or greater	10%
Moderate or greater	1.25%
Severe	0.013%

Conditions for unusually prolonged, intense CAT are noted in 6.1.3.2(iv).

HAM, Chapter 5.8

6.1.3.1 Synoptic indicators of CAT

Marked wind shear

(i) Both vertical and horizontal wind shears are important for the physical generation of the turbulent eddies that cause turbulence, and stability (or instability) of the air suppresses (or enhances) the effect.

(ii) The relative magnitude of the stability to the kinetic energy due to the vertical wind shear (Richardson number, *Ri*) is used in theoretical calculations.

(iii) The theoretical threshold for turbulence initiation is as *Ri* drops below 0.25; a value of 0.5 is more appropriate for layers resolved by a radiosonde.

Jet streams

About 60% of CAT reports are near jet streams. The most probable regions are those where rapid changes or development are occurring **(Fig. 6.2(a))**:

(i) on the cold side, near and below the core;
(ii) on the warm side, above the core;
(iii) near exits with marked curvature and diffluence;
(iv) at a confluence or diffluence of two jet streams;
(v) near sharp upper troughs;
(vi) around sharp ridges on the warm side of jets;
(vii) where one jet undercuts another;
(viii) where the tropopause height fluctuates.

Moderate/severe CAT is often associated with certain cirrus (Ci) boundaries and cloud patterns which identify jet streams accompanied by strong temperature gradients, shears, deformation, atmospheric waves and instability.

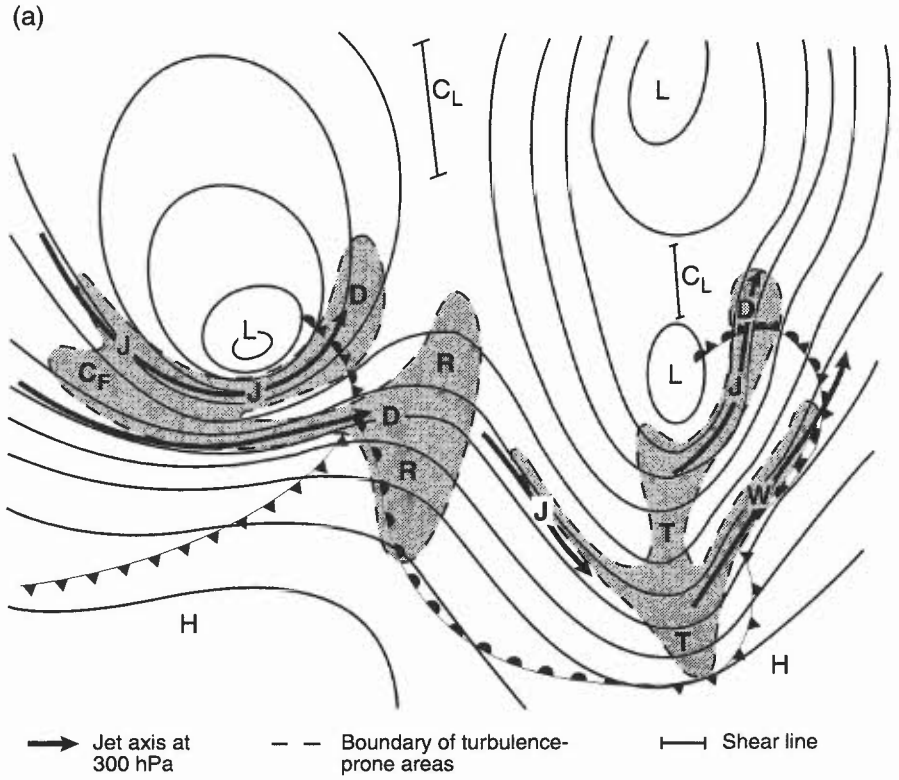

Figure 6.2(a). Main turbulence-prone areas between 500 and 200 hPa as related to features of the 300 hPa chart.

—	300 hPa contours. Fronts marked are at surface.
C_F	Region of confluence between two jet streams.
C_L	Upper-air col. Turbulence occurs in narrow bands along marked shear line.
D	Diffluent region of jet stream.
J	Jet-stream turbulence on low-pressure side.
R	Developing upper ridge.
T	Sharp upper trough.
W	Developing wave depression.

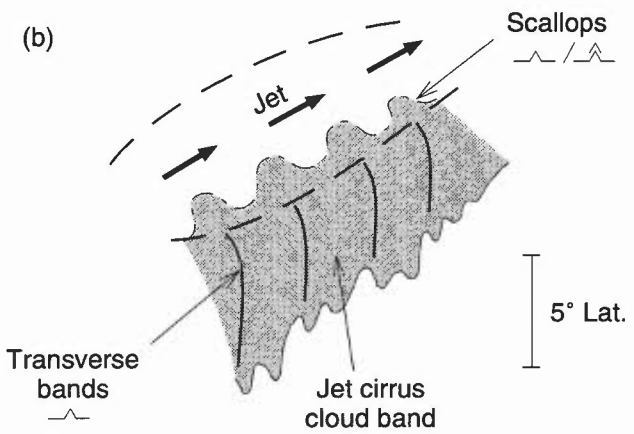

Figure 6.2(b). Model showing the relationship of turbulence to transverse bands and scallops in a jet cirrus band. Dashed lines enclose regions where moderate turbulence is likely.

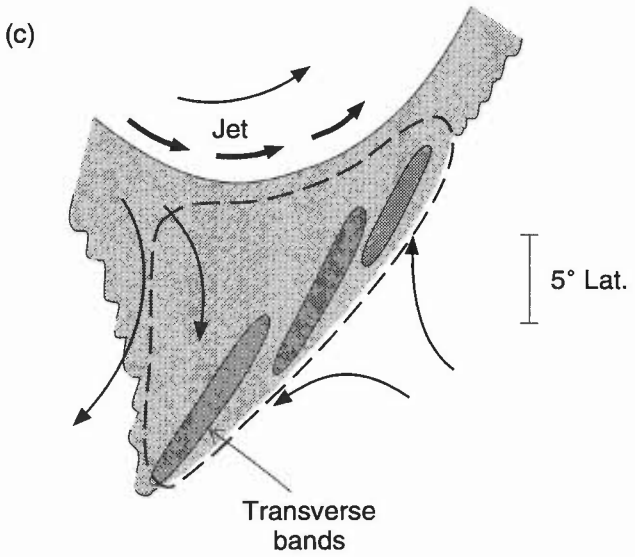

Figure 6.2(c). Model showing the relationship of turbulence to transverse bands in a delta cloud formation. The dashed line encloses a region where turbulence is likely, and thin arrows are streamlines.

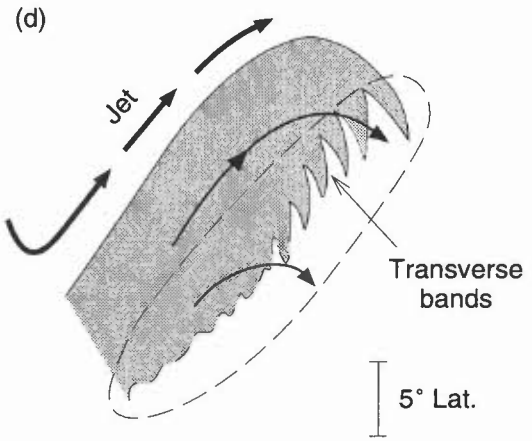

Figure 6.2(d). Model showing the relationship of turbulence to transverse bands (cirrus streamers) along the leading edge of ridge cirrus. The dashed line encloses a region of turbulence. Thin arrows are high-level streamlines.

Turbulence is usually within 3° latitude of the cloud or moisture edge. Transverse Ci bands, Ci 'scallops' and billows may indicate CAT at jet aircraft cruising level **(Fig. 6.2(b))**.

Curved flow

(i) In areas of anticyclonic curvature, where the actual wind speed approaches the critical value of twice the geostrophic wind speed.
(ii) Within 150 n mile or so of the axis of a sharp upper trough where the wind shift is over 90°.
(iii) Occasionally, across shear lines in cols where the wind direction reverses rapidly.

Turbulence in deformation zones is often associated with a transverse banding signature in Ci (**Fig. 6.2(c)**); delta- and comma-shaped clouds are a reliable indicator of moderate or severe turbulence (particularly as the comma system transforms into a vortex).

Thermal gradients

Cloud edges may provide clues as to thickness gradients; near a ridge axis transverse bands (Ci streamers indicate a turbulence area **(Fig. 6.2(d))**.

Topography

CAT is reported twice as often over land as over the sea, and is possibly ten times more frequent over mountains as over flat land.

Bader et al. (1995), Chapter 3 **Sparks et al. (1976)**
Ellrod (1990) **WMO (1977)**
Hisscott (1986)

6.1.3.2 Empirical prediction of CAT

Useful empirical rules are:

(i) Horizontal wind shear:
If shear $\geq$20 kn deg^{-1} of latitude, forecast moderate CAT
If shear $\geq$30 kn deg^{-1} of latitude, forecast severe CAT.
(ii) Vertical wind shear:
If shear $\geq$6 kn/1000 ft, forecast moderate CAT
If shear $\geq$9 kn/1000 ft, forecast severe CAT
(iii) Jet streams:
If the core speed exceeds 100 kn, and vertical wind shear 4 kn/1000 ft, forecast moderate CAT within 150 n mile.
(iv) An unusually persistent and extensive incidence of moderate to severe CAT reported over the UK in September 1985, was associated with diffluence and anticyclonic turning below a warm-frontal zone.
(v) CAT is rare above a well-defined tropopause.

CAT probability forecasts are available from numerical prediction model output.

Hisscott (1986) **WMO (1977)**

6.1.4 Intensity of turbulence and aircraft response

(i) The intensity of the turbulence reported by aircraft ('bumpiness') will be a function of the strength of the vertical currents and of various aircraft characteristics.

(ii) Individual aircraft will experience different effects, depending on their track, speed, flown profile and physical characteristics. **Table 6.3** (ICAO definitions) refers to civil aircraft while not discussing the origin of the turbulence.

Table 6.3. Definitions (ICAO) of turbulence

Description	Effect on civil aircraft
Light	Effects are less than those for Moderate intensity.
Moderate	There may be moderate changes in aircraft attitude and/or height but the aircraft remains in control at all times. Air-speed variations are usually small. Changes in accelerometer readings of 0.5–1.0 g at the aircraft's centre of gravity. Occupants feel strain against seat belts. There is difficulty in walking. Loose objects move about.
Severe	Abrupt changes in aircraft attitude and/or height. The aircraft may be out of control for short periods. Air-speed variations are usually large. Changes in accelerometer readings greater than 1.0 g at the aircraft's centre of gravity. (Military aviators regard +4 g/−2 g as severe). Occupants are forced violently against seat belts. Loose objects are tossed about.
Extreme	Effects are more pronounced than for Severe intensity.

CAA (1991, 1992)
HAM (1994), Chapter 12.3
HWF (1975), Chapter 23.3

6.2 Turbulence near the surface

The sources will be frictional and orographic; there will also be effects due to deep convection and severe storms. Forecasts required will depend on what is at risk and the nature of the wind /gust hazard.

Hunt, 1995

6.2.1 Turbulence, gusts and squalls

(i) As a rough guide: the intensity of turbulence expected in the lowest few hundred feet in windy conditions increases as surface roughness increases **(Table 6.4(a))**.

(ii) Strong sunshine added to strong wind may increase the difficulties of controlling aircraft, especially on landing and take-off.

Violent turbulence creates a most dangerous low-level hazard to aircraft. It may occur:

(i) during or preceding the passage of an active cold front;
(ii) during or preceding a thunderstorm;
(iii) in hilly or mountainous country (1.3.2, 1.3.3);
(iv) with a steep lapse rate.

At 250 feet (75 m) AGL mean winds >30 to 35 kn in unstable conditions might preclude a low-level training flight, primarily due to the dangers of parachute-induced drag should ejection be necessary. Thus a 35 kn wind can be a forecast 'threshold'. Low-level convective turbulence has been reported by aircrew to be over-forecast; the very turbulent conditions encountered by them in mountain-wave and rotor streaming conditions are reported in 1.3.3.

Cashmore (1966) **HAM (1994)**
Förchtgott (1949) **Klemp (1978)**

6.2.1.1 Criteria for forecasts of hazardous low-level wind shear/turbulence

One or more of the following to be satisfied:

(i) Mean surface wind ≥20 kn.

(ii) Magnitude of vector difference between mean surface wind and the gradient (2000 ft) wind ≥40 kn.

(iii) Thunderstorms or heavy showers within 10 km.
(iv) Significant wind shear has already been reported by aircraft in the vicinity.

MO, Heathrow(198?)

6.2.1.2 Effect of turbulence, lapse rate and wind shear

Turbulent mixing, lapse rates and wind shears are interlinked; the net result of turbulent mixing, starting with a surface inversion, is to warm the lower layers and cool the upper layers until a dry adiabat is established, sometimes forming an inversion at the top of the friction layer. If initial conditions are superadiabatic, the lapse rate will decrease. Section 5.5 discusses the case when the mixing air becomes saturated.

Criteria for forecasting low-level wind shears likely to hazard aircraft are in 6.2.1.1.

6.2.2 Gusts

Empirical and theoretical procedures have produced estimates for 'gust ratios' and gusts which are defined both in terms of the mean hourly wind, and relative to the gradient wind.

Table 6.4(a). Ratio of maximum (3-second) gust to mean hourly speed (for strong, steady 10 m winds)

Surface type	Range of ratios	Estimated average
Open sea	1.3	1.3
Isolated hill tops	1.4–1.5	1.4
Flat open country	1.4–1.8	1.6
*Rolling country (few wind-breaks)	1.5–2.0	1.7
Rolling country (numerous wind-breaks), forest areas, towns, outskirts of large cities	1.7–2.1	1.9
Centres of large cities	1.9–2.3	2.1

*Local variations, using this commonly used category, often give gusts varying widely in space and time from the estimated values, making airfield forecasting difficult, especially under isallobaric surging.

Table 6.4(b). Maximum wind speeds relative to the gradient wind, V_{grad}, in neutral conditions

	V_{grad}		
	units: m s^{-1} (kn)		
Surface type	10 (19)	20 (39)	30 (58)
Open sea	8.8 (17.0)	17.0 (33.1)	24.9 (48.1)
Flat open country	7.8 (14.8)	15.0 (27.3)	21.6 (41.8)
Rolling country (few wind-breaks)	7.1 (13.5)	13.4 (26.1)	19.5 (37.7)
Rolling country (numerous wind-breaks) forest areas, towns, outskirts of large cities	6.8 (12.9)	12.8 (25.0)	18.3 (35.4)
Centres of large cities	6.4 (12.1)	12.0 (23.4)	17.4 (33.6)

Maximum wind speed V_{max} is here defined statistically as: the mean wind speed V_{mean}, plus the fluctuating component in the direction of the mean wind speed (3 times the standard deviation).

These tables may be combined to give an estimate of the mean wind and the ratio of max/mean wind over different surfaces in neutral conditions in terms of the gradient wind **(Table 6.4(c))**.

Table 6.4(c). Estimate of the mean wind and the ratio max/mean wind over different surfaces in neutral conditions in terms of the gradient wind

	V_{grad}			
	units: m s^{-1} (kn)			
Surface type	10 (19)	20 (39)	30 (58)	V_{max}/V_{mean}
Open sea	6.8 (13.2)	13.1 (25.4)	19.2 (37.2)	1.3
Flat open country	4.9 (9.5)	9.4 (18.2)	13.5 (26.2)	1.6
Rolling country (few wind-breaks)	4.2 (8.1)	7.9 (15.3)	11.5 (22.3)	1.7
Rolling country (numerous wind-breaks) forest areas, towns, outskirts of large cities	3.6 (7.0)	6.7 (13.0)	9.6 (18.6)	1.9
Centres of large cities	3.0 (5.8)	5.7 (11.1)	8.3 (16.1)	2.1

Bradbury et al. (1994) **HWF (1975), Chapter 16.7.1**

6.2.2.1 Gusts over hills

Limited UK observations suggest that the structure of the flow over hills associated with strong, steady winds is similar to that over flat terrain, the difference between hilly and flat terrain being the magnitude of the roughness length. The gust factor appears almost independent of hill height for hills greater than 100 m. Assuming a wavelength of hills to be 1.5 km (e.g. gust ratios representative of the Welsh hills), the geostrophic gust ratio at hill height is estimated as about 0.75.

6.2.2.2 Rotor streaming

Associated with large amplitude *trapped lee waves* and *severe downslope winds (1.3.3.4)*:

(i) Surface winds often fluctuate between low and high values. The effect is considered not to extend more than 15 n mile downwind (**Fig. 6.3**).

(ii) The vertical wind/temperature profiles associated with rotor streaming are of the form:
strong winds (over 25 kn) near the ground;
a sharp decrease in wind speed, which may be accompanied by a large change in direction, at a height of 1.5 to 2 times the height of the hills;
an inversion within 1000–3000 feet of the hill tops.

Some severe cases of turbulence affecting airfields (e.g. in NW Wales) may be due to 'rotor streaming'. Initially there is a marked upwind acceleration over the hill/ridge top to 1.5 to 2 times gradient speed; speeds of some 70 kn have been encountered by helicopters. Dark lee areas in water vapour imagery can indicate the presence of hazardous, downslope surface winds.

Bader et al. (1995) Chapter 8 **Förchtgott (1949)**
Bradbury (1989) **Stull (1988)**

6.2.2.3 Gust forecasting in strong wind situations

The gales that disrupted the 1979 Fastnet Yacht Race, and the Burns' Day storm of 1990 are examples of convection occurring in the presence of strong geostrophic winds in a mid-latitude depression. Damaging winds also occur in association with thunderstorms in such depressions. Convectively generated gusts in both cases are produced by two mechanisms:

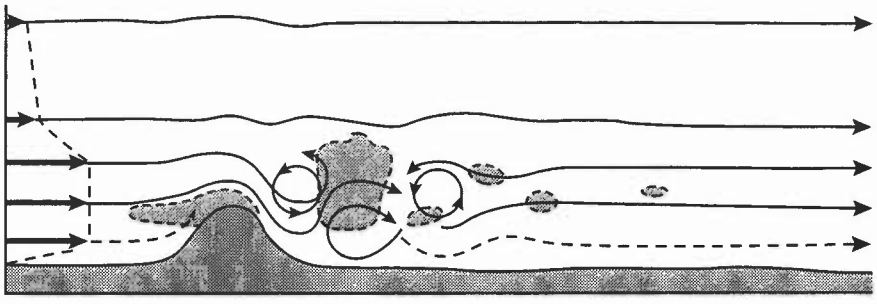

Figure 6.3. Rotor streaming (after Förchtgott). The vertical profile of the wind is shown by the bold arrows on the left.

(a) the production of horizontal momentum by pressure gradient forces as convective downdraughts are blocked by the surface and spread out horizontally,
(b) the downward transport of horizontal momentum by convective downdraughts in the presence of vertical shear.

The relative importance depends on the strengths of the vertical wind shear and the intensity of the downdraughts.

An effective approach to forecasting strong gusts is:
Are showers likely?
(i) *No*: use **Table 6.4(b)**
(ii) *Yes*: use gradient wind speed at 900 hPa as first guess of likely maximum gusts at exposed locations.
If showers are expected to be moderate or heavy, squalls (expected in association with a trough or front) or gusts might significantly exceed the gradient wind.

As a rule of thumb: $V^2_{gust} = V^2_{convection} + V^2_{gradient}$

where $V_{convection}$ is estimated using Fawbush and Miller (**Fig. 6.4**), or $V_{convection} = (gh\,\Delta T/T)^{0.5}$ and, ΔT is the surface temperature deficit in the downdraught, T the average absolute temperature and h the depth of the downdraught in metres.

More explicitly the gust is well estimated by: $V^2_{gust} = [(gh\,\Delta T/T) + V(h)^2 + 2gq_r h]$ in SI units

where h = 2000 m, T = 300 K, q_r = Rainfall rate (mm h^{-1})/(3600 × air density × precipitation fall velocity).
Air density = 1 kg m^{-3}, and fall velocity is about 5 m s^{-1} for rain and up to 10 m s^{-1} for hail. (This term is only of importance at high rainfall rates.)

It follows that a 10 m s^{-1} gust could be produced by either a ΔT of 1.7 °C, or by a rainfall rate of 45 mm h^{-1}, or by an initial wind speed at the top of the downdraught of 10 m s^{-1}.

Bradbury et al. (1994)
Nakamura et al. (1996)

6.2.2.4 Forecasting peak gusts in thunderstorms

The peak gust can be estimated using Fawbush and Miller, which relates gust strength to the negative buoyancy force in a downdraught. It is thus based mainly on the first mechanism ((a) in 6.2.2.3) (although, by its empirical nature, Fawbush and Miller may encompass elements of the second process).

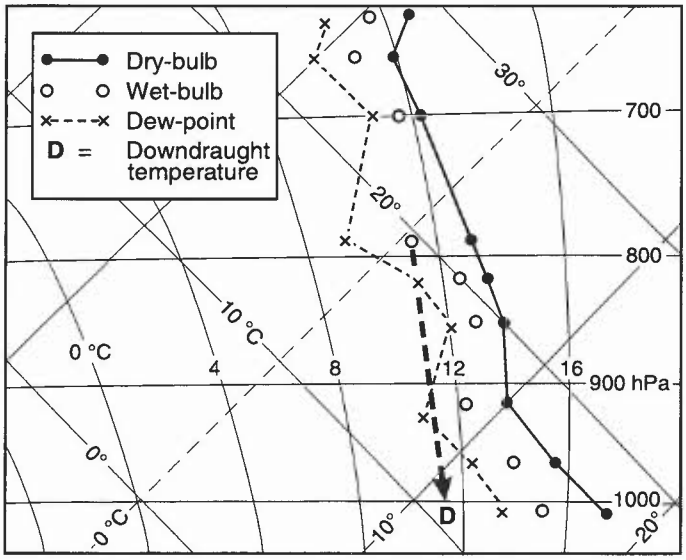

Figure 6.4. Example of a tephigram, illustrating the computation of the downdraught temperature in non-frontal thunderstorms in the USA (after Fawbush and Miller).

Procedure, in particular for summer thunderstorms when the downdraught originates near the wet-bulb freezing level (i.e. melting point for precipitation), is as follows:

(i) Peak wind speeds depend largely on the temperature difference between this cooler downdraught air and the surrounding warmer air at the surface.

(ii) Downdraught temperature may be estimated from an upper-air sounding by drawing a saturated adiabat from the level where the wet-bulb curve cuts the 0 °C isotherm to the surface pressure. **Fig. 6.4** illustrates the construction on a tephigram. **Fig. 6.5** shows the relationship between the temperature difference and the peak wind speed. A correlation coefficient of 0.86 was found in the USA (for non-frontal thunderstorms).

In wintry conditions the downdraught may originate well above the freezing level, being driven by the evaporation of snow or graupel. Such thunderstorms are usually associated with a front or trough in a depression, in which case the gust forecasting technique in the previous section is recommended.

Nakamura et al. (1996)
Fawbush & Miller, 1954

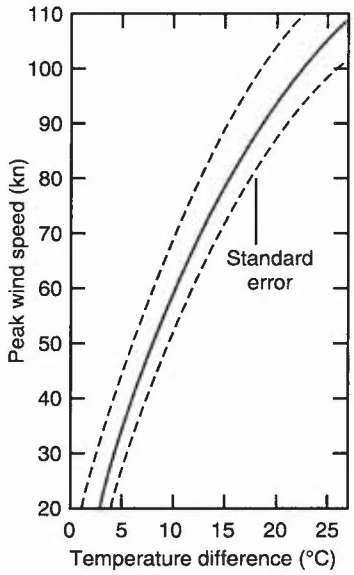

Figure 6.5. Peak wind speed at the surface related to the temperature difference between cold downdraught air and the warm surface air, during non-frontal thunderstorms in the USA.

6.2.2.5 Wind-direction changes associated with gusts

Although there is widespread belief among, for example, yachtsmen that during a surface gust the wind may veer (in the northern hemisphere) by up to 20° to 30°, studies at Cardington and elsewhere have failed to show any significant tendency for this happening at low wind speeds likely to be encountered by yachts. However, there may be a conceptual difference here; for the yachtsman a gust has to last several minutes rather than a few seconds to be of interest.

However, severe *convective gusts* (>65 kn) occasionally occur from a substantially different direction; veers of 60° have been recorded. In high gusts of convective origin at Manston between 1980 and 1990, the mean and standard deviation veers were 40° and 65°, respectively.

Bradbury et al. (1994)
Brettle (1994, 1996)
Houghton (1984)
Singleton (1981)

6.2.3 Squalls

See 6.2.2.3; also 4.7.6.

HWF (1975), Chapter 16.7.2
Ludlam (1980)

6.2.4 Tornadoes and microbursts

6.2.4.1 Tornadoes

(i) These are usually associated with the strong low-level convergence and intensification of vorticity of severe convective storms (4.7.7).
(ii) Pressure falls and wind speeds within the narrow funnel rise to exceptional levels.
(iii) In the United Kingdom modest tornadoes occur mainly in association with vigorous cold fronts or during heavy showers or thunderstorms and with convective potential vorticity advection (PVA) features (8.8).
(iv) Tornadoes normally require:
considerable depth of convective instability;
high values of θ_w (18–23 °C) in lowest layers;
marked potential instability (θ_w falling 5 °C or more up to 500 hPa);
marked vertical wind shear with winds increasing and veering with height.

HAM (1980)
Ludlam (1980)

6.2.4.2 Microbursts (downbursts)

Strong flows associated with thunderstorm downdraughts (4.7, 6.2.2.4) pose severe risks to aircraft at take-off and landing.

(i) The flows can become organized such that the aircraft encounters a 'ramp pair', on take-off/landing, a sudden headwind component being replaced by a vertical downdraught, followed by a tailwind component — all over a few kilometres.
(ii) The damaging winds are highly divergent, vertical momentum being converted to horizontal momentum; the surface outflow speed ranges from 10 m s^{-1} (19 kn) to over 25 m s^{-1} (49 kn) over a horizontal distance of 2 to 4 km (1.1 to 2.2 n mile).
(iii) The maximum speed occurs usually around 100 m above the ground.
(iv) Horizontal shears of 12.5 m s^{-1} (25 kn) km^{-1} have been measured.
(v) Radar often gives a characteristic 'spearhead-shaped' echo which may contain several potential microburst cells.
(vi) *'Wet' microbursts* are associated with shafts of intense, frozen thunderstorm precipitation falling through the melting layer. Negative buoyancy is enhanced with a high lapse rate below the melting layer.
(vii) *'Dry' microbursts* have virga visible but do not reach the surface. Evaporative cooling of the air may intensify the dry microburst downdraught, particularly if lower θ_w air at middle levels is entrained into the downdraught.

Summary of indicators for thunderstorm microbursts:
Large positive CAPE.
Little or no capping inversion.
At least 1500 m of unsaturated air beneath the convective cloud base.
A moist mid-tropospheric layer between 1500 m and 4500 m above the ground.
An elevated dry layer above an altitude of 4500 m.

Bader et al. (1995), Chapter 6.5.6.5
CAA (1991)
Caracena et al. (1989)
HAM (1994)
McCarthy & Serafin, 1984
Naylor (1995)
Waters & Collier (1995)

BIBLIOGRAPHY

CHAPTER 6 — TURBULENCE AND GUSTS

Bader, M.J., Forbes, G.S., Grant, J.R., Lilley, R.B.E. and Waters, J., 1995: Images in weather forecasting. Cambridge University Press.

Bailey, M., 1970: Mountain lee-wave incidents in Scotland. *Meteorol Mag*, **99**, 110–118.

Barry, R.G., 1981: Mountain weather and climate. Methuen.

Bradbury,T., 1989: Meteorology and flight, A & C Black.

Bradbury, W.M.S., Deaves, D.M., Hunt, J.C.R., Kershaw, R., Nakamura, K. and Hardman, M.E., 1994: The importance of convective gusts. *Meteorol Appl,* **1,** 365–378.

Brettle. M.J., 1994: An investigation of possible systematic wind-direction changes associated with sudden increases in wind speed. *Meteorol Appl*, **1**, 179–183.

Brettle, M.J., 1996: Veering winds and yachting (with reply by F. Singleton). *Weather*, **51**, 320–322.

CAA, 1991: The effect of thunderstorms and associated turbulence on aircraft operations. London, Civil Aviation Authority. Aeronautical Information Circular No. 117/1991.

CAA, 1992: Low altitude wind shear, London, Civil Aviation Authority. Aeronautical Information Circular No. 48/1992.

Caracena, F., Holle, R. and Dodswell, C.A., 1989: Microbursts, a handbook for visual identification. US Dept of Commerce.

Cashmore, R.A., 1966: Severe turbulence at low levels over the United Kingdom. *Meteorol Mag*, **95**, 17–18.

Ellrod, G.P., 1990: Use of water vapour imagery to identify CAT. NOAA/NESDIS, Satellite applications information note 90/8. Washington, Dept of Commerce.

Fawbush, E.J. and Miller, R.C., 1954: A basis for forecasting peak wind gusts in non-frontal thunderstorms. *Bull Am Meteorol Soc*, **35**, 14–19.

Förchtgott, J., 1949: Wave currents on the leeward side of mountain crests. *Bull met tchecoal, Prague*, **3,** 49–51.

Handbook of Aviation Meteorology (HAM), 1994: London, HMSO.

Handbook of Weather Forecasting (HWF), 1975: Meteorological Office, Met.O.875.

Hisscott, L.A., 1986: Prolonged CAT over the British Isles on 4 September 1985. *Meteorol Mag*, **115**, 329–331.

Houghton, D., 1992: Wind strategy. Fernhurst Books.

Hunt, J.C.R., 1995: The contribution of meteorological science to wind hazard mitigation. *In* T. Wyatt (Ed), Proceedings of the Wind Engineering Society meeting on wind hazard, May 1995.

Klemp, J.B., 1978: A severe downslope windstorm and aircraft event induced by a mountain wave. *J Atmos Sci*, **35**, 59–77.

Ludlam, F.H., 1980: Clouds and storms, Pennsylvania State University Press.

McCarthy, J. and Serafin, R., 1984: The microburst: hazard to aircraft. *Weatherwise*, **37**, 120–127.

Meteorological Glossary (MG) (6th Edition), 1991: London, HMSO.

Nakamura, K., Kershaw, R. and Gait, N., 1996: Generation of near-surface gusts by deep convection. *Meteorol Appl*, **3**, (to be published).

Naylor, D.J., 1995: A probable microburst at Weston-on-the-Green on 24 July 1994. *Weather*, **50**, 278–282.

Shutts, G.J. and Broad, A., 1993: A case study of lee waves over the Lake District in northern England. *QJR Meteorol Soc*, **119**, 377–408.

Singleton, F., 1981: Weather forecasting for sailors. Hodder and Stoughton.

Sparks, W.R., Cornford, S.G. and Gibson, J.K., 1976: Bumpiness in clear air and its relation to some synoptic-scale indices. *Geophys Mem* No. 121, Meteorological Office.

Stull, R.B., 1988: An introduction to boundary layer meteorology. Kluwer Academic Publishers.

Waters, A.J. and Collier, C.G., 1995: The Farnborough storm — evidence of a microburst. *Meteorol Appl*, **2**, 221–230.

WMO, 1977: Forecasting techniques of CAT, including that associated with mountain waves. Geneva, World Meteorological Organization, Technical Note 155.

CHAPTER 7 — FRONTS: CONCEPTUAL MODELS AND ANALYSIS; NON-FRONTAL SYSTEMS

CHAPTER 7 — FRONTS: CONCEPTUAL MODELS AND ANALYSIS; NON-FRONTAL SYSTEMS

7.1 Conceptual models — fronts and conveyor belts

Conceptual models provide the framework for the visualization and interpretation of satellite and radar imagery and are discussed in Bader et al., 1995, Chapters 4 & 5.

7.1.1 Fronts

At the most basic level a front represents the 'boundary between air masses of different thermal characteristics'. Frontogenesis is encouraged by: pressure falls on both sides of the front; convergence of two air streams; orographic influences (in particular a warm front, on approaching high ground, will intensify on the windward side). Conversely frontolysis will occur when there are pressure ~~falls~~ RISES on both sides of the front; there are divergent wind fields; and in the lee of high ground.

7.1.1.1 Ana- and kata-fronts

Warm fronts and cold fronts may have ana- or kata- characteristics depending on whether the warm air mass is rising up or subsiding down the frontal surface. A front may change from ana- to kata- at some point along its length, or at some time during its life history.

7.1.2 Conveyor belts; cyclogenetic models (Fig. 7.1)

Archetypal models are:

(i) Warm conveyor belts (ana- and kata-cold frontal situations, **Fig. 7.2**, **Fig. 7.3**, respectively).
(ii) Cold conveyor belts ahead of warm fronts.
(iii) Mesoscale rain bands — narrow and wide.
(iv) Other mid-latitude systems — comma clouds and cold-air vortices; polar trough conveyor belt and instant occlusions.

Bader et al. (1995), Chapters 4 and 5
Browning (1985)

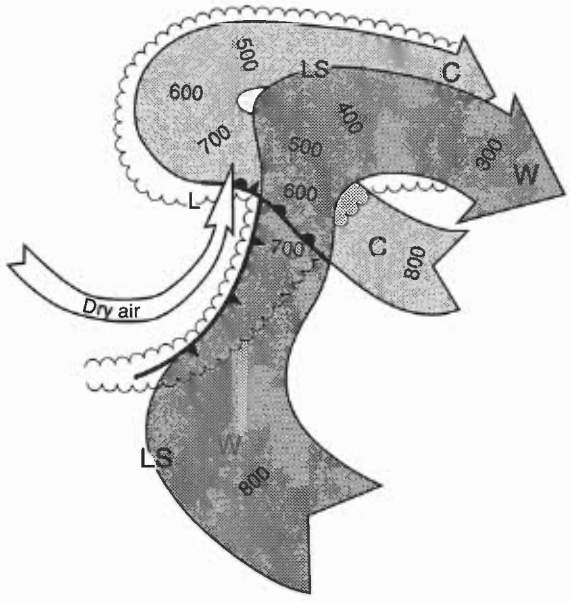

Figure 7.1. Model depicting the main features of the warm and cold conveyor belts in a mature mid-latitude depression. WW is the warm conveyor belt and CC is the cold conveyor belt. Figures within the broad arrows indicate the top of the belt in hectoPascals. The scalloped line represents the edge of the cloud produced by these flows. LS is the limiting streamline; L is the surface low.

7.1.3 The warm conveyor belt (WCB)

The dominant mechanism in frontal systems is baroclinic slantwise ascent in the form of a narrow airstream, the WCB, (**Fig. 7.1**) conveying large quantities of heat, moisture and westerly momentum. A small, but important, mainly ageostrophic, component perpendicular to the front produces two contrasting ascents: rearward and forward. Transitions from one to the other can occur along the front.

7.1.3.1 WCB with rearward-sloping ascent

This situation corresponds to the classical ana-front situation (**Fig. 7.2**); it is not as common in the UK as the forward-sloping one.

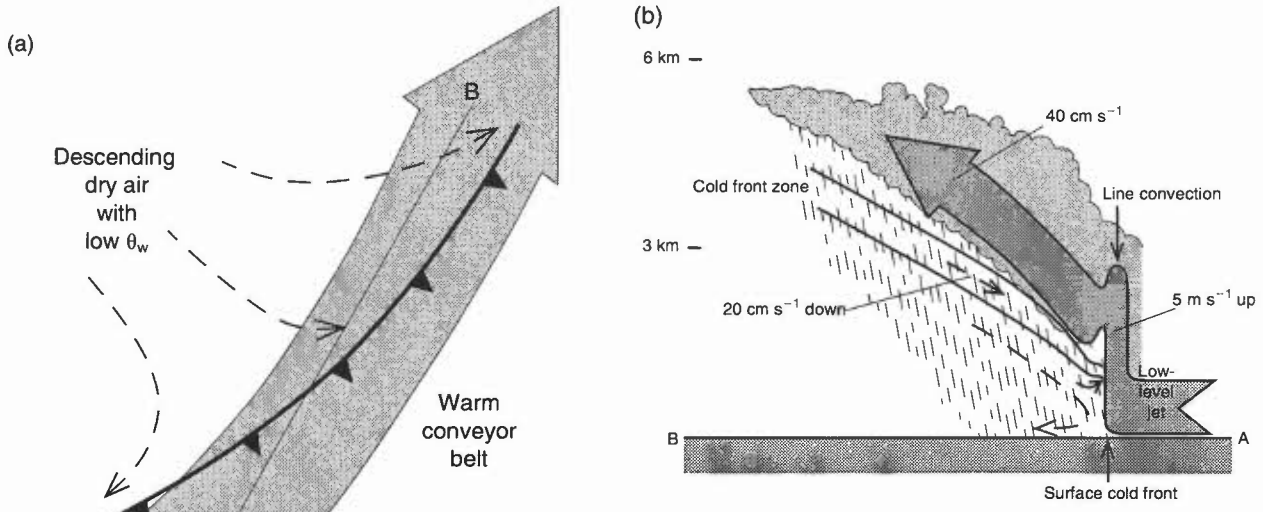

Figure 7.2. Schematic portrayal of airflow at a classical ana cold front showing the warm conveyor belt (bold arrow) undergoing rearward-sloping ascent above the cold-frontal zone with the cold air (dashed lines) descending beneath it: (a) plan view, (b) vertical section along AB in (a). LLJ marks the axis of the low-level jet. Flows are shown relative to the moving frontal system.

(i) The surface cold front tends to be sharp.

(ii) The warm boundary layer air ahead of the surface cold front is lifted abruptly some 2–3 km in a narrow strip adjacent to the cold front.

(iii) Further slantwise ascent above the cold air wedge produces two distinct precipitation patterns: a narrow band of very heavy rain at the surface cold front, and a broad belt of light-to-moderate rain behind, and often a little ahead of, the surface cold front.

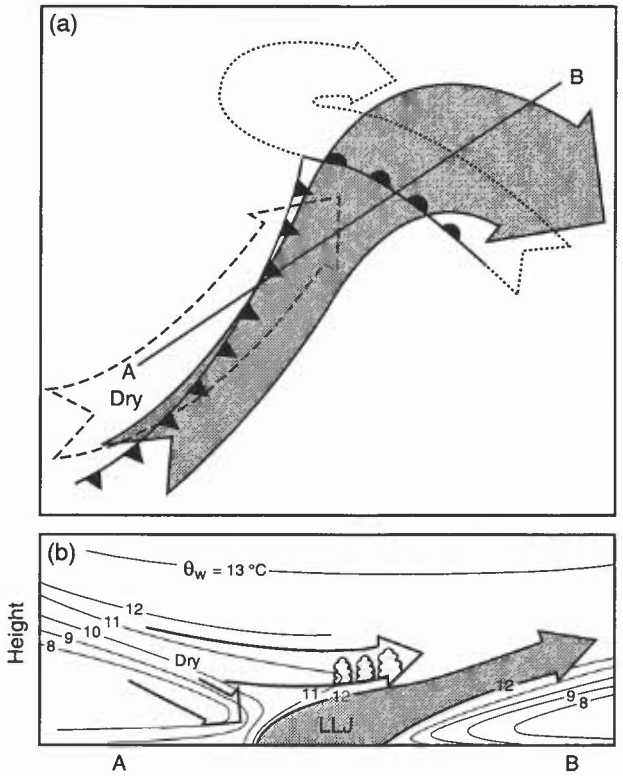

Figure 7.3. Schematic portrayal of airflow in a mid-latitude cyclone in which the warm conveyor belt (bold arrow with stippled shading) is undergoing forward-sloping ascent ahead of a kata cold front before rising above a flow of cold air ahead of the warm front (dotted arrow referred to as the cold conveyor belt). Cold middle-tropospheric air with low θ_w (dashed arrow) is shown overrunning the cold front and generating potential instability in the upper portion of the warm conveyor belt: (a) plan view, (b) vertical section along AB in (a). LLJ marks the axis of the low-level jet. Flows are shown relative to the moving frontal system.

7.1.3.2 WCB with forward-sloping ascent

This situation corresponds to the classical kata-cold front situation (**Fig. 7.3**).

(i) Low θ_w air overruns the warm conveyor belt in mid-troposphere, leading to generation of potential instability, realized later as convection (in the UK it occurs more usually as shallow convection at middle levels).

(ii) The convex-poleward boundary to this flow where it ascends and turns to the right is often clearly detectable in satellite VIS imagery from the upper-cloud shadow cast on the lower cloud layer.

(iii) The leading edge of the overrunning dry, low θ_w, air often appears as a well-defined upper cold front (**Fig. 7.4**); warm, moist air ahead, associated with organized convection, gives rise to a wide band of moderate-to-heavy rain.

(iv) The passage of the upper cold front is marked by scattered outbreaks of weakly convective rain. It may also be marked by a surface pressure trough or 'bar kick'. In general the upper cold front should be thought of as an upper wet-bulb temperature front; it is always accompanied by a decrease in humidity but not always accompanied by a significant decrease in dry-bulb temperature.

(iv) This is termed the 'split front' model because of the separate existence of the upper cold front; it is very common in the UK but can cause confusion if traditional classical frontal analysis is applied. The upper front should be identified distinctly.

Identification: compare the 700 hPa RH field with the position of the front as deduced from the 850 hPa chart; if the region of maximum RH lies forward of the frontal position, then this is likely to be a forward-sloping front.

Bader et al. (1995), Chapter 4
Browning (1995)

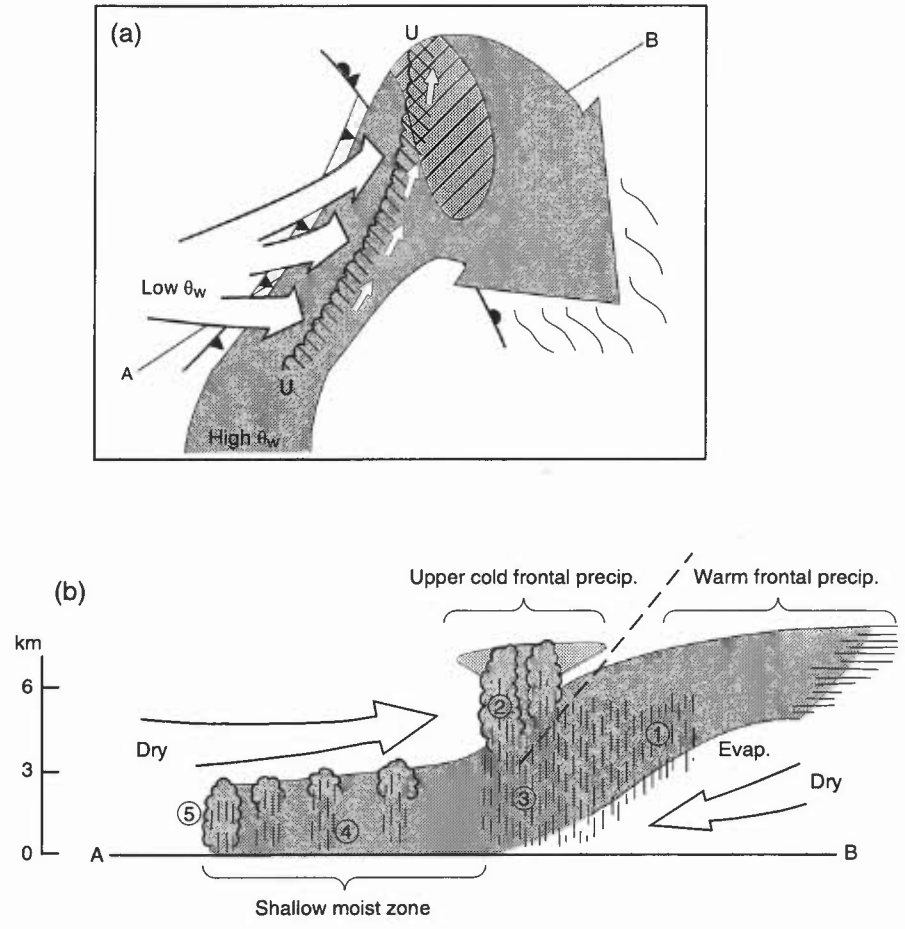

Figure 7.4. Schematic portrayal of the same situation as in Fig. 7.3, i.e. with the warm conveyor belt undergoing forward-sloping ascent, but drawing attention to the split-front characteristics and the overall precipitation distribution: (a) plan view, and (b) vertical section along AB in (a). In (a) UU represents the upper cold front. The hatched shading along UU and ahead of the warm front represents precipitation associated with the upper cold front and warm front, respectively. Numbers in (b) represent precipitation type as follows: 1, warm-frontal precipitation; 2, Convective precipitation-generating cells associated with the upper cold front; 3, precipitation from the upper cold-frontal convection descending through an area of warm advection; 4, shallow moist zone between the upper and surface cold fronts characterized by warm advection and scattered outbreaks of mainly light rain and drizzle; 5, shallow precipitation at the surface cold front itself.

7.1.4 The cold conveyor belt (CCB)

A secondary cloud-producing flow, the CCB, originates in the low-level flow to the north-east of a depression.

(i) Air in the CCB travels westwards, relatively, just ahead of the surface warm front beneath the WCB **(Figs 7.1 and 7.3)**.

(ii) Initially the air subsides and rain from the WCB, falling into it, evaporates. As it travels westwards towards the depression centre, it ascends, reaching into the middle troposphere near the apex of the warm sector.

(iii) Air near the surface warm front ascends due to frictional convergence; eventually the air may ascend slantwise out of the boundary layer into a cloud head, detectable in the satellite imagery, within which the rising air fans out, some of it ascending anticyclonically, and some of it descending cyclonically around the cyclone centre.

7.1.5 Slantwise convection and symmetric instability (2.9.10)

Motions resulting from the release of instability due to slantwise convection (symmetric instability), which can be regarded as a combination of buoyancy and ageostrophic forcing, may be responsible for, or important in:

(i) some of the detail observed in mesoscale precipitation bands;

(ii) the intense rearward ascent in ana-cold fronts;

(iii) the cloud head associated with explosive cyclogenesis.

Emanuel (1983) **Shutts (1990)**

7.1.6 Classification of mesoscale rain bands

To a first approximation, rain areas are aligned along the conveyor belt flows **(Figs 7.5 and 7.6)**. Sometimes the orientation is across the surface front when, for example, an upper cold front overruns the surface warm front. Precipitation is seldom uniform across a conveyor belt due to convective and mesoscale circulations:

(i) convection leads to groups of cells arranged in clusters, giving mesoscale precipitation areas tens of kilometres across;

(ii) The mesoscale circulations lead to banded precipitation structures which are sometimes quite uniform along their length, although more often they consist of aligned mesoscale areas.

Two principal categories of these mesoscale rain bands have been identified: narrow and wide.

7.1.6.1 Narrow rain bands

(i) The most significant occur in the cold seasons at the sharp surface cold frontal discontinuity in the situation of rearward-sloping ascent. These bands, seldom >3 km deep, are aligned along the surface front and frequently produce bursts of very heavy rain and sometimes hail **(Fig. 7.6)**.

(ii) The band of almost vertical convection, and the associated narrow cold-frontal rain band, is termed 'line convection' that can extend as an unbroken line for hundreds of kilometres, although it is more generally broken into line elements of tens of kilometres in length **(Fig. 7.7)**. Only when a full line element (as opposed to a 'gap') passes over will surface reports of transitions of temperature etc. give a realistic impression as to the nature of the front **(Fig. 7.8)**.

(iii) These rope-like cloud bands tend to occur towards the leading edge of the stratiform cloud generated by the slantwise convection. At the very edge they may be detectable by satellite imagery; although, even within the uniform stratiform mass the line convection will be clearly seen by radar.

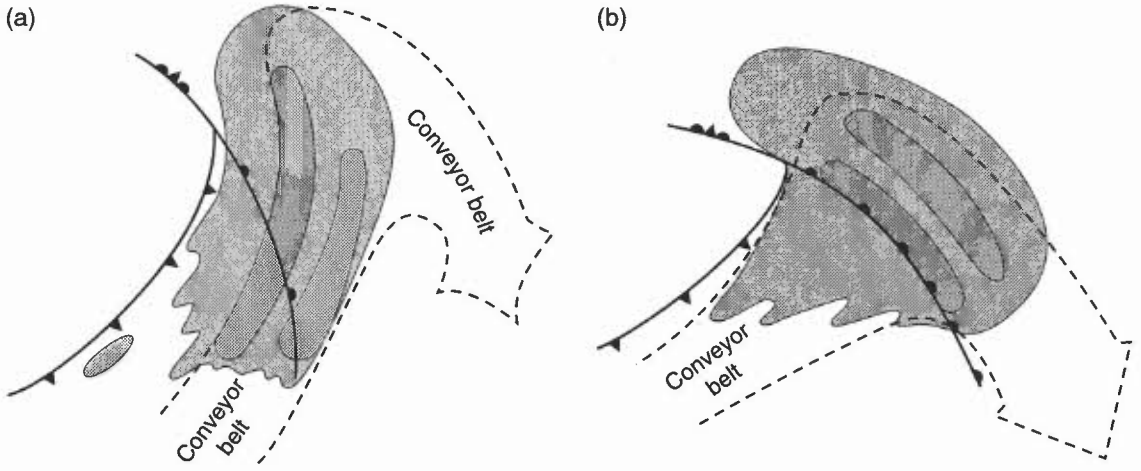

Figure 7.5. Rain areas associated with warm conveyor belts.

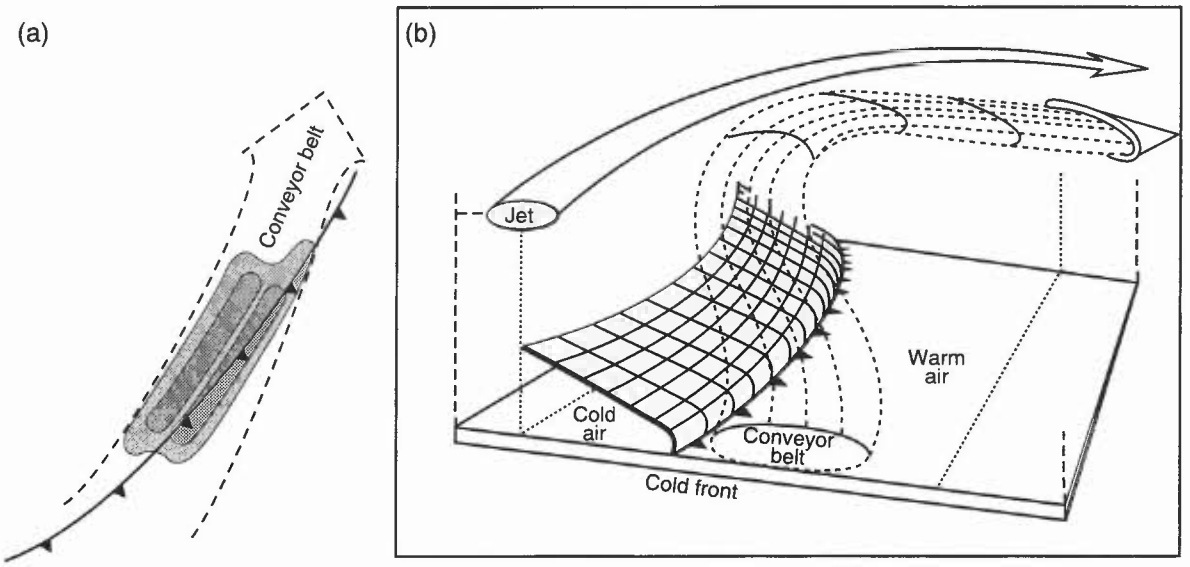

Figure 7.6. Conveyor belt ascending cold front: (a) plan view with rain areas, and (b) 3-D sketch with conveyor belt and jet stream.

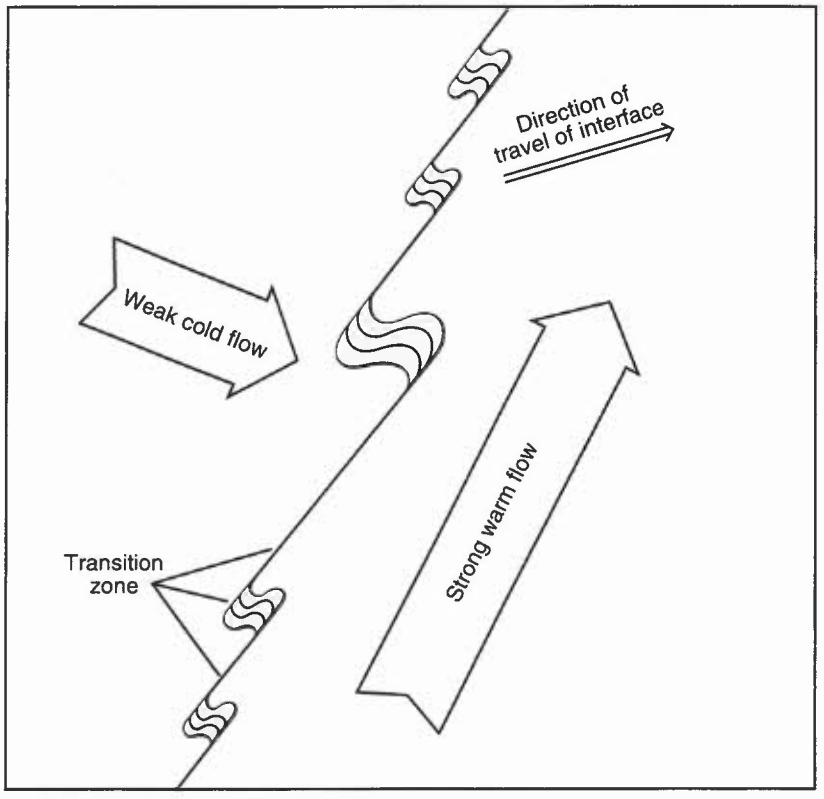

Figure 7.7. Schematic depiction of the transition zone at a sharp surface cold front. Line convection elements, with intense low-level convergence, strong updraughts and heavy precipitation, occur in the regions with a sharp transition zone. The regions where the temperature gradient is more gradual correspond to gaps between the line convection elements. The broad arrow, representing the flow at low levels on either side of the interface, are drawn relative to the ground.

7.1.6.2 Wide rain bands

There are several types: those in the warm sector are sometimes associated with squall lines, while post-frontal bands correspond to the cold-air comma clouds. The most common type is the upper-level rain band **(Fig. 7.5)**. These can occupy different positions within a frontal system, but can be considered as one dynamical type, the characteristics of which are:

(i) they are associated with the ascending parts of the WCB where its top reaches into the middle troposphere;
(ii) they may contain upper- or middle-level convective cells, often in clusters, which are generated within a shallow layer of potential instability where air with low θ_w overruns the WCB;
(iii) they are some 50 km wide and a few hundred kilometres long, orientated parallel to the baroclinicity at their level.

Bader et al. (1995), Chapter 4 **Browning (1985)**
Bradbury (1991), Chapter 3

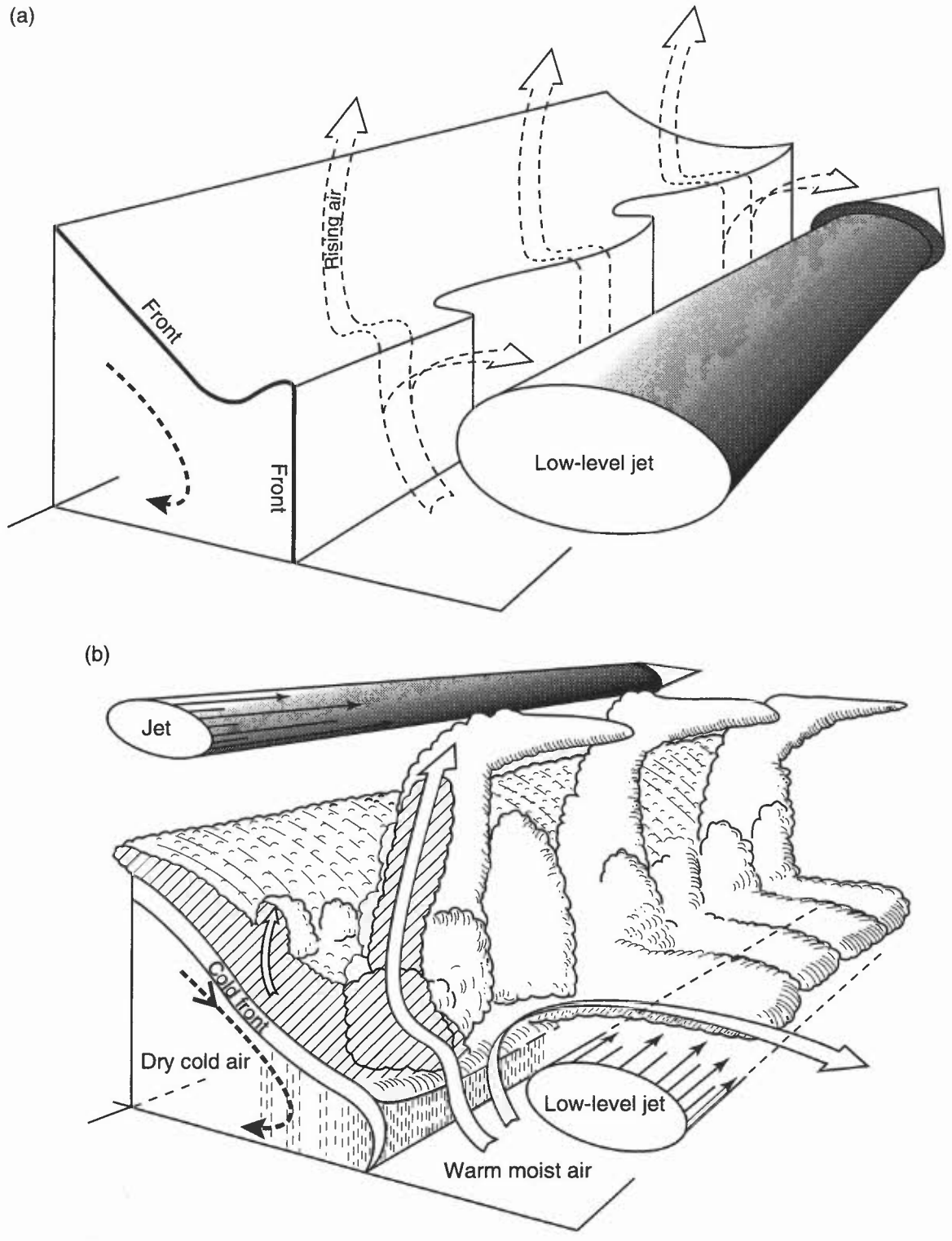

Figure 7.8. (a) Schematic 3-D structure of the cold front showing a low-level jet ahead of it, and (b) 3-D sketch of a cold front showing cloud, low- and high-level jets and patterns of air flow (after Bradbury (1991)).

7.1.7 Other mid-latitude systems

7.1.7.1 Sub-synoptic-scale comma clouds and cold-air vortices.

(i) Some phenomena classified as 'convective' can take on frontal characteristics, particularly evident in the comma-shaped cloud and sub-synoptic-scale precipitation systems associated with cold pools in polar air streams which develop most often over oceans in winter **(Fig. 7.9)**.

(ii) Baroclinicity and conditional instability coexist in the wide range of situations that occur — from conditional instability driving polar lows in very cold outbreaks over warm oceans to the case of comma-clouds due to baroclinic slantwise ascent, as in the short-wave polar troughs in westerlies behind major cold fronts approaching north-west Europe.

(iii) The comma cloud is characterized by convective precipitation and by a distinctive low-level jet as in the case of the synoptic-scale WCB.

(iv) When cloud from the preceding frontal system gets carried around the back of the cold pool (a bent-back, or wrap-around, occlusion) comma-clouds may develop from elements of this cloud as they travel around the southern flank of the pool **(Fig. 7.10)**.

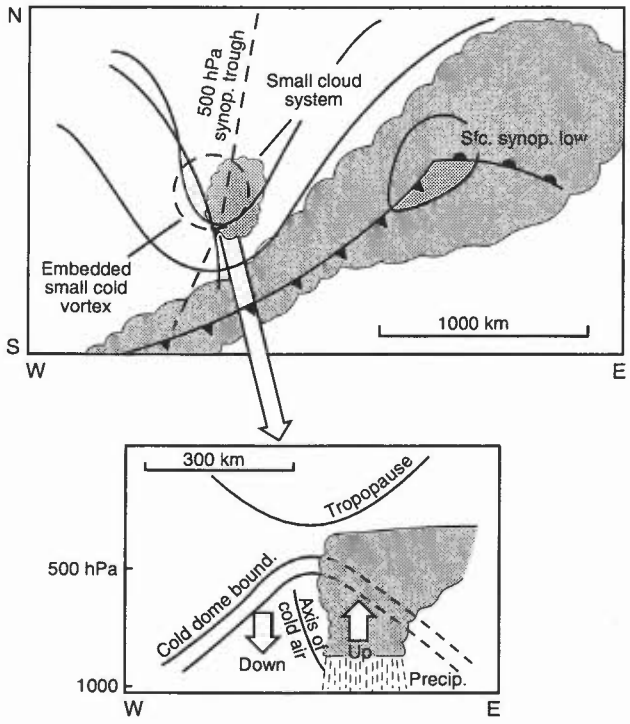

Figure 7.9. Schematic representation of a sub-synoptic-scale cold vortex.

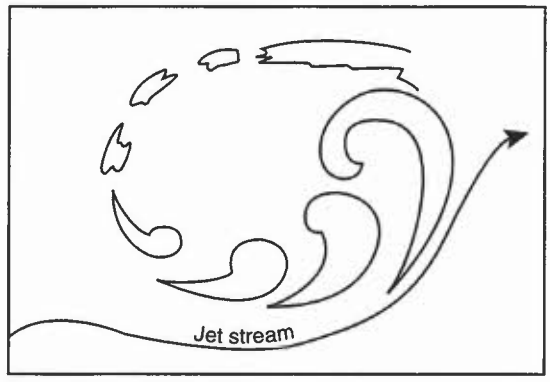

Figure 7.10. Schematic representation of successive stages in the life-cycle of a sub-synoptic-scale comma cloud as it travels around a cold pool behind an upper-level jet stream.

7.1.7.2 The polar trough conveyor belt and instant occlusion

(i) An instant occlusion is the name given to the lambda-shaped cloud pattern produced when a cloud band associated with a polar trough interacts with a cloud band associated with a polar front. The process is interpreted in terms of a dual conveyor belt configuration **(Fig. 7.11)**.

(ii) The instant occlusion is part of a spectrum of types **(Figs 7.12 and 7.13)** in which the form of the disturbance depends on the position of the short-wave trough or vorticity maximum with respect to the polar front.

(iii) The simple comma cloud development **(Fig. 7.12(a))** occurs well within the cold air, not interacting significantly with the main polar front **(Fig. 7.13(a))**.

(iv) By contrast, when the vorticity maximum is at the latitude of the polar front **(Fig. 7.12(c))**, a frontal wave forms in which the main WCB, associated with the polar front, gets involved in the circulation and dominates the cloud pattern **(Fig. 7.13(c))**.

(v) In the intermediate situation there are two distinct cloud belts, associated with the polar trough and polar front **(Figs 7.12(b) and 7.13(b))**.

Bader et al. (1995), Chapters 4 & 5 **Browning (1985)**
Bradbury (1991), Chapter 3

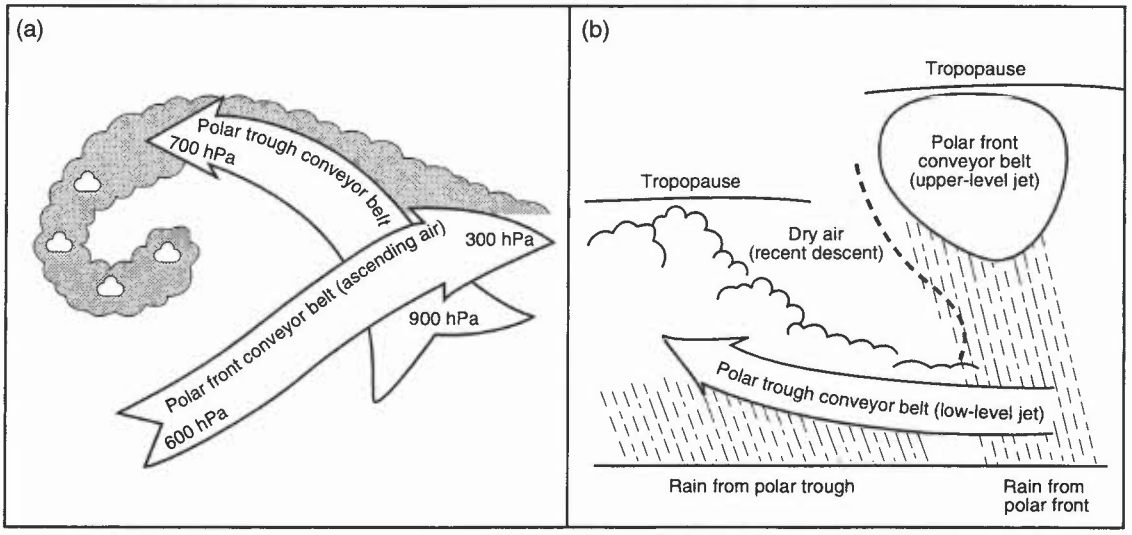

Figure 7.11. Schematic model of the lambda cloud system showing intersecting polar trough conveyor belt and polar front conveyor belt: (a) plan view, and (b) vertical section along axis of polar trough.

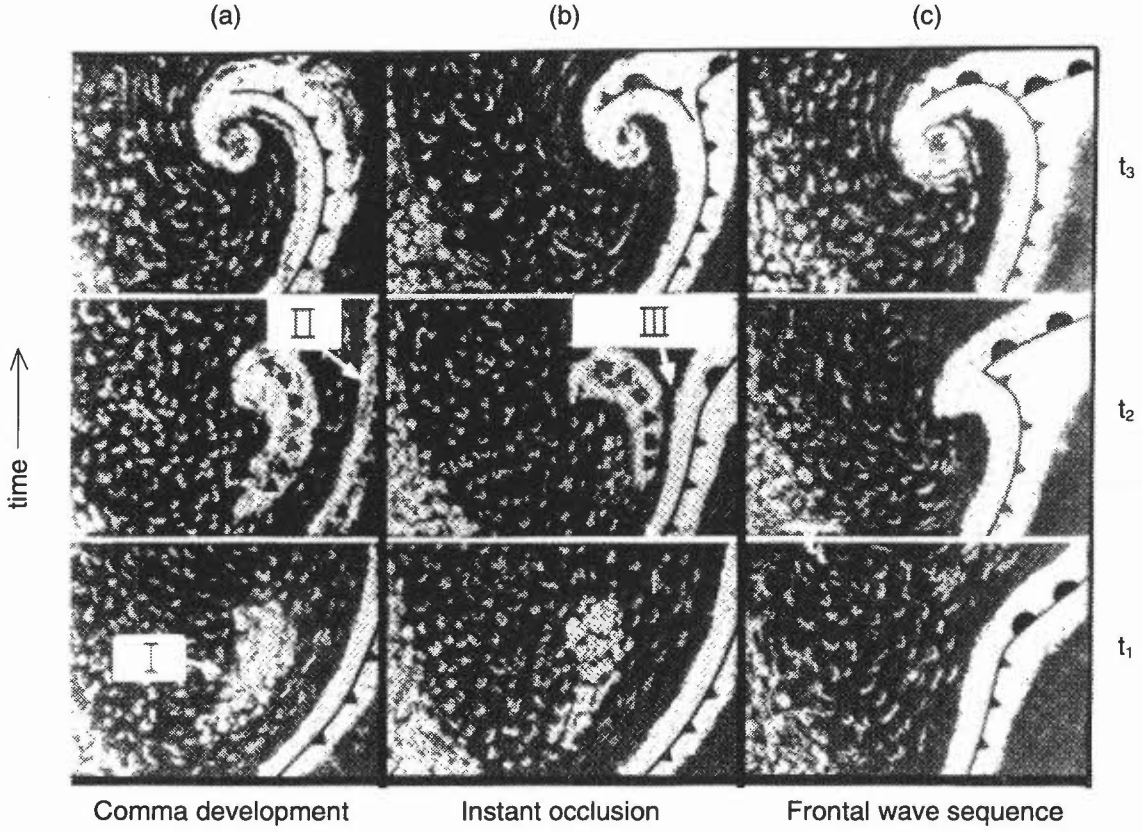

Figure 7.12. Schematic depiction of three basic sequences of vortex development evident in satellite imagery: (a) development of a comma cloud entirely within the cold air, (b) development of an instant occlusion, (c) development of a frontal wave. The figure was derived from observations over the Southern Ocean but it is printed vertically inverted so as to apply to the northern hemisphere. Frontal symbols indicate one scheme for representing the various evolution sequences using the tools of conventional frontal analysis. I, II and III, respectively, indicate a region of enhanced convection, a decaying cloud band and a convective cloud band merging with a frontal cloud band.

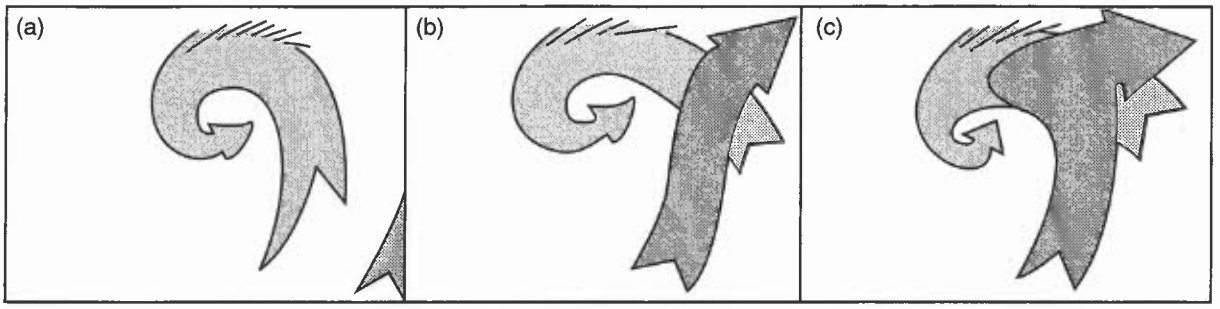

Figure 7.13. Schematic depiction of the conveyor belt flows associated with the cloud patterns at time t_1 in Fig. 7.12.

7.2 Frontal features and development

7.2.1 Features of a depression

Surface lows are usually associated with upper-level troughs; the trough line is not vertically above the surface low but displaced increasingly with height towards the region of coldest air. Upper ridges are similarly displaced from surface anticyclones.

In the lowest layers:

(i) Front lies on warm boundary of tightest θ_w gradient (**Fig. 7.14(a)**); a pronounced gradient of θ_w exists near the surface cold front with decreasing θ_w with height (potential instability) at the bottom of the cold air mass. Above 700 hPa, the pattern of the isentropes of ~~wet-bulb potential temperature~~ θ_w differ little from the pattern of ~~(Fig. 7.14(b))~~ isentropes of θ).

(ii) A steeper (cold) frontal slope at low levels, with a tendency for the cold 'nose' to override surface front, means that 850 or 900 hPa position is similar to surface position (**Figs 7.14(b, c)**). However, shallow cold intrusions may travel >100 miles ahead of the 850 hPa θ_w.gradient, especially along an active front. Surface front often lies from half to two thirds into cloud band from cold side when seen from above. It may even be on the extreme warm side in certain cases.

7.2.2 Assessment of development of frontal depressions from synoptic charts

7.2.2.1 Empirical rules

Motion of surface pressure systems

Frontal depressions move, depending on state of development, as follows:

(i) If low or wave is *without a closed circulation and is not developing* it can be moved in the direction of the 1000–500 hPa thermal wind at about 1/2 the thermal wind speed or at 1/3 speed of the 300 hPa winds above the wave tip, in the 300 hPa direction.

(ii) *Open wave depressions, usually developing,* move at about 4/5 of the geostrophic speed in the warm air and in the corresponding direction or half the 500 hPa wind speed above the wave tip and in the corresponding direction.

(iii) The mature system moves in the direction of the warm sector isobars, with the speed of the 700 hPa flow.

(iv) A low may be moved parallel to a line joining the isallobaric high and low; there are no rules for quantifying the speed.

Intensity of surface pressure systems

(i) Frontal depressions deepen as markedly cold air is drawn into the rear of their circulation and as a warm anomaly in the lower stratosphere advances from the rear. Deepening is indicated by falls of pressure in the warm sector. Deepening may continue for 6–12 hours after the occlusion process starts.

(ii) Frontal depressions start to fill some 12–24 hours after the occlusion process begins; they slow and turn to the left. Pressure rises occur in the warm sector. Secondary depressions must be at least 600 n mile (1100 km) from the primary depression in order to deepen.

(iii) Over oceans the isallobaric pattern is often difficult to define because of the scarcity of observations and the effect of ships' motions on the observed pressure tendency.

Continuity is always a useful aid.

Bader et al. (1995), Chapters 4 & 5

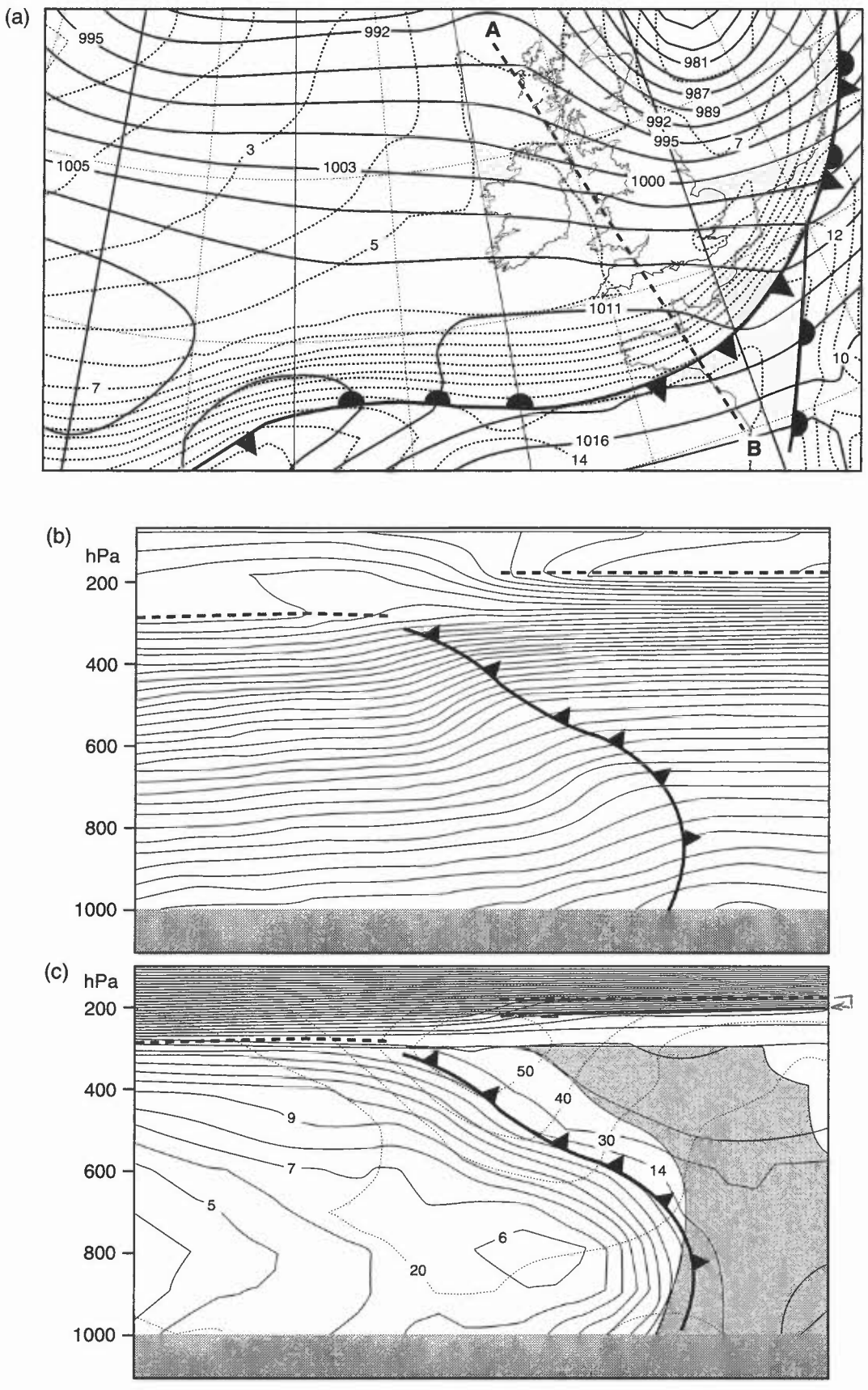

Figure 7.14. The structure of a cold front at 2100 UTC on 2 November 1992: 900 hPa WBPT every 1 °C (dotted), MSLP every 4 hPa (solid), (b) ~~potential~~ temperature (°C), and (c) cross-section through ana cold front (line AB in (a), distance 1400 km), solid lines represent WBPT every 1 °C, the shaded area frontal cloud, thin dashed lines the wind strength every 10 m s^{-1} and thick dashed lines the tropopause.

7.3 Explosive cyclogenesis (EC)

7.3.1 Definition

An explosively deepening depression is defined as a depression which deepens at a rate exceeding 24 hPa per day. Some such systems deepen at over twice that rate; falls of >10 hPa in 3 hours are often a precursor of EC.

7.3.2 Geographical and seasonal characteristics

(i) Explosive cyclogenesis (EC) is nearly always confined to oceanic regions, and predominantly occurs during the winter half of the year, with the western North Atlantic one of the world's most favoured areas.

(ii) However, EC can occur even in mid-summer and forecasters must be particularly alert to this possibility owing to the increased number of weather-sensitive activities at this time of year.

(iii) Explosively deepening depressions can develop from the remnants of ex-tropical storms in late summer and autumn.

7.3.3 Characteristic upper-air patterns

(i) The thickness gradient ahead of an upper trough interacting with a polar front is always intense prior to EC — typically 20 to 30 dam per 300 nautical miles.

(ii) A variety of upper-air patterns can lead to EC. By far the most favoured pattern is a short-wave trough or jet streak moving around a major mobile confluent trough. A general schematic of this type is shown in **Fig. 7.15**.

(iii) The importance of upper-level potential vorticity (PV) anomalies for cyclogenesis is well established.

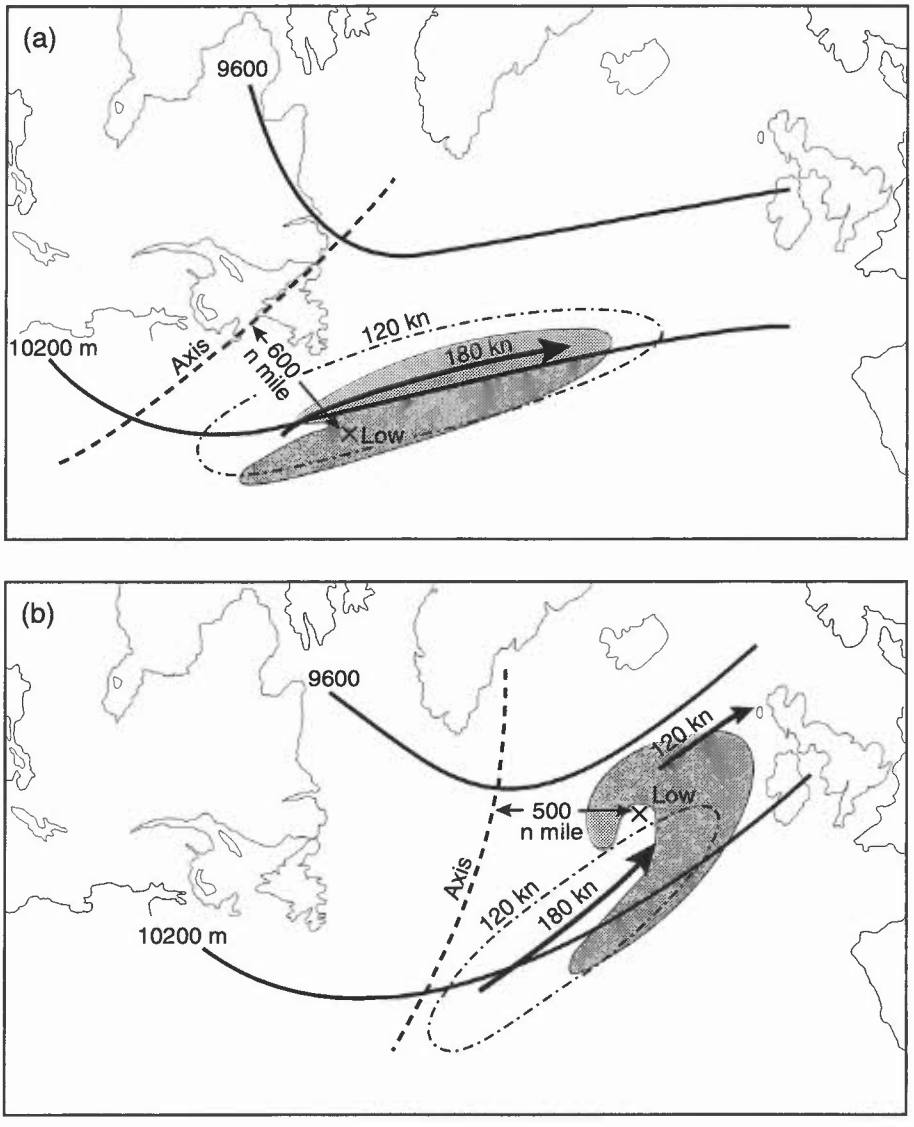

Figure 7.15. Schematic of low development ahead of a broad, mobile, confluent 250 hPa trough. Dispositions of surface centre relative to the 250 hPa pattern (a) at time of onset of rapid deepening, and (b) 24 hours later. Bold arrows are jet axes.

7.3.4 Satellite imagery

Damaging winds associated with EC are often preceded (by as much as 24 hours) by a 'cloud head', an example of which is shown in **Fig. 7.16**. This cloud head is characterized by:

(i) A very broad mass of dense layered cloud C, whose poleward edge often exhibits an 'S' shape. The cloud texture usually appears smooth on IR imagery, although VIS pictures in particular may show embedded convection arranged in transverse bands. Deep convection P in the adjacent polar air often undercuts C. The cloud head C is generated by the ascent and fanning out of air within the cold conveyor belt.

(ii) A narrow region, devoid of middle and upper cloud (but with significant sub-structure), known as the 'dry intrusion', which separates cloud head C from the adjacent band of frontal cloud F. The 'dry intrusion' consists of recently subsided air, partially stratospheric in origin, with high PV; when this air overruns a low-level baroclinic zone the effect of the overrunning high PV is to trigger cyclogenesis and ascent. Mesoscale events, including severe wind and precipitation, are closely related to the mesoscale PV maximum within the dry intrusion.

(iii) The surface depression centre is usually located within or close to the 'dry intrusion'. During deepening, the upstream tip of C evolves into a 'hook' around the surface low centre.

(iii) In addition, a rope-like cloud structure (line convection, 7.1.6.1) (often present at RR in **Fig. 7.16)** indicates the position of a new surface cold front (formally called the back-bent occlusion), which acquires the main low-level thermal gradient at the expense of the pre-existing front beneath F. Note: refer to recommended frontal analysis in Browning & Roberts (1994).

The above characteristic structures are not confined to explosive cyclogenesis.

Bader et al. (1995), Chapters 4 & 5
Browning et al. (1987)
Browning (1995)
Browning & Roberts (1994)
Monk & Bader (1988)
Norris & Young (1991)

7.3.5 Winds associated with explosive cyclogenesis

(i) Mean winds over the sea usually reach storm force, sometimes hurricane force, around a depression which has deepened explosively.

(ii) Early in the life-cycle, strongest winds are often found in the warm sector, but following explosive deepening, they occur near the hook of cloud as seen on satellite imagery, and are most likely just outside the southern edge of the hooked tip of the cloud head.

(iii) Rapid pressure rises to the rear of the depression centre in the cold air (sometimes exceeding 15 hPa in 3 hours) are a potent generator of damaging winds and are characteristic of lows developing ahead of a mobile confluent upper trough (and which is associated with the marked subsidence that typically occurs behind the confluent trough).

(iv) Such a pressure surge is not a feature of lows ahead of a major diffluent trough.

Young (1990)

7.3.6 Precipitation

Marked lowering of the freezing level (often by 1000 m) can occur in extensive heavy precipitation poleward of the depression centre, and rain may turn to snow over lowland areas when the 850 hPa wet-bulb potential temperature is 6° C or lower. Thunderstorms frequently occur at the boundary between the 'dry intrusion' and the hook of cloud late in the deepening phase.

7.3.7 Factors mitigating against EC:

(i) a rapidly relaxing upper trough;
(ii) the cloud head signature becoming ragged and ill-defined;
(iii) lack of warm air;
(iv) the depression centre moving from sea to land (possibly).

McCallum (1990)
McCallum & Norris (1990)

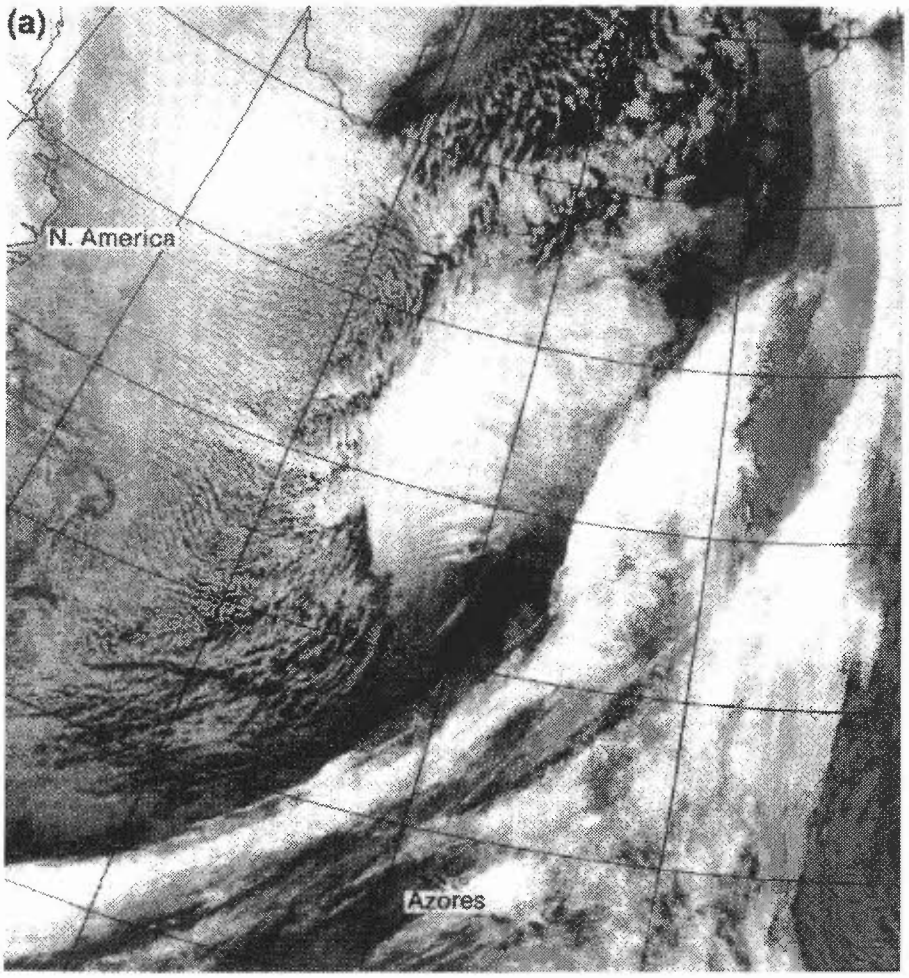

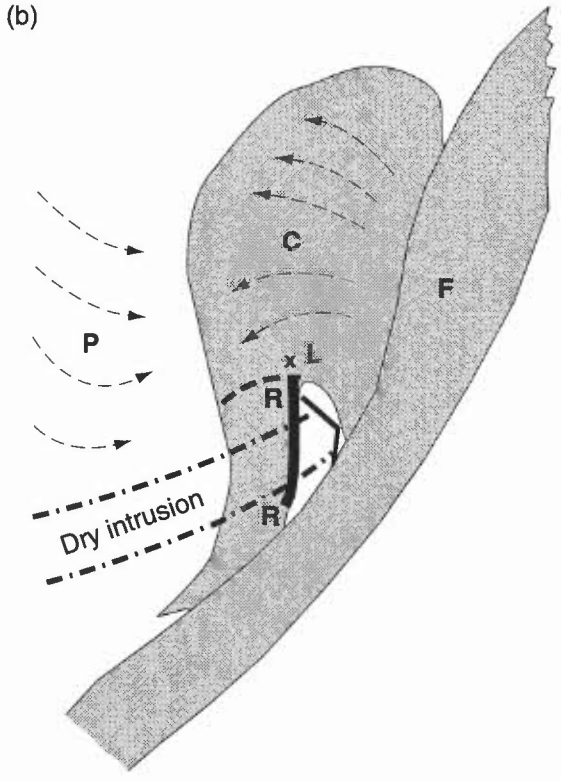

Figure 7.16. Infrared image showing cloud signature associated with early stages of EC at 1550 UTC on 2 February 1991, and (b) schematic diagram of the features described in the text.

7.4 Non-frontal systems

A number of other types of pressure system can affect the UK.

7.4.1 Old lows

(i) Circulation is present right through the depth of the troposphere; movement is slow and irregular.
(ii) It may be steered in the direction of strongest flow around it and cause other mobile features to be steered around it; sub-centres form and decay due to local convection.

7.4.2 Thermal lows

7.4.2.1 Heat lows

(i) Heat from warmed ground will extend up to, say, 850 hPa while temperature above is unaffected.
(ii) Surface pressure is therefore lower by a few hectopascals; in the UK the effect soon disappears as evening temperatures fall. Low-level convergence may trigger thunderstorms in unstable air.

7.4.2.2 Polar lows

(i) *Primary* lows develop as the result of the equatorward movement of an upper-level cold-cored vortex (or trough originating in a polar vortex region). Others are termed '*secondary*' (e.g. those forming as a by-product of normal extratropical cyclone development)
(ii) Comma clouds, waves on secondary baroclinic zones within the cold air mass, and lows that form on an occlusion are all examples of the latter type.
(iii) Sensible and latent heat input to polar lows will be continuous while over the sea; convective polar lows will usually decay rapidly after landfall.
(iv) Satellite imagery will reveal their presence in spite of their small scale (typically a few hundred kilometres in diameter).
(v) Low-level convergence, together with the strong pre-existing instability, often results in gale-force winds on the western flanks of, particularly, convective types and frequent showers or continuous precipitation resulting in significant accumulations of snow.

Significant parameter for development
Surface development is likely when a 500 hPa cold pool at -42 °C or below moves out over the open sea.

7.4.3 Orographic lows

Closed circulation lows in the lee of mountain ranges (as occurs in the Alps) are not common in the UK, though lee troughing is often observed. Lee lows frequently form to the lee of the Greenland plateau where they may alter the large-scale synoptic development of systems in the North Atlantic.

7.4.4 Old tropical depressions

Occasionally, generally in autumn, decaying tropical depressions, with very warm, moist air within their circulations, get caught up and reinvigorated in the mid-latitude westerly flow, feeding off baroclinic instability. They reach the UK as vigorous depressions giving strong winds and copious rain.

7.4.5 Summary of movement and development indicators

Non-frontal depressions move:
(i) with the strongest winds around their periphery;
(ii) around the circulation of a larger primary depression;
(iii) as a rotating system ('dumb-bell') if two (or more) equal sized lows are present. Detailed movement is difficult to forecast.

The best indicators of their development are the observed pressure tendencies.

7.4.6 Anticyclones

High pressure areas can be clear or cloudy, presenting a difficult forecasting problem for St or Sc, particularly in winter. Generally, highs will build if warm air is advected northwards on their western flank and cold air is advected southwards on their eastern flank, declining when encircled by warm air. They will move towards regions of rising pressure.

7.4.6.1 Cold anticyclones

In one type cold, dense air is confined to the lower troposphere following protracted radiation cooling over large land masses such as Canada or Siberia during winter. Another type forms between two successive depressions, but is mobile, moving with speed similar to the depressions; it is steered parallel to thickness lines.

7.4.6.2 Warm anticyclones

In this system cold, dense air is largely confined to the upper troposphere and lower stratosphere, the middle and lower troposphere often being warmer than usual. The subtropical anticyclones, such as the Azores high, are of this type. The highest MSLPs arise from cold air at low levels, exceptionally, combining with a higher-than-average tropopause.

7.4.6.3 Blocking highs

Anticyclones centred between 50 and 70° N prevent the polar front from occupying its normal position, thus blocking the progress of frontal depressions. There is a tendency for blocking highs to persist in preferred geographical areas, especially between 10 and 20° W, just to the west of the UK, and between 10 and 20° E, over Scandinavia.

7.4.7 Other synoptic features

(i) A *trough of low pressure* may occur simply as an extension of a low pressure area, or as a sharper, more well-defined feature, such as is found across a front of occasionally in unstable polar air.

(ii) A well-marked trough is often marked by lines of enhanced convection and, occasionally, by persistent rain. It will move with the component of the geostrophic wind speed across it.

(iii) The weather in a *col* tends to be calm, but diffluence in the larger-scale flow around a col can lead to frontogenesis.

Bader et al. (1995), Chapter 5
HWF (1975), Chapter 6.3

BIBLIOGRAPHY

CHAPTER 7 — FRONTS: CONCEPTUAL MODELS AND ANALYSIS; NON-FRONTAL SYSTEMS

Bader, M.J., Forbes, G.S., Grant, J.R., Lilley, R.B.E. and Waters, J., 1995: Images in weather forecasting. Cambridge University Press.

Bradbury, T.A.M., 1991: Meteorology and flight. A.C. Black.

Browning, K.A., 1985: Conceptual models of precipitation systems. *Meteorol Mag*, **114**, 293–318 (includes list of other definitive papers).

Browning, K.A., 1995: Mesoscale aspects of extratropical cyclones: an observational perspective. Joint Centre for Mesoscale Meteorology, Internal Report No. 44.

Browning, K.A., Bader, M.J., Waters, A.J., Young, M.V. and Monk, G.A., 1987: Applications of satellite imagery in nowcasting severe storms and very short range forecasts. *Meteorol Mag*, **116**, 161–179.

Browning, K.A. and Golding, B.W., 1995: Mesoscale aspects of a dry intrusion within a vigorous cyclone. *QJR Meteorol Soc*, **121**, 463–495.

Browning, K.A. and Roberts, N.M., 1994: Structure of a frontal cyclone. *QJR Meteorol Soc,* **120**, 1535–1557.

Emanuel. K., 1983: On assessing local conditional symmetric instability from atmospheric soundings. *Mon Weather Rev*, **111**, 2016–2033.

McCallum, E., 1990: The Burns' Day storm, 25 January 1990. *Weather*, **45**, 166–173.

McCallum, E. and Norris, W.J.T., 1990: The storms of January and February 1990. *Meteorol Mag*, **119**, 201–210.

Monk, G.A. and Bader, M.J., 1988: Satellite images showing the development of the storm of 15–16 October 1987. *Weather*, **43**, 130–135.

Norris, W.J.T. and Young, M.V., 1991: Satellite photographs — 2 February 1991 at 1533 UTC. *Meteorol Mag*, **120,** 115–116.

Orographic Processes in Meteorology (Pre-prints), 1993: Summer School, Meteorological Office College, Shinfield.

Shutts, G.J., 1990: SCAPE charts from NWP model fields. *Mon Weather Rev*, **118**, 2745–2751.

Young, M.V., 1990: Satellite and radar images, 0900 GMT 3 February 1990. *Weather*, **45**, 268–270.

CHAPTER 8 — USE OF DYNAMICAL CONCEPTS IN ASSESSING DEVELOPMENT

CHAPTER 8 — USE OF DYNAMICAL CONCEPTS IN ASSESSING DEVELOPMENT

8.1 Basic ideas

8.1.1 Frontogenetic flow patterns

There are two main configurations of the synoptic-scale horizontal flow in relation to a pre-existing thermal gradient which act to increase the baroclinicity. These deformation patterns fall into two categories:

(i) Diffluence in the flow across a thermal gradient. **(Fig. 8.1(a), Fig. 8.1(c)).**

(ii) Shear in the flow leading to the tilting of the orientation of a thermal gradient. **(Fig. 8.1(b), Fig. 8.1(c).** See also **Fig. 8.11.)**

Since the thermal wind is the major component of the upper tropospheric wind in baroclinic zones, these frontogenetic effects strengthen upper-level winds.

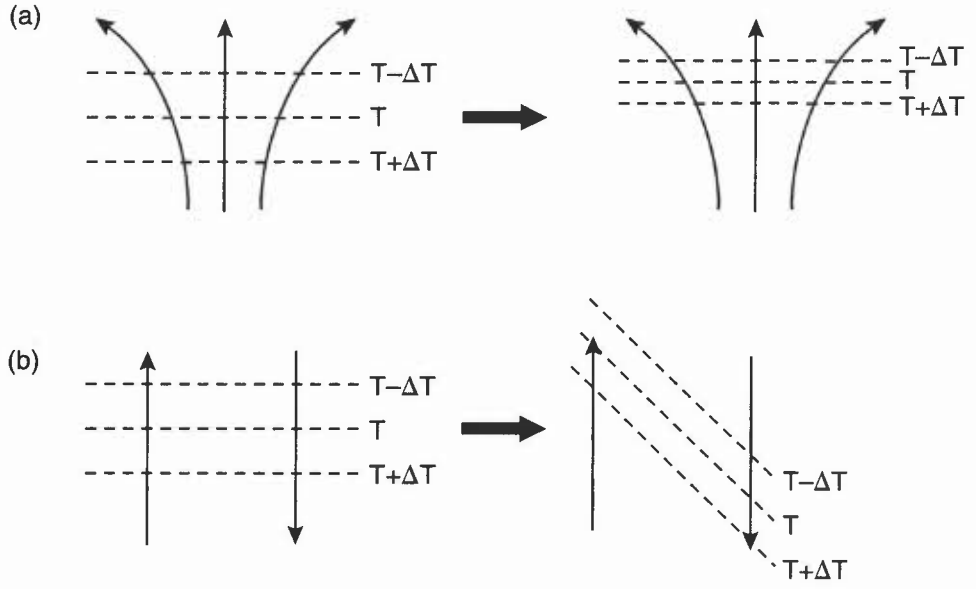

Figure 8.1. Deformation patterns associated with frontogenesis. (a) Diffluence, and (b) shear.

8.1.2 The two-layer model of the atmosphere

In situations of active development, the atmosphere may be divided into two layers of opposite divergence, separated by a level of non-divergence **(Fig. 8.2).** This simple schematic model is valid for regions with strong vertical velocity through the troposphere and marked changes in surface pressure; it has the following characteristics:

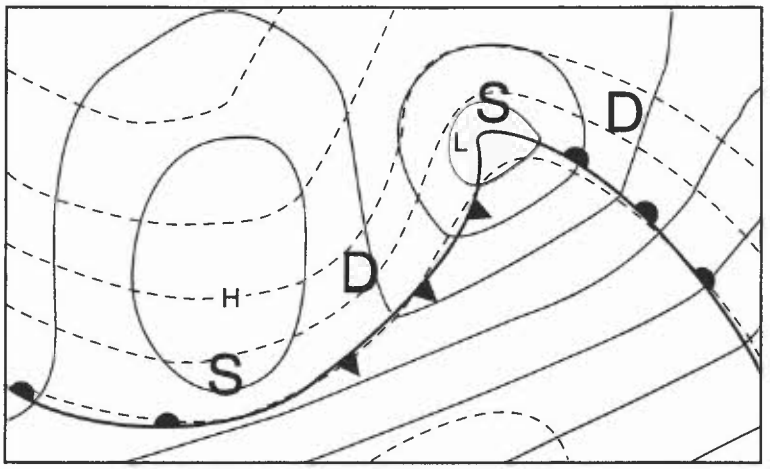

Figure 8.2. Mean sea-level pressure (solid lines) and thickness (dashed lines). Regions of diffluence and shear frontogenesis marked by D and S, respectively.

(i) The upper-level divergence is stronger than that at lower levels, and drives the circulation.
(ii) Vertical motion is at a maximum at the level of non-divergence, falling to zero at the surface and at some upper level, nominally the tropopause.

Subjective methods of assessing surface development are based on this model, and often rely on the diagnosis of upper-level divergence via either ageostrophic motion or vorticity.

8.2 Ageostrophic motion

8.2.1 Definition and significance

The ageostrophic wind is that part of the wind not in geostrophic balance, i.e. the wind associated with an imbalance between Coriolis force (acting to the right of the motion in the northern hemisphere and proportional to the wind speed) and pressure gradient force (acting down the pressure gradient). Its chief practical significance lies in the fact that by identifying it, we isolate the component of the horizontal wind field causing vertical motion.

8.2.2 Vertical motion due to friction

(i) Friction deflects the wind towards lower pressure and reduces its strength. In cyclonic (anticyclonic) flow within the boundary layer, ageostrophic motion due to friction causes convergence (divergence).
(ii) Unlike situations of large-scale ascent, the resulting vertical velocity is generally only of order of millimetres per second and is at a maximum at the top of the boundary layer, where it is proportional to the geostrophic relative vorticity.
(iii) An opposite but weaker divergence profile compensates above the boundary layer **(Fig. 8.3)**.

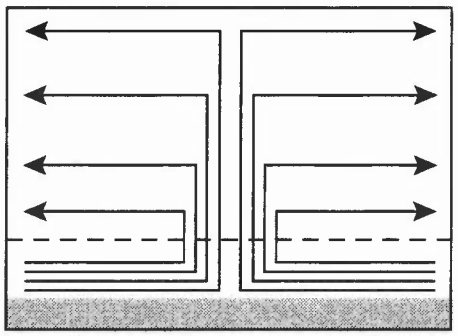

Figure 8.3. Streamlines of frictionally induced motion in cyclonic flow. (The dashed line indicates the top of the boundary layer.)

8.2.3 Ageostrophic motion due to acceleration

(i) Imbalance between Coriolis force and pressure gradient force gives ageostrophic motion with magnitude proportional to the acceleration of the flow, acting to the left of the acceleration vector in the northern hemisphere.
(ii) The total time derivative of the wind velocity, i.e. the acceleration, can be split into local and advective components, giving local, or *isallobaric* and advective, or *downwind* changes in velocity, respectively. The downwind effects can be further subdivided into along-flow acceleration and curvature effects.

8.2.3.1 Acceleration/deceleration along the flow

(i) This component of ageostrophic motion is directed across the flow, and its strength can be gauged on a chart showing gph contours and isotachs — the smaller the areas bounded by contours and isotachs, the larger the ageostrophic motion.
(ii) It results in upper-level divergence and surface cyclonic development areas at right entrances and left exits of jets, with upper-level convergence and surface anticyclonic development areas at left entrances and right exits **(Fig. 8.4)**.

8.2.3.2 Curvature

(i) This component of ageostrophic motion is directed against the flow in cyclonic curvature and with the flow in anticyclonic curvature. Adding it to the geostrophic wind gives the gradient wind.
(ii) Consideration of this effect gives upper-level divergence (convergence) and surface cyclonic (anticyclonic) developments areas where curvature is becoming more anticyclonic (cyclonic) or less cyclonic (anticyclonic) along the flow **(Fig. 8.5)**.

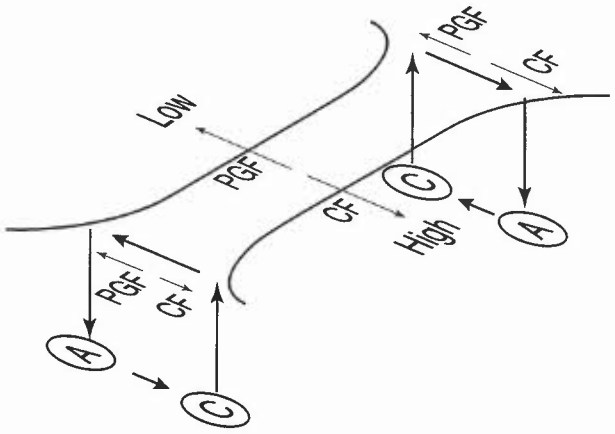

Figure 8.4. Ageostrophic motion, vertical velocity and development areas associated with a jet. Ageostrophic motion at upper levels associated with downwind acceleration, at lower levels with isallobaric effects. Also shown are changes in relative strengths of pressure gradient and Coriolis forces.

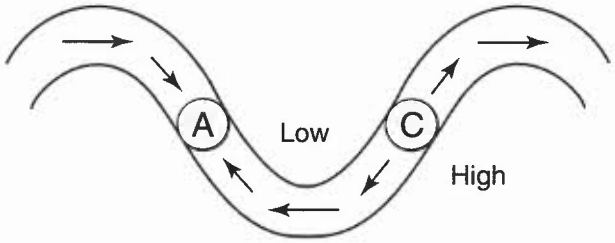

Figure 8.5. Ageostrophic motion and development areas associated with an upper trough–ridge flow pattern.

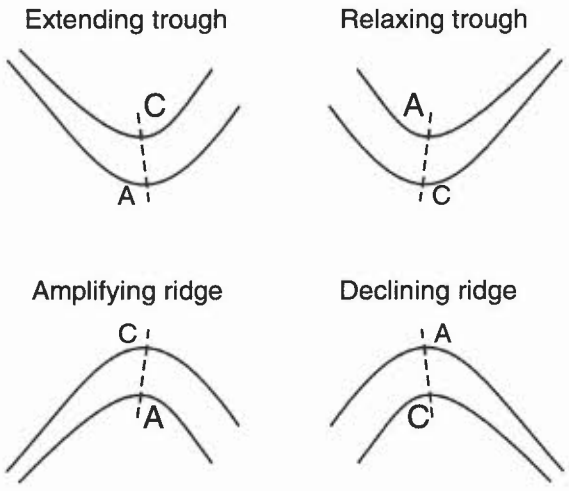

Figure 8.6. Major and minor development areas due to downwind changes. Also indicated are tendencies induced in upper-level flow patterns.

Combining the two types of downwind changes leads to major and minor cyclonic (C) and anticyclonic (A) development areas in association with the different combinations of confluence and diffluence with cyclonic and anticyclonic curvature **(Fig. 8.6)**.

8.2.3.3 Isallobaric effects

(i) These arise from local changes in the pressure gradient force; the resulting ageostrophic motion is directed down the isallobaric gradient. At the surface isallobaric flow is directed into regions of pressure falls and away from regions of pressure rises **(Fig. 8.4)**.

(ii) At upper levels, the most significant cause of isallobaric motion is horizontal variation in thermal advection.

(iii) Warm advection tends to raise upper-level geopotential height. This results in isallobaric motion directed away from the warm advection maximum, with attendant divergence aloft and ascent through the atmospheric column **(Fig. 8.7(a))**.

(iv) Cold advection has the opposite affect, with upper-level convergence and descent **(Fig. 8.7(b))**.

(v) On the edges of advection areas, the opposite sign of divergence tends to occur. For instance, cold advection behind a cold front contributes to ascent at the front **(Fig. 8.8)**.

(vi) During the process of frontogenesis, parcels of air are being accelerated, as at a jet entrance, leading to isallobaric motion from warm to cold air **(Fig. 8.7(c))**. For this reason cloud and rain are often confined to the warm side of the jet, with clear air on the cold side.

The static stability of the air modulates these motions; if the air is stable, ascent (descent) produces marked cooling (warming) which offsets the advective changes in potential temperature. In addition, sources of heat can be important in producing divergence.

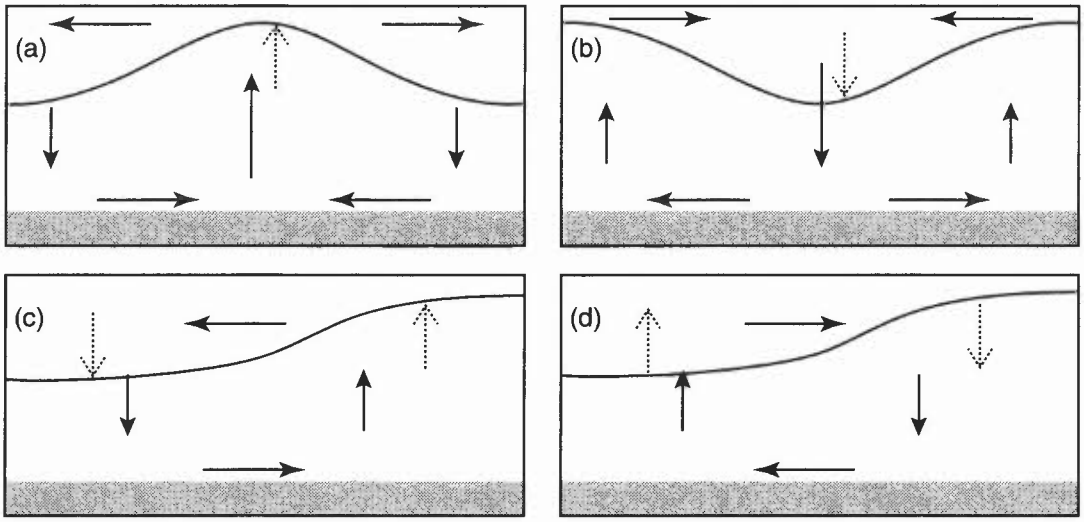

Figure 8.7. Cross-sectional views of upper-tropospheric pressure surfaces and direction of instantaneous change in height (dotted arrows). Resulting departure from geostrophic balance and induced vertical motion is shown by solid arrows. (a) Warm advection, (b) cold advection, (c) jet entrance (following motion) or frontogenesis, and (d) jet exit (following motion) or frontolysis.

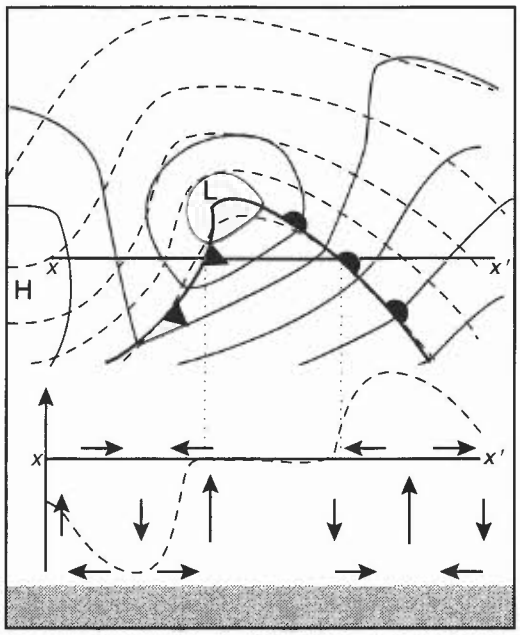

Figure 8.8. Top: contours of mean sea-level pressure (solid) and thickness (dashed) associated with a schematic developing warm-sector depression. Bottom: upper-level gph tendency due to thermal advection along line XX′ (dashed) and cross-section of resulting ageostrophic and vertical acceleration (arrows).

8.2.3.4 The latitude effect

(i) Since the geostrophic wind is inversely proportional to f, and thus to the sine of the latitude, for a given pressure gradient, the geostrophic wind will increase in strength as the equator is approached and decrease in strength as the pole is approached.

(ii) Thus cyclonic (anticyclonic) development is favoured by a strong equatorward (poleward) flow, and there is a tendency for retrogression of large-amplitude, long-wave troughs and ridges against the usual west–east current **(Fig. 8.9)**.

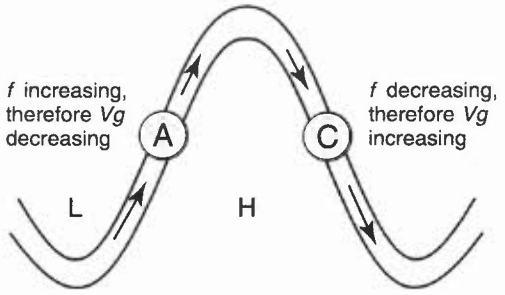

Figure 8.9. Development areas due to the divergence/convergence of the geostrophic wind with large changes in latitude, leading to tendency for retrogression.

8.3 Vorticity

8.3.1 Simplified vorticity equations

(i) A simplified vorticity equation (SVE) offers an alternative way of diagnosing divergence without reference to ageostrophic motion. It shows the fractional rate of change of absolute vorticity following the motion to be proportional to the convergence (ignoring frictional effects and the tilting of horizontal vorticity).

$$\frac{1}{\zeta + f}\,\frac{\mathrm{d}(\zeta + f)}{\mathrm{d}t} \approx -\mathrm{div}_{\mathrm{H}}\mathbf{V}$$

(ii) This equation is most easily visualized as the 'ice-skater' effect, whereby ice skaters increase their vorticity (=angular velocity) through drawing their arms in (convergence) and decrease it through stretching their arms out (divergence), e.g. convergence in the lower part of the frontogenetic circulation illustrated in **Fig. 8.7(c)** generates vorticity, manifested as a pressure trough marking the surface front.

(iii) Splitting the total rate of change of absolute vorticity into local and advective components shows that divergence is associated with the advection of vorticity and the local rate of change of vorticity.

$$-\mathrm{div}_{\mathrm{H}}\mathbf{V} \approx \frac{1}{\zeta + f}\left(\frac{\partial \zeta}{\partial t} + \mathbf{V}.\nabla(\zeta + f)\right)$$

convergence — local rate of change of vorticity — vorticity advection

8.3.2 Vorticity advection

(i) Positive (negative) vorticity advection contributes towards divergence (convergence).

(ii) Vorticity advection gives the same regions of divergence diagnosed by consideration of ageostrophic motion due to downwind acceleration. Advection of shear vorticity gives divergence due to ageostrophic motion resulting from along-flow acceleration/deceleration, whilst advection of curvature vorticity gives divergence due to ageostrophic motion resulting from curvature.

(iii) The advection of planetary vorticity (f) is also entirely equivalent to the latitude effect discussed in 8.2.3.4, e.g. a northerly flow gives positive vorticity advection and a cyclonic development area.

8.3.3 Local rate of change of vorticity

(i) Horizontal variations in thermal advection beneath an upper pressure level cause vorticity to change at a point. Over a maximum of warm (cold) advection absolute vorticity decreases (increases); the SVE shows this change to be accompanied by divergence (convergence).

(ii) Such changes have their direct equivalent in the isallobaric effects discussed in 8.2.3.3. As shown in that section, divergence of the opposite sign tends to occur on the periphery of the region of thermal advection.

(iii) It is best to consider thickness advection through a deep layer, preferably the whole of the troposphere. This can be assessed using a representation of 300 or 250 hPa gph contours superimposed on mean sea-level pressure. Low-level flow from low (high) to high (low) upper-level gph indicates cold (warm) advection, whilst the smaller the areas formed between two gph contours and two isobars, the stronger the advection.

(iv) On average, vorticity advection is more influential than thermal advection in producing mid-tropospheric vertical velocity. Thermal advection is at its most effective somewhat lower down, say at 700 hPa .

8.4 The development and movement of upper features

8.4.1 Thermal advection

(i) Thermal advection tends to induce opposite gph tendencies at lower and upper levels, e.g. warm advection is often associated with falling surface pressure but rising 300 hPa gph because of the increasing thickness. At some mid-level, the level of non-divergence (on average 500–600 hPa), it has a smaller, indeterminate effect.

(ii) Adiabatic and diabatic heating/cooling can act to offset advective changes, e.g. cold advection to the west of the UK in winter can be significantly offset by diabatic warming through convection and adiabatic warming through descent, limiting the amount of cooling in the column and thus the fall of upper-level gph.

8.4.2 Vorticity advection

(i) Positive (negative) vorticity advection favours falling (rising) surface pressure and thus, ignoring the effects of any changes in temperature in the atmospheric column, falling (rising) upper-level gph.

(ii) For example, a diffluent upper trough leads to falling surface gph downstream of its axis on its cold side, and this is reflected by a fall in gph at upper levels. Such troughs, therefore, tend to extend and sharpen. One way to look at this process is as the advection of shear vorticity and planetary vorticity into the axis of the trough, reinforcing it. **Fig. 8.6** shows this and other configurations.

(iii) The divergence field due to advection of curvature vorticity leads to progression of troughs and ridges, shorter-wavelength features moving most quickly. Similarly, the divergence field due to shear vorticity advection causes a jet to progress through the pattern.

(iv) Planetary-scale troughs and ridges tend to be slow moving or stationary under a balance between curvature and planetary vorticity advection, whereas the shorter-wavelength features associated with travelling weather systems move through the pattern. (Because of the cancellation between relative vorticity advection and planetary vorticity advection associated with the planetary-scale features, the usual configuration of 'A' and 'C' areas does not apply.)

(v) At the nominal level of non-divergence, vorticity is conserved following the motion. For this reason vorticity features are advected around and often preserve their identities longer on a 500 hPa chart than on a 250 hPa chart.

The following table summarizes and compares the factors leading to changes in geopotential height near the surface and in the upper troposphere.

Development	**Factors favouring**
Surface C area	PVA + centre of warm advection area or where cold advection area borders on region of little thermal advection.
Surface A area	NVA + centre of cold advection area or where warm advection area borders on region of little thermal advection.
Upper-level C area	PVA + cold advection.
Upper-level A area	NVA + warm advection.

NB. PVA and NVA refer to the upper-tropospheric vorticity advection.

In any instance, thermal advection may be acting to offset vorticity advection.

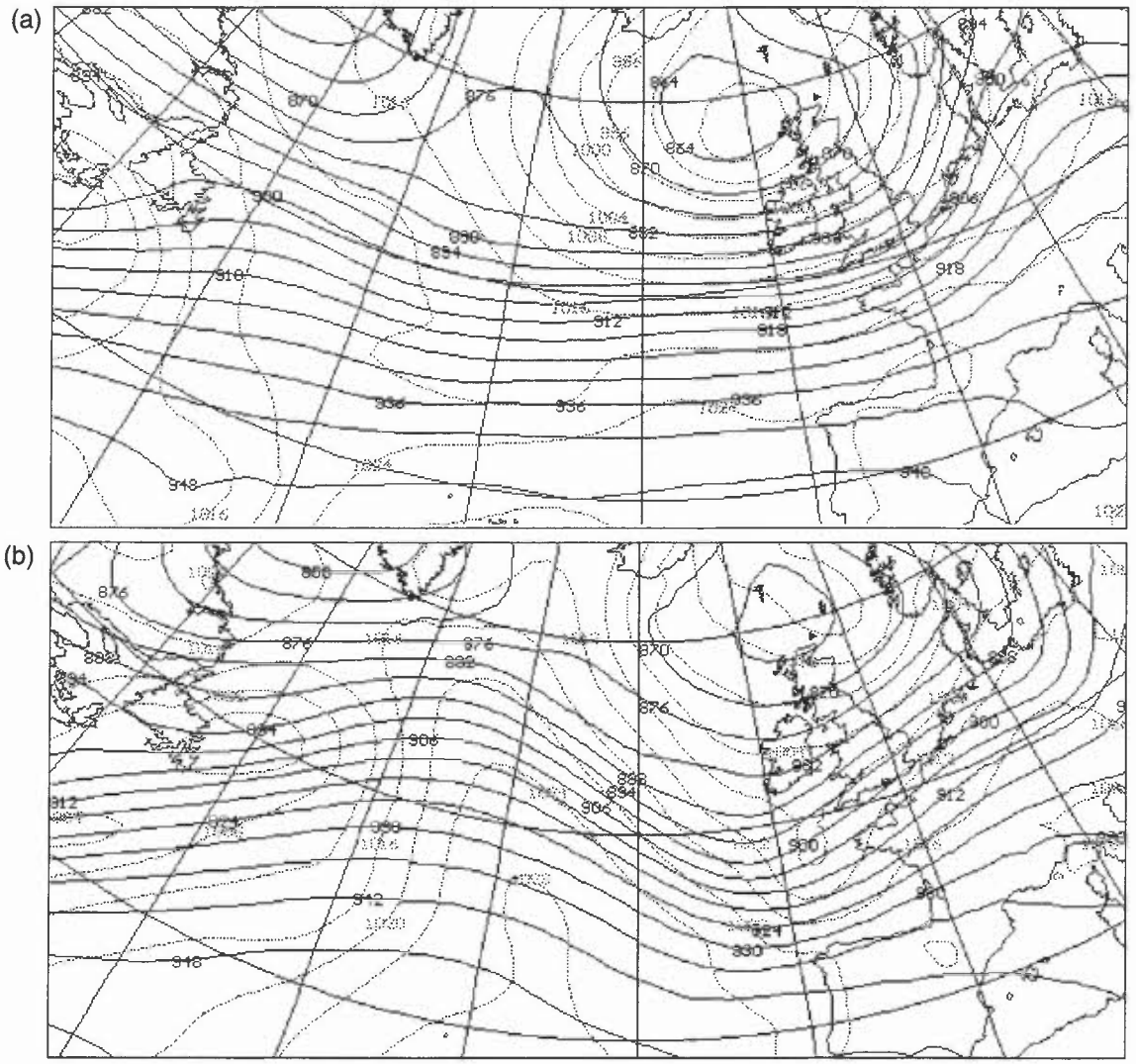

Figure 8.10. Development in the north-east Atlantic downstream of strong, warm advection in the north-west Atlantic. Dark lines; 300 hPa gph every 6 dam, lighter lines: MSLP every 4 hPa. Above 0000 UTC on 27 April 1992, below 2100 UTC on 27 April 1992. Thermal advection strength can be gauged by the smallness of the areas bounded by two MSLP and two 300 gph contours, a surface flow from high to low 300 hPa gph indicating warm advection.

8.4.3 Downstream development

Weather systems can be influenced by events upstream on a time scale shorter than that in which advective processes can account for their development. A typical process is now described:

(i) A vigorous surface depression generates much warm advection ahead of it, which builds an upper ridge.

(ii) The consequent veering of the thermal gradient downstream of the ridge axis leads to a tightening of that gradient through shear frontogenesis, so the jet strengthens.

(iii) The resulting downstream diffluent trough extends and sharpens through advection of cyclonic shear vorticity into its axis, and gives rise to a new cyclonic surface development.

(iv) The intensification of this new surface feature induces cold advection on its western flank, reinforcing the upper trough.

(v) This sequence is contributory in determining the evolution shown in **Fig. 8.10**.

8.4.4 Trough disruption

(i) Trough disruption is said to occur when the poleward portion of a trough becomes separated from the equatorward part and moves on, often having left a cut-off circulation **(Fig. 8.11)**.

(ii) This evolution sometimes follows the extension of a trough, especially if sufficient positive vorticity, both planetary and shear, is advected into the lower part of the trough, or if a cut-off region of cold air due to strong cold advection forms in the region of the trough.

(iii) The induced cyclonic circulation brings warmer air of originally lower planetary vorticity around its eastern then northern flanks, and it thus cuts itself off from the higher-vorticity polar air.

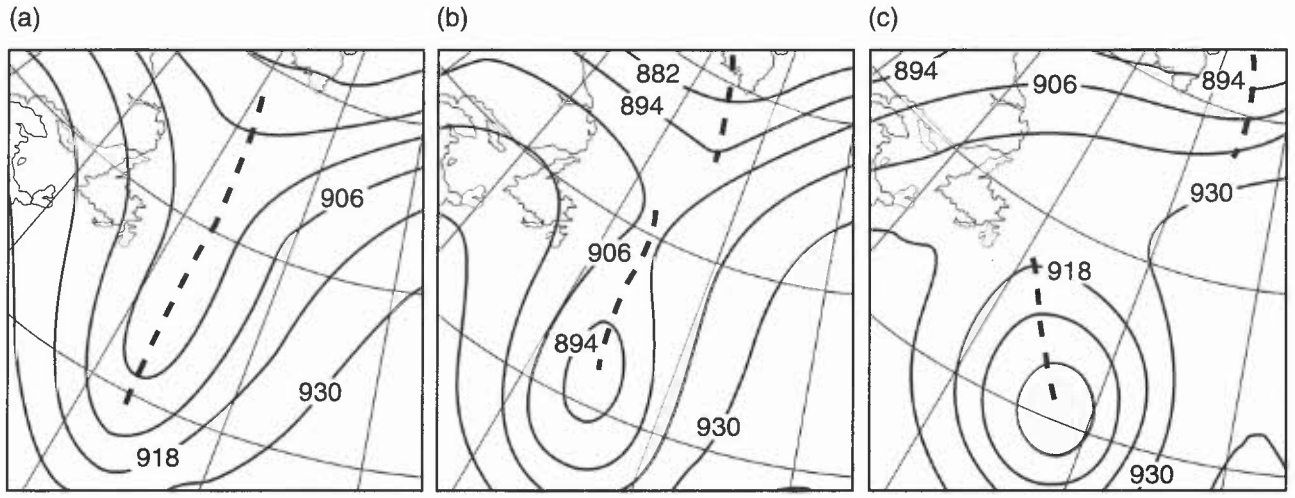

Figure 8.11. Trough disruption shown in 300 hPa gph forecast sequence. (a) T + 0 (00 UTC on 13 April 1995), (b) T + 12 (12 UTC on 13 April 1995), and (c) T + 24 (00 UTC on 14 April 1995).

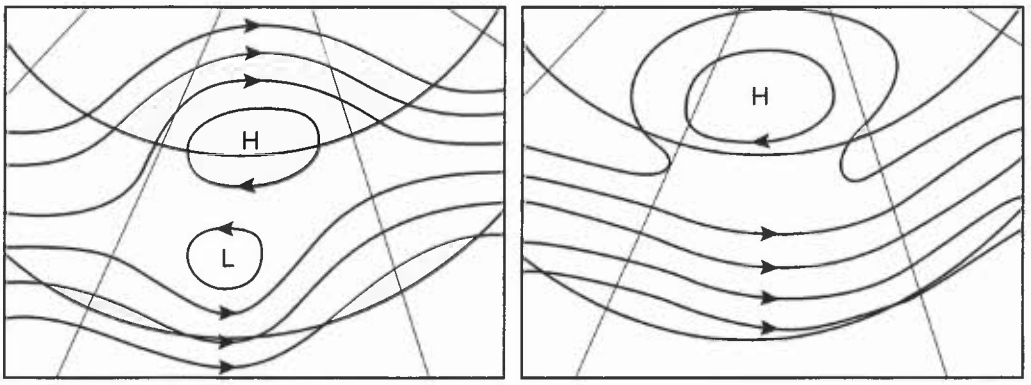

Figure 8.12. Schematic large-scale mid- or upper-tropospheric flow patterns in diffluent block (left) and omega block (right).

(iv) Surface pressure rises across the neck of the disrupting trough, and the process is sometimes referred to as anticyclonic disruption.

(v) Trough disruption is likely if the 300 hPa trough has an amplitude of 10° or more and if the jet has a strong equatorward component (340–020°).

(vi) The disruption process appears to be finely balanced, and the detail of such events is often not well predicted by NWP models.

8.4.5 Blocking

(i) Blocking patterns give rise to prolonged periods when the normal mid-latitude zonal current is replaced over a large latitude range by meridional flow. A large, stationary high is the prominent feature of such situations.

(ii) **Fig. 8.12** shows typical mid- to upper-tropospheric contour patterns associated with such situations. The usual latitudinal thickness gradient is reversed over a large area, with warm air cut off in high latitudes and pools of cold air in low latitudes.

(iii) The normal westerly flow is either split into two equal streams as it flows around what is known as a diffluent block **(Fig. 8.12(a))** or the westerly flow may be diverted to unusually low latitudes, forming what is known as an *omega block* **(Fig. 8.12(b))**.

(iv) A block visible on charts is only part of a very large-scale, deep wave pattern.

8.5 Self development

8.5.1 Interaction of PVA with surface baroclinicity

A PVA area in a barotropic region progresses downstream without developing; development and amplification of surface and upper features will generally not take place unless a zone of surface baroclinicity is engaged, allowing constructive interaction between the two via positive feedback in the following way **(Fig. 8.13)**:

(i) Falling pressure ahead of an upper trough at a surface front brings warm and cold advection into play. Cold advection reinforces the upper trough, whilst warm advection helps build the downstream upper ridge.

(ii) The intensification of the upper trough–ridge system increases the PVA, which further deepens the surface low, which increases the strength of the thermal advection, which further reinforces the upper wave and so on. The thermal advection configuration tends to strengthen the jet by shearing frontogenesis.

(iv) The relative phase (trough/ridge positions) between the lower and upper troposphere is important. In a favourable 'phase-locked' conjunction a westward-tilting, developmental configuration is established, whereas advection of the upper feature ahead of the surface feature leads to mutual weakening **(Fig. 8.14)**.

(v) In the standard sequence of events, the occlusion process removes the PVA and low centre from the baroclinic zone, reducing thermal advection strength. In addition, the circulation becomes vertically uniform since there is a much reduced contribution from the thermal wind.

(vi) The development of a closed circulation at upper levels above the surface feature reduces the PVA and makes the slope of the vorticity anomaly vertical. However, if baroclinicity can be maintained in the vicinity of the depression, e.g. by injection of fresh polar air, development can continue.

(vii) Thermal advection by the lower tropospheric circulation is very important to the self-development process. For this reason, the tighter the pre-existing low-level thermal gradient, the greater the potential for cyclonic development. Preferred regions for cyclogenesis occur over oceanic areas of large sea-surface temperature gradient, such as the north-west Atlantic and north-west Pacific, or over cold continent/warm sea boundaries in winter.

(viii) The temperature and humidity of the warm air mass is also important. High wet-bulb potential temperature air releases much latent heat on ascent, increasing upper-level divergence.

(ix) The development process is not always initiated from aloft; the formation of a low-level perturbation can trigger the self-development process.

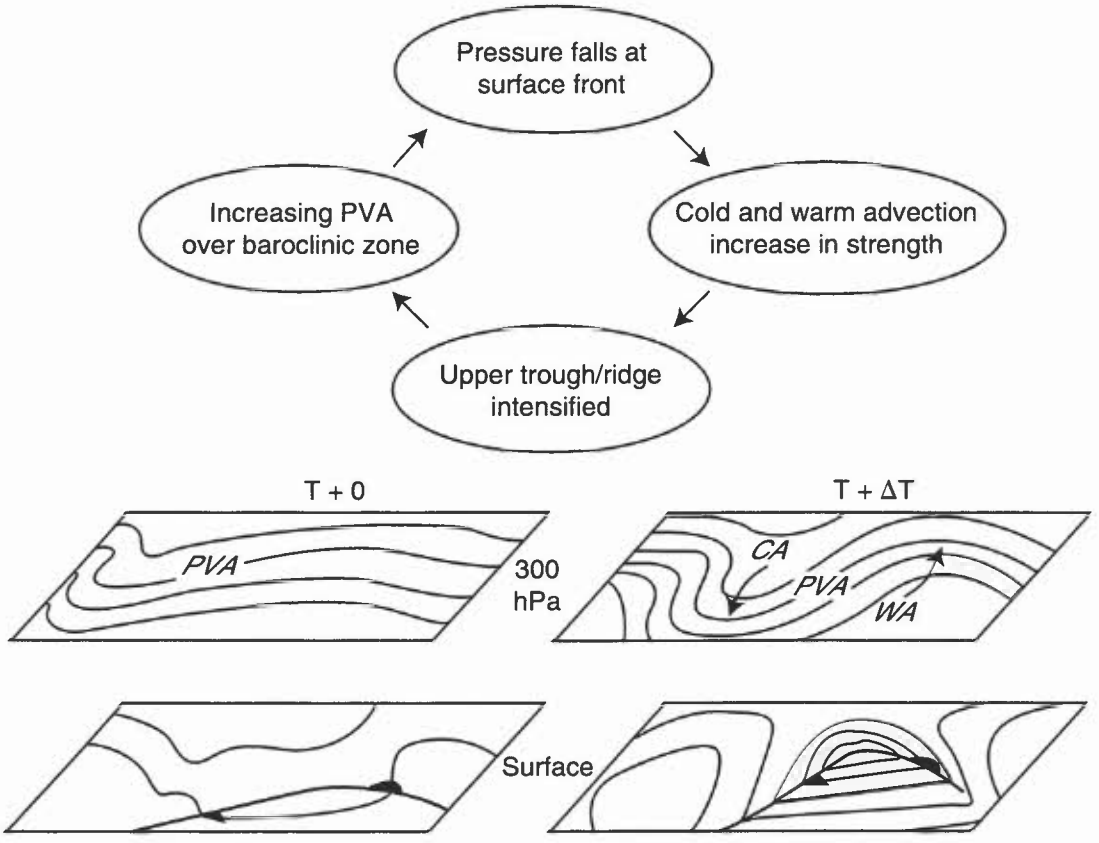

Figure 8.13. Self-development initiated by the engaging of a low-level baroclinic zone by an upper-level PVA region.

8.6 The quasi-geostrophic omega equation

8.6.1 Discussion

The diagnosis of vertical motion presented in sections 8.2 and 8.3 has the two-layer model as its basis, and is conceptual rather than mathematically rigorous. Quasi-geostrophic theory provides an objective framework for

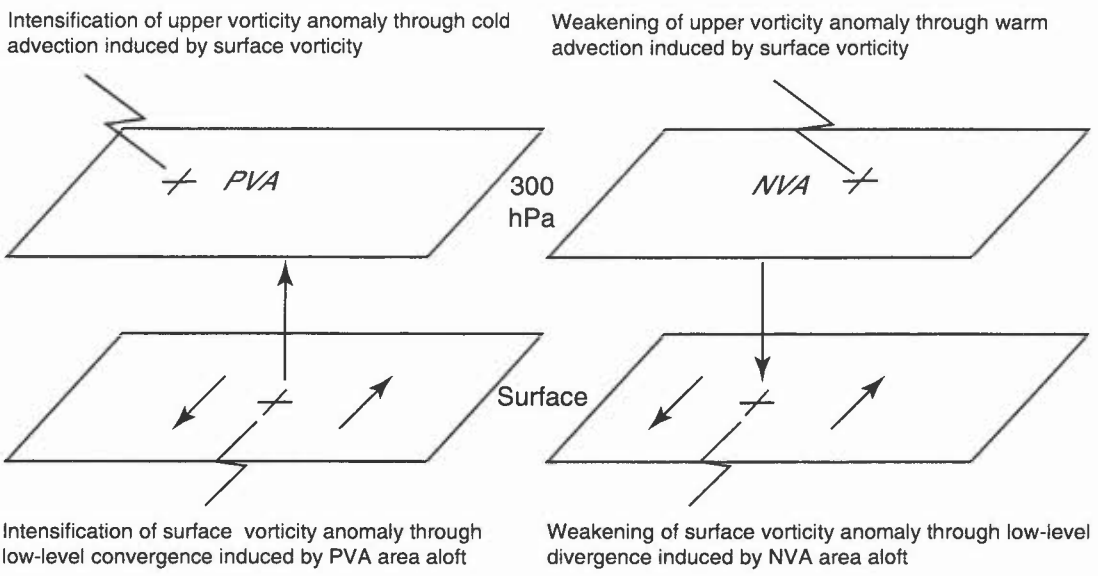

Figure 8.14. Self-developing (left) and self-destroying (right) configurations of surface and upper vorticity maxima.

calculating vertical velocity. It is based on simplified dynamics using the geostrophic advecting winds and other consistent approximations valid for synoptic-scale motion. One of its results, the omega equation, diagnoses the necessary vertical motion to adjust the vorticity and temperature fields into balance with each other in the face of thermal and vorticity advections. In its most well known form it can be given by

$$\frac{\partial^2\omega}{\partial x^2} + \frac{\partial^2\omega}{\partial y^2} + \frac{f^2}{\sigma}\frac{\partial^2\omega}{\partial p^2} = \frac{f}{\sigma}\frac{\partial}{\partial p}\mathbf{V}_g.\nabla_p(\zeta_g + f) + \frac{R}{\sigma p}\nabla_p^2(\mathbf{V}_g.\nabla_p T)$$

where σ is a stability parameter equal to $-1/(\rho\theta)\ \partial\theta/\partial p$ and ω is dp/dt, the vertical velocity in pressure co-ordinates. The form of the RHS determines the forcing, whilst that of the LHS determines the nature of the response.

Simply stated, upward (downward) motion is forced where there is PVA (NVA) in the upper troposphere and in the centres of warm (cold) advection regions, or where a region of cold (warm) advection borders on a region of little thermal advection.

However, applied subjectively it can give the wrong signal, and the following points are worth noting.

8.6.1.1 Interpretation: LHS

(i) The LHS of the equation is a three-dimensional Laplacian of vertical velocity rather than vertical velocity itself. One way to visualize this is as the curvature in three dimensions of the vertical-velocity distribution.

(ii) This Laplacian is negatively correlated with vertical velocity on the average, most reliably so near the level of non-divergence and in regions of strong ascent and descent.

(iii) There is a scale dependence in the conversion of forcing to vertical velocity. Forcing from a small-scale feature such as a front translates to much less vertical velocity than forcing of the same strength from a feature such as a depression.

(iv) The form of the equation shows ω to be dependent not just on local forcing but also on sources of forcing at a distance. The effect of forcing at lower levels is inhibited by the requirement that the vertical velocity should be small at the ground. Therefore, upper-tropospheric forcing is more influential than lower- to mid-tropospheric forcing of the same strength.

(v) The only way to estimate vertical velocity with any certainty using the omega equation is by solving it with a computer. In doing so portions of the vertical velocity at any one level may be attributed separately to forcing from different levels.

8.6.1.2 Interpretation: RHS

(i) Vertical velocity depends on the vertical variation of absolute vorticity advection and the Laplacian, or horizontal curvature, of the thermal advection field.

(ii) Since vorticity advection generally increases in strength up to jet level, in mid-troposphere the vorticity advection term is strongest directly below the strongest upper-tropospheric vorticity advection.

(iii) The Laplacian of the thermal advection field tends to be greatest in the centres of thermal advection regions, often with values of opposite sign at the edges of thermal advection anomalies.

(iv) In addition, vertical motion is greater (less) in statically stable (unstable) air. The effects of latent heating can be absorbed into the stability parameter (assumed in the form given above) or treated more explicitly by a term in the Laplacian of heating.

(v) In many situations there is a fair degree of cancellation between the terms, this cancellation increasing with the strength of the background flow — a strong PVA region embedded in a rapid westerly current, for instance, will probably be significantly offset by cold advection.

(vii) The negative correlation between the Laplacian of vertical velocity and vertical velocity itself is often poor locally, but becomes better when integrated over a large volume. Therefore, subjectively it is best to apply a vertically integrated form, so that instead of temperature advection, thickness advection through a large depth of the atmosphere is used, and upper-level vorticity advection rather than its vertical variation is applied. The method then ends up being similar to the rules derived in 8.3.

8.6.2 Q-vector form

Hoskins et al. (1978) presented a version of the omega equation with only one forcing term. This has advantages over the form given earlier, entailing no cancellation and depending on no vertical derivatives.

$$\frac{\partial^2\omega}{\partial x^2} + \frac{\partial^2\omega}{\partial y^2} + \frac{f^2}{\sigma}\frac{\partial^2\omega}{\partial p^2} = -2\nabla.\mathbf{Q}$$

(i) The vector **Q** depends on the time rate of change of the potential temperature gradient due to horizontal variation of the geostrophic wind. This form of the omega equation above shows that forcing can be related to the divergence of the **Q** field (not included in this rendering is the effect of the advection of planetary vorticity).

(ii) Convergence (divergence) of **Q** gives a forcing which would normally be associated with ascent (descent), though the points made under 8.6.1.1 still apply.

(iii) **Q** may be subjectively determined by noting the vector change in geostrophic wind along an isotherm in the direction of the thermal wind, turning this difference clockwise (in the NH) through 90° and multiplying it by the magnitude of the thermal wind **(Fig. 8.15)**.

(iv) **Q** directed from cold (warm) to warm (cold) implies that frontogenesis (frontolysis) is occurring.

Fig. 8.16 shows a map of computer-generated Q-vectors.

8.7 Sutcliffe theory

8.7.1 Discussion

Sutcliffe (1947) formulated a theory for predicting the tendency in surface vorticity based on the concept of a level of non-divergence at 500 hPa. His development equation can be manipulated to give

$$\frac{\partial}{\partial t}\zeta_{1000} \approx -(V_{1000} + \alpha V')\frac{\partial}{\partial s}\zeta_{1000} - \alpha V'\frac{\partial}{\partial s}(f + \zeta_{500})$$

where subscripts refer to the pressure levels and V' is the 1000–500 hPa thermal wind. α has an average value of 0.5, but increases towards 1 for very large or statically unstable systems and decreases towards 0 for very small systems or in situations of high static stability.

8.7.2 Interpretation

(i) The local rate of change of vorticity at 1000 hPa is shown to be dependent on:

— a steering term which is typically the wind at about half way between the 1000 and 500 hPa levels, say at 700 hPa;

— a development term which is some proportion of the advection by the 1000–500 hPa thermal wind of the absolute vorticity at 500 hPa. This term on its own can be used to indicate the vertical velocity at 500 hPa **(Fig. 8.17)**.

(ii) As with the Q-vector omega equation, there is only one development term, allowing a clear signal in situations of cancellation between vorticity and thermal advection. The form given here is more accurate and involves much less cancellation than Sutcliffe's original form, which has as its development term the advection of thermal vorticity by the thermal wind.

(iii) However, approximations made in the basic approach mean that whatever form is used, vertical velocity directly caused by deformation frontogenesis processes are not represented in Sutcliffe theory.

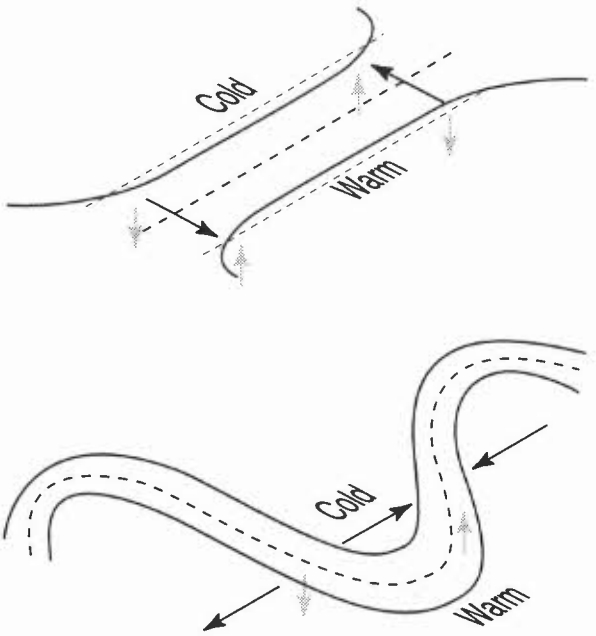

Figure 8.15. Q-vectors (dark arrows) associated with jet entrance and entrance patterns (top) and a ridge–trough–ridge pattern (bottom). Solid lines show geopotential, dashed lines temperature and light arrows implied vertical motion.

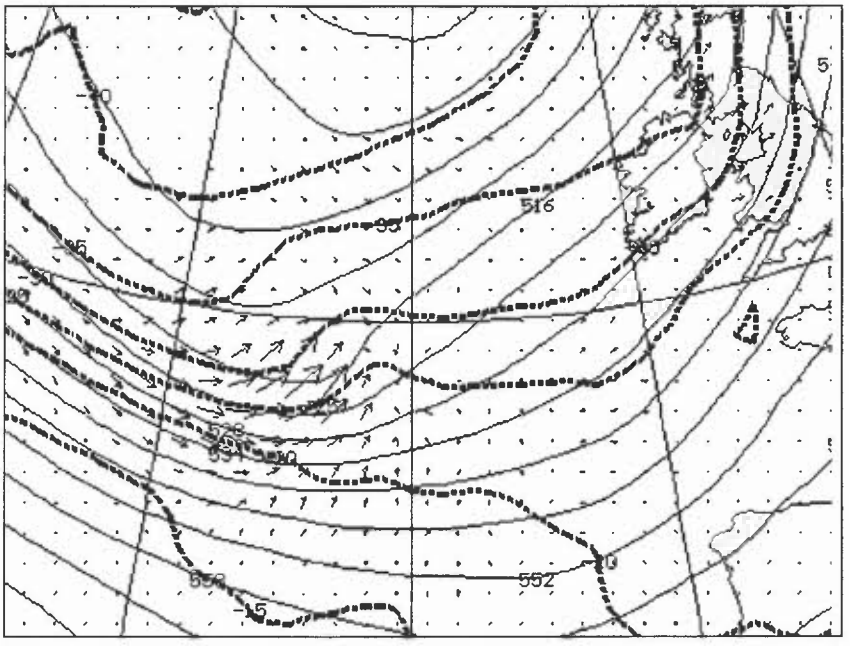

Figure 8.16. Forecast for 0000 UTC on 17 January 1995. Light solid contours show 500 hPa gph, dark dashed contours 500 hPa temperature, and Q-vectors.

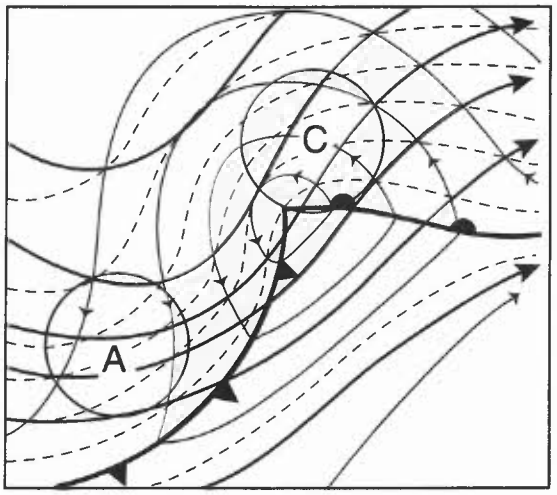

Figure 8.17. Schematic 500 hPa contours (dark solid lines), 1000 hPa contours (thin lines) and 1000–500 hPa thickness (dashed) illustrating a developing warm-sector depression. Sutcliffe development areas derived from advection of absolute vorticity by 1000–500 hPa thermal wind are marked.

8.8 Potential vorticity (PV)

8.8.1 Potential vorticity; conservation, invertibility

Potential vorticity can be expressed as

$$P = -g(\zeta_\theta + f)\frac{\partial \theta}{\partial p}$$

where ζ_θ is the vorticity of the wind on an isentropic surface and $-\partial\theta/\partial p$ is a measure of static stability, being large in conditions of high stability. PV is conserved for frictionless, dry adiabatic processes, making it a good tracer for following features. It is also invertible, in the sense that a knowledge of PV distribution and boundary conditions allows other dynamic variables (e.g. temperature, geopotential wind) to be retrieved if some further balance conditions, such as geostrophic balance, is assumed.

8.8.1.1 Orographic and latitude effects

Fig. 8.18 shows how the effects of orography on stability and meridional motion on f can cause changes in the relative vorticity of the flow.

8.8.1.2 Units and representation

(i) PV is usually measured in PV units, where 1 PV unit corresponds to $(\zeta + f) = 10^{-4}\,s^{-1}$ and $\partial\theta/\partial p = 1$ K per 10 hPa.

(ii) PV distribution is commonly either displayed as PV on an isentropic surface (e.g. $\theta = 315$ K), as θ on a PV = 2 surface (i.e. the dynamic tropopause) or as the height of the PV = 2 surface. Low (high) θ or height correspond to high (low) PV on an isentropic surface.

(iii) Unlike the other two measures, the height of the PV = 2 surface is not conserved following adiabatic, frictionless motion.

8.8.2 The PV view of development

(i) PV features can be viewed as centres of forcing which induce a response in the geopotential height field remote from their locations, in a fashion which is broadly similar to the view of the omega equation presented in section 8.6.

(ii) The strength of this remote effect is greatest with strong anomalies and in statically unstable air, and decreases with increasing distance.

(iii) Because of the high static stability of the stratosphere, it has inherently high PV (>2 units), and anomalies close to the tropopause level are important for forcing development. An upper-level cyclonic PV anomaly draws lower-level isentropic surfaces upwards and apart, reducing static stability and inducing a cyclonic circulation below it **(Fig. 8.19)**.

(iv) Lower-tropospheric temperature anomalies can be thought of as PV anomalies concentrated in a thin layer at the surface, a warm (cold) region having the same effect as a positive (negative) PV anomaly. Dynamical development is controlled by the advection of internal PV anomalies and surface-temperature anomalies. However, since cold (warm) surface air is often associated with high (low) PV aloft, it is not unusual to have conflicting influences from above and below.

(v) Cyclonic development occurs when a cyclonic upper PV anomaly engages a low-level baroclinic zone, initiating constructive interaction between the thermally induced surface circulation and the pre-existing upper trough in a way analogous to the self development described in 8.5 **(Fig. 8.20)**.

(vi) Vertical velocity can be thought of as arising from induced bulging of isentropic surfaces due to upper-level PV advection plus flow of air relative to the isentropic surfaces, i.e. thermal advection. Cyclonic (anticyclonic) PV advection at upper levels and warm (cold) advection lead to ascent (descent), but as with the traditional form of the omega equation, there can be cancellation.

(vii) Latent heat release redistributes PV by warming mid-levels and changing stability, concentrating cyclonic PV at low levels and anticyclonic PV aloft.

(viii) In some instances, stratospheric intrusions of dry, high PV air penetrate into the lower troposphere, causing marked cyclonic development at the surface.

(ix) Ultimately, the ageostrophic motion, vorticity, omega equation and PV views, though apparently different, are nearly equivalent approaches to understanding development.

A cyclogenesis situation (**Fig. 8.21**) and a trough disruption situation (**Fig. 8.22**) are presented from the PV viewpoint.

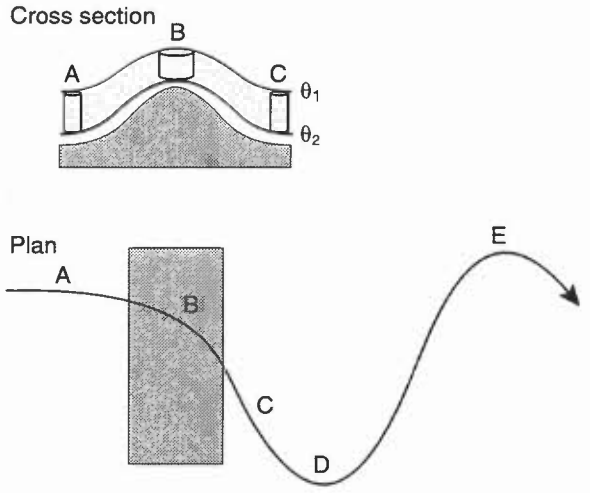

Figure 8.18. Orographic and meridional effects on flow deduced from principle of conservation of potential vorticity.
A–B: $\partial\theta/\partial p$ increases in magnitude therefore ζ decreases.
B–C: $\partial\theta/\partial p$ regains initial value therefore ζ increases.
C–D: f increases therefore ζ increases.
D–E: f increases therefore ζ decreases.

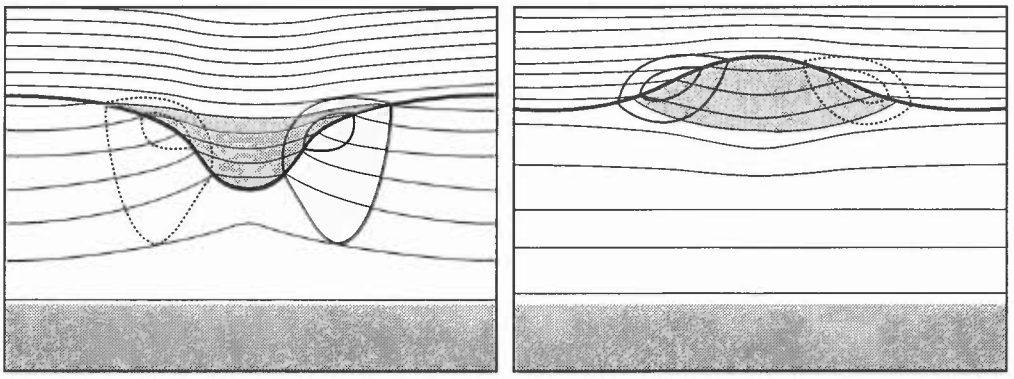

Figure 8.19. Cross-section of isentropes (thin lines, increasing in value upwards) and tropopause (thick line) associated with idealized upper-level PV anomalies, cyclonic (left) and anticyclonic (right). Also shown are anomaly positions (shaded) and isotachs (solid into page, dashed out of page).

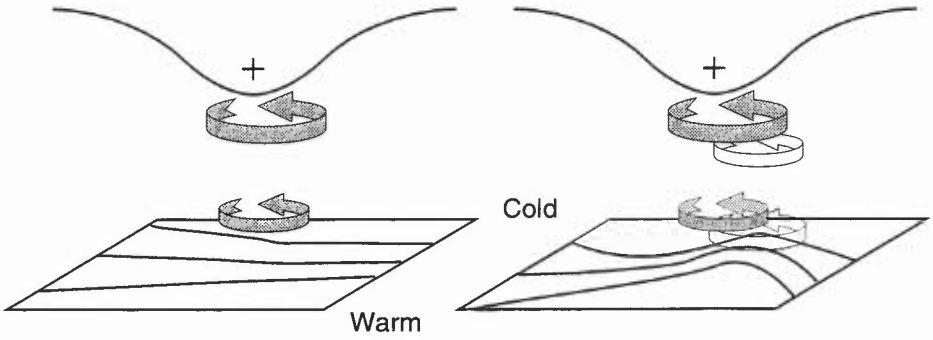

Figure 8.20. Schematic picture of cyclogenesis associated with the arrival of an upper PV anomaly over a low-level baroclinic zone. Dark line tropopause, thin lines surface isotherms. The low-level circulation induced by the cyclonic PV anomaly aloft advects warm air polewards. The resulting low-level warm anomaly induces a cyclonic flow at higher levels which advects high PV air equatorwards into the upper anomaly.

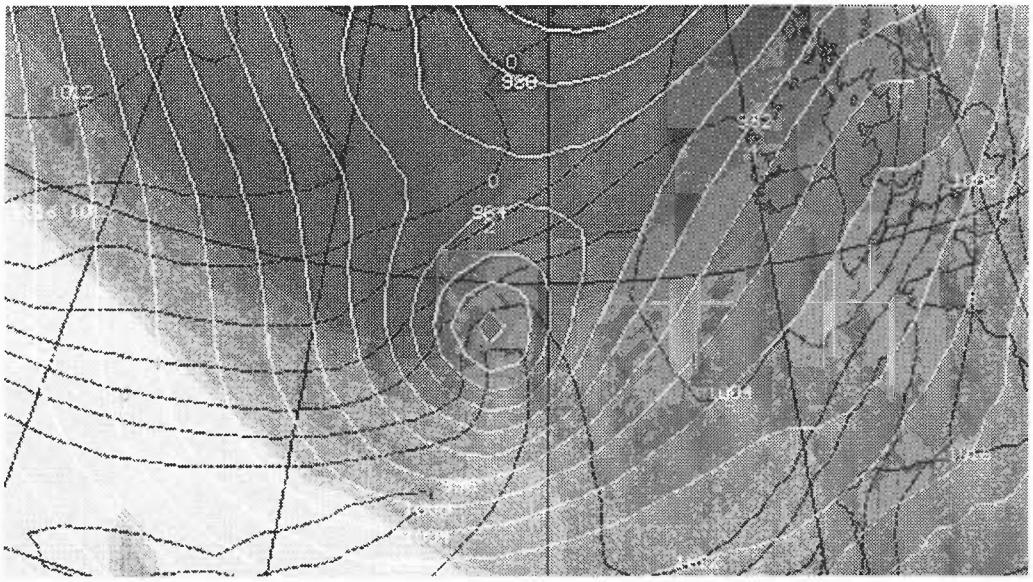

Figure 8.21. Forecast for 0000 UTC on 17 January 1995. Potential temperature on a PV = 2 surface shown by shade of background (dark cold, light warm, shades every 5 °C); PMSL (light solid); 850 hPa wet-bulb potential temperature (dark dashed, every 2 °C). Warm surface anomaly and upper positive PV anomaly combining to give strong forcing for cyclogenesis.

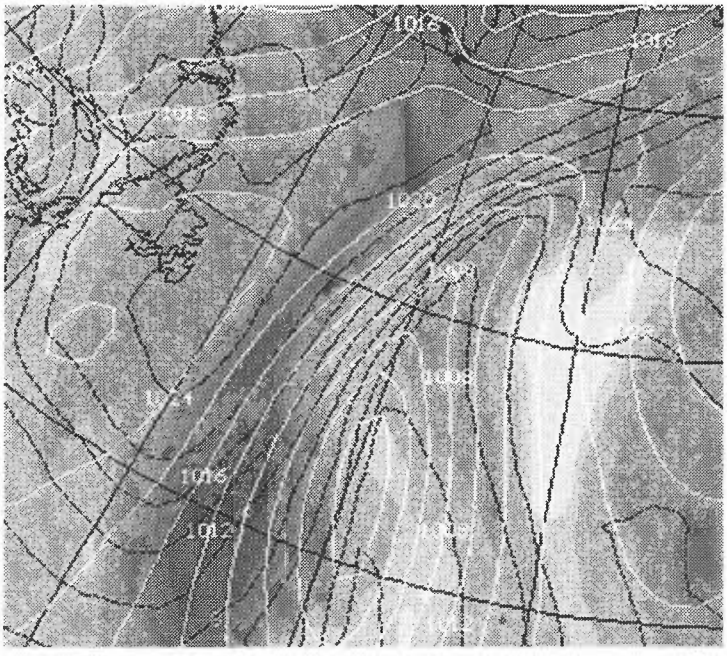

Figure 8.22. Forecast for 1200 UTC on 13 April 1995. Potential temperature on a PV = 2 surface, PMSL and 850 hPa wet-bulb potential temperature as in Fig. 8.21. The trough disruption case shown in Fig. 8.11. The surface depression lies close to a plume of warm air at low levels. The plunge of high PV aloft partly offset by advection of cold low-level air. Surface high south of Newfoundland forced by cold low-level air and low PV aloft.

BIBLIOGRAPHY

CHAPTER 8 — USE OF DYNAMICAL CONCEPTS IN ASSESSING DEVELOPMENT

Bishop, C. and Thorpe, A.J. 1995: Potential vorticity and the electrostatics analogy. *QJR Meteorol Soc*, **120**, 713–731.

Carlson, T.N., 1994: Mid-latitude weather systems. Routledge.

Carroll, E.B., 1995: Practical subjective application of the omega equation and Sutcliffe development theory. *Meteorol Appl*, **2**, 71–81.

Carroll, E.B., 1995: Diagnosis of a rapidly deepening depression: 16/17 January 1995. *Meteorol Appl*, **2**, 231–237.

Clough, S.A., Davitt, C.S.A. and Thorpe, A.J., 199?: Attribution concepts applied to the omega equation (JCMM Internal Report 47). *QJR Meteorol Soc*, to be published.

Durran, D.R. and Snellman, L.W., 1987: The diagnosis of synoptic-scale vertical motion in an operational environment. *Weather and Forecasting*, **2**, 17–31.

Hoskins, B.J., Draghici, I. and Davies, H.C., 1978: A new look at the ω-equation. *QJR Meteorol Soc*, **104**, 31–38.

Hoskins, B.J., McIntyre, M.E. and Robertson, A.W., 1985: On the use and significance of isentropic potential vorticity maps. *QJR Meteorol Soc*, **111**, 877–946.

Hoskins, B.J. and Pedder, M.A., 1980: The diagnosis of middle latitude synoptic development. *QJR Meteorol Soc*, **106**, 707–719.

Sanders, F. and Hoskins, B.J., 1990: An easy method for the estimation of Q-vectors from weather maps. *Weather and Forecasting*, **5**, 346–353.

Sutcliffe, R.C., 1947: A contribution to the problem of development. *QJR Meteorol Soc*, **73**, 370–383.

Young, M.V., Browning, K.A. and Monk, G.A., 1987: Interpretation of satellite imagery of a rapidly deepening cyclone. *QJR Meteorol Soc*, **113**, 1089–1115.

CHAPTER 9 — NUMERICAL WEATHER PREDICTION

CHAPTER 9 — NUMERICAL WEATHER PREDICTION

9.1 Operational models

The Meteorological Office operational models are increasingly sophisticated but their output should always be interpreted cautiously. Familiarity with strengths and weaknesses is vital.

9.2 Summary of types of numerical models

(i) Climate models describe the general behaviour of the troposphere and stratosphere over long periods of time.
(ii) Operational synoptic models are used for day-to-day weather forecasting. They may cover a domain that is global (GM) in extent, or may be restricted to a more limited area (LAM). Their resolution is such that they can describe the state and behaviour of synoptic-scale weather systems.
(iii) Mesoscale models (MM) are used for forecasting localized weather variations, especially those forced by topography, over a domain about the size of the UK.
(iv) Specialized models are research tools for investigating the physics of such phenomena as fog, cumulonimbus clouds, stratocumulus, low-level turbulent flow, etc. or larger-scale phenomena such as individual cyclones and the long-wave flow pattern.

Cullen (1993)

9.3 Guide to NWP Interpretation

Asynoptic data are assimilated with model forecast fields to give the best possible estimate of the initial state of the atmosphere (e.g. 4-D variational assimilation).

Lorenc et al. (1991)

9.3.1 Limits of resolution

(i) LAM grid-point spacing of 50 km effectively defines frontal position accuracy (i.e. at 15 kn this represents nearly 2 hours of movement). In practice, the frontal position will be aided by information on orientation from surrounding grid points.
(ii) Frontal waves need at least three grid lengths in order to be adequately represented; such features can occasionally be missed as a result.
(iii) More often a wave will be developed, but with uncertainty as to position and amplitude.
(iv) Artificial smoothing within the model and resulting from contouring algorithms will reduce sharpness of angles/discontinuities.
(v) Satellite imagery may provide evidence of the development of a frontal wave through the widening of the frontal band and other characteristics.

9.3.2 Precipitation

(i) It is important in forecasting the distribution and type of precipitation to deduce surface frontal positions and apply conceptual models.
(ii) The 850 hPa WBPT is useful here (Bradbury, 1977); the front, warm or cold, is likely to be situated just on the warm side of a tight WBPT gradient.
(iii) Because of frontal slopes, the frontal position at 850 hPa may not coincide with the surface frontal position.
(iv) Generally surface cold fronts coincide well with the warm side of the 850 hpa WBPT gradient because of the steeper frontal slope and the tendency for a nose of cold air to override the warm air at the surface, whereas surface warm fronts tend to be slightly back from the 850 hPa position (though not as far as the 1:150 slope would suggest) **(Fig. 9.1)**.
(v) Occlusions are positioned along ridges of WBPT.
(vi) Troughing in the forecast surface isobaric pattern is a more definitive indication of frontal surface position.
(vii) The position of a certain value WBPT isopleth may be linked to, say, a surface front, cloud sheet edge, etc. which may, in the short term anyway, be related to the movement of that isopleth.
(viii) Consistency is important in positioning surface fronts from frame to frame. A good guide in this respect is to use the ASXX chart to position fronts on the T+0 initializing frame and the FSXX to position fronts on the T+24 frame and to fill in intermediate frames accordingly.

(ix) Any differences between a precipitation forecast by the model and that expected from subjective assessment should be reconciled with, for example, WBPT analysis and checking LAM T-ϕs or global model 700 hPa RH fields against relevant satellite imagery and actual T-ϕs.

Bradbury (1977)

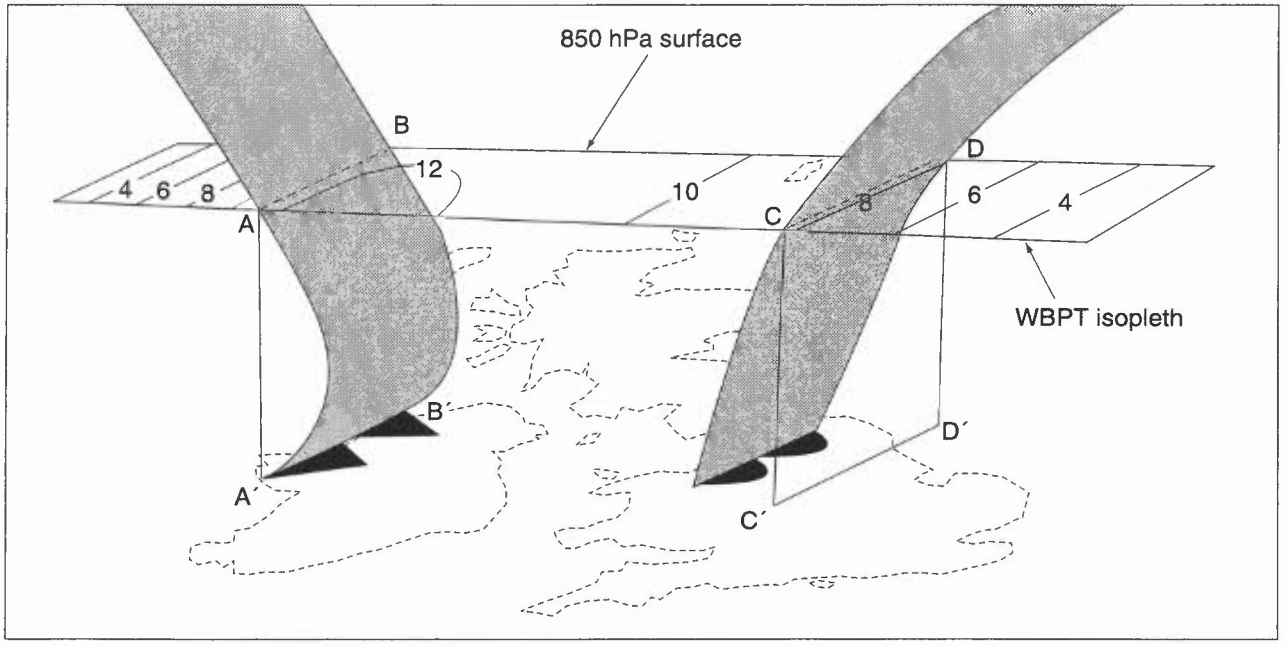

Figure 9.1. Cold- and warm-frontal positions at 850 hPa coinciding with the warm side of the WBPT gradients, given by AB and CD, respectively. These positions projected down onto the surface are A′B′ and C′D′. A′B′ gives a good estimate of surface cold-frontal position because of the cold air 'nose' overriding warm air at the surface. C′D′ is somewhat ahead of the surface warm front, but not as far ahead as a 1:150 slope would suggest because frontal slope is steeper near the surface.

9.3.2.1 Shower forecasts

(i) The convection scheme is based on parcel theory (4.2.1) ; output rain rates are averaged over a grid box so heavy showers are designated mean rate 0.5 mm h^{-1} or more.

(ii) In order to model the effect of different concentrations of condensation nuclei in continental and oceanic air masses, showers are diagnosed according to strict criteria:
showers develop if cloud depth >1.5 km over sea
>4.0 km over land
if (land or sea) cloud-top temperature < -10 °C, then critical depth is 1.0 km.

These may only just fail to be reached, so checking against the actual or forecast T-ϕs is important. The output may point to something overlooked. Correct or not, the model evolution is always internally consistent. Check accumulated as well as actual rates of precipitation.

9.3.2.2 Phase

(i) The UM differentiates between phases of the precipitation, based on temperature of the first model level.

(ii) Snow probabilities are based on the mean temperature at the 1000–850 hPa thickness and should be corrected for the height of the ground above sea level (**Fig. 9.2**).

(iii) Beware of the situation where cold air at the surface is undercutting warm (e.g. use Hand's method, 5.10.1.3).

(iv) Beware, too, of the poor vertical resolution of representative forecast tephigram, especially in the boundary layer.

(v) A downdraught scheme allows snow to reach the ground on some occasions, even when wet-bulb temperatures are several degrees above zero.

(vi) An arbitrary limit of 2 °C is set for precipitation to be output as snow.

(vi) Current boundary layer and convective schemes have led to unrealistic temperature profiles near intense cold pools.

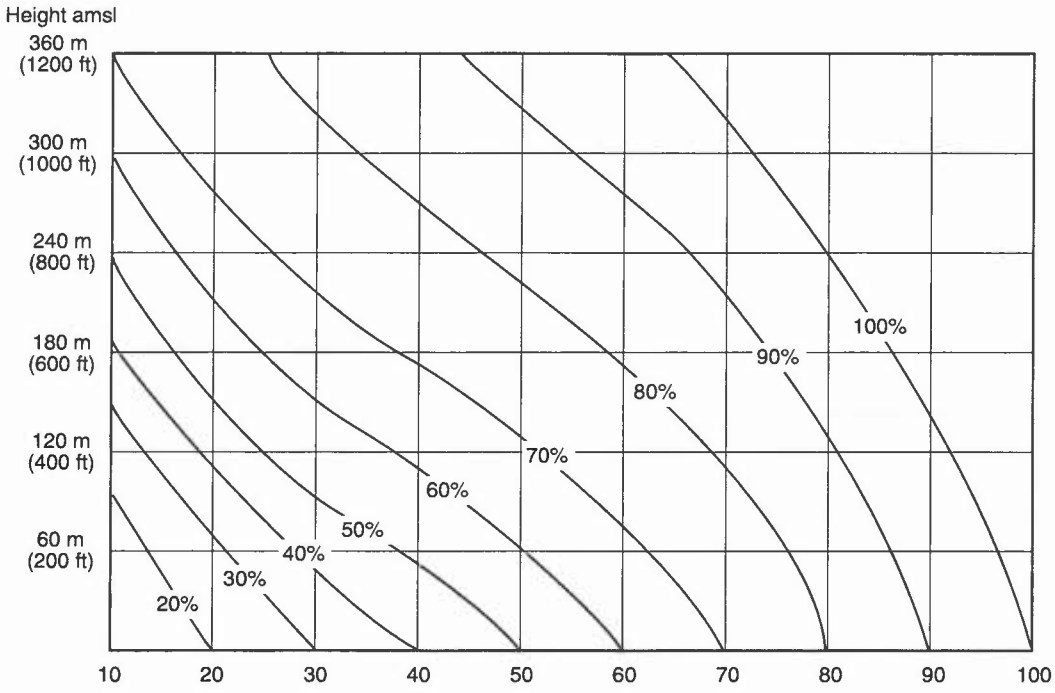

Figure 9.2. Diagram to adjust snow probability at sea level for different elevations, e.g. 20% probability at MSL represents 50% probability at 150 m AMSL.

9.3.2.3 Cloud water and dynamic precipitation

(i) Cloud water is included as a model variable, distributed between liquid and solid phases according to temperature.
(ii) Precipitation is generated by coalescence in warm clouds with the seeder–feeder mechanism modelled (5.9.5).
(iii) For dynamic rain a rate of 4 mm h^{-1} is required to produce the heavy rain symbol.
(iv) Evaporation of dynamic precipitation falling through unsaturated air is rain-rate dependent; cloud water can be advected in the GM and LAM leading to possible moisture convergence and rainfall intensification.

Davies & Hammon (1986) **Hall (1991)**

9.3.3 Surface boundary conditions

Surface hydrology includes effects of plant canopies and sub-soil characteristics; surface albedo depends on soil, canopy type, fractional vegetation cover, snow cover and temperature. Insulating effects of snow cover are modelled.

9.4 Model characteristics

9.4.1 General comments

(i) Generally the model handles cyclogenesis well; there is little evidence of systematic problems; trough disruption situations account for most errors, the model failing to capture the fine balances involved, and producing spatial and temporal errors.
(ii) Systematic under-forecasting of winds near jet cores for World Area Forecast output is noted.
(iii) Surface winds — normally too strong over land in the LAM; a little too weak in the MM.
(iv) Vertical velocity — very high grid box mean velocity often associated with intense convection; possibly due to excessive feedback between convection scheme and large-scale motion.

9.4.2 Rainfall

(i) Main problems during summer months are due to poor representation of moisture and weakly defined forcing functions.
(ii) Spurious light rain is sometimes found from shallow boundary layers driven by radiative cooling of the cloudy layer, due to lack of vertical resolution which does not allow compensating entrainment of air from above the boundary layer.

(iii) The possibility of low cloud/drizzle should not be ruled out when light rain is forecast.
(iv) The model has a tendency to change shower distribution from run to run; forecasters should treat shower symbols as indicating areas of instability that may trigger showers.
(v) Over-forecasting of showers with a high 850 hPa θ_w may be due to too high θ_w or early encroachment of instability from the south or south-west.
(vi) Under-forecasting of dynamic rain is often associated with too rapid decay of precipitation on weakening, slow moving fronts and/or poor humidity analysis (MM is better at retaining moisture).

Nicholass (1993)

9.4.3 Snow

(i) Frozen precipitation is defined as melted or frozen depending on whether the layer temperature is above or below being <0 °C.
(ii) Chart symbols depend on temperature at the lowest level; snow/rain mixture possible if rate is high enough for temperature to be lowered to 0 °C before all snow melts. Output symbol is then snow, the temperature being held at 0 °C; thus lowering of freezing level by melting snow is modelled.
(iii) Snow probability lines are derived from 1000–850 hPa thickness adjusted for MSLP; they are a better indicator of snow than using symbols directly.
(iv) Probabilities are based on past frequencies of rain or snow compared to the observed thickness, and take into account that the wet-bulb freezing level is normally lower than the dry-bulb freezing level, and the fact that wet snow can fall when both are a few hundred metres above the surface. This is not the case for snow symbols in association with dynamic precipitation.
(v) Probabilities work best in unstable, showery situations when the 1000–850 hPa thickness represents a homogeneous air mass:
the 20% line suggests rain/sleet,
80% mostly snow
50% often indicates a mixture of type and requires interpretation as to wind direction, proximity to sea, intensity, etc.
(vi) Widespread and heavy dynamical precipitation often turns to snow even with 20% or less probabilities if low-level air has a long land track over the UK or a short sea track from the continent.
(vii) Probabilities are significantly affected by height above sea level (150 m can change 20% to 50% probability, **Fig. 9.2**).

9.4.4 Temperature errors

(i) The GM and LAM tend to be too slow at warming cold air masses advecting over warmer surfaces — 500 hPa contour errors as high as 20 dam by T+96 have occurred; result — over-forecasting of snow at lower levels in polar maritime outbreaks.
(ii) Nested models within UM system tend to underestimate freezing-level height from summer to autumn — and overestimate for rest of year.
(iii) Under anticyclones, lowest layers often too cold, giving misleading MOS (2.12) from GM.

9.4.5 Humidity errors

(i) Initialized model ascents sometimes poorly represent observed moisture structure.
(ii) Humidity quality control is likely to reject information if it is significantly different from background, but intervention can support or bogus humidity observations to improve analysis.
(iii) Relative lack of model vertical resolution a problem on forecast ascents. For example, top of frontal cloud appears to be near 600 hPa.

9.4.6 Pressure over mountains

(i) Analysis and forecasts of sea-level pressure over mountainous areas is a problem. Indeed, there is no completely satisfactory way of deducing PMSL at high-level stations.
(ii) Uniform lapse rate of 6.5 °C km^{-1} from sigma level 4 (to avoid spurious effects from surface temperatures) to PMSL is assumed.
(iii) Observed PMSL is higher than the model when surface is cold. During a hot day, overland heat lows will appear deeper than model. This does not necessarily imply that the surface observations are correct.

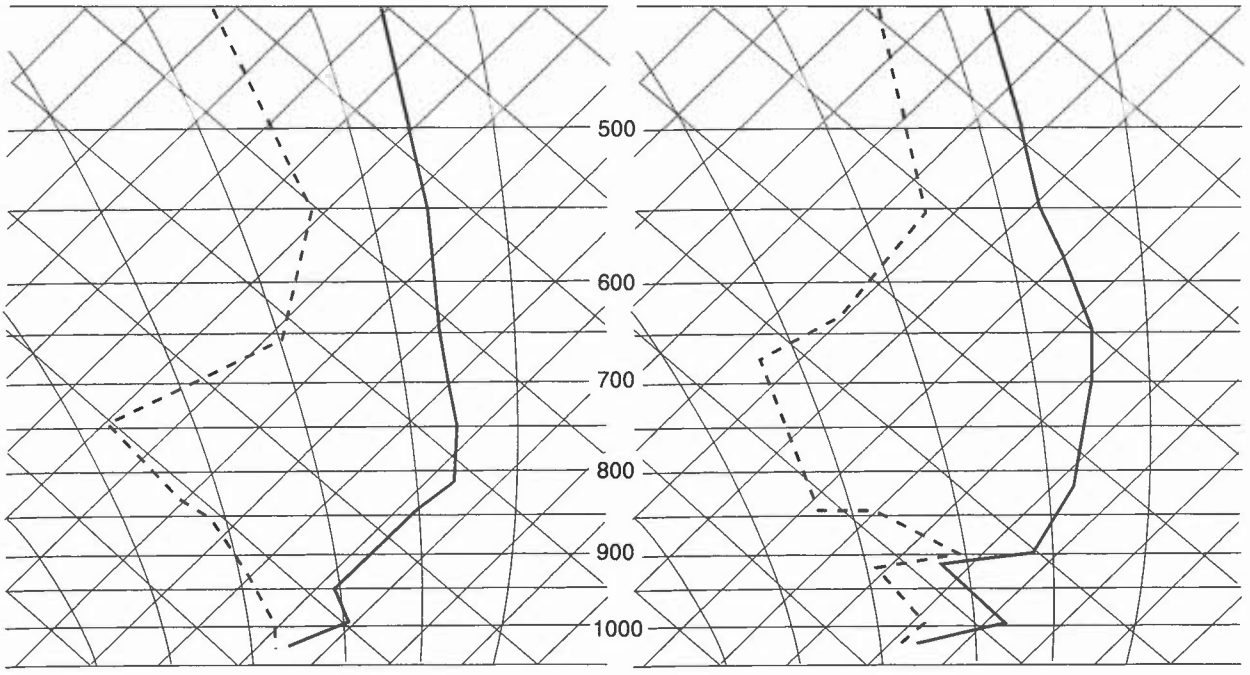

Figure 9.3. A tephigram from the initial fields of the old 15-level fine mesh (left) compared to its counterpart as measured by radiosonde. Note that although the general shape is correct, the model has completely failed to represent the sharp, moist inversion at 900 hPa.

9.4.7 T-ϕs

(i) Temperature of the lowest level is that of model ground (or sea); temperature at a model level represents mean temperature of a layer.
(ii) Thus, inversions are usually less well defined and the height will be in error when compared to the real atmosphere **(Fig. 9.3)**.
(iii) Real value of the T-ϕ may be to indicate stability and moisture changes with time at different levels.

See 5.9.8.

McCullum et al. (1995)

9.5 Guidance, confidence and verification

(i) The Synoptic Review (SR) will generally appraise the model output, with comments on the shortcomings of analysis and implications for subsequent development.
(ii) Major changes from run to run should be treated with caution.
(iii) Simple verification can include comparison of reported surface pressures with T+6 or T+12 forecasts, agreement giving confidence in subsequent evolution.
(iv) Actual versus forecast rainfall distribution can be compared; if T+6 is realistic, confidence in T+12, etc. frames will be high. The model output, anyway, should not be dismissed too hastily.
(v) Meteosat imaging is particularly useful (except during eclipses!) as it will be available at standard verification times.

9.5.1 Using Global Model output

(i) The 850 hPa WBPT allows direct comparison of the (lower-resolution) GM and LAM output. Differences, e.g. in timing, should be noted and the SR consulted.
(ii) If no specific guidance offered, the situation should be monitored for early indications of development.
(iii) The 700 hPa charts show RH at 19% intervals — mark the 76% isopleth; within this area extensive medium-level cloud and some rain is likely. The 95% line is indicative of likely medium to heavy precipitation.
(iv) The 500 hPa thickness and contour charts allow assessment of thermal advection and likely forcing for development .

(v) The 300 hPa chart has isotachs at 20 kn intervals; highest winds are slightly underestimated because the 90 km resolution is less able to cope with the large shear values around jets.
(vi) By better understanding of the model atmosphere, the dynamical processes and the features governing surface evolution, the better position the forecaster will be in a good position for extrapolating errors which become apparent early in the forecast run.
(vii) The output also allows the routine study of the 3-D relationship between the movement and development of upper and surface features.

9.5.2 Global compared to LAM

(i) The greater resolving power of the LAM will handle waves and jets more realistically (but has led to less-accurate handling of certain features) and should outperform the GM in highly developmental situations.
(ii) The GM has a later run time and may receive vital data missed by the LAM. The GM may also benefit from later intervention on the analysis.
(iii) SR will offer guidance as to which model has the preferred solution.

9.5.3 Mesoscale compared to LAM

(i) Mesoscale precipitation fields add little to LAM; by restricting diffusion to smaller scales MM allows sharper features and more active precipitation areas;
(ii) spurious signals can result due to problems with the initialization scheme for cloud and moisture;
(iii) assimilation includes humidity from surface observations with intention of improving fog treatment.

McCullum et al. (1995)

9.5.4 Model Output Statistics (2.12)

9.5.5 Ensemble forecasting (11.7)

BIBLIOGRAPHY

CHAPTER 9 — NUMERICAL WEATHER PREDICTION

Bradbury, T.A.M., 1977: The use of wet-bulb potential temperature charts. *Meteorol Mag*, **106**, 233–251.

Cullen, M.J.P., 1993: The Unified Forecast/Climate Model. *Meteorol Mag*, **122**, 81–94.

Davies, T. and Hammon, O., 1986: Snow forecasts from the Meteorological Office fine-mesh model during the winter of 1985/86. *Meteorol Mag*, **115,** 396–404.

Hall, C.D., 1991: A guide to NWP models and their output. *Central Forecasting Technical Note* 5, Meteorological Office.

Lorenc, A.C., Bell R.S. and MacPherson, B., 1991: The Meteorological Office analysis correction data assimilation scheme. *QJR Meteorol Soc*, **117**, 59–89.

McCullum, E., Mansfield, D. and Grahame, N., 1995: Model characteristics — Notes for forecasters (2nd edition), Central Forecasting Office, Meteorological Office Bracknell.

Nicholass, C.A., 1993: Forecasting difficulties in showery situations. *Meteorol Mag*, **122**, 135–139.

CHAPTER 10 — REMOTE SENSING

CHAPTER 10 — REMOTE SENSING

10.1 Meteorological satellites

Satellite imagery can give important clues as to the dynamical processes occurring, especially if they are complemented by the forecaster's ability to associate this imagery with conceptual models (7.1). The principles of remote sensing and much about the interpretation of satellite images are in **Bader et al., 1995, Chapter 1.**

Cracknell & Hayes (1991)
Scorer & Verkaik (1989)

10.2 Image interpretation

In examining imagery the following should be borne in mind:

(i) time and date — for temperature regimes and likelihood of, say, snow or ice cover which in turn will indicate physical processes likely to be occurring, e.g. fog formation, convection;

(ii) geography of the field of view — hence radiation fog is often seen filling valleys and leaving ridges clear, while sea fog and stratus often follow the coastline.

10.2.1 VIS imagery

(a) When considering albedo in VIS images, bear in mind that:
  (i) thick cloud is more reflective than thin cloud;
  (ii) water cloud is more reflective than ice cloud;
  (iii) cloud composed of small droplets is more reflective than cloud of large droplets.
  These criteria can act against each other (e.g. a Cu congestus will have a higher albedo than a glaciated Cb of the same depth).

(b) St and fog can have high albedos; oceans have low values except in diffuse or concentrated sun glint. However, absolute values are not necessarily too important — contrast is more readily discerned **(Fig. 10.1)**.

(c) Textural detail is clearest at low solar elevation (e.g. smoothness, striations, cellular or fibrous structure).

(d) Shadows and highlights are most easily seen at low solar elevation; they can help to differentiate partially superimposed cloud details at different levels.

(e) Sun glint on the polar orbiting satellite images:
  (i) The strongest reflection will be in the vicinity of the specular point where direct sunlight is reflected back to satellite.
  (ii) Sun glint increases in brightness towards latitude of overhead sun, i.e. brighter towards the south and in summer in northern latitudes.
  (iii) Clouds have enhanced brightness around the specular point; regions of calm winds or sheltered water may show up dark in the middle of sun glint.
  (iv) Absolutely calm water will give a very bright, concentrated response in a north–south oriented line. Small wavelets will give a broader, less bright response **(Fig. 10.2)**.

10.2.2 IR imagery

(i) The degree of whiteness can generally be taken to be a function of the degree of coldness and density/thickness of the underlying cloud (e.g. thin clouds will appear darker than thick layers having the same top level.

(ii) Cloud elements not completely filling pixels will be representative of a temperature between cloud top and the earth's surface and may be difficult to detect, e.g. fair-weather Cu, thin Ci.

(iii) IR image generally has less texture due to lack of shadow, highlight features and resolution.

(iv) The temperate latitude convention is for low temperatures to be displayed as white and high temperatures as black.

(v) At high latitudes over cold surfaces there is lower contrast between high and low clouds.

10.2.3 Using IR with VIS imagery

Fig. 10.3 represents a decision table relating different cloud and surface types to different VIS and IR radiances; imagery is compared in **Fig. 10.4**.

Bader et al. (1995), Chapter 1
DNOM (1982)

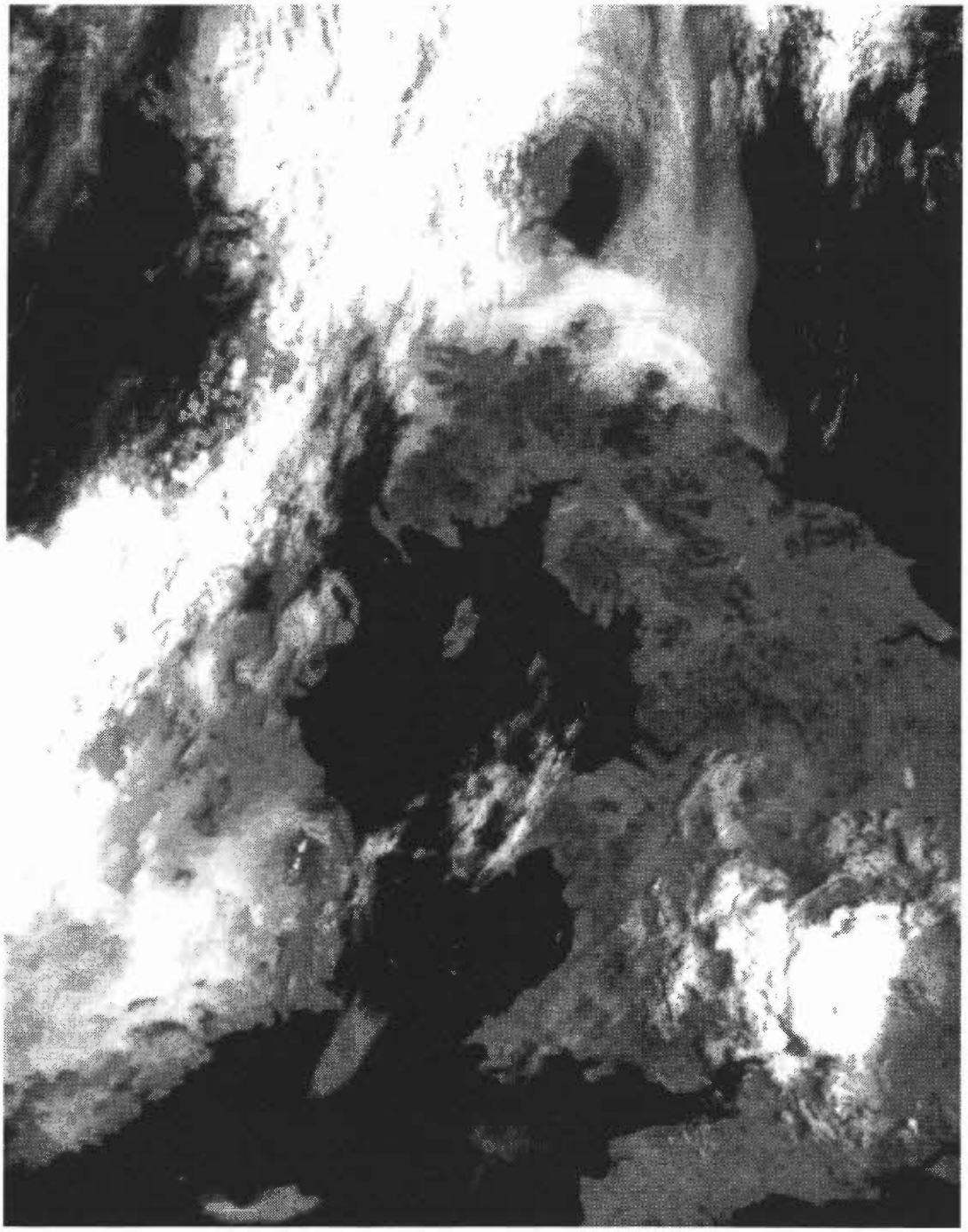

Figure 10.1. NOAA channel 2 (VIS) image at 0812 UTC on 24 May 1989. A large cumulonimbus anvil cloud over southern England shows up a small shadow cast by an overshooting top, probably extending into the stratosphere. A cold-frontal band extending from western Ireland to northern Scotland shows evidence of embedded convective activity. On the warm side of the front, sea fog is blown onto the coast of north-east England and south-east Scotland. This has rather straight, well defined edges over the sea, whereas inland its boundaries are determined by topography — the greatest inland penetration is between areas of high ground. The fog appears whiter over the land, where its albedo is little different from the much thicker clouds — this is because it is semi-transparent, and the sea is darker than the land. Much of central Ireland is also covered by fog, producing drizzle in places. The Wicklow Hills, just south of Dublin, are free of fog, and cumulus clouds have started to form due to insolation in the hilltops.

10.2.4 Water vapour imagery

10.2.4.1 Principles

(i) WV imagery is usually displayed with the emitted radiation converted to temperature (as with IR imagery);

(ii) regions of high (low) tropospheric humidity appear cold (light)/warm (dark);

(iii) when the upper troposphere is dry, the radiation reaching the satellite originates from further down in the atmosphere, where it is warmer (darker image)

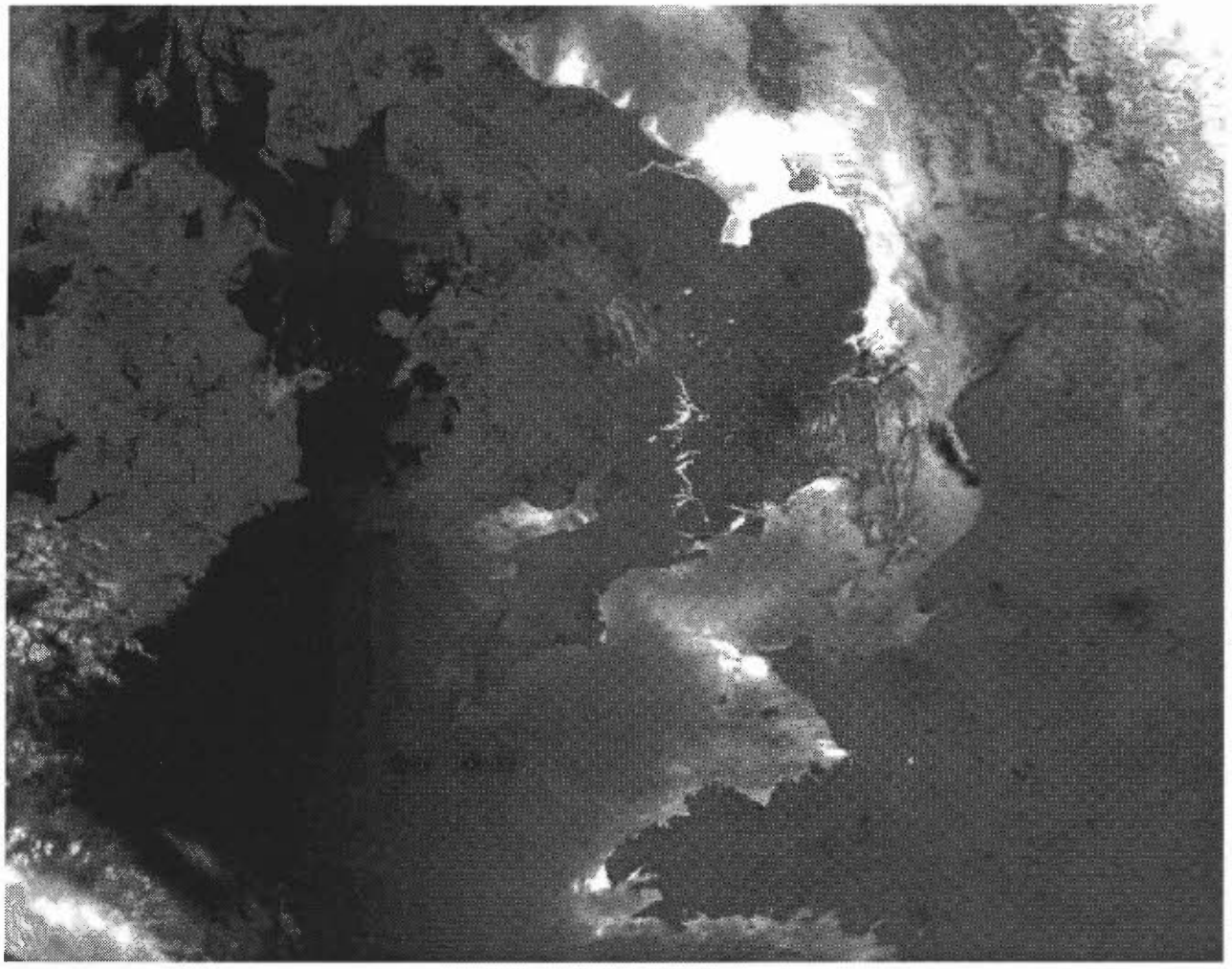

Figure 10.2. NOAA channel 2 (VIS) image at 0907 UTC on 19 July 1989. An anticyclone is centred over East Anglia. Sun glint reveals rivers and lakes in England despite their sub-pixel size. Differences in the intensity of sun glint result from variations in the smoothness of the sea. Sheltered waters near the coast show bright glint near the specular line, e.g. Brest peninsula, East Anglia, whilst slightly further from the specular line they appear dark, e.g in the Thames estuary and eastern Channel. Note that urban areas, e.g. Paris and London, as well as upland, have a lower albedo than other land surfaces.

10.2.4.2 Interpretation

(i) In a normally moist atmosphere, most of the WV radiation received by the satellite originates in the 300–600 hPa layer;
(ii) where the air is dry some radiation may come from layers as low as 800 hPa;
(iii) at higher latitudes the troposphere is colder with smaller temperature/height variations in lower latitudes, so that higher latitudes display a smaller range of grey shades;
(iv) the winter range of grey shades is less;
(v) moisture banding implies that brightness temperature may not be representative of air in lower layers — in particular, when WV imagery (dark) indicates a very dry upper troposphere (possibly low θ_w/maximum vorticity) there may well be regions of high θ_w near the surface, leading to areas of deep convection;
(vi) moist air or cloud in the lower troposphere is not well depicted in WV imagery;
(vii) thick, high clouds such as Cb anvils, stand out prominently in both WV and IR.

Bader et al. (1995), Chapter 1 DNOM (1982)

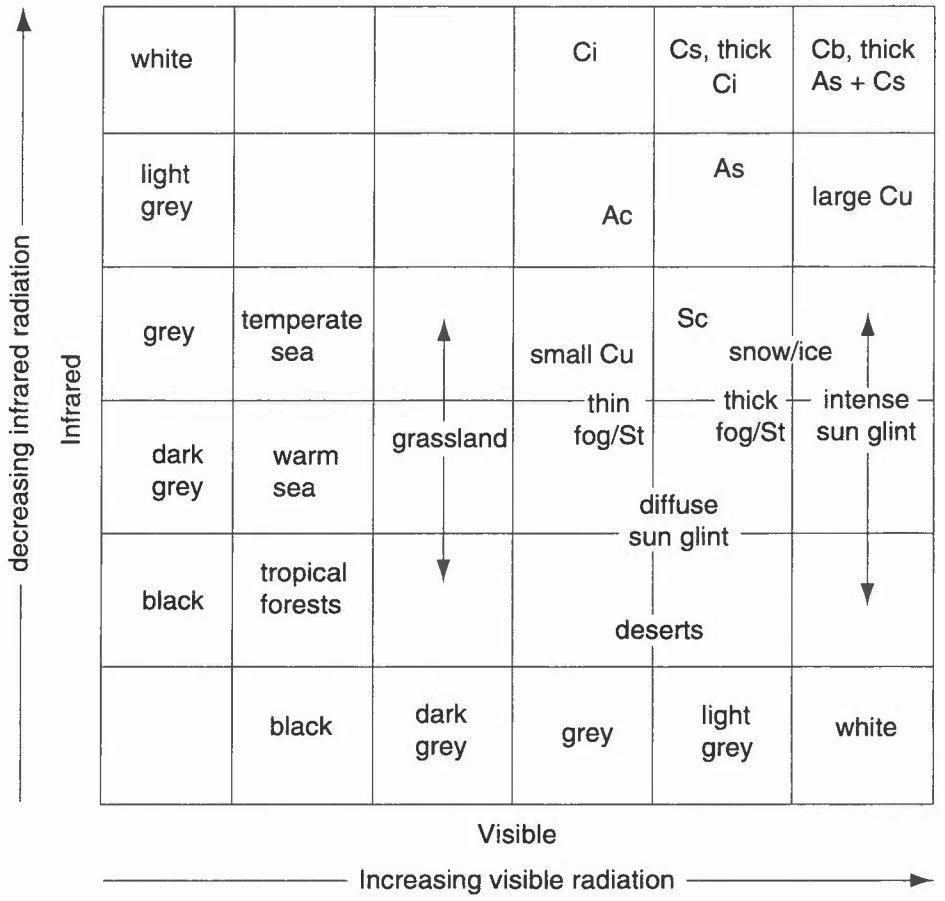

Figure 10.3. Decision table indicating typical radiances associated with clouds and different surfaces.

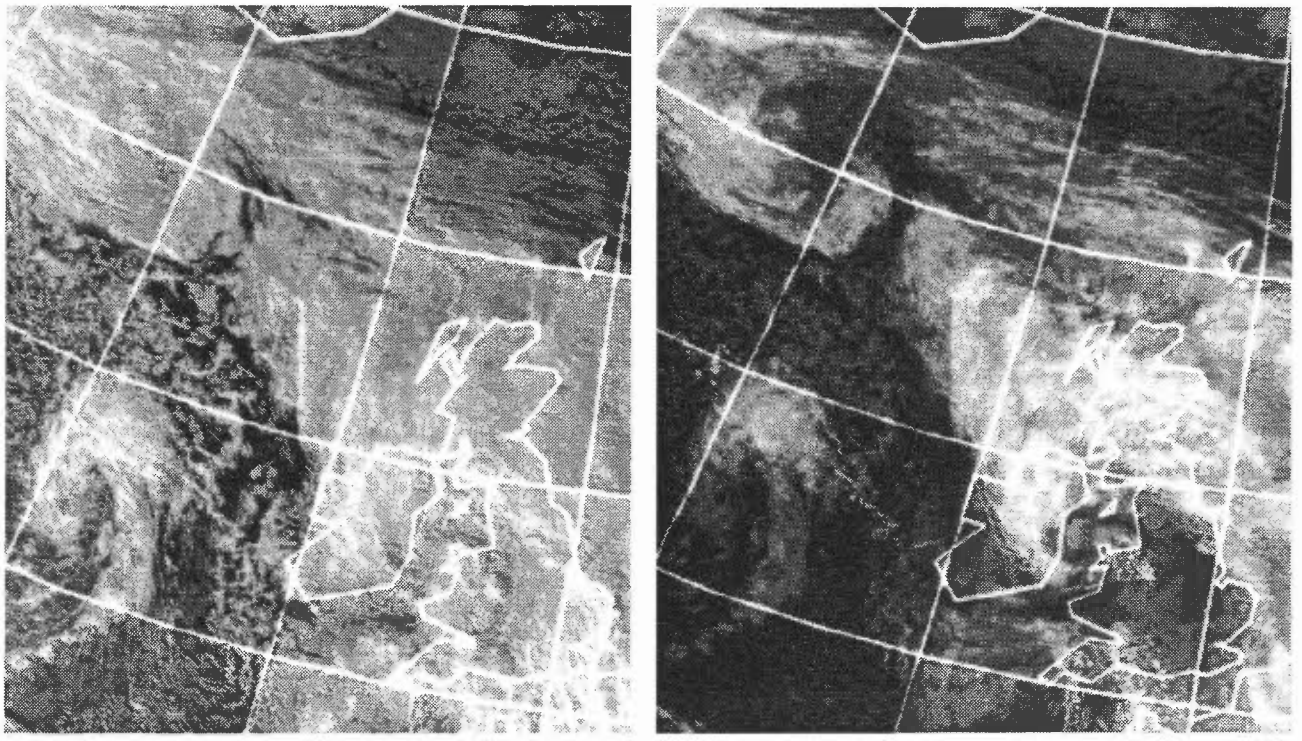

Figure 10.4. NOAA channel 2 (VIS) (left) and channel 4 (IR) (right), both at 1534 UTC on 22 October 1980. The IR image provides much detail which is not present in the VIS due to the lack of albedo contrast in the cloud features. The vortex structures to the south of Iceland and, in particular, in the Irish Sea are better represented in the IR image — these were both associated with surface depressions. The comma-shaped cloud appears to be a fairly active feature in the VIS image, whereas inspection of the IR image shows the comma tail to be of limited vertical development and therefore not likely to be associated with dynamical ascent.

10.3 Mesoscale interpretation — identification of cloud type and characteristics

10.3.1 Cumuliform

(i) VIS imagery resolves small Cu better than IR.
(ii) IR imagery provides a better indicator of vertical development through grey-scale variations.
(iii) Dry-air advection may be indicated by warm brightness temperatures on water-vapour channels.
(iv) Cb appear very white in both VIS and IR with cloud aligned along the direction of any shear between cloud base and top; a clear edge will delineate cloud edge at the base and there will be a fuzzy edge where Ci plume spreads out (**Fig. 10.1**).
(v) Clusters of large Cb, growing in a sheared environment, produce extensive Ci shields which hide the lower cloud columns.
(iv) An arc-cloud (4.7.5) may be identifiable in imagery; it is associated with the region of surface outflow from cumulonimbus clouds and is a potential zone for daughter-cell Cb development (4.7.7.5).

Bader et al. (1995), Chapter 6.4.3
Browning & Roberts (1995)

10.3.1.1 Cu patterns over land (see 4.6)

(i) In light winds, preferred areas for cloud may be related to high ground, sun-facing slopes, or in association with troughs and sea-breeze convergence.
(ii) In more windy conditions (>10 kn) organized lines may appear; topographic forcing can lead to convergence giving streams of shower-producing clouds extending hundreds of kilometres downstream. Inland penetration of a sea breeze is illustrated in **Fig. 10.5** (see 1.3.1.1).
(iii) 'Cloud streets' appear as narrow lines of small Cu aligned along the low-level wind direction above the boundary layer; upper limit of cloud top is 10,000 ft, spacing is 2 to 8 km (some 3× the cloud depth) **(Fig. 10.6)**. There is often an inversion, with dry air above limiting the vertical development and preventing the spread into Sc by continual evaporation. Inland heating produces deeper convection which flattens out at the inversion (see 4.3.2.1).

Monk (1987)

10.3.1.2 Cu patterns over sea

Cloud streets occur, more widely spaced, downstream of land masses in fresh to strong cold off-shore airstreams; again orientation is a good indicator of low-level wind direction. Regular patterns of cells form, probably due to the homogeneous temperature distribution across the sea surface.

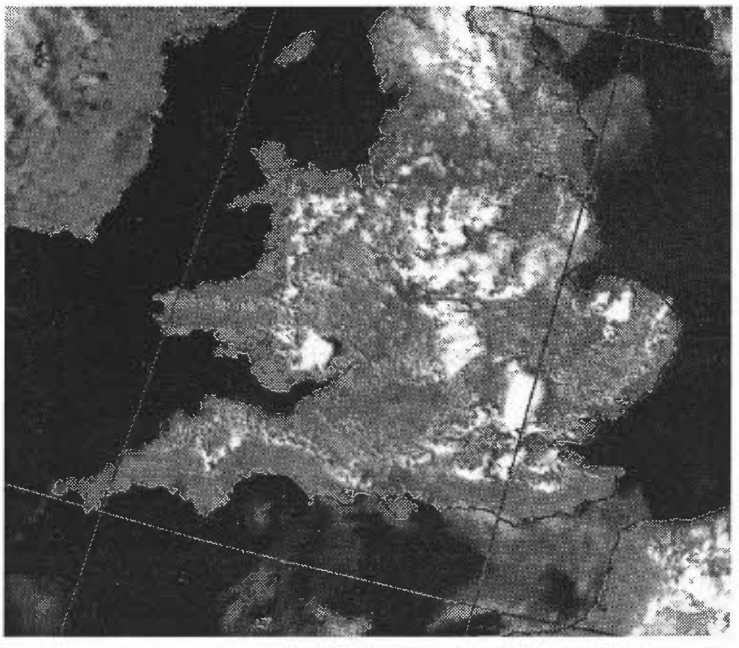

Figure 10.5. NOAA-7 AVHRR image at 1437 UTC on 7 July 1983. Inland penetration of the sea breeze around East Anglia and the south coast shown by the cloud-free margin.

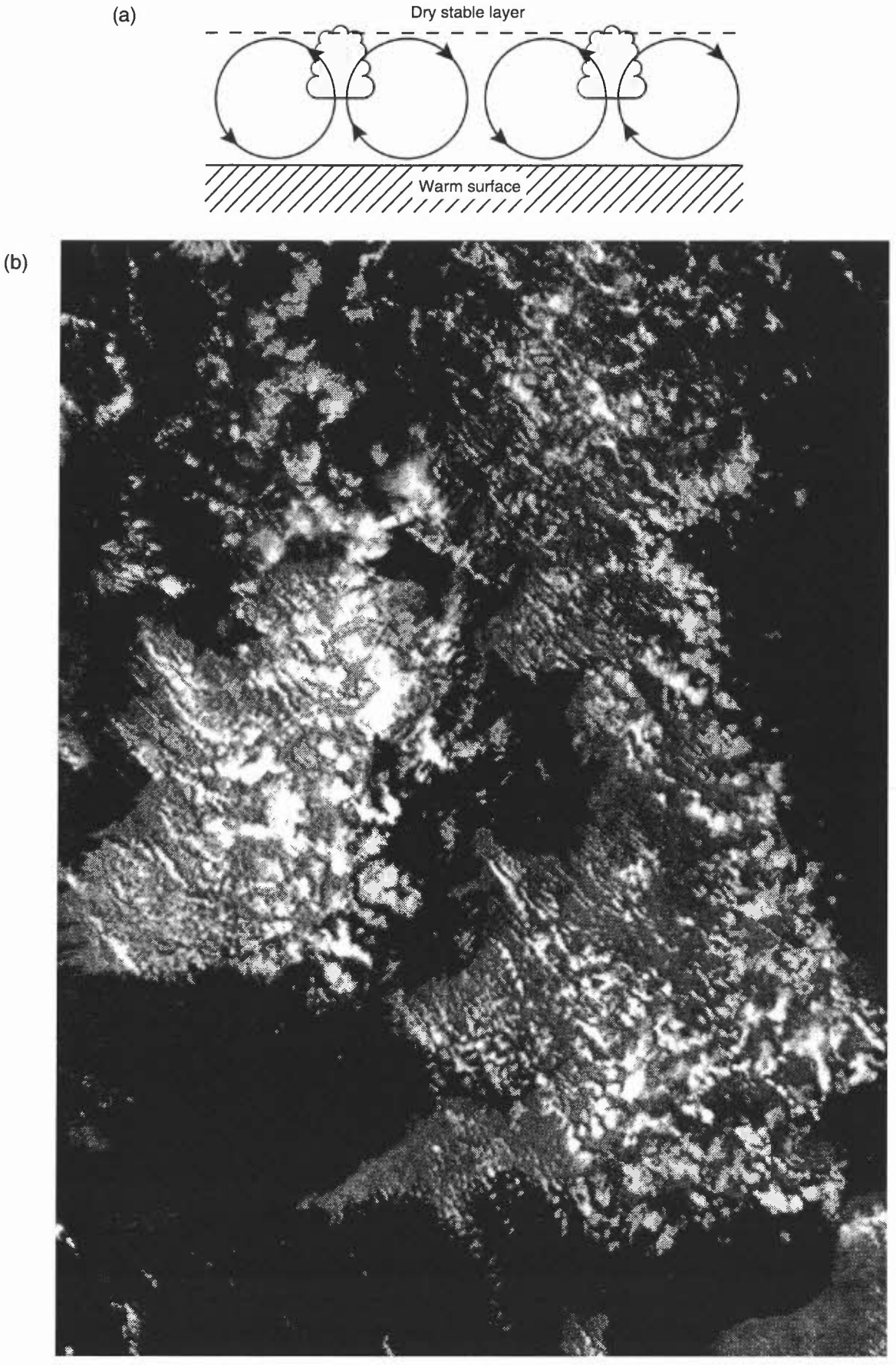

Figure 10.6. (a) Cross-section of circulations associated with cloud streets looking along the flow. Component of wind into the diagram leads to helical trajectories. (b) NOAA channel 2 (VIS) image at 1515 UTC on 16 April 1984 showing cumulus streets. It can be deduced that the low-level wind is from the WNW since the streets continue out over the southern North Sea.

Open cells **(Fig. 10.7)** characteristics:
(i) vigorous instability (through depths to 10,000 ft);
(ii) a large sea–air temperature difference;
(iii) usually cyclonic low-level flow and only small vertical wind shear;
(iv) aligned with the direction of thermal winds;
(v) open cell sizes often increase downwind with increasing instability over progressively warmer seas; however then anvils tend to obscure the polygons. The size of the cells is also related to the depth of convection (a ratio of 30:1 for cell diameter to depth of convection has been suggested).

Closed cells **(Fig. 10.7)** characteristics:
(i) an unstable layer is capped by a stable layer or inversion;
(ii) small differences in air–sea temperatures;
(iii) patterns are generally a feature of anticyclonic flow under a subsidence inversion and of areas of weak convection with low-level winds less than 20 knots.

Browning et al. (1985)

10.3.1.3 Stratocumulus

It is not unusual for Sc to display a closed cellular appearance when viewed under VIS; sensor resolution may not be good enough to resolve individual cells. In contrast IR images generally present a featureless sheet of grey which rarely displays the smoothness evident in fog or St.

10.3.2 Wave clouds, vortex sheets and lee eddies

When conditions are right for *lee waves* (1.3.21), Sc can take on a wave pattern on passing over high ground **(Fig. 10.8)**. *Bow waves* can be triggered by isolated, steep-sided, mountainous islands for a wind speed greater than 30 kn **(Fig. 10.9).**

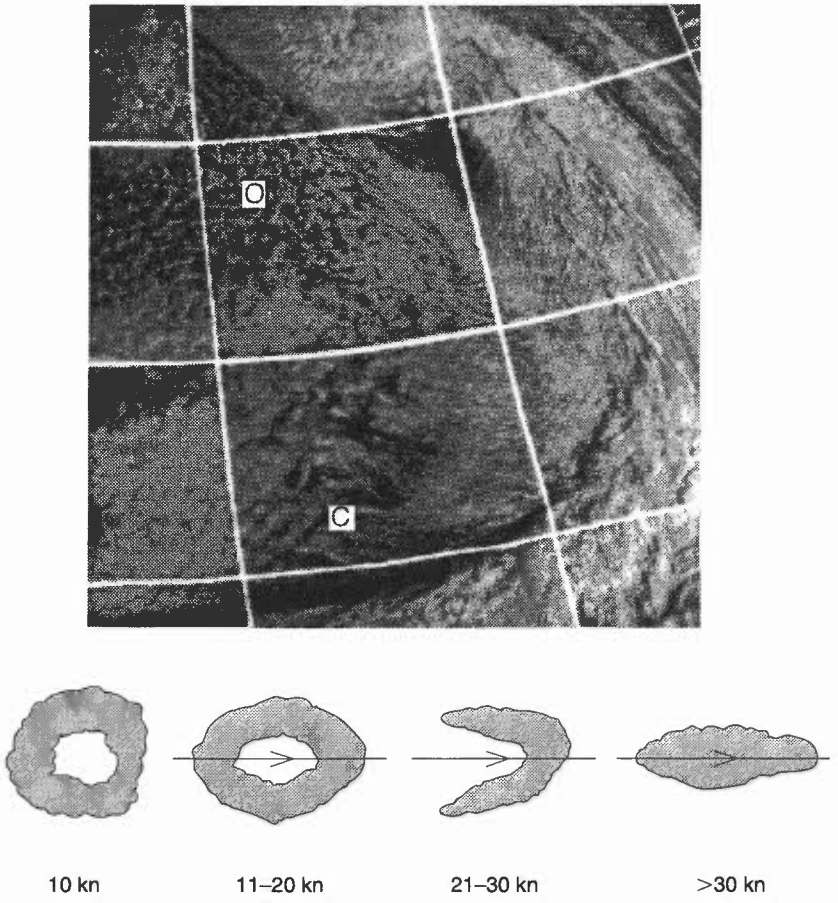

Figure 10.7. (top) NOAA channel 2 (VIS) image at 0927 UTC on 12 October 1980. Open (O) and closed (C) cell convection to the west of an Atlantic highlighted from the east by the morning sun. (bottom) Open cell shapes in different surface wind regimes.

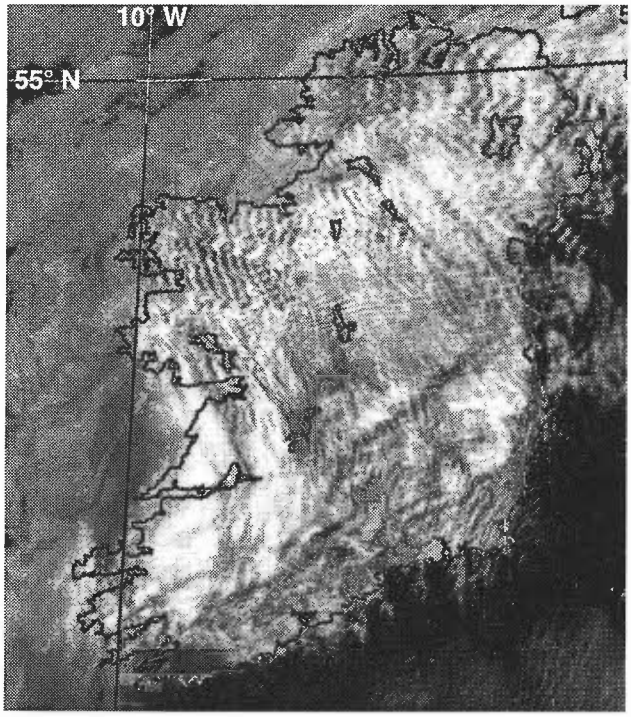

Figure 10.8. NOAA-11 VIS image at 1404 UTC on 20 May 1991 showing lee wave clouds over Ireland, and billow clouds.

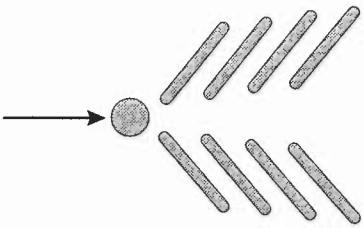

Figure 10.9. Bow waves forming downstream of an island.

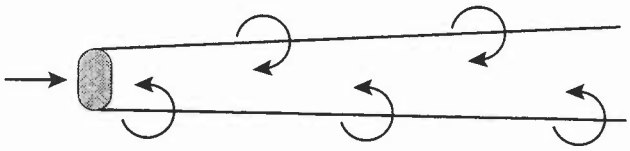

Figure 10.10. Vortex shedding from a steep-sided island.

Families of mesoscale *vortices* can be shed when there is:

(i) a strong inversion below obstacle height;
(ii) constant wind speed (10-30 kn) and direction with height.

The shedding generally appears with Sc cover; vortex shedding can sometimes be seen on the cold side of a frontal band downwind of Cape Farewell (southern tip of Greenland) **(Fig 10.10)** and frequently to the lee of the Canaries and Madeira, where they can extend for hundreds of kilometres downwind.

Bader et al. (1995), Chapter 8
Scorer (1989)

10.3.3 Stratus and fog

(i) St/fog in a VIS image shows as a flat, uniformly textured surface and appears white or light grey. Boundaries are often sharply defined and coincide with topographical features **(Fig. 10.1)**.
(ii) In IR, St/fog appears as a uniformly grey field similar to Sc and is very difficult to identify, especially when thin.
(iii) St and Sc can be distinguished by the greater detail present in the VIS image. The lighter colour in IR imagery is associated with Sc.
(iv) Cloud over the sea having edges following the coastline (or with well defined edges far from land) is a sure sign of St/fog. However, with little depth, the St/fog may be hard to detect in IR since cloud-top temperatures and sea temperatures are similar.
(v) Vortex patterns similar to those associated with Sc are sometimes seen in St/fog fields.

Fog may be detected with the Advanced Very High Resolution Radiometer (AVHRR) by comparing brightness temperatures of the two channels 3 and 4 (providing there is no upper cloud):
(i) fog water drops have lower emissivity in Ch 3 (Ch 3<Ch 4);
(ii) land and sea surfaces have similar emissivity in Ch 3 and Ch 4 (Ch 3 = Ch 4);
(iii) thin, high cloud looks brighter in Ch 3 (Ch 3>Ch 4).

Thus at night white represents water cloud, grey — land or sea, and black — ice cloud.

10.3.4 Medium-level clouds

(i) Altostratus produces a smooth, white response in a VIS image, mostly in association with frontal clouds when there is little to distinguish it from thick Cs. (It is often difficult to gauge the vertical extent of frontal cloud.)
(ii) The change from Ci to As is sometimes apparent at low solar elevation; at high elevation only the IR images will identify the individual cloud layers.
(iii) With no underlying cloud As appears light grey in VIS but cloud below will increase the whiteness of the image.
(iv) Ac is difficult to distinguish from As in VIS and IR since individual elements are too small to be resolved by sensors.
(v) Ac elements produced in the crests of lee waves will be clearly visible.
(vi) Convective elements associated with medium-cloud instability (Ac cast) appear similar to Cu clouds but produce brighter IR responses than are received from surface-based convection elements of similar size.

10.3.5 High-level clouds

(i) Ci generally appears as mid- to light-grey in VIS imagery but thin Ci can be difficult to detect; IR response will be better. Increasing Ci thickness leads to a progressively whiter image.
(ii) In IR thin, patchy Ci may have a fibrous appearance and darker due to radiation from below.
(iii) Increasing Ci thickness leads to a progressively whiter VIS image, and Ci shields associated with frontal systems can be a brilliant white.
(iv) In IR, very thin, patchy Ci may have a fibrous, streaky appearance, but extensive formations tend to produce a continuous response, since IR radiation is effectively absorbed by ice.

10.3.5.1 Contrails

Contrails can have a sub-pixel response enough to be resolved; they are more likely to be resolved in IR imagery than VIS when the temperature difference with the background surface provides good contrast, although, in VIS, they sometimes cast noticeable shadows on lower cloud decks. Straight line appearance, sometimes criss-crossing, is unmistakable.

Bader et al. (1995), Chapter 1

10.3.6 Other features

10.3.6.1 Snow and ice cover

Snow appears white to light grey in VIS depending on depth and freshness:
(i) reflectivity falls off rapidly as solar elevation to surface falls below 45°;
(ii) the older the snow the lower its reflectivity;
(iii) fresh snow at high solar elevation has an albedo of 85 to 90%; old snow 70% or less.

Underlying vegetation will influence the albedo:
(i) snow-covered forest has a lower albedo than snow-covered grassland, appearing mottled.
(ii) flat terrain appears smooth;
(iii) the 'dendritic' appearance of snow-free (or perhaps tree-filled) valleys in a mountainous terrain is unmistakable.

However, uniform snow fields are difficult to distinguish from cloud in VIS:
(i) they will have well defined edges and change only slowly with time;
(ii) clouds may by distinguished by shadows and change in detail between one image and another.

Off-shore winds, breaking up an ice field, will leave a characteristic dark band mapping the coastline.

10.3.6.2 Ships' trails

The seeding of clouds by particulates in ships' exhausts (principally in lower latitudes) can result in a narrow line of cloud sometimes extending for hundreds of kilometres. The trails, best seen in the VIS image, show up as an elongated bright region within the cloud, or as isolated streamers of cloud.

Bader et al. (1995), Chapter 1

10.3.6.3 Dust clouds and smoke plumes

Rising dust or sand may show as a blurring or brightening of the VIS image and also sometimes as an extensive cool area on IR, where VIS shows no cloud; they will show up well when blown over sea. Similarly smoke plumes from major fires and volcanoes can be detected in the VIS channel.

10.4 Image signatures of meso- and synoptic-scale processes

(i) Animated imagery from geostationary satellites is essential for identifying developments.
(ii) Overlaying appropriate model output with satellite imagery can reveal important phase or amplitude errors in the early stages of model runs (9.5).
(iii) Features of the imagery are useful in detecting model errors and giving advance warning of important developments, animated imagery being particularly useful.
(iii) Imagery, related to conceptual models (7.1), will help to identify significant cloud and the dynamical processes involved.

McPherson et al. (1992)

10.4.1 Relationship between the jet axis, frontal location and cloud-band structure

10.4.1.1 Locating cold fronts

(i) **Fig. 10.11** shows the positioning, relative to cold-frontal cloud bands, of the ana- and kata- cold front.
(ii) If 'rope' clouds are visible the cold front is best placed along them.
(iii) If not visible, then the ana-cold front is best placed ⅔ the way across the cloud band from the rear of the band and the kata-cold front towards the rear of the band.

10.4.1.2 Locating warm fronts

Although more difficult to position than cold fronts, the warm front is roughly 300 n mile from the leading edge of the frontal cirrus (**Fig. 10.12(a)**).

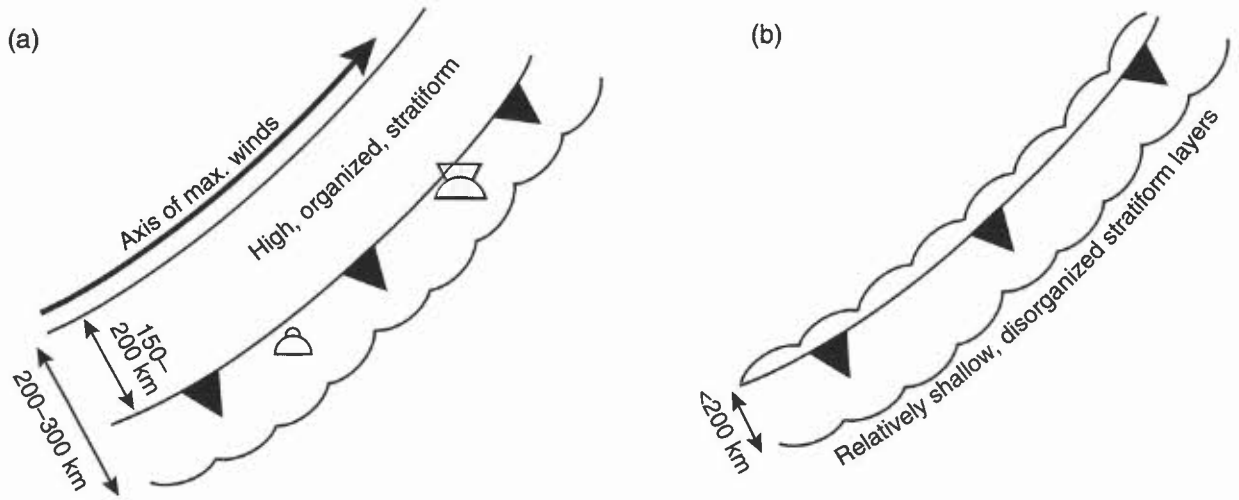

Figure 10.11. The cold front is best placed along 'rope' clouds, if visible. If these are not visible then the front is best placed, (a) ⅔ of the way across cloud band of an ana-cold front, and (b) towards the rear of cloud band of a kata-cold front.

10.4.1.3 Locating occlusions

It is suggested that the occlusion is placed 50 to 100 km in from the rear edge of the frontal band (**Fig. 10.12(a)**).

10.4.1.4 Frontal cloud-band structure in relation to jet configuration

Fig 10.12 shows the nature of frontal cloud structure in relation to the configuration of the jet axis; the more active the front, the smaller the angle between the cold front and the jet (e.g. **Fig 10.12(b) & (c)**).

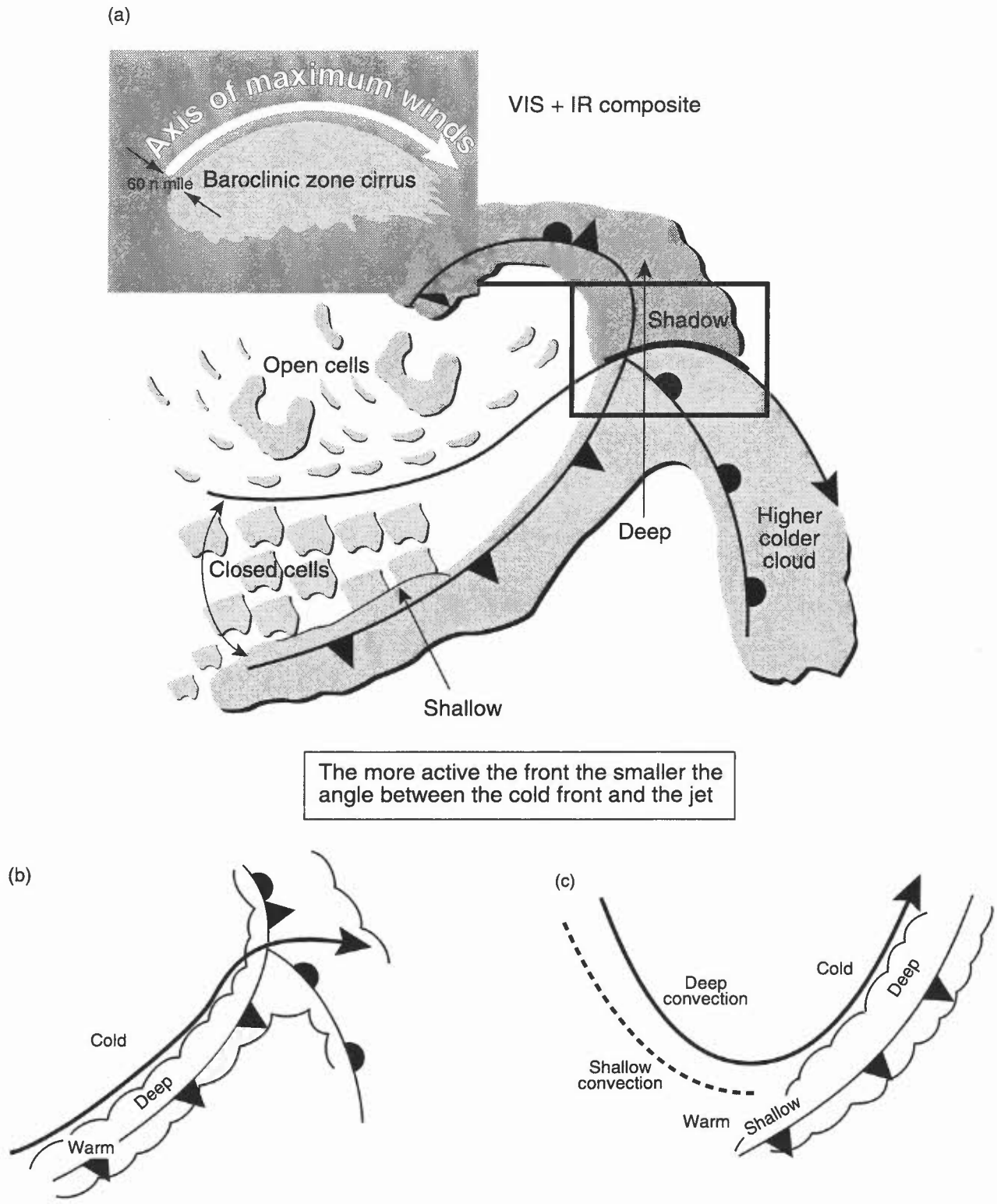

Figure 10.12. Satellite interpretation. (a) Positioning jet streams, (b) jet axis parallel to cloud band. Cloud vertically deep. Cloud edge aligned along jet axis but not necessarily in direction of jet winds. (c) Where jet is parallel to frontal band, cloud is deep and wide.

10.4.1.5 Troughs and fronts over the ocean

The upper trough may be difficult to position using satellite imagery. Here are clues as to its position:

(i) Where the trough intersects the front the cloud tops will often lower or fragment **(Fig. 10.13(a))**.

(ii) When the PVA ahead of the upper trough reaches 350 n mile upstream of a cold front, formation of a wave on the front can be expected **(Fig. 10.13(b))**.

(iii) Enhanced cumulus occurs in association with PVA ahead of an upper trough.

(iv) The relationship between comma-cloud formation, maximum vorticity areas and the diffluent thermal trough is shown in **Fig. 10.13(c)**. (Note: the comma shape is due to circulation within the relative airflow; vectorially adding the system translation velocity may give a trough relative to the earth's surface rather than a circulation.)

Boyden (1963)

10.5 Diagnosis of cyclogenesis

The 3-D detail required to forecast accurately the evolution of explosive cyclogenesis is very sensitive to initial conditions and not always correctly assimilated in the NWP initial conditions. There are characteristic image signatures which are not only associated with these intense storms, but more importantly from the forecasting point of view, precede the onset of winds of storm force 10 or more by as much as 24 hours (7.3.4).

10.5.1 Image features

10.5.1.1 The baroclinic cloud leaf

(i) Even if no cloud head is apparent the elongated 'S' shape of the cold side of the frontal cloud and the broadening of the band are characteristic of incipient cyclogenesis (the 'cloud leaf').

(ii) Only a small minority of cloud leaves develop into cloud heads.

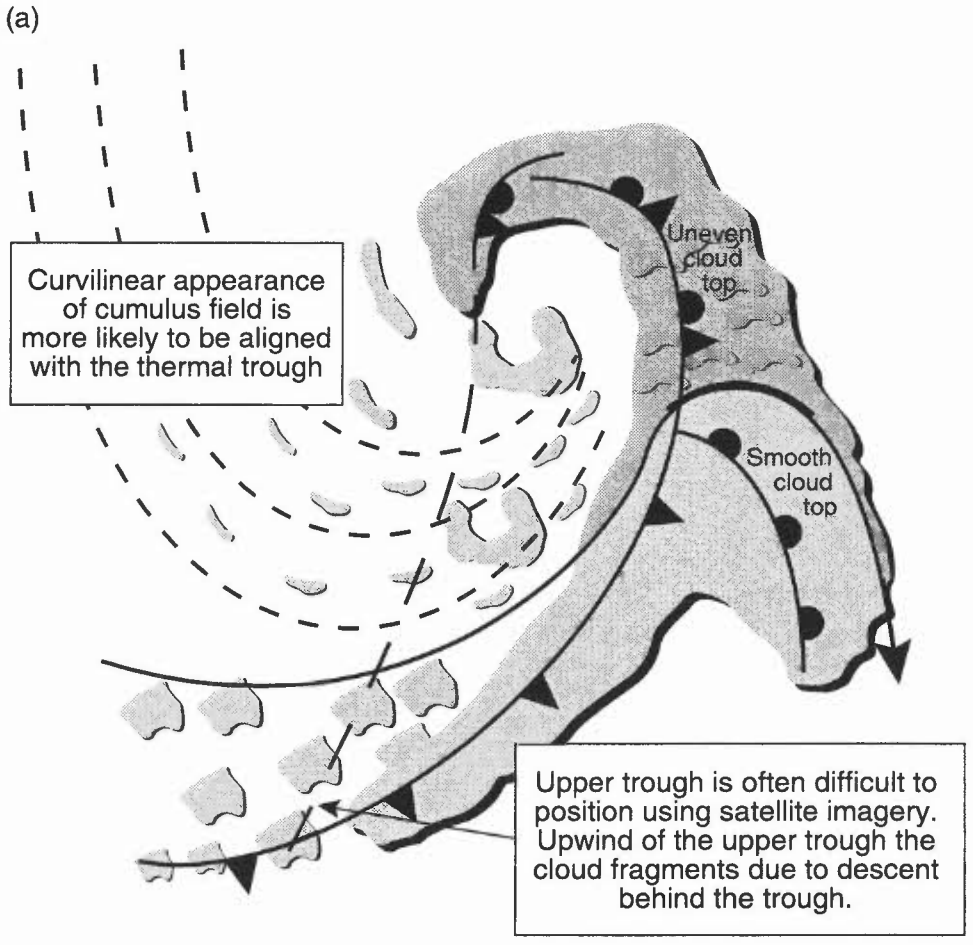

Figure 10.13. Satellite interpretation. (a) Troughs and fronts over the oceans, (b) upper troughs and frontal waves, and (c) troughs over the oceans — comma cloud.

(b)

The relationship between upper troughs and waves.

When the PVA ahead of the upper trough reaches 350 n mile upstream of a cold front, formation of a wave on the front can be expected.

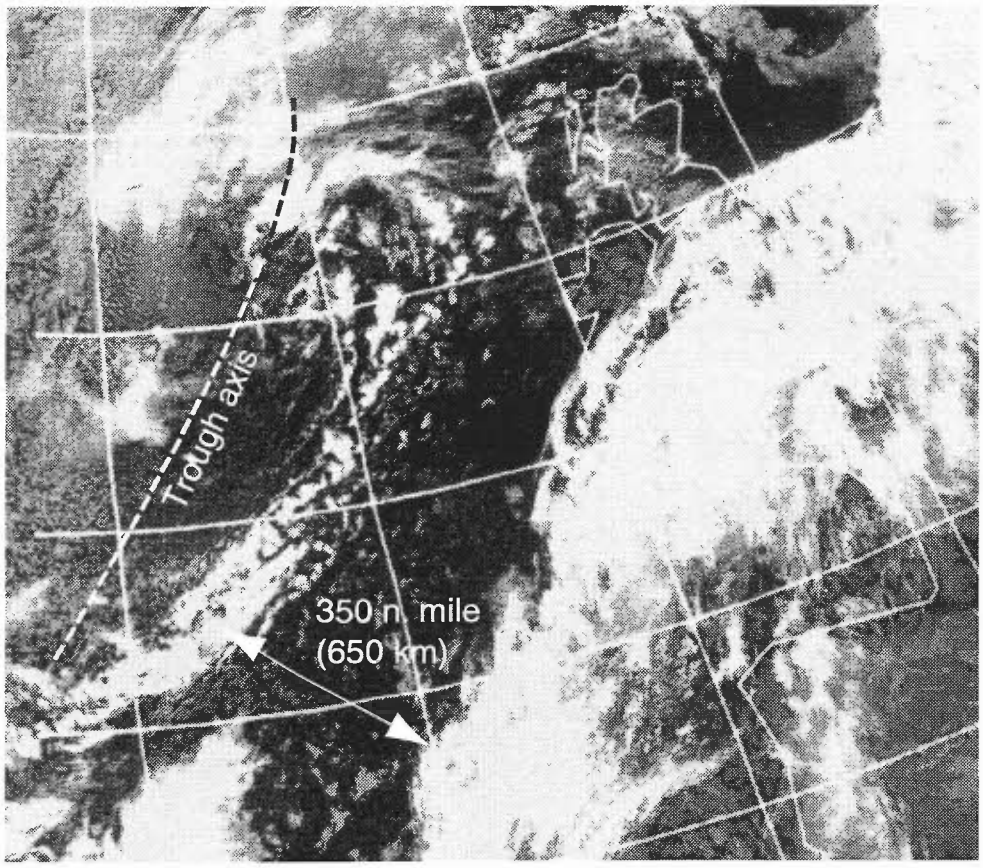

(c)

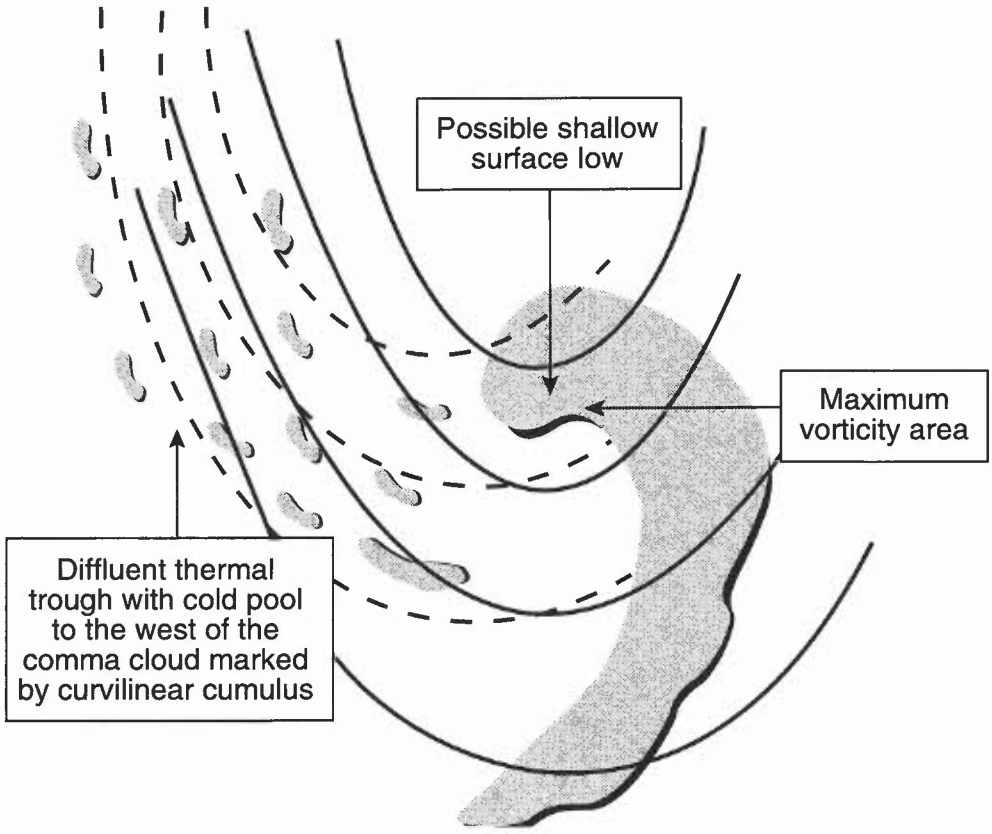

Figure 10.13. (Continued).

Fig. 10.14 shows an IR image of a baroclinic cloud leaf associated with a depression (the surface front is unlikely to be significantly 'waved' in the early stages, despite the shape of the cloud structure (which is associated with upper flow and induced mid-tropospheric ascent)).

Estimating the position of the new low centre (**Fig. 10.15**):

(i) **Fig. 10.15** shows a schematic sequence of IR images at 6-hourly intervals of a vigorous cyclonic development over the north-eastern Atlantic.
(ii) Identify the point of inflection on the cold side of the the frontal boundary (P).
(iii) Draw a line perpendicular to the forward boundary of the cloud pattern.
(iv) The developing surface low (L) is likely to be along the warm side of the cloud boundary, about 2° latitude poleward of the intersection of the line with the cloud edge.
(v) With a PVA area close to the frontal zone, development is to be expected and the depression will take up a more central position underneath the cloud canopy (but still near the point of inflection).
(vi) If a dry slot forms, the surface low-pressure centre is likely to have migrated to a position under the cold boundary of the frontal band just behind the leading edge of the dry wedge.

Weldon & Holmes (1991)

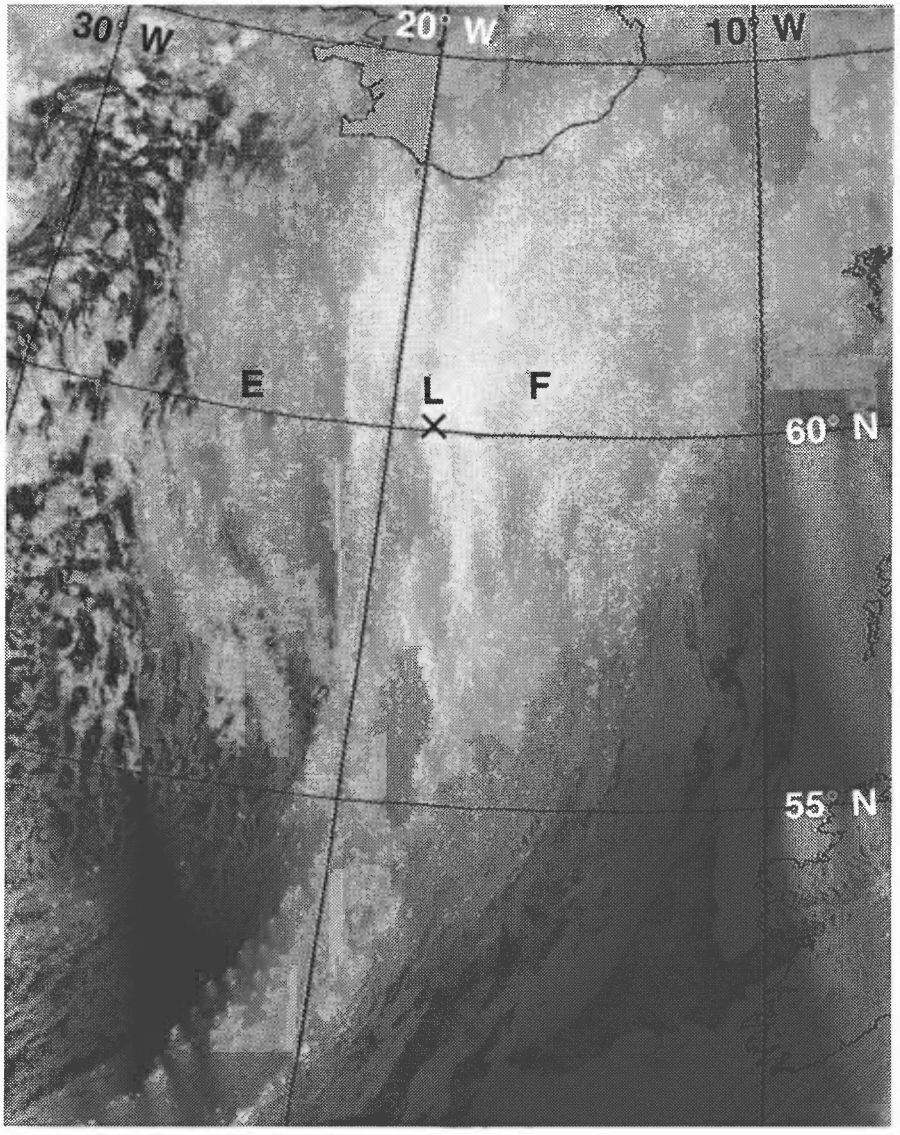

Figure 10.14. NOAA-11 IR image at 1336 UTC on 21 December 1988. Example of frontal cloud, F, and middle-level cloud, E (emergence of E is a sign of cyclogenesis). L is the developing surface low.

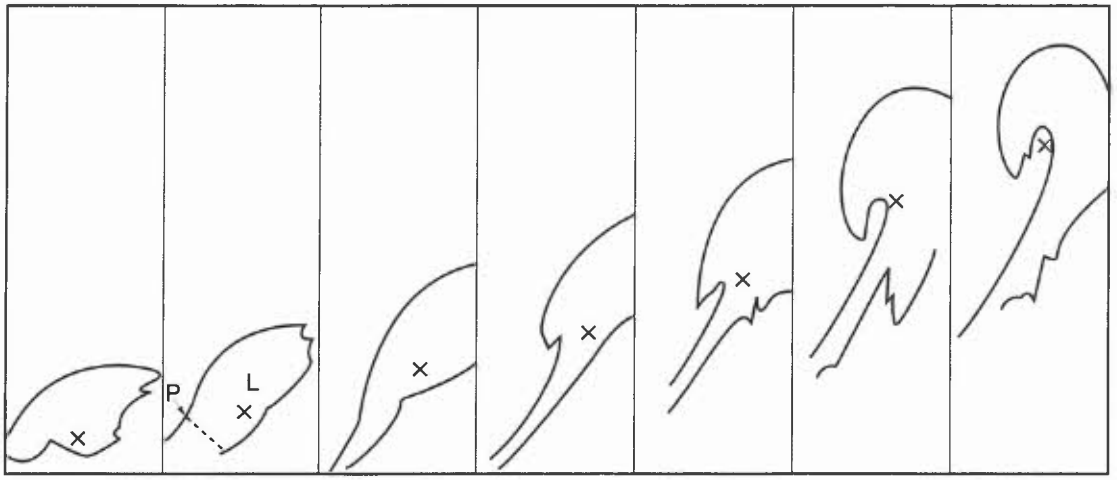

Figure 10.15. Sequence of schematic IR images associated with a developing depression. Images at 6-hourly intervals mark the surface depression. See 10.5.1.1 for explanation of construction on second image.

10.5.1.2 Development

As cyclogenesis proceeds, a cloud E emerges from beneath the main frontal cloud F (**Fig. 10.16).** The shape of E and F will depend on the middle- and upper-tropospheric patterns (i.e. whether upper trough is confluent, diffluent, large or small amplitude). **Fig. 10.17(a)** shows seven types of cyclogenesis, **Fig. 10.17(b)** is the associated cyclogenesis decision tree; when E becomes particularly large and well-organized (a 'cloud head', see below), rapid deepening is more likely.

Bader et. al (1995), Chapter 5.2
McLennan & Neil (1988)
Young (1993)

10.5.1.3 The cloud head

(i) Rapid cyclogenesis over the eastern Atlantic is invariably preceded by the cloud head, a cold-topped cloud structure extending polewards of, and separated from, the main frontal band (but elongated along a similar orientation, with a convex curved poleward edge); the cloud head is especially seen in confluent trough development.
(ii) The frontal development in **Fig. 10.18** has proceeded no further than the wave stage.
(iii) The head is indicative of rapid ascent, leading to the creation of low-level vorticity through vortex stretching and release of latent heat (7.3).

Note that in American terminology a cloud head is referred to as a 'comma' cloud and is not to be confused with the 'frontal comma cloud'.

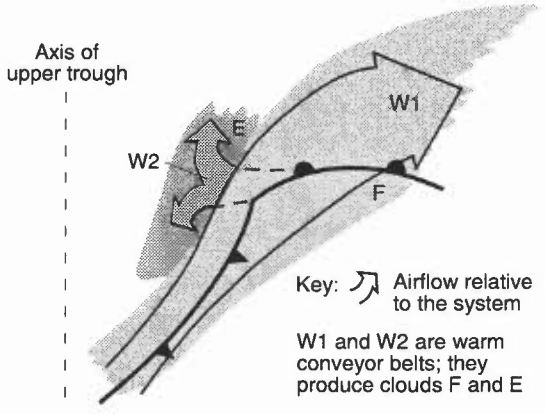

Figure 10.16. Emergence of cloud E is a sign that cyclogenesis is proceeding (after Bader et. al (1995), Chapter 5).

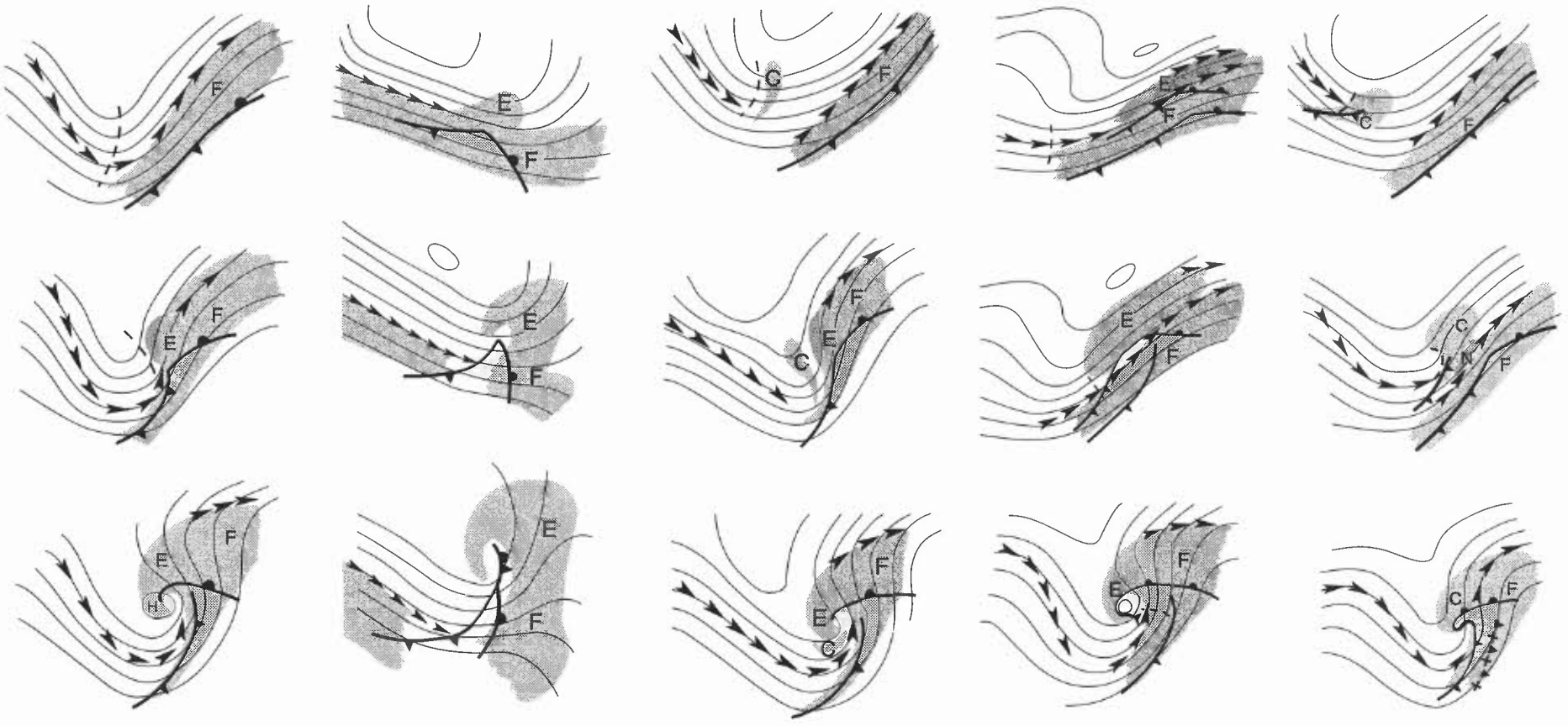

Figure 10.17(a). The shape of clouds E and F associated with cyclogenesis will depend on middle- and upper-tropospheric patterns; seven types are illustrated (after Bader et. al (1995), Chapter 5). The diagrams aid your use of the decision tree (**Fig, 10.17(b)**).

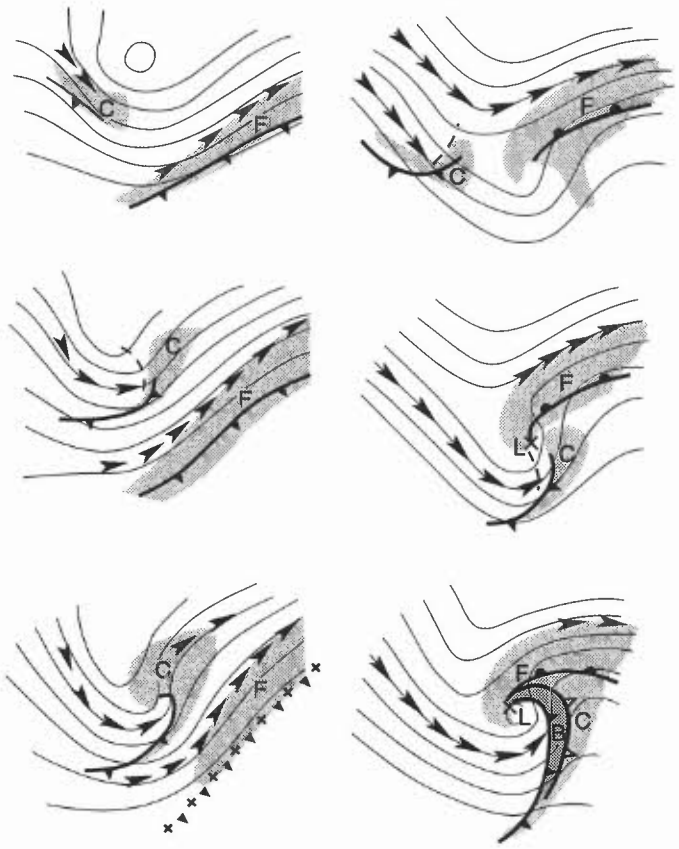

Cold air Split flow

Figure 10.17(a). (Continued).

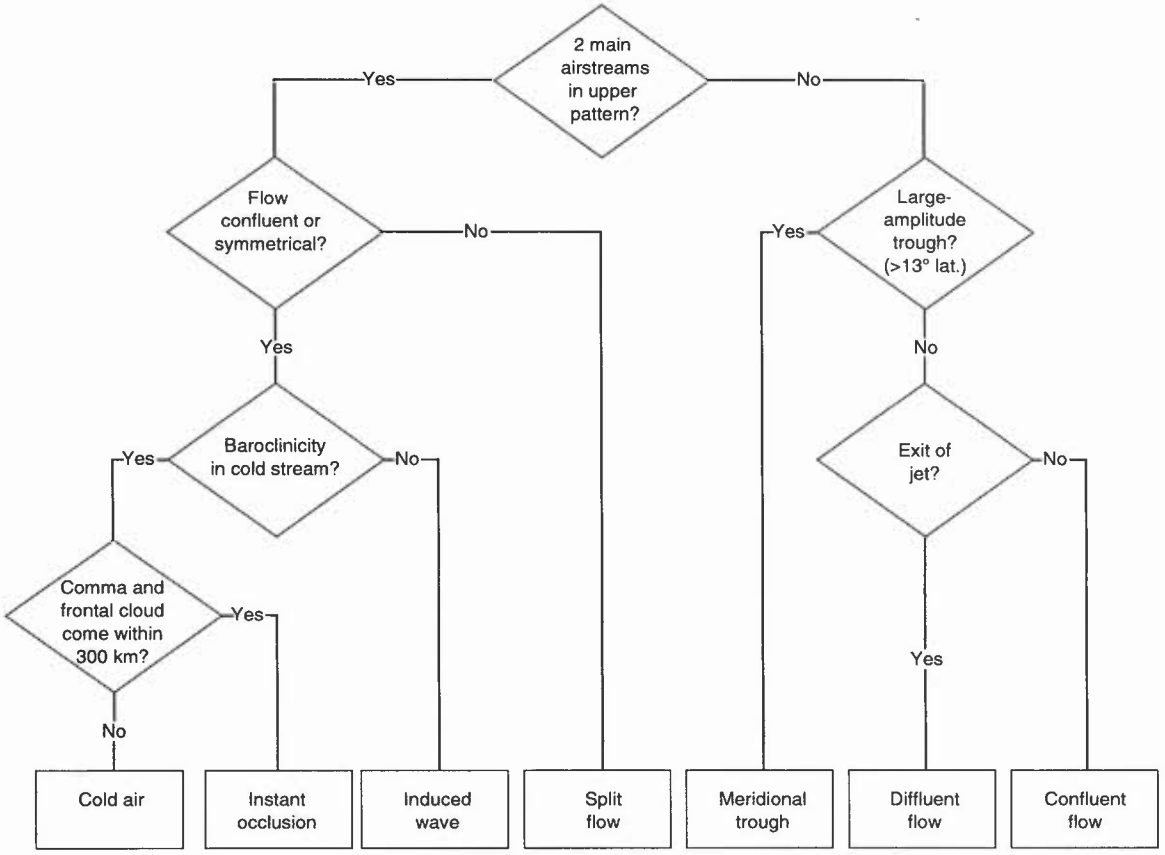

Figure 10.17(b). Decision tree for determining cyclogenesis type. A decision tree can be used to determine the appropriate archetype for cyclogenesis. It uses as input the characteristics of the cloud pattern and the upper flow. The path through the tree depends on whether the airflow around the upper trough is a single airstream (as in 'meridional trough') or has two separated streams (as in 'cold air').

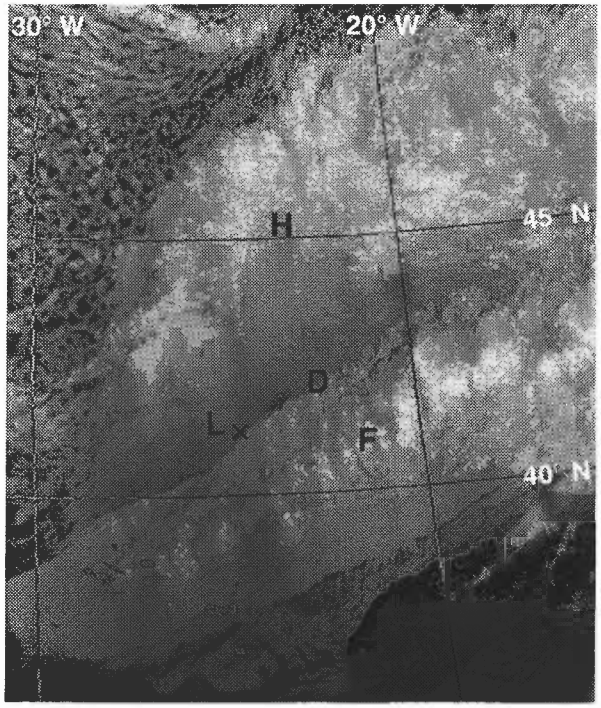

Figure 10.18. NOAA IR image for 0453 UTC on 15 October 1987. H marks the cloud head, D the dry slot and F the frontal cloud band.

10.5.1.4 The dry wedge

(i) Separating the cloud head (H) from the frontal band is a slot of relatively cloud-free air (dry slot or wedge), which forms upstream of the cloud head and becomes pronounced as it drives forwards (D in Fig 10.18).

(ii) The water vapour channel shows the dry wedge as a darkening feature, indicating stratospheric descent which accompanies upper tropospheric spin-up.

(iii) Clues to this dry air show up better in IR than VIS images since there is often warm-topped cloud with quite high albedo beneath the mid- to upper-tropospheric dry air.

(iv) Conducive to strong development also is the presence of deep convective cloud extending right up to and beneath the poleward edge of the cloud head; this indicates the close proximity of deep cold air and hence the strength of the baroclinicity.

Bader et al. (1995), Chapter 5
Hewson (1993)

10.6 Radar rainfall measurements

10.6.1 Rainfall radar data limitations

Although the display provides real-time information on the location of precipitation and associated frontal and convective development, the data have a number of limitations due to:

(a) spurious, non-meteorological echoes;
(b) radar rainfall not necessarily being that measured by a gauge at the surface;
(c) technical and meteorological causes (some of which are illustrated in **Fig. 10.19**), *particularly*:
  (i) beam sampling at ever-increasing heights above the ground **(Fig. 10.20)** (important in cases of precipitation growth or evaporation below radar beam);
  (ii) uncertainties in the radar reflectivity (Z)/rainfall-rate relationship (note that Z is proportional to the 6th power of the drop radius, R). Real-time calibration against gauges reduces errors by identifying the radar-to-gauge data for distinct rainfall regimes.
  However: the intensity of convective rain is often *overestimated* by a factor of 1.5,
  the intensity of melting snow by up to a factor of 4.
  Drizzle intensity is *underestimated* by a factor of up to 1.5.
  Frontal rain and dry snow are usually well estimated;

(iii) from the 6th power relationship above it follows that drizzle and light rain are not detected even at short range;
(iv) orographic enhancement when pre-existing upper-level precipitation falls through very moist low-level air;
(v) detection at long range less likely with shallow precipitation and a low freezing level (this implies radar range performance is likely to be best in summer;
(vi) low-level evaporation, particularly ahead of warm fronts giving overestimate of surface rainfall and an error in the forecasting of beginning of precipitation;
(vii) large hail, causing serious overestimation;
(viii) an intense 'flare echo' may result due to multi-reflection of beam from hail and ground;
(ix) anomalous propagation — refraction of the radar beam can occur with a combination of a temperature inversion and, more important, a steep hydrolapse, for example, when there is a well-marked surface-based nocturnal cooling inversion. The most severe 'anaprop' occurs in anticyclonic conditions beneath a marked surface inversion; it rarely occurs when an inversion is more than 1200 m above the radar. Rain and anaprop can co-exist, especially when medium-level instability is present, in warm sectors, or when a cold front arrives following anticyclonic or ridge conditions (data from conventional observations must be monitored);
(x) signal attenuation on passing through rainfall (worse at shorter wavelengths, e.g. 3 cm compared with 10 cm) or behind hills (clutter may be mapped and electronically eliminated). Rainfall rates in cluttered areas can be estimated by interpolation. Higher beam elevation at close range can be used.
(xi) the 'bright band' due to beam intersecting the melting layer leading to overestimates in inferred surface rainfall;
(xii) radar sensitivity drift (perhaps over an hour or over many months).

In addition there can be interference from other radars, and a build-up of precipitation on the radome.

10.6.2 Meteorological features

(i) Animation can show major changes in the horizontal wind field through convergence of rain cells or rotation of cells about a vortex centre.
(ii) The smallest rain areas are usually short-lived (1–2 hours); clusters of cells often persist longer.
(iii) Mesoscale rain areas, typically in bands, are frequently observed with lengths 50–500 km and persist for some time.
(iv) Large-scale rain areas have mesoscale features buried within them, typically one or two bands (often displaced from the surface front).
(v) These bands often travel faster than the organized rain area, with individual cells, in turn, moving faster than the band.
(vi) The cells within a band often have a major component of motion along the band. Mesoscale rainfall patterns thus reveal much about the fine-scale structure of the large-scale systems.
(vii) Showers are rarely totally random, but occur in organized convective areas that may persist well into the night (4.6).
(viii) A rain band can often be linked to a minor synoptic feature or to a line of convergence due to a sea-breeze front or to a topographical feature.
(ix) Extrapolation of well-defined entities can be effective to 6 hours ahead, some modification being allowed for development.
(x) Intense but rapidly moving cells may contribute little to point rainfall, but intense, slow moving cells or bands can give large accumulations.

The local forecaster should be aware of these limitations and features when monitoring rainfall areas and intensities; at the very least the display will be a valuable qualitative guide to precipitation distribution, to be used cautiously in conjunction with NWP and satellite data.

Atlas (1990)
Bader et al. (1995), Chapter 2
Brown et al. (1991)
Collier (1989)
Conway & Browning (1988)
Kitchen et al. (1994)

10.7 Sferics (see 4.7.4 — Lightning)

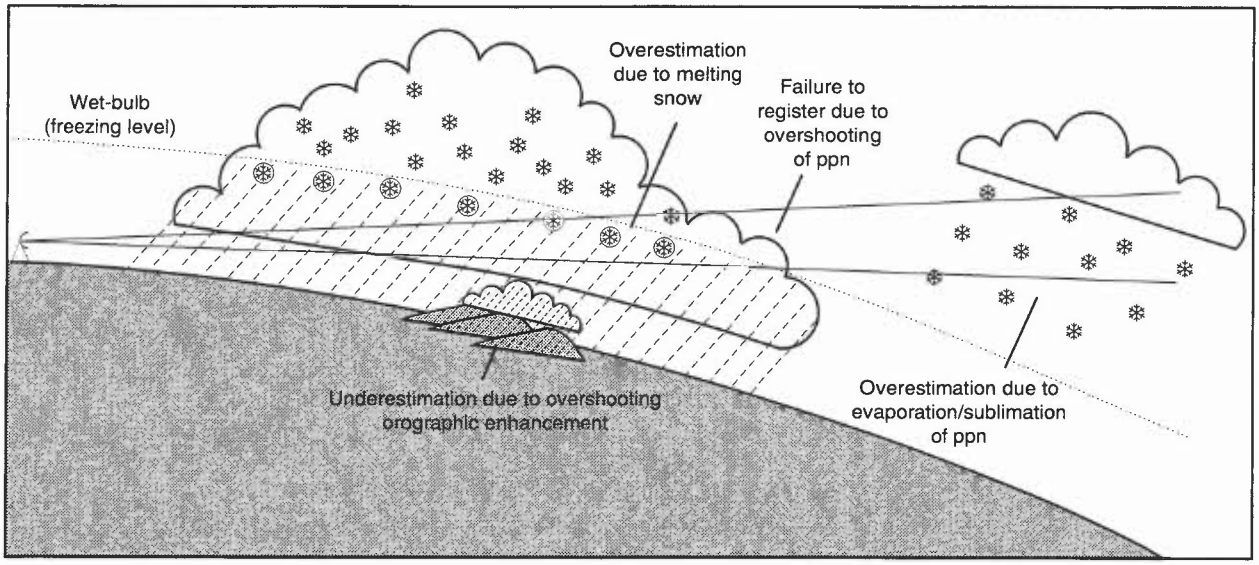

Figure 10.19. Some of the errors in surface precipitation rate estimates caused by sampling of precipitation away from the ground.

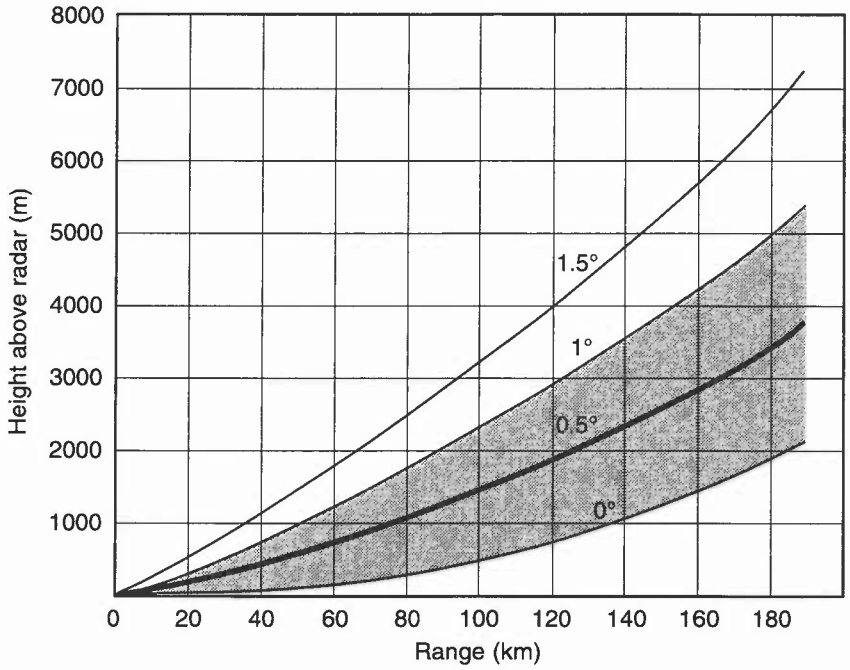

Figure 10.20. Height versus range for various beam elevations.

BIBLIOGRAPHY

CHAPTER 10 — REMOTE SENSING

Atlas, D, (Ed), 1990: Radar in meteorology. Proceedings of the Battan Memorial and 40th Anniversary Radar Meteorology Conference. Boston, American Meteorological Society.

Bader, M.J., Forbes, G.S., Grant, J.R., Lilley, R.B.E. and Waters, J., 1995: Images in weather forecasting. Cambridge University Press.

Boyden, C.J.,1963: Jet streams in relation to fronts and the flow at low levels. *Meteorol Mag*, **92**, 319–328.

Brown, R., Sargent, G.P. and Blackall, R.M., 1991: Hydrological applications of radar. pp. 219–228. Publisher: Ellis Horwood.

Browning, K.A. and Roberts, N.M., 1995: Use of satellite imagery to diagnose events leading to frontal thunderstorms: part 1 of a case study. *Meteorol Appl*, **1**, 303–310.

Browning, K.A., Eccleston, A.J. and Monk, G.A., 1985: The use of satellite and radar imagery to identify persistent shower bands downwind of the North Channel. *Meteorol Mag*, **114**, 325–331.

Collier, C.G., 1989: Applications of weather radar systems. Ellis Horwood.

Conway, B.J and Browning, K.A., 1988: Weather forecasting by interactive analysis of radar and satellite imagery. *Philos Trans R Soc Lond*on, **A324**, 299–315.

Cracknell, A.P. and Hayes, L.W.B., 1991: Introduction to remote sensing. Taylor and Francis.

DNOM, 1982: Weather satellite picture interpretation. Vols 1 and 2. DNOM memo 1/82. London, MoD, Directorate of Naval Oceanography and Meteorology.

Hewson, T.D. (Editor), 1993: The Fronts 92 Experiment: A Quicklook Atlas. Joint Centre for Mesoscale Meteorology, University of Reading, *Internal Report* No. 15.

Kitchen, M., Brown, R. and Davies, A.G., 1994: Real-time correction of weather data. *QJR Meteorol Soc*, **120**, 1231–1254.

McLennan, N. and Neil, L., 1988: Marine bombs program (phase II). Pacific Region tech. note 88-002.

McPherson, B., Wright, B.J. and Maycock, A.J., 1992: Formulation of the new Mesoscale Model data assimilation scheme. *Forecasting Research Paper* No. 143.

Monk, G.A., 1987: Topographically related convection over the British Isles. *Workshop on Satellite and Radar Imagery Interpretation,* pp. 305–324, Meteorological Office College.

Scorer, R.S. and Verkaik, A, 1989: Spacious skies. David and Charles.

Weldon, R.B. and Holmes, S.J., 1991: Water vapor imagery: interpretation and applications to weather analysis and forecasting. NOAA, Technical Report NESDIS 57.

Young, M.V., 1993: Cyclogenesis: interpretation of satellite and radar images for the forecaster. Bracknell, Meteorological Office, Forecasting Research Division Technical Report No. 73.

CHAPTER 11 — PROBABILITY FORECASTS

CHAPTER 11 — PROBABILITY FORECASTS

11.1 Basic concepts

Most forecasts give a categorical estimate of what various weather elements will be for a particular place/region and time/period. In reality uncertainty is inherent because:
(i) Observations do not provide a complete description of the state of the atmosphere.
(ii) Numerical models do not completely represent atmospheric processes (9.1).
(iii) Various assumptions are made in deriving expected weather from model forecasts.

The uncertainty can be implied by using such words as 'perhaps' (with the wide variations in meaning which can be attached to them) or expressed either qualitatively or quantitatively.

Probability forecasts are becoming more widely used because:
(i) They provide quantitative information for customers in uncertain situations.
(ii) They express inherent uncertainty in a precise and unambiguous manner.

11.1.1 Interpretation of probabilities

Probabilities can be interpreted in two ways:
(i) Relative frequency interpretation.
(ii) Subjective interpretation.

Thus consider a 'probability of precipitation (PoP) forecast of 30%':
(i) Relative interpretation: the present meteorological situation, observed on a large number of occasions, would give rise to precipitation on 30% of the time.
(ii) Subjective interpretation: the forecaster's judgement is that the odds against precipitation are 7 to 3 (odds against no precipitation being 3 to 7). Generally, if p is the probability, the odds against the event are:
$(1/p - 1)$ to 1.
(iii) The subjective interpretation gives a practical way of thinking about probabilities.

11.2 Types of probability measure

Three types of probability are in use:
(i) *Point probability*: probability that an event will occur at a particular point within a specified period of time.
(ii) *Average point probability*: the average point probability over a defined area.
(iii) *Area probability*: probability that the event will occur somewhere in the defined area within a specified period.

Point probability is easiest for interpretation and verification; average point probabilities, sometimes used for large areas by the media, can be misleading if there is a wide variation of point probability across the area.

The *area probability*, P_a, and *average point probability*, P_p, are related:

$$P_p = P_a\, a_c$$

where a_c is the proportion of the areal coverage if precipitation does occur.
(i) Note: $P_a \geq P_p$; and when precipitation is certain ($P_a = 1$), then $P_p = a_c$, i.e. the expected areal coverage of precipitation.
(ii) This area probability concept, P_a, can be very helpful when deriving P_p. Thus, if there is a 20% chance of precipitation reaching an area, $P_a = 0.2$, but if it does reach the area there will be precipitation everywhere (so that $a_c = 1$), then the average point probability, P_p, is 20%.
(iii) Similarly, if showers are certain in an area, $P_a = 1$, but if they do occur they will be scattered ($a_c = 0.2$ say), then again $P_p = 20\%$.

Conditional probabilities must be correctly identified and used.
(i) For example, if P(precip) is the probability of precipitation and P(precip|snow) is the conditional probability of snow (the probability of snow if precipitation occurs), then the probability of snow is given by:
P(snow) = P(precip) P(precip|snow).
(ii) The difference between P(snow) and P(precip|snow) is important; it is essential that the user knows which figure is being given.

11.3 Practical considerations

11.3.1 Determination of probabilities

Successful determination of probabilities depends upon the skill and experience of the forecaster. A few general points worth considering are given:

(i) Discussion between forecasters about probabilities is likely to be beneficial.

(ii) It may be useful to assess area probability of precipitation and conditional areal coverage separately before combining them to give the average point probability.

(iii) Although forecasters are likely to start with central guidance, in principle it is beneficial to make an independent assessment and then try to reconcile this with the guidance. In practice, there may not be sufficient time available to do this.

(iv) Most effort should be put into improving on the guidance for the early forecast period; later the value of local knowledge decreases rapidly.

11.3.2 Time period

A probability forecast must refer to a particular period. However, there are some pitfalls that must be avoided, as illustrated with the PoP forecasts:

(i) PoP can change discontinuously between periods so a continuous change should not be implied. Thus '80% chance of rain this evening *but only* a 30% chance tonight' is preferable to '80% chance of rain this evening *decreasing to* a 30% chance tonight'.

(ii) Periods should not be combined. Thus, '30% chance of rain today and tonight' is ambiguous. Does the 30% refer to each period separately or to them combined?

(iii) Do not use terms that leave the time period unclear, e.g. '20% chance of rain *by* this evening'.

(iv) Avoid using a period unhelpful or ambiguous to the user, e,g. 'late this evening'.

11.3.3 Incorporating probabilities into forecasts

The following are general guidelines for probability forecasts, especially PoP forecasts, to the general public (although not necessarily applicable to specialized services):

(i) Use 'chance' rather than 'probability' and avoid reference to 'threat of' or 'risk of'.

(ii) Give only one probability for each location. Thus '10% chance of showers this morning and a 60% chance of rain this evening' is to be avoided.

(iii) Do not combine probabilities about extent and duration. Thus, '30% of scattered showers' or '40% chance of occasional rain' should be avoided.

(iv) It is important that it is clear about the type of 'precipitation' to be expected.

(v) PoP should separate different types of precipitation, e.g. 'occasional rain with the possibility of an afternoon thunderstorm. 70% chance of rain'.

(vi) When a change of precipitation type is forecast, the PoP should refer to the chance of precipitation not the chance of the type changing, e.g. 'rain, possibly turning to snow this afternoon. 70% chance of precipitation'. Statements such as: '70% chance of rain turning to snow' should *not* be used.

11.3.4 Improving probability forecasts

Effective and timely feedback from a verification scheme can increase the reliability of probability forecasts. Common problems that arise when making probability forecasts are:

(i) Over-confidence, excessive use being made of very high/low probabilities.

(ii) Probabilities are not changed when a forecast is updated or even when developing as expected.

(iii) Range of probabilities available for a fixed period decreases with the length of the forecast. 100% PoP might be reasonable for day 1 of a forecast, but not for day 5.

(iv) Some probabilities are over- or under-used.

(v) There is a tendency to over-forecast probabilities for relatively infrequent events.

Reliability of forecasts (11.4.2.1) can be improved by identifying and remedying these problems. However, accuracy must not be compromised by artificially using 'under used' probabilities.

11.3.4.1 Characteristics of a reliable probability forecast

A reliable probability forecast is characterized by the following:

(i) When an event is infrequent at a particular location the probabilities tend to be lower than at locations where the event is frequent.

(ii) Probabilities tend to be lower the shorter the length of the period.

(iii) Probabilities tend to be less extreme as the lead time to the forecast period increases. For large lead times the range of probabilities reduces to the climatological frequency.

11.4 Verification

An assessment made of the extent of the agreement of a forecast with the actual state, using entirely *objective* methods, is termed an objective verification process.

11.4.1 Characteristics

The three characteristics of the verification process that are useful to assess are:
(i) Reliability.
(ii) Accuracy.
(iii) Skill.

(Another useful characteristic is 'factorization', discussed in 11.6).

However, before considering any summary measures from the verification scheme, it is important that the basic data are examined.

11.4.2 Display of information

Information about probability forecasts can be displayed in a contingency table. In the example a PoP of 0.4 was forecast on 264 occasions, with precipitation occurring 114 times and not occurring 150 times. The table also shows that a probability of 0.4 was forecast on 264 occasions out of a total of 8699 (this is referred to as the frequency of use).

Table 11.1. Contingency table

PoP	0.0	0.1	0.2	0.3	0.4	0.5	0.6	0.7	0.8	0.9	1.0	Total
Precipitation	120	132	162	215	114	173	174	358	380	85	1172	3485
No precip	2619	739	492	398	150	168	126	211	132	102	77	5214
Total	2739	871	654	613	264	341	300	569	512	587	1249	8699

Often the climatological frequency of an event is not known. In this case the best estimate of the frequency can be derived from the contingency table. In the example the frequency of occurrence of precipitation was $P_o = 3485/8699 = 0.401$.

11.4.2.1 Reliability

The *reliability* is a measure of the degree of correspondence between the average of a set of forecasts and the corresponding average of a set of observations. The *bias* is one measure of reliability.

The forecasts are reliable (i.e. unbiased) if, for each forecast probability, the frequency with which an event occurs is the same as the forecast probability.

Consider the bias of the 0.4 probability forecasts. The contingency table shows that 0.4 was forecast on 264 occasions and of these precipitation was observed on 114 occasions. Therefore, on the occasions for which 0.4 was forecast, the observed frequency of precipitation was 114/264 = 0.432. This shows that there is a small bias in the 0.4 probability forecasts. The bias can be calculated in a similar way for each forecast probability.

A convenient way of displaying information about reliability is to use a reliability diagram (analogous to a scatter diagram) — a plot of frequency with which an event occurs when a particular probability is forecast against the forecast probability. Forecasts are perfectly reliable when points lie on a 45° line; points falling below/above the line indicate over-forecasting/under-forecasting **(Fig. 11.1(a))**

The frequency-of-use histogram is helpful in assessing whether the points on the reliability diagram are subject to significant sampling errors **(Fig. 11.1(b))**.

The frequency-of-use histogram is also useful in assessing whether the forecasts try to distinguish between different events — this property is called *sharpness.* The forecasts would be completely sharp if only probabilities of 0 and

1 were used. However, there would be no sharpness if a climatological probability was used because the forecasts would not distinguish between days with or without precipitation.

Note that if climatology is always used the forecasts would be perfectly reliable, but have no sharpness. In general forecasts should be reliable and quite sharp.

The reliability diagram is a very effective way of displaying information. However, it is convenient to be able to summarize the reliability with a single figure which represents the overall bias. There are two related measures that can be used:

$$\text{Bias} = [(\overline{P} - P_o)/P_o] \times 100\% \qquad \text{or Bias} = \overline{P}/P_o$$

where: $\overline{P}$ is the mean forecast probability and P_o is the frequency with which the event occurred.

(i) For the first measure, Bias = 0% for perfectly reliable forecasts, with positive values indicating over-forecasting and negative ones indicating under-forecasting.
(ii) For the second measure, Bias = 1.0 for perfectly reliable forecasts, with values greater than one indicating over-forecasting and values less than one indicating under-forecasting.
(iii) For the example, $\overline{P} = (2739 \times 0.0 + 871 \times 0.1 + ...)/8699 = 0.396$ and $P_o = 0.401$, giving a bias of -1.3% or 0.99 depending upon the measure used.

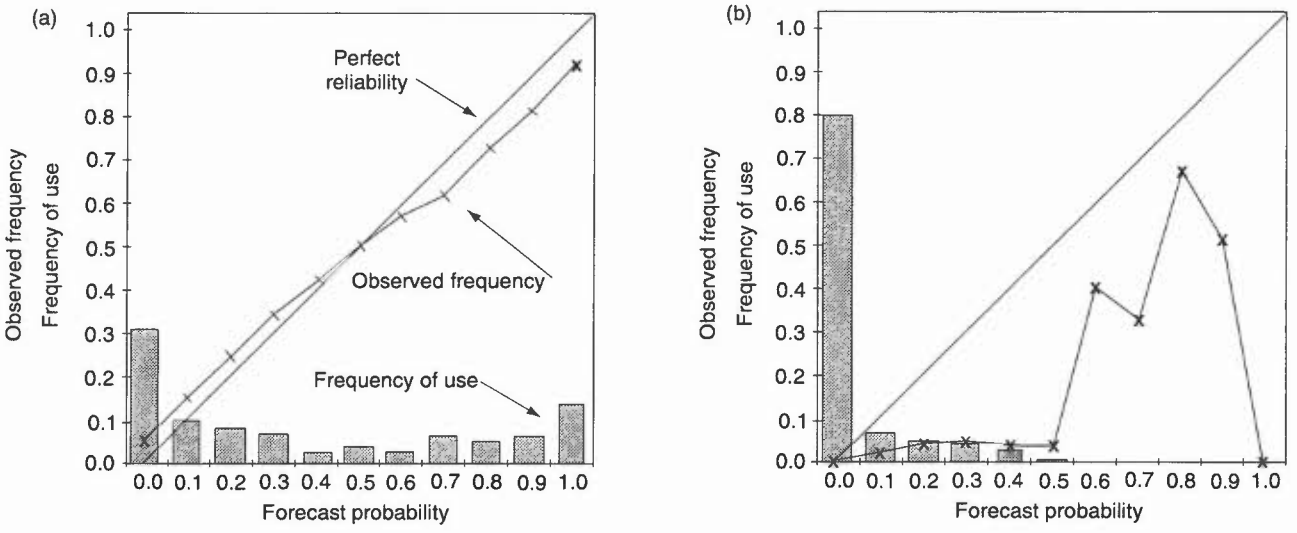

Figure 11.1. Reliability diagram and frequency of use histogram for (a) the PoP forecasts given in Table 1, and (b) for a set of forecasts of probability of fog.

11.4.2.2 Accuracy

Accuracy is defined as the average degree of correspondence between individual forecasts and what actually occurs.

The Brier Score is the most widely used measure of the accuracy of probability forecasts. It is a measure of the mean square probability error and is computed in essentially the same way as the Mean Square Error.

(i) First consider the case where the probability forecast refers to an event that falls into one of two categories (e.g. precipitation which either does or does not occur). PoP forecasts are of this type.
(ii) For a set of N forecasts, the Brier Score (BS) is given by:

$$BS = 1/N\,[\Sigma^N (F_i - O_i)^2]$$

where: F_i is the forecast probability of the event occurring.
O_i indicates whether the event occurred ($O_i = 1$ if it did and $O_i = 0$ if it did not).

With this scheme:
(i) $BS = O$ when all the forecasts are completely accurate (only probabilities 0 and 1 are forecast and $F_j = 0$ when $O_j = 0$ and $F_j = 1$ when $O_j = 1$).

(ii) $BS = 1$ when all the forecasts are completely wrong (only probabilities 0 and 1 are forecast and $F_i = 0$ when $O_i = 1$ and $F_i = 1$ when $O_i = 0$).

The Brier Score can easily be computed from the information used to produce the reliability diagram and the frequency of use histogram. The contribution to the Brier Score by forecasts of probability F is given by:

$$BS_F = \phi_F (F - 1)^2 + (1 - \phi_F)F^2$$

where: F is the forecast probability,
ϕ_F is the frequency the event occurred when probability F was forecast.

The overall Brier Score is then given by the sum of the individual contributions weighted by the frequency of use.

It should be noted that the Brier Score has three particularly desirable properties:
(i) Reliable forecasts are rewarded.
(ii) A willingness to discriminate between events is rewarded by penalizing forecasts in the mid-probability range (i.e. hedging).
(iii) The accuracy is maximized if and only if the forecaster makes a prediction that corresponds to his/her judgement about whether an event will occur.

The form of the Brier Score given above only applies when the event being forecast falls into one of two categories. If there are more than two categories (K say), the Brier Score for N sets of forecasts is given by:

$$BS = 1/2N \, [\Sigma^N \Sigma^K (F_{ij} - O_{ij})^2]$$

where: F_{ij} is the ith forecast for the jth category.
O_{ij} is the corresponding observation (1 if the event occurred and 0 if it did not).

When there are only two categories this expression reduces to the one given earlier.

The Brier Score has a negative orientation (the larger the score the lower the accuracy). If a positive orientation is required the Probability Score can be used:

$$PS = 1 - BS$$

11.4.2.3 Skill

The *skill* is a measure of the accuracy of a forecast relative to some reference such as persistence or climatology.

The *Probability Skill Score* (*PSS*) is based on the Brier Score of the forecasts (*BS*) relative to that based on climatology (BS_c)

$$PSS = (BS_c - BS)/BS_c$$

For a set of perfect forecasts $BS = 0$ giving $PSS = 1$, but if $BS = BS_c$ then $PSS = 0$.

One of the drawbacks of the *PSS* is its sensitivity to the accuracy of the climatological forecast. If the BS_c is small (i.e. the denominator in the expression for *PSS* is small) any difference between the forecast and climatological prediction is amplified. This makes the score rather unstable so it is essential that a large sample is used.

Ideally the value of the probability used as the climatological forecast should be the long-term frequency of the event. In reality this is often not available so the frequency of the event during the period of the forecasts is often used.

Suppose P_o is the observed frequency of an event. A forecast of P_o would lead to a contribution to the Brier Score of:
(i) $(1 - P_o)^2$ if the event occurred and the proportion of occasions on which this would happen is P_o.
(ii) $(0 - P_o)^2$ if the event did not occur and the proportion of occasions on which this would happen $(1 - P_o)$.
(iii) Therefore the reference Brier Score based on the observations from the period is given by:

$$BS_C = P_o (1 - P_o)^2 + (1 - P_o)P_o^2 = P_o (1 - P_o).$$

For the data in Table 11.1, $P_o = 0.401$, giving $BS_C = 0.240$. As $BS = 0.129$, the *PSS* is 0.463. Therefore the skill of the forecasts is 46.3% relative to climatology.

11.5 Making comparisons

Use of the Probability Skill Score is the most effective way of comparing two sets of probability forecasts. However, care still has to be taken in making such comparisons. For example, there is evidence that the skill of PoP forecasts sometimes depends upon the climatological frequency of precipitation, with the dependency being more marked in winter than in summer.

It has been argued that it would be expected the skill would be a maximum when the climatological frequency is about 50%, and approach zero as the climatological frequency approaches zero or 100%. These considerations suggest the following.

(i) Comparison of PoP forecasts from different stations should be avoided unless both sets of forecasts apply to regions with a similar frequency of precipitation.

(ii) Comparison for PoP forecasts produced by different forecasters at a station for the same location or area should produce meaningful results.

In both cases a large sample should be used in making a comparison. For example, for the comparison of individual forecasters about two years' worth of forecasts are required.

11.6 Factorization

11.6.1 Joint frequency distribution

Consider a set of PoP forecasts from the Central Forecasting Office. Information about the forecasts and observations ean be summarized in a contingency table.

Table 11.2. Contingency Table

PoP	0.0	0.1	0.2	0.3	0. 4	0.5	0.6	0.7	0.8	0.9	1.0	Total
Precip	120	132	162	215	114	173	174	358	380	85	1172	3485
No precip	2619	739	492	398	150	168	126	211	132	102	77	5214
Total	2739	871	654	613	264	341	300	569	512	587	1249	8699

The joint frequency distribution ean be derived by dividing each entry in the contingency table by the total number of forecasts. This distribution contains information about the forecasts, the observations and the relationship between them.

Table 11.3. Joint frequency distribution

PoP	0.0	0.1	0.2	0.3	0.4	0.5	0.6	0.7	0.8	0.9	1.0	Occurrence
Precip	0.014	0.015	0.019	0.025	0.013	0.020	0.020	0.041	0.044	0.056	0.135	0.401
No precip	0.301	0.085	0.057	0.046	0.017	0.019	0.014	0.024	0.015	0.012	0.090	0.599
Total	0.315	0.100	0.076	0.071	0.030	0.039	0.034	0.065	0.059	0.067	0.144	1.000

The joint frequency distribution can be factorized in two ways to give the conditional distributions.

11.6.2 Reliability factorization

Dividing each element in a column by the corresponding frequency of use gives the conditional distribution that indicates how often an event was observed when a particular probability was forecast. This is called the reliability factorization.

Table 11.4. Reliability factorization

PoP	0.0	0.1	0.2	0.3	0.4	0.5	0.6	0.7	0.8	0.9	1.0
Precip	0.044	0.152	0.248	0.351	0.432	0.507	0.580	0.629	0.712	0.826	0.938
No precip	0.956	0.848	0.752	0.649	0.568	0.493	0.420	0.371	0.258	0.174	0.062

This shows that on the occasions on which a probability of 0.4 was forecast, precipitation was observed with a frequency 0.432 (given by 0.013/0.030). This factorization is useful in assessing the reliability of forecasts — hence its name.

11.6.3 Likelihood factorization

Dividing each element in a row by the corresponding frequency of occurrence gives the conditional distribution that indicates how often an event was forecast with a particular probability when the event occurred (these are referred to as likelihoods). The whole process is called likelihood factorization.

Table 11.5. Likelihood factorization

PoP	0.0	0.1	0.2	0.3	0.4	0.5	0.6	0.7	0.8	0.9	1.0
Precip	0.034	0.038	0.046	0.062	0.033	0.050	0.050	0.103	0.109	0.139	0.336
No precip	0.502	0.142	0.094	0.076	0.029	0.032	0.024	0.040	0.025	0.020	0.015

This shows that on the occasions on which precipitation was observed, a probability of 0.4 was forecast with a frequency of 0.033 (given by 0.013/0.401). This factorization is useful in assessing whether the forecasts discriminate between observed events (high values of forecast probability would be expected more often when an event occurs and low values when it does not).

Discrimination is the degree to which forecasts discriminate between occasions on which events occur. This can be assessed by examining the likelihood that particular probabilities were forecast when an event occurred. This information is provided by the likelihood factorization. A plot of the likelihood functions on a graph give a visual indication of the degree of discrimination.

For PoP forecasts there are two likelihood functions. The forecasts are not very discriminatory if, for each value of forecast probability, the likelihood functions are similar. However, if high probabilities are forecast when precipitation occurs and low values are forecast when it does not, there will be little overlap between the likelihood functions and the forecasts will be highly discriminatory — this is a desirable characteristic.

The likelihoods indicate the additional information provided by the forecast beyond that provided by a forecast based on climatology.

11.7 Ensemble forecasting and predictability

The current state of the atmosphere is never precisely known; the sensitivity of an NWP forecast to the adopted initial conditions varies from occasion to occasion. The *ensemble technique* involves running a large number of numerical forecasts (32 in the ECMWF scheme) to 10 or more days ahead, each with slightly differently perturbed initial conditions.

The perturbations are chosen to provide a good sampling of the major modes of error growth. The degree to which the individual members of the ensemble are consistent from day to day is, in turn, indicative of the amount of reliance that can be placed on the 'unperturbed' forecast.

The forecasts of 850 hPa temperature, total precipitation and 500 hPa height can be grouped into clusters, defined with respect to behaviour over selected regions and time intervals, to show the evolution of cluster average fields over 4 to 7 days. As a simple example of the application of the technique, the ensemble might divide into two clusters by day 6, which present in the one case (consisting of 60% of the whole) a strong likelihood of precipitation at day 6, the other group indicating no precipitation. The form of presentation of the forecast will depend on the customer and their requirements .

In one case the customer may only need to be told that there is a 'fair chance of rain towards the end of the week'; the other customer, with a specific interest in the outcome of rainfall, can be told that there is a 3 in 5 chance of rain at day 6.

Molteni, et al. (1996)

BIBLIOGRAPHY

CHAPTER 11 — PROBABILITY FORECASTS

Gordon, N., 1993: Verification of terminal forecasts. Am Meteorol Soc, Conference on Aviation Meteorology, Vienna (Virginia), USA.

Halsey, N.G.J., 1995: Setting verification targets for minimum road temperature forecasts. *Meteorol Appl*, **2**, 193–197.

Molteni, F., Buizza, R, Palmer, T.N. and Petroliagis, T., 1996: *QJR Meteorol Soc*, **122**, 73–119.

Murphy, A.H. and Katz, R.H., 1985: Probability, statistics and decision making in the atmospheric sciences. Westview Press (Boulder, Colorado).

Stanski, H.R., Wilson, L.J. and Burrows, W.R., 1989: Survey of Common Verification Methods in Meteorology. WMO. World Weather Watch Technical Report No. 8.

Wilks, D.S., 1995: Statistical methods in the atmospheric sciences. San Diego, Academic Press.

CHAPTER 12 — AIR QUALITY AND ATMOSPHERIC DISPERSION

CHAPTER 12 — AIR QUALITY AND ATMOSPHERIC DISPERSION

12.1 Air quality

At times during both summer and winter, air quality deteriorates significantly in the UK (see 3.9 for guidance on haze occurrence and visibility forecasting). Under these conditions, the Government has asked the Meteorological Office to prepare air quality bulletins to give advance notice to the general public; these bulletins are issued through NETCEN to the media.

12.1.1 Emission of airborne pollutants

An air pollutant is a substance which, between the points of discharge into the atmosphere and ultimate removal, causes harm to the target. Because emission densities are higher in urban compared with rural areas, air pollutant concentrations are usually higher in urban areas.

Urban air quality reflects the balance between opposing tendencies of emissions to increase concentrations, and meteorology to disperse pollution and ventilate urban areas. The environmental harm caused by air pollutants may occur over spatial scales from the urban, to long-range transport and global scales.

Lyons & Scott (1990) **Smith (1992)**

12.1.2 Type of emissions

Emissions may be classified by type (e.g. CFC, hydrocarbon) and source; they come from a variety of natural sources and from human activities:

(i) *Particulates* — Urban concentrations of particles have caused a significant public health concern. Motor traffic, particularly diesel vehicles, are the major source but others include (stationary) combustion and industrial processes. Particles with particles with diameters less than 10 μm are of the greatest interest and this includes particles of natural origins: sea salt, wind-blown dust, pollen and spores.

(ii) *Sulphur compounds* — Sources from human activities (released mainly from the burning of coal and oil) wholly predominate over natural sources (dimethyl sulphide from decaying algal blooms) in the northern hemisphere.

(iii) *Carbon monoxide* — is produced by incomplete combustion of carbonaceous fuels, the main source being the internal combustion engine. There are large sources of carbon monoxide from the oxidation of methane and other hydrocarbons.

(iv) *Carbon dioxide* — is not normal regarded as a pollutant; sources are both natural and anthropogenic, including plants, animals and the burning of fossil fuels. Vegetation and oceans provide the main sinks. Since CO_2 is a major absorber of long-wave radiation, increased concentrations are expected to lead to an enhanced greenhouse effect.

(v) *Hydrocarbons* — Combustion and evaporation of fuels such as oil and petrol lead to emissions of highly reactive hydrocarbons which contribute to ozone formation in summertime episodes; some hydrocarbons (benzene and 1,3-butadiene) are cancer-inducing agents. There are large natural sources of hydrocarbons.

(vi) *Oxides of nitrogen* — NO_X emissions occur principally from motor traffic and combustion in power stations and industrial plants; the emissions readily oxidizes to NO_2, which is important in urban areas. Lightning and biomass burning are important global sources.

(vii) *Methane* — Main sources of CH_4 are rice production, cattle rearing, coal mining and the venting and leaking of natural gas. After CO_2, methane is the most important greenhouse gas; the bulk of the methane is removed in the lower atmosphere where it is an important source of tropospheric ozone, an important greenhouse gas in its own right. On entering the stratosphere methane breaks down and oxidizes to form water vapour, raising the stratospheric frost point and making polar stratospheric cloud production more likely.

(viii) *Chlorofluorocarbons* — CFCs have been used as refrigerants etc. only since the 1930s. They are essentially inert until they reach the stratosphere, where the reactive chlorine is is released by photodissociation. CFCs have been identified as major contributors to the destruction of the ozone layer over the (particularly Antarctic) winter poles.

(ix) *Other species* — dioxins and other toxic organic micropollutants are released in small quantities or restricted to certain localities but can be highly toxic.

Note that the hydroxyl radical (OH) is not an emission, being formed by chemical reaction in the atmosphere. However, it plays a significant role in many important chemical reactions, cleansing the troposphere by oxidizing trace gases to harmless products or to those more readily removed from the atmospheric circulation.

Bertorelli & Derwent (1995) **Derwent (1994, 1995)**

12.1.3 Smog

(i) *Wintertime UK smogs* — In conditions of light winds and high boundary-layer stability, particulate matter provides condensation nuclei for fog formation, for which the term 'smog' was termed after severe incidents in earlier decades. Urban wintertime smogs persist with elevated concentrations of nitrogen dioxide and particles which are associated with detectable short-term changes in public health.

(ii) *Tropospheric ozone and photochemical smog* — During summertime conditions, chemical reactions driven by sunlight, involving hydrocarbons and oxides of nitrogen, give rise to elevated concentrations of ozone which have some general public health significance.

Topography, onshore winds and other factors which will block dispersion, all contribute to making certain (low-latitude) cities infamous for their photochemical smogs. Even at higher latitudes summer days when days are long and solar radiation stronger, ozone can become a problem in anticyclonic weather.

12.1.4 Acid rain

SO_2 is readily oxidized to sulphuric acid which, having a low saturation vapour pressure, readily forms droplets that can serve as condensation nuclei. These droplets have an important acidifying influence on cloud water, rain and snow. Rainfall with a PH as low as 4 (even 2 in extreme cases) has been measured.

Chalk and limestone neutralize low PH rainfall and percolating water, but many upland areas of the UK (e.g. Cambrian Hills) are on geologically hard rock. This, combined with an evergreen forest catchment and spring snow-melt can lead to large surges in acidity which can leach out toxic aluminium from the soil, destroying, for example, whole aquatic ecosystems.

Although pollution sources causing major 'events' are likely to be local, long-range transport is an important element of environmental acidification in Europe. The influence of the UK, for example, on acidic deposition in Norway has been well characterized by both modelling and monitoring. Transport from the USA will give a low but, nevertheless, steady influx of pollution, particularly to western areas.

Smith (1991c)

12.1.5 Chemical and nuclear releases

Emissions from chemical and nuclear releases will generally differ in the following ways:

(a) *Chemical*
- (i) release(s) with gradual reduction over a period of hours;
- (ii) finite store of material released;
- (iii) density/buoyancy of gas at release is important;
- (iv) chemical interactions may change nature of emission with time.

(b) *Nuclear*
- (i) release(s) with gradual reduction over days;
- (ii) effectively an infinite store of material;
- (iii) neutral buoyancy;
- (iv) gas/particle release;
- (v) overseas, as well as domestic releases, may affect UK.

12.2 Dispersion on various scales

This section discusses the various dispersion and deposition mechanisms on the short-, meso-, and long-range to aid forecasters to more authoritatively offer advice under pollution scenarios and, particularly, under the CHEMET (Chemical Meteorology), PACRAM (Procedures and Communications in the event of the Release of Nuclear Material) and NAME (Nuclear Accident Model) emergency procedures (for details of which refer to *Commercial and Public Services Handbook*, Met.O.868, chapter 22). Procedures are also in place for providing the Ministry of Agriculture, Fisheries and Food with areas at risk in the event of outbreaks of, for example, foot and mouth disease.

CPSH
Gloster (1983)

12.2.1 Short-range dispersion

Over short ranges (out to 30 km) wind speed and direction, etc. can be assumed to be approximately constant and is dominated by turbulence (generated by wind shear, and by insolation) within the boundary layer (**Fig. 12.1**), the depth of which can be estimated from a nomogram (**Fig. 12.2**). Eventually fine-scale variations are smoothed by molecular diffusion; the result is that concentrations can be very patchy.

The peaks can be important for toxic or inflammable material, or for odours. Most models predict mean concentrations. Dispersion depends on natural mixing processes due to stability as follows:

(a) *unstable boundary layer* — convection rapidly disperses emission into a large volume, diluting it. Near-ground sources lead to lower concentrations of a plume than in neutral or stable conditions; elevated sources can lead to higher ground concentrations than in the latter conditions.
(b) *stable boundary layer* — turbulence is suppressed, resulting in high concentrations for near-ground sources. Unless an elevated plume impacts on downwind topography, ground-level pollution from elevated sources will not be significant.

Wind — high wind increases the dilution at source and reduces the influence of stability.
(i) speed influences distance of travel and concentration;
(ii) there will be directional variability;
(iii) light winds and high stability favour high pollutant concentrations at ground level although unstable conditions can give concentration peaks under 'looping' conditions (**Fig. 12.3**).

Pasquill & Smith (1983)
Stull (1988)

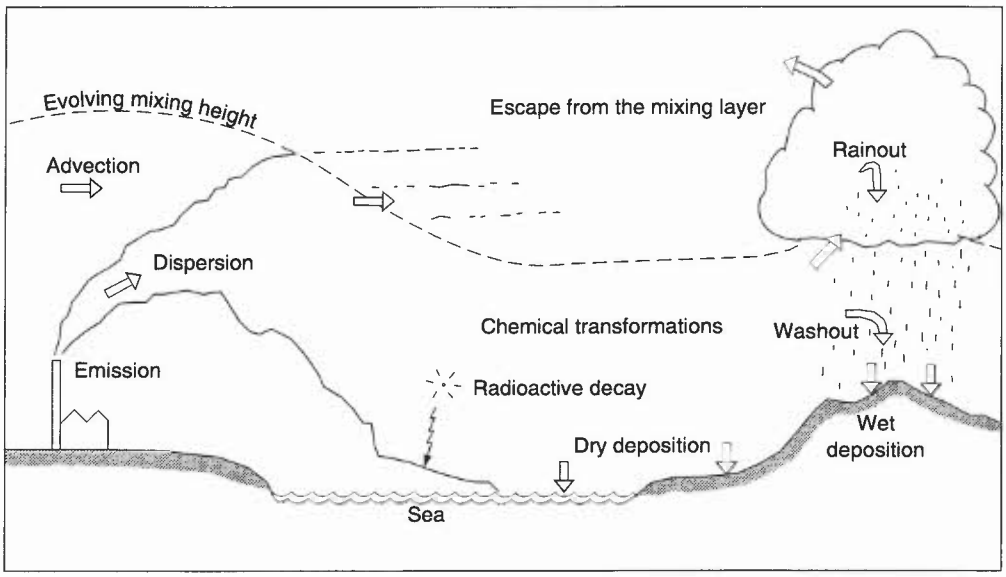

Figure 12.1. Some of the processes affecting airborne pollution.

12.2.1.1 Pasquill stability criteria

Pasquill combined wind speed, insolation and state of sky to categorize the influence of stability on the (horizontal and vertical) dispersion of a pollutant; these stability criteria are used in many short-range dispersion models out to 100 km and are required for the forecast information form in the PACRAM procedure (*Commercial and Public Services Handbook* Met.O.868, chapter 22, Annex D — the criteria are presented in **Table 12.1**.and the dispersion diagrams in **Fig. 12.4**). However, recourse is increasingly made to a method that characterizes the height at which stability effects become important (Monin–Obukhov technique).

Table 12.1. Stability categories in terms of wind speed, insolation and state of sky

Surface wind speed ($m\ s^{-1}$)	Insolation			Night	
	Strong	Moderate	Slight	Thinly overcast or ≥4/8 low cloud	≤3/8 cloud
<2	A	A–B	B	E	F
2–3	A–B	B	C	E	F
3–5	B	B–C	C	D	E
5–6	C	C–D	D	D	D
>6	C	D	D	D	D

Strong insolation corresponds to sunny midday in midsummer England, slight insolation to similar conditions in midwinter. Night refers to the period from 1 hour before sunset to 1 hour after dawn. For A–B take averages for A and B etc. The neutral category D should also be used, regardless of wind speed, for overcast conditions during day or night, and for any sky conditions during the hour preceding or following the night as defined above.

CPSH
Pasquill& Smith (1983)

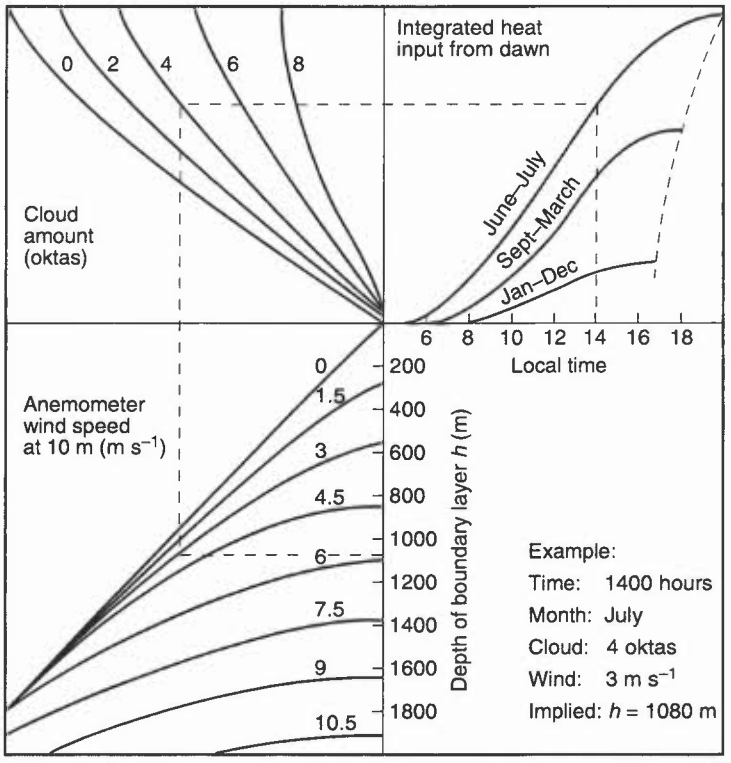

Figure 12.2. A nomogram for estimating the depth of the mixed layer in daytime conditions typical of the United Kingdom, assuming no marked advective effects or basic changes in weather conditions. The broken line shows how the diagram is to be used.

12.2.1.2 Plume characteristics from an elevated stack

Characteristic forms of plumes from an elevated stack are illustrated in **Fig. 12.3**:

(a) *Looping* — daytime conditions on fine summer day. Large eddies dominate which are larger than plume diameter and transport it up and down; high concentrations at ground level close to emission may result.

(b) *Coning* — characteristic of windy/cloudy conditions in near-neutral stability. Small-scale friction-generated eddies from forced convection. Similar lateral and vertical spread; plume may reach ground but further down wind than in looping.

(c) *Fanning* — under very stable conditions. Very weak turbulence; thin plume but may fan horizontally; plume can remain unchanged for 100 km or more downwind. Ground-level pollution virtually nil.

(d) *Lofting* — the most favourable dispersion condition; stable layer below plume inhibits downward transport while instability aloft encourages dispersion.

(e) *Fumigation* — reverse of lofting; buoyant mixing at low levels while inversion above plume inhibits upward dispersion. Occurs most commonly in the morning when nocturnal inversion is being eroded by surface heating. Once mixing layer reaches the plume high concentrations may be brought to the surface simultaneously at various locations along the plume.

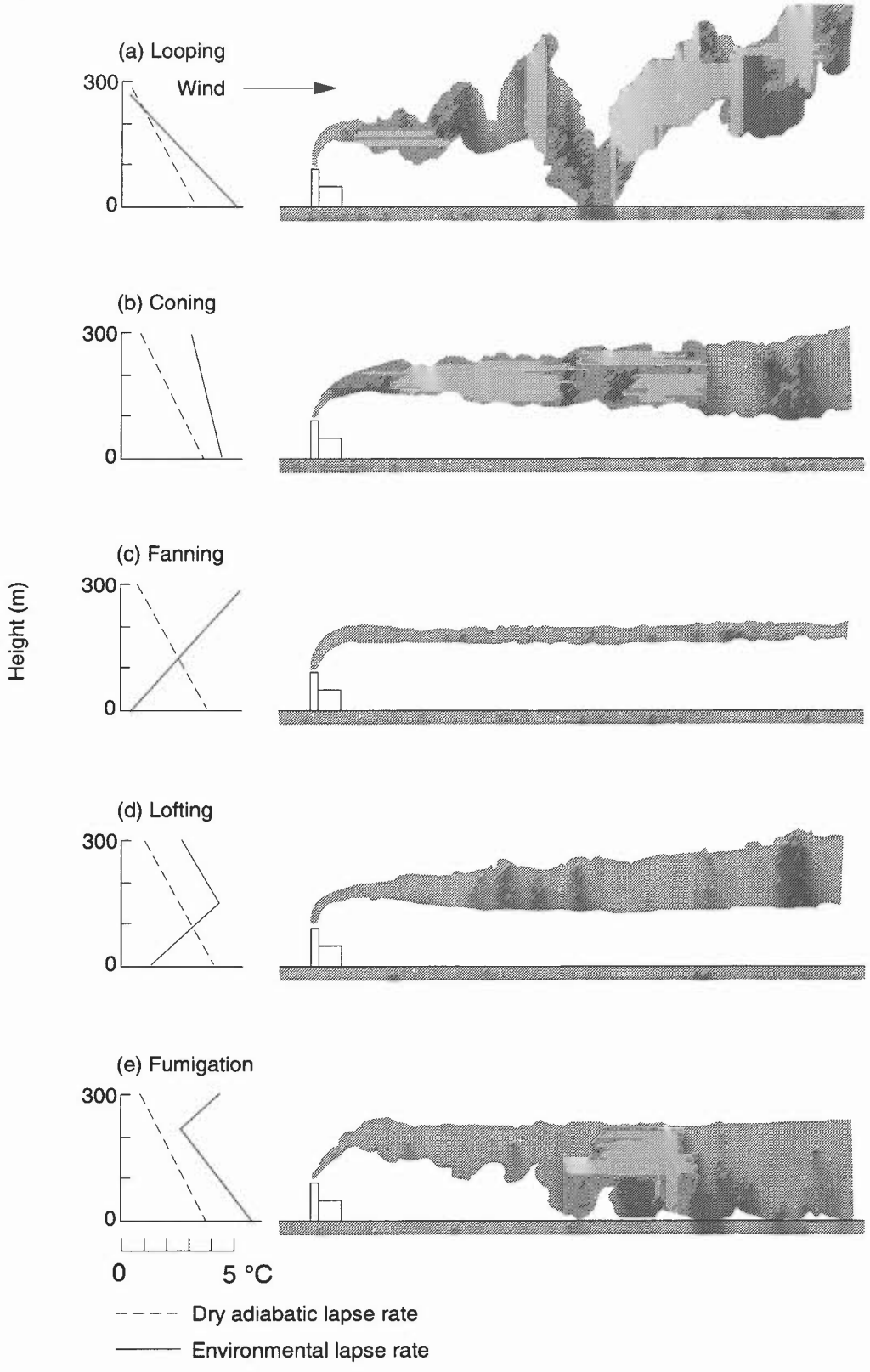

Figure 12.3. Characteristic plume patterns under different stability conditions.

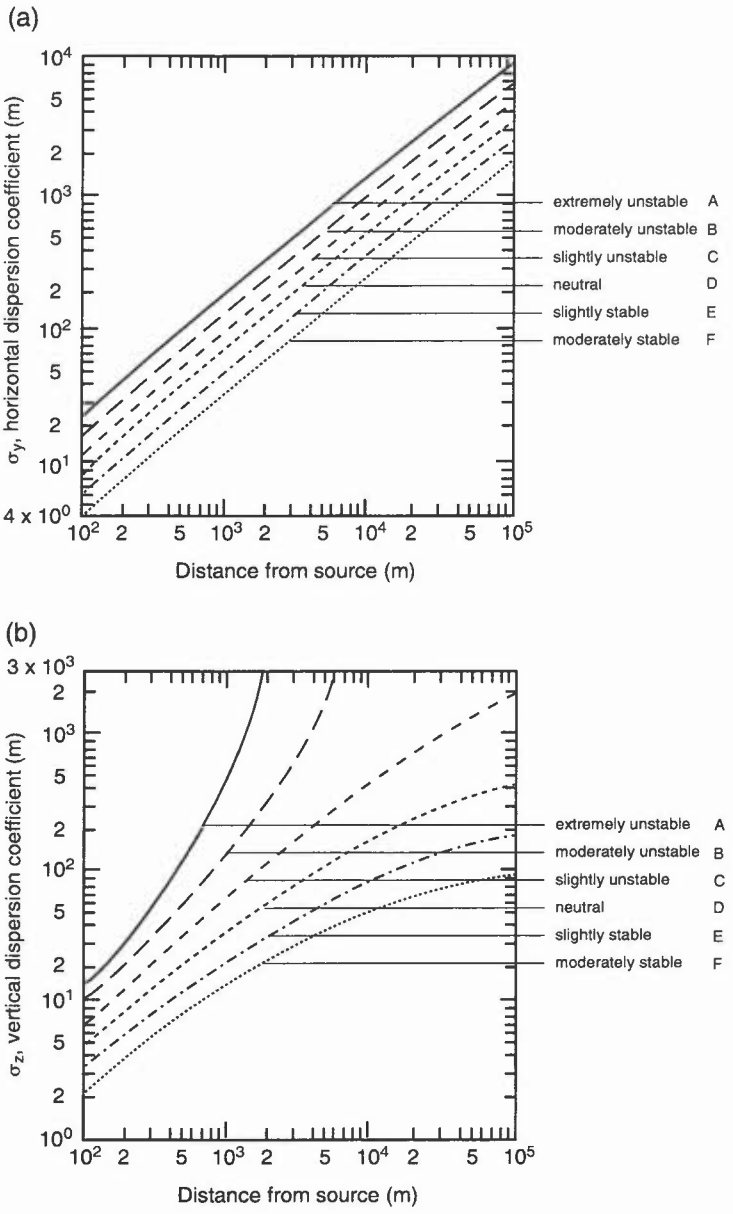

Figure 12.4. Pollutant dispersion diagrams, due to Pasquill–Gifford, illustrating standard deviation, σ, of the concentration about the central line maximum — the dispersion coefficient — for (a) horizontal and (b) vertical dispersion as a function of Pasquill stability criteria (Table 12.1).

12.2.2 Mesoscale dispersion

Examples of mesoscale circulations are sea and land breezes, flows associated with large convective cloud systems, urban circulations and topographically induced flows.

12.2.2.1 Sea and land breezes, storms, and urban circulation (1.3)

Sea breezes can:

(i) suppress convective dispersion through the introduction of cold air at low levels;

(ii) bring down high pollution concentrations, in particular by fumigation from coastal stacks where the plume is engaged by the turbulent internal boundary layer forming in the onshore breeze;

(iii) incorporate emissions from various coastal sources through circulations which cycle the same air repeatedly.

Land breezes

Down-slope flows may reinforce the land breeze under slack pressure gradients and virtually cloudless conditions. Generally, though, land breezes will carry pollution out to sea where, however, the pollutant may constitute a 'reservoir', ready to be engaged by the next sea breeze.

Storms

(i) Large storms will break down normal boundary-layer structure.
(ii) Pollution will be dispersed to other levels and there will be washout of much of the soluble and particulate pollutants.
(iii) A deposition 'episode' may result when heavy precipitation follows a period of stagnation, during which pollutant emissions have accumulated.

Urban circulation

Increased surface roughness and the 'heat island' effect will affect dispersion in several ways:
(i) there will be an increase in vertical mixing;
(ii) it will be difficult to ascribe wind speeds and turbulence levels.

12.2.2.2 Topography

The effect of hills on pollution dispersion is complex; here are guidelines for simple topographic models.

(i) the wind speed-up factor at the top of an isolated hill of height, h, is $2h/l$, where l is the 'half-width' of the hill at height $0.5h$ (1.3.2);
(ii) turbulence levels are increased in proportion: $1 + 2h/l$;
(iii) for slopes >1 in 3 near-neutral airflows tend to separate from the surface and closed eddies can be set up. If a pollution source lies inside one of these eddies (or if pollutant gets into such an area) then high concentrations will be found within it with a relatively slow escape to the main external flow;
(iv) for a source upwind of a hill the dispersion and resulting ground level concentration will depend very much on stability;
(v) unstable and neutral air flows can flow over the hill; under stable conditions there may be a critical height, h_c, below which air will stagnate or be forced around the hill and above which flow over the hill is possible **(Table 12.2)**;
(vi) High and low surface concentrations may be experienced on the forward side of the hill as the airflow responds to upstream variations in flow while on the lee side, complex separated flows may result in a point being continuously subjected to high dosages;
(vii) a persistent single vortex may form and stretch downwind from an isolated hill; the stability of the vortex may inhibit dispersion of material entrained beyond its own dimensions;
(viii) an area of high ground may generate mesoscale horizontal eddies on the sub-synoptic scale with closed circulations inhibiting dispersion (e.g. emissions from Eggborough Power Station have been monitored circulating within the lee eddy generated by North York Moors).

12.2.2.3 Flows near fronts

'Conveyor belt' and associated flows can advect pollution from behind the cold front to ahead of the warm front etc. (see Chapter 7). Wet deposition and rain out (removal as condensation nucleus (12.3)) processes will be important.

Table 12.2. The height below the hill crest ($h-h_c$) at which the airflow has just sufficient kinetic energy to rise over the hill in stable conditions

		$\Delta\theta$ Increase in potential temperature over 100 m				
		0.1	0.3	0.5	1	3
	1	172	100	77	55	32
wind	2	344	199	154	109	63
speed	4	688	397	308	217	126
u	6	1032	596	461	326	188
(m s^{-1})	8	1375	794	615	435	251
	10	1719	993	769	544	314

12.2.3 Long-range dispersion

(i) Initially dispersion is governed by turbulent and mesoscale diffusive processes.
(ii) After about a day the dispersion is controlled by differential ('chaotic') advection, the plume being stretched into 'tendrils', folded and sheared into 'whorls'.
(iii) Persistent anticyclones may form a barrier to this 'stirring' process, provided the source is outside the circulation.

(iv) Eventually plumes lose coherence as they are stirred by successive wind regimes; the plume has been effectively diffused on a hemispherical or even global scale.
(v) Gradually the material becomes uniformly mixed, assuming it has not been removed by the depletion processes long before then.

Maryon (1994)
Smith & Hunt (1978)
Smith (1988)

12.3 Deposition processes

The persistence of a pollutant within the boundary layer depends on:
(i) the synoptic conditions in which it is released;
(ii) its interception by rain-bearing systems.

Typical lifetime of pollution within the boundary layer is 3 to 4 days, depending on weather type (10 to 20 days in the troposphere and much longer in the stratosphere).

Within the boundary layer the three pathways for deposition are:
(i) *dry deposition* which accounts for ⅓ of all deposition through gravitational settling (particles <1 mm), impaction and surface absorption from a near-surface plume;
(ii) *wet deposition* which accounts for about ⅔ of all deposition through wash-out by impact with raindrops and by occult deposition (see below).

Wet deposition is vastly more efficient than dry — 1 hour of rain is equivalent to 2 or 3 days of dry deposition. Thus upland areas have the greatest potential for pollution deposition compared with lowland areas.

Falling snow scavenges pollutants more efficiently than rain, the seeder-feeder rate being about three times that for rainfall at the equivalent rainfall rate.

In turbulent (occult) deposition pollutants act as condensation nuclei within cloud formed by upslope motion. Some 90% of the mass is captured within cloud droplets. This is a source of deposition of acid species on, particularly, European upland forests.

There are other depletion processes, such as chemical transformations and radioactive decay, which do not involve deposition.

Chamberlain (1960)
Mason (1992)
Smith (1991a, 1991b, 1991c, 1992)

BIBLIOGRAPHY

CHAPTER 12 — AIR QUALITY AND ATMOSPHERIC DISPERSION

Bertorelli, V. and Derwent, R. 1995: Air quality A to Z. A directory of air quality data for the United Kingdom in the 1990s. Bracknell, Meteorological Office.

Chamberlain, A.C., 1960: Aspects of the deposition of radioactive and other gases and particles. *Int J Air Poll*, **3**, 63–88.

CPSH: Commercial and Public Services Handbook, Met.O.868, Chapter 22.

Derwent, R.G., 1994: Second generation abatement strategies for NO_x, NH_2, SO_2 and VOCs. *Ambio*, **23**, 425–433.

Derwent, R.G., 1995: Air chemistry and terrestrial gas emissions: a global perspective. *Philos Trans R Soc London*, **A351**, 205–217.

Gloster, J. 1983: Forecasting the airborne spread of Foot and Mouth Disease and Newcastle Disease. *Philos Trans R Soc London*, **B302**, 535–541.

Lyons, T. and Scott, W., 1990: Principles of air pollution meteorology, Bellover Press, London.

Maryon. R.H., 1994: Modelling long-range transport of radio-nuclides following a nuclear accident. *Nuclear Energy*, **33**, 119–128.

Mason, B.J., 1992: Acid rain: Its causes and its effects on inland waters. Oxford University Press.

Pasquill, F. and Smith, F.B., 1983: Atmospheric Diffusion. Ellis Horwood.

Smith, F.B., 1988: Lessons from the dispersion and deposition of debris from Chernobyl. *Meteorol Mag*, **117**, 310–317.

Smith, F.B., 1991a: A scheme for estimating fluctuations in concentration of an airborne pollutant. *Meteorol Mag*, **120**, 124–132.

Smith, F.B., 1991b: Deposition processes for airborne pollutants. *Meteorol Mag*, **120**, 173–182.

Smith, F.B., 1991c: An overview of the acid rain problem. *Meteorol Mag*, **120**, 77–91.

Smith, F.B., 1992: The first 50 years in the study of atmospheric dispersion. *Meteorol Mag*, **121**, 135–141.

Smith, F.B. and Hunt, R.D., 1978: Meteorological aspects of the transport of pollution over long distances. *Atmos Environ,* **12**, 461–478.

Stull, R. B., 1988: An introduction to boundary layer meteorology. Kluwer Academic Publishers.

CHAPTER 13 — SEA WAVES AND SURGES

CHAPTER 13 — SEA WAVES AND SURGES

13.1 Sea waves and swell

Terminology is in section 13.3.

13.1.1 Forecasting wind-wave heights and periods

13.1.1.1 Waves in deep water (WMO nomogram)

(i) **Fig. 13.1** is an adaptation of a WMO nomogram which is suitable for forecasting in the Atlantic and in the northern and central parts of the North Sea. For given values of wind speed and fetch, **Fig. 13.1(a)** may be used to forecast the Significant Wave Height and **Fig. 13.1(b)** the corresponding Wave Period.

(ii) The dashed lines indicate the duration in hours after which the waves will attain the computed state. If the duration is limited, the waves will not develop beyond the point given by the intersection of the wind speed and the duration on the graph.

Golding (1983) **Holt (1994)**

13.1.1.2 Waves in shallow waters (Darbyshire–Draper graphs)

Fig. 13.2 is suitable for forecasting waves in shallow coastal waters and in the southern North Sea. The layout and use of the graphs are the same as **Fig. 13.1**.

Darbyshire & Draper (1963)

13.1.2 Wave conditions at the shoreline; refraction

(a) Waves generally approach a beach with crests parallel to it. The angle between wave crests and the beach is reduced through the effect of wave refraction as the wave moves into shallower water, so that waves approach the beach with their crests more nearly aligned parallel to the depth contours (**Fig. 13.3**). The wave height increases and the wave breaks, how and when depending on the beach steepness, wind and other factors.

(b) Wave period is similar to that in the open sea, but can be significantly altered on passing through a zone of breaking waves (e.g. over an offshore sand-bar). Longer-period waves, which may seem insignificant off shore, may become the most prominent waves on breaking, as the effect of shoaling will increase the wave height relative to the shorter-wavelength/shorter-period waves.

(c) Waves may be refracted by variations in water depth and by current gradients; the process is important for several reasons:
   (i) Refraction (and shoaling) determines wave height and hence distribution of wave energy along the coast.
   (ii) Change in wave direction along wave front results in convergence or divergence of wave energy and thus on forces exerted on structures.
   (iii) Refraction affects bottom topography through the erosion and deposition of material.

There are PC-based techniques for transferring near-shore model forecasts to the beach zone. Details of forecasting the effects of tides and currents and surf etc. are in the DNOM Memorandum referenced.

DNOM (1984) **Shore Protection Manual (1984)**
Sanderson (1982)

13.1.3 Forecasting swell heights and periods

(a) The difficult task of forecasting in detail the range of wave heights and periods spreading out from a distant storm (which is both moving and developing in strength) is reduced by the practical limitations of the known data. These normally comprise little more than the distance of the storm, the maximum wave period generated in the storm area and the duration of wave generation in the direction from the storm to the forecast location.

(b) The information that is required includes:
   (i) the arrival time of the first swell from the direction of the storm;
   (ii) the height of the swell;
   (iii) the range of wave periods and wavelengths at any given time.

(c) **Fig. 13.4** may be used for estimating some of the properties of the swell from a distant storm. The initial data are entered on the horizontal and vertical axes, and from their point of intersection estimates of the swell travel time, the ratio of the swell height to the initial wave-height, and the swell period can be read off.

The height of the total sea generated by a combination of wind waves and swell is:

$$= \sqrt{[(\text{significant wave height})^2 + (\text{swell height})^2]}$$

Bretschneider (1973)

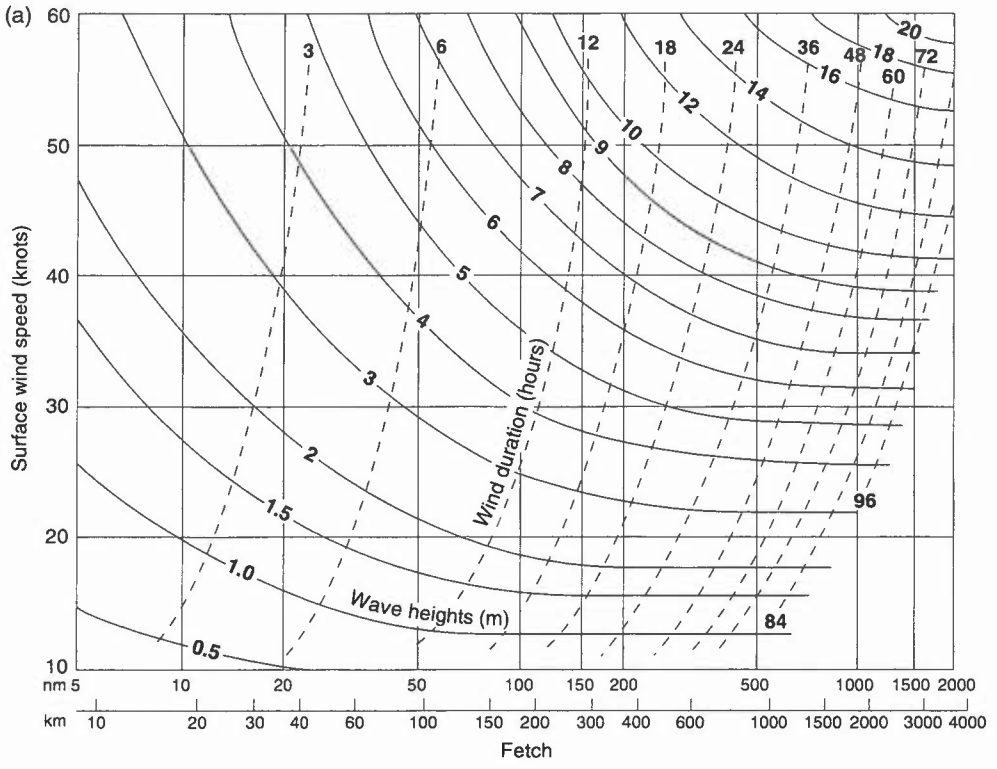

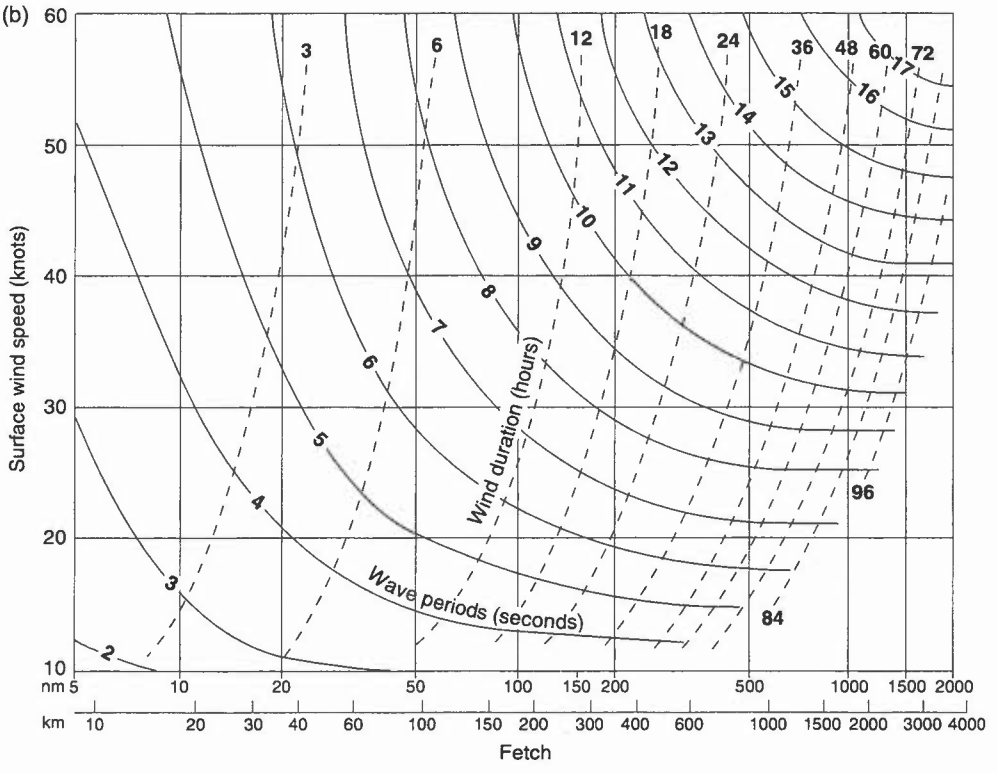

Figure 13.1. (a) Significant heights, and (b) periods, of deep-water waves (adapted from WMO nomograms).

13.1.4 Forecasting maximum waves

13.1.4.1 Wind waves

The most likely maximum wave height is 1.67 × the significant wave height. **Fig. 13.5** gives the maximum wave height corresponding to a given value of the significant wave height.

13.1.4.2 Swell waves

Swell height only varies a little, and for practical forecasting it may be considered as constant.

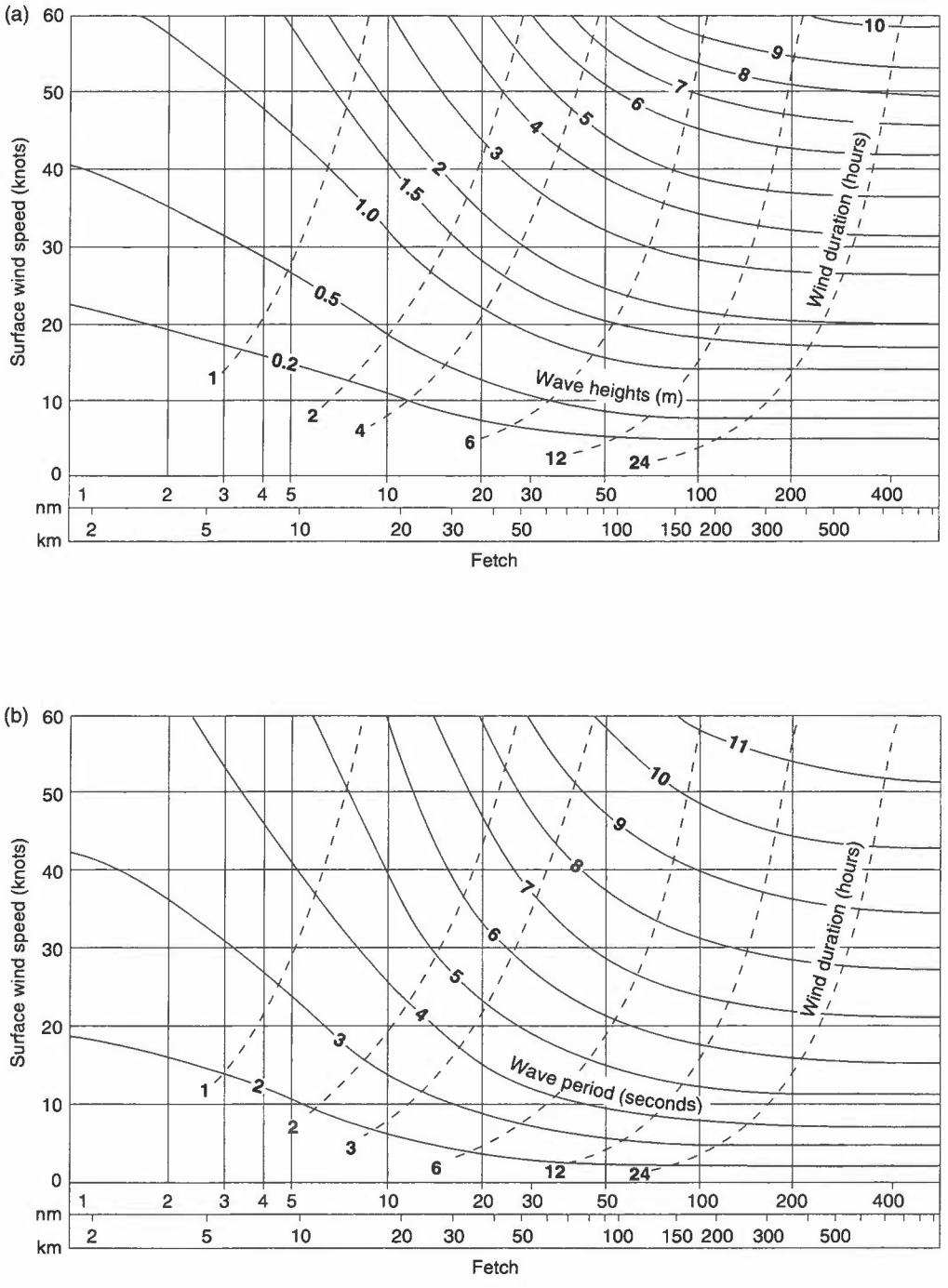

Figure 13.2. (a) Significant heights, and (b) periods, of shallow-water waves.

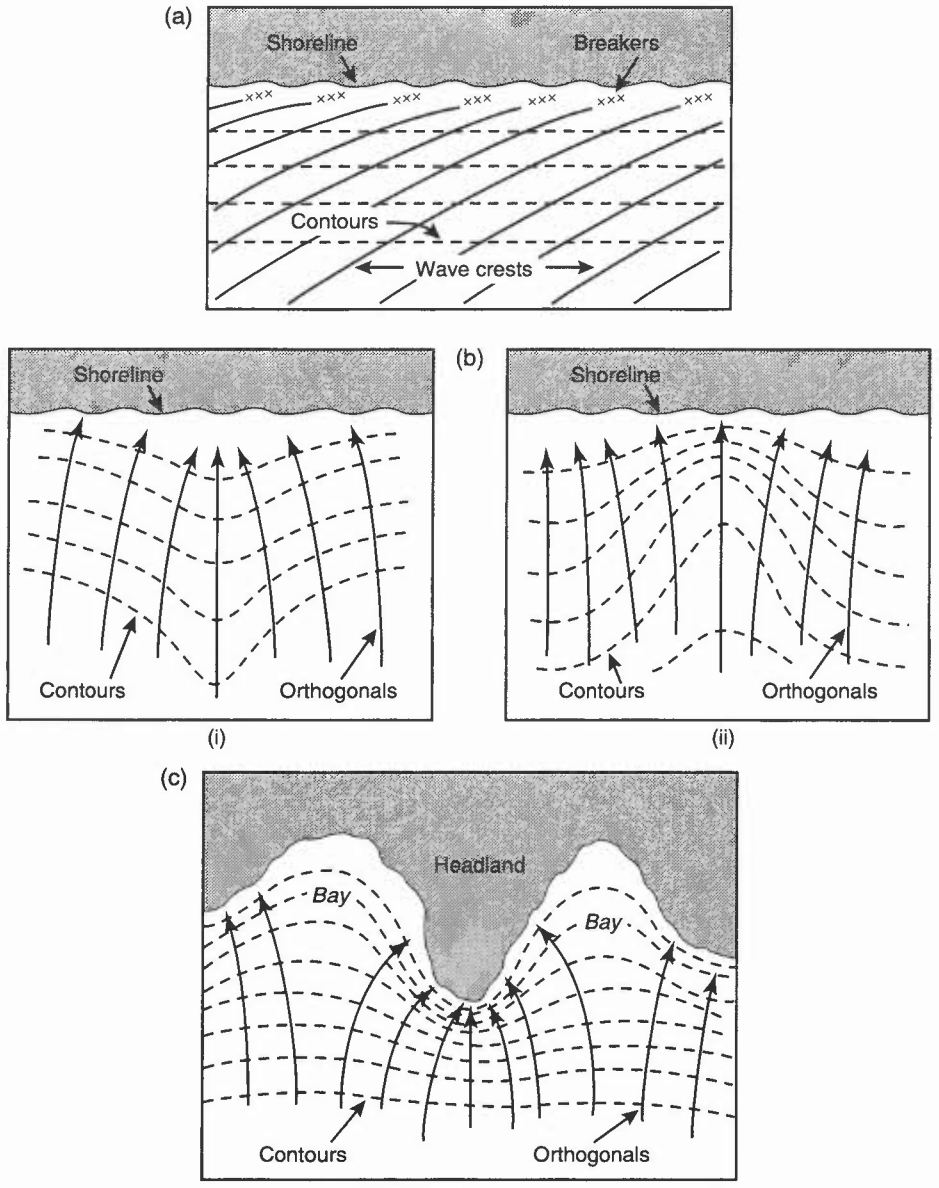

Figure 13.3. (a) Refraction along a straight beach with parallel bottom contours. (b) Refraction, (i) by a submarine ridge, and (ii) by a submarine canyon. (c) Refraction along an irregular shoreline.

13.1.4.3 Wind waves and swell waves combined

The maximum wave in a combined sea with wind waves and swell is:

$$\sqrt{[(\text{maximum wind wave})^2 + (\text{swell})^2]}$$

13.1.4.4 Extreme waves

When gales persist for long periods and the fetch is long, the 'maximum' wave height may be exceeded. **Fig. 13.5** gives an estimate of the 'extreme' waves which may be generated under these conditions.

DNOM (1984)
Open University (1991)

13.1.5 Tidal currents and waves

It is basic knowledge to mariners that waves become steeper and more of a hazard to shipping when the tide sets against the wind. Waves, generated in the sea before the tide has changed, have to reduce wavelength in order to conserve energy and must therefore increase amplitude.

Suthows (1945)

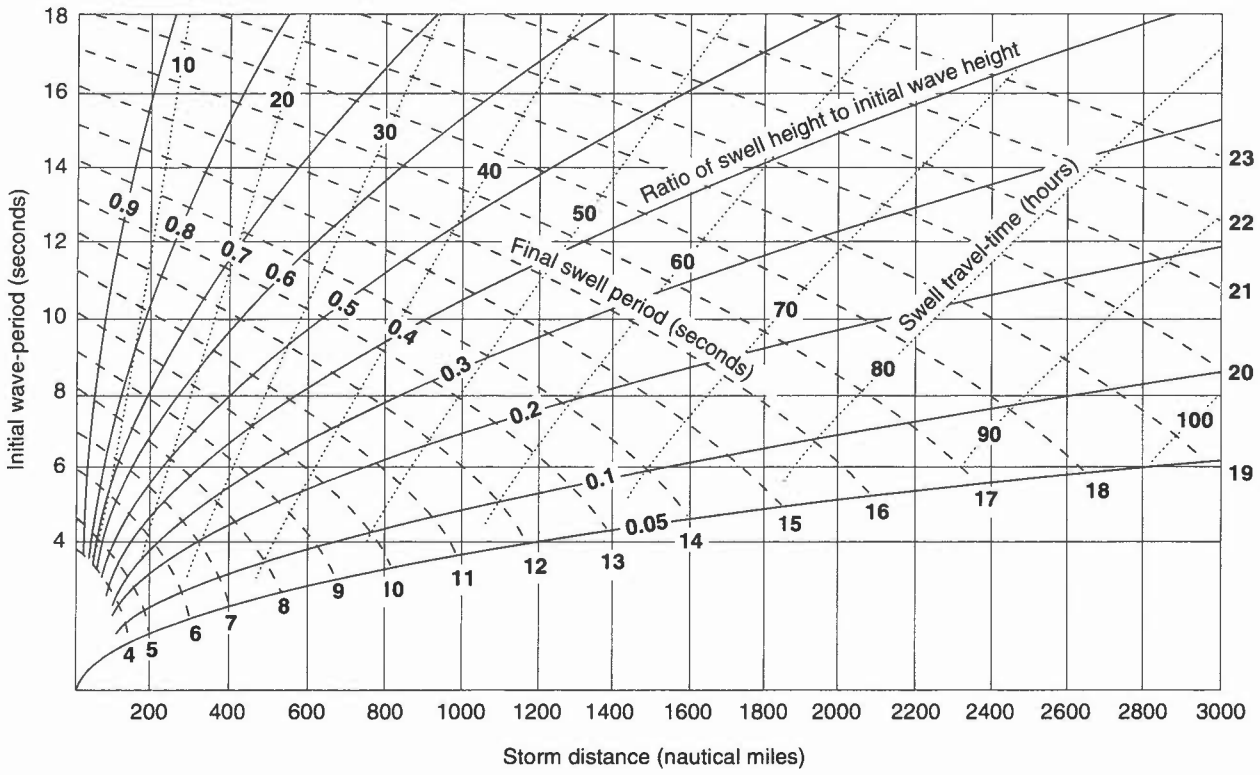

Figure 13.4. Forecasting swell height.

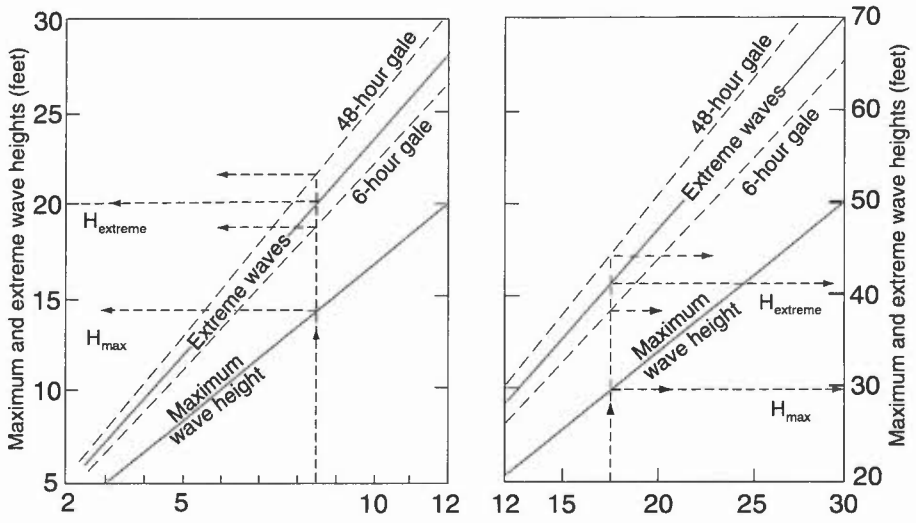

Figure 13.5. Forecasting maximum wave heights and extreme waves.

13.2 Storm surges

Storm surges are caused by particular combinations of wind, atmospheric pressure, waves and tides; the wind stress effects associated with a mobile low-pressure system dominate the surge effect due to any change in sea level due to the pressure system alone. This effect can be important along the south coast during prolonged periods of low pressure. Large anticyclones may depress tidal levels by up to 0.3 m.

Thus, levels in the Thames Estuary will comprise an element of the surge experienced in northern Scotland 12 hours earlier plus any surge generated within the North Sea; on occasion there may also be an element of surge that has propagated from the English Channel and through the Strait of Dover.

13.2.1 Causes and effects of storm surges

13.2.1.1 Atmospheric pressure

A change in atmospheric pressure of 1 hPa has the potential to cause a change in sea level of 1 cm. The response is not instantaneous but can be clearly observed when the UK is under the influence of an anticyclone, and coastal wind strengths are light. Tidal levels may then be depressed by as much as 0.3 m; areas of low pressure, similarly, has a tendency to raise tidal levels, although the transient nature of these systems means that the full response is not often seen.

13.2.1.2 Wind stress

The drag on the sea surface is assumed to be a function of the (10 m) wind speed and air density:

$$\text{stress} = \text{Drag coefficient} \times \text{air density} \times (\text{wind velocity})^2.$$

Typically the drag coefficient = 0.63.

13.2.1.3 Wind set-up

The effect of the wind on the slope of the sea surface in a narrow channel of constant depth is dependent on the water depth and density:

$$\text{Surge elevation} = \text{stress}/[g \times \text{water density} \times \text{depth}]$$

The effect is thus greater in shallow water. For a force 9 wind (22 m s^{-1}) blowing for 200 km over water of 30 m depth the rise in the level would be 0.85 m; an increase to force 11 (30 m s^{-1}) would result in a surge residual of 1.6 m.

13.2.1.4 Coriolis effect

The currents resulting from wind stress increase with depth as the current speed decreases so that the current profile describes an Ekman spiral.

Pugh (1987) **WMO (1988)**

13.2.2 Types and effects

13.2.2.1 North Sea surges

In a typical surge a 'positive' phase is preceded by a lowering of tidal levels at the southern end of the North Sea, due to the influence of southerly winds and to the Strait of Dover restricting flow into and out of this area. The strongest surges often result from depression on a south-easterly track crossing northern England or Scotland; the surge then can be wholly generated in the North Sea. Such surges will affect the eastern end of the English Channel.

13.2.2.2 'Negative' surges

Strong southerly winds in the North Sea may result in tidal levels much lower than tidal table predictions in the southern end of the North Sea, the Strait of Dover and the Thames Estuary (levels of over 2 m below predictions have been recorded). Such reductions in tidal levels pose a risk of grounding to deep-draught shipping with low under-keel clearance approaching port.

13.2.2.3 Frequency and extremes

(i) On east and west coasts there are about 20 events each winter with surge levels exceeding 0.6 m; negative surges in the Thames Estuary number about 15.
(ii) The 50-year return period surge is 1 m in the Hebrides, 3 m in the Thames Estuary, 1 m at Land's End.
(iii) Surge peaks only infrequently coincide with high water.

13.2.2.4 Areas at risk

(i) Low-lying southern and eastern areas are at greatest risk from tidal flooding. The east coast experiences an average of 19 surges with amplitudes exceeding 0.6 m each winter.
(ii) Flooding of susceptible areas of western Britain are generally associated with strong south-westerly winds ahead of depressions approaching from the west of Ireland. The surges may also affect the western end of the Channel.
(iii) Storm surges around the Scottish coast are usually <1 metre and will generally only cause concern when combined with periods of extreme river flow. Local conditions in areas such as the Clyde may result in larger surges and associated flooding.

Pugh (1987)

13.2.3 Forecasting surge levels

(i) The Meteorological Office's Storm Tide Warning Service monitors the National Tide Gauge Network, comprising over 40 gauges around the coasts of the British Isles. It makes use of data from the European Wave Model and uses NWP data to force surge models that are routinely run twice-daily.

(ii) Empirical techniques are available for key locations on the east coast (no similar methods are available for the west coast, although the 'Lennon' criteria give an indication of a major event in the Bristol Channel or Liverpool areas).

(iii) 2-D modelling of the shelf area surrounding the UK on a 12 km mesh gives output in the form of port tables of surge residuals (effects due to meteorological influences) for 36 hours ahead.

(iv) Data can be provided for offshore locations, together with wind-induced currents and *tidal stream velocities* (periodic, generally horizontal, movements due to periodic forces).

(v) Customer demand has resulted in fine-mesh local-area models: a model of the Bristol Channel uses a 4 km grid and runs in concert with a Severn Estuary model with a 1.3 km grid.

13.3 Terminology

Amplitude. The vertical distance between mean water level and wave crest.

Currents. Non-periodic movements of water, generally horizontally.

Duration (D). The time during which a given wind persists. Waves take time to build but, for a given wind speed, D is not a relevant factor once a mature wave system is established.

Fetch. The length of the traverse of an airstream across a sea or ocean. Fetch limits the height which waves can attain.

Maximum wave height (H_{max}). The highest wave to be expected in every 100 consecutive waves. For wind waves it has been found that $H_{max} = 1.67\ H_{sig}$.

Meteorological residual. Deviations from astronomically predicted tidal levels resulting from meteorological influences.

Neap tides. The semi-diurnal tides of smallest range in a semi-lunar cycle of 15 days.

Period. The time between successive wave crests (or troughs).

Significant wave height (H_{sig}). The mean of the highest third of the waves in a wave train, over a period of 10–20 minutes. This happens to correspond to what is normally reported as the mean wave height.

Spring tides. The greatest semi-diurnal tide in a semi-lunar cycle of 15 days.

Storm surge. Large change in sea level resulting from a major meteorological event.

Swell. represents wind waves (sea) which have travelled out of the area in which they were generated, or can no longer be sustained by the winds in the generating area.

Tide. Periodic movement in the level of sea or ocean surfaces due to periodic astronomical forcing.

Tidal streams. Periodic movements of water, generally horizontal, due to periodic forcing.

Wave height (H). The vertical distance between a wave crest and the following trough.

Wavelength. The distance between successive wave crests (or troughs).

Wind waves. are the waves caused by the local wind system (the 'wind-sea').

BIBLIOGRAPHY

CHAPTER 13 — SEA WAVES AND SURGES

Bretschneider, C.L., 1973: Prediction of waves and currents. *Look Laboratory, Hawaii*, **3**, 1–17.

Darbyshire, M. and Draper, L., 1963: Forecasting wind-generated sea waves. *Engineering*, **195**, 482–484.

DNOM: Forecasting sea swell and surf: Directorate of Naval Oceanography and Meteorology, Memorandum No 2/84.

Golding, B., 1983: A wave prediction system for real time sea state forecasting. *QJR Meteorol Soc*, **109**, 393–416.

Holt, M.W., 1994: Improvements to the UKMO wave model swell dissipation and performance in light winds. Meteorological Office FR Tech. Report No. 119.

Open University, 1991: Waves, tides and shallow-water processes. Pergamon Press/Open University.

Pugh, D.T., 1987: Tides, surges and mean sea level. Wiley and Sons.

Sanderson, R., 1982: Meteorology at sea. London, Stanford Maritime.

Shore Protection Manual (4th edition), 1984: Coastal Engineering Research Center, Dept. of the Army, Mississippi, USA.

Suthows, Commander, 1945: The forecasting of sea and swell waves. Met. Branch Memo 135/45, p. 72.

WMO, 1988: Guide to wave analysis and forecasting. Geneva, World Meteorological Organization, Pub No. WMO-702.

APPENDIX I — UNITS

1. S I units

Quantity	Name (symbol)	Definition
Basic units:		
Length	metre (m)	
Mass	kilogram (kg)	
Time	second (s)	
Temperature	Kelvin (K)	
Derived units:		
Force	newton (N)	kg m s^{-2}
Pressure	pascal (Pa)	N m^{-2}
Energy	joule (J)	N m
Power	watt (W)	J s^{-1}
Frequency	hertz (Hz)	s^{-1}

2. Multiples of units

Multiple	Prefix	(symbol)	Multiple	Prefix	(symbol)
10^{-1}	deci	(d)	10	deca	(da)
10^{-2}	centi	(c)	10^{2}	hecto	(h)
10^{-3}	milli	(m)	10^{3}	kilo	(k)
10^{-6}	micro	(μ)	10^{6}	mega	(M)
10^{-9}	nano	(n)	10^{9}	giga	(G)
10^{-12}	pico	(p)	10^{12}	tera	(T)

APPENDIX II — CONVERSION TABLES

1. Temperature

Table A1. Celsius to Fahrenheit

°C	−40	−35	−30	−25	−20	−15	−10	−5	0	5	10	15	20	25	30	35	40	45	50
°F	−40	−31	−22	−13	−4	5	14	23	32	41	50	59	68	77	86	95	104	113	122

differences

°C	1	2	3	4	5
°F	2	4	5	7	9

Table A2. Fahrenheit to Celsius

°F	−40	−30	−20	−10	0	10	20	30	40	50	60	70	80	90	100	110	120	130	140
°C	−40	−34	−29	−23	−18	−12	−7	−1	4	10	15	21	27	32	38	43	49	54	60

differences

°F	1	2	3	4	5	6	7	8	9
°C	1	1	2	2	3	3	4	4	5

2. Distance

1 inch	= 25.4 mm	1 cm	= 0.39 inch
1 foot	= 30.48 cm	1 m	= 3.28 feet
1 mile	= 1.61 km	1 km	= 0.62 mile
1 n.mile	= 1.85 km	1 km	= 0.54 n mile

Table A3. Nautical miles to kilometres

n mile	10	20	30	40	50	60	70	80	90	100
km	18	37	56	74	93	111	130	148	167	185

Table A4. Kilometres to nautical miles

km	10	20	30	40	50	60	70	80	90	100
n mile	5	11	16	22	27	32	38	43	49	54

3. Area

1 hectare = $(100\ m)^2$ = 2.47 acres

$(1\ km)^2$ = 100 hectares = 247 acres

4. Speed

Table A5. Knots to metres/second and kilometres/hour

knots	1	2	3	4	5	10	20	30	40	50	60	70	80	90	100
m s^{-1}	0.5	1	1.5	2	2.5	5	10	15	21	26	31	36	41	46	51
km h^{-1}	1.8	3.7	5.6	7.4	9.3	19	37	56	74	93	111	130	148	167	185

1 knot = 0.515 m s^{-1} = 1.85 km h^{-1}

Table A6. Miles/hour to knots and kilometres/hour

m.p.h.	1	2	3	4	5	10	20	30	40	50	60	70	80	90	100
knots	0.9	1.7	2.6	3.5	4.4	9	17	26	35	44	52	61	70	78	87
km h^{-1}	1.6	3.2	4.8	6.4	8.1	16	32	48	64	81	97	113	129	145	161

1 m.p.h. = 0.87 knot = 1.61 km h^{-1}

Table A7. Metres/second to kilometres/hour and knots

$m\ s^{-1}$	1	2	3	4	5	10	20	30	40	50	60	70	80	90	100
$km\ h^{-1}$	3.6	7.2	10.8	14.4	18.0	36	72	108	144	180	216	252	288	324	360
knots	1.9	3.9	5.8	7.8	9.7	19	39	58	78	97	117	136	155	175	194

$1\ m\ s^{-1} = 3.60\ km\ h^{-1} = 1.94$ knots

Table A8. Kilometres/hour to knots and metres/second

$km\ h^{-1}$	1	2	3	4	5	10	20	30	40	50	60	70	80	90	100
knots	0.5	1.1	1.6	2.2	2.7	5	11	16	22	27	32	38	43	49	54
$m\ s^{-1}$	0.3	0.6	0.8	1.1	1.4	3	5	8	11	14	17	19	22	25	28

$1\ km\ h^{-1} = 0.54$ knots $= 0.28\ m\ s^{-1}$

Table A9. Feet/minute to knots and metres/second

$ft\ min^{-1}$	10	25	50	75	100	200	300	400	500	1000
knots	0.10	0.25	0.49	0.74	1.0	2.0	3.0	3.9	4.9	9.9
$m\ s^{-1}$	0.05	0.13	0.25	0.38	0.5	1.0	1.5	2.0	2.5	5.1

$1000\ ft\ min^{-1} = 9.87$ knots $= 5.08\ m\ s^{-1}$

Table A10. Runway cross-wind components

		Angle between wind direction and runway heading (deg. true)								
		10	20	30	40	50	60	70	80	90
	5	1	2	2	3	4	4	4	5	5
	10	2	3	5	6	7	8	9	9	10
	15	3	5	7	9	11	13	14	14	15
	20	3	7	10	13	15	17	18	19	20
	25	4	8	12	16	19	22	23	24	25
Wind	30	5	10	15	19	23	26	28	29	30
	35	6	12	17	22	26	30	32	34	35
speed	40	7	14	20	25	30	35	37	39	40
in	45	8	15	22	29	34	39	42	44	45
	50	9	17	25	32	38	43	47	49	50
knots	55	10	19	27	35	42	48	52	54	55
	60	10	20	30	38	46	52	56		
	65	11	22	32	42	50	56			
	70	12	24	35	45	54				
	75	13	26	37	48					
	80	14	27	40						

APPENDIX III — PHYSICAL TABLES AND CONSTANTS

1. The Earth

Dimensions

Equatorial radius	6378 km (3963 miles	
Polar radius	6357 km (3950 miles)	
Rate of rotation (Ω)	7.29×10^{-5} s^{-1}	
Total surface area	510×10^6 km^2	
Land surface area	150×10^6 km^2	(29.2% of total area)
Ocean surface area	360×10^6 km^2	(70.8% of total area)

Table A11. Gravity at mean sea level

Latitude (deg)	0	50	60	90
g (m s^{-2})	9.78	9.81	9.82	9.83

Table A12. Distance of sea horizon from viewpoint at given heights

Height (ft)	6	10	20	30	50	100	200	400	600	800
Distance (n mile)	2.8	3.6	5.1	6.3	8.1	11	16	23	28	32

Table A13. Distance corresponding to 1 degree of longitude at given latitudes

Latitude (deg)	0	15	30	45	50	55	60	75	85	90
Distance (n mile)	60.4	58.3	52.2	42.6	38.7	34.5	30.1	15.5	5.2	0

Table A14. Value of Coriolis Parameter ($f = 2\Omega\sin\varphi$)

	Latitude (φ) degrees								
	0	15	30	45	50	55	60	75	90
f (10^{-4} s^{-1})	0.00	0.38	0.73	1.03	1.12	1.19	1.26	1.41	1.46
f (h^{-1})	0.00	0.14	0.26	0.37	0.40	0.43	0.45	0.51	0.52
$\partial f/\partial y$ (10^{-11} m^{-1} s^{-1})	2.29	2.12	1.98	1.62	1.47	1.31	1.14	0.59	0.00

2. The atmosphere

(a) **Some physical properties**

Mass of atmosphere = 5.27×10^{18} kg

Surface pressure:
1 'atmosphere' = 1.03 kg cm^{-2} = 14.7 lb in^{-2} = 29.9 in Hg
1 millibar = 100 dynes cm^{-2} = 100 N m^{-2} = 1 hPa

Speed of light = 2.998×10^8 m s^{-1}

Speed of sound in dry air

Temperature (°C)	−40	−20	0	20	40
Speed (m s^{-1})	306	318	331	343	354

(b) **Specific heats (J deg^{-1} kg^{-1}) of atmospheric constituents:**

Dry air (c_p)	1004
Dry air (c_v)	717
Water vapour (c_p)	1952
Water vapour (c_v)	1463
Liquid water (0°C)	4218
Ice (0°)	2106

(c) **Latent heats (J kg^{-1}) of water substances**

Vapour/Liquid	2 500 000
Liquid/Solid	334 000
Solid/Vapour	2 834 000

Table A15. ICAO Standard atmosphere (dry air)

Pressure	Temperature	Density	Height		Thickness of 1 hPa layer	
hPa	°C	g m^{-3}	m	ft	m	ft
1013.2	15.0	1225	0	0	8.3	27
1000	14.3	1212	111	364	8.4	28
950	11.5	1163	540	1773	8.8	29
900	8.6	1113	988	3243	9.2	30
850	5.5	1063	1457	4781	9.6	31
800	2.3	1012	1949	6394	10.1	33
750	−1.0	960	2466	8091	10.6	35
700	−4.6	908	3012	9882	11.2	37
650	−8.3	855	3591	11780	11.9	39
600	−12.3	802	4206	13801	12.7	42
550	−16.6	747	4865	15962	13.7	45
500	−21.2	692	5574	18289	14.7	48
450	−26.2	635	6344	20812	16.1	53
400	−31.7	577	7185	23574	17.7	58
350	−37.7	518	8117	26631	19.7	65
300	−44.5	457	9164	30065	22.3	75
250	−52.3	395	10363	33999	25.8	85
200	−56.5	322	11784	38662	31.7	104
150	−56.5	241	13608	44647	42.3	139
100	−56.5	161	16180	53083	63.4	208
90	−56.5	145	16848	55275	70.5	231
80	−56.5	128	17595	57726	79.3	260
70	−56.5	112	18442	60504	90.6	297
60	−56.5	96	19419	63711	105.7	347
50	−55.9	80	20576	67507	127.0	417
40	−54.5	64	22000	72177	160	525
30	−52.7	47	23849	78244	215	706
20	−50.0	31	26481	86881	326	1072
10	−45.4	15	31055	101885	669	2195

Table A16. The Sun

Date	Noon sun overhead (lat.)	Noon solar altitude 50° N (deg.)	Noon solar altitude 60° N (deg.)	Sunrise/sunset times (UTC) London	Manchester	Glasgow	Lerwick
Jan. 1	23° S	17	7	0805/1600	0825/1600	0850/1555	0925/1440
Jan. 16	21° S	19	9	0800/1620	0815/1620	0835/1615	0905/1500
Feb. 1	17° S	23	13	0740/1650	0755/1650	0810/1650	0830/1540
Feb. 16	13° S	27	17	0715/1715	0725/1720	0740/1720	0745/1625
Mar. 1	8° S	32	22	0645/1740	0700/1745	0710/1750	0700/1705
Mar. 16	2° S	38	28	0615/1805	0625/1815	0630/1820	0620/1745
Apr. 1	4° N	44	34	0535/1835	0545/1845	0550/1855	0535/1825
Apr. 16	10° N	50	40	0505/1855	0510/1910	0510/1925	0450/1910
May 1	15° N	55	45	0435/1925	0435/1935	0435/1955	0410/1945
May 16	19° N	59	49	0405/1945	0405/2005	0405/2025	0340/2010
June 1	22° N	62	52	0350/2005	0345/2025	0340/2050	0310/2030
June 16	23° N	63	53	0340/2020	0340/2040	0330/2105	0255/2105
July 1	23° N	63	53	0345/2020	0345/2040	0335/2105	0310/2100
July 16	21° N	61	51	0400/2010	0400/2030	0355/2050	0325/2045
Aug. 1	18° N	58	48	0420/1950	0425/2005	0420/2025	0345/2010
Aug. 16	14° N	54	44	0445/1920	0450/1935	0450/1950	0420/1930
Sept. 1	8° N	48	38	0510/1850	0515/1900	0520/1915	0500/1850
Sept. 16	3° N	43	33	0535/1815	0545/1825	0550/1835	0545/1810
Oct. 1	3° S	37	27	0600/1740	0610/1745	0620/1755	0630/1730
Oct. 16	8° S	32	22	0625/1705	0635/1710	0650/1715	0710/1645
Nov. 1	14° S	26	16	0655/1635	0705/1640	0720/1640	0755/1600
Nov. 16	18° S	22	12	0720/1610	0735/1610	0755/1610	0835/1525
Dec. 1	22° S	18	8	0745/1555	0800/1555	0820/1550	0910/1500
Dec. 16	23° S	17	7	0800/1550	0820/1550	0840/1545	0930/1440

Table A17. Rossby Long Waves — wavelength of stationary waves

Latitude (deg.)	Mean zonal wind speed (knots)									
	10	20	30	40	50	10	20	30	40	50
	wavelength									
	kilometres					degrees of longitude				
70	5100	7200	8800	10200	11400	134	190	232	268	300
60	4200	6000	7300	8400	9400	76	108	132	152	170
50	3700	5300	6400	7400	8300	52	74	90	104	116
40	3400	4800	5900	6800	7600	40	57	69	80	90
30	3200	4500	5600	6400	7200	33	47	57	66	74

APPENDIX IV — FORECASTING WEATHER BELOW 15,000 FT

In order to prepare a low-level forecast of weather for a short period ahead (e.g.6–12 hours) for a specific region, the following elements must be considered:

- visibility (Chapter 3)
- cloud (4.3; 4.6; 5.1; 5.2; 5.4–5.6; 5.8)
- weather, including fog/hill fog (3.3; 3.4; 3.5.2; 3.6)
- low-level turbulence (6.2)
- lee-wave activity (1.3.2)
- icing and turbulence in cloud (2.9; 6.1.1)
- variations in freezing level, with possible sub-zero layers, across the area (2.9.7; 2.9.8; 2.9.9; 2.9.10)

A brief ten-point summary of the main aspects of preparing a low-level aviation chart is as follows:

- Must know weather and cloud distribution now
- How does model represent weather at data time?
- Make necessary adjustments throughout forecast period.
- Check upper-air pattern — as above, is model correct?
- Allow for possible changes in development/decay, e.g. of large rain or shower areas; use trajectories.
- Consider effects of clearing skies — fog formation.
- Check gradient wind forecasts — consider turbulence.
- Run/modify lee-wave program results according to wind direction and vertical shear in relation to topography.
- Always examine actual and forecast ascents or profiles.
- Consider sub-zero layer(s) when calculating freezing levels.

Bibliography

Hall, B.A. 1996: Forecasting weather below 15,000 feet. 4th Joint UK Met. Office/WMO Aeronautical Forecasting Seminar, Meteorological Office College, July 1996.

FORECASTERS' REFERENCE BOOK — INDEX

C

D

E

F

G

H

I

J

K

L

M

N

O

P

Q

R

S

T

U

V

W

Fig 3.6 (FRB 3-11, Source 3-12)
The abscissa scale in the **middle** (upper and lower) pair of graphs ('Part 2') should read $T_2 + T_1$, (NOT $T_2 - T_1$). However, abscissa scale in 'Part 1' pair of graphs stands as $T_2 - T_1$

7.1.1 Fronts (7-1)

Third sentence: " Conversely frontolysis will occur when there are pressure **rises** on both sides of the front; ....." (*not* falls)

7.2.1 (7-9) and corresponding Fig. 7.14 (7-10)

7.2 Frontal features and development

7.2.1 Features of a depression (Fig 7.14)
Surface lows ...etc as in text.

In the lowest layers:
(i) Front lies on warm boundary of tightest θ_w gradient (**Fig. 7.14(a)**); *a pronounced gradient of* θ_w *exists near the surface cold front with decreasing* θ_w *with height (potential instability) at the bottom of the cold air mass (Fig. 7.14(c)). (Above about 700 hPa the pattern of isentropes of* θ_w *differ little from the pattern of isentropes of* θ*).*

(ii) as in text

Fig 7.14 (7-10): Isotherm values at 10°C intervals are added to (b); the legend for (b) is correspondingly changed to read 'temperature' NOT 'potential temperature'. In (c) the position of the tropopause in the warm air near B has been redrawn.
(See overpage for re-drawn Fig 7.14).

JRS
14/1/98

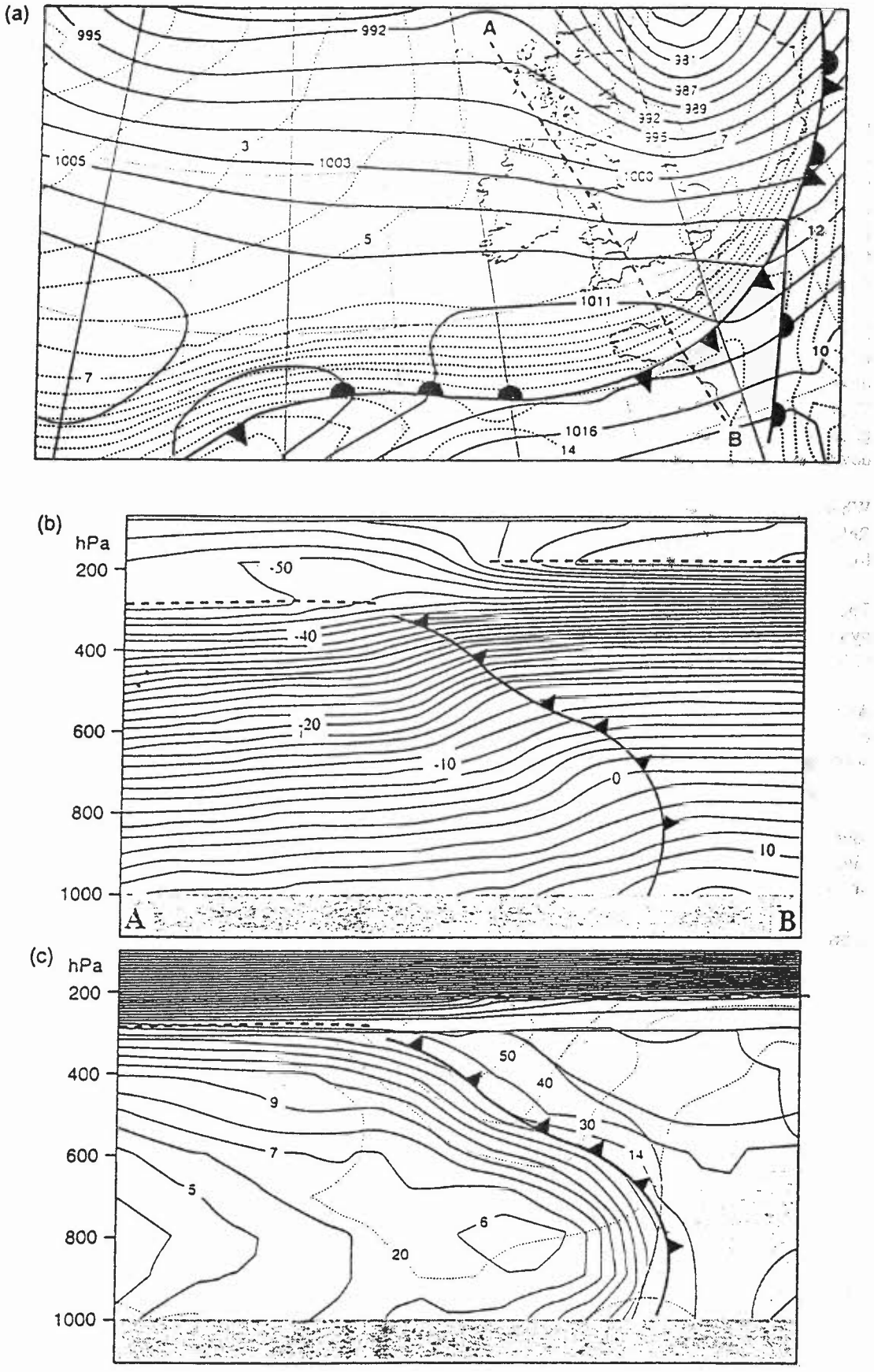

Figure 7.14. The structure of a cold front at 2100 UTC on 2 November 1992: 900 hPa WBPT every 1 °C (dotted), MSLP every 4 hPa (solid), (b) temperature (°C), and (c) cross-section through ana cold front (line AB in (a), distance 1400 km), solid lines represent WBPT every 1 °C, the shaded area frontal cloud, thin dashed lines the wind strength every 10 m s^{-1} and thick dash lines the tropopause.